Universidad de Córdoba

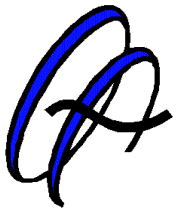

Departamento de Química Analítica

CONTRIBUCIONES ANALÍTICAS A LA CARACTERIZACIÓN Y DETERMINACIÓN DE NANOPARTÍCULAS

ANALYTICAL CONTRIBUTIONS TO THE CHARACTERIZATION AND DETERMINATION OF NANOPARTICLES

Tesis Doctoral

Ángela Inmaculada López Lorente

Córdoba, 2013

TITULO: *Contribuciones analíticas a la caracterización y determinación de nanopartículas. Analytical contributions to the characterization and determination of nanoparticles*

AUTOR: *Ángela Inmaculada López Lorente*

© Edita: Servicio de Publicaciones de la Universidad de Córdoba. 2014
Campus de Rabanales
Ctra. Nacional IV, Km. 396 A
14071 Córdoba

www.uco.es/publicaciones
publicaciones@uco.es

CONTRIBUCIONES ANALÍTICAS A LA CARACTERIZACIÓN Y DETERMINACIÓN DE NANOPARTÍCULAS

EL DIRECTOR,

Fdo. **Miguel Valcárcel Cases**
Catedrático del Departamento
de Química Analítica de la
Universidad de Córdoba

Trabajo presentado para aspirar al grado de Doctor en Ciencias

LA DOCTORANDA,

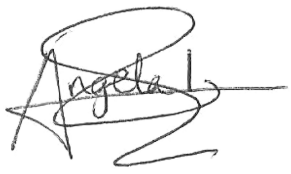

Fdo. **Ángela Inmaculada López Lorente**
Licenciada en Química

Miguel Valcárcel Cases, Catedrático del Departamento de Química Analítica de la Universidad de Córdoba,

EN CALIDAD DE:

Director de la Tesis Doctoral presentada por la Licenciada en Química ÁNGELA INMACULADA LÓPEZ LORENTE, titulada "Contribuciones analíticas a la caracterización y determinación de nanopartículas",

CERTIFICA:

1) Que el trabajo experimental de la Tesis Doctoral ha sido desarrollado en los laboratorios del Departamento de Química Analítica de la Universidad de Córdoba (España) y en el Institut für Analytische und Bioanalytische Chemie de la Universität Ulm (Alemania).

2) A mi juicio, reúne todos los requisitos exigidos a este tipo de trabajo.

3) ÁNGELA LÓPEZ es la primera autora de todos los trabajos científicos presentados en la Tesis. De acuerdo a la normativa de la Universidad y los acuerdos internos de nuestro grupo de investigación, el primer autor es el responsable por completo de la implementación del trabajo experimental y de la producción de la primera versión del artículo. Además, ella ha participado activamente en las reuniones con el director para comprobar y discutir el progreso del trabajo doctoral.

Córdoba, a 15 de Noviembre de 2013.

Miguel Valcárcel Cases

Miguel Valcárcel Cases, Full Professor of Analytical Chemistry of the University of Córdoba,

IN QUALITY OF:

Supervisor of the Doctoral Thesis of ÁNGELA INMACULADA LÓPEZ LORENTE, entitled "Analytical contributions to the characterization and determination of nanoparticles",

CERTIFIES THAT:

1) The experimental work of the PhD thesis has been developed in the laboratories of the Department of Analytical Chemistry of the University of Córdoba (Spain) and the Institute of Analytical and Bioanalytical Chemistry of the University of Ulm (Germany).

2) According to my judgment the thesis meets all the requirements of this type of scientific work.

3) ÁNGELA LÓPEZ is the first author of all the scientific papers presented in the thesis. According to the University rules and the internal agreements in our research group, the first author of a paper is the full responsible for the implementation of the experimental work and also to produce the first draft of the paper. In addition, she has also actively participated in the meetings with the supervisor to check and discuss the progress of the doctoral work.

Córdoba, 15th November 2013

Miguel Valcárcel Cases

TÍTULO DE LA TESIS: CONTRIBUCIONES ANALÍTICAS A LA CARACTERIZACIÓN Y DETERMINACIÓN DE NANOPARTÍCULAS

DOCTORANDO/A: Ángela Inmaculada López Lorente

INFORME RAZONADO DEL/DE LOS DIRECTOR/ES DE LA TESIS

La doctoranda Ángela Inmaculada López Lorente cursó brillantemente los estudios del Máster en Química Fina Avanzada, obteniendo excelentes calificaciones en las asignaturas del mismo. El trabajo fin de Máster se publicó en la revista Analyst, situada en el primer cuartil del área de conocimiento.

La temática de la tesis se encuadra en una línea de investigación puntera, como es la Nanociencia y Nanotecnología Analíticas. En este sentido, se han desarrollado métodos de caracterización y determinación de nanopartículas en matrices medioambientales y biológicas, dado el déficit de técnicas analíticas para dichos fines.

La realización de la investigación recogida en la Memoria que se presenta, ha permitido a la doctoranda adquirir una sólida formación analítica, adiestrándose en el manejo de técnicas de separación electroforéticas, espectroscopias Raman e infrarroja, microscopías de barrido, transmisión y fuerza atómica, entre otras. Asimismo, se han estudiado nanopartículas de distinta naturaleza en diversas matrices medioambientales y biológicas, lo que ha permitido completar la formación integral de la doctoranda en el ámbito analítico. Todo ello ha dado lugar a 14 artículos científicos publicados o en vías de publicación en revistas del primer cuartil del área de Química Analítica, y a la publicación de un capítulo de libro. También han sido fruto de esta Tesis Doctoral 23 comunicaciones a Congresos nacionales e internacionales, ocho de ellas orales/flash.

La estancia realizada en el grupo de investigación del Prof. Mizaikoff (Universidad de Ulm, Alemania) durante el desarrollo de la Tesis Doctoral ha completado de forma satisfactoria dicha formación, profundizando en nuevos procedimientos de síntesis y caracterización de nanopartículas de oro.

Por todo ello, considero que la investigación desarrollada y recogida en esta Memoria, reúne todos los requisitos necesarios en cuanto a originalidad, innovación y calidad, y autorizo la presentación de la Tesis Doctoral de Dª Ángela Inmaculada López Lorente.

Córdoba, a 15 de Noviembre de 2013

Firma del/de los director/es

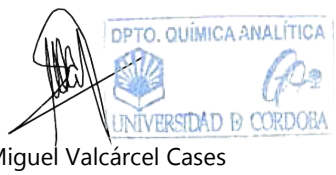

Fdo.: Miguel Valcárcel Cases

MENCIÓN DOCTORADO INTERNACIONAL

Mediante la defensa de esta Memoria de Tesis Doctoral se pretende optar a la obtención de la Mención de "Doctorado Internacional" habida cuenta de que el doctorando reúne los requisitos para tal mención (R.D. 99/2011, de 28 de Enero):

1. Cuenta con los informes favorables de dos doctores pertenecientes a instituciones de Enseñanza Superior de países distintos a España.

2. Uno de los miembros del tribunal que ha de evaluar la Tesis pertenece a un centro de Enseñanza Superior de otro país distinto a España.

3. Parte de la defensa de la Tesis Doctoral se realizará en una lengua distinta de las lenguas oficiales en España.

4. La doctoranda ha realizado una estancia de cuatro meses en el Institut für Analytische und Bioanalytische Chemie de la Universität Ulm (Alemania), gracias a la concesión de una ayuda para estancias en el extranjero asociada a una beca de Formación de Profesorado Universitario del Ministerio de Educación, Cultura y Deporte, que ha contribuido a su formación y permitido desarrollar parte del trabajo experimental de esta Memoria.

Agradezco al Ministerio de Educación, Cultura y Deporte la concesión de una beca de Formación de Profesorado Universitario (FPU) que ha hecho posible mi dedicación a este trabajo durante los últimos cuatro años.

ÍNDICE/INDEX

ACRÓNIMOS/ABBREVIATIONS 1

OBJETO/AIM 7

BLOQUE I. INTRODUCCIÓN 13

I.1. ANALYTICAL NANOSCIENCE AND NANOTECHNOLOGY 15

I.2. TYPES OF NANOPARTICLES 25

2.1. Organic nanoparticles

2.2. Inorganic nanoparticles

2.3. Hybrid nanoparticles

Capítulo 1. Analytical potential of hybrid nanoparticles. 35

I.3. NANOPARTICLES AS TOOLS IN ANALYTICAL CHEMISTRY 71

I.4. NANOPARTICLES AND NANOSTRUCTURED MATERIALS AS ANALYTICAL OBJECTS 78

4.1. Microscopic techniques for the analysis of nanoparticles

4.2. Spectroscopic and related techniques for the analysis of nanoparticles

4.3. Methods of separation and purification of nanoparticles

4.4. Determination of nanoparticles in environmental, food and biological samples

Capítulo 2. Determination of nanoparticles in biological matrices. 91

BLOQUE II. HERRAMIENTAS ANALÍTICAS 143

II.1. Nanomateriales 145

II.2. Reactivos y muestras 146

II.3. Instrumentación 148

II.4. Aparatos y material 151

II.5. Síntesis y funcionalización de nanopartículas 153

II.6. Procedimientos de dispersión, extracción y preconcentración de nanopartículas 157

BLOQUE III. SÍNTESIS DE NANOPARTÍCULAS **161**

Introducción

Capítulo 3. Characterization of stainless steel assisted bare gold nanoparticles and their analytical potential. 165

Capítulo 4. Continuous flow synthesis and characterization of tailor-made bare gold nanoparticles for analytical applications. 189

BLOQUE IV. CARACTERIZACIÓN DE NANOPARTÍCULAS **211**

IV.1. ESPECTROSCOPIA RAMAN 213

Introducción

Capítulo 5. Raman spectroscopic characterization of single-walled carbon nanotubes: influence of sample aggregation state. 217

Capítulo 6. Qualitative detection and quantitative determination of single-walled carbon nanotubes in mixtures of carbon nanotubes with a portable Raman spectrometer. 245

IV.2. ESPECTROSCOPIA INFRARROJA 273

Introducción

Capítulo 7. Infrared attenuated total reflection spectroscopy as a tool for the characterization of gold nanoparticles in solution 275

IV.3. ELECTROFORESIS CAPILAR 301

Introducción

Capítulo 8. Electrophoretic methods for the analysis of nanoparticles. 303

Capítulo 9. Capillary electrophoresis separation of citrate-capped silver and gold nanoparticles by interaction with thiol compounds as additives in buffer solution. 343

BLOQUE V. DETERMINACIÓN DE NANOPARTÍCULAS EN MUESTRAS AMBIENTALES Y BIOLÓGICAS **369**

V.1. MICROEXTRACCIÓN LÍQUIDO-LÍQUIDO CON LÍQUIDO IÓNICO 372

Introducción

Capítulo 10. Rapid analysis of gold nanoparticles in liver and river water samples. 375

Capítulo 11. Determination of carboxylic SWCNTs in river water by microextraction in ionic liquid and determination by Raman spectroscopy. 401

V.2. DETERMINACIÓN MEDIANTE ESPECTROSCOPIA RAMAN AMPLIFICADA EN SUPERFICIE (SERS) 421

Introducción

Capítulo 12. Bare gold nanoparticles mediated surface-enhanced Raman spectroscopy determination and quantification of carboxylated single-walled carbon nanotubes. 423

V.3. PRECONCENTRACIÓN EN MEMBRANAS MODIFICADAS CON NANOTUBOS DE CARBONO 449

Introducción

Capítulo 13. The potential of carbon nanotube membranes for analytical separations. 451

Capítulo 14. Sequential preconcentration and on-membrane Raman determination of carboxylic single-walled carbon nanotubes in river water samples. 479

BLOQUE VI. RESULTADOS Y DISCUSIÓN **503**

VI.1. Carbon nanoparticles 509

VI.2. Metallic nanoparticles 520

VI.3. Facets of nanoparticles in Analytical Nanoscience and Nanotechnology 529

CONCLUSIONES/CONCLUSIONS **533**

AUTOEVALUACIÓN CIENTÍFICA DE LA TESIS DOCTORAL/SCIENTIFIC SELF-ASSESSMENT OF THE PhD THESIS **547**

ANEXOS: PRODUCCIÓN CIENTÍFICA **561**

Anexo A. Publicaciones científicas derivadas de la Tesis Doctoral 563

Anexo B. Presentación de comunicaciones a congresos 569

Anexo C. Pósters 577

ACRÓNIMOS

ABBREVIATIONS

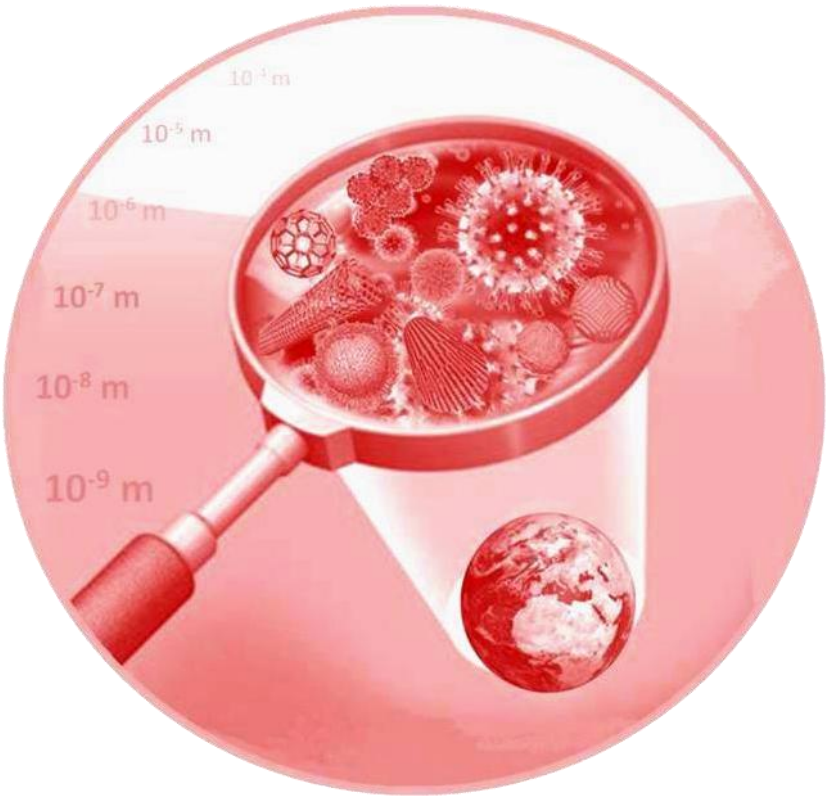

AAS	Espectroscopia de absorción atómica/ Atomic absorption spectroscopy
AFM	Microscopía de fuerza atómica/ Atomic force microscopy
AgNPs	Nanopartículas de plata/ Silver nanoparticles
AN&N	Nanociencia y Nanotecnología Analíticas/ Analytical Nanoscience & Nanotechnology
AuMPC	Monocapa de oro protegida/ Gold monolayer-protected cluster
AuNPs	Nanopartículas de oro/ Gold nanoparticles
BGE	Tampón electroforético/ Electrophoretic buffer
BMIM PF_6	1-butil-3-metil imidazolio hexafluorofosfato/ 1-butyl-3-methyl imidazolium hexafluorophosphate
BSA	Albúmina de suero bovino/ Bovine serum albumin
CAPS	Ácido 3-ciclohexilamino-1-propanosulfónico/ 3-cyclohexylamino-1-propanesulfonic acid
CDs	Nanopuntos de carbono / Carbon dots
CE	Electroforesis capilar/ Capillary electrophoresis
CEC	Electrocromatografía capilar/ Capillary electrochromatography
CGE	Electroforesis capilar en gel/ Capillary gel electrophoresis
CLSM	Microscopía de barrido de láser confocal/ Confocal laser scanning microscopy
CNFs	Nanofibras de carbono/ Carbon nanofibers
CNOs	Nanocebollas de carbono/ Carbon nano-onions
CNTs	Nanotubos de carbono / Carbon nanotubes
CRM	Microscopio Raman confocal/ Confocal Raman microscope
c-SWNTs	Nanotubos de carbono monocapa carboxilados/ Carboxylated single walled carbon nanotubes
CTAB	Bromuro de hexadeciltrimetilamonio/ Cetyltrimethylammonium bromide
CTAC	Cloruro de hexadeciltrimetilamonio/ Cetyltrimethylammonium chloride
CVD	Deposición química de vapor/ Chemical vapor deposition
CZE	Electroforesis capilar de zona/ Capillary zone electrophoresis
DAD	Detector de diodos en fila/ Diode array detector
DEP	Dielectroforesis/ Dielectrophoresis
DF	Dendrofullereno [60]/ Dendro[60] fullerene
DLS	Dispersión dinámica de luz/ Dynamic light scattering
DMF	Dimetilformamida/ Dimethylformamide
DMSO	Dimetilsulfóxido/ Dimethyl sulfoxide
DNs	Nanocristales de diamante / Diamond nanocrystals
DOC	Desoxicolato sódico/ Sodium deoxycholate
DOX	Doxorrubicina/ Doxorubicin
DSB	Destiobiotina/ Desthiobiotin
DWNTs	Nanotubos de carbono de doble capa/ Double-walled carbon nanotubes
EDC	Acoplamiento con etilen carbodiimida/ Ethylene carbodiimide coupling

EDTA	Ácido etilendiamino tetraacético/ Ethylenediaminetetraacetic acid
EDX/EDS	Espectroscopia de energía dispersiva de rayos X/ Energy dispersive X-ray spectroscopy
EELS	Espectroscopia de pérdida de energía de electrones/ Electron energy loss spectroscopy
EM	Microscopías electrónicas/ Electron microscopies
EOF	Flujo electroosmótico/ Electroosmotic flow
ESEM	Microscopio de barrido electrónico ambiental/ Environmental scanning electron microscopy
ESI-MS	Espectrometría de masas con electrospray/ Electrospray-mass spectrometry
ETAAS	Espectroscopia de absorción atómica electrotérmica/ Electrothermal atomic absorption spectroscopy
FACS	Clasificación de células activadas por fluorescencia/ Fluorescence-activated cell sorting
FFF	Fraccionamiento de flujo de campo/ Field-flow fractionation
FITC	Isotiocianato de fluoresceína/ Fluorescein isothiocyanate
FRET	Transferencia de energía de resonancia de fluorescencia/ Fluorescence resonance energy transfer
FT-IR	Infrarrojo con transformada de Fourier/ Fourier transform-infrared
FWHM	Ancho a mitad del máximo/ Full width at half maximum
GC	Cromatografía de gases/ Gas chromatography
GFAAS	Espectrometría de absorción atómica en horno de grafito/ Graphite furnace atomic absorption spectrometry
GQDs	Puntos cuánticos de grafeno / Graphene quantum dots
HDC	Cromatografía hidrodinámica/ Hydrodynamic chromatography
HMIM PF_6	1-hexil-3-metil imidazolio hexafluorofosfato/ 1-hexyl-3-methyl imidazolium hexafluorophosphate
HPLC	Cromatografía líquida de alta resolución/ High performance liquid chromatography
HPMC	Hidroxipropilmetilcelulosa/ Hydroxypropyl methyl cellulose
HR-TEM/HTEM	TEM de alta resolución/ High resolution TEM
IC	Cromatografía iónica/ Ion chromatography
ICP-AES	Plasma de acoplamiento inductivo con espectroscopia de emisión atómica/ Inductively coupled plasma with atomic emission spectroscopy
ICP-MS	Plasma de acoplamiento inductivo con espectrometría de masas/ Inductively coupled plasma with mass spectrometry
ICP-OES	Plasma de acoplamiento inductivo con espectroscopia de emisión óptica/ Inductively coupled plasma with optical emission spectroscopy
IEF	Enfoque isoeléctrico/ Isoelectric focusing
ILs	Líquidos iónicos/ Ionic liquids
IR-ATR	Espectroscopia infrarroja con reflexión total atenuada/ Infrared attenuated total reflection spectroscopy
IUPAC	Unión Internacional de Química Pura y Aplicada/ International Union of Pure and Applied Chemistry

K-NN	K nearest neighbours
LAMMS	Espectrometría de masas con microsonda láser de una partícula/ Single-particle laser microprobe mass spectrometry
LC	Cromatografía de líquidos/ Liquid chromatography
LIBS	Espectroscopia de plasma inducido por láser/ Laser-induced breakdown spectrocopy
LIF	Fluorescencia inducida por láser/ Laser-induced fluorescence
LLE	Extracción líquido-líquido/ Liquid-liquid extraction
LODs	Límites de detección/ Limits of detection
LSPR	Plasmón de resonancia superficial localizado/ Localized surface plasmon resonance
LVSS	Inyección de grandes volúmenes de muestra/ Large volumen sample stacking
MALLS	Dispersión de luz láser multiángulo/ Multiangle laser light scattering
MEKC	Cromatografía electrocinética micelar/ Micellar electrokinetic chromatography
MHNs	Nanopartículas híbridas micelares/ Micellar hybrid nanoparticles
MiNDECK	Cromatografía electrocinética micelar con dispersión de nanopartículas/ Micellar nanoparticle dispersion electrokinetic chromatography
MIPs	Polímeros de impresión molecular/ Molecularly imprinted polymers
MNPs	Nanopartículas magnéticas/ Magnetic nanoparticles
MNPs (chapter 8)	Nanopartículas metálicas/ Metallic nanoparticles
MRI	Imagen por resonancia magnética/ Magnetic resonance imaging
MS	Espectrometría de masas/ Mass spectrometry
MWNTs	Nanotubos de carbono multicapa/ Multiwalled carbon nanotubes
NAs	Ácidos nucléicos/ Nucleic acids
NIR	Infrarrojo cercano/ Near-infrared
NMR	Resonancia magnética nuclear/ Nuclear magnetic resonance
NPs	Nanopartículas / Nanoparticles
NSOM	Microscopio óptico de barrido de campo cercano/ Near-field scanning optical microscopy
PAGE	Electroforesis en gel de poliacrilamida/ Polyacrylamide gel electrophoresis
PAHs	Hidrocarburos aromáticos policíclicos/ Polycyclic aromatic hydrocarbons
PCA	Análisis por componentes principales/ Principal component analysis
PCs	Componentes principales/ Principal components
PEG	Polietilenglicol/ Polyethylene glycol
PLS	Calibrado por mínimos cuadrados parciales/Partial least square modelling
PTFE	Politetrafluoroetileno (Teflón)/ Polytetrafluoroethylene
PVA	Alcohol polivinílico/ Polyvinyl alcohol
PVDF	Polifluoruro de vinilideno/ Polyvinylidene fluoride
QDs	Puntos cuánticos/ Quantum dots

RBM	Modos de respiración radiales/ Radial breathing modes
REPSM	Modo de concentración con polaridad de electrodo reversa/ Reversed-electrode polarity-stacking mode
RSD	Desviación estándar relativa/ Relative standard deviation
SAED	Difracción de electrones en área seleccionada/ Selected area electron diffraction
SAMs	Monocapas autoensambladas/ Self-assembled monolayers
SAXS	Dispersión de rayos X de ángulo pequeño/ Small angle X-ray scattering
SC	Colato sódico/ Sodium cholate
SDBS	Dodecilbenceno sodio sulfonato/ Sodium dodecylbenzene sulfonate
SDS	Dodecil sulfato sódico/ Sodium dodecyl sulfate
SEC	Cromatografía de exclusión por tamaños/ Size-exclusion chromatography
SECM	Microscopía de barrido electroquímica/ Scanning electrochemical microscopy
SEIRA	Absorción infrarroja amplificada por superficie/ Surface-enhanced infrared absorption
SEM	Microscopía de barrido electrónico/ Scanning electron microscopy
SERS	Dispersión Raman amplificada por superficies/ Surface enhanced Raman scattering
SLS	Dispersión de luz estática/ Static light scattering
SPM	Microscopías de sonda de barrido/ Scanning probe microscopies
SPR	Resonancia de plasmón superficial/ Surface-plasmon resonance
STEM	Microscopio electrónico de barrido y transmisión/ Scanning transmission electron microscopy
STP	Planta de tratamiento de aguas residuales/ Sewage treatment plant
STXM	Microscopía de rayos X de transmisión y barrido/ Scanning transmission X-ray microscopy
SWNHs	Nanocuernos de carbono monocapa/ Single-walled carbon nanohorns
SWNTs	Nanotubos de carbono monocapa/ Single-walled carbon nanotubes
TA	Ácido tióctico/ Thioctic acid
TA-AuNPs	Nanopartículas de oro funcionalizadas con ácido tióctico/ Thioctic-acid functionalized gold nanoparticles
TCA	Ácido tricloroacético/ Trichloroacetic acid
TEM	Microscopía de transmisión electrónica/ Transmission electron microscopy
TERS	Dispersión Raman amplificada en punta/ Tip-enhanced Raman scattering
TGA	Análisis termogravimétrico/ Thermogravimetric analysis
TMA	Ácido tiomálico / Thiomalic acid
TOPO-TOP	Óxido de trioctilfosfina-Trioctilfosfina/ Tri-n-octyl-phosphine oxide-Tri-n-octyl-phosphine
UV-Vis	Ultravioleta visible/ Ultraviolet visible
XRM	Microscopía de rayos X/ X-ray microscopy

OBJETO

AIM

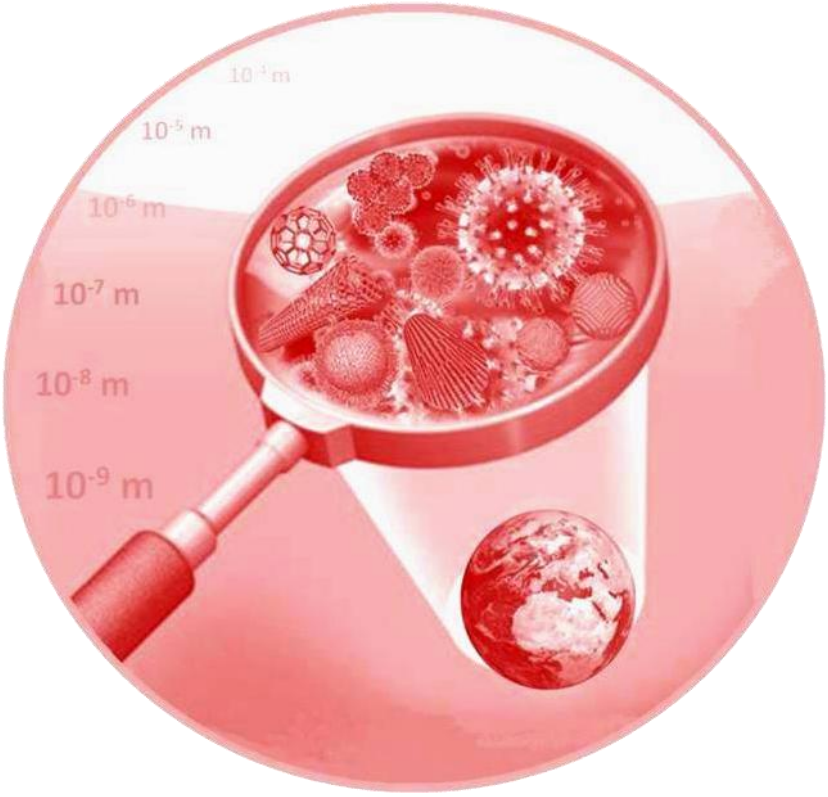

Actualmente nos encontramos en plena expansión de la Nanociencia y Nanotecnología. Millones de toneladas de nanopartículas (NPs) se producen anualmente con fines comerciales o como subproductos de la actividad humana. La creciente producción y el uso de nanomateriales conducirán a su acumulación en el medio ambiente, generando potenciales implicaciones negativas para la salud humana y animal. Sin embargo, la evaluación de los efectos de los nanomateriales en la salud y el medio ambiente es difícil ya que los métodos analíticos y herramientas necesarias están aún en desarrollo. En comparación con los contaminantes clásicos y otros emergentes, las nanopartículas están planteando desafíos ambientales y analíticos desconocidos.

Uno de los roles de la Química Analítica en este contexto es el análisis y caracterización de dichas nanopartículas. Se pueden definir dos facetas clave en la Nanociencia y Nanotecnología Analítica, por un lado, la consideración de las nanopartículas y el material nanoestructurado como herramientas para la innovación y mejora de los procesos (bio)químicos de medida, aspecto más desarrollado hasta la fecha, y por otro, su consideración como objetos, faceta en la que se enmarca la presente Tesis Doctoral. Como interfase entre ambas existe una tercera opción que consiste en que las nanopartículas se empleen como herramientas en procesos analíticos para caracterizar/determinar otros nanomateriales.

La consideración de la nanomateria como analito-diana requiere de métodos analíticos que permitan detectar y/o cuantificar nanopartículas en diferentes tipos de muestras, así como el desarrollo y puesta a punto de metodologías

para su caracterización química. Si bien puede afirmarse que hay un déficit de técnicas analíticas que permitan su caracterización rápida, la situación se agrava aún más cuando se pretenden determinar en matrices complejas como medioambientales y biológicas.

Teniendo en cuenta lo anteriormente expuesto, el objetivo principal de la Tesis Doctoral que se presenta en esta Memoria es el desarrollo de metodologías analíticas que permitan la caracterización y determinación de nanomateriales en matrices ambientales y biológicas. Con este objetivo global, los objetivos específicos de la investigación a desarrollar son los siguientes:

- Desarrollo de nuevos procedimientos de síntesis de nanopartículas de forma simple, económica, buena con el medio ambiente, así como el acoplamiento de los procedimientos de síntesis para su producción en flujo continuo.
- Caracterización de las nuevas nanopartículas obtenidas mediante diversas técnicas microscópicas y espectroscópicas, además de la evaluación de su potencial analítico como herramientas para la mejora de los sistemas de detección y determinación de otros nanomateriales.
- Desarrollo de metodologías para la caracterización rápida de nanomateriales, tanto de productos de síntesis como mezclas de nanopartículas con distintas propiedades, mediante el empleo de técnicas espectroscópicas y de separación.
- Desarrollo de métodos para la preconcentración, determinación y cuantificación de nanomateriales en matrices ambientales –agua de río- o biológicas –hígado de pollo.

De la amplia variedad de nanopartículas descritas hasta la fecha, esta Tesis Doctoral se ha centrado en las más populares y representativas dentro de las metálicas y de carbono, como son las nanopartículas de oro y plata y los nanotubos de carbono, respectivamente.

Nowadays, we are immersed in a full expansion of Nanoscience and Nanotechnology. Millions of tonnes of nanoparticles (NPs) are produced annually for commercial purposes or as by-products of human activity. The growing production and use of nanomaterials will inevitably lead to their accumulation in the environment, which can have major implications for human and animal health. However, assessing the effects of nanomaterials on health and the environment is difficult since analytical methods required are still under development. Compared with classical and other emerging contaminants, nanoparticles are posing previously unknown environmental and analytical challenges.

One of the roles of Analytical Chemistry in this context is the analysis and characterization of such NPs. Two key facets of Analytical Nanoscience and Nanotechnology can be defined, on the one side, the consideration of nanoparticles and nanostructured materials as tools for the innovation and improvement of (bio)chemical measurement processes, which is the aspect more developed until date, and, on the other hand, their consideration as objects, facet in which this Doctoral Thesis is framed. A third option exists as interface between both of them, which consists on nanoparticles being employed as tools in analytical processes for the characterization/determination of other nanomaterials.

The consideration of nanomatter as target-analyte requires analytical methods that enable the detection and/or quantification of nanoparticles in different kind of samples, as well as the development and refinement of methodologies for their chemical characterization. While it can be affirmed that there is a lack of analytical techniques that allow their rapid characterization, the situation is

further aggravated when trying to determine them in complex matrices such as environmental or biological.

Based on the foregoing, the primary aim of this doctoral work is the development of analytical methodologies that enable the characterization and determination of nanomaterials in environmental and biological matrices. The specific objectives derived from this general objective are as follows:

- *Development of new simple, inexpensive, environmentally friendly procedures for the synthesis of nanoparticles, as well as their coupling for continuous flow production.*
- *Characterization of the new obtained nanoparticles by means of diverse microscopic and spectroscopic techniques, in addition to the evaluation of their analytical potential as tools for the improvement of detection and determination systems of other nanomaterials.*
- *Development of methodologies for the rapid characterization of nanomaterials, both products of synthesis and mixtures of nanoparticles with different properties, by employing spectroscopic and separation techniques.*
- *Development of methods for the preconcentration, determination and quantification of nanomaterials in environmental –river water- and biological –chicken liver- matrices.*

Among the wide variety of nanoparticles described until date, this Doctoral Thesis has focused on the most popular and representative within metallic and carbonaceous, such as gold and silver nanoparticles and carbon nanotubes, respectively.

INTRODUCCIÓN

INTRODUCTION

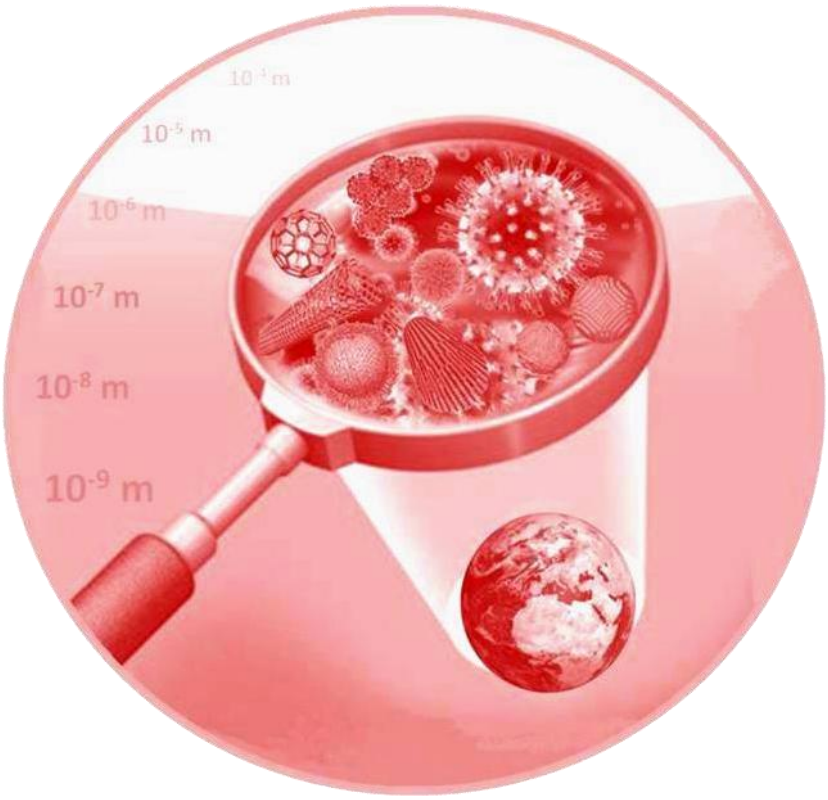

BLOQUE I

1

I.1. ANALYTICAL NANOSCIENCE AND NANOTECHNOLOGY

The common characteristic of Nanoscience and Nanotechnology (N&N) is the size of the target objects, which are comprised in the so-called "nanometric scale", typically between 1 and 100 nm.

Nanoscience has multiple complementary definitions, such as: "*the science of the synthesis, analysis and manipulation of materials at atomic or molecular level, where the characteristics or physical or chemical properties are substantially different to those shown by the same material at a higher scale (micro or macro)*[1]", or, simply: "*the science based on the diverse structures of materials which have dimensions of a billionth part of the meter*[2]".

On the other hand, **Nanotechnology** "*deals with the design, characterization and use of structures, devices and systems, whose shape and size are controlled in the nanoscale*[1]".

A substantial aspect of Nanoscience and Nanotechnology (N&N) is their multidisciplinary as well as transversal and convergent character. Physicists, chemists and engineers are the scientists and professionals more directly

[1] M. Valcárcel. Las nanoestructuras de carbono en la nanociencia y nanotecnología analíticas. *Discurso de recepción como académico de número de la Real Academia de Ciencias* (2010).
[2] P. Poole, F.J. Owens. Introduction to nanotechnology (2003). Wiley, Hoboken, NJ.

involved, but their convergence with other areas such as information technology and communication, biotechnology and materials science, in a first approach, and medicine, pharmacy, agrifood and diverse types of industries such as textile or energetic, in another, has to be pointed out.

Analytical Science cannot be left out of N&N[3] and, in fact, it is even present in many definitions of N&N since reliable information about the nanoworld is crucial to make well founded scientific and technical decisions in this area. Words belonging to analytical discipline such as "analysis" or "characterization" and other shared with other disciplines such as "use" or "employment" summarize the two key facets of the relationship between Analytical Chemistry and Nanoscience and Nanotechnology, namely: i) the consideration of nanoparticles and nanostructured materials as objects (analytes) or ii) tools for the innovation and improvement of the (bio)chemical measurements processes. These two facets of Analytical Chemistry in the context of Nanoscience and Nanotechnology will be dealt in depth later.

The major application areas of nanotechnology can be classified in four groups[3], namely: i) nanobiotechnology and nanomedicine, ii) nanomaterials, iii) nanoelectronics, and iv) nanosensors/nanodevices, nanotechnological instrumentation and nanometrology. The last area is directly related to analytical science, which also plays an essential role in the other three, for example dealing with the monitoring of production processes or both the characterization and use of end products.

Overview of Analytical Nanoscience and Nanotechnology

There are several emerging possibilities when introducing Nanoscience and Nanotechnology in the analytical scope. Because of that, a multiple classification

[3] M. Valcárcel, B.M. Simonet, S. Cárdenas, Anal. Bioanal. Chem. 391 (2008) 1881-1887.

based on four complementary criteria has been done, which is shown schematically in Figure I.1.1. and following commented on.

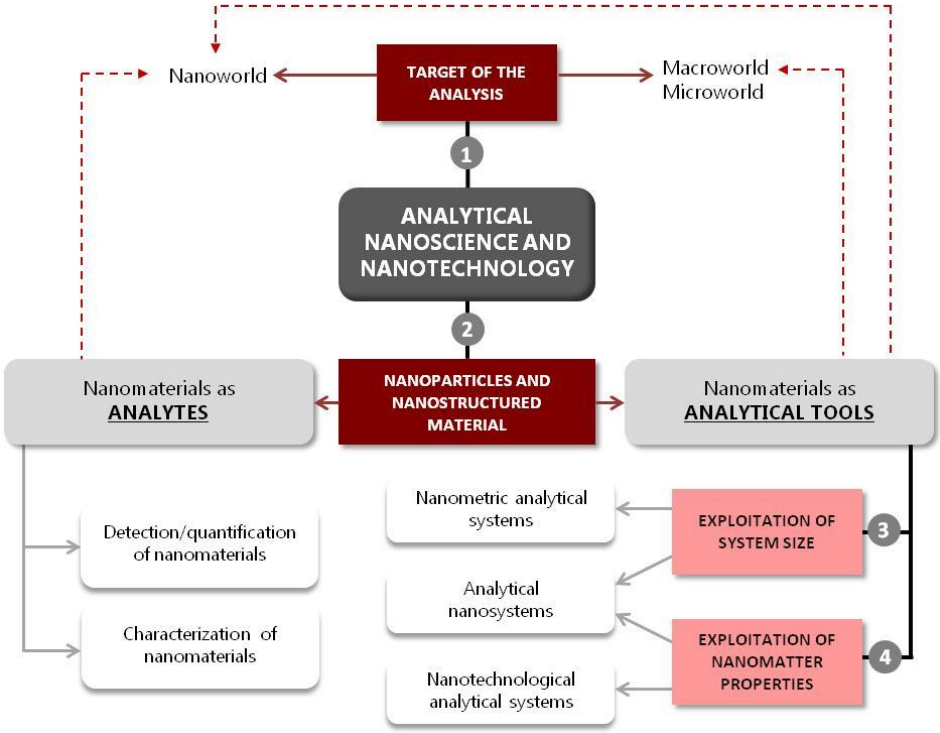

Figure I.1.1. Inherent classifications of Analytical Nanoscience and Nanotechnology taking into account four criteria: 1) Target of the analysis; 2) According to the consideration of the nanomatter; 3) According to the exploitation of the nanosize; 4) According to the exploitation of the nanomatter properties. For details, see the text.

The first criterion (Figure I.1.1.(1)) considers the type of material analyzed, which can be conventional (macro or micro in size), or nanomaterials. In the first case, nanoparticles can be involved in the analytical process, conferring it nanotechnological character. An example is the use of quantum dots functionalized with antibodies, which can be injected in organisms in order to

detect carcinogenic processes[4]. In the second possibility the target is the own nanoworld, which coincides with the consideration of nanomaterials as analytes. Along this thesis different approaches to the analysis of the nanoworld will be presented, some of them also employing nanoparticles as tools in order to improve the analytical process of determination of nanomaterials.

The second criterion (Figure I.1.1.(2)) relies on the analytical consideration of nanoparticles and nanostructured materials as objects –analytes- or tools involved in the analytical process. The extraction of chemical information from the structured nanomaterials (composition, chirality, reactivity, etc.) is an indispensable complement to the physical characterization, which is more well-known (dimensions, topography, etc.)[5]. On the other hand, nanomaterials can be used as analytical tools to develop new analytical processes or to improve existing ones (i.e. development of optical sensors, development of stationary and pseudostationary phases in chromatography and capillary electrophoresis, mechanical sensors, etc.).

Criteria 3 and 4 (Figure I.1.1.(3) y (4)) are based on exploitation in the analytical scope of the exceptional properties of nanomaterials, in exploiting the nanosize, or both, which leads to the definition of three types of analytical systems related to Nanoscience and Nanotechnology: nanotechnological analytical systems, nanometric analytical systems, and analytical nanosystems[6]. *Nanotechnological analytical systems* exploit the exceptional physicochemical properties of nanomaterials (although they are in micro/macro analytical systems) accounting for the most current uses of analytical nanoscience. *Nanometric analytical systems* which are based exclusively on the nanosize of the devices involved are

[4] A. Zajac, D. Song, W. Qian, T. Zhukov, Colloids and Surf B: Biointerfaces, 58 (2007) 309-314.
[5] R. Lucena, B.M. Simonet, S. Cárdenas, M. Valcárcel, J. Chromatogr. A, 1218 (2011) 620-637.
[6] M. Valcárcel, B.M. Simonet, Anal. Bioanal. Chem 399 (2011) 1-2.

exemplified by nano-chip liquid chromatography systems[7] exploting the advantages of working with flow rates as low as few nanolitres per minute, a nanopipette[8] or levitated nanodrops as analytical containers[9]. Finally, *Analytical nanosystems* successfully integrate previous two types of systems, by exploiting both the nanosize and nanomaterials properties (e.g. individual carbon nanotubes for use as electrodes[10], supramolecular systems that selectively recognize an analyte[11], and the so called lab-on-a-particle[12]).

How to reach the nanoscale

Nanomaterials can exist in the environment from a natural source, such as organic colloids, magnetite, aerosols, iron oxides, etc. The nanotechnological revolution is posed in a change of paradigm in the fabrication of products. Two approaches can be used to raise nanosize, namely: i) "Top-down" strategies, based on methodologies which achieve nanosize materials from macromaterials: nanoparticles are directly generated from bulk materials via the generation of isolated atoms usually involving physical methods such as milling or attrition, repeated quenching and photolithography[13]; and ii) "Botttom-up" strategies, based on the creation of complex nanostructures from atomic or molecular functional elements. They comprise molecular components as starting materials linked with chemical reactions, nucleation and growth processes to promote the formation of clusters. Numerous kinds of nanoparticles have been produced by liquid-phase synthesis, using techniques such as co-precipitation

[7] R.A. Brennen, H. Yin. K.P. Killeen, Anal. Chem. 79 (2007) 9302-9309.
[8] M.G. Schrlau, E.M. Falls, B.L. Ziober, H.H. Bau, Nanotechnology 19 (2008) 15101.
[9] N. Leopold, M. Haberkorn, T. Laurell, J. Nilsson, J.R. Baena, B. Lendl, Anal. Chem. 75 (2003) 2166-2171.
[10] H. Boo, R.A. Jeong, S. Park, K.S. Kim, K.H. Am, Y.H. Lee, J.H. Han, H.C. Kim, T.D. Chung, Anal. Chem. 78 (2006) 617-620.
[11] A. Burns, H. Ow, U. Wiesner, Chem. Soc. Rev. 35 (2006) 1028-1042.
[12] A.B. Descalzo, R. Martínez-Mañez, F. Sancenon, K. Hoffmann, K. Rurack, Angew. Chem. Int. Ed. 45 (2006) 5924-5948.
[13] G. Cao, Nanosctructures and nanomaterials. Synthesis, Properties & Applicationd. Imperial College Press; London (2004).

of sparingly soluble products by addition, exchange and reduction reactions, oxidation, hydrolysis[14], sol-gel processing[15], microemulsions[16], etc. The latter approach is generally considered to be far more promising due to the higher level of control offered[17]. Figure I.1.2 shows a scheme of the different strategies ("top-down" and "bottom-up") used to achieve the nanoscale.

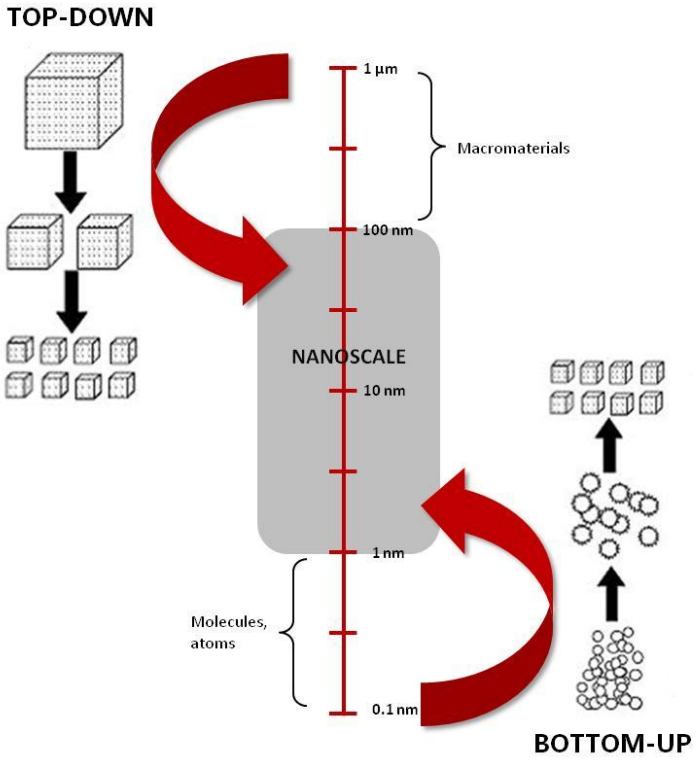

Figure I.1.2. Scheme of the two approaches employed in the fabrication of nanomaterials: "top-down" and "bottom-up".

[14] B.L. Cushing, V.L. Kolesnichenko, C.J. O'Connor, Chem. Rev. 104 (2004) 3893-3946.
[15] B.G. Trewing, I.I. Slowing, S. Giri, H.T. Chen, V.S.Y. Lin, Accounts of Chemical Research 40 (2007) 846-853.
[16] J. Eastoe, M.L. Hollamby, L. Hudson, Adv in Colloids and Interf Sci 128 (2006) 5-15.
[17] C.X. Zhao, L. He, S.Z. Qiao, A.P.J. Middelberg, Chem. Eng. Sci. 66 (2011) 1463-1479.

The added value of nanometric material

The "nanoscale" has introduced a new scenario where impressive changes in physicochemical principles, laws and properties are observed as regards macro and micromaterials.

Two especially significant differences have been described: the surface/volume ratios and chemical reactivities of nanostructured matter in comparison to macro- and microscale matter. In addition, quantum effects are enhanced by effect of the configuration of molecular orbitals (similar to that of atomic orbitals), and, as consequence, chemical, optical, electrical, thermal and magnetic characteristics are unique on the nanoscale. Such changes have shaped the impact of nanotechnology on a number of scientific, technical and industrial fields.

Scientific-technical evolution and limits

Nanoscience and Nanotechnology unarguably have promising prospects. A report of the US National Science Foundation[18] predicted that a new revolution based on the bio-nano-info triangle will shortly surpass the present evolution of the computer-info binomial.

The scientific and industrial impact of Nanoscience and Nanotechnology has grown dramatically in recent years. The exponential growth of the number of papers on this topic published in the last ten years in the SciFinder and the vast amount of economic resources invested in industrial technological developments each year[19] constitute the best support for the brilliant present and promising future of Nanoscience and Nanotechnology. It should be pointed

[18] NSF (2001) Societal applications of the nanoscience and nanotechnology. US National Science Foundation (NSF), Arlington, VA.
[19] A. Hullmann (European Commission, DG Research) "The economic development of nanotechnology. An indicator based analysis". Bruselles, 2006.

out that there are more than one million of scientific papers published on this topic.

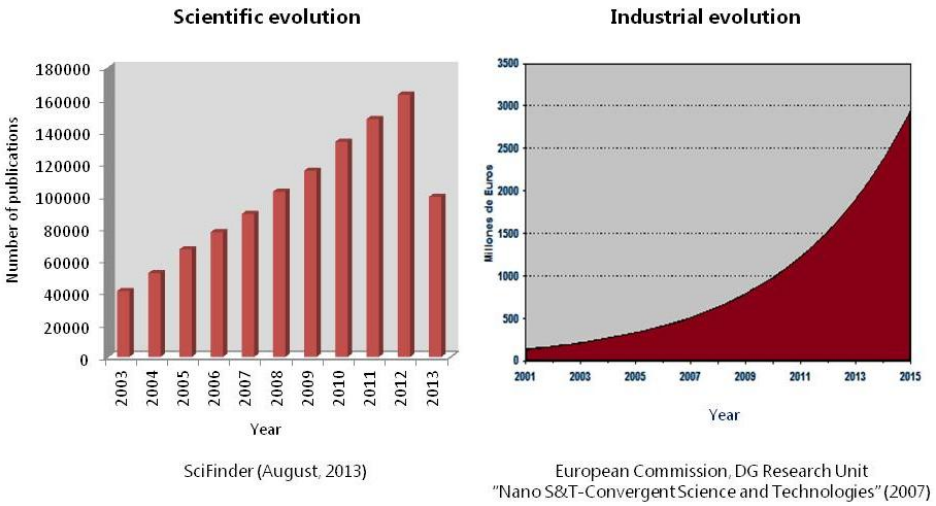

Figure I.1.3. Scientific and industrial evolution of Nanoscience & Nanotechnology: (left) number of publications per year; (right) millions of euros involved in European nanotechnological industry.

The impact of nanotechnology leaves no shadow of doubt. Hassan[20] emphasized that the most crucial aspect in this respect is the small things-big changes binomial. Analytical chemistry should play a major role in the coming advances in N&N, particularly in these aspects: i) the environmental and toxicological impacts of nanotechnology, ii) the need for homogeneous, pure, well-characterized nanoparticles, iii) the need to address nanometrology, and iv) nanomedicine, in the development of biomeasurement nanosystems and the characterization and monitoring of nanostructured pharmaceuticals[3].

Regarding Analytical Nanoscience and Nanotechnology, the use of nanomaterials as analytical tools is the most developed field. Although more than one half of reported applications relate to the use of nanoparticles, the

[20] M.H.A. Hassan, Science 309 (2005) 65-66.

balance is bound to change over the next few years due to the growing significance of the characterization of nanomaterials and the development of new instruments based on nanotechnological approaches.

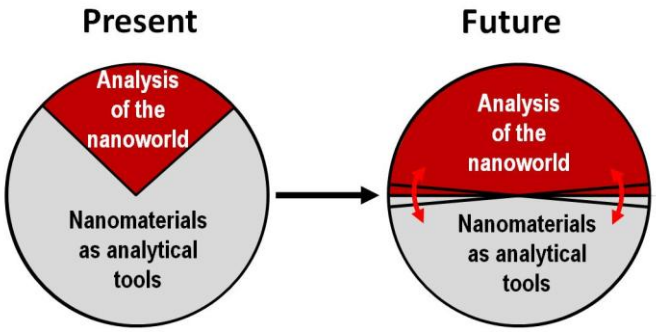

Figure I.1.4. Present situation and trends in the two facets of Analytical Nanoscience and Nanotechnology: nanomaterials as analytical tools and analysis of the nanoworld.

Nowadays, the prefix "nano" is opening many doors, which leads to many authors misusing it to their advantage. The prefix "nano" should be used in connection to nanomaterials, nanostructures and nanodevices that exploit not only the size but also the exceptional properties of nanoworld. The same happened in the past with other overexploited keywords such as "sensor". Fortunately, this terminological abuse has vanished over time.

Ethical and social implications

Nanotechnology has been deemed as a key emerging technology for fulfilling the "Grand Challenges of our Time" (Lund Declaration[21]) in areas such as health care, energy production, environmental protection and potable water procurement. However, it shows two contradictory connotations, namely: the

[21] Lund declaration (2009): http://www.vr.se/download/18.7dac901212646d84fd38000336/ (accessed on 30/07/2013)

production of new materials with outstanding mechanical, optical, electric, and magnetic properties for a wide variety of uses, which is highly positive; and its uncertain effects on human health and the environment, which is highly negative[22].

There are two major deficiencies regarding the impact of nanotechnology. One is that the risks and ethical implications of nanotechnology[23] in the production and industrial domains have not been considered. The other is that, although the potential hazards of nanotechnological products has been described, their toxicity remains uncertain due to the lack of scientific consensus in many cases.

Nanoethics, which is the term used to designate ethics in the development of nanosized objects, comprises three different fields of study, the former two of which are closely related: ecotoxicity, nanotoxicity, and violation of privacy. Ecotoxicity is related to the potential environmental damage of nanomaterials, whereas nanotoxicity focuses on the effects of nanoparticles on health. Assessing the risks of nanomateriales is especially important in nanomedicine, where they are used to prevent, diagnose, and treat specific diseases[24]. The violation of privacy field is associated with the production of nanosensors. The development of new communication technologies may result in an increasing invasion of privacity and violation of personal rights[22].

Government's concern about this issue is raised, as well as of various prestigious scientific and technical organizations. No doubt that this is a pending issue of Nanotechnology, which is the key for future consolidation. Recently, an integral approach to the social responsibility of Nanoscience and Nanotechnology[22] has been reported, which proposes a framework for conducting responsible research in Nanoscience.

[22] E. Caballero-Díaz, B.M. Simonet, M. Valcárcel, J. Nanopart. Res. 15 (2013) 1534.
[23] G. Hunt, M. Mehta, Nanotechnology risks, ethics and laws. Routledge, Oxford (2006).
[24] M. Mahmood, D. Casciano, Y. Xu, A.S. Biris, J. Appl. Toxicol. 32 (2012) 10-19.

I.2. TYPES OF NANOPARTICLES

According to the IUPAC Glossary of terms, a nanoparticle is a microscopic particle whose size is measured in nanometers, often restricted to so-called nanosized particles (NPs; < 100 nm in aerodynamic diameter), also called ultrafine particles[1]. With the expected increase in the applications of nanotechnology, more and more products will be manufactured containing components which will fit the commonly used definition of the nanoscale, as having a size between approximately 1 and 100 nanometers. These wide varieties of nanostructures have been classified in multiple ways in the literature. Figure I.2.1 shows the most relevant types of nanostructures in Analytical Nanoscience and Nanotechnology classified following four nonexclusive criteria.

Nanoparticles can be classified as natural, antrophogenic (incidental) or engineered in origin[2] (Figure I.2.1(1)). Nanoparticles belonging to each of these groups depending on their source are explained in depth in Chapter 2 of this thesis (see section 1.1. of such chapter).

From a practical point of view it is important to know the homogeneity of the nanostructured materials both for scientific studies as well as industrial applications. Homogeneity can be referred in terms of chemical composition or dimensionality (Figure I.2.1(2)). Identical nanoparticles are those with the same chemical composition and dimensions. Contrary, nanoparticles with the same

[1] http://sis.nlm.nih.gov/enviro/iupacglossary/glossaryn.html (accessed on 18/05/2013).
[2] A.M. Thayer. Chem. Eng. News 86 (2008) 10-15.

chemical composition but different dimensions usually present different properties.

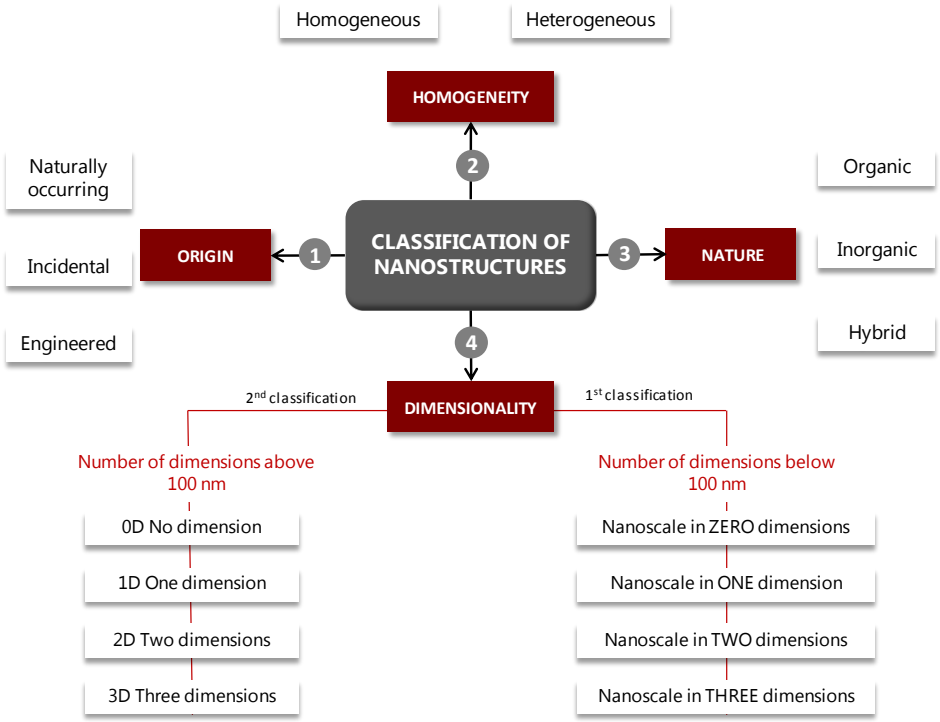

Figure I.2.1. Classification of nanostructures according to their origin (1), homogeneity (2), nature (3) and dimensionality (4). For details, see text.

Concerning the nature or chemical composition of nanostructures those can be classified (Figure I.2.1(3)) as inorganic (e.g. noble metal nanoparticles, quantum dots, etc.), organic (fullerenes, carbon nanotubes, dendrimers, molecular imprinted polymers, etc.) or mixed (gold nanoparticles modified with calixarenes, carbon nanotubes functionalized with ferrocene, etc.). In this context, there is a growing interest in the development of hybrid nanoparticles, which can be defined as well-organized nanomaterials consisting of two or

more types of individual nanocomponents[3]. This type of nanoparticles will be thoroughly analyzed in Chapter 1 of this thesis.

The last classification of nanomaterials is based on dimensionality criteria (Figure I.2.1(4)). As shown in the Figure, two classifications may be done, taking into account both the strict dimensions (in the nanoscale) of the nanostructure that give rise to those exceptional properties and the dimensions of the material where nanostructures are present.

The Royal Society of Chemistry and the Royal Academy of Engineering classified nanostructures in function of the number of dimensions in the nanoscale (below 100 nm)[4], distinguishing three types of nanostructures: i) nanoscale in one dimension, such as surfaces with nanometric thickness (e.g. graphene sheets); ii) nanoscale in two dimensions, such as carbon nanotubes, inorganic nanotubes, nanowires, etc.; iii) nanoscale in three dimensions, which includes metallic nanoparticles and their oxides, quantum dots, fullerenes, dendrimers. Classification of nanoscale at zero dimensions can also be added, such as materials composed by dispersed nanoparticles.

Other authors[5] have classified nanostructures depending on the number of dimensions which exceed 100 nm, being above the nanoscale, nanostructures being thus categorized as 0D, 1D, 2D or 3D. A 0D nanostructure is a material with all its dimensions comprised in the nanometric scale (e.g. metallic nanoparticles, quantum dots, etc.). Carbon nanotubes are an example of 1D nanostructures, which have one dimension of micro/macrometric size, such as nanowires or nanorods. 2D nanostructures have two dimensions above nanoscale while one of them is below 100 nm. That is the case of surface

[3] A.I. López-Lorente, B.M. Simonet, M. Valcárcel, Anal. Bioanal. Chem. 399 (2011) 43-54.
[4] http://www.nanotec.org.uk (accessed on 18/05/2013).
[5] A. Daniszewska, W. Lojkowski, H. Fecht, K.J. Kurzydlowski, U. Narkiewicz, G.A. Salishchev, M.J. Zehetbauer, M. Kulczyk, M. Chmielecka, D. Kuzmenko, Solid State Phenomena 114 (2006) 345-391.

nanocoatings or thin films of molecular monolayers[6]. Finally, 3D nanostructures are those whose three dimensions escape from the nanoscale, but the material is comprised by a set of nanoparticles forming a block of micro/macrometric size (e.g. nanoporous materials, powders).

Herein, we will focus on engineered nanoparticles, which are employed from an analytical point of view as tools or determined in different samples. They have been classified according to their nature as organic, inorganic or hybrid.

2.1. Organic nanoparticles

2.1.1. Carbon nanomaterials

Graphitic forms include 0D fullerene, 1D CNT and 3D graphite, and the 2D case comes to the graphene, a single layer of carbon atoms formed in honeycomb lattice.

Graphene is an open, flat, two dimensional structure composed of carbon atoms organized in a network of hexagons attached to each other. This is possible owing to sp^2 hybridization of the carbon atoms present in this sheet. It has a large specific surface area and can be easily modified with functional groups, especially via graphene oxide. Graphene quantum dots (GQDs), as a new kind of quantum dots, have emerged and ignited tremendous research interest. GQDs are defined as graphene sheets with lateral dimensions less than 100 nm in single-, double- and few- (3 to <10) layers. GQDs show low cytotoxicity, excellent solubility, chemical inertia, stable photoluminescence, better surface grafting, thus making them promising in optoelectronic devices, sensors, bioimaging, etc[7].

[6] R. Madueño, M.T. Räisänen, C. Silien, M. Buck, Nature 454 (2008) 618-621.
[7] L. Li, G. Wu, G. Yang, J. Peng, J. Zhao, J.-J. Zhu, Nanoscale 5 (2013) 4015-4039.

Another two examples of 0D carbon-based fluorescent nanomaterials are diamond nanocrystals (DNs) and carbon dots (CDs), which have also drawn numerous attention in recent years. In general, DNs consist of about 98% carbon with residual hydrogen, oxygen, and nitrogen, they possess a sp^3 hybridized core, and have small amounts of graphitic carbon on the surface. Luminescent CDs comprise discrete, quasi-spherical carbon nanoparticles with sizes below 10 nm.

Fullerenes are closed-cage carbon molecules containing pentagonal and hexagonal rings. They comprise a wide range of isomers and homologous series, from the most studied C_{60} and C_{70} to the so-called higher fullerenes like C_{240}, C_{540} and C_{720}. They possess relatively high electron affinity, hydrophobic surface and high surface/volume ratio.

Carbon nanotubes have received special attention ever since their discovery by Iijima in 1991[8]. They are tubular in shape and consist entirely of covalently bonded carbon atoms. As explained in more detail in Chapter 2 section 1.1., they can be described as hollow graphitic nanomaterials comprising one (single-walled carbon nanotubes, SWNTs), two (double-walled carbon nanotubes, DWNTs) or multiple (multi-walled carbon nanotubes, MWNTs) layers of graphene sheets. They possess non-polar bonds and high aspect ratios, which make them insoluble in water and facilitated their aggregation.

Carbon nano-onions (CNOs) are nanoparticles with a diameter between 20-100 nm composed by several layers of concentric fullerenes and constitute the spherical version of MWNTs. They were described by Ugarte[9] in 1992, although few applications have been reported.

[8] S. Iijima, Nature 354 (1991) 56-58.
[9] D. Ugarte, Nature 359 (1992) 707-709.

Moreover, carbon nanofibers (CNFs) are solid carbon fibers with lengths in the order of a few microns and diameters below 100 nm. CNFs differ from CNTs in the absence of a hollow cavity, and the diameters of CNFs are generally higher than those of the corresponding CNTs[10].

Finally, carbon nanocones were first synthesized by vapor condensation of carbon atoms on a graphite substrate[11]. The disclination of each structure corresponds to the presence of a given number of pentagons in the seed from which it grew: disks (no pentagons), five types of cones (one to five pentagons) and open tubes (six pentagons). The unique electronic distribution, which is provided by these pentagonal rings to the carbon nanocones, results in an enhanced local density at the cone apex. One major class of cone structures are single-walled carbon nanohorns (SWNHs) with the narrowest opening angle with five pentagonal rings in its apex.

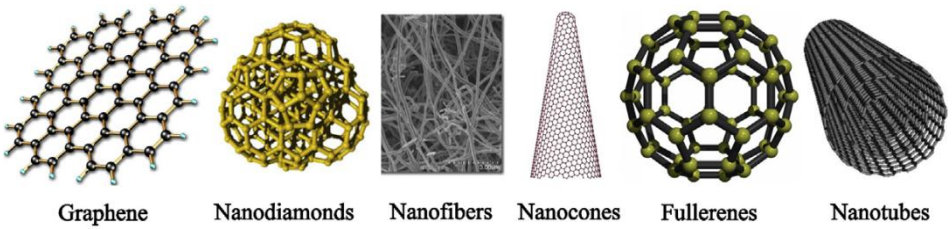

Figure I.2.2. Main types of carbon-based nanomaterials. Adapted from ref[10].

2.1.2. Other organic nanomaterials

Organic polymeric nanoparticles are prepared from polymers and considered potential drug delivery devices. Dendrimers are one kind of polymeric

[10] B.-T. Zhang, X. Zheng, H.-F. Li, J.-M. Lin, Anal. Chim. Acta 784 (2013) 1-17.
[11] M.H. Ge, K. Sattler, Chem. Phys. Lett. 220 (1994) 192–196.

nanoparticles constructed by the successive addition of layers of branching groups.

Molecularly imprinted polymers (MIPs) are a specific class of selective sorbents that are built-in functionalized in order to achieve the complementary recognition of a given chemical compound[12]. Although MIP particles can be nanometric in size, they usually fall in the micrometric range.

In addition, an increasing number of diverse nanomaterials are emerging for biopharmaceutical applications, such as liposomes, nanomicelles, nanovesicles. nanoemulsions, etc[13].

2.2. Inorganic nanoparticles

Inorganic nanoparticles cover a broad range of substances including elemental metals, metal oxides and metal salts. Silver nanoparticles (AgNPs) are used in many products as bactericide, whereas gold nanoparticles (AuNPs) are explored for many possible applications owing their catalytic activity. Both silver and gold nanoparticles possess the so-called surface Plasmon owing to the collective oscillation of the electrons, which provide them excellent optical properties and a large enhancement of the electric field on their surface.

Quantum dots (QDs) are semiconductor nanocrystals with all three dimensions falling in the 1–10 nm size range. In many respects, these luminescent nanocrystals constitute a transitional stage between bulk semiconductors and single atoms. The QD core is made up of elements from the II–VI (e.g. CdSe, CdTe, CdS, ZnSe), III–V (e.g. InP, InAs) or IV–VI (e.g. PbSe) group[14]. They have

[12] F. Kolarov, K. Niedergall, M. Bach, G.E.M. Tovar, G. Gauglitz, Anal. Bioanal. Chem. 402 (2012) 3245-3252.
[13] T. Elbayoumi, V. Weissig, J. Biomed. Nanotechnol. 5 (2009) 620-633.
[14] C. Carrillo-Carrión, S. Cárdenas, B.M. Simonet, M. Valcárcel, Chem. Commun. (2009) 5214-5226.

aroused widespread interest by virtue of their exceptional optical, electronic, electrochemical, photophysical, redox and catalytic properties.

Nanoparticulate metal oxides are widely used, such as TiO_2, Al_2O_3, ZrO_2, MnO and CeO_2, as well as iron oxides (FeOx) nanoparticles. It should be pointed out the increasingly used magnetic nanoparticles, which have been synthesized with a number of different compositions and phases, including iron oxides, such as Fe_3O_4 and Y-Fe_2O_3, pure metals, such as Fe and Co, spinel-type ferromagnets, as well as alloys[15]. Moreover, silica nanoparticles (SiO_2) are characterized by presenting high surface areas and exhibit intrinsic surface reactivity which allows chemical modifications[16].

Nano-sized zeolite, clays and ceramics are other nanoparticles that have been proposed for various applications[17].

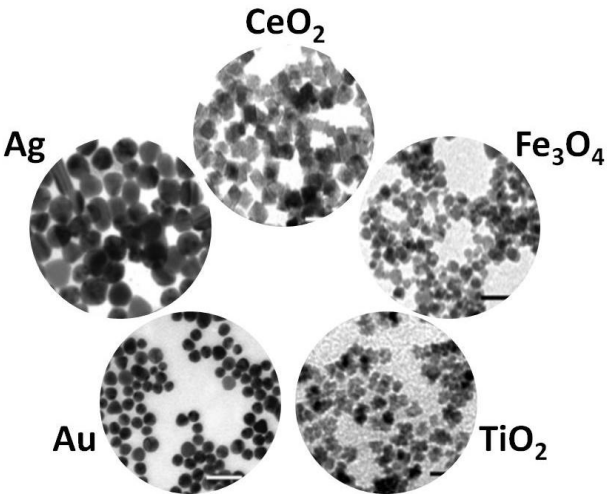

Figure I.2.3. Transmission electron microscopy images of model inorganic nanoparticles, namely: Ag, Au, TiO_2, Fe_3O_4, CeO_2 NPs. Adapted from ref[18].

[15] A.-H. Lu, E.L. Salabas, F. Schüth, Angew. Chem. Int. Ed. 46 (2007) 1222 – 1244.
[16] R. Lucena, B.M. Simonet, S. Cárdenas, M. Valcárcel, J. Chromatogr. A 1218 (2011) 620-637.
[17] B. Nowack, T.D. Bucheli, Environm. Pollut. 150 (2007) 5-22.

2.3. Hybrid nanoparticles

Hybrid nanoparticles are raising growing interest. In general, hybrid nanoparticles can be classified into two different types according to the combined properties, namely: i) Properties of the isolated nanoparticles are different but complementary, and ii) Properties of the isolated nanoparticles are of the same nature but their combination produces important synergistic effects.

Chapter 1 of this Thesis is a review concerning the potential of hybrid nanoparticles in Analytical Chemistry.

[18] A. Sánchez, S. Recillas, X. Font, E. Casals, E. González, V. Puntes, Trends Anal. Chem. 30 (2011) 507-516.

Capítulo 1

Analytical potential of hybrid nanoparticles

Analytical Bioanalytical Chemistry 399 (2011) 43-54

Springer Link

Analytical Bioanalytical Chemistry
399 (2011) 43-54

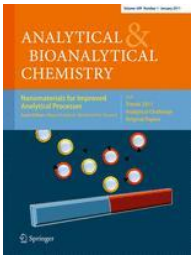

Analytical potential of hybrid nanoparticles

A. I. López-Lorente, B. M. Simonet, M. Valcárcel

Department of Analytical Chemistry, University of Córdoba. 14071 Córdoba, Spain.

The growing use of nanoparticles in the analytical process in recent years has set a new trend towards the simplification of analytical methods and improvement of their performance. Miniaturization and nanotechnology have allowed new analytical challenges to be met. Hybrid nanoparticles in particular possess exceptional properties enabling further improvement of analytical methods. Despite the continuous developments in their synthesis and characterization, hybrid nanomaterials have scarcely been used in analytical chemistry, however. This paper discusses the analytical potential of hybrid nanoparticles in terms of their special characteristics and properties, and describes their analytical applications.

Keywords: Nanoparticles, Nanotechnology, Hybrid nanoparticle, Analytical tools

1. Introduction

Nanotechnology has evolved extremely rapidly and expanded into a broad variety of areas in the medical, industrial, chemical, and physical fields in recent years. One area of particular interest is the synthesis of nanoparticles, which can be defined as particles having at least one dimension on the nanosize scale. There have been strong endeavors at improving synthetic procedures and developing straightforward purification techniques for the production of (usually) heterogeneous nanoparticles. In fact, the production of multicomponent materials is an important emerging target for nanoscience. Combining two materials with different properties in the same particle provides a unique hybrid nanoparticle with new functionalities.

Chemically, nanostructures may be inorganic (silica nanospheres, borazine inorganic nanotubes, quantum dots), organic (fullerenes, carbon nanotubes, dendrimers, molecular imprinted polymers), or mixed (e.g., gold nanoparticles modified with calixarenes, carbon nanotubes functionalized with ferrocene, gold monoparticles functionalized with cyclodextrines). The nanoparticles addressed in this review consist of two different types of materials, so they can be considered hybrid nanoparticles.

Nanoparticles are widely assumed to be smaller than 100 nm in all three dimensions. While such is the case with metallic nanoparticles and their oxides, for example, the word “nanoparticle” is generally used to refer to particles with two or even only one dimension falling off the nanoscale (e.g., carbon nanotubes, nanowires, biopolymers).

The greatest advantage of nanotechnology is a result not only of the small “size” of nanoparticles—at least one dimension of which falls in the range 1–100 nm—but also the exceptional properties they exhibit by virtue of their reduced size. Thus, while properties usually vary in a linear manner at the macroscopic level,

they change dramatically when the nanoscale threshold is crossed. This is the origin of the revolution that nanoscience and nanotechnology have brought about.

2. Intrinsic properties of individual nanoparticles

This section discusses the main properties of metallic, semiconductor, and carbon nanoparticles, which provide the basis for hybrid nanomaterials. Nanoparticles are being extensively used by virtue of their exceptional properties. The properties of a nanomaterial are strongly dependent on its particle size and shape. For example, some properties of nanosized particles are a result of asymmetry at the interface or of electron confinement, both which vary nonlinearly with particle size. As noted earlier, the nanoscale (1–100 nm) encompasses collections of atoms or molecules the properties of which depart from those of their individual constituents and the bulk. Since such properties depend on the size of particles rather than on the nature of the material, a single material can be used to modulate properties in a continuous manner.

Metallic nanoparticles exhibit fascinating properties that differ markedly from those of individual atoms, surfaces, and bulk materials. They are a focus of interest for fundamental science and, by virtue of their vast potential in nanotechnology, they have been the subject of strong research efforts in a wide spectrum of disciplines. Gold nanoparticles have a characteristic red color, whereas silver spheres are yellow. The color of nanoparticles is due to collective oscillation of electrons in the conduction band, “surface plasmon oscillation”, which occurs at a frequency usually in the visible region for gold and silver, and results in strong surface plasmon resonance absorption. Gold nanoparticles, for instance, are widely used in biomedical imaging and diagnostic tests by virtue of the high chemical stability of Au(0) [1] against, for example, cancer [2]. They have also been used as catalysts [3] on the grounds of their ability to lower the activation energy barriers or increase the rates of some reactions—and the

yields of the target products as a result. Also, they have been employed in many biological applications [4] and for uses based on the enhanced optical properties of nanoparticles such as absorption, fluorescence of chromophores in close proximity and nanoparticles themselves, and enhanced Rayleigh scattering and surface enhanced Raman scattering (SERS) of adsorbed molecules.

The excellent electrical, thermal, catalytic, and optical properties of nanosized silver colloids (e.g., their ability to sustain resonant collective electron oscillations excited in the near-ultraviolet or visible range of the electromagnetic spectrum) have aroused much interest in recent years for various potential uses (conductors, catalysts, chemical sensors) [5]. Also, silver colloids have been tested as conducting inks for inkjet printers.

Metal oxide nanoparticles are attractive for a large variety of applications including catalysis, sensors, (opto)electronic materials, and environmental remediation. For instance, titanium dioxide, the optical properties of which are governed by its refractive index and grain size, is widely used as a white pigment. In fact, TiO_2 micrometric particles are generally opaque to visible light, whereas smaller (nanosized) particles are transparent to visible light but still block UV light. One other important property of TiO_2 is its superhydrophobicity, which is a result of its near-zero contact angle with water. This has facilitated the development of easy-to-clean surfaces and, where a natural source of water exists, self-cleaning surfaces [6]. Nanometric silicon dioxide (nano-SiO_2), which is among the most popular nanomaterials, is used for a variety of purposes including industrial manufacturing, packaging, high-molecule composite and ceramics production, disease labeling, drug delivery, cancer therapy, and biosensor development.

Iron oxide nanoparticles provide valuable benefits for in vivo biomedical applications thanks to their size-dependent superparamagnetism and nontoxic, metabolizable nature. Superparamagnetic iron oxide nanoparticles are clinically

used as contrast media in magnetic resonance imaging and have been assessed for a variety of applications such as magnetic drug delivery, cell tracking, and hyperthermia. The particles consist of iron oxide magnetic cores coated with a protective layer providing stability and dispersibility, and yet are often found in agglomerated forms spanning a wide range of sizes from nanometric to micrometric.

One other important group is that of semiconducting nanoparticles, which have their three dimensions in the ca. 1–10 nm size range and are known as quantum dots (QDs). Quantum dots are spherical in shape, mostly direct band gap materials, and can hold hundreds or thousands of atoms depending on their final size. In many respects, these luminescent nanocrystals constitute a transitional stage between bulk semiconductors and single atoms. Their nanometric size is important in this context as it allows quantum confinement of electrons. As particle size decreases below the Bohr radius of a semiconductor material, electrons are increasingly confined within particles. This increases the band gap energy and causes the valence and conduction bands to split into quantized energy levels [7]. Photoluminescence in QDs arises from radiative exciton recombination. QDs have a symmetric, narrow bandwidth of ca. 30 nm full width at half maximum fluorescence, which enables emission of pure color. Since the spectroscopic properties of QDs are size-dependent, they can be tuned over a continuum in preparation procedures. The smaller QDs are the more blueshifted (hypsochromic) are their absorption and emission. QDs are currently being investigated in various fields including biology, electronics, and optoelectronics. Applications in these fields have so far relied on various types of materials including InP, InAs, GaAs, and GaN, as well as porous Si and Si/Ge dots [8]. In addition, the family of II–VI compounds (e.g., ZnS and ZnSe QDs) have their absorption and emission spectra restricted to the UV and blue regions. In this respect, QDs containing heavier atoms (CdTe, HgSe) and hybrids

consisting of PbSe have aroused special interest by virtue of their optical properties extending into the near-infrared region.

As regards carbon nanoparticles, carbon nanotubes (CNTs) have received special attention from scientists ever since their discovery [9]. Carbon nanotubes belong to the fullerene family of carbon allotropes. They are tubular in shape as implied by their name and consist entirely of covalently bonded carbon atoms. CNTs possess nonpolar bonds and high aspect ratios (length-to-diameter ratios), which makes them insoluble in water and facilitates their spontaneous aggregation. This tendency to aggregate, together with their high flexibility, enhances their ability to bundle and close-pack. CNTs are adequately soluble only in a limited number of solvents such as dimethylformamide, dimethylacetamide, and dimethylpyrrolidone [10]. Also, they can be covalently functionalized [11]. In general, CNTs are not especially reactive, but can be made to react under strong chemical conditions (e.g., by incorporating hydroxyl or carboxyl groups onto their side walls) [12]. Single-walled nanotubes (SWNTs) possess a good surface area-to-volume ratio. The fact that they contain no atoms in their lumina, together with their excellent van der Waals physisorption properties, make them especially good candidates for gas filtration, sensing, and energy storage devices [13]. CNTs exhibit excellent thermal stability in inert atmospheres, where they remain stable at temperatures up to 1,200°C, and possess a π complex both above and below the plane containing the carbon atoms that is the origin of their high electron mobility and electrical conductivity [14]. Also, they are plastic and more elastic than carbon steel, and can carry large electric currents for their size with minimal resistance.

C_{60} fullerenes are another type of carbon nanostructure possessing unique surface properties for use in analytical chemistry. Fullerenes comprise a wide range of isomers and homologous series from the most widely studied C_{60} or C_{70} to the so-called higher fullerenes (C_{240}, C_{540}, and C_{720}). Ever since

buckminsterfullerene C_{60} was first reported [15], a wide variety of analytical applications of fullerenes have been reported including their use as chromatographic stationary phases [16], sorbents for solid-phase extraction [17], electrochemical sensors [18], and electron mediators [19]. Worth special note among their properties is their relatively high transition temperature (33 K for C_{60}), which makes them suitable for superconductivity studies [20]. One other interesting property of fullerenes and fullerene-like materials is their photoactivity, which makes them potentially useful for solar energy conversion. The biological potential of fullerenes has attracted increasing attention despite the low solubility of carbon spheres in physiological media. In fact, the unique characteristics of fullerenes make them promising candidates for use in biological applications.

In addition to CNTs and C_{60}, nanodiamond has aroused growing interest in the last few years. This form of diamond carbon has recently come into focus as a new potential material for quantum engineering, biological and electronic applications, as well as in composite materials. Nanoscale diamond, which can be obtained by detonating some explosives [21], possesses a variety of surface functionalities that can be used to adsorb or graft functional groups or much more complex moieties (e.g., proteins, DNA) onto the diamond surface. Nanoscale diamond particles have recently been used in a variety of biological applications. Newly developed production, purification, and functionalization techniques have enabled their use in a number of ways. In addition, their apparently low cytotoxicity makes them an attractive alternative to other, widely used nanoparticles such as cadmium-containing quantum dots [22].

3. Hybrid nanoparticles

3.1. Definition and classification

Hybrid nanoparticles can be defined as well-organized nanomaterials consisting of two or more types of individual nanocomponents (Fig. 1). The nanocompounds integrating hybrid nanoparticles can be bound via organic/inorganic molecular bridges or directly attached to one another. For example, two quantum dot nanoparticles can be attached via a dithiol compound or a quantum dot in order to facilitate nucleation and crystal growth on a CNT surface. Apart from the special type of bonding between the nanocompounds, the exceptional properties of hybrid nanoparticles are due to the highly organized arrangement of the nanoconstituents.

One major goal in materials science is the preparation of an artificially designed structure of nanoparticles with new properties. Nanoparticles possess excellent properties that can be boosted or supplemented by combining two or more types of materials into a hybrid nanocomposite. Well-defined ordered solids prepared from tailored nanoparticles have provided new opportunities for optimizing the properties of materials and exposed interesting, potentially useful new collective physical phenomena. Combining two different types of nanoparticles may (a) produce a synergistic effect leading to a combination or improvement of the properties of the two nanomaterials or (b) allow the individual exploitation of the properties of one or both materials. This distinction is probably the most analytically useful. For example, a gold nanoparticle coated with a nanometric layer of silica possesses the typical optical properties of gold nanoparticles and the chemical properties of silica as regards stability. This is a clear example of the combination of properties from the two nanoconstituents. On the other hand, silver nanoparticles attached to quantum dots combine the intrinsic electromagnetic field of each

nanoconstituent, which results in a hybrid nanoparticle with an increased activity in SERS. There is thus a synergistic effect.

Although synergy and complementariness between nanoparticles have scarcely been exploited, they can provide a promising area for research. This section describes selected types of hybrid nanoparticles and their applications.

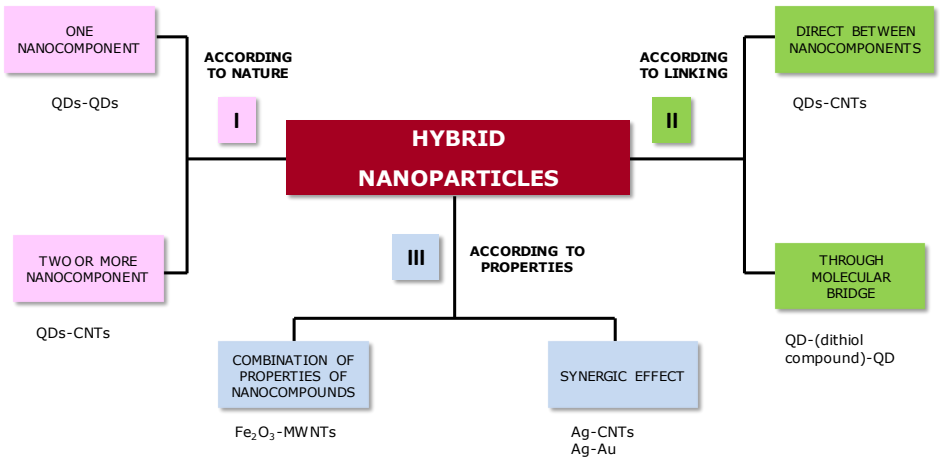

Figure 1. Classification of hybrid nanoparticles according to three different criteria

3.2. Main types of hybrid nanomaterials

3.2.1. Noble metal–magnetic nanoparticle hybrids

Some noble metals have been used in combination with magnetic materials in order to improve the SERS signals for some molecules. Kim et al. [23] developed a one-step fabrication process for Ag-deposited Fe_2O_3 particles. The amount of Ag deposited onto iron oxide can be adjusted simply by varying the mole ratio of $AgNO_3$ to butylamine. The $Ag@Fe_2O_3$ particles thus prepared were readily recovered from the solution phase by means of a magnet. The magnetic particles were irregularly shaped before and after silvering at a 1:1 mole ratio of

Ag^+ to butylamine. For silver deposition, the Fe_2O_3 particles were dispersed in a reaction mixture consisting of ethanolic $AgNO_3$ and butylamine (Fig. 2).

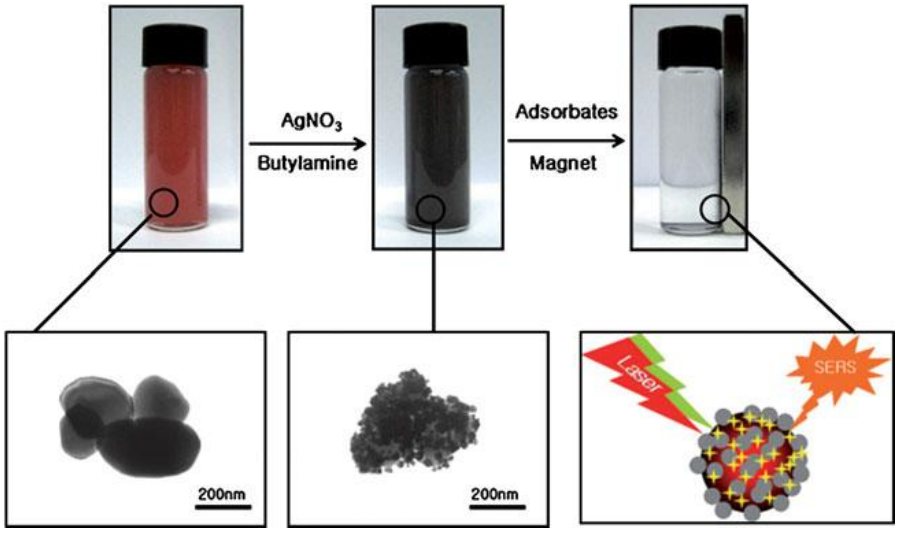

Figure 2. Schematic depiction of a novel one-step fabrication procedure for $Ag@Fe_2O_3$ particles by soaking Fe_2O_3 in ethanolic solutions of $AgNO_3$ and butylamine, and of their use as SERS substrates for the analysis of various model compounds. The insets show the individual Fe_2O_3 particles before and after Ag deposition, respectively.

Magnetic/gold composites prepared in various ways have also been reported. Thus, Lin et al. [24] used inverse micelles to form crystalline iron cores, treatment of which with chlorauric acid and sodium borohydride provided gold-coated iron. Stoeva et al. [25] synthesized three-layer nanoparticles ca. 200 nm in diameter containing a Fe_2O_3 layer between a SiO_2 core and an outer gold shell in a two-phase process. Once in the aqueous phase, the particles were functionalized with oligonucleotides and shown to reversibly bind via DNA hybridization. Wang et al. [26] followed a similar synthetic route to obtain iron oxide/gold core/shell nanorods with a final length of 250 nm.

Hou et al. [27] reported a SERS substrate consisting of magnetic Fe_3O_4 and Au nanoparticles. Figure 3 shows scanning electron microscopy (SEM) images of the Fe_3O_4 nanoparticle modified substrate, and the Fe_3O_4 and Au nanoparticle co-modified substrate. Fe_3O_4 nanoparticles organize as a uniform, compact surface when dropped on glass. By virtue of their relatively small size, Au nanoparticles added onto a surface consisting of Fe_3O_4 nanoparticles spread gradually onto it to form a new active surface.

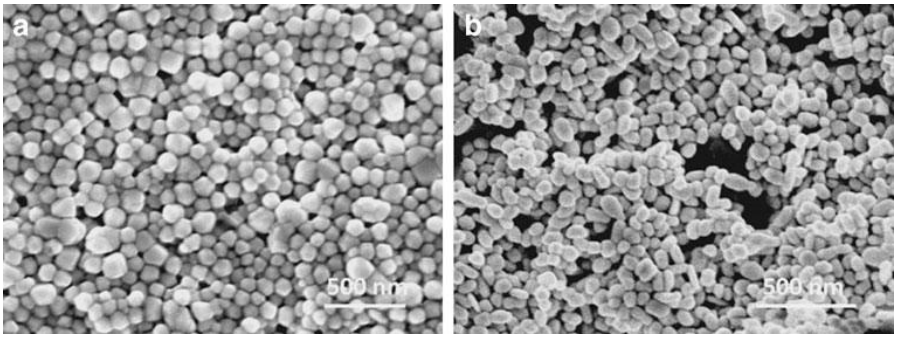

Figure 3. SEM images of a Fe_3O_4 nanoparticle modified surface (a), and Fe_3O_4 and Au nanoparticle co-modified surface (b). Adapted, with permission, from Ref. [27]

Arruebo et al. [28] developed a synthetic method for antibody-conjugated superparamagnetic nanoparticles with an inorganic shell. The nanoparticles consisted of an inner iron oxide core coated with a silica shell that was in turn functionalized with amine or carboxyl groups and covalently bonded to a monoclonal antibody (anti-hCG; hCG = human chorionic gonadotropin) for use as enhanced contrast agents in magnetic resonance imaging applications. Microscopically, the product appears as a relatively homogeneous collection of nanoparticles of average size 80 nm consisting of an iron oxide core encapsulated in a microporous silica shell (Fig. 4).

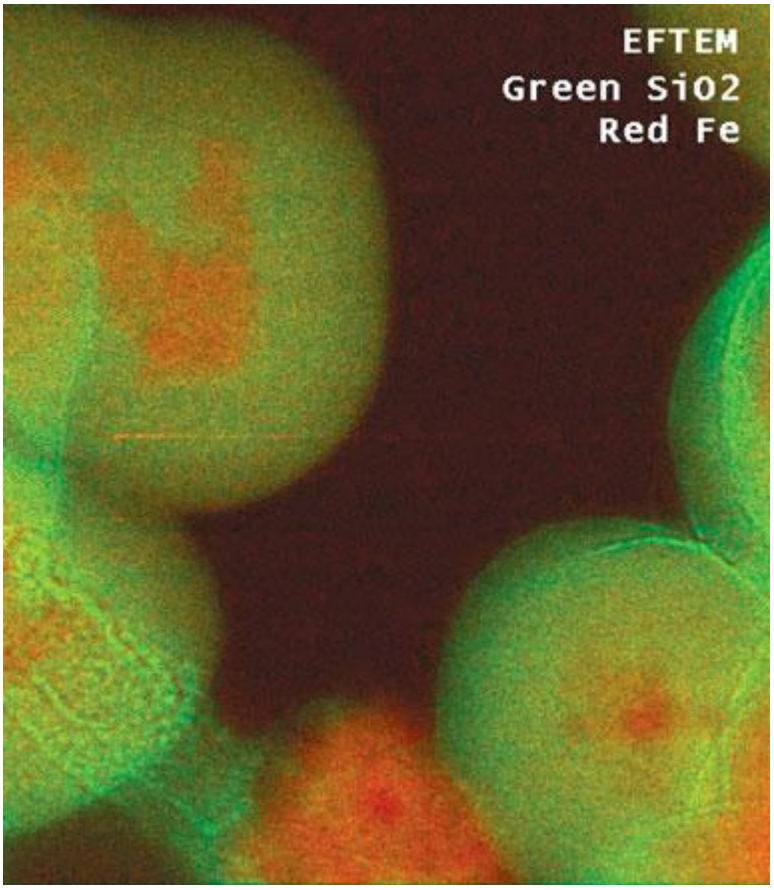

Figure 4. Energy-filtered transmission electron microscopy (EFTEM) color map showing the iron (red) atomic distribution (in this case, forming the Fe_3O_4 nanoparticles), and the silicon (green) distribution, as part of the shells. Adapted, with permission, from Ref. [28]

3.2.2. Carbon nanotube-based magnetic nanoparticles

Magnetic carbon nanotube composites are hybrids of magnetite (Fe_3O_4) and/or maghemite (γ-Fe_2O_3) with single-walled (SWCNTs) or multiwalled carbon nanotubes (MWCNTs) [29]. These composites combine the unique optical, electrical, and mechanical properties of carbon nanotubes (CNTs) with the paramagnetic or ferromagnetic properties of magnetic nanoparticles (MNPs) at room temperature. This has enabled their use as tips for magnetic force

microscopes, separators in wastewater treatment, biosensors, drug delivery systems, and biomanipulators. These hybrid nanoparticles have been obtained with a variety of synthetic methods [30–32] and can be rapidly isolated from the dispersion with the aid of an external magnetic field (117.7 N). No free MWCNTs remain in solution after the magnetic field is applied to the side wall of the vessel, which can be especially useful for analytical purposes. No spectral differences between MWCNT and MWCNT–MNP composites have been detected; this reflects the dominance of the properties of CNTs in the hybrid material, which, however, exhibits magnetic properties not present in the pure MWCNTs.

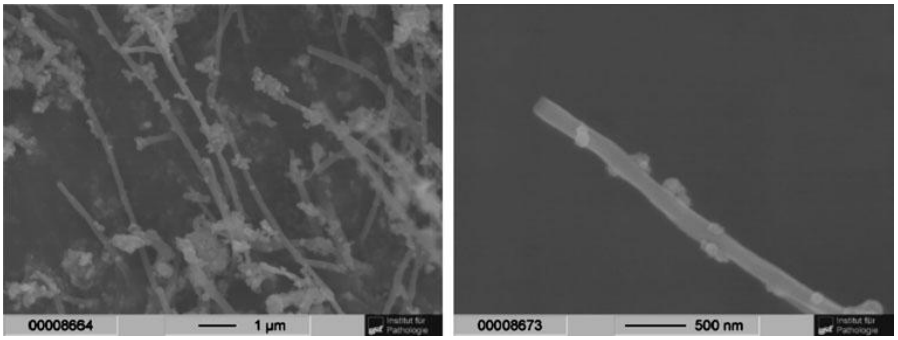

Figure 5. SEM images of the nanoparticles at the micrometric scale, and detail at the 500-nm scale, of an MWCNT–MNP composite. Adapted, with permission, from Ref. [29]

Figure 5 is a micrograph of an MWCNT–MNP composite material. The detailed views (500-nm scale) clearly reveal that the MNPs attach onto nanotube surfaces and look like nodes growing from the tubes. MNP–CNT binding in the composite is strong enough to resist applied mechanical energy such as that of manual shaking or sonication. The overall tubular structure of the MWCNTs remains intact after in situ decoration. Because the nanotubes are not completely covered, the composite can be expected to possess sorption properties of both MNPs and MWCNTs.

3.2.3. Magnetic nanoparticle–quantum dot hybrids

Some hybrid nanosystems of this type allow multimodal imaging. Magnetic nanocrystals and quantum dots have been extensively used in the biomedical field as contrast enhancement agents in magnetic resonance imaging, magnetic carriers for drug delivery systems, biological labels, and diagnostic media. Formulations containing quantum dots (QDs) and magnetic iron oxide nanoparticles (MNPs) provide a means for simultaneous fluorescence optical imaging and magnetic resonance imaging (MRI). Park et al. [33] obtained long-circulating, micellar hybrid nanoparticles (MHNs) containing MNPs, QDs, and the anticancer drug doxorubicin (DOX) within a single poly(ethylene glycol) (PEG)–phospholipid micelle (Fig. 6) and provided an example of simultaneous targeted drug delivery, and of dual-mode near-infrared (NIR) fluorescence imaging and MRI of diseased tissue, both in vitro and in vivo. In vitro studies have shown that drug molecules and MNPs can be effectively incorporated within micelles in order to confirm drug delivery by MRI [34, 35]. Also, micellar preparations containing single-component nanomaterials such as QDs and carbon nanotubes have proved stable enough for in vivo use [36, 37].

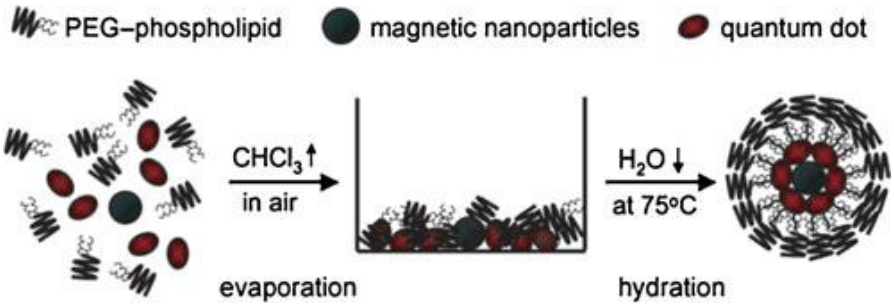

Figure 6. Synthetic procedure used to prepare micellar hybrid nanoparticles for encapsulating magnetic nanoparticles and quantum dots within a single PEG-modified phospholipid micelle. Adapted, with permission, from Ref. [33]

Yi et al. [38] developed similar hybrid nanoparticles. Thus, they synthesized a novel water-soluble hybrid material consisting of quantum dots (QDs) and magnetic nanoparticles (MNPs) encapsulated in a silica shell. Kim et al. [39] prepared monodisperse magnetite (Fe_3O_4) nanocrystals embedded in mesoporous silica spheres, as well as magnetite nanocrystals and CdSe/ZnS quantum dots embedded in mesoporous silica spheres. The spheres were used for the uptake and controlled release of drugs.

Sathe et al. [40] developed silica microbeads embedded with both semiconductor quantum dots (QD) and iron oxide (Fe_3O_4) nanocrystals as a new class of dual-function carriers for optical encoding and magnetic separation. The embedding (doping) process involves simultaneous or sequential addition of quantum dots and iron oxide (Fe_3O_4) nanocrystals in solution. The procedure is expeditious and quantitative; however, incorporation of the iron oxide strongly attenuates the signal intensity of QD fluorescence. This is not the result of conventional fluorescence quenching, but rather of the broad optical absorption spectrum for mixed-valence Fe_3O_4. For improved biocompatibility and reduced nonspecific binding, the encoded beads can be further coated with amphiphilic polymers such as octylamine poly(acrylic acid). On the basis of the results, the polymer-coated beads are well suited to target capturing and enrichment as they provide magnetic separation efficiencies above 99%. The combination of the multiplexing capabilities of QDs and the superparamagnetic properties of iron oxide nanocrystals is expected to make these encoded beads useful for a number of high-throughput and multiplexed biomolecular assays.

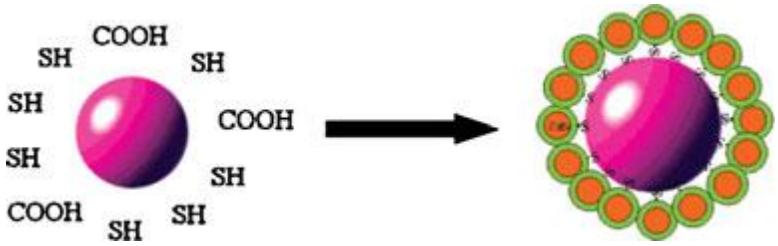

Figure 7. Thiol- and carboxy-modified γ-Fe_2O_3 beads reacted with CdSe/ZnS QDs to form luminescent/magnetic nanocomposite particles. Adapted, with permission, from Ref. [41]

Wang et al. [41] synthesized nanocomposite nanoparticles consisting of polymer-coated γ-Fe_2O_3 superparamagnetic cores and a CdSe/ZnS quantum dot (QD) shell. A single layer of QDs was bound to the surface of thiol modified magnetic beads through thiol–metal bonds to form luminescent/magnetic nanocomposite particles (Fig. 7). A threefold decrease in luminescence quantum yield for the luminescent/magnetic particles and a slight blue shift in their emission peaks compared to individual luminescent QDs were observed. However, the particles were bright and easily observed under a conventional fluorescence microscope. In addition, no apparent broadening of the luminescence peak for the QDs was observed. These nanoparticles might be useful in a variety of bioanalytical assays involving luminescence detection and magnetic separation.

3.2.4. Quantum dot–carbon nanotube hybrids

Some novel strategies aimed at altering the physical properties of CNTs by surface modification with organic, inorganic, and biological species have been developed in recent years. These functional CNT-based composites may open up eminent prospects for new applications in a wide variety of areas. One is the binding of semiconductor nanocrystals to CNTs. Combining quantum dots (QDs) with carbon nanotubes (CNTs) is expected to produce composite

materials blending the selective wavelength absorption capabilities of the former with the charge transfer and efficient electron transport capabilities of the latter. CdSe(SWCNT) nanocomposites [42] have been found to exhibit a high quantum yield and long lifetime relative to fluorescent molecules, and also to disperse highly efficiently in aqueous media; however, covalently attaching a fluorescent molecule to a CNT has the disadvantage that it causes a rapid decay of the lifetime and reduces the quantum yield of the fluorescent label.

Single amine-functionalized CdSe quantum dots have been coupled to individual acid chloride modified singlewalled carbon nanotubes via amide bonds [43]. For SWNTs less than 200 nm long, QDs were bound at nanotube ends; longer nanotubes, however, exhibited signs of sidewall attachment. The number of QDs bound per nanotube can be relatively efficiently controlled by adjusting the quantum dot/nanotube mass ratio. These quantum dot–nanotube complexes may provide the basis for future nanoelectronic devices.

Various types of QD–CNT composites have so far been reported including CNT–QD junctions using CdSe in ozonized CNTs [44, 45], CNT/CdS core-shell nanowires produced by chemical reduction, and heterojunctions of amine-terminal ZnS-coated CdSe/ZnS on acid-oxidized CNTs [46]. The electronic interaction between the CNTs and the external active semiconductor layer is believed to be of the same importance since it plays a crucial role in constructing optoelectronic devices. One of the main drawbacks of covalently attaching a fluorescent molecule to a CNT is the rapid decay of the lifetime and reduced quantum yield of the fluorescent label. This problem can be overcome by using quantum dots, which are superior substitutes for organic fluorescent molecules. Ravindran et al. [47] reported the controlled synthesis of multiwalled carbon nanotube–quantum dot (CNT–QD) heterojunctions by using the ethylene carbodiimide coupling procedure (EDC). Thiol-stabilized ZnS-capped CdSe quantum dots containing amino terminal groups (QD–NH_2) were

conjugated with acid-treated multiwalled carbon nanotubes (MWCNTs) ranging from 400 nm to 4 μm in length.

3.2.5. Quantum dot–metal nanoparticle hybrids

Quantum dots have also been attached to TiO_2 nanoparticles [48]. The observation of efficient electron injection from photoexcited CdS QDs into TiO_2 nanoparticles, leading to the formation of long-lived charge-separated states, has provided further evidence that these materials may find application in QD-sensitized solar cells or QD sensitized photocatalysts. TiO_2 nanoparticles have also been attached to CNTs via controlled hydrolysis and condensation of titanium bis(ammonium lactate)dihydroxide in water [49].

3.2.6. Fullerene–metal nanoparticle hybrids

Gold/C_{60}(/C_{70}) nanoclusters have been fabricated [50] in order to improve the Raman spectra of fullerenes via the SERS effect of the metal. In fact, the surface enhanced resonance resulting from the presence of Au was found to facilitate detection of fullerenes. Gold/C_{60} (/C_{70}) nanoclusters were deposited onto floppy disk and hard disk pieces, using pyridine as transfer solvent. The floppy disk or hard disk piece, as a new and effective substrate for SERS, provided a plank for C_{60}/C_{70} molecules to adsorb on the gold nanoparticles.

The properties of nanoscale materials have been boosted with the development of semiconductor/semiconductor [51], metal/metal, and metal/semiconductor hybrids. Mokari et al. [52] prepared a metal/semiconductor material by using a simple method for the selective growth of gold tips on the apexes of colloidal semiconductor nanorods and tetrapods. This combination endows nanostructures with new functionalities the most important of which is the formation of natural anchor points that can serve as a recognition element for directed self-assembly and for imprinting onto electrical circuitry. A transition

from two to one-sided gold growth was observed at increased gold concentrations. Zhao et al. [53] developed a metal/semiconductor hybrid material consisting of Au/TiO_2 nanoparticles.

3.2.7. Core-shell bimetallic nanoparticles

Core-shell bimetallic nanoparticles have received considerable attention on account of their special photochemical and photophysical properties [54]. One important example is bimetallic Au/Pd nanoparticles, which exhibit improved catalytic activity as compared to monometallic mixtures of Pd and Au nanoparticles [55]. There are also Ag@TiO_2 nanoparticles [56], Au/TiO_2 hybrid nanoparticles in silicate film [57], water-soluble silica/PAAc hybrid nanoparticles embedded with silver QDs [58], water-soluble $SiO_{1.5}$/TiO_2 hybrid nanoparticles [59], gold@silica- and magnetite@silica- type nanoparticles obtained by embedding Au nanoparticles protected by captopril or magnetite nanoparticles protected by alanine into larger silica nanoparticles [60], and high-density Au/Pt hybrid nanoparticles supported on a silica nanosphere [61] (Au-Pt/SiO_2). Metallic iron nanoparticles have been synthesized within micron-sized mesoporous molecular sieves with 2.9-nm pores and hollow silica microcapsules with pores 2.7 or 15 nm in size [62].

Kim et al. [63] demonstrated the co-encapsulation of magnetic (Fe_2O_3 and Fe_3O_4), semiconductor (CdSe/ZnS), and metal (Au) nanoparticles in various combinations to form multicomponent micelles that retained the distinct properties of the precursor particles.

The preparation of core-shell nanoparticles, in which the core of the particle is inorganic and the shell is an organic polymer, has been the subject of much research inasmuch as it allows different properties to be combined in one particle by adjusting the composition of the core and shell [64]. The core often shows the relevant property while the shell helps to stabilize the core, make it

compatible with the environment, promote hydrocarbon dispersion [65], or alter the charge, functionality, or reactivity of a surface [66]. The organic polymer shell dictates the chemical properties of such materials and their interaction with the environment, whereas the size and shape of the inorganic core, and the surrounding organic layer, govern their physical properties [67]. The resulting nanocomposites have found wide use in coatings, adhesives, optics, and electronics, as well as in biomedical and environmental applications [68].

3.2.8. Carbon nanotube–metal nanoparticle hybrids

A simple approach to decorating carbon nanotubes (CNTs) with silver nanoparticles (Ag-NPs) was developed to enhance the electrical conductivity of CNTs [69]. To this end, nanotubes were functionalized with ball milling in the presence of ammonium bicarbonate, followed by reduction of silver ions in N,N-dimethylformamide, which produced silver-decorated CNTs. The resulting Ag@CNTs were used as conducting filler in epoxy resin in order to produce electrically conducting polymer composites. The electrical conductivity of composites containing 0.10 wt% Ag@CNTs was more than four orders of magnitude higher than that of composites containing the same amount of pristine and functionalized CNTs, which confirms the advantage of Ag@CNTs as an effective conducting filling material.

Ag-coated CNT hybrid nanoparticles (Ag/CNTs) have been also prepared by ultrasonic irradiation of dimethylformamide (DMF) and silver(I) acetate precursors in the presence of CNTs [70]. A study of antibacterial activity in Ag-coated CNTs, commercial Ag, neat Nylon-6, and plain CNTs revealed that nylon nanocomposite fibers infused with Ag-coated CNTs possess substantial activity. New nanoscale photocatalysts based on silver and CNTs/TiO_2 have been successfully prepared by photoreduction [71]; the presence of Ag nanoparticles was found to increase the photocatalytic efficiency of CNTs/TiO_2 and the photocatalysis reaction to follow a first-order kinetics.

4. Analytical applications of hybrid nanoparticles exploiting synergy between their nanoconstituents

Ag-deposited Fe_2O_3 particles [23] have proved efficient SERS substrates for the vibrational spectroscopic characterization of molecular adsorbates prepared similarly on silver surfaces. Using benzenethiol as a model compound revealed that the SERS activity of the $Ag@Fe_2O_3$ particles is greater than that of the commercially available μAg powders by a factor about 3×10^6. Since the magnetic particles are readily isolated from the solution phase without centrifugation and/ or filtering, the resulting SERS-active magnetic particles can be especially useful for the Raman spectroscopic analysis of organic species in aqueous solutions.

The Fe_3O_4 and Au nanoparticle co-modified substrate developed by Hou et al. [27] allowed a high-quality SERS spectrum of C_{60} to be obtained. Gold nanoparticles are known to exhibit good SERS activity for fullerene molecules and it is impossible to obtain an SERS spectrum for C_{60} simply with a Fe_3O_4 nanoparticle modified surface or a bare glass surface. Dropping Au nanoparticles onto a magnetic surface consisting of Fe_3O_4 nanoparticles allows more extensive information to be obtained from the SERS spectrum derived from the co-modified substrate (Fig. 8). On reaching the Au nanoparticle surface, the laser produces an excited localized surface plasmon that creates a high local electromagnetic field in the vicinity of the Au nanoparticles. Introducing Fe_3O_4 nanoparticles onto the substrate leads to their coupling with Au nanoparticles around them by virtue of their unique magnetism. Through magnetic coupling, Fe_3O_4 and Au nanoparticles interact in a number of ways. Possibly, the magnetic Fe_3O_4 nanoparticles play a prominent role in magnifying the local electromagnetic field near the Au nanoparticle surface through their mutual interaction. This effect cannot be achieved with conventional single noble metal nanoparticles. The magnetic Fe_3O_4 nanoparticles have a

concomitant impact on the electron cloud distribution of adsorbed C_{60} molecules. This reduces the symmetry of C_{60} molecules and increases the number of vibrational modes observed in the SERS spectrum.

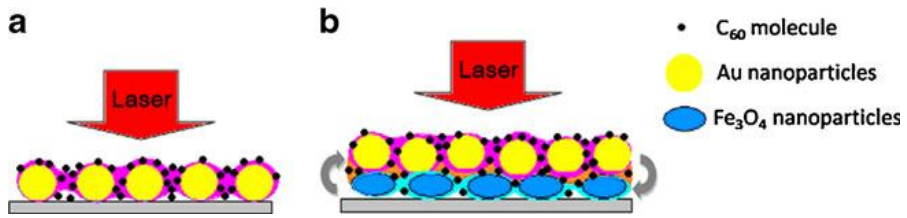

Figure 8. (a) Sketch maps for the SERS mechanism on an Au nanoparticle modified substrate and (b) a Fe_3O_4 and Au nanoparticle co-modified substrate. Adapted, with permission, from Ref. [27].

Core-shell Au@Pd nanoparticles have been prepared by chemical deposition of Pd on preformed gold seeds of variable size [72]. Worth special note here is the ability to modify the entire surface of the gold seeds with a thickness controllable, pinhole-free Pd shell as thin as one monolayer. This provides an effective method for using Au@Pd nanoparticles to enhance SERS activity to practical levels by optimizing the shell thickness and core size while preserving the properties of the shell metal and avoiding potential interferences from the core metal underneath. Experimental results indicate that the underneath SERS active Au core further enhances the SERS signals for adsorbates such as CO on the one or few Pd layers by more than two orders of magnitude through long-range electromagnetic interactions.

Semiconductor QDs have a great potential as future photonic materials, provided some hindrances are overcome [43]. For example, the quantum efficiencies of hybrid conducting polymer–QD light-emitting devices (LEDs) are

in the region of 0.25%. The relative inefficiency of these QD devices is largely due to the difficulty in effectively transferring charge carriers into (LEDs) or away from (solar cells) the CdSe nanoparticles constituting the device. On the other hand, the unique electrical transport properties of carbon nanotubes suggest that they can have many advantages over conventional materials for use as superior nanometer-scale wires. Raising the efficiency of QD devices to practical levels will require the development of effective techniques to facilitate direct charge transport to quantum dots. For example, attachment of conducting SWNTs to CdSe QDs can be used to bring a metallic wire into direct chemical contact with a quantum dot surface and the resulting metallic SWNT could then promote direct charge transport and efficient charge transfer to the quantum dot. This system has the potential to significantly increase the efficiency of the device.

The addition of small amounts of dodecylamine-capped Au nanoparticles into the active layer of organic bulk heterojunction solar cells consisting of poly(3-octylthiophene) (P_3OT) and C_{60} was recently suggested to have a positive impact on performance through improved electron transport [73]. The performance of the poly(3-hexylthiophene) P_3HT/ [6,6]-phenyl C_{61}-butyric acid methyl ester (PCBM) solar cells was found to be degraded by the addition of Au particles to the active layer, which is therefore an unsuitable strategy for the P_3HT/PCBM system.

Electrochemical storage of hydrogen in Ag–CNT electrodes was studied with the potentiostat/galvanostat method [74]. Using foamed silver as a mattress for the CNTs improved connections between the nanotubes and metal, thereby leading to an increased hydrogen storage capacity caused by the effect of two competitive phenomena: (a) realignment of the CNTs and (b) oxidation of the electrode surface.

5. Analytical applications of hybrid nanomaterials combining selected properties of their nanoconstituents

Magnetic nanoparticles and nanocomposites have been the subject of both fundamental and applied research [75] even though they lack the surface tunability required for biocompatible applications. Coating magnetic particles with a gold shell provides an intriguing class of biomaterials with the potential to overcome this drawback since the well-established surface chemistry and biological reactivity of gold can be used to endow magnetic particles with the desired chemical or biomedical properties [76]. As illustrated in Fig. 9, the immobilization of antibodies on gold-coated magnetic nanoparticles and the subsequent recognition of specific antigens provide an effective means for the separation of proteins under a magnetic field. Similar strategies can also be used for DNA separation. Lim et al. [77] reported the surface functionalization of highly monodispersed Au nanoparticles and magnetic nanoparticles coated with gold shells (M/Au) by proteins and spectroscopic labels, e.g., protein A (A), anti-rabbit IgG (Ab), and bovine serum albumin (BSA), and Raman labeling, e.g., 11-mercaptobenzoic acid (L, MBA), for the production of SERS nanoprobes.

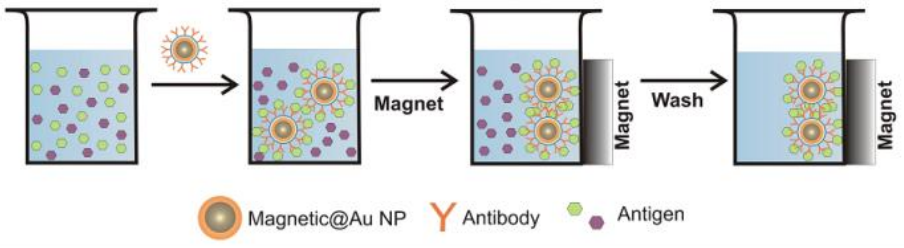

Figure 9. Idealized illustration of bio-recognition using labeled magnetic M/Au nanoparticles, and of protein separation by application of a magnetic field. Adapted, with permission, from Ref. [77].

Arruebo et al. [28] developed various types of inorganic (silica) coated magnetic nanoparticles to exploit their major advantages as contrast agents for magnetic resonance imaging applications. The silica shell provided a biocompatible, nontoxic coating, as well as a hydrophilic surface that helped to delay nanoparticle clearance by macrophages in the reticuloendothelial system. Silanol groups on the silica coating provide many possibilities for surface functionalization. The silica shell helps to avoid electrostatic agglomeration; because the isoelectric point of silica is reached at pH 2–3, silica nanoparticles exhibit significant negative surface charge at blood pH.

Morales-Cid et al. [29] synthesized hybrid magnetic–carbon nanotube nanoparticles for the preconcentration of (fluoro)quinolones in human plasma. Since the sorption properties of the magnetic nanoparticles by themselves failed to ensure reliable sample preparation, the authors tested an alternative material capable of efficiently adsorbing aromatic compounds (carbon nanotubes, which can also be used in combination with MNPs). They chose to use MWCNT in preference to SWCNT in order to obtain an effective hybrid material (a composite) in terms of adsorption on the grounds that MWCNTs possess a higher adsorption capacity than do SWCNTs [78]; that MWCNTs are less prone to aggregating [79]; and that MWCNTs are more widely used for solid-phase extraction (SPE) than are SWCNTs [80]. This hybrid nanomaterial combines the magnetic properties of MNPs at room temperature and the extremely high sorption capacity of MWCNTs. This advantage could therefore be used for the convenient, effective sampling and clean-up of the target components in a single step, even from a complex matrix. The recoveries obtained by using the composite to treat the analytes in a standard solution were better than those obtained with MNPs and MWCNTs alone, which suggests that both materials contribute similarly to the adsorption characteristics of the composite. Also, the magnetic MWCNTs exhibited a lower sedimentation rate and less marked aggregation by virtue of their net-like structure. Using a sorbent phase with

magnetic susceptibility has the advantage that it facilitates separation of the solid material from the solution by means of an externally applied magnetic field, which can considerably simplify sample preparation procedures.

SWNT–QDs hybrids were used to determine trace levels of polycyclic aromatic hydrocarbons (PAHs) in water [42]. Some analytes including pyrene, benzo[a]pyrene, benzo[a]anthracene, and perylene exhibited a dramatic increase in intrinsic fluorescence in the presence of the metallic nanoparticles. The concomitant increase in intrinsic fluorescence of the analytes and decrease in the typical fluorescence of CdSe—which was only observed when using photoactivated nanoparticles—can be ascribed to a fluorescence resonance energy transfer (FRET) process. Such a process originates from energy transfer from the nanoparticles to the analyte energy levels being much faster than fluorescence generation by the former. Because the FRET rate depends very strongly on the distance between the donor and acceptor, only those acceptor analyte molecules in close proximity to the donor QDs will take part in the FRET process. For this reason, the main constraint on the development of effective strategies based on the use of QDs as FRET donors is that if the QD site–acceptor distance is greater than the Förster radius then the FRET efficiency will be very low. Accordingly, the more marked increase in acceptor fluorescence observed with SWCNT(CdSe) can be probably ascribed to adsorption of the analyte (acceptor) onto the CNT surface bringing the acceptor and donor (CdSe) closer, and raising the FRET efficiency as a result. The broader absorption spectrum for SWCNT(CdSe) and high excitation cross sections are the most likely origins of the extensive spectral overlap and high FRET efficiency. These nanocomposites may open up new prospects for developing nanosensors inasmuch as they combine the exceptional optical properties of QDs with the also exceptional sorption capabilities of carbon nanostructures.

In micellar hybrid nanoparticles containing MNPs, QDs, and the anticancer drug DOX within a single PEG-modified phospholipid micelle [33], the strong interaction of hydrophobic chains in PEG–phospholipids with hydrophobic chains attached to the MNPs and QDs was found to increase dispersibility and stability for in vitro and in vivo applications. Increasing the ratio of MNPs to QDs within a micelle was found to decrease the fluorescence intensity from the MHN assembly with no significant spectral shift or line broadening in the emission spectrum. The loss of fluorescence intensity can be ascribed to a reduced number of QDs per micelle and to optical absorption by the MNPs. In addition, the proximity of MNPs and other QDs in the MHNs is likely to have caused fluorescence quenching through nonradiative energy or charge transfer. Despite the quenching effect observed, the fluorescence was strong enough to enable the detection of MHNs at subnanomolar QD concentrations. These inorganic QDs containing hybrid systems can be excited and observed with high photostability in the NIR spectral region, which is a substantial advantage over MNPs labeled with organic fluorophores. MHNs retain the superparamagnetic characteristics of individual MNPs. Thus, they are detectable by both MRI and fluorescence at submicromolar Fe and subnanomolar QD concentrations, which testifies to their usefulness for bimodal applications. Simultaneous dual-mode diagnosis and therapy with this type of hybrid system may enable more effective early detection and treatment of various types of cancer.

Another example of the combination of magnetic nanoparticles with quantum dots was reported by Wang et al. [41], who synthesized water-soluble nanocomposite particles consisting of a magnetic core (γ-Fe_2O_3) and a shell of luminescent quantum dots (CdSe/ZnS QDs). The material was water soluble, exhibited a high emission quantum yield, and was easily separated from solution by means of a permanent magnet. An increase in excited state lifetime ascribed to quenching interactions between the magnetic nanoparticles and the luminescent QDs, or between the close packed QDs, was observed. The drop in

the emission quantum yield could also be ascribed to the solvent change and to potential changes in electron density on the surface of the QDs caused by their immobilization onto the magnetic particles, which might allow electrons to leak to the surface of the dots and to the polymer-coated magnetic core particle. The utility of this material was demonstrated by using it to immobilize anticyclin E antibodies on their surface in order to separate MCF-7 breast cancer cells from serum solutions. Anticyclin E antibodies bind specifically to cyclin, a protein that is specifically expressed on the surface of breast cancer cells. The separated breast cells were easily observed by fluorescence imaging microscopy thanks to the strong luminescence of the luminescent/magnetic nanocomposite particles.

Aaron et al. [81] developed an approach to in vitro molecular specific optical imaging that combines the advantages of molecularly targeted plasmonic nanoparticles and magnetic actuation. The hybrid nanoparticles consisted of a superparamagnetic core coated with a gold layer. The nanoparticles were conjugated with monoclonal antibodies for molecular recognition. The hybrid nature of these particles provides new opportunities for optical contrast enhancement. The addition of the gold layer introduces three important advantages: (1) enhancement of optical signals, which facilitates detection and digital processing; (2) optical resonance tunability; and (3) the availability of a convenient surface for conjugation of probe molecules. The iron oxide core provides a magnetically susceptible component which can be exploited to periodically actuate the magnetic particles attached to cells in the field of view, thereby enabling the use of an external magnetic field to modulate the optical signal.

6. Conclusions and outlook

In recent years, nanotechnology has opened up new prospects for analytical chemistry through the exceptional characteristics of nanoparticles. However, hybrid nanoparticles possess an even greater potential inasmuch as they

combine the properties of their nanoconstituents, which can be highly useful towards simplifying analytical methods and exploring new challenges and applications relying on their synergistic effects. Hybrid nanoparticles can therefore be expected to gain increasing ground in analytical chemistry in the near future.

Acknowledgments

The authors would like to express their gratitude to Spain's Ministry of Innovation and Science, and the Andalusian Regional Government, for funding Projects CTQ2007-60426 and FQM02300, respectively. A. L.-L. also wishes to thank the Ministry for award of a Research Training Fellowship.

References

[1] Baptista P, Pereira E, Eaton P, Doria G, Miranda A, Gomes I, Quaresma P, Franco R (2008) Anal Bioanal Chem 391:943–950

[2] CaiW, Gao T, Hong H, Sun J (2008) Nanotechnol Sci Appl 1:17–32

[3] Eustis S, El-Sayed MA (2006) Chem Soc Rev 35:209–217

[4] Sperling RA, Rivera-Gil P, Zhang F, Zanella M, Parak WJ (2008) Chem Soc Rev 37:1896–1908

[5] Magdassi S, Bassa A, Vinetsky Y, Kamyshny A (2003) Chem Mater 15:2208–2217

[6] Marchisio DL, Omegna F, Barresi AA (2009) Chem Eng J 146:456–465

[7] El-Sayed MA (2004) Acc Chem Res 37:326–333

[8] Ozkan M (2004) Drug Discov Today 9:1065–1071

[9] Iijima S (1991) Nature 354:56–58

[10] Kim B, Lee YH, Ryu JH, Suh KD (2006) Colloid Surf A 273:161–164

[11] Georgakilas V, Kordatos K, Prato M, Guldi DM, Holzinger M, Hirsch A (2002) J Am Chem Soc 124:760–761

[12] Wang Y, Iqbal Z, Malhotra SV (2005) Chem Phys Lett 402:91–101

[13] Raffaelle RP, Landi BJ, Harris JD, Bailey SG, Hepp AF (2005) Mater Sci Eng B 116:233–243

[14] Baughman RH, Lui C, Zakhidov AA, Iqbal Z, Baisci JN, Spinks GM, Wallace GG, Mazzoldi A, de Rossi D, Rinzler AG, Jaschinski O, Roth S, Hertesz M (1999) Science 284:1340–1344

[15] Kroto HW, Heath JR, O'Brien SC, Curl RF, Smalley RE (1985) Nature 318:162–163

[16] Stalling DL, Guo CY, Saim S (1993) J Chromatogr Sci 31:265–278

[17] Muñoz J, Gallego M, Valcárcel M (2004) J Chromatogr A 1055:185–190

[18] Shih JS, Chao YC, Sung MF, Gau GJ, Chiou CS (2001) Sens Actuators B 76:347–353

[19] Wang LG, Wang X, Ottova AL, Tien HT (1996) Electroanalysis 8:1020–1022

[20] Tanigaki T, Kuroshima S, Fujita J, Ebbesen TW (1993) Appl Phys Lett 63:2351–2353

[21] Dolmatov VY (2001) Russ Chem Rev 70:607–626

[22] Krueger A (2008) Chem A Eur J 14:1382–1390

[23] Kim K, Janga HJ, Shin KS (2009) Analyst 134:308–313

[24] Lin J, Zhou W, Kumbhar A, Wiemann J, Fang J, Carpenter EE, O'Connor CJ (2001) J Solid State Chem 159:26–31

[25] Stoeva SI, Huo F, Lee JS, Mirkin CA (2005) J Am Chem Soc 127:15362–15363

[26] Wang H, Brandl DW, Le F, Nordlander P, Halas NJ (2006) Nano Lett 6:827–832

[27] Hou X, Zhang X, Fang Y, Chen S, Zhou Q (2010) Chem Phys 372:1–5

[28] Arruebo M, Fernández-Pacheco R, Velasco B, Marquina C, Arbiol J, Irusta S, Ibarra MR, Santamaría J (2007) Adv Funct Mater 17:1473–1479

[29] Morales-Cid G, Fekete A, Simonet BM, Lehmann R, Cárdenas S, Zhang X, Valcárcel M, Schmitt-Kopplin P (2010) Anal Chem 82:2743–2752

[30] Korneva G, Ye HH, Gogotsi Y, Halverson D, Friedman G, Bradley JC, Kornev KG (2005) Nano Lett 5:879–884

[31] Georgakilas V, Tzitzios V, Gournis D, Petridis D (2005) Chem Mater 17:1613–1617

[32] Gao C, Li WW, Morimoto H, Nagaoka Y, Maekawa T (2006) J Phys Chem B 110:7213–7220

[33] Park JH, Maltzahn G, Ruoslahti E, Bhatia SN, Sailor MJ (2008) Angew Chem Int Ed 47:7284–7288

[34] Jain TK, Morales MA, Sahoo SK, Leslie-Pelecky DL, Labhasetwar V (2005) Mol Pharm 2:194–205

[35] Nasongkla N, Bey E, Ren J, Ai H, Khemtong C, Guthi JS, Chin SF, Sherry AD, Boothman DA, Gao J (2006) Nano Lett 6:2427–2430

[36] Dubertret B, Skourides P, Norris DJ, Noireaux V, Brivanlou AH, Libchaber A (2002) Science 298:1759–1762

[37] Liu Z, Cai WB, He LN, Nakayama N, Chen K, Sun XM, Chen XY, Dai HJ (2007) Nat Nanotechnol 2:47–52

[38] Yi DK, Selvan ST, Lee SS, Papaefthymiou GC, Kundaliya D, Ying JY (2005) J Am Chem Soc 127:4990–4991

[39] Kim J, Lee JE, Lee J, Yu JH, Kim BC, An K, Hwang Y, Shin CH, Park JG, Kim J, Hyeon T (2006) J Am Chem Soc 128:688–689

[40] Sathe TR, Agrawal A, Nie S (2006) Anal Chem 78:5627–5632

[41] Wang D, He J, Rosenzweig N, Rosenzweig Z (2004) Nano Lett 4:409–413

[42] Carrillo-Carrión C, Simonet BM, Valcárcel M (2009) Anal Chim Acta 652:278–284

[43] Haremza JM, Hahn MA, Krauss TD, Chen S, Calcines J (2002) Nano Lett 2:1253–1258

[44] Banerjee S, Wong SS (2004) Chem Commun 1866–1867

[45] Banerjee S, Wong SS (2002) Nano Lett 2:195–200

[46] Cao J, Sun JZ, Hong J, Li HY, Chen HZ, Wang M (2004) Adv Mater 16:84–87

[47] Ravindran S, Chaudhary S, Colburn B, Ozkan M, Ozkan CS (2003) Nano Lett 3:447–453

[48] Dibbell RS, Watson DF (2009) J Phys Chem C 113:3139–3149

[49] Lee SW, Sigmund WM (2003) Chem Commun 780–781

[50] Zhixun L, Yan F (2006) Chem Phys 321:86–90

[51] Tallman RE, Weinstein BA, Trallero-Giner C, Sahoo Y, Prasad PN (2009) Phys Stat Sol B 246:477–481

[52] Mokari T, Costi R, Sztrum CG, Rabani E, Banin U (2006) Phys Stat Sol B 243:3952–3958

[53] Zhao S, Chen S, Wang S, Quan Z (2000) J Coll Interf Sci 221:161–165

[54] Cao L, Diao P, Zhu T, Liu Z (2004) J Phys Chem B 108:3535–3539

[55] Scott RWJ, Wilson OM, Oh SK, Kenik EA, Crooks RM (2004) J Am Chem Soc 126:15583–15591

[56] Zhang D, Song X, Zhang R, Zhang M, Liu F (2005) Eur J Inorg Chem 1643–1648

[57] Kawazu M, Nara M, Tsujino T (2004) J Sol–Gel Sci Technol 31:109–112

[58] Jiang L, Wang W, Wu D, Zhan J, Wang Q, Wu Z, Jin R (2007) Mater Chem Phys 104:230–234

[59] Mori H, Miyamura Y, Endo T (2009) Mater Chem Phys 115:287–295

[60] Ionita G, Maganu M, Caproiu MT, Ionita P (2009) J Inorg Organomet Polym 19:228–233

[61] Guo S, Zhai J, Fang Y, Dong S, Wang E (2008) Chem Asian J 3:1156–1162

[62] Arruebo M, Galán M, Navascués N, Téllez C, Marquina C, Ibarra MR, Santamaría J (2006) Chem Mater 18:1911–1919

[63] Kim BS, Taton TA (2007) Langmuir 23:2198–2202

[64] Marini M, Toselli M, Borsacchi S, Mollica G, Geppi M, Pilati F (2008) J Polym Sci A Polym Chem 46:1699–1709

[65] Pedroso MAS, Dias ML, Azuma C, San Gil RM, Mothe CG (2003) Colloid Polym Sci 281:19–26

[66] Burgeat-Lami EJ (2001) Nanosci Nanotechnol 2:1–24

[67] Wang TL, Ou CC, Yang CH (2008) J Appl Polym Sci 109:3421–3430

[68] Daigle JC, Claverie JP (2008) J Nanomater. doi:10.1155/2008/609184

[69] Ma PC, Tang BZ, Kim JK (2008) Carbon 46:1497–1505

[70] Rangari VK, Mohammad GM, Jeelani S, Hundley A, Vig K, Singh SR, Pillai S (2010) Nanotechnology 21:095102

[71] Wang S, Gong Q, Zhu Y, Liang J (2009) Appl Surf Sci 255:8063–8066

[72] Hu JW, Li JF, Ren B, Wu DY, Sun SG, Tian ZQ (2007) J Phys Chem C 111:1105–1112

[73] Topp K, Borchert H, Johnen F, Tunc AV, Knipper M, von Hauff E, Parisi J, Al-Shamery K (2010) J Phys Chem A 114:3981–3989

[74] Khoshnevisan B, Behpour M, Kaveh D (2009) Physica B 404:1733–1736

[75] Wang LY, Luo J, Maye MM, Fan Q, Rendeng Q, Engelhard MH, Wang CM, Lin YH, Zhong CJ (2005) J Mater Chem 15:1821–1832

[76] Grubisha DS, Lipert RJ, Park HY, Driskell J, Porter MD (2003) Anal Chem 75:5936–5943

[77] Lim IS, Njokil PN, Park HY, Wang X, Wang L, Mott D, Zhong CJ (2008) Nanotechnology 19:305102

[78] Valcárcel M, Cárdenas S, Simonet BM (2007) Anal Chem 79:4788–4797

[79] Dai L (2006) Carbon nanotechnology: recent developments in chemistry, physics, material science and device applications. Elsevier, Amsterdam

[80] Valcárcel M, Cárdenas S, Simonet BM, Moliner-Martínez Y, Lucena R (2008) Trends Anal Chem 27:34–43

[81] Aaron JS, Oh J, Larson TA, Kumar S, Milner TE, Sokolov KV (2006) Opt Express 14:12930–12943

I.3. NANOPARTICLES AS TOOLS IN ANALYTICAL CHEMISTRY

One of the main goals of Analytical Chemistry is the development of new methodologies which improve existing ones and meet new demands of (bio)chemical information posed by the present social and economic problems. The growing demand of (bio)chemical information requires the development of new tangible and intangible tools to support analytical processes. Improvements in analytical processes can be measured in terms of analytical properties: capital, basic and productivity-related[1] (see Figure I.3.1).

The new scene created by the growth of Nanoscience and Nanotechnology has had an impact in the field of Analytical Chemistry. Nanotechnological tools have been used in analytical methods by exploiting the excellent properties of nanoparticles in order to improve well-established analytical methods or to develop others for new analytes or matrices. The use of nanoparticles should lead to improved selectivity, sensitivity, rapidity, miniaturizability or portability of the analytical system. This facet of Analytical Nanotechnology is the most extensively explored[2].

[1] M. Valcárcel, A. Ríos, Anal. Chem. 65 (1993) 781A-787A.
[2] M. Valcárcel, B.M. Simonet, S. Cárdenas, Anal. Bioanal. Chem. 391 (2008) 1881-1887.

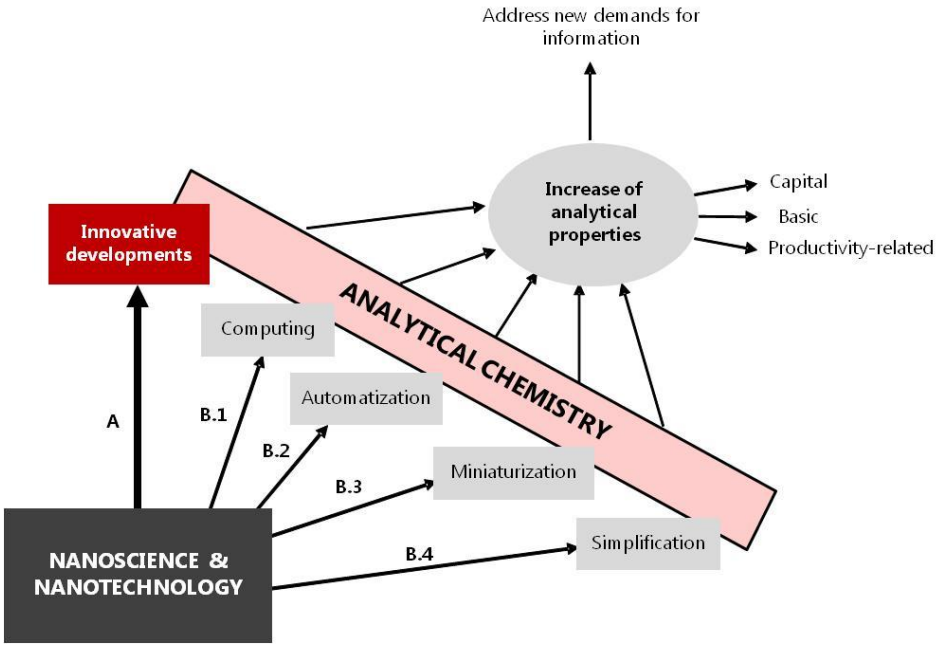

Figure I.3.1. The multiple role of Nanotechnology in Analytical Science: (A) Direct impact, and (B) Indirect impact through their role as support of other scientific-technical advances.

Nanotechnology-based analytical processes can exploit both the nanosize and exceptional properties of structured nanomatter. In this sense, as it was previously introduced (see Figure I.1.1 and related text), analytical systems based on Nanoscience and Nanotechnology can be classified in three types[3], namely: i) *nanometric analytical systems*, based on nanosize and/or nanofluidics, for example nano-chip liquid chromatography, however, some authors have placed them outside the scope of nanotechnology, ii) *nanotechnological analytical systems*, which exploit the exceptional physicochemical properties of nanomaterials, and iii) *analytical nanosystems*, which integrate previous two systems, for example individual carbon nanotubes for use as electrodes.

[3] M. Valcárcel, B.M. Simonet, Anal. Bioanal. Chem 399 (2011) 1-2.

The most widely used nanoparticles in analytical sciences include (a) silica nanoparticles, (b) metallic nanoparticles (quantum dots, gold nanoparticles, etc.), (c) carbon nanoparticles (mainly fullerenes and carbon nanotubes), (d) organic polymer nanoparticles (e.g. molecular imprinted polymers) or (e) supramolecular aggregates (nanomicelles, nanovesicles), as depicted in Figure I.3.2. The explored nanoparticle property can be electrical, optical, thermal, magnetic or chemical. Frequently, however, two or more properties are explored at once.

An analytical process can be divided into several steps, as represented in Figure I.3.2, namely: sample preparation (including sampling), chromatographic (LC, GC) and capillary electrophoretic techniques, detection and data handling and treatment to offer the results as required. The role of nanoparticles differs between the different steps of the analytical process. Figure I.3.2 shows the proportion of described analytical procedures in which nanoparticles are involved.

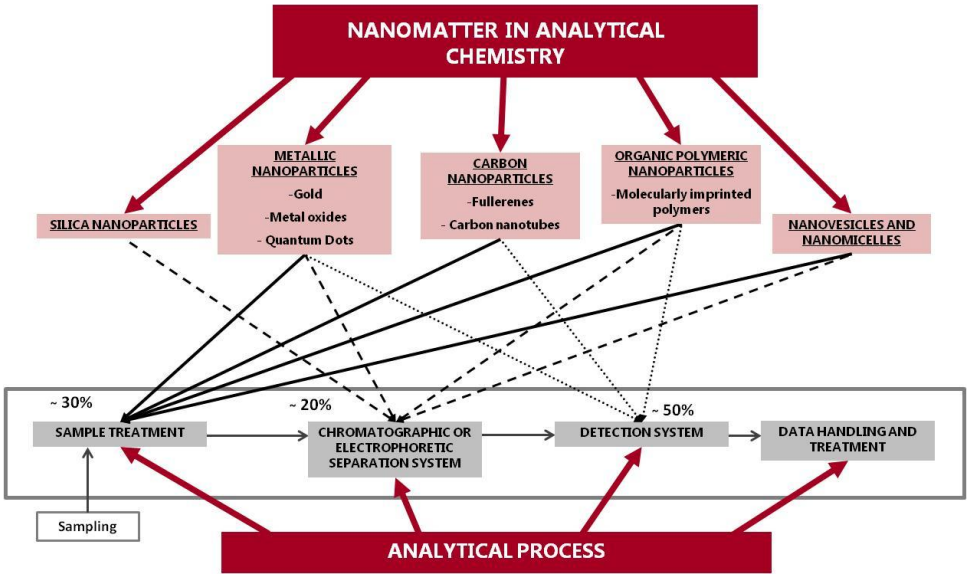

Figure I.3.2. The role of nanoparticles in different steps of analytical process.

Detection

Detection is the analytical step in which nanoparticles have been more widely used by virtue of their ability to replace conventional materials as well as the advantages of electrochemical biosensors. In this sense, biomolecules are stabilized by the nanoparticles, which increase active surfaces and facilitate electron transfer. In addition, the development of optical nanosensors has been fostered by the exceptional optical properties of metallic nanoparticles derived from their plasmon resonance, as well as photofluorescent properties in the case of semiconducting nanoparticles (quantum dots)[4], carbon dots[5,6] (CDs) or graphene quantum dots[7].

Quantum dot-based sensors for chemical and biological detection have been widely developed[8] by virtue of the special optical and electronic properties of the component QDs[9] plus the possibility to relatively easily functionalize them with a wide variety of biological as well as relevant molecules for other important applications[10].

Gold nanoparticles have been also widely used by virtue of their optical properties. For example, mercury traces have been detected by ultraviolet-visible spectroscopy using gold nanoparticles functionalized with

[4] L. Wang, W. Ma, L. Xu, W. Chen, Y. Zhu, C. Xu, N.A. Kotov, Mater. Sci. Eng. R 70 (2010) 265–274.
[5] L. Cao , X. Wang , M.J. Meziani , F. Lu , H. Wang , P.G. Luo , Y. Lin ,B.A. Harruff , L.M. Veca , D. Murray, S.-Y. Xie , Y.-P. Sun, J. Am. Chem. Soc. 129 (2007) 11318–11319.
[6] S.-T. Yang, X. Wang, H. Wang, F. Lu, P.G. Luo, L. Cao, M.J. Meziani, J.-H. Liu, Y. Liu, M. Chen, Y. Huang, Y.-P. Sun, J. Phys. Chem. C 113 (2009) 18110–18114.
[7] S. Zhu, J. Zhang, C. Qiao, S. Tang, Y. Li, W. Yuan, B. Li, L. Tian, F. Liu, R. Hu, H. Gao, H. Wei, H. Zhang, H. Sun, B. Yang, Chem. Commun. 47 (2011) 6858-6860.
[8] Z. Yue, F. Lisdat, W.J. Parak, S.G. Hickey, L. Tu, N. Sabir, D. Dorfs, N.C. Bigall, ACS Appl. Mater. Interfaces 5 (2013) 2800-2814.
[9] W.J. Parak, T. Pellegrino, C. Plank, Nanotechnology 16 (2005) R9–R25.
[10] W.J. Parak, D. Gerion, T. Pellegrino, D. Zanchet, C. Micheel, S.C. Williams, R. Boudreau, M.A. Le Gros, C.A. Larabell, A.P. Alivisatos, Nanotechnology 14 (2003) 15–27.

complementary DNA sequences, which are intensely coloured and are present as colloidal dispersion[11].

Carbon nanotubes and gold nanoparticles are the types of nanoparticles most widely used for developing electrochemical (bio)sensors[12,13]. CNT-based sensors can be used to detect changes in their electronic properties resulting from the sorption of molecules on their surface. The electronic properties of CNTs encourage their use as electrodes to mediate electron-transfer reactions with electroactive species in solution[14]. Combining gold nanoparticles and carbon nanotubes was found to enhance some electrocatalytic properties of electrodes[15].

Sample preparation

Sample preparation has also profited from the use of nanomaterials, albeit a lesser extent than detection. The incorporation of nanoparticles in the sample treatment step, in general, helps to simplify it. For example, conventional sorbents for solid-phase extraction and solid-phase microextraction have been replaced by nanomaterials. Nanoparticles, according to their participation and role in the sample treatment step can be classified as follows[16]: i) nanoparticles acting as sorbent agents[17], where direct interaction between the analyte and the nanoparticle takes place; ii) nanoparticles acting as an inert support, such as a silica nanoparticle functionalized with a complexation agent; iii) nanoparticles

[11] J.S. Lee, M.S. Han, Ch.A. Mirkin, Angew. Chem. (Int. Ed.) 46 (2007) 4093-4096.
[12] E.J. Parra, F.X. Rius, P. Blondeau, Analyst 138 (2013) 2698-2703.
[13] G.A. Zelada-Guillén, A. Tweed-Kent, M. Niemann, H.U. Göringer, J. Riu, F.X. Rius, Biosensors and Bioelectronics 41 (2013) 366-371.
[14] M. Trojanowicz, Trends Anal. Chem. 25 (2006) 480-489.
[15] J. Manso, M.L. Mena, P. Yáñez-Sedeño, J. Pingarrón, J. Electroanal. Chem. 603 (2007) 1-7.
[16] R. Lucena, B.M. Simonet, S. Cárdenas, M. Valcárcel, J. Chromatogr. A, 1218 (2011) 620-637.
[17] I. Márquez-Sillero, E. Aguilera-Herrador, S. Cárdenas, M. Valcárcel, J. Chromatogr. A 1217 (2010) 1-6.

having special magnetic properties, which can either directly adsorb the analyte or can be functionalized with organic groups, the use of a magnetic field can simplify the analytical procedure; iv) nanoparticles acting as ionizations agent for the direct analysis of samples by ion secondary mass spectrometry.

Carbon nanomaterials have focused attention thanks to their singular π-π electron configuration, as well as metal oxides by virtue of their high surface area. In this sense, carbon nanotubes have been widely used as sorbents for solid-phase extraction[18,19]. Packed nanotubes tend to aggregate to some extent, their inclusion as a nanoscience application requires that aggregation be avoided and interactions between analytes and isolated nanoparticles favoured[20]. Conical carbon nanoparticles, such as single-walled nanohorns (SWNHs)[21] or carbon nanocones/disks[22] have been also used for solid-phase (micro)extraction. In addition to solid-phase extraction, nanoparticles have been used in other sample treatments such as membrane filtration, for example with membranes composed or modified by carbon nanotubes, as it will be explained in deep in chapter 13 of this memory[23] and applied to the determination of other nanomaterials in chapter 14 of this Doctoral Thesis.

Separation science

Furthermore, nanostructured materials are being increasingly used in *separation science* as stationary phases in gas and liquid chromatography or electrochromatography, and also as pseudo-stationary phases in electrokinetic chromatography. The use of nano-sized materials in electro-driven separation

[18] B. Suárez, B.M. Simonet, S. Cárdenas, M. Valcárcel, J. Chromatogr. A 1159 (2007) 203-207.
[19] B. Suárez, B. Santos, B.M. Simonet, S. Cárdenas, M. Valcárcel, J. Chromatogr. A 1175 (2007) 127-132.
[20] M. Valcárcel, S. Cárdenas, B.M. SImonet, Y. Moliner-Martínez, R. Lucena, Trends Anal. Chem. 27 (2008) 34-43.
[21] J.M. Jiménez–Soto, S. Cárdenas, M. Valcárcel, Anal. Chim. Acta 714 (2012) 76-81.
[22] J.M. Jiménez–Soto, S. Cárdenas, M. Valcárcel, J. Chromatogr. A 1216 (2009) 5626-5633.
[23] A.I. López-Lorente, B.M. Simonet, M. Valcárcel, Anal. Chem. 82 (2010) 5399-5407.

systems has received more attention than in laminar flow liquid and gas chromatographic (LC and GC) systems[24]. As novel stationary phases and dynamic coatings, NPs greatly enhance separation performance in relation to resolution, selectivity and efficiency. They display a large surface area-to-volume ratio, which is ideal for low mass-transfer effects in chromatography[25].

So far, nanoparticles have found extensive use in capillary electrophoresis (CE), packed capillary electrochromatography (CEC), open tubular CEC formats and microchip CE. Several nanoparticles have been employed as pseudostationary phases in capillary electrophoresis[26], such as SWNHs, CNTs and fullerenes[27] or graphene[28]. A new electrophoretic mode designated as micellar nanoparticle dispersion electrokinetic chromatography (MiNDEKC) has been developed which proved to be effective in the separation of aromatic compounds[29] or even chiral compounds[30].

There are also some reports of the use of nanoparticles in LC, ion chromatography (IC) and GC[31]. Nanoparticles for GC are usually packed into a tubular column. As an alternative to packing, CNTs can be self-assembled into a gas chromatographic column[32]. NPs have been also inserted into a monolithic column in LC[33].

[24] E. Guihen, Trends Anal. Chem. 46 (2013) 1-14.
[25] C. Nilsson, S. Birnbaum, S. Nilsson, J. Chromatogr. A 1168 (2007) 212.
[26] C. Nilsson, S. Nilsson, Electrophoresis 27 (2006) 76-83.
[27] Y. Moliner-Martinez, M. Barrios, S. Cárdenas, M. Valcárcel, J. Chromatogr. A 1194 (2008) 128-133.
[28] S. Benítez-Martínez, B.M. Simonet, M. Valcárcel, Electrophoresis, 34 (2013) 2561-2567.
[29] B. Suárez, B.M. Simonet, S. Cárdenas, M. Valcárcel, Elecctrophoresis 28 (2007) 1714-1722.
[30] Y. Moliner-Martínez, S. Cárdenas, M. Valcárcel, Electrophoresis 28 (2007) 2573-2579.
[31] D. Sýkora, V. Kasicka, L. Miksik, P. Rezanka, K. Záruba, P. Matejka, V. Kral, J. Sep. Sci. 33 (2010) 372-387.
[32] C. Saridara, S. Mitra, Anal. Chem. 77 (2005) 7094-7097.
[33] Y. Li, Y. Chen, R. Xiang, D. Ciuparau, L.D. Pfefferle, C. Horvath, J.A. Wilkins, Anal. Chem. 77 (2005) 1398-1406.

I.4. NANOPARTICLES AND NANOSTRUCTURED MATERIALS AS ANALYTICAL OBJECTS

The development of analytical methodologies for extracting quality information from nanoparticles or nanostructured compounds is of high interest due to the poor knowledge available about their actual composition and characteristics, as well as their presence in environmental, biological or agrifood matrices. Developing effective analytical methods for the rapid, accurate characterization of nanoparticles is mandatory with a view to advancing nanotechnology[1].

This topic has clear connotations of interface between physics and chemistry, as can be inferred from Figure I.4.1, where the physical (size, properties, topography) and chemical characteristics (composition, chirality, reactivity and type of bond) are reflected. It should be pointed out in this context the increasing interest of biological characteristics (diffusion through membranes, toxicity[2], biotransformations, nanoparticles interaction with cells and microorganisms[3]) derived from the chemical reactivity of the nanomatter. Among the types of characterization that are needed, perhaps none is more challenging than chemical characterization[4].

[1] M. Valcárcel, B.M. Simonet, S. Cárdenas, Anal. Bioanal. Chem. 391 (2008) 1881-1887.
[2] A.K. Suresh, D.A. Pelletier, M.J. Doktycz, Nanoscale, 5 (2013) 463-474.
[3] P.R. Leroueil, S. Hong, A. Mecke, J.R. Baker Jr., B.G. Orr, M.M.B. Holl, Acc. Chem. Res. 40 (2007) 335–342.
[4] M.R. Winchester, R.E. Sturgeon, J.M. Costa-Fernández, Anal. Bioanal. Chem. 396 (2010) 951-952.

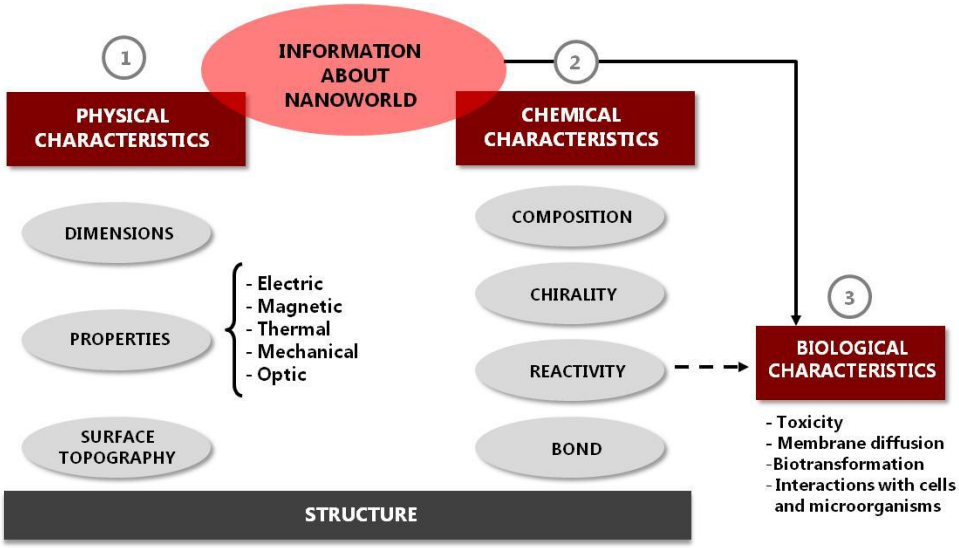

Figure I.4.1. Types of information about nanomatter according to the nature of its characteristics.

Extracting information from the nanoworld entails measuring dimensions of only a few nanometers. So-called nanometrology is therefore a hot topic. Although nanometrology is of special concern to physicists, analytical chemists can make substantial contributions to its advancement.

Several types of techniques are available to characterise NPs[5] and their surface chemistry[6,7,8]. Herein, the different techniques have been classified as microscopic, spectroscopic and separation ones.

[5] R. Zenobi, Anal. Bioanal. Chem. 390 (2008) 215-221.
[6] B. Zhang, B. Yan, Anal. Bioanal. Chem. 396 (2010) 973-982.
[7] D.R. Baer, D.J. Gaspar, P. Nachimuthu, S.D. Techane, D.G. Castner, Anal. Bioanal. Chem. 396 (2010) 983-1002.
[8] K.A. Wepasnick, B.A. Smith, J.L. Bitter, D.H. Fairbrother, Anal. Bioanal. Chem 396 (2010) 1003-1014.

4.1. Microscopic techniques for the analysis of nanoparticles

Microscopic techniques include optical, electron and scanning probe microscopy. The most used techniques for the characterization of NPs are electron microscopies (EM) -transmission electron microscopy (TEM), high-resolution TEM and scanning electron microscopy (SEM)-, and scanning probe microscopies (SPM), namely, atomic force microscopy (AFM) and scanning tunneling microscopy (STM). Depending on the technique, resolutions down to the sub-nanometer range can be achieved. Besides the imaging of nanoparticles, these methods enable the determination of the aggregation, dispersion, size, structure and shape of NPs. In addition, SEM and AFM offer three dimensional images of nanoparticles.

However, microscopic techniques present shortcomings in sample preparation as well as the statistical uncertainty due to the human subjectivity implied when deciding which parts of the grid are photographed. In order to measure an accurate size distribution of nanoparticles it is necessary to count and measure thousand of particles in order to obtain a reliable counting statistics. Regarding sample preparation, SEM and TEM have to operate in vacuum, and therefore only dry, solid samples can be investigated. The transfer of the sample from dispersion to dried state changes the size distribution as well as the aggregation state of the nanoparticles or leads to the precipitation of salts. Furthermore, electron microscopy is usually a destructive method, meaning that the same sample cannot be analyzed twice or by another method for validation. Also, biological samples often need treatment, such as heavy metal staining, for improved contrast. In this case, a scanning transmission electron microscope (STEM) belonging to the group of TEMs can be of use.

In order to image NPs in more natural conditions, environmental scanning electron microscopy[9] (ESEM) has been developed. Although its sample chamber and detector cannot achieve atmospheric pressure, nanoparticles can be visualized under almost natural conditions[10], with residual hydration water still on the particles. This water layer also serves as a conductor on the surface so the sample does not need to be conductively coated[11].

AFM is one of the most common nanometrology methods and has numerous applications[12,13,14]. With this technique it is possible to analyze samples under moist conditions or even in liquids, which affords minimum perturbation. Under liquid conditions particles can eventually stick to the cantilever, which leads to imaging artifacts. This smearing effect could be minimized by using a non-contact scanning mode where the tip is not touching the nanoparticles but only feels its forces.

When combined with analytical methods, additional information can be gained about the elemental composition of the sample. Electron microscopy methods can be combined to perform energy dispersive X-ray spectroscopy (EDX or EDS) and electron energy loss spectroscopy (EELS) for the elemental analysis of the nanoparticles, whereas selected area electron diffraction (SAED) gives information about the crystalline properties of NPs[15].

[9] D.J. Stokes, Philos. Trans. R. Soc. London, Ser. A 361 (2003) 2771-2787.
[10] K. Tiede, A.B.A. Boxall, S.P. Tear, J. Lewis, H. David, M. Hassellöv, Food Addit. Contam. 25 (2008) 795-821.
[11] M. Hassellöv, J.W. Readman, J.F. Ranville, K. Tiede, Ecotoxicology, 17 (2008) 344-361.
[12] J.H. Hafner, C.L. Cheung, A.T. Woolley, C.M. Lieber, Prog. Biophys. Mol. Biol. 77 (2001) 73-110.
[13] P. West, N. Starostina, Adv. Powder. Metall. Part. Mater. (2006) 2/17-2/28.
[14] J.R. Viguie, J. Sukmanowski, B. Nolting, F.X. Royer, Colloids Surf. Physicochem. Eng. Aspects 302 (2007) 269-275.
[15] D. Mavrocordatos, W. Pronk, M. Boller, Water. Sci. Technol. 50 (2004) 9-18.

X-ray microscopy (XRM) can provide spatial resolution imaging of a specimen in the aqueous state without the need for sample preparation[16]. A variation of the XRM is the scanning transmission X-ray microscopy (STXM), which has been used, for example, to characterize metallic Fe particles for remediation purposes[17].

Moreover, near-field scanning optical microscopy (NSOM), with a resolution between 50 and 100 nm, can be used to image aggregates of nanoparticles[18]. A modification of confocal microscopy –confocal laser scanning microscopy (CLSM)- is able to detect fluorescent samples and can be used to characterize colloids, since it is able to image thick samples[10].

4.2. Spectroscopic and related techniques for the analysis of nanoparticles

Spectroscopic methods also have a wide range of applications for the analysis of nanomaterials. Fluorescence-based techniques are used for the analysis of nanoparticles with a strong native fluorescence, such as quantum dots (QDs), or more recently, carbon dots[19] (CDs) or graphene quantum dots[20,21], which can be characterized from their absorption or fluorescence spectra. The position of emission bands can be correlated with particle size and is commonly used to monitor size in the synthesis of QDs[22], for example. In describing the UV-Vis absorption spectra of metal NPs, the term surface Plasmon is used, which describes the oscillating electron clouds present at the metal-solution interface.

[16] J. Thieme, I. McNulty, S. Vogt, D. Paterson, Environ. Sci. Technol. 41 (2007) 6885–6889.
[17] J.T. Nurmi, P.G. Tratnyek, V. Sarathy, D.R. Baer, J.E. Amonette, K. Pecher, C.M. Wang, J.C. Linehan, D.W. Matson, R.L. Penn, M.D. Driessen, Environ. Sci. Technol. 39 (2005) 1221–1230.
[18] A.D. Maynard, Philos. Trans. R. Soc. Lond. A 358 (2000) 2593-2609.
[19] Y.-P. Sun, B. Zhou, Y. Lin, W. Wang, K.A.S. Fernando, P. Pathak, M.J. Meziani, B.A. Harruff, X. Wang, H. Wang, P.G. Luo, H. Yang, M.E. Kose, B. Chen, L.M. Veca, S.-Y.Xie, J. Am. Chem. Soc. 128 (2006) 7756–7757.
[20] Y. Li, Y. Hu, Y. Zhao, G. Shi, L. Deng, Y. Hou, L. Qu, Adv. Mater. 23 (2011) 776-780.
[21] D. Pan, J. Zhang, Z. Li, M. Wu, Adv. Mater. 22 (2010) 734-738.
[22] Q.Q. Yu, L. Qu, W. Guo, X. Peng, Chem. Mater. 15 (2003) 2854-2860.

Particle concentrations can be quantified from absorption measurements provided the optical constants for the nanoparticles are known[23,24].

Vibrational spectroscopies, both Raman and infrared, are useful for the analysis of nanoparticles, especially carbon nanoparticles. The two techniques differ in the excitation source used, the way signals are monitored and the selection rules employed on vibrational modes. At present, Raman spectroscopy is the most important technique for the analysis of carbon nanotubes[25], since Raman measurements are simple, can be done at room temperature and under ambient pressure, are quick, non-destructive and non-invasive[26], and it is possible to find sophisticated laboratory equipments as well as less expensive portable ones. Their widespread acceptance relies on their usefulness to provide information about vibrational properties that can be correlated with the structure and electronic properties of the nanotubes. Tip-enhanced Raman scattering (TERS) has been also used for carbon nanotubes[27], for example. In the case of SWNTs, NIR-fluorescence[28] is a technique widely used for their characterization according to their chirality[29] as well as their quantitative analysis in aquatic environment[30].

The average bulk chemical composition of a sample can be determined by using spectroscopic techniques such as atomic absorption spectroscopy, inductively coupled plasma with atomic emission spectroscopy (ICP-AES), optical emission

[23] W.W. Yu, L. Qu, W. Guo, X. Peng, Chem. Mater. 15 (2003) 2854-2860.
[24] W. Haiss, N.T.K. Thanh, J. Aveyard, D.G. Ferning, Anal. Chem. 79 (2007) 4215-4221.
[25] M.S. Dresselhaus, G. Dresselhaus, A. Joiro, J. Phys. Chem. C 111 (2007) 17887-17893.
[26] A. Jorio, M.A. Pimenta, A.G. Souza Filho, R. Saito, G. Dresselhaus, M.S. Dresselhaus, New J. Phys. 5 (2003) 1.1-1.17.
[27] N. Hayazawa, T. Yano, H. Watanabe, Y. Inouye, S. Kawata, Chem. Phys. Lett. 376 (2003) 174-180.
[28] R.B. Weisman, Anal. Bioanal. Chem. 396 (2010) 1015-1023.
[29] S. Maruyama, Y. Miyauchi, Y. Murakami, S. Chiashi, New J. Phys. 5 (2003) 149.1–149.12.
[30] A. Schierz, A.N. Parks, K.M. Washburn, G.T. Chandler, P.L. Ferguson, Environ. Sci. Technol. 46 (2012) 12262-12271.

spectroscopy (ICP-OES)[31] and mass spectrometry (ICP-MS)[32,33,34] especially for the analysis of metallic nanoparticles. These techniques feature good limits of detection, providing compositions results which are sample averages and they also afford multielement analysis. However, they are destructive and subject to matrix interferences[35]. Mass spectrometry techniques are gaining growing importance thanks to their compatibility with any type of sample, their extremely high sensibility and easy coupling with separation techniques to obtain real-time information[36].

Light scattering is a very commonly used method to determine particle size. Among the scattering techniques, dynamic light scattering (DLS) is widely used for sizing of NPs and determining their aggregation in suspensions[37]. The advantages of DLS are the rapid and simple operation, readily available equipment, and minimum perturbation of the sample. The limitations are the interpretation and critical review of the data obtained, especially for polydisperse systems[11]. Turbidimetry and nephelometry have been also employed to measure particle concentration[38].

Laser-based methods worth mentioning are the small angle X-ray scattering (SAXS), which is able to characterize mono- and polydisperse systems, and laser-induced breakdown spectroscopy (LIBS), which has a very low detection limit and is suitable for the size and concentration analysis of colloids. Nuclear

[31] S. Elzey, D.-H. Tsai, S.A. Rabb, L.L. Yu, M.R. Winchester, V.A. Hackley, Anal. Bioanal. Chem. 403 (2012) 145–149.
[32] A. Scheffer, C. Engelhard, M. Sperling, W. Buscher, Anal Bioanal Chem 390 (2008) 249–252.
[33] A. Helfrich, W. Brüchert, J. Bettmer, J. Anal. At. Spectrom. 21 (2006) 431–434.
[34] R. Allabashi, W. Stach, A. de la Escosura-Muñiz, L. Liste-Calleja, A. Merkoçi, J Nanopart Res 11 (2009) 2003–2011.
[35] B.M. Simonet, M. Valcárcel, Anal. Bioanal. Chem. 393 (2009) 17-21.
[36] A.R. Montoro-Bustos, J. Ruiz-Encinar, A. Sanz-Medel, Anal. Bioanal. Chem. 405 (2013) 5637-5643.
[37] A. Ledin, S. Karlsson, A. Ker, B. Allard, Water Res. 28 (1994) 1539-1545.
[38] J.A. Sene, M.V.B. Pinheiro, K. Krambrock, P.J.S. Barbeira, Talanta 78 (2009) 1503-1507.

magnetic resonance (NMR) spectroscopy[39] is used to determine the dynamics and three-dimensional structure of the samples, whereas X-ray spectroscopy provides crystallographic information which can be used for the characterization of NP surfaces and coatings[40].

4.3. Methods of separation and purification of nanoparticles

Separation techniques such as size-exclusion chromatography (SEC), hydrodynamic chromatography (HDC), capillary electrophoresis (CE), dielectrophoresis (DEP) and field-flow fractionation (FFF) can also be used to characterize NPs. These methods are sensitive and enable further analysis of the sample.

The most employed method is SEC[41], which, combined with detection techniques such as voltammetric, ICP-MS, DLS, multiangle laser light scattering (MALLS) also called static light scattering (SLS), can be applied to the characterization of AuNPs, QDs and SWNTs, for example. A drawback of SEC is that irreversible adsorption onto the stationary phase may occur.

Separation and characterization of NPs with hydrodynamic chromatography is based on their hydrodynamic radius. Liquid chromatography coupled to voltammetric detection has been also employed for the separation of metal nanoparticles[42].

Capillary electrophoresis (CE) has emerged as a useful technique, with fewer surface effects than in other techniques (e.g. SEC) and with low consumption of

[39] D.J. Nelson, C.N. Brammer, Anal. Bioanal. Chem. 396 (2010) 1079-1086.
[40] M. Farré, K. Gajda-Schrantz, L. Kantiani, D. Barceló, Anal. Bioanal. Chem 393 (2009) 81-95.
[41] G.T. Wei, F.K. Liu, J. Chromatogr. A 836 (1999) 253-260.
[42] Y. Song, M.LAV Heien, V. Jimenez, R.M. Wightman, R.W. Murray, Anal. Chem. 76 (2004) 4911-4919.

sample and reagents, for the characterization of nanoparticles[43]. CE has been used to separate a variety of differently sized materials, including gold[44] and silver nanoparticles[45], CNTs[46], QDs[47], among others. Different modalities have been employed such as isoelectric focusing (IEF) or gel electrophoresis. Chapter 8 of this Thesis delves in the electrophoretic characterization of nanoparticles.

Dielectrophoresis (DEP) has also emerged as a powerful technique in order to manipulate nanoparticles[43]. Special emphasis is given to the dielectrophoretic separation of CNTs, due to its usefulness in discriminating metallic ones from semiconductor[48], since it is capable of separate species not only by size but also by dielectric constant. However, DEP is further from routine analytical application than gel or capillary electrophoresis.

Field-flow fractionation separates nanoparticles according to particle size in terms of their diffusion coefficients in a very thin open channel. Separation relies on the combination of an applied field and a longitudinal carrier flow. It has been successfully used to analyze a wide range of NPs[49,50] including SiO_2, CNTs, QDs, gold and silver.

Other separation techniques used in this field are centrifugation[51], ligand-assisted extraction[52], solid-phase extraction[53], microextraction with ionic liquids

[43] A.I. López-Lorente, B.M. Simonet, M. Valcárcel, Comprehensive Analytical Chemistry 59 (2012) 33-89.
[44] F.-K. Liu, Y.-Y. Lin, C.-H. Wu, Anal. Chim. Acta 528 (2005) 249-254.
[45] F.-K. Liu, F.-H. Ko, P.-W. Huang, C.-H. Wu, T.-C. Chu, J. Chromatogr. A 1062 (2005) 139-145.
[46] B. Suárez, B.M. Simonet, S. Cárdenas, M. Valcárcel, J. Chromatogr. A 1128 (2006) 282-289.
[47] C. Carrillo-Carrión, Y. Moliner-Martínez , B.M. Simonet, M. Valcárcel, Anal. Chem. 83 (2011) 2807-2813.
[48] R. Krupke, F. Hennrich, H. v. Löhneysen, M.M. Kappes, Science 301 (2003) 344-347.
[49] F. von der Kammer, S. Legros, T. Hofmann, Trends Anal. Chem. 30 (2011) 425-436.
[50] M. Baalousha, B. Stolpe, J.R. Lead, J. Chromatogr. A. 1218 (2011) 4078-4103.
[51] O. Akbulut, C.R. Mace, R.V. Martinez, A.A. Kumar, Z. Nie, M.R. Patton, G.M. Whitesides, Nano Lett. 12 (2012) 4060-4064.
[52] L. Li, K. Leopold, Anal. Chem. 84 (2012) 4340-4349.

(see chapters 10 and 11 of this thesis), microfiltration[54], dialysis[55], and cloud-point extraction[56] of different nanomaterials.

Table I.4.1. Specifications of methods for analysis and characterization of nanoparticles. Adapted from ref.[11]

Method	Approximate size range (nm)	Limit of detection[a]	Level of sample perturbation
AFM	0.5 to >1000	ppb-ppm	Medium
Centrifugation	10 to >1000	(d.d.)[b]	Low
Dialysis	0.5-100	(d.d.)[b]	Low
DLS	3 to >1000	ppm	Minimum
Electrophoresis	3 to >1000	ppm	Minimum
EM-EELS/-EDX	Analysis spot size: ~1 nm	ppm	High
ESEM	40 to >1000	ppb-ppm	Medium
FFF	1-1000	(d.d.)[c]	Low
HDC	5-1200	(d.d.)[b]	Low
ICP-MS	Depends on fractionation	ppt-ppb	
LIBS	5 to >1000	ppt	Minimum
Microfiltration	100 to >1000	(d.d.)[b]	Low-medium
SEC	0.5-10	(d.d.)[b]	Medium
SEM	10 to >1000	ppb-ppm	High
SLS/MALLS	50 to >1000		Minimum
TEM/HR-TEM	1 to >1000	ppb-ppm	High
TEM-SAED	Analysis spot size: 1 nm		High
Turbidimetry/nephelometry	50 to >1000	ppb-ppm	Minimum
XRD	0.5 to >1000	Dry powder	High

[a]For comparison mass concentration limit of detection for 100 nm particles are estimated.
[b](d.d.)= detection dependant
[c] (UV: ppm, Fluo/ICP-MS: ppb)

[53] B. Suárez, Y. Moliner-Martínez, S. Cárdenas, B.M. Simonet, M. Valcárcel, Environ. Sci. Technol. 42 (2008) 6100-6104.
[54] S. Bandow, A.M. Rao, K.A. Williams, A. Thess, R.E. Smalley, P.C. Eklund, J. Phys. Chem. B 101 (1997) 8839-8842.
[55] S.F. Sweeney, G.H. Woehrle, J.E. Hutchison, J. Am. Chem. Soc. 128 (2006) 3190-3197.
[56] J.-B. Chao, J.-F. Liu, S.-J. Yu, Y.-D. Feng, Z.-Q. Tan, R. Liu, Y.-G. Yin, Anal. Chem. 83 (2011) 6875-6882.

Other techniques

In addition to those techniques, electrochemical methods[57] of analysis of nanoparticles have been also employed for their analysis such as voltammetry[58,59]. Thermogravimetric analysis (TGA) has been also utilized, for example, as a bulk characterization method for determining carbon nanotubes quality after manufacturing[60] and/or after oxidation processes[61].

Nowadays, there is a tendency to combine microscopic and spectroscopic techniques in order to obtain information about both the size and chemical composition of materials. Examples are the combination of AFM-ATR-IR[62], AFM-Raman[63] or AFM-SECM (scanning electrochemical microscopy)[64]. These techniques may be also useful in the case of the analysis of nanomaterials.

4.4. Determination of nanoparticles in environmental, food and biological samples

The increasing use of engineered nanoparticles in industrial and household applications will probably lead to the release of such materials into the environment as well as their accumulation in biological systems. In spite of this fact, there are still few analytical methods for their quantification in environmental matrices.

[57] Y.-G. Zhou, N.V. Rees, R.G. Compton, Angew. Chem. Int. Ed.50 (2011) 4219 –4221.
[58] D. Hernández-Santos, M.B. González-García, A. Costa-García, Electrochimica Acta 46 (2000) 607–615.
[59] M. Pumera, M. Aldavert, C. Mills, A. Merkoçi, S. Alegret, Electrochimica Acta 50 (2005) 3702–3707.
[60] E. Mansfield, A. Kar, S.A. Hooker, Anal. Bioanal. Chem. 396 (2010) 1071-1077.
[61] L.S.K. Pang, J.D. Saxby, S.P.Chatfield, J. Phys. Chem. 97 (1993) 6941–6942.
[62] M. Brucherseifer, C. Kranz, B. Mizaikoff, Anal. Chem. 79 (2007) 8803-8806.
[63] C.E. Harvey, E.M. v.S. Lantman, A.J. G. Mank, B.M. Weckhuysen, Chem. Commun. 48 (2012) 1742-1744.
[64] J. Wiedemair, J.-S. Moon, D.E. Eaton, B. Mizaikoff, C. Kranz, IFMBE Proceedings 25 (2010)372-375.

Effectively monitoring nanoparticles in environmental samples entails meeting several requirements. One is using analytical methods capable of detecting environmentally relevant concentrations, which fall in the nanogram per litre or the picogram per litre range, and another is avoiding the potential interference of natural nanoparticles frequently present in environmental samples.

Most of the methods described above have been applied to the determination of nanoparticles in environmental matrices. A detailed description of the different examples of analysis of nanoparticles in environmental matrices is out of the scope of this introduction, further information about this issue may be found in the following reviews[11,35,40].

Applications of nanomaterials in food, food additives and food-contact materials have been described, in this sense, analytical approaches suitable to address food-safety issues related to nanotechnology are being developed. Several reviews collect described methods for these food matrices[65,66,67].

Chapter 2 of this Doctoral Thesis describes a general overview of the most relevant analytical techniques for the analysis of nanoparticles in biological matrices.

[65] C. Blasco, Y. Picó, Trends Anal. Chem. 30 (2011) 84-99.
[66] R. Peters, G. ten Dam, H. Bouwmeester, H. Helsper, G. Allmaier, F. vd Kammer, R. Ramsch, C. Solans, M. Tomaniová , J. Hajslova, S. Weigel, Trends Anal. Chem. 30 (2011) 100-112.
[67] K. Tiede, A.B.A. Boxall, S.P. Tear, J. Lewis, H. David, M. Hassellöv, Food Addit. Contam. 25 (2008) 795-821.

Capítulo 2

Determination of nanoparticles in biological matrices

Frontiers in Bioscience E4 (2012) 1024-1042

[Frontiers in Bioscience E4, 1024-1042, January 1, 2012]

Determination of nanoparticles in biological matrices

A. I. López-Lorente, B. M. Simonet, M. Valcárcel

Department of Analytical Chemistry, University of Córdoba. 14071 Córdoba, Spain.

Human exposure to nanoparticles has increased considerably due to anthropogenic activities dominated by coal and diesel oil fuel combustion. Not only the inhalation of nanoparticles, which nowadays is considered to be the most significant via of exposure to nanomaterials, but also the gradually more employment of nanoparticles in products such as cosmetics, deodorants, textiles, or even food is broadening the exposure to those materials. Developing the previous applications will obviously require the use of analytical methodologies to analyze biological matrices in order to assess potential risks in their use and take appropriate corrective actions. This chapter describes a general overview of the most important analytical techniques for the analysis of nanoparticles in biological matrices.

Keywords: Nanoparticles, Biological Samples, Nanotoxicology, Review

1. Introduction

Nanomaterials are defined as products with at least one dimension less than 100 nm. A number of common products and processes currently use or produce nanomaterials. This increasing use of engineered nanoparticles in research and product development engenders a growing need to understand their properties and behaviors as well as the health, safety, and environmental impact of them in both their synthesized form and when they evolve through application or environmental interaction.

Millions of tones of such materials are entering the commercial market in products ranging from cosmetics, catalyst, semiconductors, fillers and drug carriers or as byproducts of human activity. Commercial nanoparticle-based products include titania nanoparticles for sunscreens, paints or self-cleaning windows, silica nanoparticles used as solid lubricants, protein-based nanomaterials for soaps and detergents, metal nanoparticles for environmental remediation, carbon nanoparticles for composites, and nanoparticles in electronic devices or pharmaceuticals. On the other hand, by-products in the form of nanoparticles typically come from emissions due to incomplete combustion of diesel fuel or nanosized minerals resulting from acid drainage in mining operations.

It is widely recognized that as particle size decreases to the nanometer scale, their physical and chemical properties differ from those shown in their bulk form. Because of their size and those unique physical and chemical properties, determination of nanomaterials represents a challenge. The increasing use of nanoparticles in industrial applications will inevitably lead to the release of such materials into the environment. Accurately assessing the environmental risks posed by nanoparticles requires using effective quantitative analytical methods to determine their mobility, reactivity, ecotoxicity and persistency, many of which have still to be developed. Moreover, their accumulation in the

environment might have major implications for both human and environmental health. Studies have indicated that some nanomaterials can travel through the human body, deposit themselves in target organs and trigger injury to the cells; while other nanomaterials are being designed to enter the body in order to deliver drugs to a specific location.

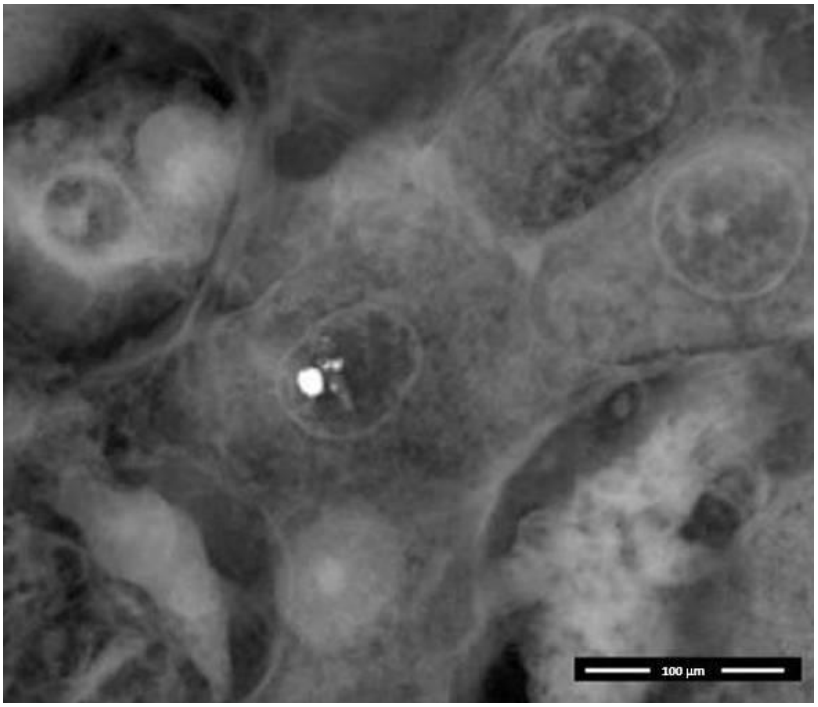

Figure 1. Electron microscopy image of a cancerous tissue of liver with a living cell containing metallic nanoparticles in the nucleus. Reproduced with permission from [1].

Human exposure to nanoparticles has considerably increased due to anthropogenic activities dominated by coal and diesel oil fuel combustion. As example, Figure 1 shows the image of a metallic nanoparticle located in a liver cell [1]. Furthermore, the exponential growth of nanotechnology is contributing with another source of aerial pollution via engineered nanomaterials. Not only

the inhalation of nanoparticles, which nowadays is considered to be the most significant via of exposure to nanomaterials, but also the gradually more employment of nanoparticles in products such as cosmetics, deodorants, textiles, or even food is broadening the exposure to those materials. Consequently, there are being carried out several studies of the ecotoxicity of nanoparticles and the impact of them on human health since there are many medical advances that imply the use of nanoparticles. The possible secondary effects of their use are a controversial issue. Anyway, there is a lack of methods currently available to do reliable measurements in the presence of small particulate contaminations present in biological fluids.

Reliable methods of characterization of nanoparticles in biological fluids and tissues are necessary for development and use of precise drug delivery technologies with nanosized carriers. While more work was devoted to nanoparticles investigation in water suspensions, there is still a lack of characterization techniques in biological liquids and tissues.

Effectively monitoring nanoparticles in biological samples entails meeting several requirements. One is using analytical methods capable of detecting biologically relevant concentrations, and another is avoiding the potential interference of small particles present in biological fluids. A drawback associated with the determination of nanoparticles is the heterogeneous nature of biological fluids, such as serum, containing for example serum albumin, lipoproteins, inmuno-, γ- and macroglobulins, and oleic acid, which can give significant background signals, whereas sizing techniques based on conventional light scattering require minimum levels of background noise for generation of accurate results. This make necessary in most of the cases the extraction or separation of the nanoparticles from their matrix.

1.1. Type of nanoparticles

The general term nanoparticle (NP) is used to define any particle less than 100 nm in at least one dimension. Nanoparticles can be generally classified as natural, anthropogenic or engineered in origin.

Nanoparticles are naturally present in the environment, commonly formed as either weathering by-products of minerals such as biogenic products of microbial activity, or by growth in super-saturated fluids. Many inorganic growth mechanisms are responsible for nanoparticle formation, for instance crystal growth, aggregation [2], and redox triggered crystallization based on changes in mineral solubility [3].

Natural nanoparticles can be biogenic, geogenic, atmospheric or pyrogenically produced. For example, there are fullerenes with interstellar origin that have been brought to earth by comets or asteroids [4], the majority is believed to have formed from polycyclic aromatic hydrocarbons (PAH) derived from algal matter during metamorphosis at temperatures between 300 and 500 ºC and in the presence of elemental sulfur [5], or during natural combustion processes.

Inorganic NPs are present everywhere in soils and geologic systems [6,7]. NPs are also ubiquitous aerosols in the atmosphere and they are precursors for the formation of larger particles, which are known to strongly influence global climate, atmospheric chemistry, the visibility and regional and global transport of pollutants [8]. Primary atmospheric NPs are, for example, soil dust and sea salt, although the major mass fraction is composed of coarse particles. The average particle size of airborne mineral dust, based on mass, is between 2 and 5 mm. However, based on the number of particles, the average size is approximately 100 nm with a considerable number below this value [9].

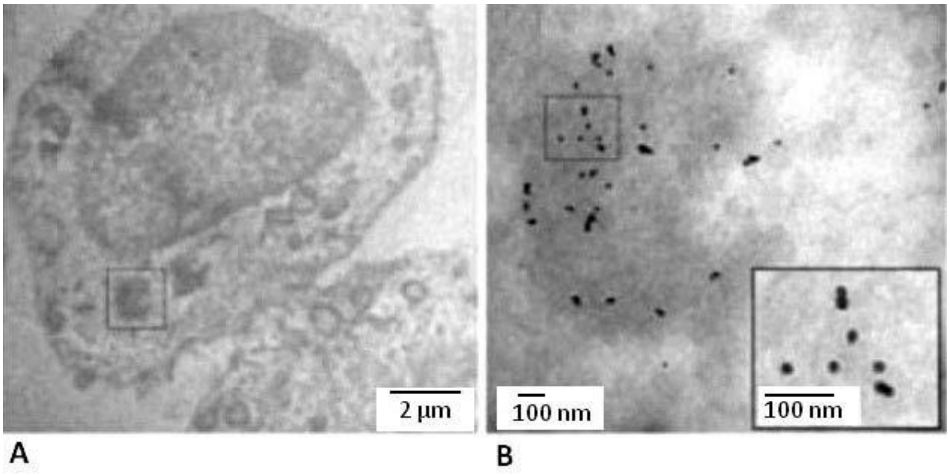

Figure 2. Electron micrographs at different magnifications of a cell containing nanoparticles. Cells were exposed to nanoparticles for 24 h to gold nanoparticles. A) Image at 8000x magnification of a representative cell with nanoparticles subcellularly localized. The small box represents the area magnified in (B) image at 60000x magnification of gold nanoparticles within cells. The inset is a 150000x magnification of the gold nanoparticles. Reproduced with permission from [11].

Biogenic nanoparticles are sometimes formed directly by the organism as a metabolic requirement, such as the case of magnetite which is formed by bacteria in response to a need of mobility [10]; or indirectly as a result of the microbial activity. Nanocrystalline mineral phase may precipitate during the redox transformation of a metal induced by a microorganism. Other routes of mineralization are promotion by other metabolites or by microbial cell surfaces acting as organic templates. Anthropogenic nanoparticles are those which are unintentionally produced as by-product of the human activity. These nanoparticles can be also internalized in the cells (see Figure 2) [11]. They are predominately combustion derived, formed by automobile exhaust gases or as consequence of the industrial fabric. Some of those combustion-derived nanoparticles, such as diesel exhaust particles, carbon black and fly ash are environmental hazards. Diesel exhaust particles account for up to 80% of the

mass of PM10 collected in urban areas. They contain toxic metals and organics and this, in combination with their large surface area, leads to the production of reactive oxygen species. Carbon black is a low-solubility particle produced industrially from the incomplete thermal decomposition of hydrocarbons. Moreover, fly ash is a generic term for particulate matter from mineral and metal contaminants of organic fuels [12].

Another class of unintentionally produced NP is composed of platinum and rhodium containing particles produced from automotive catalytic converters. Although most Pt and Rh are attached to coarser particles, about 17% was found to be associated with the finest aerosol fraction (<0.43 mm) [13].

The design of novel NPs has been the basis of many advances in technology for the last decade. Nanoparticles can be produced by a huge range of procedures which can be grouped into top-down and bottom up strategies. Top-down approaches are defined as those by which NPs or well-organized assemblies are directly generated from bulk materials via the generation of isolated atoms by using various distribution techniques [14]. The majority of the top-down strategies involve physical methods such as milling or attrition, repeated quenching and photolithography [15]. Bottom-up strategies involve molecular components as starting materials linked with chemical reactions, nucleation and growth process to promote the formation of more complex clusters [16].

Carbon nanotubes (CNT) represent one of the best examples of novel nanostructures derived by bottom up chemical synthesis approaches. Carbon nanotubes can be considered to be hollow graphitic nanomaterials comprising one (single-walled carbon nanotubes, SWNT) or multiple (multi-walled carbon nanotubes, MWNT) layers of graphene sheets. The lengths of the nanotubes can range from several hundred nanometers to several micrometers and the diameters from 0.2 to 2 nm for SWNT and from 2 to 100 nm for coaxial MWNT [17]. Depending on the synthesis method, the technique used for the separation

from the amorphous by-products, subsequent cleaning steps, and finally different functionalizations, a variety of different CNT are obtained that have very different properties [18]. Most CNTs reported to date have been prepared by using arc discharge [19], laser ablation [20], or chemical vapor deposition (CVD) techniques [21]. The former two use a solid-state carbon precursor for nanotube growth. On the other hand, CVD uses hydrocarbon gases as sources for carbon atoms and metal catalyst particles as seeds for CNT growth.

The high potential of CNTs has promoted much study aimed at elucidating their properties (particularly those of SWNTs). Based on structure, CNTs possess nonpolar bonds and high aspect ratios (length to diameter ratio) and are thus insoluble in water. This results in the spontaneous aggregation of CNTs. This affinity to aggregation combined with their high flexibility increases the possibility of bundling and closing packing [22]. As opposed to aqueous solutions, hydrophobic CNTs are expected to be wetted by organic solvents and, therefore, to assemble less in bundles and ropes. However, CNTs were shown to exhibit a sufficient solubility only in a limited number of solvents, such as dimethyl formamide, dimethyl acetamide, and dimethyl pyrrolidone [23]. Like other organic molecules, CNTs can be functionalized covalently [24]. SWNTs possess a good surface area to volume ratio and an excellent thermal stability in inert atmospheres. They also possess a π complex both above and below the plane containing the carbon atoms that is the origin of their high electron mobility and electrical conductivity [25]. They present excellent plasticity and elasticity and the sharp tip of the end of a SWNT results in a locally boosted electrical field upon application of a potential.

Fullerenes are polyhedral carbon cages in which sp^2 carbons are bonded to three carbon neighbors in an arrangement of five-membered and six-membered rings [26]. C_{60} has been extensively studied since its discovery in 1985, it present low electron delocalization over the spherical surface with a

resonance structure, being a good electron acceptor, so it can form charge-transfer complexes with compounds with donor groups. A drawback is their low solubility in aqueous and organic solvents, which limit their applications and focus lot of research to functionalization [27]. Fullerenes have been proposed to be used in fullerene polymer combinations, as thin films, in electro-optical devices and in biological applications [28].

Engineered inorganic NP also cover a broad range of substances including elemental metals, metal oxides and metal salts.

Colloidal gold nanoparticles have been used technologically since ancient times due to their optical properties, in particular for staining glass [29]. Gold spheres have a characteristic red color, which is due to the collective oscillation of the electrons in the conduction band, known as the surface Plasmon oscillation. The oscillation frequency is usually in the visible region for gold and silver giving rise to the strong surface Plasmon resonance absorption. Therefore, the origins of properties on the nanoscale are different for metal nanoparticles than for semiconductor nanoparticles.

Many applications became possible due to the large enhancement of the surface electric field on the metal nanoparticles surface. The plasmon resonance absorption has an absorption coefficient orders of magnitude larger than strongly absorbing dyes. Anisotropic shapes have plasmon resonance absorptions that are even stronger, leading to increased detection sensitivity. Metal nanoparticles generate enhanced electromagnetic fields that affect the local environment.

Silver nanoparticles have been widely used as bactericide [30], whereas gold nanoparticles are mainly used for optical sensors or to exploit its catalytic activity [31]. The use of nanoscale zero-valent iron for groundwater remediation ranks as the most widely investigated environmental nanotechnological

application. Nanoparticles having magnetic properties are the most interesting in this field. To this end, metallic iron is very effective in degrading a wide variety of common contaminants such as chlorinated methanes, brominated methanes, trihalomethanes, chlorinated ethenes, chlorinates benzenes, other polychlorinated hydrocarbons, pesticides and dyes [32].

Today, nanoparticulated metal oxides are among the most used NPs [33]. Bulk materials of TiO_2, SiO_2 and aluminum and iron oxides have been produced for many years. However, recently they have also been manufactured in nano-sized form and have already entered the consumer market, e.g. ZnO in sunscreens [34]. TiO_2 NPs are widely used for applications such as photocatalysis, pigments and cosmetic additives. Two methods are commonly used to prepare oxide-based nanomaterials: stabilized precipitation and flame pyrolysis [35,36]. Nano-sized zeolites [37], clays [38] and ceramics [39] are other NPs that have been proposed for various catalytic applications. Several non-carbon nanotubes have also been synthesized [40], for example, TiO_2.

Nanoparticles synthesized from organic polymers have gained widespread interest in medicine as carriers for drugs. The possibility to control size, surface charge, morphology and composition make polymers especially well suited for designing NPs with tailored properties based on selective recognition. These NPs are taken up by a wide variety of cells and are studied for their ability to cross the blood-brain barrier [41].

Polymeric nanoparticles have also been developed and synthesized to be used in soil and groundwater remediation. For example, micelle like amphiphilic polyurethane particles have a hydrophilic outer side and a hydrophobic inner core and are therefore very well suited for the removal of hydrophobic pollutants (e.g. phenanthrene) from soils [42]. Another related polymeric nanoscale material is dendrimers that function as water soluble chelators [43].

Metal and semiconductor nanoparticles in the 2–6 nm size range are of considerable current interest, not only because of their unique size-dependent properties but also because of their dimensional similarities with biological macromolecules (e.g. nucleic acids and proteins) [44]. These similarities could allow an integration of nanotechnology and biology, leading to major advances in medical diagnostics, targeted therapeutics, molecular biology and cell biology. Quantum dots (QDs) are inorganic semiconductor nanocrystals with interesting luminescent and electrochemical properties extensively used in numerous bioassays [45,46]. These NPs show broad excitation profiles and narrow emission peaks and can emit in a range of wavelengths by changing their size and composition. Also, they lack photobleaching and have long fluorescence lifetimes. However, QDs can show blinking characteristics when they are excited with high intensity light, which could be a limiting factor for fast scan systems, such as flow cytometry. Other limitations are toxicity, size variation, agglomeration and non-specific binding. Surface oxidation of QDs can occur under combined exposure to aqueous/UV-light excitation, which can lead (e.g., in CdSe-based QDs) to the release of cadmium ions, so that these NPs are inadequate for *in vivo* applications, such as *in vivo* drug delivery assays. However, they offer better imaging results than those achieved by organic dyes in cell-based or tissue-based drug studies. Luminescence emission from QDs is detected at concentrations comparable to organic dyes by using conventional fluorescence methods, and individual QDs and QD-bioconjugates are easily observable by confocal microscopy [47]. In particular, CdSe- ZnS core-shell QDs exhibit size-dependent tunable photoluminescence (PL) with narrow emission bandwidths that span the visible spectrum and broad absorption spectra that allow simultaneous excitation of several particle sizes at a single wavelength (48). These nanoparticles have a high quantum yield and a high resistance to photodegradation. Quantum dots have potential in biomedical applications, but concerns persist about their safety.

The particles can be further separated based on their chemical composition into carbon-containing and inorganic NPs. In fact, in order to describe the different approaches for the analysis of nanoparticles in this review we have distinguished between metallic and metal oxide nanoparticles, carbon-based nanoparticles and nanodrug or nano food-additives.

1.2. Effects of nanoparticles in biological systems

Human exposure to nanoparticles is inevitable as they become more widely used. This has given rise to a new division of toxicology, namely "nanotoxicology", which involves the safety evaluation of engineered nanostructured and nanodevices. As it has been previously reported, human exposure is not limited to engineered nanoparticles, since there is anthropogenic sources which unintentionally release nanoparticles to the environment, such as industrial activity or combustion processes. In contrast to nanoparticle exposure through use of consumer products (such as textiles, cosmetics, deodorants), emerging biomedical applications of nanoparticles as drug delivery agents, biosensors, or imaging contrast agents involve direct ingestion or injection of nanoparticles into the body. Therefore, understanding the properties of nanoparticles and their effect on the body is crucial before clinical use can occur. A number of authors have reviewed characterization, fate, and toxicological information for nanomaterials and proposed research strategies for safety evaluation of nanomaterials [49,50].

A factor influencing potential toxicity in the case of carbon nanoparticles is their complexity and variety in size, shape, charge, methods of production, chemical compositions, surface chemistry/functionalization and aggregation tendency. Most practical carbon nanomaterial samples are highly complex, containing the desired structure (e.g. single-wall nanotubes) mixed with amorphous or graphitic nanoparticulated byproducts, other nanotube varieties, and metallic catalyst residues of unknown chemical form (metal, oxide, carbide), in complex

association with carbon (within nanotube cavities or as particles partially or wholly encapsulated by carbon shells). The toxicity indicators associated with any given material may just as well be related to these impurities as to the properties of the nanomaterials in question. The catalyst residues in vapor-grown carbon nanotubes include Fe, Ni, Co, and less often Y, Mo, and other metals, many of which would pose health risks of their own in the form of nanophase powders. Ideally, toxicological assays would be accompanied by characterization of all the biologically relevant properties of these complex materials—size, shape, surface chemistry (hydrophobicity/philicity), and the amount, form, and encapsulation state of metals. Some of these properties can be measured by routine techniques (overall metal contents by atomic absorption or emission techniques; size and shape by scanning and transmission electron microscopies) but others are not standard (surface chemistry, metal form and encapsulation) and require experts [51].

Moreover, a given nanomaterial can be produced by different processes which lead to derivatives of the same material, for instance the case of SWNTs which have different physical-chemical properties, namely size, shape, composition and consequently different ecological and toxicological impact [52]. Alternative methods for measuring properties of nanomaterials may need to be developed both quickly and cost effectively.

Cytotoxicity studies [53] have demonstrated that, in general, cells can survive short-term exposure to low concentrations (<10 mg mL^{-1}) of nanoparticles. It is important to remark that the effect is mainly produced by the small dimension of the nanoparticle than its nature. However, at high doses, several groups have found cytotoxic effects to emerge in a dose- and time-dependent manner for carbon-, metal-, and semiconductor-based nanoparticles. The generation of reactive oxygen species and the influence of cell internalization of nanoparticles

are two common found causes for the increase in cell death observed at higher concentrations and longer exposure times.

Gold nanoparticles have been reported to induce little toxicity, around 15% reduction in cell viability, at 200 mg mL^{-1} [54-56]. While higher concentrations could elicit a cytotoxic effect, many substances become toxic at high concentrations. Therefore, it may be reasonable to conclude that the results from cytotoxicity testing of other nanoparticle types suggest low toxicity if those results are similar for gold-nanoparticle solutions containing relatively the same size particles at the same concentration.

Many nanoparticles are not water soluble. However, the most important applications are performed in aqueous media. For that, the addition of a hydrophilic surface coating is required. However, as seen in MWNTs and QDs studies, adding certain hydrophilic molecules results in lower cell viability as the functional groups themselves were toxic [57-60]. Although it is difficult to establish a general rule, surface charge also plays a role in toxicity with cationic surfaces being more toxic than anionic, and neutral surfaces being most biocompatible [61] because of the affinity of cationic particles to the negatively charged cell membrane. Therefore, adding a coating that makes the nanoparticle more cationic could make the nanoparticle appear more toxic than it inherently is.

Complexation of metallic nanomaterials may have important effects on biological availability and photochemical reactivity since it reduces the availability by reducing free metal ion concentrations and dissolved metal, for instance iron, which is quantitatively complexed by organic ligands. Solar UV radiation can also interact with these processes through photoreactions of the complexes [62]. Particle aggregation has also been suggested to be a factor in nanoparticle cytotoxicity. Wick *et al.* aimed to determine how agglomeration influenced SWNT cytotoxicity and [63] found that aggregation occurred in all

SWNT fractions except the well-dispersed SWNT bundles. Correspondingly, the SWNT bundles did not induce adverse cellular effects, and as this was the only solution where agglomerates were not formed, this corroborates the hypothesis that SWNT agglomeration leads to cytotoxic effects. However, an earlier study by Tian *et al.*, testing an unrefined SWNT solution and a SWNT solution with the metal catalysts removed, found lower cytotoxicity with the unrefined SWNTs (64) which was proposed to be a result of their aggregation into larger, and therefore less toxic, particles. This contradicts the reasoning of Wick *et al.*, so the effect of SWNT aggregation is still questionable.

2. Tools for the analysis of nanoparticles in biological samples.

In spite of the increase in the use of nanoparticles, there are still few analytical methods for their quantification in environmental or biological matrices due to their unique physical and chemical properties. Their capacity to form colloidal phases and aggregates, their different ad- and absorption characteristics and their shape and size variety make their quantification difficult.

It is necessary to consider features of biological samples, connected with the presence of macromolecules, having the sizes comparable with investigated nanoparticles, and various effects of interaction of these particles with the components of biological sample.

Considering the complexity of biological samples as well as the number of potential interferences and the number of interactions that can be established between the nanoparticles and the sample, liquid-liquid extraction techniques are the most usefulness. The excess of the solvent and chelating agent helps to break the interactions of nanoparticles with biomolecules. To this end, the use of ionic liquids has been recently proposed for the analysis of gold nanoparticles in tissues. Ionic liquids, especially those derivates from imidazolium groups have a high affinity to interact and solubilize nanoparticles.

Preliminary results obtained in our research group pointed out that the BMIM-PF_6 can extract gold nanoparticles from liver tissue homogenates. Nanoparticles were directly quantified in the IL by UV-Vis and Raman spectroscopy. Other sample treatment systems involve the use of surfactants. Supramolecular complexes of surfactant have also a high tendency to extract nanoparticles from aqueous systems.

There is no doubt that sample treatment is a key step in the analysis of biological samples for the analysis of nanoparticles since sample treatment need to provide selectivity in addition to a high capacity to preconcentrate the nanoparticles. In addition to liquid-liquid extraction other treatments such as centrifugation, dielectrophoresis or field flow fractionation have been also applied. In general, it must be point out that these techniques have been applied to the study of the interaction of nanoparticles with biomolecules in order to determine and characterize the interaction established between the nanoparticle and the biomolecule. Although these techniques are a good alternative to analyze simple systems, there are not a real alternative for the analysis of complex biological samples. The most reliable attempt to extract and preconcentrate nanoparticles based on solid phase extraction is with the use of modified filters based on carbon nanotubes. The modified filters have a high capacity to adsorb carbon nanotubes. This methodology has been applied to the preconcentration of soluble carboxylic carbon nanotubes from waste water [65]. It will be also applicable to biological samples, but for that it is necessary the addition of chelating agents to avoid and minimize the interaction of nanoparticles with biomolecules.

A large number of detection techniques have been applied to the analysis of nanoparticles, some of them focused on the assessment of its toxicity [66]. A general overview in presented in Figure 3. In general, three groups can be distinguished:

i. Microscopic techniques

ii. Spectroscopic techniques

iii. Electrochemical techniques

In general, it can be affirmed that for the detailed characterization of nanoparticles or nanoobjects in general, such as subcellular compartments, and other very small biological structures, currently there is a lack of methods for chemical diagnostics and characterization, in particular of the molecular composition. Traditional methods with nanoscale lateral resolution (viz, standard atomic force microscopy, scanning tunneling microscopy and electron microscopy) typically yield very little or no chemical information, whereas traditional methods for chemical analysis (for example, mass spectrometry, spectrochemical analysis performed with microscope, etc.) are in many cases far from achieving nanoscale lateral resolution.

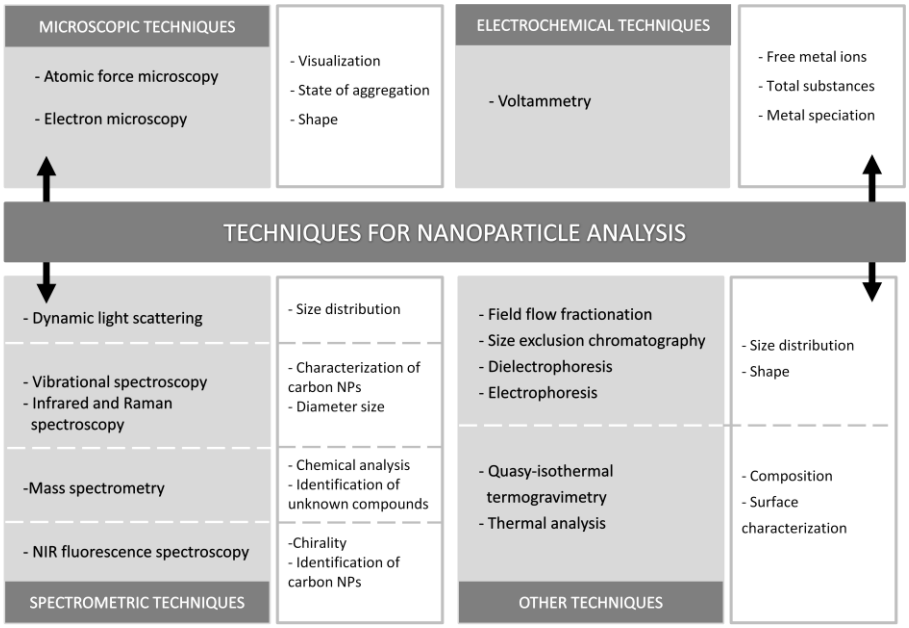

Figure 3. General overview of analytical techniques for the analysis of nanoparticles in biological samples.

Microscopy-based techniques capable of analyzing nanoparticles include the well-known scanning and transmission electron microscopy (SEM and TEM) and atomic force microscopy (AFM) of the group of scanning probe microscopes [67]. These techniques allow exact information about type and characteristics (shape, size, etc.); however, one of their most important shortcomings is the low representativity of the results due to the small sample volume that are analyzed. Besides, sample preparation involves drying, which might result in aggregation of the sample and, thus, a false representation of the sample size in tissue. As well, inference of the three-dimensional structure from two-dimensional images is very difficult [68], but can be accomplished in some cases with stereological transformation [69]. Eventually, in-situ 3D characterization should be possible by nano-coupled tomography [70]. As advantage, by using classifical sample treatments applied to tissues it is possible to analyze biological samples. Although this technique can be applied to a wide number of nanoparticles, its use is mainly limited to the analysis of metallic nanoparticles due to resolution capacity. Because metals scatter light efficiently, electron microscopy is the technique of choice for physical characterization of colloidal gold nanoparticles [71]. However, many biological compounds (e.g., proteins) are invisible to TEM without heavy metal staining procedures, because these compounds do not sufficiently deflect an electron beam.

Atomic force microscopy (AFM) relies on tapping a particle (either in solution or dried to a surface) and so has limited resolution of flexible compounds (e.g., proteins), which may move under the force applied by the instrument tip. Their use for the analysis of carbon nanoparticles in biosamples such as tissue is limited.

Apart from providing information on particle aggregation, dispersion, size, structure and shape, additional elemental information can be obtained by coupling EMs to energy-dispersive spectrometry (EDS), which was employed to

confirm the presence of silver nanoparticles within cells [72] or to electron energy loss spectrometry (EELS), used in conjunction with TEM for elemental confirmation of carbon nanotube uptake [73]. The combination of these techniques is indispensable when it comes to the characterization of nanoparticles and other nano-structured materials.

Spectroscopic techniques involve a large number of techniques: UV/Vis techniques, fluorescence techniques, NIR-fluorescence, infrared spectroscopy and Raman spectroscopy. These techniques provide a large level of information about nanoparticles. UV/Vis and fluorescence spectroscopy are the most useful for the analysis of metallic, oxide derivates and semimetallic nanoparticles. Fluorescence spectroscopy is useful in both the quantitative assessment of nanoparticle uptake as well as the qualitative assessment of nanoparticle localization. Quantitative assessment can be achieved through use of bulk fluorescence [74] or on a cell-to-cell basis using confocal fluorescence [75]. Non-natively fluorescent nanostructures can still be evaluated using fluorescence methods after applying one of many available labeling techniques in order to study the uptake in toxicological assays, although in the case of natural samples there is no a label that allows their detection. These studies also require additional control experiments to account for effects of the fluorescent surface dyes or incorporated species.

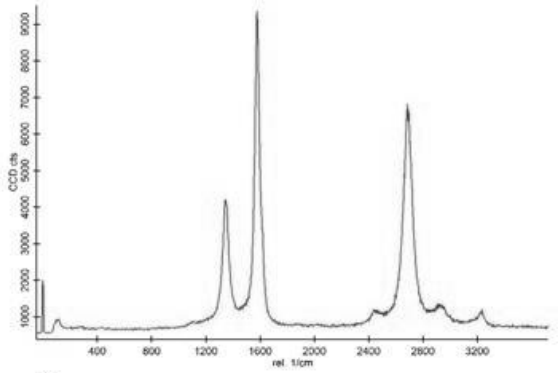

A Multi-walled carbon nanotube

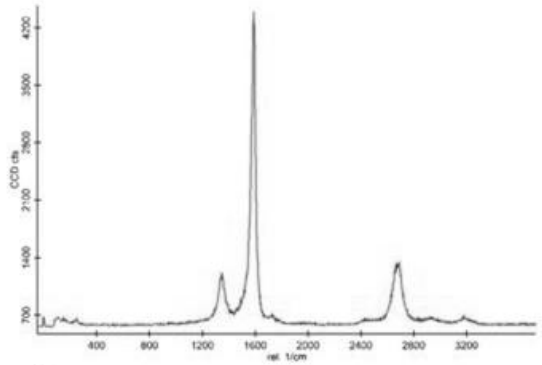

Figure 4. Characteristic Raman spectrum of a A)- multiwalled and B)- single walled carbon nanotubes.

Contrary, Raman spectroscopy is the most important technique for the analysis of carbon nanoparticles. Figure 4 shows the characteristic spectrum of single walled and multiwalled carbon nanotubes. The spectrum reported is characteristic of the nanoparticle and its intensity can be related with concentration. Information about interaction and state of aggregation can be also obtained from the spectrum. In the case of single walled carbon nanotubes, NIR-fluorescence is a technique with a high capacity to classify the nanoparticles according to their chirality (see Figure 5) [76]. Optical-spectral methods are rather informative and practical for nanoparticles characterization. Good representativity of sample, simplicity of sample preparation, high productivity of analysis, opportunity of its automation and price availability of measurement instruments are among the advantages of these methods. The majority of optical spectral techniques also give the opportunity to measure nanoparticles parameters directly in a liquid. In a number of cases it is necessary to process the results received by optical-spectral methods together with the data of high resolution microscopy.

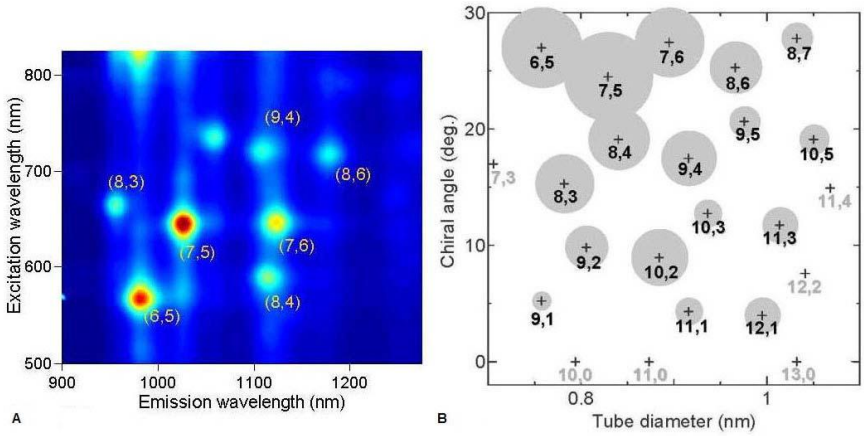

Figure 5. Classification of single walled carbon nanotubes according their chirality by NIR-fluorescence spectroscopy. A) Tridimensional spectrum and B) classification according to carbon nanotube chirality. Reproduced with permission from [76].

Sizing of nanoparticles can be done using methods such as scanning and transmission electron microscopy, dynamic light scattering, and size-exclusion chromatography; however, the size values obtained can vary between these methods. A standard technique for measuring and reporting the hydrodynamic sizes of nanoparticles would be valuable. Available technologies for the size fractionation and collection of nanoparticle fractions in liquid mediums include the above mentioned size-exclusion chromatography as well as ultrafiltration and field flow fractionation [77]. Field-flow fractionation (FFF) is a high-resolution method that can be an ideal candidate for direct separation, detection, and size characterization of nanoparticles in biological samples, because it allows for the separation of nanoparticles in a liquid matrix of desired composition and as a separation technique, provides a size distribution instead of an average value. FFF has been widely used to separate carbon nanotubes [78], particles [79], cells, bacteria, viruses, and natural organic matter. Unlabeled inorganic nanoparticles extracted from biological media have been characterized, separated and quantified by this technique [80]. Probably, the

most important shortcoming of this technique is the need of standards to calibrate the FFF equipment. The use of polymeric nanoparticles is the most useful approximation described to date.

On-line particle size analysis in liquid mediums can be done using dynamic light scattering to obtain a particle size distribution [81]. Because dynamic light scattering (DLS) measures hydrodynamic diameter, it provides a fundamentally different measure of particle size from TEM or AFM. DLS is very sensitive to "soft" flexible biological molecules such as polymers, proteins, and antibodies because they cause significant frictional drag [82], which can dramatically influence the rate of the particle's motion under Brownian diffusion. DLS is therefore appropriate for measurement of the hydrodynamic size of protein bound nanoparticles. Complementary size characterization by TEM and AFM can be useful in resolving ambiguities due to the different measurement techniques. For example, the DLS-measured size may be influenced by particle agglomeration, and further analysis by TEM is required to ensure that the DLS-measured sizes represent primary particle size (i.e., discrete particle size), and not the size of an agglomerate [83]. For polydispersed samples, the task is more difficult, since the signal intensity has a power relationship with size and the average size can be overestimated if some larger particles exist in the sample. Therefore, although DLS is a common method for measuring nanoparticle size ex-situ, it is not appropriate for nanoparticle analysis in-situ or in a digested biological sample, because of the multiple scattering issues.

Since many nanomaterials are constructed of materials not found natively in the body, uptake of these nanomaterials can be quantified by determining the mass or concentration of these non-native elements within cells. Inductively coupled plasma atomic emission spectroscopy (ICP-AES) is a powerful technique for the quantification of internalized nanoparticle (NP) elemental composition [84,85] and has been used to quantify nanoparticle uptake.

Advantages of ICP-AES are sub-ppb detection limits, high precision, and a dynamic range of five orders of magnitude or more. But this technique is limited in biological systems to metallic nanoparticles since it is unable to characterize the uptake of carbonaceous nanoparticles (e.g. polymeric NPs and carbon nanotubes) because it cannot distinguish between cellular and nanoparticle sources of carbon. It also cannot differentiate between elements confined within the nanostructure and solvated ions that had leached from the nanomaterial as well as spatial information about the location of nanoparticles. In addition, conversion of the ICP-AES measurement to standard nanoparticle dosing units requires a well-characterized crystalline lattice and nanoparticle monodispersity as well as the assumption that the nanostructure does not change upon exposure to the cellular environment. Using similar procedures, samples can be also analyzed by ICP-MS. Mass spectrometry is a detector with a higher sensitivity than the optical emission spectroscopy (OES). In addition to its higher sensitivity, MS detectors can analyze isotopes and can perform multianalysis in a simple run. Furthermore, single-particle laser microprobe mass spectrometry (LAMMS) can provide chemical composition data on single particles from a collected fraction [86].

Determining the concentration of nanoparticles in solution is more difficult. Concentration can be calculated from the optical density using the Beer–Lambert law given the extinction coefficient of the nanoparticle. However, as Yu *et al.* pointed out, the extinction-coefficient values published for quantum dots differ between groups by an order of magnitude [87]. Cryogenic TEM was used as an alternative method of determining concentration. This method involves direct counting of particles in a relatively fixed volume. As concentration or dose plays a significant role in biomedical applications of nanoparticles, having a standard technique of calculating this value is important.

After this general overview, several examples of the analysis of different types of nanoparticles in biological matrices are described below. In order to facilitate the text to readers, examples have been classified according to the nature of the nanoparticle because it is clearer than a classification based on the detection system.

3. Analysis of metallic oxides and metallic nanoparticles

While a lot of work was devoted to nanoparticles investigation in water suspensions, development of nanoparticles characterization techniques in biological liquids and tissues began more recently. Typically, nanoparticles can be detected in cells and tissues if they have been labeled with radioactive [88], magnetic [89], or fluorescent markers [90]. However, the inorganic nanosized powders being produced as bulk chemicals or the ultrafine particles produced by combustion processes do not have a convenient label that allows for their detection. As well, discrimination between nanoparticles, sub-micron particles, and soluble species with the same nominal elemental composition is a very difficult task. This complexity in detection and characterization of unlabeled nanoparticles in biological systems poses a major limitation for current research on environmental and occupational health effects of nanoparticles.

An example of the determination of labeled nanoparticles is the use of fluorescent silica-capped NPs containing a CdSe-CdS core for the study of uptake and loss of these silica nanoparticles in living human lung epithelial cells [91]. A number of other luminescent silica NPs have been employed for labeling, and as long as there is not leakage of luminescent materials from the NPs, they have been shown to be compatible for *in vitro* testing. Examples of them are fluorescein isothiocyanate (FITC) in silica [92], FITC–silica coatings for iron oxide NPs [93], and encapsulation of other organic fluorophores for two-photon-fluorescence imaging [94].

A rapid, high-resolution methodology for characterization, separation, and quantification of unlabeled inorganic nanoparticles extracted from biological media, based on sedimentation filed-flow fractionation and light scattering detection, [80] has been developed. Silica nanoparticles were added to human endothelial cell lysate and rat lung tissue homogenate and incubated. The nanoparticles were extracted by acid digestion with nitric acid and then separated and characterized by sedimentation field-flow fractionation. Fraction collected at the peak maxima was analyzed by transmission electron microscopy (TEM) to verify their size and shape. A linear relationship between the particle number and the area under the fractogram was found.

Many techniques have been used to identify and characterize natural inorganic NPs [95]. The ones most often used are transmission electron microscopy and scanning probe microscopy; images of individual NPs can be obtained with both techniques. However, only a minute fraction of material is characterized, which means that it can be extremely difficult to ensure that a representative sample is examined. Elemental analysis methods such as Atomic Absorption Spectroscopy (AAS) or Mass spectrometry (MS) can quantify nonlabeled nanoparticles, but do not provide direct information on the primary particle size or aggregation state. Besides, sample preparation can involve drying, which might result in aggregation of the sample and thus a false representation of the sample size in tissue.

Dynamic light scattering is another common method for the size characterization of nanoparticles, although may be not appropriate for in-situ measurements or in a digested biological sample, because of the multiple scattering issues [96]. The heterogeneous nature of fluid such as serum can give rise to significant background signals. Moreover, samples of polymer/DNA complexes are typically dilute in nature and often contain large fractions of free polymer [97], which can interact with serum proteins and form aggregates that

strongly interfere with size measurements by conventional light scattering techniques [98]. However, Xie et al. [99] have developed a quantitative method for the estimation of gold nanoshell concentrations in whole blood and estimate the actual delivered dose of intravenously injected nanoparticles using dynamic light scattering. Triton X-100 was added to blood samples containing gold nanoshells to act as a quantitative scattering standard and blood lysing agent. Au nanoshells are similar in size and shape to other types of nanoparticles delivered intravascularly in biomedical applications, and given the pervasiveness of DLS in nanoscale particle manufacturing, this simple technique should have wide applicability toward estimating the circulation time of other solid nanoparticles. It has some limitations; one is that it is critical that the nanoparticles solution of interest remain unaggregated, since only separate, unattached particles will produce a scattering profile identical to the stock particles enabling concentration calibration. For in vivo oncology applications, however, this is often the goal for therapeutic reasons, and this technique primarily quantitates individual nanoparticles that remain in circulation and that are expected to produce a size dependent accumulation. Also, the use of Triton X-100 surfactant may limit the protocol to solid nanoparticles. Micellar or liposomal systems may be subject to breakdown or aggregation in the presence of this agent, rendering further analysis useless.

Dynamic light scattering has been also employed to evaluate secondary TiO_2 nanoparticles size for *in vitro* toxicity assessment [100]. However, when using DLS to determine the hydrodynamic diameter of the nanoparticles in a biological media, it must be taken in account the fact that for example citrate-stabilized gold colloids in the bloodstream are quickly coated by serum proteins. Dobrovolskaia *et al.* [101] demonstrated that after incubation with plasma the intensity-weighted average particle diameters increased, and trypsin digestion of the particle-bound plasma proteins returns the colloids to approximately their pre-incubation sizes. This measurement can be also

influenced by particle agglomeration, so TEM or AFM measurements are useful to determine if the increase could be attributed to a change in agglomeration state.

Optical-spectral methods have been useful for the characterization of nanoparticles in biological fluids and tissues. Absorbance spectroscopy and resonant light scattering spectroscopy were used for determination of nanoparticles number concentration. Gold nanoparticles surface Plasmon resonance peaks are clearly visible on absorption and scattering spectra. Levin and coworkers from the Russian Scientific Research Institute for Optical and Physical Measurements in 2009 in the International Nanotechnology Forum Rusnanotech presented an overview on the characterization of nanoparticles in biological fluids and tissues with optical methods. Concretely, they executed measurements for nanoparticles suspensions in water, phosphate buffer solution (PBS), whole blood and plasma. Directly before measurement the filtration of solution through membrane filters with pore size about 0.2 microns was made. It was necessary to exclude light scattering on red blood cells, for this purpose lysis of red blood cells was made by dilution of blood with surfactant Triton X-100.

In order to know NPs penetration efficiency through biological barriers it is necessary to define their concentration in organs and tissues. A possible method in this case is atomic absorption spectrometry with electrothermal atomization. Such approach is possible, if nanoparticle's composition includes at least one element contained in organism not more then on trace level. Penetration of gold nanoparticles through skin of laboratory animals was investigated. Samples of liver and spleen from rats were subjected by autoclave mineralization and gold concentration in mineralized solution was measured using atomic absorption spectrometer with electrothermal atomization.

Moreover, electrothermal atomic absorption spectrometry (GFAAS) with Zeeman background correction has been used to measure the Ag concentration permeated through human abdominal full thickness skin [102]. Experiments were performed using the Franz diffusion cell method with intact and damaged human skin. Physiological solution was used as receiving phase and silver nanoparticles coated with polyvinylpirrolidone dispersed in synthetic sweat were applied as donor phase to the outer surface of the skin for 24 h. The receptor fluid measurements were performed by electrothermal atomic absorption spectroscopy (ETAAS). Human skin penetration was also determined by using transmission electron microscope (TEM) to verify the location of silver nanoparticles in exposed membranes.

Electrophoretic methods, both gel and capillary electrophoresis are being widely employed for separation of nanoparticles, mainly as a function of their size, but in case of functionalized nanoparticles, the charge and pKa of the group attached to the NPs plays an important role in their separation.

For instance, Hanauer *et al.* [103] demonstrated separation of gold and silver nanoparticles according to their size and shape by agarose gel electrophoresis after coating them with a charged polymer layer. The separation was monitored optically using the size- and shape dependent Plasmon resonance and confirmed by transmission electron microscopy (TEM). In other work, Xu *et al.* [104] also used agarose gel electrophoresis for preparative separation of gold nanoclusters with sizes of 5, 15 and 20 nm. Gold balls, plates and long rods could also be separated according to shape. Liquid chromatography (LC) and gel electrophoresis can also be coupled to inductively coupled plasma (ICP)-MS [105] for the separation of gold nanoparticle standards by size.

The suitability of CE for the separation of metallic nanoparticles such as Au [106-111], Ag [110, 111], maghemite (γ-Fe_2O_3) [112, 113], semiconductors (quantum

dots) [114-116], and mixtures of metal oxides such as TiO_2, Fe_2O_3, Al_2O_3 and Fe_3O_4 [117, 118] has been also reported.

Flow cytometry allows high-resolution size distribution analysis of multimodal populations of nanoparticles directly in biological fluids and a proof of principle for preparative fractionation of polydisperse samples in the submicron range. Flow cytometry integrates light scattering and fluorescence measurements to gather information regarding size, shape, morphology of cells, which are their originally target analytes, although recently this technique has been exploited to study submicron matter, including unilamellar synthetic vesicles, liposomes, viral particles and nucleic acid containing nanoparticles [119]. It is also possible to correlate nanoparticle counting directly with cell numbers or sort cells based on nanoparticle uptake using a flow cytometry technique such as fluorescence-activated cell sorting (FACS) [120].

Inductively coupled plasma mass spectrometry (ICP-MS) has been also employed to quantitatively measure the presence of gold distribution in rats [121]. Gold suspensions were diluted by adding phosphate buffer saline in order to obtain a physiological solution for intravenous injection. One milliliter of each freshly prepared solution was injected in the tail vein. At 24 h after injection, blood and the following organs were collected: adrenals, aorta, brain, heart, kidney, liver, lung, lymph nodes (mesenteric and popliteal), spleen, testis, thymus, and vena cava. Organs were weighed, and tissue samples were homogenized and frozen for determination of gold content by inductively coupled plasma mass spectrometry.

Many *in vitro* nanotoxicity studies have used ICP-AES to assess nanoparticle uptake of gold, [122,123,124], cerium-oxide [125], and iron-oxide nanomaterials [126] among others. Generally, sample preparation includes isolation of cells from culture media followed by acidic sample digestion before dilution and ICP-AES analysis. In some instances, the mass concentrations obtained from ICP-AES

are converted into nanoparticle numbers after estimating the mass of a single nanoparticle using the atomic weight, the crystal lattice unit length and the well defined geometry of the nanoparticle [127].

The inherent fluorescent properties of some nanoparticles allow for facile analysis of uptake such as the recently reported uptake of quantum dots (QDs) by stem cells [128]. Recent advances in confocal light collection, such as spinning-disk confocal microscopy, can be used to monitor the trafficking of quantum dot trajectories [129] within cells with sub-second time resolution.

4. Analysis of carbon nanoparticles

In this section we will focus mainly in the analysis of fullerenes and carbon nanotubes since they are the most used carbon-based nanoparticles. Both carbon nanotubes and fullerenes are poor soluble in water, however, aggregates of fullerene nanoparticles can be dispersed in water solutions as well as carbon nanotubes, which are dispersed in water in the presence of surfactants. The concentrations of these nanoparticles in biological media as consequence of systemic exposure could be very low, so trace analysis will be required in order to develop toxicological studies of the nanomaterials.

While a range of methods is accessible for detection and characterization of nanomaterials, a number of challenges will arise when analyzing these materials in biological matrices due to the analytical artifacts caused by sample preparation, lack of reference materials and the matrix of the sample. Few methods have been reported.

One of the proposed methods for trace analysis of fullerenes in biological samples is a simplified liquid-liquid extraction (LLE) prior to high-performance liquid chromatography [130]. LLE is a usually choice in method development for complicated biological samples, although it has a longstanding problem:

emulsion. Xia *et al.* have demonstrated that the conventional LLE protocols could not be used for trace analysis of fullerenes in biological samples. The large amounts of proteins, lipids and surfactants in the biological samples would create a heavy emulsion that would interfere with the extraction. The emulsion problem is overcome by adding glacial acetic acid in order to solubilize the proteins and surfactants without causing significant analyte losses. Magnesium perchlorate was used to destabilize the nano-C_{60} particles in the water solution and promote the solvent extraction, since it is known that once nano-C_{60} is in water is difficult to be extracted back into the toluene phase. They found a serious drop in extraction efficiency at low concentrations. Several reasons could cause this problem including protein adsorption, glassware adsorption, or reconstitution loss. The glassware adsorption could cause analyte loss and extraction efficiency drop in trace analysis of small chemicals. Deactivation of the glassware is a routine practice to reduce the analyte loss. It was observed that glassware silanization only provided limited improvement. The extraction efficiency drop could be due to the C_{60} adsorption to the glassware or aggregation during dryness evaporation, which could not be re-dissolved into toluene even under sonication. Procedures of evaporation to dryness and reconstitution with a solvent are routine practice in chemical analysis; however, it cannot be used for trace analysis of fullerenes in biological and environmental samples. This method was evaluated with samples of BSA media and porcine plasma.

Quantification of C_{60} can be performed by UV-Vis measurements for high concentrations; by using absorption bands of C_{60} which are located at 336, 407, 540, and 595 nm. HPLC is used for the detection of low concentrations of C_{60} [131] but also a method for the direct analysis by electrospray time-of-flight mass spectrometry has been developed [132].

Optical spectroscopies are particularly useful for the analysis of homogeneous samples containing one type of nanoparticles. However, samples subjected to the analysis are often composed of populations of polydispersed nanoparticles. It is often necessary to study parameters such as size, shape and surface modification. If separation of subpopulations of nanoparticles present in the sample is required, application of techniques such as chromatography or electrophoresis should be considered [133]. For example, fullerenes can readily be separated and quantified by LC coupled to ESI-MS [134].

Electrophoresis has been also employed for the separation of single-walled carbon nanotubes, based on tube length [135], or diameter-selective CE separation for bundled and individual carbon nanotubes [136]. Gel electrophoresis has been useful for the separation of nucleic acid-carbon nanotube complexes [137]. Recently, Wang *et al.* [138] have developed a method to measure the concentration of SWNTs extracted from biological tissue. They employed polyacrylamide gel electrophoresis (PAGE) followed by quantification of SWNT bands by measure of the intensity from digitized images of these bands, which showed to be proportional to the amount of SWNTs loaded onto the gel. Normal rat kidney cells in culture were allowed to take up SWNTs upon exposure to medium containing various concentrations of BSA-SWNTs for different times and temperatures. When BSA-SWNT dispersions were subjected to sodium dodecyl sulfate (SDS)-PAGE, BSA passed through the stacking gel, entered the resolving gel, and migrated towards the anode; however, SWNTs accumulated in a sharp band at the interface between the loading wall and the stacking gel.

It has been also demonstrated the suitability of the combination of capillary electrophoresis with Raman spectroscopy or with scanning probe microscopy for individual single-walled carbon nanotube analysis [139]. This system could

be applied to the characterization of nanoparticles extracted from biological samples.

CNT quantification is normally performed by UV-Vis spectrometry at high concentrations [140, 141]. CNT show strong absorption in the UV and visible region with peaks at 253 nm, 266 nm, 350 nm and strong absorption extending up to 1200 nm [142]. Wrapping of CNT with conventional fluorophores, fluorescent polymers or with DNA- oligonucleotides allowed their detection in biomedical applications. SEC with UV-detection was used for the separation of CNT from impurities and amorphous carbon.

A work evaluated extraction of carboxylic CNTs from surface water using a filter modified with MWCNTs as a preconcentrator [65]. To prepare the filters, a dispersion of MWCNTs prepared in Triton X-100 was filtered through a nylon filter with a pore size of 0.45 μm. They were then washed with methanol and dried under air stream. MWCNTs can interact with SWCNTs through π-π interactions, showing a high capacity to adsorb SWCNTs. Similar methodologies can be adapted to be applied to biological samples.

5. Analysis of nanodrug and nano-food additives

Two aspects of nanotoxicology should be mentioned, which concerns the safety of nanodrugs. First, the patients will use the nanodrug particles, and it explains the need to examine their toxic profile not only in healthy organism, but also on animal models of particular diseases. Second, the wide spread of the genetic polymorphisms in human population suggests that some part of this population can be extremely sensitive to the action of nanoparticles [143]. This hypothesis agrees with the preliminary data on the role of oxidative stress in the realization of the toxic effects of nanoparticles and genetically determined heterogeneity of the antioxidant and other protective systems [144].

6. Future trends

One challenge for analytical chemists is the area of nanoparticle characterization. Firstly, most of the current techniques used for physical nanoparticle characterization provide only limited information before or after engineered nanoparticles are in the biological environment. In next years, it is expected the development of new methods to extract and preconcentrate the nanoparticles from the biological matrix before their physico-chemical characterization. Electron microscopy, scanning probe microscopy, and dynamic light scattering are techniques commonly used for this purpose, which reveal nanoparticle size and distribution but give no information about aggregation/agglomeration that may occur within the biological environment, adsorption of biomolecules, or degradation of the nanoparticle itself (biotransformation), all of which may change during residence within the biological system and would greatly influence nanoparticle uptake and/or behavior. These concerns suggest the future development of a new area among the field of nanotoxicology, which could be called as "nanomaterial speciation". It will be focus on the determination of the nanoparticles taking into account their possible biotransformation. So, it is expected that nanoparticles having different biocoatings will have different effects from the toxicological point of view.

Acknowledgements

The authors wish to thank Spain's Ministry of Innovation and Science for funding Project CTQ2007- 60426 and Junta de Andalucía for Project FQM02300. A.I. López-Lorente also wishes to thank the Ministry for the award of a Research Training Fellowship (Grant AP2008-02939).

References

[1] http://ec.europa.eu/research/quality-oflife/ka4/pdf/report_nanopathology_en.pdf

[2] Alexandra Navrotsky: Energetic clues to pathways to biomineralization: Precursors, clusters, and nanoparticles. *Proc. Natl. Acad. Sci. USA* 101, 12096–12101 (2004)

[3] John M Zachara, Steve M Heald, Byong-Hun Jeon, Ravi K Kukkadapu, Chongxuan Liu, James P McKinley, Alice C Dohnalkova, Dean A Moore: Reduction of pertechnetate (Tc (VII)) by aqueous Fe (II) and the nature of solid phase redox products. *Geochim Cosmochim Acta* 71, 2137–2157 (2007)

[4] Luann Becker, Robert J Poreda, Jeffrey L Bada: Extraterrestrial helium trapped in fullerenes in the Sudbury impact structure. *Science* 272, 249-252 (1996)

[5] D Heymann, L W Jenneskens, J Jehlicka, C Koper, E Vlietstra: Terrestrial and extraterrestrial fullerenes. *Fuller Nanotub Carbon Nanostruct* 11, 333-370 (2003)

[6] Jillian F Banfield, Hengzhong Zhang: Nanoparticles in the environment. *Reviews in Mineralogy & Geochemistry* 44, 1-58 (2001)

[7] Glenn A Waychunas, Christopher S Kim, Jillian F Banfield: Nanoparticulate iron oxide minerals in soils and sediments: unique properties and contaminant scavenging mechanisms. *J Nanopart Res* 7, 409-433 (2005)

[8] Cort Anastasio, Scot T Martin: Atmospheric nanoparticles. *Reviews in Mineralogy & Geochemistry* 44, 293-349 (2001)

[9] Michael F Hochella, Andrew S Madden: Earth's nanocompartment for toxic metals. *Elements* 1, 199-203 (2005)

[10] Dennis A Bazylinski, Richard B Frankel: Magnetosome formation in prokaryotes. *Nat Rev Microbiol* 2, 217–230 (2004)

[11] Ellen E. Connor, Jugith Mwamuka, Anand Gole, Catherine J. Murphy, Michael D. Wyatt: Gold nanoparticles are taken up by human cells but do not cause acute cytotoxicity. *Small* 1, 325–327 (2005)

[12] Kelly BéruBé, Dominique Balharry, Keith Sexton, Lata Koshy, Tim Jones: Combustion-derived nanoparticles: mechanisms of pulmonary toxicity. *Clin Exp Pharmacol Physiol* 34, 1044-1050 (2007)

[13] Fathi Zereini, Clare Wiseman, Friedrich Alt, Juergen Messerschmidt, Juergen Muller, Hans Urban: Platinum and rhodium concentrations in airborne particulate matter in Germany from 1988 to 1998. *Environ Sci Technol* 35, 1996-2000 (2001)

[14] Christof M Niemeyer: Nanoparticles, proteins, and nucleic acids: biotechnology meets materials science. *Angew Chem Int Ed* 40 (22), 4128–58 (2001)

[15] Guozhong Cao: Nanostructures and nanomaterials. Synthesis, Properties & Applications. *Imperial College Press*; London (2004)

[16] Vincent Rotello: Nanoparticles: Building Blocks for Nanotechnology. *Springer*, NY (2003)

[17] Peter J F Harris: Carbon nanotubes and related structures: New materials for the 21st Century. *Cambridge University Press*, Cambridge (1996)

[18] Hongjie Dai: Carbon nanotubes: synthesis, integration, and properties. *Acc Chem Res* 35, 1035-1044 (2002)

[19] C Journet, W K Matser, P Bernier, L Laiseau, S Lefrant, P Deniard, R Lee, J E Fischer: Large-scale production of single-walled carbon nanotubes by the electric-arc technique. *Nature* 388, 756-758 (1997)

[20] Andreas Thess, Roland Lee, Pavel Nikolaev, Hongjie Dai, Pierre Petit, Jerome Robert, Chunhui Xu, Young Hee Lee, Seong Gon Kim, Andrew G Rinzler, Daniel T Colbert, Gustavo E Scuseria, David Tománek, John E Fischer, Richard E Smalley: Crystalline ropes of metallic carbon nanotubes. *Science* 276, 483-487 (1996)

[21] Emmanuel Flahaut, Christphe Laurent, Alain Peigney: Catalytic CVD synthesis of double and triple-walled carbon nanotubes by the control of the catalyst preparation. *Carbon* 43, 375-383 (2005)

[22] Linda Vaisman, H Daniel Wagner, Gad Marom: The role of surfactants in dispersion of carbon nanotubes. *Adv Colloid Interface Sci* 128-130, 37-46 (2006)

[23] Bumsu Kim, Yun-Ho Lee, Jee-Hyun Ryu, Kyung-Do Suh: Enhanced colloidal properties of single-wall carbon nanotubes in α-terpineol and Texanol. *Colloid Surf A* 273, 161-164 (2006)

[24] Vasilios Georgakilas, Konstantinos Kordatos, Maurizio Prato, Dirk M Guldi, Michael Holzinger, Andreas Hirsch: Organic functionalization of carbon nanotubes. *J Am Chem Soc* 124, 760-761 (2002)

[25] Ray H Baughman, Changxing Cui, Anvar A Zakhidov, Zafar Iqbal, Joseph N Barisci, Geoff M Spinks, Gordon G Wallace, Alberto Mazzoldi, Danilo De Rossi, Andrew G Rinzler, Oliver Jaschinski, Siegmar Roth, Miklos Hertesz. Carbon nanotube actuators. *Science* 284, 1340-1344 (1999)

[26] Miguel Valcárcel, Soledad Cárdenas, Bartolomé M Simonet, Yolanda Moliner-Martínez, Rafael Lucena: Carbon nanostructures as sorbent materials in analytical processes. *Trends Anal Chem* 27, 34-42 (2008)

[27] Fred Wudl: Fullerene materials. *J Mater Chem* 12, 1959-1963 (2002)

[28] Maurizio Prato: Fullerene Materials. *Top Curr Chem* 199, 173-187 (1999)

[29] Travis Jennings, Geoffrey Strouse: Past, present, and future of gold nanoparticles. *Adv Exp Med Biol* 620, 34–47 (2007)

[30] Jose Ruben Morones, Jose Luis Elechiguerra, Alejandro Camacho, Katherine Holt, Juan B Kouri, Jose Tapia Ramirez, Miguel Jose Yacaman: The bactericidal effect of silver nanoparticles. *Nanotechnol* 16, 2346-2353 (2005)

[31] Mathias Brust, Christopher J Kiely: Some recent advances in nanostructure preparation from gold and silver particles: a short topical review. *Colloids Surf A* 202, 175-186 (2002)

[32] Wei-Xian Zhang: Nanoscale iron particles for environmental remediation: an overview. *J Nanopart Res* 5, 323-332 (2003)

[33] R J Aitken, M Q Chaudhry, A B A Boxall, M Hull: Manufacture and use of nanomaterials: current status in the UK and global trends. *Occup Med* 56, 300-306 (2006)

[34] M N Rittner: Market analysis of nanostructured materials. *Am Ceram Soc Bull* 81, 33-36 (2002)

[35] Douglas C Hague, Merrilea J Mayo: Controlling crystallinity during processing of nanocrystalline titania. *J Am Ceram Soc* 77, 1957–1960 (1994)

[36] S R Dhage, R Pasricha, V Ravi: Synthesis of ultrafine TiO_2 by citrate gel method. *Mat Res Bull* 38, 1623–1628 (2003)

[37] O Larlus, S Mintova, T Bein: Environmental syntheses of nanosized zeolites with high yield and monomodal particle size distribution. *Micropor Mesopor Mater* 96, 405-412 (2006)

[38] Dana Yaron-Marcovich, Yona Chen, Shlomo Nir, Rene Prost: High resolution electron microscopy structural studies of organo-clay nanocomposites. *Environ Sci Technol* 39, 1231-1238 (2005)

[39] Markys Cain, Roger Morrell: Nanostructured ceramics: a review of their potential. *Appl Organomet Chem* 15, 321-330 (2001)

[40] Vladimir V Pokropivnyi: Non-carbon nanotubes (review). Part 2. Types and structure. *Powder Metallurgy and Metal Ceramics* 40, 582-594 (2001)

[41] Joanna Koziara, Paul R Lockman, David D Allen, Russell J Mumper: *In situ* blood-brain barrier transport of nanoparticles. *Pharm Res* 20, 1772-1778 (2003)

[42] Ju-Young Kim, Sun-Bo Shim, Jin-Kie Shim: Enhanced desorption of phenanthrene from aquifer sand using amphiphilic anionic polyurethane nanoparticles. *J Ind Eng Chem* 10, 1043-1051 (2004)

[43] Yinhui Xu, Dongye Zhao: Removal of copper from contaminated soil by use of poly (amidoamine) dendrimers. *Environ Sci Technol* 39, 2369-2375 (2005)

[44] Manoj Nirmal, Louis Brus: Luminescence photophysics in semiconductor nanocrystals. *Acc Chem Res* 32, 407-414 (1999)

[45] Matthias Seydack: Nanoparticle labels in immunosensing using optical detection methods. *Biosens Bioelectron* 20, 2454-2469 (2005)

[46] Jose Manuel Costa-Fernandez, Rosario Pereiro, Alfredo Sanz Medel: The use of luminescent quantum dots for optical sensing. *Trends Anal Chem* 25, 207-218 (2006)

[47] Hedi Mattoussi, J Matthew Mauro, Ellen R Goldman, George P Anderson, Vikram C Sundar, Frederic V Mikulec, Moungi G Bawendi: Self-assembly of CdSe-ZnS quantum dot bioconjugates using an engineered recombinant protein. *J Am Chem Soc* 122, 12142-12150 (2000)

[48] C B Murray, D J Norris, M G Bawendi: Synthesis and characterization of nearly monodisperse CdE (E = sulfur, selenium, tellurium) semiconductor nanocrystallites. *J Am Chem Soc* 115, 8706-8715 (1993)

[49] Kara Morgan: Development of a Preliminary Framework for Informing the Risks Analysis and Risk Management of Nanoparticles. *Risk Anal* 25, 1-15 (2005)

[50] Joyce S Tsuji, Andrew D Maynard, Paul C Howard, John T James, Chiu-Wing Lam, David B Warheit, Annette B Santamaria: Research Strategies for Safety Evaluation of Nanomaterials, Part IV: Risk Assesment of Nanoparticles. *Toxicol Sci* 88, 12-17 (2006)

[51] Robert H Hurt, Marc Monthioux, Agnes Kane: Toxicology of carbon nanomaterials: Status, trends, and perspectives on the special issue. *Carbon* 44 1028-1033 (2006)

[52] Karluss Thomas, Philip Sayre: Research strategies for safety evaluation of nanomaterials, Part I: Evaluating Human Health Implications for exposure to Nanomaterials. *Toxicol Sci* 87, 316-321 (2005)

[53] Nastassja Lewinski, Vicki Colvin, Rebekah Drezek: Cytotoxicity of nanoparticles. *Small* 4, 26-49 (2008)

[54] Wei Fu, Dinesh Shenoy, Jane Li, Curtis Crasto, Graham Jones, Charles Dimarzio, Srinivas Sridhar, Mansoor Amiji: Biomedical applications of gold nanoparticles functionalized using hetero-bifunctional poly (ethylene glycol) spacer. *Mater Res Soc Symp Proc* 845, 223-228 (2005)

[55] Dinesh Shenoy, Wei Fu, Jane Li, Curtis Crasto, Graham Jones, Charles Dimarzio, Srinivas Sridhar, Mansoor Amiji: Surface functionalization of gold nanoparticles using heterobifunctional poly (ethylene glycol) spacer for intracellular tracking and delivery. Int J Nanomed 1, 51–57 (2006)

[56] Aliasger K Salem, Peter C Searson, Kam W Leong: Multifunctional nanorods for gene delivery. Nat Mater 2, 668–671 (2003)

[57] Massimo Bottini, Shane Bruckner, Konstantina Nika, Nunzio Bottini, Stefano Bellucci, Andrea Magrini, Antonio Bergamaschi, Tomas Mustelin.: Multi-walled carbon nanotubes induce T lymphocyte apoptosis. Toxicol Lett 160, 121–126 (2006)

[58] Arnaud Magrez, Sandor Kasas, Valérie Salicio, Nathalie Pasquier, Jin Won Seo, Marco Celio, Stefan Catsicas, Beat Schwaller, Lázló Forró: Cellular Toxicity of Carbon-Based Nanomaterials. Nano Lett 6, 1121–1125 (2006)

[59] Christian Kirchner, Tim Liedl, Stefan Kudera, Teresa Pellegrino, Almudena Munoz Javier, Hermann E Gaub, Sonja Stolzle, N Fertig, Wolfgang J Parak: Cytotoxicity of Colloidal CdSe and CdSe/ZnS Nanoparticles. Nano Lett 5, 331–338 (2005)

[60] Akiyoshi Hoshino, Kouki Fujioka, Taisuke Oku, Masakazu Suga, Yu F Sasaki, Toshihiro Ohta, Masato Yasuhara, Kazuo Suzuki, Kenji Yamamoto: Physicochemical Properties and Cellular Toxicity of Nanocrystal Quantum Dots Depend on Their Surface Modification. Nano Lett 4, 2163–2169 (2004)

[61] Catherine M Goodman, Catherine D. McCusker, Tuna Yilmaz, Vincent M Rotello: Toxicity of Gold Nanoparticles Functionalized with Cationic and Anionic Side Chains. Bioconjugate Chem 15, 897–900 (2004)

[62] Gemma Reguera, Kevin D McCarthy, Teena Mehta, Julie S Nicoll, Mark T Tuominen, Derek R Lovley: Extracellular Electron Transfer Via Microbial Nanowires. Nature 453, 1098-1101 (2005)

[63] Peter Wick, Pius Manser, Ludwing K Limbach, Ursula Dettlaff-Weglikowska, Frank Krumeich, Siegmar Roth, Wendelin J Stark, Arie Bruinink: The Degree and Kind of Agglomeration Affect Carbon Nanotube. Toxicol Lett 168, 121-131 (2007)

[64] Furong Tian, Daxiang X Cui, Heinz Schwarz, Giovani Gomez Estrada, Hisatashi Kobayashi: Cytotoxicity of single-wall carbon nanotubes on human fibroblasts. Toxicol In vitro 20, 1202–1212 (2006)

[65] Beatriz Suarez, Yolanda Moliner-Martinez, Soledad Cardenas, Bartolome M Simonet, Miguel Valcarcel: Monitoring of carboxylic carbon nanotubes in surface water by using multiwalled carbon nanotube-modified filter as preconcentration unit. *Environ Sci Technol* 42, 6100-6104 (2008)

[66] Bryce J Marquis, Sara A Love, Katherine L Braun, Christy L Haynes: Analytical methods to assess nanoparticle toxicity. *Analyst* 134, 425–439 (2009)

[67] Andrew D Maynard: Overview of methods for analyzing single ultrafine particles. *Phil Trans R Soc Lond A* 358, 2593-2610 (2000)

[68] Barbara Rothen-Rutishauser, Christian Muhlfeld, Fabian Blank, Claudia Musso, Peter Gehr: Translocation of particles and inflammatory responses after exposure to fine particles and nanoparticles in an epithelial airway model. *Part Fibre Toxicol* 4, 9 (2007)

[69] Chen-Luh Lin, Jan D Miller: The development of a PC image based on-line particle size analyzer. *Miner Metall Proc* 2, 29–35 (1993)

[70] Christian Mühlfeld, Barbara Rothen-Rutishauser, Dimitri Vanhecke, Fabian Blank, Peter Gehr, Matthias Ochs: Visualization and quantitative analysis of nanoparticles in the respiratory tract by transmission electron microscopy. *Part Fibre Toxicol* 4, 11 (2007)

[71] Barbara Pergolese, Adriano Bigotto, Maurizio Muniz-Miranda, Giuseppe Sbrana: Gold/palladium and silver/palladium colloids as novel metallic substrates for surface enhanced Raman scattering. *Appl Spectrosc* 59, 194-9 (2005)

[72] P V Asharani, Yi Lian Wu, Zhiyuan Gong, Suresh Valiyaveettil: Toxicity of silver nanoparticles in zebrafish models. *Nanotechnology* 19, 255102 (2008)

[73] Alexandra E Porter, Mhairi Gass, Karin Muller, Jeremy N Skepper, Paul A Midgley, Mark Welland: Direct imaging of single-walled carbon nanotubes in cells. *Nat Nanotechnol* 2, 713–717 (2007)

[74] Vaishali Bagalkot, Liangfang Zhang, Etgar Levy-Nissenbaum, Sangyong Jon, Philip W Kantoff, Robert Langer and Omid C. Farokhzad: Quantum Dot-Aptamer Conjugates for Synchronous Cancer Imaging, Therapy, and Sensing of Drug Delivery Based on Bi-fluorescence Resonance Energy Transfer. *Nano Lett* 7, 3065–3070 (2007)

[75] Evangelia Chnari, Jessica S Nikitczuk, Kathryn E Uhrich, Prabhas V Moghe: Nanoscale Anionic Macromolecules Can Inhibit Cellular Uptake of Differentially Oxidized LDL. *Biomacromolecules* 7, 597–603 (2006)

[76] Shigeo Maruyama, Yuhei Miyauchi, Yoichi Murakami, Shohei Chiashi: Optical characterization of single-walled carbon nanotubes synthesized by catalytic decomposition of alcohol. *New Journal of Physics* 5, 149.1–149.12 (2003)

[77] Bailin Chen, John P Selegue: Separation and Characterization of Single-Walled and Multiwalled Carbon Nanotubes by Using Field-Flow Fractionation. *Anal Chem* 74, 4774-4780 (2002)

[78] Jie Liu, Andrew G Rinzler, Hongjie Dai, Jason H Hafner, R Kelley Bradley, Peter J Boul, Adrian Lu, Terry Iverson, Konstantin Shelimov, Chad B Huffman, Fernando Rodriguez-Macias, Young-Seok Shon, T Randall Lee, Daniel T Colbert, Richard E Smalley: Fullerene pipes. *Science* 280, 1253–1256 (1998)

[79] J Calvin Giddings, S Kim Ratanathanawongs, Bhajendra N Barman, Myeong Hee Moon, Guangyue Liu, Brenda L Tjelta, Marcia E Hansen: Characterization of colloidal and particulate silica by field-flow fractionation. *Advances in Chemistry* 234, 309–340 (1994)

[80] Soheyl Tadjiki, Shoeleh Assemi, Cassandra E Deering, John M. Veranth, Jan D Miller: Detection, separation, and quantification of unlabeled silica nanoparticles in biological media using sedimentation field-flow fractionation. *J Nanopart Res* 11, 981-988 (2009)

[81] Pratim Biswas, Chang-Yu Wu: Nanoparticles and the Environment. *J Air Waste Manage Assoc* 55, 708-746 (2005)

[82] Kevin W Powers, Scott C Brown, Vijay B Krishna, Scott C Wasdo, Brij M Moudgil, Stephen M Roberts: Research strategies for safety evaluation of nanomaterials. Part VI.

Characterization of nanoscale particles for toxicological evaluation. *Toxicol Sci* 90, 296-303 (2006)

[83] Richard C Murdock, Laura Braydich-Stolle, Amanda M Schrand, John J Schlager, Saber M Hussain: Characterization of nanomaterial dispersion in solution prior to *in vitro* exposure using dynamic light scattering technique. *Toxicol Sci* 101, 239-53 (2008)

[84] Joanna Szpunar: Bio-inorganic speciation analysis by hyphenated techniques. *Analyst* 125, 963–988 (2000)

[85] Kunnath S Subramanian: Determination of metals in biofluids and tissues: sample preparation methods for atomic spectroscopy techniques. *Spectrochim Acta Part B* 51, 291–319 (1996)

[86] P H McMurry: A Review of Atmospheric Aerosol Measurements. *Atmospheric Environ* 34, 1959-1999 (2000)

[87] William W Yu, Emmanuel Chang, Joshua C Falkner, Junyan Zhang, Ali M Al-Somali, Christie M Sayes, Judah Johns, Rebekah Drezek, Vicki L Colvin: Forming biocompatible and nonaggregated nanocrystals in water using amphiphilic polymers. *J Am Chem Soc* 129, 2871–2879 (2007)

[88] A Nemmar, P H M Hoet, B Vanquickenborne, D Dinsdale, M Thomeer, M F Hoylaerts, H Vanbilloen, L Mortelmans, B Nemery: Passage of inhaled particles into the blood circulation in humans. *Circulation* 105, 411–414 (2002)

[89] Jun Sung Kim, Tae-Jong Yoon, Kyeong Nam Yu, Byung Gul Kim, Sung Jin Park, Hyun Woo Kim, Kee Ho Lee, Seung Bum Park, Jin-Kyu Lee, Myung Haing Cho: Toxicity and tissue distribution of magnetic nanoparticles in mice. *Toxicol Sci* 89, 338–347 (2006)

[90] Jung-Taek Kwon, Soon-Kyung Hwang, Hua Jin, Dae-Seong Kim, Arash Minai-Tehrani, Hee-Jeong Yoon, Mansoo Choi, Tae-Jong Yoon, Duk-Young Han, Young-Woon Kang, Byung-Il Yoon, Jin-Kyu Lee, Myung-Haing Cho: Body distribution of inhaled fluorescent magnetic nanoparticles in the mice. *J Occup Health* 50, 1–6 (2008)

[91] Isaac Stayton, Jeffrey Winiarz, Katie Shannon, Yinfa Ma: Study of uptake and loss of silica nanoparticles in living human lung epithelial cells at single cell level. *Anal Bioanal Chem* 394, 1595-1608 (2009)

[92] Xinli Xing, Xiaoxiao He, Jiaofeng Peng, Kemin Wang, Weihong Tan: Uptake of silica-coated nanoparticles by HeLa cells. *J Nanosci Nanotechnol* 5, 1688–1693 (2005)

[93] Chen-Wen Lu, Yann Hung, Jong-Kai Hsiao, Ming Yao, Tsai-Hua Chung, Yu-Shen Lin, Si-Han Wu, Szu-Chun Hsu, Hon-Man Liu, Chung-Yuan Mou, Chung-Shi Yang, Dong-Ming Huang, Yao-Chang Chen: Bifunctional Magnetic Silica Nanoparticles for Highly Efficient Human Stem Cell Labeling. *Nano Lett* 7, 149–154 (2007)

[94] Sehoon Kim, Haridas E Pudavar, Adela Bonoiu, Paras N Prasad: Aggregation-enhanced fluorescence in organically modified silica nanoparticles: a novel approach toward high-signal-output nanoprobes for two-photon fluorescence bioimaging. *Adv Mater* 19, 3791–3795 (2007)

[95] David J Burleson, Michelle D Driessen, R Lee Penn. On the characterization of environmental nanoparticles. *J Environ Sci Health Part A* 39, 2707-2753 (2004)

[96] Charlie Yu Ming Hsu, Hasan Uludag: Effects of size and topology of DNA molecules on intracellular delivery with non-viral gene carriers. *BMC Biotechnol* 8, 23 (2008)

[97] Jean Pierre Clamme, Joel Azoulay, Yves Mely: Monitoring of the formation and dissociation of polyethylenimine/DNA complexes by two photon fluorescence correlation spectroscopy. *Biophys J* 84, 1960–1968 (2003)

[98] Jong-Yuh Cherng, Petra van de Wetering, Herre Talsma, Daan J Crommelin, Wim E Hennink: Effect of size and serum proteins on transfection efficiency of poly ((2-dimethylamino) ethyl methacrylate)-plasmid nanoparticles. *Pharm Res* 13, 1038–1042 (1996)

[99] Huan Xie, Kelly L Gill-Sharp, D Patrick O'Neal: Quantitative estimation of gold nanoshell concentrations in whole blood using dynamic light scattering. *Nanomedicine: Nanotechnology, Biology, and Medicine* 3, 89-94 (2007)

[100] Haruhisa Kato, Mie Suzuki, Katsuhide Fujita, Masanori Horie, Shigehisa Endoh, Yasukazu Yoshida, Hitoshi Iwahashi, Kayori Takahashi, Ayako Nakamura, Shinichi Kinugasa: Reliable size determination of nanoparticles using dynamic light scattering method for *in vitro* toxicology assessment, *Toxicol In vitro* 23, 927-934 (2009)

[101] Marina A Dobrovolskaia, Anil K Patri, Jiwen Zheng, Jeffrey D Clogston, Nader Ayub, Parag Aggarwal, Barry W Neun, Jennifer B Hall, Scott E McNeil: Interaction of colloidal gold nanoparticles with human blood: effects on particle size and analysis of plasma protein binding profiles. *Nanomedicine: Nanotechnology, Biology, and Medicine* 5, 106-117 (2009)

[102] Francesca Filon Laresea, Flavia D'Agostin , Matteo Crosera, Gianpiero Adami, Nadia Renzi, Massimo Bovenzi, Giovanni Maina: Human skin penetration of silver nanoparticles through intact and damaged skin. *Toxicology* 255, 33–37 (2009)

[103] Matthias Hanauer, Sebastien Pierrat, Inga Zins, Alexander Lotz, Carsten Sonnichsen: Separation of nanoparticles by gel electrophoresis according to size and shape. *Nano Lett* 7, 2881 – 2885 (2007)

[104] Xiaoyou Xu, Kenneth Caswell, Elizabeth Tucker, Saswat Kabisatpathy, K Lisa Brodhacker, Walter A Scrivens: Size and shape separation of gold nanoparticles with preparative gel electrophoresis. *J Chromatogr A*, 1167, 35 – 41 (2007)

[105] Andreas Helfrich, Wolfram Bruechert, Jorg Bettmer: Size characterisation of Au nanoparticles by ICP-MS coupling techniques. *J Anal At Spectrom* 21, 431 – 434 (2006)

[106] Ursula Schnabel, Christian-Herbert Fischer, Ernst Kenndler: Characterization of colloidal gold nanoparticles according to size by capillary zone electrophoresis. *J Microcolumn Sep* 9, 529 – 534 (1997)

[107] Fu-Ken Liu, Guor-Tzo Wei: Adding sodium dodecylsulfate to the running electrolyte enhances the separation of gold nanoparticles by capillary electrophoresis. *Anal Chim Acta* 510, 77 – 83 (2004)

[108] Fu-Ken Liu, Ying-Ying Lin, Chien-Hou Wu: Highly efficient approach for characterizing nanometer-sized gold particles by capillary electrophoresis. *Anal Chim Acta* 528, 249 –254 (2005)

[109] Fu-Ken Liu: A high-efficiency capillary electrophoresis-based method for characterizing the sizes of Au nanoparticles. *J Chromatogr A* 1167, 231 – 235 (2007)

[110] Fu-Ken Liu, Fu-Hsiang Ko: Separation and study of the optical properties of silver nanocubes by capillary electrophoresis. *Chem Lett* 33, 902 – 903 (2004)

[111] Fu-Ken Liu, Fu-Hsiang Ko, Pei-Wen Huang, Chien-Hou Wu, Tieh-Chi Chu: Studying the size/shape separation and optical properties of silver nanoparticles by capillary electrophoresis. *J Chromatogr A* 1062, 139 – 145 (2005)

[112] Natalia G Vanifatova, Boris Ya Spivakov, Juergen Mattusch, Ulrich Franck, Rainer Wennrich: Investigation of iron oxide nanoparticles by capillary zone electrophoresis. *Talanta* 66, 605 – 610 (2005)

[113] Chung Keung Lo, Man Chin Paau, Dan Xiao, Martin M F Choi: Capillary electrophoresis, mass spectrometry, and UV-Visible absorption studies on electrolyte-induced fractionation of gold nanoclusters. *Anal Chem* 80, 2439 –2446 (2008)

[114] Xiangyi Huang, Jifang Weng, Fuming Sang, Xingtao Song, Chengxi Cao, Jicun Ren: Characterization of quantum dot bioconjugates by capillary electrophoresis with laser-induced fluorescent detection. *J Chromatogr A* 1113, 251 – 254 (2006)

[115] Mark Pereira, Edward P C Lai, Bryan Hollebone: Characterization of quantum dots using capillary zone electrophoresis. *Electrophoresis* 28, 2874 – 2881 (2007)

[116] Ute Pyell: CE characterization of semiconductor nanocrystals encapsulated with amorphous silicium dioxide. *Electrophoresis* 29, 576 – 589 (2008)

[117] C Quang, Steven L Petersen, G R Ducatte, Nathan E Ballou: Characterization and separation of inorganic fine particles by capillary electrophoresis with an indifferent electrolyte system. *J Chromatogr A* 732, 377 – 384 (1996)

[118] Steven L Petersen, Nathan E Ballou: Separation of micrometer-size oxide particles by capillary zone electrophoresis. *J Chromatogr A* 834, 445 – 452 (1999)

[119] E V B van Gaal, G Spierenburg, W E Hennink, D J A Crommelin, E Mastrobattista: Flow cytometry for rapid size determination and sorting of nucleic acid containing nanoparticles in biological fluids. *J Control Release* 141, 328–338 (2010)

[120] Yu Pan, Sabine Neuss, Annika Leifert, Monika Fischler, Fei Wen, Ulrich Simon, Guenter Schmid, Wolfgang Brandau, Willi Jahnen-Dechent: Size dependent cytotoxicity of gold nanoparticles. *Small* 3, 1941–1949 (2007)

[121] Wim H De Jong, Werner I Hagens, Petra Krystek, Marina C Burger, Adriënne J A M Sips, Robert E Geertsma: Particle size-dependent organ distribution of gold nanoparticles after intravenous administration. *Biomaterials* 29, 1912-1919 (2008)

[122] Tanya S Hauck, Arezou A Ghazani, Warren C W Chan: Assesing the effect of surface chemistry on gold nanorod uptake, toxicity, and gene expression in mammalian cells. *Small* 4, 153–159 (2008)

[123] B Devika Chithrani, Warren C W Chan: Elucidating the mechanism of cellular uptake and removal of protein-coated gold nanoparticles of different sizes and shapes. *Nano Lett* 7, 1542–1550 (2007)

[124] Joseph A Ryan, K Wesley Overton, Molly E Speight, Chistine N Oldenburg, Lina Loo, Wayne Robarge, Stefan Franzen, Daniel L Feldheim: Cellular uptake of gold nanoparticles passivated with BSA-SV40 large T antigen conjugates. *Anal Chem* 79, 9150–9159 (2007)

[125] Swanand Patil, Amanda Sandberg, Eric Heckert, William Self, Sudipta Seal: Protein adsorption and cellular uptake of Cerium oxide nanoparticles as a function of zeta potential. *Biomaterials* 28, 4600–4607 (2007)

[126] Shy Chyi Wuang, Koon Gee Neoh, En-Tang Kang, Daniel W Pack, Deborah E Leckband: HER-2-mediated endocytosis of magnetic nanospheres and the implications in cell targeting and particle magnetization. *Biomaterials* 29, 2270–2279 (2008)

[127] B. Devika Chithrani, Arezou A Ghazani, Warren C W Chan: Determining the size and shape dependence of gold nanoparticle uptake into mammalian cells. *Nano Lett* 6, 662–668 (2006)

[128] Oleksandr Seleverstov, Olga Zabirnyk, Mattias Zscharnack, Larysa Bulavina, Marcin Nowicki, Jean-Michael Heinrich, Maksym Yezhelyev, Frank Emmrich, Ruth O'Regan, Augustinus Bader: Quantum dots for human mesenchymal stem cells labeling. A size-dependent autophagy activation. *Nano Lett* 6, 2826–2832 (2006)

[129] Gang Ruan, Amit Agrawal, Adam I Marcus, Shuming Nie: Imagin and tracking of Tat peptide-conjugated quantum dots in living cells: new insights into nanoparticle uptake, intracellular transport, and vesicle shedding. *J Am Chem Soc* 129, 14759–14766 (2007)

[130] Xin-Rui Xia, Nancy A Monteiro-Riviere, Jim E Riviere: Trace analysis of fullerenes in biological samples by simplified liquid-liquid extraction and high-performance liquid chromatography. *J Chromatogr A* 1129, 216-222 (2006)

[131] J D Fortner, D Y Lyon, C M Sayes, A M Boyd, J C Falkner, E M Hotze, L B Alemany, Y J Tao, W Guo, K D Ausman, V L Colvin, J B Hughes: C_{60} in water: nanocrystal formation and microbial response. *Environ Sci Technol* 39, 4307-4316 (2005)

[132] V Kozlovski, V Brusov, I Sulimenkov, A Pikhtelev, A Dodonov: Novel experimental arrangement developed for direct fullerene analysis by electrospray time-of-flight mass spectrometry. *Rapid Commun. Mass Spectrom* 18, 780-786 (2004)

[133] Mark C Hersam: Progress towards monodisperse single-walled carbon nanotubes. *Nat Nanotechnol* 3, 387 –394 (2008)

[134] Carl W Isaacson, Crystal Y Usenko, Robert L Tanguay, Jennifer A Field: Quantification of fullerenes by LC/ESI-MS and its application to *in vivo* toxicity assays. *Anal Chem* 79, 9091 – 9097 (2007)

[135] Stephen K Doorn, Robert E Fields, Hui Hu, Mark A Hamon, Robert C Haddon, John P Selegue, Vahid Majidi: High resolution capillary electrophoresis of carbon nanotubes. *J Am Chem Soc* 124, 3169 – 3174 (2002)

[136] Stephen K Doorn, Michael S Strano, Michael J O'Connell, Erik H Haroz, Kristy L Rialon, Robert H Hauge, Richard E Smalley: Capillary electrophoresis separations of bundled and individual carbon nanotubes. *J Phys Chem* 107, 6063 – 6069 (2003)

[137] Alexandre A Vetcher, Srimeenakshi Srinivasan, Ivan A Vetcher, Semen M Abramov, Mikhail Kozlov, Ray H Baughman, Stephen D Levene: Fractionation of SWNT/nucleic acid complexes by agarose gel electrophoresis. *Nanotechnology* 17, 16, 4263 – 4269 (2006)

[138] Ruhung Wang, Carole Mikoryak, Elena Chen, Synyoung Li, Paul Pantano, Rockford K Draper: Gel electrophoresis method to measure the concentration of single-walled carbon nanotubes extracted from biological tissue. *Anal Chem* 81, 2944-2952 (2009)

[139] Tatsuhiro Yamamoto, Yoichi Murakami, Jin Motoyanagi, Takanori Fukushima, Shigeo Maruyama, Masaru Kato: An analytical system for single nanomaterials: combination of capillary electrophoresis with Raman spectroscopy or with scanning probe microscopy for individual single-walled carbon nanotube analysis. *Anal Chem* 81, 7336-7341 (2009)

[140] Masahito Sano, Junko Okamura, Seiji Shinkai: Colloidal nature of single-walled carbon nanotubes in electrolyte solution. The Schulze-Hardy rule. *Langmuir* 17, 7172-7173 (2001)

[141] Linqin Jiang, Lian Gao, Jing Sun: Production of aqueous colloidal dispersions of carbon nanotubes. *J Colloid Interface Sci* 260, 89-94 (2003)

[142] Sandeep S Karajanagi, Hoichang Yang, Prashanth Asuri, Edward Sellitto, Jonathan S Dordick, Ravi S Kane: Protein-assisted solubilization of single-walled carbon nanotubes. *Langmuir* 22, 1392-1395 (2006)

[143] A D Durnev: Toxicology of nanoparticles. *Bulletin of experimental biology and medicine* 145, 72-74 (2008)

HERRAMIENTAS ANALÍTICAS

ANALYTICAL TOOLS

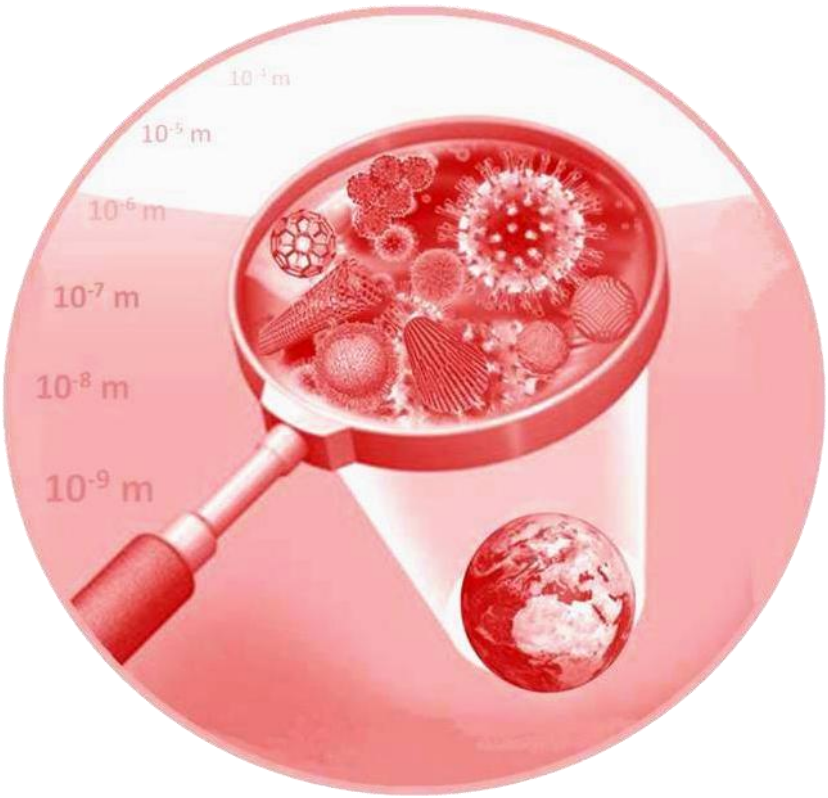

BLOQUE II

II

En el desarrollo experimental de la presente Tesis Doctoral se han empleado diferentes herramientas analíticas, que se describen brevemente en este Bloque. Tal es el caso de nanopartículas y nanomateriales, reactivos y muestras, la instrumentación empleada, aparatos y otros materiales. Por último, se describen los métodos utilizados para la síntesis de nanopartículas así como los procedimientos de dispersión y extracción de nanomateriales.

II.1. NANOMATERIALES

Los nanomateriales empleados durante el desarrollo experimental de esta Tesis Doctoral son los que se detallan a continuación:

1.1. Nanotubos de carbono

Se han empleado nanotubos de carbono de pared simple (SWNTs) así como de pared múltiple (MWNTs) obtenidos de diversas casas comerciales. La tabla II.1 muestra las principales características de cada tipo de nanotubo.

Tabla II.1. Características de los nanotubos de carbono objeto de estudio.

	Diámetro (nm)	Longitud (μm)	Funcionalización
MWNTs-1	10-30	10-30	2.5 (wt)% OH
MWNTs-2	10-30	10-30	1.6 (wt)% COOH
MWNTs-3	10-30	10-30	-
MWNTs-4	5-20	1-10	-
MWNTs-5	10-20	5-15	-
MWNTs-6	9.5	1.5	-
SWNTs	<2	5-15	-

MWNTs-1, 2 y 3 fueron suministrados por Cheap Tubes Inc. (Brattleboro, Vermont, EEUU), con >90% de pureza en peso, y un contenido en cenizas <1.5% en peso. MWNTs-4 fueron proporcionados por Bayer Material Science (Alemania), MWNTs-5 por Shenzhen Nanotech Port Co. Ltd (NTP, China) y MWNTs-6 por Nanocyl (Bélgica).

Nanotubos de carbono de pared simple (SWNTs) fueron proporcionados por Shenzhen Nanotech Port Co. Ltd (NTP), China, con una pureza superior al 90%, y un área superficial específica de 500-700 m^2g^{-1}.

1.2. Nanopartículas metálicas

Se han empleado nanopartículas de oro y plata recubiertas con citrato, nanopartículas de oro funcionalizadas con ácido tióctico, así como nanopartículas de oro sin ligandos en superficie obtenidas mediante la síntesis propuesta en la presente Tesis Doctoral. En el apartado II.5 de este bloque se detallan los procedimientos de síntesis empleados.

II.2. REACTIVOS Y MUESTRAS

Durante el desarrollo de la Tesis Doctoral se han utilizado los siguientes reactivos:

- Reactivos para la síntesis de nanopartículas: ácido tetracloroaúrico ($HAuCl_4$), cloruro de oro(III), citrato sódico dihidrato 99.5%, nitrato de plata, de Sigma-Aldrich.
- Líquidos iónicos: 1-hexil-3-metilimidazolio hexafluorofosfato (HMIM PF_6), 1-butil-3-metilimidazolio hexafluorofosfato (BMIM PF_6).
- Tensioactivos: Dodecil sulfato sódico (SDS), de Sigma-Aldrich; y Tritón X-100, cloruro de cetiltrimetilamonio (CTAC) y bromuro de cetiltrimetilamonio (CTAB), de Fluka.
- Sales: nitrato potásico y cloruro sódico, de Sigma-Aldrich.

- Ácidos: ácido nítrico, ácido clorhídrico, ácido sulfúrico y ácido tricloroacético (TCA), de Panreac; ácido etilendiaminotetraacético (EDTA) y ácido 3-(ciclohexilamino)-1-propano sulfónico (CAPS), de Sigma-Aldrich.
- Bases: hidróxido sódico e hidróxido potásico, de Sigma-Aldrich.
- Disolventes: Etanol (Fluka), acetona, metanol (Sigma-Aldrich y J.T. Baker), óxido de deuterio (D_2O), de VWR y agua ultrapura (MilliQ a través de un sistema Millipore).
- Compuestos tiólicos: ácido tiomálico (o mercaptosuccínico) (Sigma-Aldrich) y ácido tióctico (lipoico o 6,8-ditioctanoico) (Fluka).
- Otros reactivos: 1,10-fenantrolina (VWR), ácidos húmicos (Sigma-Aldrich).

Todos los estándares, reactivos y disolventes empleados a lo largo de la investigación fueron de pureza analítica o superior.

2.1. Muestras

Para llevar a cabo el estudio de la utilidad analítica de los distintos métodos de determinación de nanopartículas desarrollados para su aplicación en muestras medioambientales y biológicas, se seleccionaron muestras de agua de río y muestras de tejido de hígado de pollo, respectivamente.

Las muestras de agua de río recolectadas se almacenaron en frascos de vidrio ámbar sin dejar espacio de cabeza a 4ºC. Las muestras se recogieron de varios efluentes del Rio Guadalquivir a su paso por Córdoba (Andalucía).

Las muestras de hígado de pollo fueron adquiridas de una carnicería local. Las muestras se secaron con acetona y se pulverizaron hasta tener una mezcla uniforme.

II.3. INSTRUMENTACIÓN

En el desarrollo experimental de la presente Tesis Doctoral se ha hecho uso de diferentes equipos instrumentales, los cuales se describen a continuación.

3.1. Espectrofotometría UV-Vis

Para llevar a cabo las medidas UV-Vis se empleó una lámpara de halógeno como fuente de excitación y el monocromador y detector fotónico de un Espectrofluorímetro PTI *QuantaMaster*™ como detector (Photon technology International) controlado por el software FeliX32.

3.2. Espectrómetros Raman portátil

Para la caracterización de nanotubos de carbono y la determinación de los mismos así como de nanopartículas de oro se empleó un espectrómetro Raman portátil de B&W TEK Inc., conocido como i-Raman BWS415 (Raman portátil 1), que lleva acoplado un láser de diodo con una longitud de onda de 785 nm y una potencia máxima en el puerto de excitación de 354 mW±15%.

Se ha trabajado además con un modelo posterior del mismo, denominado inno-Ram (Raman portátil 2), también de la compañía B&W TEK Inc., con un láser de 785 nm y una potencia de láser máxima en el puerto de excitación de 348 mW y 285 mW en la sonda.

Para tratar los datos se utilizó el software OPUS 5.0 y Unscrambler 9.1 (Camo).

3.3. Microscopio Raman confocal

Se ha utilizado un microscopio Raman confocal (CRM) alpha500 de WITec GmbH. El microscopio confocal requiere una fuente de luz (láser), que se enfoca sobre la muestra. La luz reflejada (Raman) se recoge con el mismo objetivo y se enfoca hacia un *pinhole* hacia el detector. De esta manera sólo la señal

procedente del plano focal llega al detector, lo que incrementa el contraste de la imagen y la resolución. El sistema combina la alta eficiencia del espectrómetro Raman con la alta resolución del microscopio óptico confocal, de manera que es posible combinar la información química con resolución lateral en el rango del sub-micrómetro. El equipo permite obtener el espectro Raman en un punto determinado, así como crear imágenes Raman de una superficie de la muestra.

Para la excitación se utilizó un láser de doble frecuencia de Nd:YAG de 532 nm (segundo armónico), que resulta en una profundidad de penetración en silicio de 0.5 µm. Los espectros Raman se registraron con una rejilla de difracción de 600 g/mm. El haz del láser se enfoca sobre la superficie de la muestra usando objetivos de 20x/0.4 de Zeiss y de 100x/0.95, 50x/0.80 en aire, y de 100x/1.25 de inmersión en aceite, de Nikon.

Figura II.1. Microscopio Raman confocal acoplado con AFM de WITec.

3.4. Microscopía de fuerza atómica (AFM)

En cuanto a microscopía AFM se utilizó el microscopio AFM acoplado con el equipo alpha500 de WITec descrito anteriormente, utilizando el modo contacto intermitente. Para ello se empleó un cantiléver con recubrimiento reflectante

con una constante de fuerza de 42 Nm^{-1} y una frecuencia de resonancia de 285 KHz.

Asimismo también se empleó un microscopio AFM5500 de Agilent equipado con cantiléver SPM con sonda de silicio *NCL-W Point.* Se utilizó modo contacto intermitente con una frecuencia de resonancia de 190 KHz y una constante de fuerza de 48 Nm^{-1}.

3.5. Microscopía electrónica (TEM y SEM)

Para la caracterización de las nanopartículas se utilizaron los siguientes equipos de microscopía electrónica:

- Microscopía de barrido electrónico: i) microscopio electrónico de barrido (SEM) JEOL JSM 6300 (Isaza, Alcobendas, España) con una capacidad de aumento de entre 70x y 300.000x y una resolución de 3~4 nm (a 30 Kv); ii) microscopio de barrido electrónico a Quanta 3D FEG, FEI Company (Eindhoven, Países Bajos) equipado con un detector de rayos X por dispersión de energía.

- Microscopía de transmisión electrónica: i) microscopio electrónico de transmisión PHILIPS CM-10, el cual permitió obtener imágenes aumentadas de 18x a 450.000x; ii) microscopio electrónico de transmisión JEOL JEM-1400; y iii) microscopio Electrónico de Transmisión de alta resolución JEOL JEM 2010 (con sistema de microanálisis de rayos X por dispersión de energía).

Los microscopios que se han utilizado, a excepción del Quanta 3D FEG, pertenecen al servicio centralizado de apoyo a la investigación (SCAI) de la UCO.

3.6. Electroforesis capilar

La separación de nanopartículas por electroforesis capilar se realizó utilizando un equipo P/ACE MDQ Beckman Coulter (Palo Alto, CA, EE.UU.) equipado con un detector UV-Vis de diodos en fila (DAD). Los capilares de sílice fundida utilizados fueron de 75 µm de diámetro interno. El equipo dispone del software 32 Karat (versión 8.0) para el control del instrumento y la recogida y tratamiento de datos.

3.7. Espectroscopia infrarroja

Las medidas de infrarrojo se llevaron a cabo usando un espectrómetro FT-IR Vertex 70 equipado con una unidad BioATRCell-II y un detector de mercurio-cadmio-telurio (MCT) refrigerado con nitrógeno líquido (Bruker Optics, Ettlingen, Alemania). Las medidas se realizaron en la modalidad de reflexión total atenuada (ATR). El equipo está acoplado a un sistema que permite controlar la temperatura de la cámara ATR. La adquisición y tratamiento de los datos se llevó a cabo con el software OPUS 6.5 (Bruker Optics, Ettlingen, Alemania).

3.8. Espectroscopia de emisión óptica con plasma de acoplamiento inductivo (ICP-OES)

Para investigar el mecanismo de la síntesis propuesta de nanopartículas de oro se utilizó un equipo Ultima2 Horiba Jobin Yvon de espectroscopia de emisión óptica con plasma de acoplamiento inductivo.

II.4. APARATOS Y MATERIAL

Durante el desarrollo del trabajo experimental realizado en esta Tesis Doctoral, se emplearon los siguientes **aparatos**:

- Baño de agua termostatizado de circulación FRIGITERM (J.P. Selecta, Barcelona, España).
- Bomba peristáltica Gilson Miniplus-3 (Middleton, Estados Unidos).
- Ultracentrífuga controlada por microprocesador (Centronic BL-II, J.P. Selecta, Barcelona, España).
- Baño de ultrasonidos 50 W, 60 Hz (J.P. Selecta, Barcelona, España).
- Sonda ultrasonidos Vibracell^{TM} 75041(750 W, 20 KHz, Bioblock Scientific, Illkirch, Francia), equipada con una sonda de 3 mm.
- Agitador Vortex (Heidolph, Mérida, España).
- Agitador magnético (Velp Científica, Milán, Italia).
- Placa calefactora con agitación magnética Agimatic-N (J.P. Selecta, Barcelona, España)
- Horno cromatográfico HP 5890 (Agilent Technologies, Palo Alto, CA, USA).
- pH-metro (Crison, modelo micropH 2000).
- Balanza analítica Cobos AI-220CB (Cobos, Barcelona, España).
- Balanza analítica de precisión OHAUS Explorer (OHAUS, Nänikon, Suiza).
- Equipo de agua Milli-Q (Millipore, Bedford, MA, EEUU).
- Sistema de microfiltración de diseño propio y construido por Inmeco (Córdoba). El diámetro de filtración es de 1.3 mm.

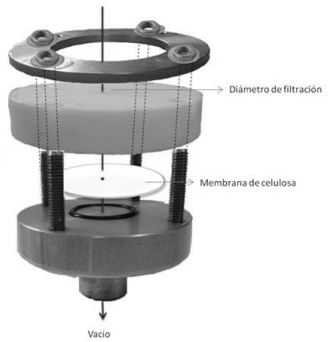

Figura II.2. Sistema de microfiltración *home-made* con un diámetro de filtración de 1.3 mm.

Asimismo se ha empleado el siguiente **material**:

- Membranas de acetato de celulosa de tamaño de poro de 0.2 µm (Sartorius Stedim Biotech, Alemania).
- Membranas de celulosa de tamaño de poro de 5 µm (Millipore).
- Membranas de nylon de tamaño de poro de 0.45 µm (Supelco, USA) y filtros de nylon de 0.45 µm (Análisis vínicos, España).
- Pieza de acero inoxidable 304.
- Tubo de acero inoxidable de 1.5 m de longitud con un diámetro externo de 1/8'' y 2 mm de diámetro interno (Análisis Vínicos, España).
- Microjeringa Hamilton de 250 µL (Análisis Vínicos, España).
- Micropipetas.
- Cubeta ultramicro de Hellma con un paso óptico de 10 mm.
- Material de vidrio de laboratorio, clase A.

II.5. SÍNTESIS Y FUNCIONALIZACIÓN DE NANOPARTÍCULAS

5.1. Síntesis de nanopartículas de oro con citrato

Las nanopartículas de oro se sintetizaron de manera análoga al método propuesto por Turkevich et al.[1] con algunas modificaciones. En primer lugar se limpia todo el material que se va a emplear en la síntesis con agua regia (mezcla 1:3 de HNO_3:HCl), se enjuaga con agua ultrapura y se seca con aire. Las disoluciones de $HAuCl_4$ y citrato sódico se prepararon en agua ultrapura y se filtraron antes de su empleo. Se preparan 50 mL de una disolución de $HAuCl_4$ 0.01% y se ponen a calentar con agitación magnética. Una vez que esté hirviendo la disolución se añaden 0.254 mL de una disolución de citrato sódico al 1%. Se deja reaccionar durante 15 minutos. Al cabo de este tiempo se añaden

[1] J. Turkevich, P.C. Stevenson, J. Hillier, J. Discuss. Faraday Soc. 11 (1951) 55-75.

5mL de $HAuCl_4$ 0.01% caliente y a continuación 0.254 mL de citrato sódico 1%. Se deja reaccionar otros 15 minutos. Una vez transcurrido este tiempo, se apaga el calentador de la placa y se mantiene la agitación mientras se enfría hasta temperatura ambiente. La disolución se guardó en un frasco de color topacio y se almacenó a 4ºC.

Modificando la cantidad de citrato que se añade para la reducción del ácido tetracloroaúrico se obtienen nanopartículas de oro de distinto tamaño, como puede verse en la Figura II.3.

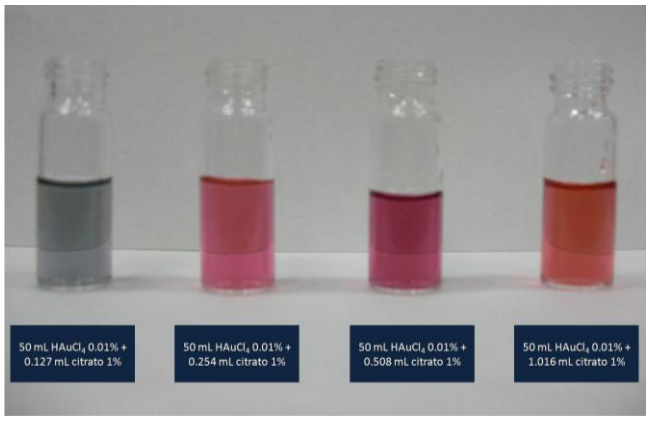

Figura II.3. Nanopartículas de oro de distinto tamaño obtenidas mediante reducción con citrato añadiendo distinta cantidad del mismo. El tamaño de las nanopartículas determina el color de la disolución coloidal.

5.2. Síntesis de nanopartículas de oro mediada por acero inoxidable

Las nanopartículas de oro se sintetizaron mediante la reducción del $HAuCl_4$ en condiciones ambiente mediada por acero inoxidable. Todo el material de vidrio se lavó con agua regia recién preparada (mezcla 1:3 HNO_3:HCl) y con agua destilada. Se introdujo una pieza de acero inoxidable 304 (con una superficie de 12,9 mm^2) en 100 µL de una disolución 0.2 $mgmL^{-1}$ de $HAuCl_4$. La reacción tiene lugar a temperatura ambiente, el substrato de acero inoxidable se usó

simultáneamente como agitador durante la síntesis. Las nanopartículas se almacenaron a 4ºC. Si se incrementa la temperatura, la reacción se acelera significativamente. Se ha comprobado que tanto acero como acero inoxidable conducen a la formación de AuNPs, sin embargo, dada su utilidad y disponibilidad, los estudios se limitaron a acero inoxidable.

El procedimiento de síntesis se ha automatizado para su obtención en flujo continuo. La disolución de $HAuCl_4$ se introduce en un tubo de acero inoxidable (1/8'' diámetro externo, 2 mm diámetro interno, 1.5 m longitud) usando una bomba peristáltica, que controló los flujos entre 0.041 y 3.63 mL min^{-1}. El tubo de acero inoxidable está sumergido en un baño termostatizado que controla la temperatura de reacción. Las nanopartículas se recogen al final del tubo en un vial de cristal y se almacenan a 4ºC. Tras la reacción, el tubo de acero inoxidable se limpia con una mezcla 1:3 de ácido nítrico y clorhídrico para eliminar posibles restos de oro en las paredes, se llena con agua y se seca con aire.

5.3. Síntesis de nanopartículas de plata con citrato

Las nanopartículas de plata se prepararon de acuerdo con el método descrito por Lee y Meisel[2]. Se disolvieron 9 mg de nitrato de plata en 50 mL de agua ultrapura y se calentaron hasta ebullición. Entonces, se añadieron 5 mL de una disolución 1% de citrato sódico y la disolución se dejó hervir a reflujo durante 90 minutos. Tras enfriarlo a temperatura ambiente se obtiene una disolución amarilla-gris que contiene las nanopartículas de plata (AgNPs), que se almacenaron en un frasco de color topacio a 4ºC.

5.4. Funcionalización de nanopartículas de oro con ácido tióctico

La funcionalización de las nanopartículas de oro con ácido tióctico (TA) tiene lugar a través de un enlace Au-S con el derivado tiol por adsorción química en

[2] P.C. Lee, D. Meisel, J. Phys. Chem., 86 (1982) 3391.

la superficie de la nanopartícula. La disolución de AuNPs obtenidas con citrato se trató con un exceso de ácido tióctico (1:3 Au/tiol) añadiendo pequeñas cantidades del mismo a la vez que se reajusta el pH a 8 para evitar que precipiten las nanopartículas. La dispersión se mantuvo agitando 12 horas y se purificó mediante diferentes etapas de lavado con agua ultrapura y dietil éter sometiendo la dispersión a centrifugación (14489 g) para eliminar posibles ligandos que no hayan reaccionado. Las nanopartículas permanecieron estables en disolución sin aglomerarse a temperatura ambiente durante un periodo de 6 meses.

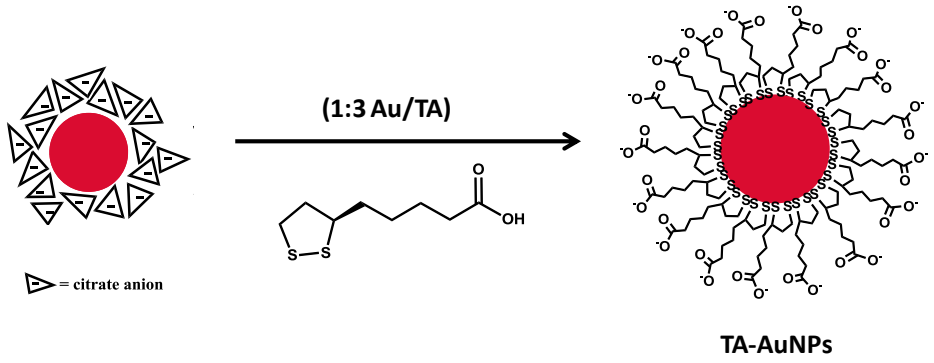

Figura II.4. Esquema de la reacción de intercambio de ligandos para la funcionalización con ácido tióctico de nanopartículas de oro obtenidas mediante síntesis con citrato.

5.5. Funcionalización de nanotubos de carbono (SWNTs)

Se carboxilaron nanotubos de carbono monocapa (SWNTs) añadiendo en un matraz de vidrio 100 mg de SWNTs y 20 mL de una mezcla 3:1 de H_2SO_4/HNO_3. La mezcla se mantuvo en reflujo durante 1 hora. A continuación, fracciones diluidas de la mezcla se centrifugaron a 10062 g durante 10 minutos y se lavaron con agua hasta que el sobrenadante dejó de tener pH ácido. Finalmente, los nanotubos de carbono monocapa carboxilados (c-SWNTs) se

secaron a 60ºC en una estufa. Después del tratamiento ácido, los c-SWNTs están cargados negativamente con grupos carboxilos en las paredes y los extremos abiertos, lo que los hace solubles en agua. El método de carboxilación está basado en el descrito por Xue y Cui[3], con algunas modificaciones.

II.6. PROCEDIMIENTOS DE DISPERSIÓN, EXTRACCIÓN Y PRECONCENTRACIÓN DE NANOPARTÍCULAS

6.1. Dispersión de nanotubos de carbono

Los nanotubos de carbono son insolubles en agua y tienen una gran tendencia a la agregación. En la presente Tesis Doctoral se han seguido dos estrategias para lograr dispersiones estables de este nanomaterial: i) funcionalización mediante la carboxilación de SWNTs, como se ha explicado anteriormente; y ii) dispersión con ayuda de tensioactivos. En este sentido se ha demostrado la posibilidad de dispersar SWNTs y MWNTs con ayuda de Tritón X-100, dodecil sulfato sódico (SDS) o bromuro de cetiltrimetilamonio (CTAB). Más detalles sobre la dispersión con tensioactivos se encuentran en el capítulo 6 de esta Memoria.

6.2. Microextracción líquido-líquido con líquidos iónicos

La microextracción líquido-líquido en líquido iónico se ha empleado para la extracción y preconcentración de nanopartículas de oro y nanotubos de carbono.

Para las nanopartículas de oro el procedimiento general consiste en poner en contacto 3 mL de agua de río fortificada con las nanopartículas de oro y CTAC hasta concentración 1.67 mM, con 0.3 g de líquido iónico (BMIM PF_6). El sistema se agita manualmente durante 30 segundos y se deja reposar para favorecer la

[3] W. Xue, T. Cui, Nanotechnology, 18 (2007) 145709/1-145709/7

separación de fases (Figura II.5). El procedimiento se modificó para el caso de las muestras de hígado de pollo. En ese caso se añadió ácido tricloroacético (TCA) 0.15 M, para desnaturalizar las proteínas y que precipiten de modo que no interfieran en las medidas posteriores, y EDTA 3.33 mM, como agente complejante de posibles iones interferentes, a 3 mL de agua ultrapura, que se pusieron en contacto con 2 mg de hígado de pollo pulverizado. Dicha suspensión se fortificó con AuNPs y se agitó durante 1 hora. Después se separó la fase sólida mediante centrifugación a 1370 g durante 5 minutos. El sobrenadante se trató con CTAC 1.67 mM y 0.3 g de BMIM PF_6 para extraer las nanopartículas.

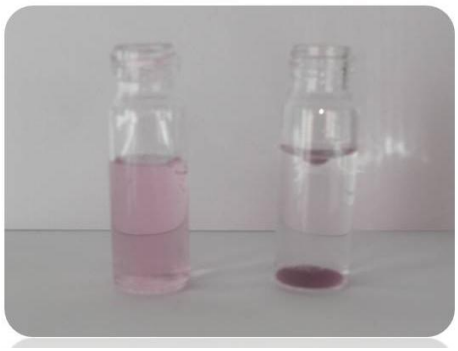

Figura II.5. Microextracción de nanopartículas de oro en líquido iónico BMIM PF_6.

En el caso de nanotubos de carbono, el procedimiento genérico consiste en poner en contacto 2 mL de agua de río (que contiene los CNTs) a la que se le añade CTAC hasta una concentración final 3.12 mM y a pH ajustado a 1.4 con 0.1 g de líquido iónico (BMIM PF_6). El sistema se agita manualmente durante 30 segundos y se deja reposar para favorecer la separación de fases.

6.3. Preconcentración de c-SWNTs sobre un sustrato SERS.

Se han preconcentrado c-SWNTs en muestras acuosas sobre un sustrato activo en SERS compuesto por nanopartículas de oro sin ligandos en superficie mediada por acero inoxidable (propuesta en el capítulo 3) microfiltradas sobre una membrana comercial de acetato de celulosa con un tamaño de poro de 0.2 µm. La muestra que contiene los nanotubos de carbono carboxilados es microfiltrada, usando el dispositivo de la figura II.2., quedando los nanotubos adsorbidos y concentrados sobre las nanopartículas de oro previamente depositadas.

6.4. Preconcentración de c-SWNTs en membranas modificadas con MWNTs.

Se han preconcentrado c-SWNTs en muestras acuosas mediante el uso de una membrana de celulosa modificada con MWNTS, que actúan como sorbente. Para ello se microfiltraron 5 mL de muestra acuosa usando el dispositivo de microfiltración casero anteriormente mostrado (Figura II.2) con ayuda de una bomba peristáltica para mantener un flujo constante. Posteriormente se pasan 5 mL de una disolución de KOH a pH 12 para eliminar posibles interferencias de ácidos húmicos, y, finalmente, se pasa 1 mL de agua ultrapura.

SÍNTESIS DE NANOPARTÍCULAS

SYNTHESIS OF NANOPARTICLES

BLOQUE III

III

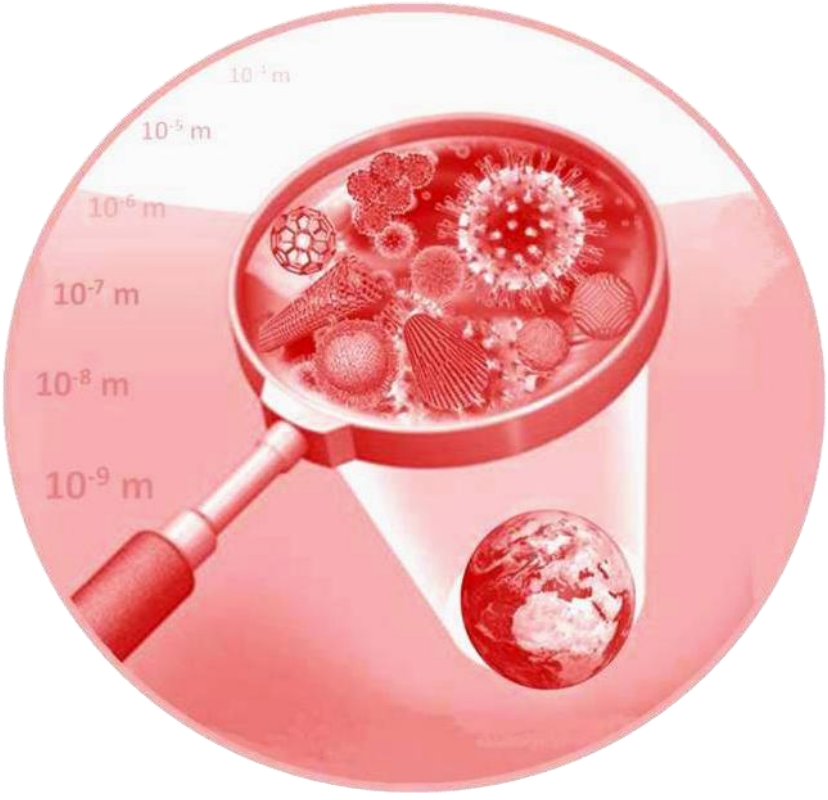

Las nanopartículas de oro se han usado ampliamente en diversos campos gracias a las extraordinarias propiedades que exhiben, lo que atraído un creciente interés hacia los métodos de síntesis de las mismas. Los métodos convencionales de síntesis de nanopartículas de oro se basan en la reducción química de Au(III) requiriendo reactivos químicos y ligandos que pueden inducir toxicidad biológica en los productos finales o causar problemas en futuras funcionalizaciones[1]. Para evitar estos inconvenientes, generalmente, las nanopartículas se someten a una etapa de purificación tras la síntesis[2]. Por otro lado, los reactivos usados para la reducción y estabilización de nanopartículas pueden ser contaminantes[3].

Como alternativa, en los últimos años se han desarrollado métodos que implican el uso de extractos de plantas o microorganismos de modo que no sean dañinos con el medio ambiente[4]. Asimismo, nanopartículas de oro sin ligandos en superficie se han sintetizado por medios físicos y/o electroquímicos (ej. irradiación láser)[5]. Por otro lado, otra tendencia en cuanto a la síntesis de nanomateriales, es el uso de sistemas de síntesis en continuo como microreactores[6], ya que se obtienen disoluciones de nanopartículas más homogéneas, y pueden escalarse fácilmente siendo procesos más eficientes energéticamente.

[1] M. C. Daniel, D. Astruc, Chem. Rev. 104 (2004) 293–346.
[2] C. J. Ackerson, P. D. Jadzinsky, G. J. Jensen, R. D. Kornberg, J. Am. Chem. Soc. 128 (2006) 2635–2640.
[3] S. F. Sweeney, G. H. Woehrle, J. E. Hutchison, J. Am. Chem. Soc. 128 (2006) 3190–3197.
[4] T. Panda, K. Deepa, J. Nanosci. Nanotechnol. 11 (2011) 10279-10294.
[5] V. Amendola, M. Meneghetti, J. Mater. Chem. 17 (2007) 4705–4710.
[6] C.X. Zhao, L. He, S.Z. Qiao, A.P.J. Middelberg, Chem. Eng. Sci. 66 (2011) 1463-1479.

En este bloque de la memoria de la Tesis Doctoral se presenta un nuevo método de síntesis de nanopartículas de oro a partir de ácido tetracloroaúrico utilizando acero inoxidable como agente reductor, que puede recuperarse de la disolución y ser reutilizado (**capítulo 3**). Las nanopartículas obtenidas a través de este nuevo procedimiento de síntesis han sido caracterizadas por diversas técnicas microscópicas y espectroscópicas, proponiéndose un posible mecanismo de reacción. Además, se ha demostrado el potencial de dichas nanopartículas para su uso como substrato SERS, aplicación que se verá con mayor profundidad posteriormente en el capítulo 12.

Por otro lado, en el **capítulo 4** se describe la producción en flujo continuo de dichas nanopartículas, usando un reactor tubular de acero inoxidable que conduce a la reducción del ácido tetracloroaúrico. De este modo la síntesis tiene lugar de modo automatizado y continuo. Modificando las condiciones del reactor, como la temperatura o velocidad de flujo, se obtienen nanopartículas con distinto tamaño como se ha demostrado mediante estudios de espectroscopia UV-Vis y de microscopía TEM.

Capítulo 3

Characterization of stainless steel assisted bare gold nanoparticles and their analytical potential

Talanta 118 (2014) 321-327

Talanta

118 (2014) 321-327

Characterization of stainless steel assisted bare gold nanoparticles and their analytical potential

A. I. López-Lorente[1,2], B. M. Simonet[1], M. Valcárcel[1], S. Eppler[2], R. Schindl[2], C. Kranz[2], B. Mizaikoff[2]

[1]*Department of Analytical Chemistry, University of Córdoba, E-14071 Córdoba, Spain.*

[2]*Institute of Analytical and Bioanalytical Chemistry, University of Ulm, Ulm, Germany.*

A simple, environmentally friendly, one-pot method to synthesize highly stable bare gold nanoparticles (AuNPs) has been developed. AuNPs have been synthesized from tetrachloroauric acid solution using steel or stainless steel as solid reducing agent, which can be reused. The proposed method yields bare gold nanoparticles at atmospheric pressure and room temperature for potentially producing large quantities. The obtained AuNPs have been characterized by SEM, TEM and AFM finding an average diameter of around 20 nm, polygonal yet nearly spherical shape and a narrow size distribution. The mechanism of reaction has been investigated by UV-vis spectroscopy, ICP-OES and EDX analysis. The obtained dispersed gold nanoparticles proved to be stable if stored a 4ºC for over four months without the addition of a stabilizing agent. Their analytical potential as SERS substrate has been demonstrated and their performance compared with that showed by citrate-coated gold nanoparticles. Thanks to their unique properties, their use as analytical tools provides analytical processes with enhanced selectivity and precision.

Keywords: bare gold nanoparticles, stainless steel, synthesis, characterization, surface enhanced Raman spectroscopy, carbon nanotubes.


$AuCl_4^-$
Au^0
H^+
H_2
H^+
Fe^0
Fe^{2+}

1. Introduction

Noble metal nanoparticles -gold nanoparticles (AuNPs) being included among them- have arouse great attention, offering huge potential for their application in fields such as nanomedicine and nanotechnologies as they provide several opportunities in imaging, diagnostics, and therapies [1,2].

In general, the synthetic routes leading to nanoparticles can be grouped into top-down and bottom-up strategies. In the so-called top-down approaches, nanoparticles are directly generated from bulk materials via the generation of isolated atoms usually involving physical methods such as milling, attrition, repeated quenching and photolithography [3]. Bottom-up strategies comprise molecular components as starting materials linked with chemical reactions, nucleation and growth process to promote the formation of clusters. Usually, they rely on the chemical reduction of metal salts, electrochemical pathways, or the controlled decomposition of metaestable organometallic compounds [4].

Among all the methods described, colloidal gold is most often prepared by reduction of gold halides (for example $HAuCl_4$) with the use of chemical reducing agents in solution such as sodium citrate [5,6,7] -also in the presence of tannin [8,9]-, sodium borohydride [10,11], ascorbic acid [12], ethylenediaminetetraacetic acid (EDTA) [13] or cyanoborohydride [14], which usually requires stabilizers or ligands. In most of these cases, the solution will be composed by the metallic particle, a counterion, the reductant or its byproducts (such as ketoglutaric acid for example in the case of citrate reduction [15]) and, in some cases, an organic stabilizer. The presence of those adsorbates may affect the optical characteristics of nanoparticles [16] as well as their photochemical reactivity [17], limiting future functionalizations [18] and causing interferences in cytotoxicity studies [19]. Moreover, chemicals employed for both reduction or stabilization of nanoparticles can be waste pollutants [20]. In

the last years, several so-called "green" synthetic methods involving the use of plant extracts as well as microorganism have been proposed [21,22].

While less commonly applied, bare gold nanoparticles without impurities within the metal particle surface have been also synthesized via physical (based on ultrasonic, UV, IR or ionizing radiation or laser photolysis) [23,24,25,26] and electrochemical methods [27]. The advantages of those methods are that impurities of chemical compounds are absent on the metal particle surface.

Laser ablation has been used for the synthesis of gold nanoparticles in liquid solution [26,28], obtaining AuNPs without chemical reagents or ligands. Those particles are electrically charged, thus, the resulting solution being stable for up to several months. However, it does not allow good control of size and size distribution. The formation of colloidal unmodified gold nanoparticles has been also achieved by irradiation of a precursor solution with X-rays from a synchrotron source, without the need of pre-added stabilizers [29]. Furthermore, gold nanoparticles have been produced by H_2 reduction of Au(III) oxide without any addition of stabilizer or counterion other than the metal ions and water dissociation ions [30].

This study demonstrates the possibility to synthesize bare gold nanoparticles (AuNP) from tetrachloroauric acid solution using steel or stainless steel as solid reducing agent. This green method avoids the use of a reductant in solution. Furthermore, the proposed synthesis method yields bare AuNPs at atmospheric pressure and room temperature for potentially producing large quantities, whereas the methods described to date to achieve nanoparticles without ligands usually require more complex instrumentation or reaction conditions such as e.g., molecular hydrogen at a pressure slightly higher than atmospheric conditions [30]. The analytical potential of these bare gold nanoparticles has been demonstrated for their use as substrates in surface enhanced Raman scattering (SERS) spectroscopic determination of carboxylated single walled

carbon nanotubes (c-SWNTs).Their performance has been compared with that of gold nanoparticles reduced by citrate.

2. Experimental

2.1. Materials and reagents

$HAuCl_4$ (Sigma Aldrich) was used to synthesize the gold nanoparticles. Before synthesis the material were washed with a mixture of nitric acid and hydrochloric acid (PANREAC). 1,10-phenantrolin was purchased from VWR (Germany). Sodium citrate dihydrate 99.5% (Sigma Aldrich) were used to synthesize citrate-coated gold nanoparticles in order to be compared with those obtained with the proposed method. A flat piece of 304-stainless steel was employed as solid reductant of gold salt in order to form gold nanoparticles.

Single walled carbon nanotubes (SWNTs) used to investigate SERS properties of synthesized nanoparticles were purchased from Shenzhen Nanotech Port Co. Ltd (NTP) (China), with a purity over 90%, an outer diameter of <2 nm, a length of 5-15 μm and a special surface area of 500-700 m^2/g. Acetate of cellulose membranes of 0.2 μm pore size were purchased from Sartorius Stedim Biotech (Germany).

2.2. Equipments

Characterization of the nanoparticles was performed using an AFM 5500 by Agilent equipped with NCL-W Point probe-Silicon SPM-cantilevers. For AFM studies of AuNPs, a piece of silicon wafer was covered with AuNP suspension, dried, and then imaged by AFM in tapping mode with a resonance frequency of 190 KHz and a force constant of 48 N m^{-1}. SEM measurements were performed with a Quanta 3D FEG, FEI Company (Eindhoven, Nederland) equipped with an energy dispersive x-ray spectroscopy (EDX) detector. TEM images were recorded using a PHILIPS CM-10 system. UV/Vis measurements were performed using a

halogen lamp as light source, and a monocromator combined with a photonic detector of a PTI Fluoresecence Master System as detector. In order to investigate the mechanism of the reaction and the involved constituents an Ultima2 Horiba Jobin Yvon ICP-OES was used.

Raman measurements were performed with a portable Raman spectrometer system (inno-Ram) from B&W TEK Inc. with a wavelength of 785 nm and a maximum laser output power of 285 mW in the probe. Laser power was set to 5.7 mW for measurements, using a 1 s acquisition and accumulating a total of 10 spectra.

2.3. Stainless steel assisted synthesis of bare gold nanoparticles

Gold nanoparticles were synthesized by a novel method, which is based on the reduction of the $HAuCl_4$ mediated by stainless steel at ambient conditions. All glassware were cleaned with freshly prepared aqua regia (HNO_3:HCl 1:3 mixture) and then rinsed thoroughly with distilled H_2O prior to use. A piece of 304-stainless steel (12.9 mm^2 of total surface) was introduced into 100 µL of a 0.2 mg mL^{-1} aqueous solution of $HAuCl_4$. The reaction is carried out at room temperature and the stainless steel substrate was simultaneously used as stirrer during the reaction. By increasing the temperature, the reaction is significantly accelerated. Higher concentrations of $HAuCl_4$ have also been tested; a 10-fold higher concentrated $HAuCl_4$ solution (2mg mL^{-1}) leads to more rapidly obtaining gold nanoparticles, yet, the stability of the solution is reduced.

It should be noted that both steel and stainless steel may act as reducing agent. Due to its utility and availability, the current study was limited to stainless steel as solid reducing agent.

2.4. Synthesis of gold nanoparticles by citrate reduction

Gold nanoparticles obtained via $HAuCl_4$ reduction mediated by sodium citrate were also prepared according to the method described by Turkevich et al.[5] with some modifications as described elsewhere [31]. All glassware were cleaned with freshly prepared aqua regia (HNO_3:HCl 1:3 mixture) and then rinsed thoroughly with distilled H_2O prior to use. $HAuCl_4$ and sodium citrate solutions were filtered through a 0.45 μm nylon membrane prior use. 0.254 mL of a 15 sodium citrate solution were added to a 0.01% boiling solution of $HAuCl_4$. The system was then left to react while being stirred for 15 min. Afterwards, 5mL of 0.01% $HAuCl_4$ solution were added to the system followed by 0.254 mL of 1% sodium citrate solution and it was stirred at heating for 15 min. Then the heater was switched off and the solution was kept stirred until cool to room temperature. Gold nanoparticles were stored at 4ºC in an amber bottle.

2.5. SERS measurements

In order to prove the analytical potential of these nanoparticles obtained through the proposed procedure, SERS spectra of carboxylated single walled carbon nanotubes were measured. Carboxylated carbon nanotubes (c-SWNTs) were prepared by adding 100 mg of SWNTs to 20 mL of 3:1 H_2SO_4/HNO_3 mixture in a glass flask, as described elsewhere [32]. After refluxed for 1 hour, c-SWNTs were washed with water and centrifuged at 10062 g for 10 minutes until the pH were neutral. Finally, carboxylated carbon nanotubes were dried in a heater set at 60ºC. Carboxylic groups present in nanotube sidewalls and open ends provide them solubility in water.

SERS measurements were carried out by depositing 10 μL of gold nanoparticles solution on acetate of cellulose membrane (pore size of 0.2 μm) by using a home-made filtration device with a filtration diameter of 1.3 mm. Then, aqueous stock solutions of c-SWNTs were filtered and nanotubes adsorbed on previously

deposited gold nanoparticles. The intensity of carbon nanotubes G band around 1583 cm^{-1} was selected as analytical signal to prove the suitability of bare gold nanoparticles as SERS substrate.

3. Results and discussion

3.1. UV-vis spectroscopic characterization

If steel or stainless steel is inserted into a tetrachloroauric acid solution, the homogenous formation of gold nanoparticles in solution is observed along with a small amount of AuNPs formed at the surface of the solid reducing agent. The kinetics of the synthesis of AuNPs may be directly observed via UV/Vis spectroscopy in a cuvette (Fig. 1) since gold nanoparticles provide a characteristic absorption due to their plasmon resonance bands [33]. The solution was stirred at low velocity in order to assure homogeneity. The own stainless steel acts as stir bar as synthesis of the nanoparticles takes place in a vial placed on a magnetic stirrer.

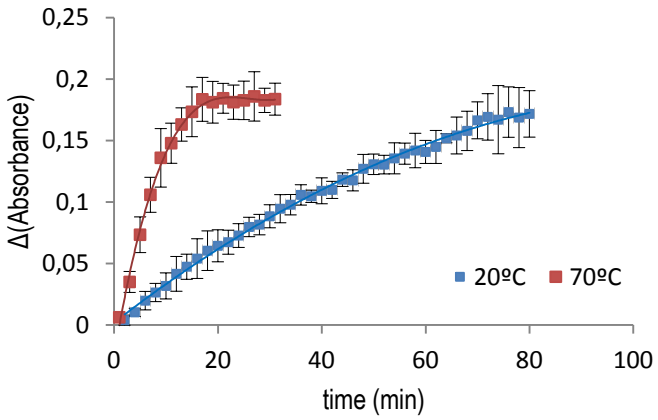

Figure 1. Kinetics of the stainless steel assisted synthesis of AuNPs performed in a UV/Vis cuvette under stirring at two different temperatures. The initial concentration of $HAuCl_4$ was 0.2 mg mL^{-1}. The graph represents the increment in absorbance of the maximum and the base of the peak.

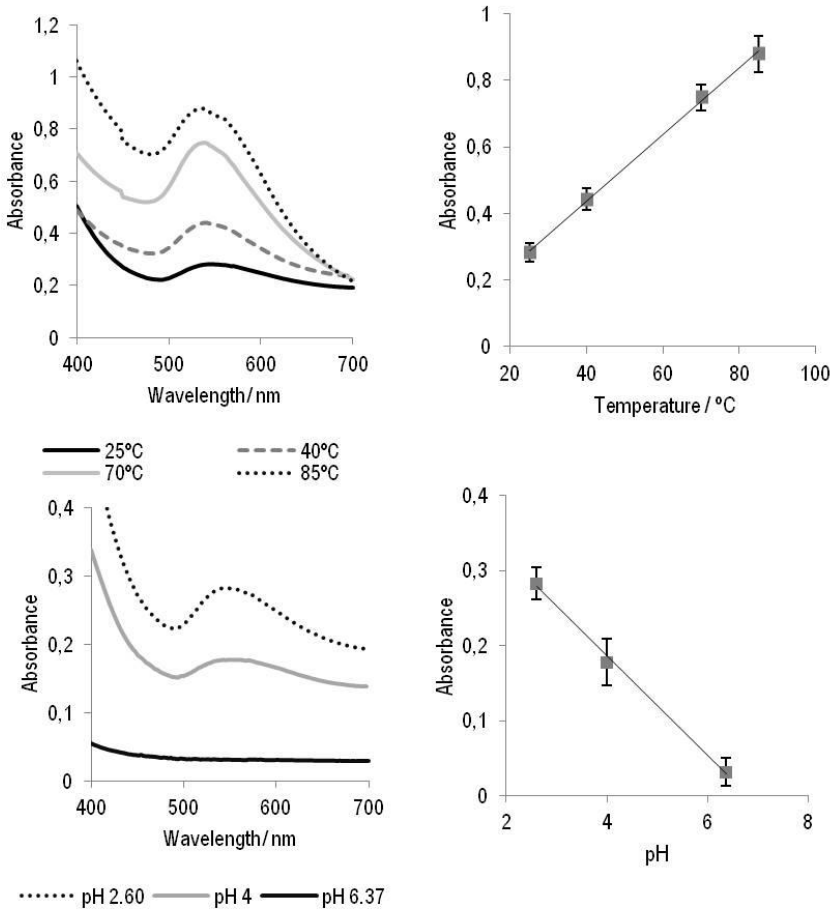

Figure 2. Effect of temperature for a reaction time of 3 min (top): the left image depicts the absorbance band of gold nanoparticles solution measured 3 min after introducing the stainless steel piece into the tetrachloroauric solution, the right image show the linear dependence of the band height with temperature conditions. Influence of the pH in the reaction for a temperature of 40ºC and 3 min of reaction (bottom): left image shows UV-vis spectra of gold nanoparticles solutions synthesized at different pH conditions, the right image depicts the dependence of band height with pH.

As can be seen in Figure 1, the reaction is almost completed after 70 minutes when it is performed at room temperature (~20ºC). In addition to the UV/Vis spectra evolution shown in Figure 1, in order to corroborate the quantitative

production of gold nanoparticles, synthesized gold nanoparticles were centrifuged at 10062 g. Then, the supernatant was analyzed showing no absorption at around 320 nm typical of Au(III) species (visually it can be also observed that the yellowish colour typical of Au(III) was not present).

The influence of temperature on the performance of the synthesis was studied. It was found that when temperature was increased until 70ºC, the reaction was accelerated to only 15 min until completion. Figure 2 (top) also depicts the dependence of formation rate of gold nanoparticles at four different temperatures, namely: 25, 40, 70 and 85ºC. As can be seen, the absorbance intensity of gold nanoparticles solutions for a reaction time of 3 minutes increases linearly when increasing temperature, which means that nanoparticles are being synthesized faster and a higher concentration of them are present in solutions at higher temperature for a certain time in comparison with those at lower temperatures.

Moreover, the effect of pH was studied in the range of 2.6-6.37. The chemical stability of $HAuCl_4$ constitutes the high pH limit. Figure 2 (bottom) shows the behavior observed, being low pH most appropriate to perform the synthesis since leads to high rates of formation of nanoparticles. A pH of 2.6 was selected for further experiments. As can be seen in Figure 2, at pH 6.37 the formation of gold nanoparticles has not started after 3 minutes of reaction, probably due to Au(III) instability. The pH of the solution was monitored during the synthesis of gold nanoparticles observing that pH value keeps almost constant around a value of 2 (using a starting $HAuCl_4$ solution of 200 mg dL^{-1}).

3.2. Microscopic characterization

The obtained gold nanoparticles have been characterized by scanning electron microscopy (SEM), transmission electron microscopy (TEM), and atomic force microscopy (AFM) in order to determine their size and shape. From the TEM

images, also the size distribution has been calculated (Figure 3). The obtained AuNPs appear homogeneous in shape and size and of polygonal yet nearly spherical shape. Of particular interest is also the fact that thus obtained AuNPs are well dispersed with neither aggregates nor rods observed. The average diameter of the nanoparticles was determined to be 20 ± 6 nm.

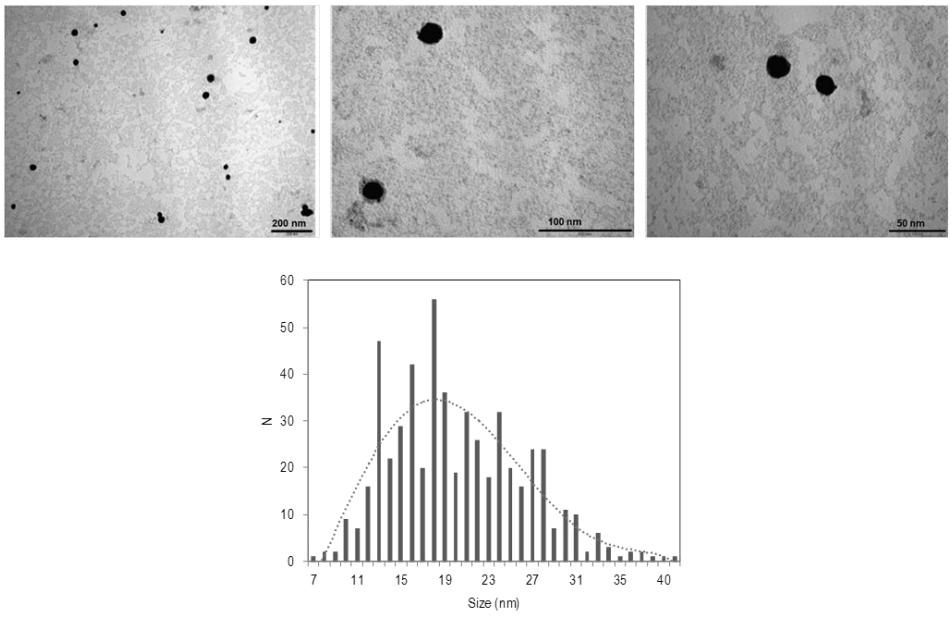

Figure 3. Top: TEM images of collected individual gold nanoparticles obtained during stainless steel assisted synthesis. Bottom: Size distribution of the particles resulting in d_{ave}= 20 ± 6 nm.

AFM studies have confirmed the nominal colloid size for the obtained nanoscale particles (Figure 4). The average size of the nanoparticles derived from AFM studies was 21 ± 9 nm, which is comparable to the results obtained using TEM.

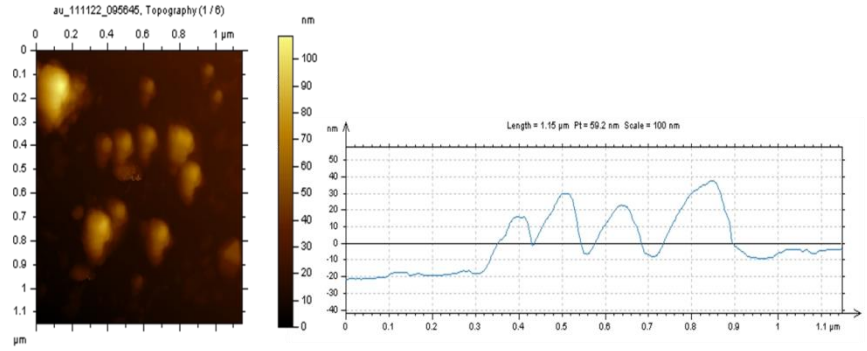

Figure 4. AFM image of the gold nanoparticles deposited on silicon wafer and dried measured in tapping mode with a resonance frequency 190 KHz and a force constant 48 Nm^{-1}. The right figure shows a representation of the topography of an image cross section of the picture.

3.3. Inductively coupled plasma atomic emission spectroscopy studies

Inductively coupled plasma optical emission spectroscopy (ICP-OES) was used to analyze which metals were present in solution after the synthesis. A systematic study of the solutions containing gold nanoparticles synthesized by introducing the stainless steel piece in a tetrachloroauric solution was performed at different pH values, as shown in Figure 5. It was found that after Au –forming the nanoparticles- Fe is the dominant metal species complemented by trace levels of Cr, Ni, Mn, and Mo(Fig. 5).

Additionally, the release of metals from stainless steel in acidic conditions was investigated by using HCl solutions at different pH values. Fe was found to be also released from the stainless steel in higher concentration as low as pH is. This behavior is similar to that observed with $HAuCl_4$ solutions. Nevertheless, Fe concentrations found in the case of HCl at the same pH than $HAuCl_4$ are lower. Thus, the oxidative character of $AuCl_4^-$ ions may play a role in the oxidation of Fe.

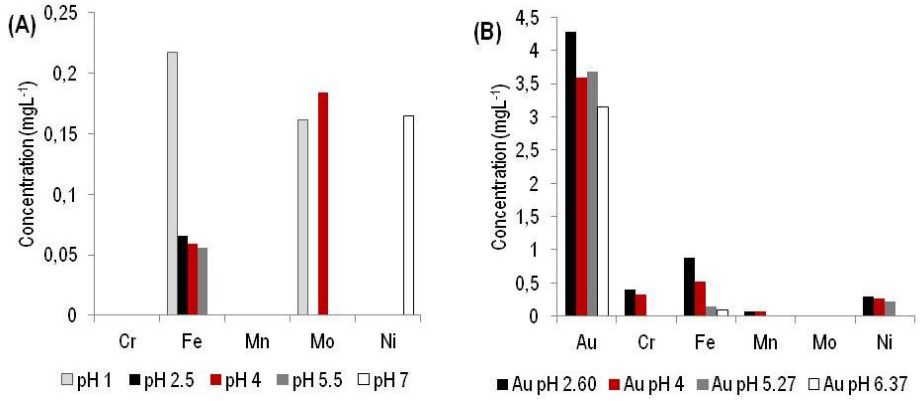

Figure 5. Inductively coupled plasma optical emission spectroscopy (ICP-OES) analysis of metals determined in aqueous solutions of (A) HCl, and (B) $HAuCl_4$ at different pH levels after insertion of a stainless steel substrate.

3.4. Energy dispersive X-ray spectroscopic characterization

In order to investigate if metals released from the stainless steel surface are subsequently incorporated into the AuNPs, EDX studies were performed corroborating that the obtained nanoparticles were only composed of gold. When recording EDX spectra of AuNPs collected while the reaction is still in progress, gold salt residues are still evident as indicated by chlorine ions present within salt crystals. In contrast, EDX spectra collected at gold nanoparticles after the reaction was complete only revealed a gold line.

3.5. Proposed mechanism of the reaction

Stainless steel promotes the reduction of Au(III) to Au(0) as nanoparticles. ICP-OES analysis proved the release of metals from the stainless steel mesh. The oxidative character of $AuCl_4^-$ ions may play a significant role in their oxidation and excretion since higher amounts of Fe are released into a $HAuCl_4$ solution as compared to neat HCl solution of the same pH. Once the stainless steel piece

was analyzed by EDX, it was found that in addition to the formation of AuNPs in solution, a small amount of AuNPs were also formed at their surface.

In order to corroborate the hypothesis of the proposed reaction mechanism, a qualitative assay was performed adding 1,10-phenantrolin (a coloured redox indicator) to the solution during the synthesis, which results in the formation of an orange-coloured complex upon the insertion of the stainless steel substrate into the acidic solution of both HCl and $HAuCl_4$, which in turn confirms the release of Fe(II) into the solution. Thus, one possible mechanism of formation of AuNPs is the reduction of Au(III) by the electron liberated from the oxidation of stainless steel Fe(0) to Fe(II) in higher amounts as well as due to other metals (Ni, Cr) yet at to a lesser extent.

In addition, the efficiency of iron mesh to produce gold nanoparticles similarly to stainless steel production was proved. In this case, the reduction of Au(III) to Au(0) as a thin gold layer above the iron surface was observed, as previously reported [34], while stainless steel yields nanoparticles with a reproducible size instead of a gold layer. On the other hand, the reaction mainly occurs in the bulk of the solution. This fact leads to the hypothesis that hydrogen, which is formed as a consequence of the reduction of protons of the acidic media mediated by the steel substrate, reduces $AuCl_4^-$ ions yielding AuNPs (Fig. 6). The formation of gold nanoparticles via hydrogen has been previously described in literature [30], although it yields AuNPs that are significantly larger than those synthesized with the novel methodology presented herein. If we evaluate the potential of reduction of the pairs H^+/H_2 (E=0 V), Fe^{2+}/Fe^0 (E=-0.440 V), Ni^{2+}/Ni^0 (E=-0.250 V) and Cr^{2+}/Cr^0 (E=-0.912 V), it can be hypothesized that during the oxidation of these metals when released from the stainless steel the reduction of H^+ ions present in the acidic solution may take place. When monitoring the pH of the solution during the reaction we have observed that the pH was maintained almost constant during the formation of the gold nanoparticles at

acidic value (around 2), thus -in order to maintain the pH value- H_2 formed may be oxidized again to H^+ while reducing the remaining Au(III) in solution. An evaluation of the potential of such reaction showed that this reaction could take place since $E(AuCl_4^-/Au)=1.002$ V and $E(H^+/H_2)=0$ V.

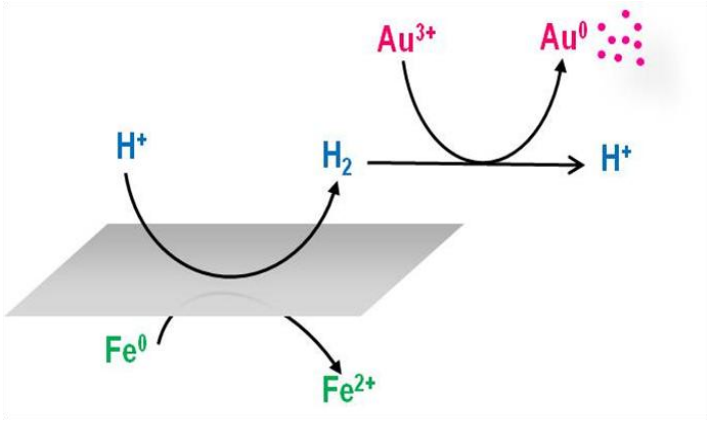

Figure 6. Proposed scheme of stainless steel mediated AuNPs synthesis mechanism.

The performance of the reaction appears best for stainless steel as the generation of H_2 mediated by it appears to occur at just the right rate, and is lower than e.g., in the case of using iron metal, which leads to the formation of instable nanoparticles that do not remains in solution (data not shown).

If only H_2 is bubbled through a solution of $HAuCl_4$ in absence of a stainless steel substrate at ambient conditions, the reduction of Au(III) is observed, yet there is no formation of gold nanoparticles evident. Instead, if H_2 is bubbled through the solution in addition to inserting a stainless steel substrate, gold is reduced at the end of the polymer tube bubbling H_2 into the solution instead of generating AuNPs. Consequently, the release rate of H_2 mediated by stainless steel plays a crucial role for successfully synthesizing stable AuNPs at ambient conditions. Hence, we may summarize the reaction as

$2\ HAuCl_4 + 3\ H_2 \rightarrow 3\ Au\ (nanoparticles) + 8\ HCl$ (1)

with a global standard redox potential of ΔE_o = 1.002 V, which implies that the reaction will spontaneously evolve (Fig. 6).

3.6. Stability of bare gold nanoparticles

A main characteristic of nanoparticles is that the number of atoms at the surface is higher than the number of internal atoms. Consequently, the stability of NPs depends on the number of surface atoms, i.e., for stable equilibrium conditions there must be sufficient atoms at the surface to stabilize the colloid (providing charges), yet enough atoms within the nanoparticle core to provide the required thermodynamic stability. Apparently, the conditions provided by the present synthetic rout facilitates slow AuNP growth until an optimal size is achieved, thus enabling stable positively charged gold nanoparticles with a narrow size distribution.

As an exceptional feature of this novel synthesis strategy, the obtained gold nanoparticles proved to be stable if stored at 4ºC for over four months. At room temperature, thus obtained AuNPs slowly precipitate at the bottom of the vial (i.e., the solution still remains stable over a period of approximately 20 days) due to agglomeration. During conventional AuNPs synthesis using e.g., citrate as reducing agent, an additional clean-up step is required for removing residual ligands. It has been described that the stability of thus purified 20-nm AuNPs synthesized with citrate is 20 days stored at 4ºC in darkness, and that aggregates are already observed after 6 days of storage at room temperature [15]. Thus, the AuNPs stability against aggregation achieved with the present method is improved as compared to conventional citrate reduction after ligand removal. The presence of ions in solution, which may interact with the positively charged nanoparticles will influence their stability. While there are no citrate ligands present in the synthesis bound to the nanoparticle surface, chloride ions

are in abundance, and may shield thus obtained nanoparticles. It is thus hypothesized that a chloride shell prevents nanoparticle agglomeration and facilitates the stabilization of the solution due to the achieved spacing between individual NPs. Finally, low ionic strength media support the stability of NPs in solution [35], which is also the case during the present synthesis.

3.7. Analytical potential of bare gold nanoparticles

Gold nanoparticles have been extensively related to Analytical Science and Technology in two complementary approaches. On the one hand, they have been the objects of the analysis by applying a variety of analytical techniques for their characterization, as it has been shown in the previous sections of this paper.

On the other hand, gold nanoparticles have been successively used as useful tools to implement a variety of functions in (bio)chemical measurement processes (i.e. as components of electrodes, as SERS substrates, as components of (bio)sensors, etc).

Two great advantages of the use of bare gold nanoparticles as analytical tools arise from the fact that there are not potential interferences from the excess of reductant used in their synthesis than act as ligands (i.e. citrate) in the suspension; and that those bare gold nanoparticles are produced with a narrow size distribution. Thus, two crucial analytical properties attributed to analytical processes involving gold nanoparticles are enhanced: selectivity and precision.

The analytical potential of these novel bare gold nanoparticles as SERS substrates has been proved. They enable the determination of carboxylated single walled carbon nanotubes by surface enhanced Raman scattering (SERS) spectroscopy mediated by the nanoparticles. The enhancement factor, calculated from the Raman signal of 5 μL of 100 mgL^{-1} solution of c-SWNTs

compared to that obtained when 5 µL of a 8 mgL^{-1} solution is placed on gold nanoparticles substrate, was found to be 39±1.

The analytical results obtained from two analytical processes involving citrate surrounded and bare gold nanoparticles as SERS substrates were compared. The same analytical procedure was carried out with the two types of gold nanoparticles. As it can be seen in Figure 7, at higher carbon nanotube concentrations citrate gold nanoparticles showed a slightly better performance in terms of enhancement, although the reproducibility of those membranes were less accurate, being observed small aggregates of nanoparticles.

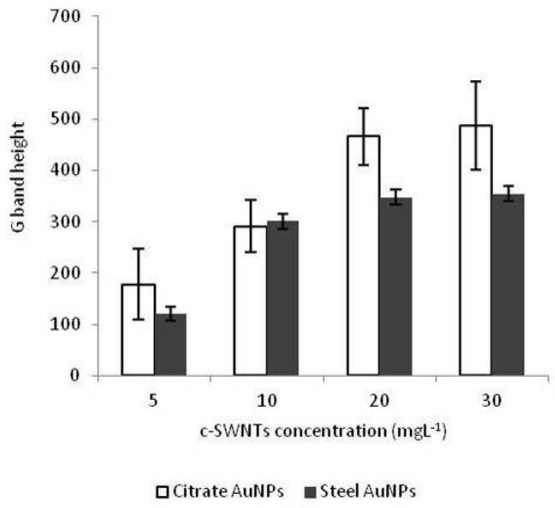

Figure 7. Comparison of SERS response, in terms of carbon nanotube G band height, at different concentrations of c-SWNTs provided by citrate-coated and stainless steel assisted synthesized gold nanoparticles.

The similar behavior observed for citrate reduced gold nanoparticles and those obtained through the proposed methodology suggest that they are suitable for being used as SERS substrate for the determination of several analytes in different analytical applications.

4. Conclusions

The main contribution of this paper is the use of a solid reducing agent –a stainless steel piece- which can be recovered from the solution, for the production of bare gold nanoparticles. The process is simple and easily scalable. 20 nm size, nearly spherical shaped nanoparticles are obtained, which have been characterized by SEM, TEM, AFM and EDX analysis. Our approach leads to bare gold nanoparticles without any ligand in their surface, obtained through an inexpensive and environmentally friendly synthesis procedure avoiding the use of harsh chemicals. A highlight of the procedure is that leads to highly stable gold nanoparticles –for more than four months when stored at 4ºC- despite the absence of stabilizing ligands on their surface, just mediated by the chloride ions present in solution which may shield thus obtained nanoparticles.

Gold nanoparticles obtained through this novel procedure are good candidates for be used as SERS substrate since they showed a similar behavior than that synthesized with citrate when applied to the SERS determination of carboxylated carbon nanotubes. The use of these bare gold nanoparticles in Analytical Science and Technology provides analytical processes with enhanced sensitivity and selectivity, owing to their stability, the absence of potential interferences from the excess of reductant and their narrow size distribution.

Acknowledgments

A.I. López-Lorente, B.M. Simonet, and M. Valcárcel wish to thank Spain's Ministry of Innovation and Science for funding Project CTQ2011-23790 and Junta de Andalucía for Project FQM4801. A.I. López-Lorente also wishes to thank the Ministry for the award of a FPU Research Training Fellowship (Grant AP2008-02939), and gratefully acknowledges funding of her stay in Germany at the University of Ulm to conduct the research reported in this paper. The authors

also thank the Focused Ion Beam Center UUlm at the University of Ulm for SEM and EDX measurements.

References

[1] R.A. Rippel, A.M. Seifalian, J. Nanosci. Nanotechnol. 11 (2011) 3740-3748.

[2] W. Lu, A.K. Singh, S.A. Khan, D. Senapati, H. Yu, P.C. Ray, J. Am. Chem. Soc. 132 (2010) 18103-18114.

[3] G. Cao Nanostructures and nanomaterials. Synthesis, Properties & Applications, Imperial CollegePress, London, 2004.

[4] J. Zhou, J. Ralston, R. Sedev, D.A. Beattie, J. Colloid Interface Sci. 331 (2009) 251-262.

[5] J. Turkevich, P.C. Stevenson, J. Hillier, Discuss. Faraday Soc. 11 (1951) 55-75.

[6] G. Frens, Nature Phys. Sci. 241 (1973) 20-22.

[7] K.C. Grabar, R.G. Freeman, M.B. Hommer, M.J. Natan, Anal. Chem. 67 (1995) 735-743.

[8] H. Mühlpfordt, Experientia 38 (1982) 1127-1128.

[9] J.W. Slot, H.J. Geuze, Eur. J. Cell Biol. 38 (1985) 87-93.

[10] G. Schmid, Chem. Rev. 92 (1992) 1709-1727.

[11] M. Brust, M. Walker, D. Bethell, D.J.Schiffrin, R. Whyman, J.Chem. Soc. Chem. Commun. (1994) 801-802.

[12] E.C. Stathis, A. Fabricanos, Chem. Ind. 27 (1958) 860-861.

[13] A. Fabrikanos, S. Athanassiou, K.H. Leiser, Z. Naturforsch 186 (1963) 612-617.

[14] R.G. DiScipio, Anal. Biochem. 236 (1996) 168-170.

[15] S.K. Balasubramanian, L.Yang, L.Y.L. Yung, C.N. Ong, W.Y. Ong, L.E. Yu, Biomaterials 31 (2010) 9023-9030.

[16] U. Kreibig, L. Genzel, Surf. Sci. 156 (1985) 678-700.

[17] P.L. Redmond, X. Wu, L. Brus, J. Phys. Chem. C 111 (2007) 8942-8947.

[18] N. Pernodet, X. Fang, Y. Sun, A. Bakhtina, A. Ramakrishnan, J. Sokolov, A. Ulman, M. Rafailovich, Small 2 (2006) 766-773.

[19] C. Uboldi, D. Bonacchi, G. Lorenzi, M.I. Hermanns, C. Pohl, G. Baldi, R.E. Unger, C.J. Kirkpatrick, Part. Fibre Toxicol. 6 (2009) 18.

[20] S.F. Sweeney, G.H. Woehrle, J.E. Hutchison, J. Am. Chem. Soc. 128 (2006) 3190-3197.

[21] T. Panda, K. Deepa, J. Nanosci. Nanotechnol. 11 (2011) 10279-10294.

[22] J.Y. Song, H.K. Jang, B.S. Kim, Process Biochem. 44 (2009) 1133–1138.

[23] K. Mallick, M.J. Witcomb, M.S. Scurrell, Appl. Phys. A 80 (2005) 395-398.

[24] Z. Wei, C.J. Liu, Mater. Lett. 65 (2011) 353–355.

[25] F. Mafune, J. Kohno, Y. Takeda, T. Kondow, H. Sawabe, J. Phys. Chem. B 105 (2001) 5114-5120.

[26] V. Amendola, M. Meneghetti, J. Mater. Chem. 17 (2007) 4705-4710.

[27] H. Ma, B. Yin, S. Wang, Y. Jiao, W. Pan, S. Huang, S. Chen, F. Meng, Chem. Phys. Chem. 5 (2004) 68-75.

[28] V. Amendola, S. Polizzi, M. Meneghetti, J. Phys. Chem. B 110 (2006) 7232-7237.

[29] C.H. Wang, C.C. Chien, Y.L. Yu, C.J. Liu, C.F. Lee, C.H. Chen, Y. Hwu, C.S. Yang, J.H. Jeg, G. Margaritondo, J. Synchrotron Radiat. 14 (2007) 477–482.

[30] G. Merga, N. Saucedo, L.C. Cass, J. Puthussery, D. Meisel, J. Phys. Chem. C 114 (2010) 14811-14818.

[31] A.I. López-Lorente, B.M. Simonet, M. Valcárcel, Analyst 137 (2012) 3528-3534.

[32] A.I. López-Lorente, B.M. Simonet, M. Valcárcel, Talanta 105 (2013) 75-79.

[33] S. Eustis, M.A. El-Sayed, Chem. Soc. Rev. 35 (2006) 209-217.

[34] J. Feng, M. Sun, H. Liu, J. Li, X. Liu, S. Jiang, J. Chromatogr. A 1217 (2010) 8079–8086.

[35] L.A. Dykman, V.A. Bogatyrev, Russ. Chem. Rev. 76 (2007) 181-194.

Capítulo 4

Continuous flow synthesis and characterization of tailor-made bare gold nanoparticles for analytical applications

Submitted to Microchimica Acta

Springer Link

Microchimica Acta

Submitted

Continuous flow synthesis and characterization of tailor-made bare gold nanoparticles for analytical applications

A. I. López-Lorente[1], M. Valcarcel[1], B. Mizaikoff[2]

[1]*Department of Analytical Chemistry, University of Córdoba, E-14071 Córdoba, Spain.*

[2]*Institute of Analytical and Bioanalytical Chemistry, University of Ulm, Ulm, Germany.*

This paper describes the synthesis of bare gold nanoparticles in a stainless steel continuous flow tubular reactor using tetrachloroauric acid as precursor without using a classical reducing agent. Gold (III) is reduced by stainless steel to form gold nanoparticles which are collected at the end of the coil. A single-phase system, which generates dispersed nanoparticles without the presence of residual reducing agents in their surface, is proposed. By controlling the conditions of the synthesis (i.e. flow rates, temperature) the size of the nanoparticles can be tuned. The reproducibility of the synthesis was investigated, relative standard deviation of both the wavelength of the maximum of the peak and intensity of Surface Plasmon Resonance were calculated and found to be 0.15% and 6.5%, respectively. We have demonstrated that the flow synthesis is an excellent alternative to produce bare, stable, tailor-made gold nanoparticles in an efficiently way that showed good properties for their use as surface enhanced Raman scattering (SERS) substrates. In fact, those bare gold nanoparticles can be used for the SERS determination of carboxylated single walled carbon nanotubes.

Keywords: bare gold nanoparticles, flow synthesis, microreactor, characterization, stainless steel, surface enhanced Raman spectroscopy.

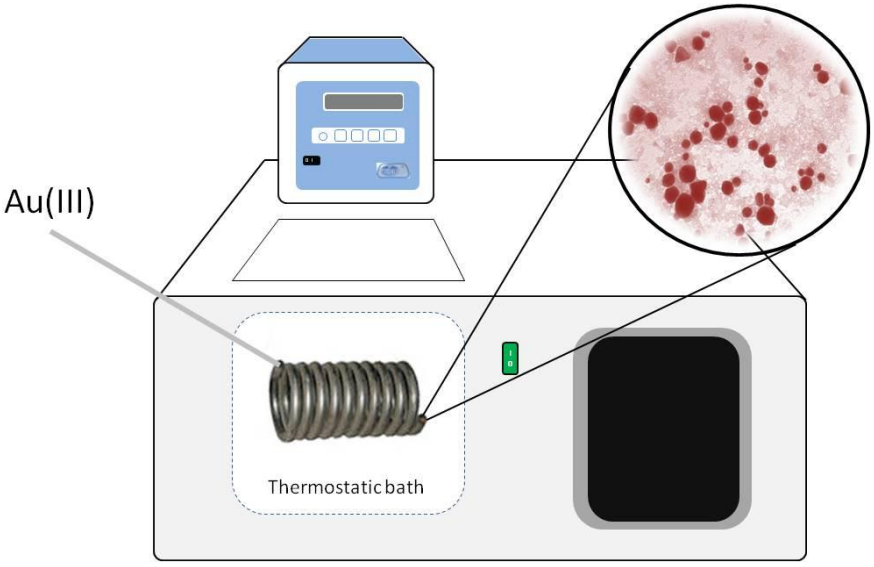
Au(III)
Thermostatic bath

1. Introduction

Gold nanoparticles (AuNPs) have been widely used in diverse fields due to the fascinating properties they exhibit [1]. Increasing interest has been, thus, attracted to their synthesis procedures [2-10]. Generally, nanosize can be reached by the so called top-down and bottom-up strategies. Top-down strategies are based on methodologies which achieve nanosized materials from macromaterials, while bottom-up strategies rely on the creation of complex nanostructures from atomic or molecular functional elements. AuNPs are most often prepared by reduction of gold(III) halides by using chemical reducing agents in solution such as sodium citrate [11-13], sodium borohydride [14, 15], ascorbic acid [16], cyanoborohydride [17], *etc.*, which usually requires the addition of stabilizers or ligands in order to preserve nanoparticles. Nanoparticles are obtained usually in a batch process, which is often limited to small-scale synthesis, and also lacks precise control over the mixing, nucleation and growth process, and thus final particle size or size distribution [18].

Continuous-flow systems have been synergistically combined with nanoparticles for the preconcentration of analytes [19]. They are promising for continuous synthesis of nanoparticles since microreactors are more productive and able to improve the homogeneity of reaction solutions, which leads to a more uniform product [20]. Another advantage is than can be easily scaled-up, shortening the development time from laboratory to commercial production [21]. In addition, it is a more energy efficient process when compared with batch synthesis systems reducing energy consumption of heating-up and cooling-down intermittently [18]. However, microfluidic devices have proven to be susceptible to irreversible blockage during nanoparticle synthesis [22-25]. Silver nanoparticles [26], star-like core-shell AuAg nanoparticles [27] or thiol functionalized AuNPs [28] have been prepared using microfluidic systems. Zhao *et al* [18] have summarized developments in the synthesis of nanoparticles in microfluidic reactors.

Recently, Lohse *et al.* [22] have developed a reactor system which facilitates the aqueous gram-scale synthesis of a variety of functionalized AuNPs by mixing of a growth solution and a reaction initiator solution, which will require well mixing of solutions [29].

In this paper, we demonstrate the synthesis of bare gold nanoparticles from tetrachloroauric acid in a stainless steel tubular flow reactor, where the own stainless steel acts as reducing agent, avoiding mixing of two or more solutions. We have previously demonstrated the possibility of synthesizing such AuNPs without ligands in their surface using stainless steel as solid reducing agent in batch process [30]. Unlike the commonly employed methods for the synthesis of AuNPs, we propose a single-phase system, which generate dispersed nanoparticles without the presence of residual reducing agents in their surface. By controlling the conditions of the synthesis (i.e. flow rates, temperature) the size of the nanoparticles can be tuned. A highlight of the procedure is its simplicity and the high throughput production of AuNPs.

2. Experimental

2.1. Materials and reagents

$HAuCl_4$ (Sigma Aldrich) was used to synthesize the gold nanoparticles. Before synthesis the material were washed with a mixture of nitric acid and hydrochloric acid purchased from Panreac (Barcelona, Spain). Stainless steel coil 1.5 m length with a 1/8'' OD and 2 mm ID was supplied by Analisis Vinicos (Tomelloso, Spain).

2.2. Equipment

UV/Vis measurements were performed using a halogen lamp as excitation and the monochromator and photonic detector of a PTI fluorescence Master system as a detector. Transmission electron microscopy (TEM) images were acquired with a JEOL JEM-1400 transmission electron microscope. Energy dispersive X-ray analysis (EDX) was performed with an Inca energy microanalysis system coupled to a JEOL JEM 2010 high resolution transmission electron microscope, with a SiLi window (SATW) detector and a resolution of 136 eV.

For the flow synthesis of the gold nanoparticles a Gilson Minipuls 3 peristaltic pump was employed as well as a thermostatic bath (Frigiterm model, Selecta).

2.3. Stainless-steel assisted flow synthesis of gold nanoparticles

$HAuCl_4$ solution is introduced into a stainless steel tubular coil (1/8'' o.d., 2 mm i.d., 1.5 m length) using a peristaltic pump. Figure 1 shows a scheme of the experimental setup. The flow rates were controlled by using the peristaltic pump in a range between 0.041 and 3.63 mL min^{-1}. The stainless steel coil is immersed in a thermostatic bath in order to control the reaction temperatures which were set between 40-80ºC. Stainless steel assists the reduction of gold(III) into gold nanoparticles. The product was collected at the end of the tubular coil in a glass vial and stored at 4ºC. After the reaction, the stainless steel tube was cleaned with a 1:3 mixture of nitric and hydrochloric acid in order to remove possible remainders of gold on the tube walls, and further rinsed with water and dry with air.

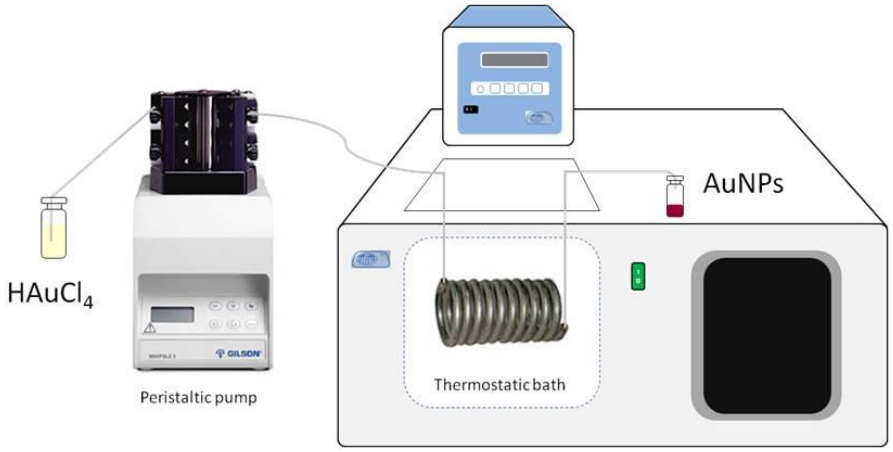

Figure 1. Experimental setup for the flow synthesis of gold nanoparticles in a tubular reactor immersed in a thermostatic bath.

2.4. Characterization of synthesized gold nanoparticles

Transmission electron microscopy images were recorded with a JEOL JEM-1400 microscope. A drop of the gold nanoparticle suspension obtained was drop-cast on a copper TEM grid with a Carbowax forward. The particle size distribution was analyzed by measuring between 200 and 1700 nanoparticles based on TEM micrographs using ImageJ Software.

The ultraviolet-visible spectra of gold nanoparticles were recorded from a solution prepared by diluting 25 µL of as-synthesized solution with 100 µL of ultrapure water. Measurements were carried out in an ultramicro Hellma cell with an optical length of 10 mm, measuring the difference between the absorbance at the maximum of the peak and the base of the peak, in order to amend baseline shifts between measurements.

3. Results and discussion

The proposed setup for the synthesis of gold nanoparticles is entirely assembled from commercially available components, namely: a peristaltic pump, thermostatic bath, polytetrafluoroethylene (PTFE) connecting tubes and a stainless steel coil, which leads the formation of gold nanoparticles. Figure 1 shows a scheme of the experimental setup. Variables such as flow rate or temperature have been evaluated between 0.041 and 3.63 mL min^{-1} and 40-80ºC, respectively.

As tetrachloroauric acid water solution is introduced by the peristaltic pump into the tubular reactor immersed in the thermostatic water bath at a designed temperature, the color of the solution turned from yellowish to red, indicating the formation of gold nanoparticles. Gold nanoparticles did not need of further stabilizing agent for long-term storage as they stay stable in solution when stored at 4ºC. The formation of gold nanoparticles was confirmed by transmission electron microscopy. Figure 2 shows TEM images of obtained gold nanoparticles obtained at flow rates of 0.2407, 0.556 and 0.7662 $mLmin^{-1}$. Temperature in these cases was set to 60ºC and initial concentration of $HAuCl_4$ $1gL^{-1}$.

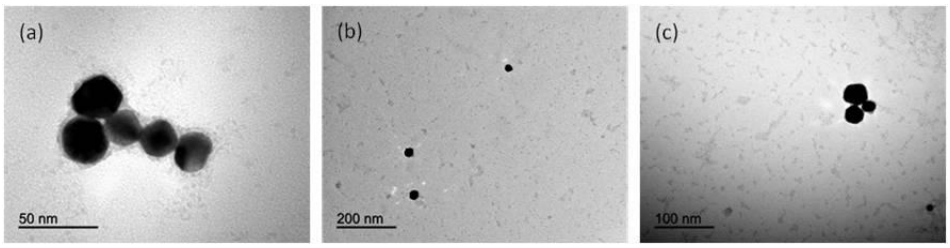

Figure 2. TEM images of gold nanoparticles obtained at a flow rate of (a) 0.2407 $mLmin^{-1}$, (b) 0.556 $mLmin^{-1}$, (c) 0.7662 $mLmin^{-1}$. Temperature was set to 60ºC and initial concentration of $HAuCl_4$ $1gL^{-1}$.

3.1. Study of the concentration of gold precursor

The concentration of tetrachloroauric solution employed as gold precursor was studied in the range 0.5-2 gL^{-1}. The concentration of gold nanoparticles in solution was shown to be proportional to the amount of gold(III) in the initial solution. This indicates that the synthesis of gold nanoparticles is quantitative. At higher concentrations the reduction of Au(III) is not complete, finding that if the solution containing the synthesized gold nanoparticles is ultracentrifugated at 10062 g, the supernatant still contains Au(III) ions reflected in a slight yellowish colour in contrast to uncolored supernatants observed in the other cases.

3.2. Study of the influence of flow rate

The flow rate, flow pattern, and reactor temperature could affect the size and size distribution of obtained gold nanoparticles. The influence of flow rate has been investigated in the range 0.04-3.63 $mLmin^{-1}$. As it can be seen in Figure 3a and 3b, the intensity of absorbance of gold nanoparticles solutions varies with flow rate. As slow as the flow rate is, the higher absorbance intensity is observed, meaning a major concentration of gold nanoparticles synthesized. The resident time of the fluids in the tube reactor, τ, is a critical factor leading the formation of gold nanoparticles. When increasing the flow rate, the resident time of precursor solution in the reactor is fewer, as it can be seen in Table 2 which shows the resident times calculated for the different flow rates based on the length of the reactor (1.30 m). At higher flow rates the resident time of the precursor solution is not enough to quantitatively reduce Au(III) into Au(0) in form of gold nanoparticles. Flow rates as from 3.63 mL min^{-1} did not result in the formation of gold nanoparticles.

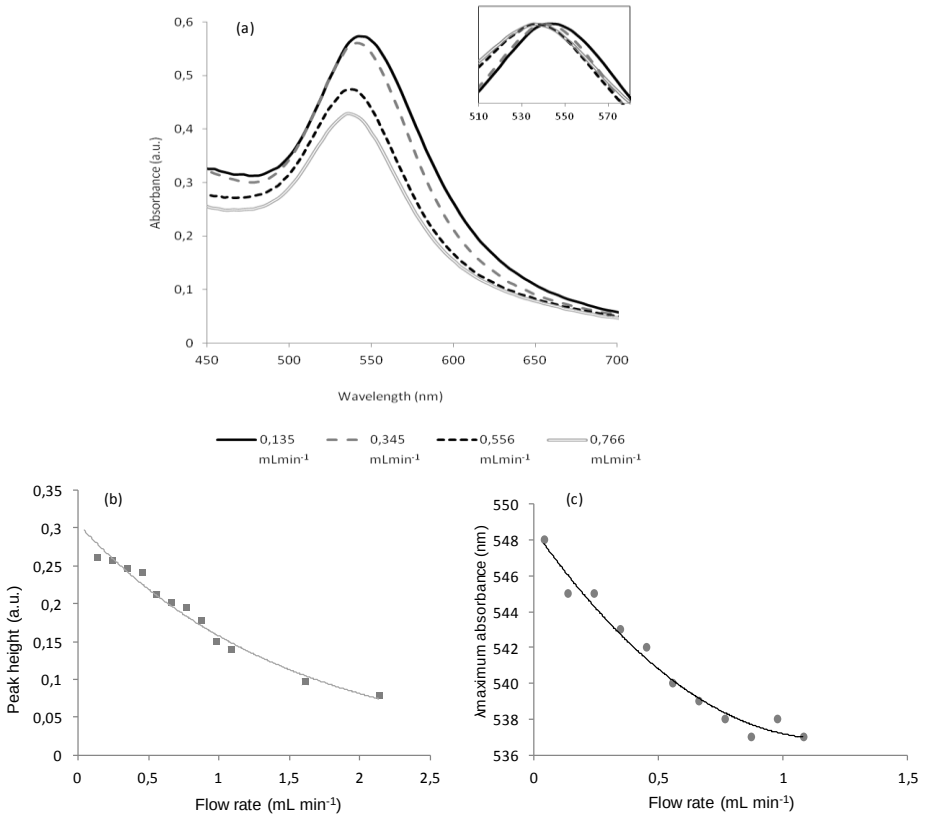

Figure 3. (a) Uv-vis spectra of solutions of gold nanoparticles obtained through the proposed synthesis at a temperature of 60ºC at different flow rates: 0.135, 0.345, 0.556 and 0.766 mL min^{-1}. The inset shows the maximum of the peak normalized where a shift in wavelength with flow rate can be observed. (b) Influence of flow rate on absorbance intensity of gold nanoparticles dispersions, which is related to their concentration in solution. Nanoparticles were synthesized at different flow rates at a temperature of 60ºC. (c) Influence of flow rate on the wavelength of the Surface Plasmon Resonance band of gold nanoparticles synthesized at 60ºC

In addition to the reduced formation of gold nanoparticles, a shift in the wavelength of the Surface Plasmon Resonance (SPR) peak is also observed (see Figure 3a inset and 3c). At higher flow rates seeds of gold nanoparticles are formed, although the less extent time of resident prevent from nucleation in order to obtain larger nanoparticles, which is confirmed by wavelengths about

535 nm. On the other hand, at slower flow rates, the nucleation process is dilatory leading to larger gold nanoparticles. In this case a bathochromic shift in the surface Plasmon band is observed.

3.3. Study of the influence of temperature

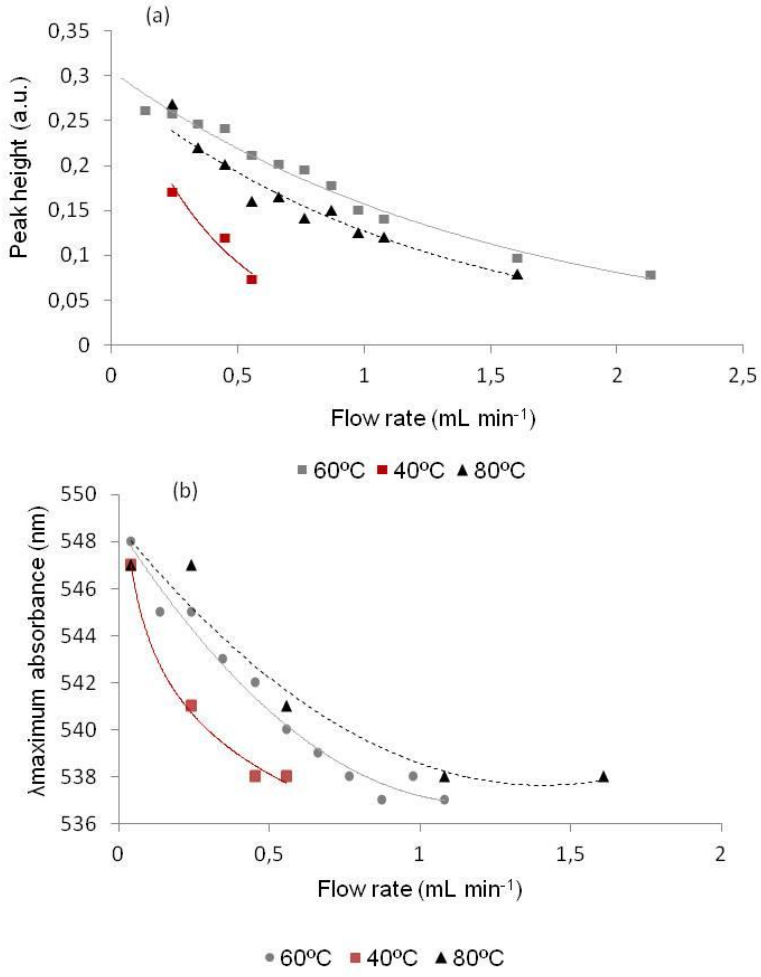

Figure 4. (a) Influence of flow rate on absorbance intensity of gold nanoparticles solutions synthesized at 40, 60 and 80ºC. (b) Influence of flow rate on the wavelength of the surface Plasmon resonance band of gold nanoparticles synthesized at 40, 60 and 80ºC

Moreover, the influence of temperature of the reactor on the performance of the synthesis procedure has been investigated. Three set temperatures, namely 40, 60 and 80ºC have been employed to obtain gold nanoparticles at various flow rates. The tendencies observed at 60ºC for absorbance intensities and SPR wavelengths are reproduced at 40 and 80ºC. Again when increasing flow rate the amount of gold nanoparticles obtained is smaller. At a fix flow rate, it can be seen in Figure 4a, that at 40ºC the formation of gold nanoparticles occurs in less extent than for 60 or 80ºC, which provided closer values of absorbance intensity. With regards to the wavelength of peak maximum, again values are similar for 60 and 80ºC temperatures, while at 40ºC smaller wavelengths are observed for a certain flow rate when compared to the other temperatures studied, which means smaller nanoparticles.

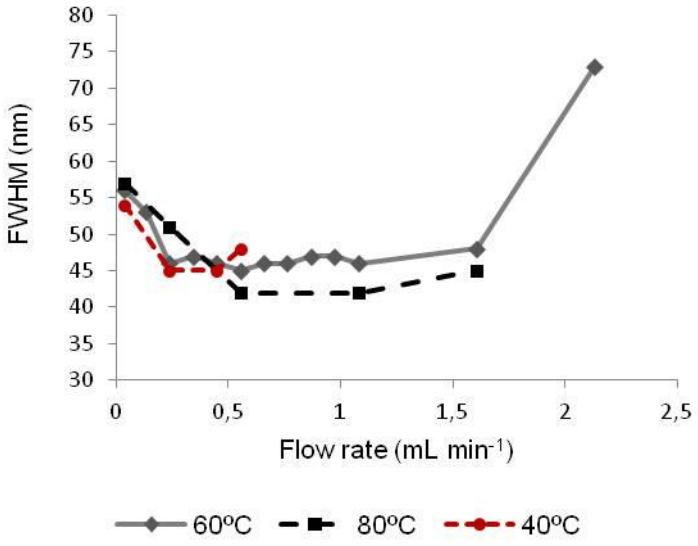

Figure 5. Calculated full width at half-maximum from the UV-Vis spectra of gold nanoparticles solutions obtained at different temperatures.

The values of full width at half-maximum (FWHM) for samples at various flow rates and temperatures are shown in Figure 5. As it can be seen, there is a broadening in absorbance at high flow rates which suggests that nanoparticles became polydisperse. The lower values of FWHM are observed at medium flow rates values for the three temperatures, indicating that at those conditions nanoparticles with a narrower size distribution are obtained. At slow flow rates, polydispersity is slightly higher due to the major residence time in the reactor which could destabilize larger nanoparticles.

3.4. Flow pattern characteristics

The following equation was used to determine the flow patterns, Reynolds numbers, Re, of the fluids:

$$Re = uD/\nu$$

Where u is the linear flow velocity, D is the inert diameter of the tube, and ν is kinematic viscosity of the fluid. In this study, the fact that solutes did not drastically change the viscosity of the fluid has been assumed and the values tabulated for water has been employed. Table 1 shows the values of Reynolds number calculated at each temperature and flow rate investigated. In all the cases studied the flows were laminar since values of Re were below 2100. Therefore, the velocity profile is parabolic and those nanoparticles formed in the center move faster than those in the wall region. This parabolic behavior could be the responsibly of the polydispersity observed when increasing the flow rate. It also agrees with the observation of higher polydispersity of obtained gold nanoparticles at higher temperatures.

Table 1. Volumetric and linear flow rates, Reynolds numbers and resident times of the fluids in the flow tubular reactor.

Flow rate (mL min^{-1})	u ($m\ s^{-1}$)·10^{-3}	Re (T=40ºC)	Re (T=60ºC)	Re (T=80ºC)	τ (s)
0.041	0.217	0.661	0.916	1.192	5975.24
0.135	0.719	2.186	3.028	3.941	1807.11
0.240	1.276	3.881	5.376	6.996	1018.05
0.345	1.834	5.576	7.724	10.052	708.63
0.450	2.392	7.270	10.071	13.107	543.45
0.556	2.949	8.965	12.419	16.162	440.72
0.661	3.507	10.660	14.767	19.217	370.66
0.766	4.064	12.355	17.114	22.272	319.81
0.871	4.622	14.049	19.462	25.328	281.24
0.976	5.179	15.744	21.810	28.383	250.96
1.081	5.737	17.439	24.157	31.438	226.57
1.607	8.525	25.913	35.896	46.714	152.48
2.132	11.313	34.386	47.634	61.990	114.90

3.5. Microscopic characterization

Synthesized gold nanoparticles solutions were investigated by TEM microscopy in order to calculate the average size of nanoparticles as well as their size distribution. Figure 6 shows TEM photographs of gold nanoparticles obtained at different conditions and their corresponding size distribution histograms. From the TEM images the disaggregation state of nanoparticles can be inferred. No aggregates are observed in the solutions, consisting of separated gold nanoparticles. Gold nanoparticles obtained at 80ºC and 0.240 mL min^{-1} flow rate are more polydisperse than those obtained at 40 or 60ºC, as the size distribution histogram at such conditions shows. This observation from microscopy images agrees with the values of FWHM obtained through UV-Vis spectroscopy measurements for that condition (Figure 5).

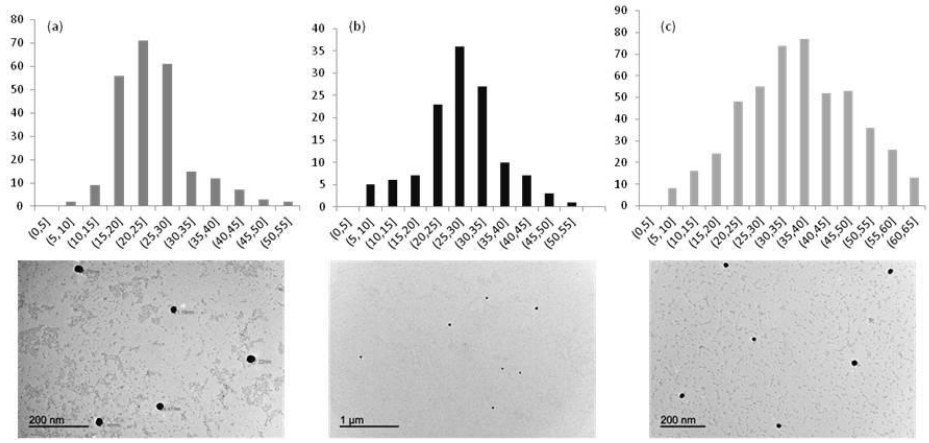

Figure 6. TEM image and the corresponding particle size distribution analysis of the Au nanoparticles synthesized in the tubular reactor (a) 60ºC 0.135 mL min^{-1}, (b) 40ºC 0.556 mL min^{-1}, (c) 80ºC 0.240 mL min^{-1}.

The average diameter of synthesized gold nanoparticles has been calculated from TEM images, as well as the standard deviation. Table 2 summarizes the values found for nanoparticles obtained at different conditions of flow rate and temperature. Size calculated from TEM images agree with UV-Vis measurements showing higher values of wavelengths those nanoparticles with larger diameter.

Energy dispersive X-ray analysis (EDX) was performed which revealed that there are small amounts of iron and chromium released from stainless steel in the solution. It could be thought that part of the released iron could have been incorporated into gold nanoparticles, in such case it has to be point out that the relative concentration found of gold to iron is ~ 20:1.

Table 2. Particle size analysis based on TEM microscopy study of Au nanoparticles synthesized at different flow rates and temperatures.

Flow rate (mL min^{-1})	Temperature (ºC)	Particle size (nm)	
		Average diameter	Standard deviation
0.041	40	35	16
0.240	40	33	15
0.556	40	27	8
0.135	60	29	7
0.556	60	24	9
1.081	60	25	10
0.240	80	36	12
0.556	80	28	11
1.607	80	26	9

3.6. Study of reproducibility of the synthesis and stability of gold nanoparticles

The reproducibility of the synthesis was investigated by preparing several solutions of gold nanoparticles at a flow rate of 0.2407 mL min^{-1} and the temperature set at 60ºC. RSD of both the wavelength of the maximum of the peak and intensity of surface Plasmon resonance were calculated and found to be 0.15% and 6.5%, respectively.

Finally, a study of stability of gold nanoparticles suspensions was conducted. The stability of nanoparticles relies on the number of atoms on nanoparticle surface regards those at nanoparticle core to provide thermodynamic stability. The presence of ions in solution interacting with the nanoparticles will influence their stability. In this case there are not citrate neither surfactant ligands bound to nanoparticles surface. Thus, chloride ions present in solution may shield obtained nanoparticles preventing them from agglomeration. In addition, low ionic strength media support the stability of nanoparticles in solution [31].

Gold nanoparticles solutions were measured by ultraviolet-visible spectroscopy 15 days after synthesis was performed. Variations in absorbance intensity observed along this interval of time resulted in RSD between 1.3 and 5.9%, for different flow rates conditions of synthesis. Stability of gold nanoparticles can also be proven attending to the SPR maximum. RSD values of wavelength peak maximum have been calculated being in the range 0.1-0.5%. Thus, the stability of as-synthesized gold nanoparticles solutions is good when stored at 4ºC.

3.7. Analytical application of bare gold nanoparticles

Gold nanoparticles can be considered within the Analytical Nanoscience and Nanotechnology scope as objects of the analysis –as reported above where synthesized nanoparticles have been characterized by microscopic or spectroscopic techniques- and analytical tools involved in different steps of the analytical process (i.e. as components of electrodes, as SERS substrates, as components of (bio)sensors, etc).

An advantage of the use of bare gold nanoparticles as analytical tool arise from the fact that there are not potential interferences from the excess of reducing agents used in their synthesis attached as ligands on the surface of the nanoparticles (i.e. citrate) or in suspension. Thus, further functionalization of the surface of gold nanoparticles for analytical applications is easier and do not requires a purification step prior it.

The analytical potential of these novel bare gold nanoparticles as SERS substrates has been proved. They enabled the determination of carboxylated single walled carbon nanotubes by surface enhanced Raman scattering (SERS) spectroscopy mediated by the nanoparticles. The enhancement factor, calculated from the Raman signal of 5 µL of 100 mgL^{-1} solution of c-SWNTs compared to that obtained when 5 µL of a 8 mgL^{-1} solution is placed on gold nanoparticles substrate, was found to be 39±1, as reported in [30]. The

continuous flow production of those bare gold nanoparticles may enable the automated formation of the gold nanoparticles and SERS measurements in a flow system.

4. Conclusions

In summary, gold nanoparticles can be synthesized in a continuous flow tubular reactor in which the own stainless steel walls of the reactor acts as reducing agent leading to the reduction of Au(III) ions into Au(0) in the form of gold nanoparticles. This continuous flow reactor can be useful for the scale-up production of gold nanoparticles without ligands on their surface. Variables affecting the synthesis process have been investigated and their influence on size and size distribution of nanoparticles evaluated. Nanoparticles obtained through the proposed methodology proved to be stable for long term storage.

Acknowledgments

The authors wish to thank Spain's Ministry of Innovation and Science for funding Project CTQ2011-23790 and Junta de Andalucía for Project FQM4801. A.I. López-Lorente also wishes to thank the Ministry for the award of a Research Training Fellowship (Grant AP2008-02939).

References

[1] Eustis S, El-Sayed MA (2006) Why gold nanoparticles are more precious than pretty gold: Noble Metal Surface Plasmon Resonance and its Enhancement of the Radiative and Nonradiative Properties of Nanocrystals of Different Shapes. Chem. Soc. Rev. 35:209-217.

[2] Sun Y, Xia Y (2002) Shape-Controlled Synthesis of Gold and Silver Nanoparticles. Science 298:2176-2179.

[3] Liu K, Nie Z, Zhao N, Li W, Rubinstein M, Kumacheva E (2010) Step-Growth Polymerization of Inorganic Nanoparticles. Science 329:197-200.

[4] Sau TK, Murphy CJ (2004) Room Temperature, High-Yield Synthesis of Multiple Shapes of Gold Nanoparticles in Aqueous Solution. J. Am. Chem. Soc. 126:8648-8649.

[5] Jana NR, Gearheart L, Murphy CJ (2001) Seed-Mediated Growth Approach for Shape Controlled Synthesis of Spheroidal and Rod-like Gold Nanoparticles Using a Surfactant Template. Adv. Mater. 13:1389-1393.

[6] Huang H, Yang X (2004) Synthesis of Polysaccharide-stabilized Gold and Silver Nanoparticles: a Green Method. Carbohydr. Res. 339:2627-2631.

[7] Daniel MC, Astruc D (2004) Gold Nanoparticles: Assembly, Supramolecular Chemistry, Quantum-Size-Related Properties, and Applications toward Biology, Catalysis, and Nanotechnology. Chem. Rev. 104:293−346.

[8] Huang CC, Yang Z, Lee KH, Chang HT (2007) Synthesis of Highly Fluorescent Gold Nanoparticles for Sensing Mercury(II). Angew. Chem. 119:6948-6952.

[9] Pang X, Zhao L, Han W, Xin X, Lin Z (2013) A General and Robust Strategy for the Synthesis of Nearly Monodisperse Colloidal Nanocrystals. Nature Nanotechnology 8:426-431.

[10] Wei H, Wang Z, Zhang J, House S, Gao YG, Yang L, Robinson H, Tan LH, Xing H, Hou C et al (2011) Time-Dependent, Protein-Directed Growth of Gold Nanoparticles within a Single Crystal of Lysozyme. Nature Nanotechnology 6:93-97.

[11] Turkevich J, Stevenson PC, Hillier J (1951) A Study of the Nucleation and Growth Processes in the Synthesis of Colloidal Gold. Discuss. Faraday Soc. 11:55-75.

[12] Frens G (1973) Controlled Nucleation for Regulation of Particle-Size in Monodisperse Gold Suspensions. Nature Phys. Sci. 241:20–22.

[13] Grabar KC, Freeman RG, Hommer MB, Natan MJ (1995) Preparation and Characterization of Au Colloid Monolayers. Anal. Chem. 67:735–743.

[14] Schmid G (1992) Large Clusters and Colloids Metals in the Embryonic State. Chem. Rev. 92:1709–1727.

[15] Brust M, Walker M, Bethell D, Schiffrin DJ, Whyman R (1994) Synthesis of Thiol Derivatized Gold Nanoparticles in a 2-phase Liquid–liquid System. J. Chem. Soc. Chem. Commun. 801–802.

[16] Stathis EC, Fabricanos A (1958) Preparation of Colloidal Gold. Chem. Ind. (London) 27:860-861.

[17] DiScipio RG (1996) Preparation of Colloidal Gold Particles of Various Sizes Using Sodium Borohydride and Sodium Cyanoborohydride. Anal. Biochem. 236:168-170.

[18] Zhao CX, He L, Qiao SZ, Middelberg APJ (2011) Nanoparticle Synthesis in Microreactors. Chem. Eng. Sci. 66:1463-1479.

[19] Acebal CC, Simonet BM, Valcárcel M (2013) Nanoparticles and continuous-flow systems combine synergistically for preconcentration. TrAC, Trends Anal. Chem. 43:109-120.

[20] Jahn A, Reiner JE, Vreeland WN, DeVoe DL, Locascio LE, Gaitan M (2008) Preparation of Nanoparticles by Continuous-Flow Microfluidics. J. Nanopart. Res. 10:925-934.

[21] Ying Y, Chen GW, Zhao YC, Li SL, Yuan Q (2008) A High Throughput Methodology for Continuous Preparation of Monodispersed Nanocrystals in Microfluidic Reactors. Chem. Eng. J. 135:209-215.

[22] Lohse SE, Eller JR, Sivapalan ST, Plews MR, Murphy CJ (2013) A Simple Millifluidic Benchtop Reactor System for the High-Throughput Synthesis and Functionalization of Gold Nanoparticles with Different Sizes and Shapes. ACS Nano 7:4135-4150.

[23] Song YJ, Hormes J, Kumar CSSR (2008) Microfluidic Synthesis of Nanomaterials. Small 4:698–711.

[24] Richmond CJ, Miras HN, de la Oliva AR, Zang H, Sans V, Paramonov L, Makatsoris C, Inglis R, Brechin EK, Long DL et al (2012) Flow-System Array for the Discovery and Scale Up of Inorganic Clusters. Nat. Chem. 4:1037–1043.

[25] Wagner J, Tshikhudo TR, Koehler JM (2008) Microfluidic Generation of Metal Nanoparticles by Borohydride Reduction. Chem. Eng. J. 135:S104–S109.

[26] Lin XZ, Terepka AD, Yang H (2011) Synthesis of Silver Nanoparticles in a Continuous Flow Tubular Microreactor. Nano Lett. 4:2227-2232.

[27] Köhler JM, Romanus H, Hübner U, Wagner J (2007) Formation of Star-Like and Core-Shell AuAg Nanoparticles during Two- and Three-Step Preparation in Batch and in Microfluidic Systems, J. Nanomaterials 98134.

[28] Shalom D, Wootton RCR, Winkle RF, Cottam BF, Vilar R, deMello AJ, Wilde CP (2007) Synthesis of Thiol Functionalized Gold Nanoparticles Using a Continuous Flow Microfluidic Reactor. Mater. Lett. 61:1146–1150.

[29] Yen BKH, Stott NE, Jensen KF, Bawendi MG (2003) A Continuous-Flow Microcapillary Reactor for the Preparation of a Size Series of CdSe Nanocrystals. Adv. Mater. 15:1858-1862.

[30] López-Lorente AI, Simonet BM, Valcárcel M, Mizaikoff B (2013) Bare Gold Nanoparticles Mediated Surface-Enhanced Raman Spectroscopic Determination and Quantification of Carboxylated Single-Walled Carbon Nanotubes, Anal. Chim. Acta 788:122-128.

[31] Dykman LA, Bogatyrev VA (2007) Gold Nanoparticles: Preparation, Functionalisation and Applications in Biochemistry and Immunochemistry. Russ. Chem. Rev. 76:181-194.

BLOQUE IV

IV

CARACTERIZACIÓN DE NANOPARTÍCULAS

CHARACTERIZATION OF NANOPARTICLES

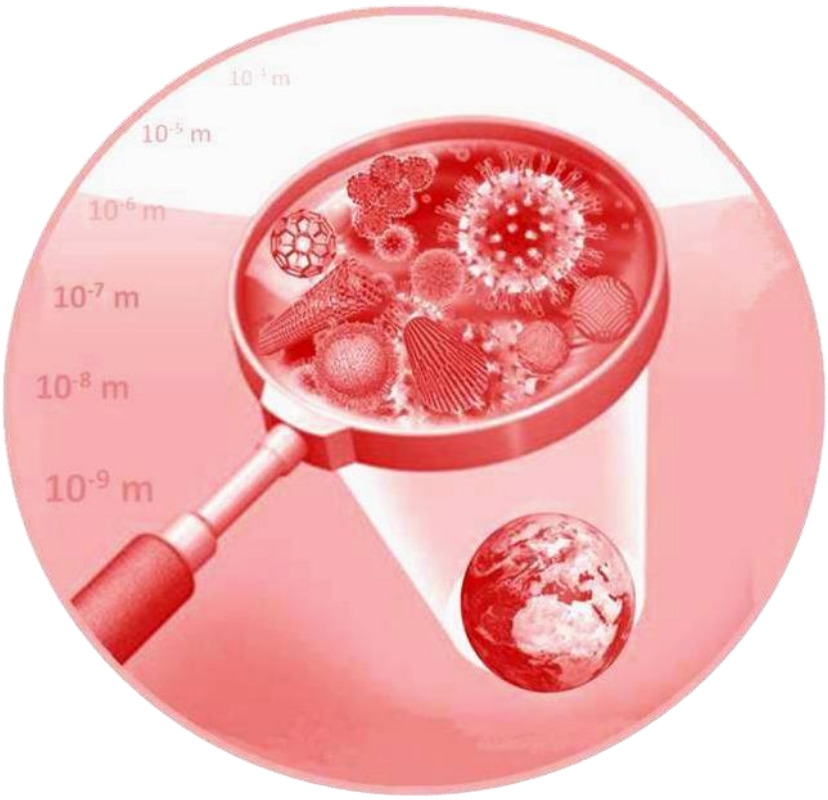

En este bloque se describen los métodos de caracterización de nanopartículas desarrollados a lo largo de la presente Tesis Doctoral. Para ello se han utilizado, además de las técnicas microscópicas y la espectroscopia UV-Vis, que ya en el bloque anterior nos sirvieron para caracterizar y evaluar los procesos de síntesis de nanopartículas de oro, las espectroscopias Raman e infrarroja así como la electroforesis capilar. A continuación se detalla el papel de cada una de ellas.

IV.1. ESPECTROSCOPIA RAMAN

Desde la primera observación de CNTs de pared múltiple en 1991 por Iijima[1], la espectroscopia Raman se ha utilizado para caracterizar los procesos de síntesis y purificación de CNTs así como estudiar sus propiedades[2]. Fue a partir de 1997[3] cuando realmente se comenzó a vislumbrar el enorme potencial de la técnica al demostrarse por vez primera la dependencia del espectro de los SWCNTs con la energía del láser de excitación como consecuencia de que tiene lugar un proceso Raman resonante que depende del diámetro del nanotubo. Además de proporcionar información detallada sobre la estructura geométrica, electrónica y vibracional de los diferentes CNTs presentes en la muestra[4], otras ventajas que han impulsado su uso extendido son que se trata de una técnica no invasiva, que no requiere preparación de la muestra y que permite versatilidad de condiciones de medida.

[1] S. Iijima, Nature 354 (1991) 56-58.
[2] D. Tasis, N. Tagmatarchis, A. Bianco, M. Prato, Chem. Rev. 106 (2006) 1105-1136.
[3] A. M. Rao, E. Richter, S. Bandow, B. Chase, P. C. Eklund, K. A. Williams, S. Fang, K. R. Subbaswamy, M. Menon, A. Thess, R. E. Smalley, G. Dresselhaus, M. S. Dresselhaus, Science 275 (1997) 187-191.
[4] M. S. Dresselhaus, G. Dresselhaus, R. Saito, A. Jorio, Phys. Rep. 409 (2005) 47-99.

Los principales modos de vibración en el espectro Raman de CNTs son las bandas de respiración radiales (RBM, 100-300 cm^{-1}), características de SWNTs, cuya energía (o número de onda) depende del diámetro de los nanotubos. En algunas ocasiones, si se establecen condiciones muy buenas de resonancia, pueden observarse en MWNTs. El modo tangencial (banda G, 1400-1700 cm^{-1}) es el de mayor energía en el caso de SWNTs, pudiéndose emplear asimismo para la caracterización del diámetro de los CNTs o de su carácter metálico. Dicha banda tiende a dividirse en dos (G^+ y G^-) en el caso de SWNTs, mientras que en MWNTs el efecto es menos pronunciado. La banda D, asociada al desorden, se observa entre 1300-1400 cm^{-1}, pudiéndose observar su sobretono, conocido como banda G', a 2600-2800 cm^{-1}. Cabe destacar que el espectro Raman de SWNTs ha sido hasta la fecha más ampliamente estudiado que el de MWNTs.

La figura muestra el espectro Raman de SWNTs, indicando las principales bandas comentadas que pueden observarse en el mismo. (Adaptada de ref.[5])

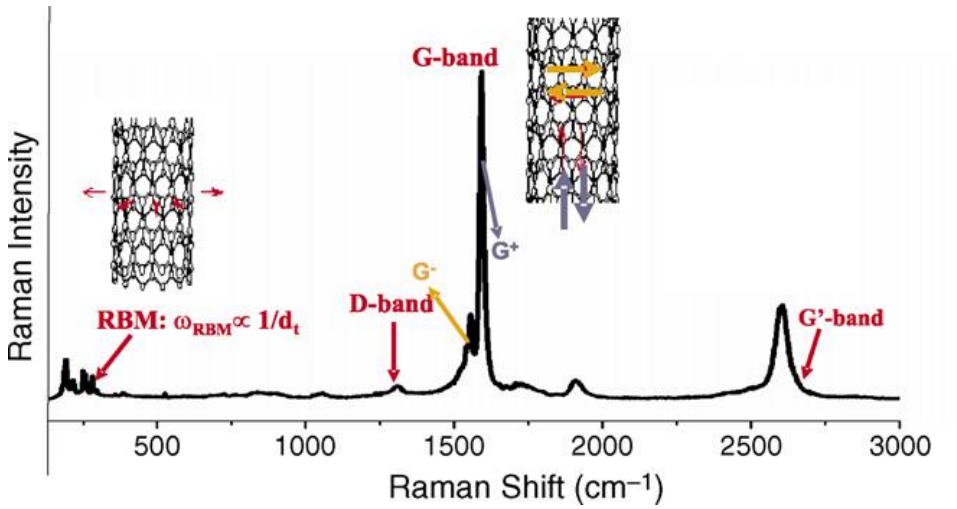

[5] M.S. Dresselhaus, G. Dresselhaus, M. Hofmann, Vibrational Spectroscopy 45 (2007) 71–81.

Un análisis en mayor profundidad de la relación de las bandas Raman de CNTs con la estructura geométrica, electrónica y vibracional (fonónica) de los nanotubos de carbono, así como la aparición de las singularidades de van Hove en su correspondiente densidad de estados electrónicos, queda fuera del alcance de la presente Tesis Doctoral. La caracterización Raman de nanotubos de carbono es un tema de gran interés, siendo un campo muy interdisciplinar abarcando en gran medida el campo de la física. En nuestro caso, hemos utilizado dicha herramientas para su explotación desde un punto de vista analítico.

En este apartado se describen dos aproximaciones analíticas a la caracterización Raman de nanotubos de carbono. En el **capítulo 5**, se demuestra la influencia del estado de agregación de SWNTs en la relación de intensidades de las bandas G y D de los mismos. Por tanto, es necesario tener en cuenta la preparación de la muestra para evitar la agregación de los nanotubos con el fin de obtener una buena representatividad de las medidas. En este sentido se propone la dispersión de los nanotubos con ayuda de tensioactivos. En el caso de MWNTs el efecto del estado de agregación sobre la relación de intensidades de las bandas G y D es menos notorio.

En el **capítulo 6** se muestra un estudio detallado de los espectros Raman de nanotubos de carbono de diferente naturaleza dispersados con ayuda de tensioactivos. Se ha llevado a cabo un estudio del número de onda al que aparecen las bandas así como la intensidad relativa de las bandas D y G. El método propuesto permite la caracterización y (semi)cuantificación de la presencia de SWNTs en mezclas de SWNTs y MWNTs.

Capítulo 5

Raman spectroscopic characterization of single-walled carbon nanotubes: influence of sample aggregation state.

Analyst, DOI: 10.1039/C3AN00642E

RSC Publishing

Analyst

DOI: 10.1039/C3AN00642E

Raman spectroscopic characterization of single-walled carbon nanotubes: influence of sample aggregation state

A. I. López-Lorente, B. M. Simonet, M. Valcárcel

Department of Analytical Chemistry, University of Córdoba, E-14071 Córdoba, Spain.

Raman spectroscopy has been employed in analytical sciences for purity determination of carbon nanotube samples based on the consideration of G-/D-band intensity ratio. This work demonstrates the role of aggregation in these feature bands, which, in the case of single-walled carbon nanotubes (SWNTs), has proved to be crucial for G-/D-band intensity ratio measurements. We have found variation in the relative intensities of G- and D-band across a sample of SWNTs without any other treatment, discarding the possible influence of laser beam or sample focusing. In the case of multiwalled carbon nanotubes (MWNTs), this effect is less notorious. Thus, for a good representativeness of Raman measurements, it is important to consider sample preparation procedure in order to avoid aggregation, which has effect over the signals, making difficult the subsequent interpretation of results.

Keywords: Raman spectroscopy, multiwalled carbon nanotubes, single-walled carbon nanotubes, aggregation.

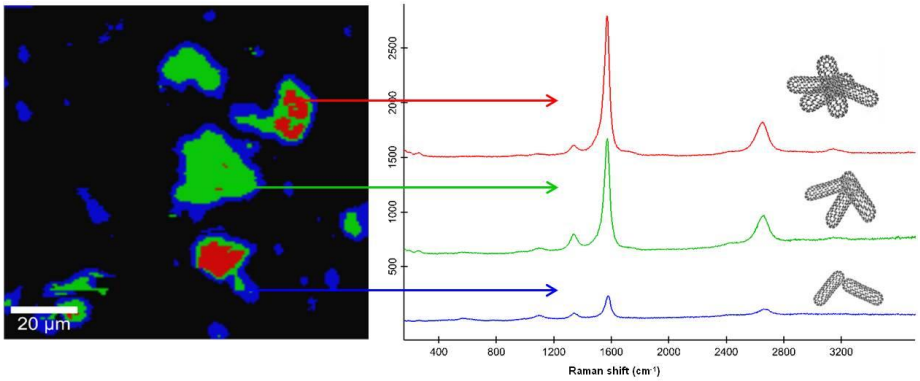
20 µm
2500
2000
1500
1000
500
400
800
1200
1600
2000
2400
2800
3200
Raman shift (cm-1)

1. Introduction

Carbon nanotubes have attracted much attention due to their huge potential in many fields. Potential applications of these nanostructures include use in nanoelectronics [1], energy storage [2], battery and field-emitting-display technologies [3], also showing great potential for sensors [4], composites [5], catalytic supports [6], and as membrane materials for analytical separations [7]. This increased use of these nanostructures opens up new challenges to analytical chemistry since new methods for their characterization are needed. Microscopy-based techniques such as scanning and transmission electron microscopy (SEM and TEM) and atomic force microscopy (AFM) provide exact information about shape and size, however, some of their most important shortcomings are the low representativeness of the results due to the small sample volumes that are analyzed, as well as sample preparation, which involves drying, and might result in their aggregation.

Ultraviolet-visible-near-infrared (UV-vis-NIR) spectroscopy has been employed for distinguish individualized dispersions of single-walled carbon nanotubes from bundles of them by visualization of the broadening and red-shift of the absorption peaks [8]. The UV-vis absorption value at 500 nm has been used to quantify different SWNTs dispersions [9], although it is difficult to distinguish SWNTs contributions from other carbonaceous impurities or the dispersing agents. Near infrared luminiscence studies performed on individual SWNTs revealed spectral variations within a given (n,m) type of nanotubes [10], which allow the determination of chirality/diameter distribution present in individually dispersed nanotubes. However, metallic nanotubes produce quenching and surfactants might influence the peak.

Raman spectroscopy has been widely employed for the characterization of carbon nanotubes. The resonant Raman scattering from SWCNTs generates an intense and easily measurable signal. The main strengths of Raman are its

simplicity [11], versatility of measurement conditions, rapidity and non-destructive neither invasive nature. The information provided about vibrational properties can be correlated with the structure and electronic properties of the nanotubes. Carbon nanotube dispersions have been quantified by Raman spectroscopy normalizing the spectra with respect to the area of a solvent peak [12], analyzing carboxylated single-walled carbon nanotubes (c-SWNTs) previously preconcentrated in ionic liquid and retained on a membrane [13] or measuring c-SWNTs preconcentrated on MWNT-modified membranes [14]. Raman spectroscopy has been also used for purity and defect characterization of SWNTs [15] since its mode around 1350 cm^{-1} is sensitive to structural defects in the graphitic sp^2 network typical of carbonaceous impurities, such as amorphous carbon particles [16].

The intensity ratio of the tangential mode of SWCNTs (G-band) to the D-band has been used to discuss the purity [17, 18, 19]. As has been reported, the evaluation based on the G-/D-band intensity ratio has uncertainty as to whether the D-band intensity reflects the amount of impurity particles or the defect density on the sidewalls. For example, when the D-band mainly reflects carbonaceous impurities in a sample, the G-/D-band intensity ratio becomes a good index of SWCNT purity. Meanwhile, when there are fewer carbon impurities in the sample, the G-/D-band intensity ratio can be used to discuss SWCNT defects [20].

In this work, we aim to point out the need of carefully considering operational conditions when measuring Raman spectra of SWNTs. Usually, Raman measurements are acquired at a specific position of the carbon nanotube sample, and this study indicates the importance of sample treatment for the debundling of aggregates of nanotubes. In fact, aggregation state of the sample takes an important role in the featured bands, as in the case of G-/D-band intensity ratio, which may lead to an ambiguity in the consideration of different

purities of samples when actually the differences are just in aggregation. If it is not taken into account mistakes may be committed. Differences in RBM bands of SWNTs spectra [21-24] or a G-band broadening [25] have been described to occur when samples with different aggregation state are measured [21, 22]. Herein we have proved that a sample of SWNTs produces spectra with different G-/D-band intensity ratio just by variation of their aggregation distribution across the sample itself, discarding the possible influence of impurities in the sample, laser beam or sample focusing. Thus, in order to achieve a good representativeness in Raman measurements for quality assessment it is necessary to control aggregation state. As far as we are concerned the relation of G-/D-band intensity with the different aggregation states along a carbon nanotube sample has not been previously reported. Dispersion of carbon nanotube sample with the aid of surfactants is proposed as an effective methodology to control aggregation of bundles of carbon nanotubes. This effect has been observed in the case of single walled carbon nanotubes while for the multiwalled carbon nanotubes investigated the effect of aggregation is less significant.

2. Materials and methods

2.1. Chemicals

Carbon nanotubes of different nature were studied in this work, namely single walled carbon nanotubes (SWNTs) purchased from Shenzhen Nanotech Port Co. Ltd (NTP) (Shenzhen, China), with a purity over 90%, an outer diameter of <2 nm, a length of 5-15 μm and a special surface area of 500-700 m^2g^{-1}. Multiwalled carbon nanotubes (MWNTs) were provided by CheapTubes (Brattleboro, USA) with an outer diameter of 10-30 nm, a length of 10-30 μm, >90% purity in weight, and ashes content <1.5% in weight. Ethanol and Triton X-100 were provided by Fluka (Buchs, Switzerland).

2.2. Equipment

For Raman measurements a confocal Raman equipment (alpha500, manufactured by WITec GmbH) was employed. For excitation a frequency double Nd:YAG laser at 532 nm (second harmonic generation) was used, which resulted in a penetration depth in silicon of about 0.5 μm. Raman spectra were collected using a 600 g mm^{-1} diffraction grating. The laser beam was focused on the sample surface onto a spot of 1 or 3.45 mm in diameter using a 100x/0.95 Nikon or 20x/0.4 Zeiss objectives, respectively. Laser powers were measured directly on the sample stage and were typically between 0.5 and 1.5 mW. Measurement time was about 20 ms for each point of a mapping, which typically consisted of 150×150 points.

An ultrasound bath without heating (Ultrason model, Selecta, 50 W, 60 Hz) was employed for sample preparation. A Vibracell™ 75041 ultrasonic probe (750 W, 20 KHz, Bioblock Scientific, Illkirch, France) equipped with a 3 mm probe was also employed to prepare the dispersions. Transmission electron microscopy (TEM) images were acquired with a JEOL JEM-1400 transmission electron microscope. AFM image was acquired with alpha500 WITec AFM microscope using tapping mode.

2.3. Sample treatment and preparation

As received single walled carbon nanotubes were dispersed in ethanol and ultrasonicated to remove impurities of the sample. Ethanol is a pure solvent which does not leave residuals when evaporating. Ultrasonication conditions were soft (50 W, 10 min) in order to not introduce defects in carbon nanotubes that will affect to the intensity of Raman D-band. It could be checked by comparison of the Raman spectra of solid samples with the dispersed one that there is no functionalization or degradation of the latter carbon nanotubes. Immediately after ultrasound step, the dispersion was drop-dried on a

microscope glass slide. Nanotubes aggregated as ethanol was evaporating, although the size of aggregates is smaller than in an untreated solid sample. Thus, aggregates can be found in the slide, but also free nanotubes at the edges of the aggregates and in the inter-aggregates regions above the crystal surface of the specimen.

Single-walled carbon nanotubes were also dispersed in 5 wt/vol% Triton X-100 solution by using an ultrasonic probe for 10 minutes (750 W, 20 KHz) equipped with a 3 mm probe set at 20% amplitude. Pulses of energy of 20 s on and 20 s off were employed in order to avoid sample heating. No degradation or shortening of carbon nanotubes was observed after sonication treatment.

2.4. Raman measurements

Both acquisition time and accumulated spectra for measuring single Raman spectra were optimized. Raman spectrum at a certain point of the sample was acquired with an integration time of 1 second being the spectrum the sum of 20 acquisitions.

Raman images in the case of the Raman study to evaluate the influence of aggregation state showed in Figure 4 were obtained by measuring a total of 150 points per line and 150 lines per image over a scan width and height of 110 μm x 110 μm with an integration time of 0.05 s. Raman image of single-walled carbon nanotubes dispersed in Triton X-100 (Fig. 6a) was acquired by measuring 250 points per line and 250 lines per image at a scan area of 50 x 50 μm with an integration time of 0.1 s. The image shown in Figure 7, in which more isolated nanotubes are shown, was acquired by measuring 100 points per line and 100 lines per image at a scan area of 8 x 8 μm with an integration time of 0.1 s. In the case of multi-walled carbon nanotubes the Raman image (Fig. 8a) was obtained measuring a total of 90 points per line and 90 lines per image at a surface of 72 x 72 μm with an integration time of 0.05 s. Finally, the depth scan

shown in Figure 3a were acquired measuring 50 points per line and 100 lines per image for a scan width of 10 μm and a scan depth of 50 μm, with an integration time of 0.05 s.

3. Results and discussion

3.1. Raman spectra of solid as received pristine single-walled carbon nanotubes

Raman spectra of a solid sample of pristine single-walled carbon nanotubes without any modification or purification step have been recorded at different points of the sample. Differences in G-/D-band intensity ratio were found as can be seen in Figure 1a. The sensitivity of D band to structural defects in the graphitic sp^2 network typical of carbonaceous impurities, such as amorphous carbon particles, has been described [15, 16]. The sample has not been purified, and, although the supplier states that the purity of carbon nanotubes is over 90%, it could be thought that differences are produced by carbonaceous impurities present in solid sample. These impurities could be closely entangled with SWNTs or stick on the outer surface of carbon nanotubes. The presence of impurities in carbon nanotubes subject of this study was discarded by microscopy measurements.

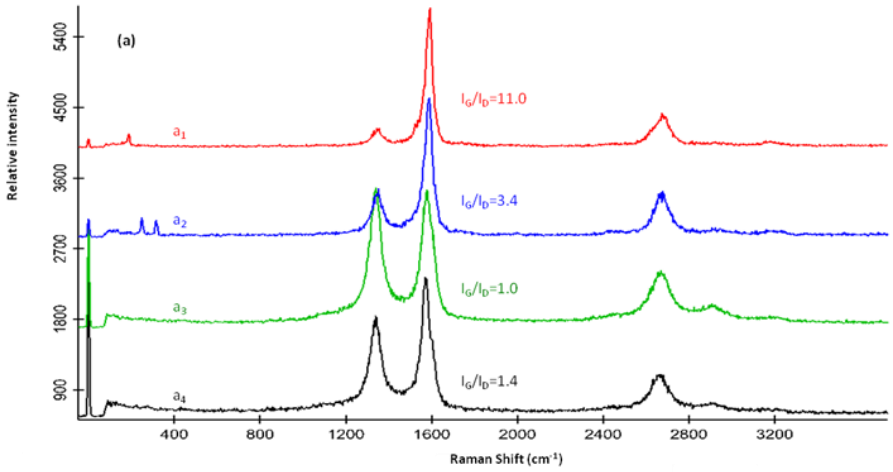

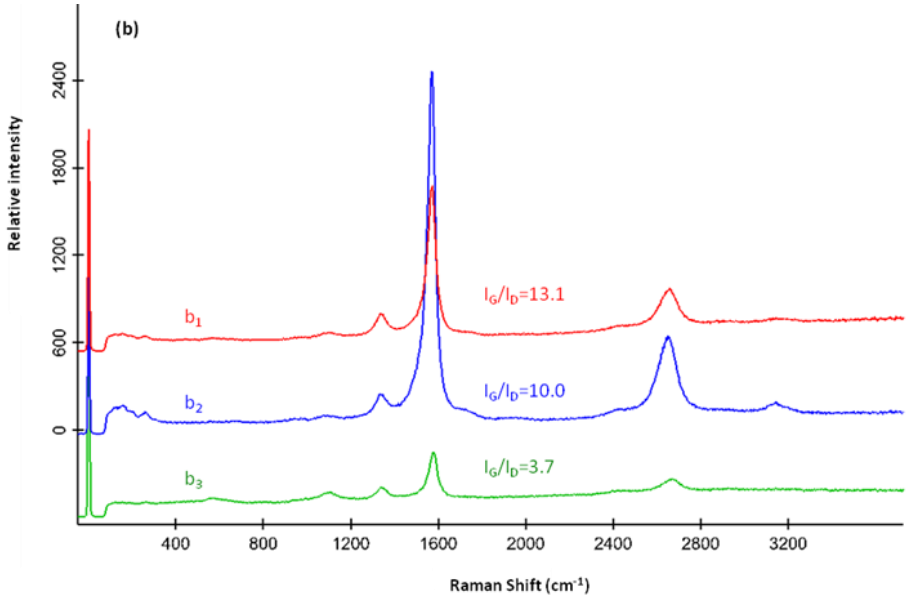

Figure 1. Raman spectra of (a) as received solid pristine single-walled carbon nanotubes (spectra normalized to G band, changes in the relative intensity of D band are observed) and (b) SWNTs after dispersion in ethanol and subsequently deposited in a glass support (normalized to D band, changes are observed for the G band). Each spectrum (a1-a4 and b1-b3) was taken at a different position of the same sample. Spectra were taken with an integration time of 1 second and accumulating 20 spectra with an EMCCD Gain output amplifier.

3.2. Raman spectra of single-walled carbon nanotubes after dispersion in ethanol

In order to eliminate a hypothetical contribution of impurities, carbon nanotubes were previously suspended in ethanol and ultrasonicated as previously explained for sample treatment. Figure 2 shows a TEM photograph of the nanotube sample after ethanol treatment once solvent evaporated. As can be seen, there are bundles of aggregated carbon nanotubes but also more isolated nanotubes at the edges of such aggregates. We acquired spectra at different locations within this sample, in which aggregated and non-aggregated

carbon nanotubes are present, and the previously observed differences in G-/D-band intensity ratio for untreated samples persisted (Figure 1b).

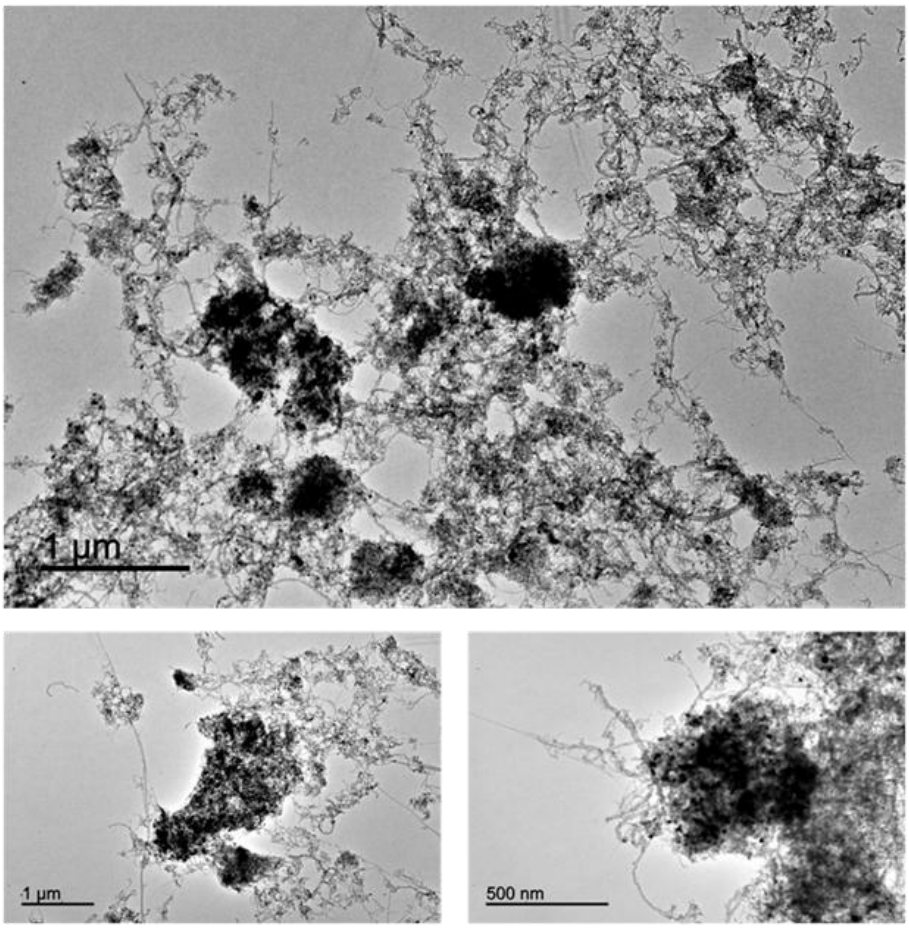

Figure 2. Transmission electron microscopy (TEM) photograph carried out with JEOL JEM-1400 transmission electron microscope. The sample was prepared by placing one drop of a solution of SWNTs in ethanol onto a copper TEM grid with a Carbowax forward.

For purity evaluation using Raman spectroscopy, the G band peak around 1593 cm^{-1}, which derives from the longitudinal optical (LO) phonons of semiconducting SWCNTs [15], has been used [26] due the fact that it is less

sensitive to excitation laser energy than the RBM intensity, and there is no significant diameter dependence of the G-band intensity for the LO phonon of semiconducting SWCNTs, while the RBM intensity is more sensitive to their diameter and chirality. Itkis et al. [18] have described that the G-band area is proportional to the relative purity. In addition to the G band, G-/D-band intensity ratio has been also employed as index of purity for characterization of carbon nanotubes in terms of defects density. The intensity ratio of G-band to D-band reflects both the purity and defect density of a SWNT sample. Pure SWNTs can also have considerable D-band intensity due to structural defects, thus, evaluation of purity through G-/D-band intensity ratio has uncertainty as to whether the D-band reflects the amount of impurity particles or the defect density on SWNTs sidewalls [15].

As can be observed in Figure 1b, RBM bands also change in the spectra. Their dependence on the aggregation state of carbon nanotubes has been previously described [20] since some modes which are initially off resonance in individually dispersed material, with aggregation, as transitions shift to lower energy, are brought into resonance while others move away. The intensity of the peak at 267 cm^{-1} has shown to be proportional to the degree of aggregation [22]. It has been also reported that the influence of aggregation on the apparent metallic to semiconductor ratio of dielectrophoretically deposited SWNTs can compromise conclusions based on Raman alone [27]. Moreover, the linewidths of G′ band for solubilised SWNTs has been observed to monotonously decrease with sonication energy density and can be used to monitor the gradual solubilisation of SWNTs [25]. Liu et al. [28] employed simultaneously Raman measurements and photoluminescence spectroscopy to evaluate the bundling states of SWNTs by using again the 267 cm^{-1} band and the sum of photoluminescence to G-band intensity ratio.

We have focused on changes of G-/D-band intensity ratio and their dependence on aggregation state, parameter which, as far as we are concerned, had not been considered until date. As will be explained below, changes in G-/D-band intensity ratio observed in this work are not a consequence of changes in purity or sample focusing, nor are a problem of laser damaging of the sample. It can be concluded that observed changes are due to different aggregation states across the sample.

3.3. Influence of laser beam

The influence of laser power in the spectra of the nanotubes has been studied. The optimum power selected for recording the spectra was 1.0 mW for a laser wavelength of 532 nm using a 20x lens. The laser power is low in order to not damaging the sample when acquiring the spectra. It has been described the use of higher laser power when measuring dispersions of carbon nanotubes in a solution, which allows better heat dissipation [29]. In addition, the laser power to measure the Raman spectrum of bundles of carbon nanotubes must be lower than for isolated nanotube samples due to the poor inter-tube thermal conductivity in CNT bundles [30].

Since it had been previously described in literature that laser beam may affects the bands [15, 31, 32], the influence of laser irradiation during a period of time over the sample was studied. In addition, laser irradiation is known to cause shifts in Raman bands due to thermal effects which leads to an increase in D peaks [31]. We have found that there is no change in the profile of the considered bands during the exposure windows usually employed for measurements. Spectra of untreated solid SWNTs with different times of laser exposure (0, 3, 6 and 9 min, respectively), showed a G-/D-band intensity ratio almost constant. An upshift of baseline was observed, having no influence when normalizing spectra. This observation agrees with observations of almost constant G-/D-band intensity ratio for subsequent measurement after the first

power sweep [33]. In any case, measurements have been carried out using the same laser power for all the studies presented in this work.

3.4. Influence of focusing

We are measuring in a relatively large area of the sample, which implies the presence of bundles of carbon nanotubes, which may have different heights. Sample focusing affects to the intensity of the spectra, usually by increasing or decreasing the whole bands of it. The possible influence on the considered parameter (G-/D-band intensity ratio) of measuring at different heights across a sample was investigated. . The small diameter of the multi-mode fiber (50 μm) of our Raman spectrometer acts as a pinhole allowing for confocal microscopy and hence increasing spatial resolution. This allows performing Raman spectra capture of a depth profile of the sample. When acquiring spectrum at different heights, no significant differences were found in G-/D-band intensity ratio.

In addition, Figure 3a shows the Raman image of a SWNT sample across its whole diameter. In this case, instead of acquiring discrete spectra at a series of points, a Raman image was formed by measuring at different points in an x- and z-axis area (50 points per line and 100 lines per image for a scan width of 10 μm and a scan depth of 50 μm, with an integration time of 0.05 s). The image depicted corresponds to the intensity of the G band. In order to corroborate our observations, the collection of spectra were subjected to cluster analysis by K-Nearest Neighbors (KNN) at the same conditions explained as follows and, as can be observed in Figure 3b, the spectrum of each cluster are very similar, so we can conclude that focusing is not the source of variations in G-/D-band intensity ratio in the spectra. Figure 3c depicts the regions of the image which corresponds to the spectrum in Figure 3b with the same colour.

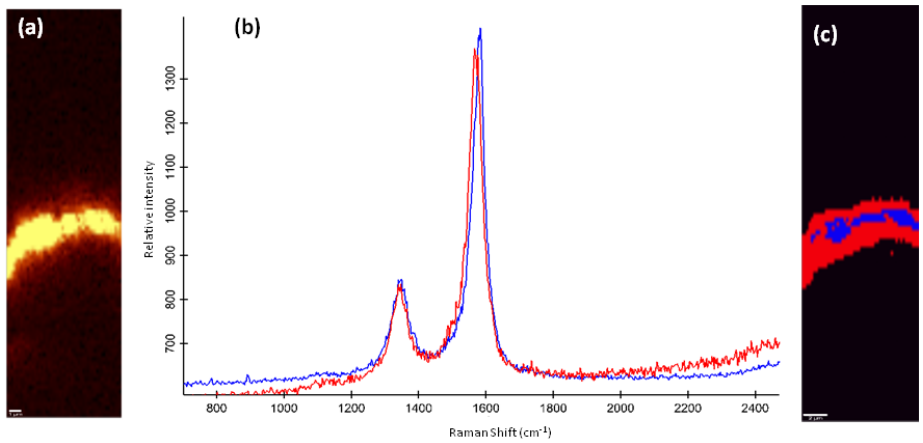

Figure 3. (a) Raman image which represent areas with a high intensity of G-band (yellow) where nanotubes are present. The scan was taken in depth, by measuring in a XZ plane. (b) Raman spectra result of cluster analysis of the spectra collection. There is little influence of focusing on D/G relation. (c) Distribution of the cluster in the sample. The color code of the cluster and Raman spectrum is the same.

3.5. Influence of aggregation state

In order to investigate the source of the observed variations, a Raman image which is composed by spectra acquired point by point in a surface was recorded. Figure 4a shows an optical microscope photograph of the sample analyzed. Nanotubes were treated with ethanol and ultrasonicated as previously explained. Specifically, a total of 150 points per line and 150 lines per image with a scan width and height of 110 μm x 110 μm with an integration time of 0.05s were measured. From the set of spectra we can see differences in the collected spectra.

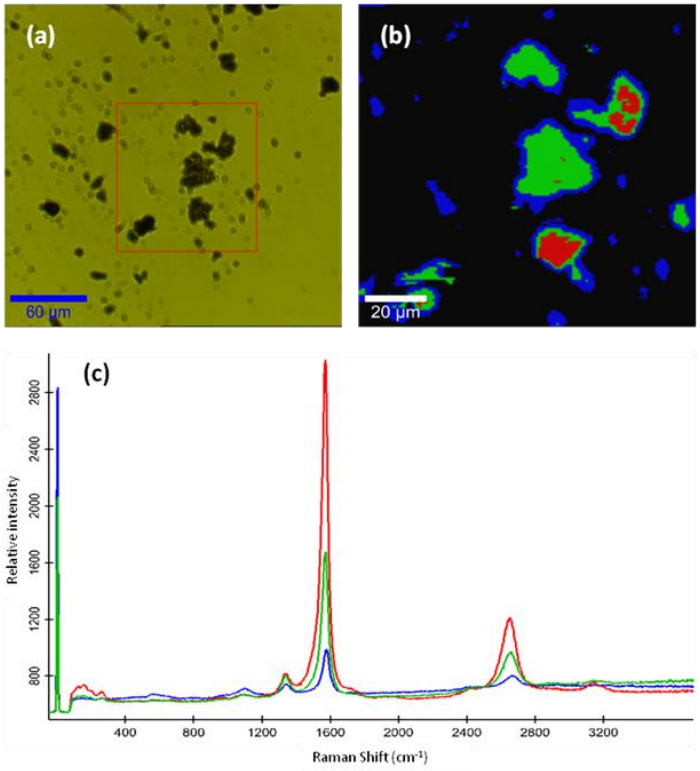

Figure 4. (a) Photography acquired with an optical microscope employing a 20x objective of a SWNTs sample ultrasonicated in ethanol and drop-dried on a glass support. (b) Distribution across sample of the different clusters classified when the set of spectra corresponding to a Raman image was submitted to K-NN analysis. (c) Corresponding spectrum of each cluster.

To prove if it is possible to cluster spectra with similar G-/D-band intensity ratio and then relate them with different properties of the sample, the whole set of spectra were submitted to K-NN cluster analysis. K-nearest Neighbors is a discriminant, non-parametric technique, based on the distance between objects in a space of dimension equal to the number of variables explored. The sample is assigned to a class where the samples of the training set closest to it have been classified. Only the K closest objects are used to make the assignment. The distance criterion used was Euclidean distance. Initially, a classification model was constructed in which all spectra were used as the training set. In a second

stage, to validate the classification model thus obtained and its stability in predicting, a cross-validation step was performed with five cancellation groups (the spectra are randomly divided into five groups, each of them containing 20% of the total), four of which were used as training set and the fifth as the prediction set. To perform this cross-validation procedure, the same process was repeated five times with the five different training and predictions sets, ensuring that all the samples were included at least once in the prediction set.

K-NN cluster analysis differenced three regions in the image (see Figure 4b) which possesses spectra with different G-/D-band intensity. As depicted in Figure 4b, the regions correspond to the nuclei of the aggregates and concentric outer regions, so it seems logical to think that changes may be produced by the different aggregation inside bundles and around them, which may affect to the resonance of carbon nanotubes. In fact, regions which have a low density of carbon nanotubes between aggregates, whose dimensions oscillate between 7-25 μm of width, have a spectrum similar to bundles edges, in which nanotubes are less aggregated.

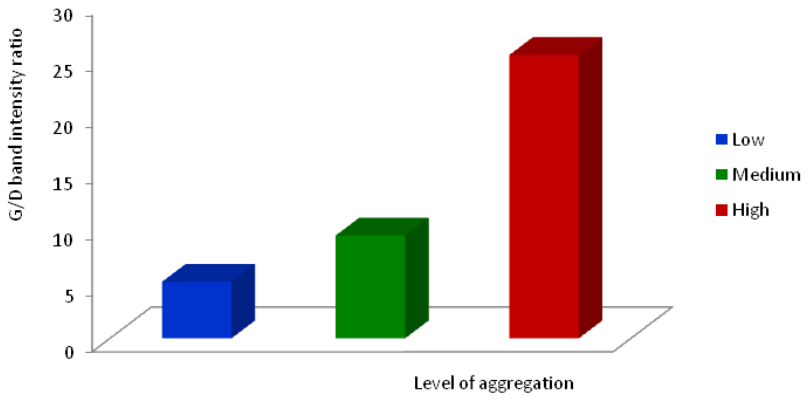

Figure 5. Representation of the G/D ratio obtained from their maximum peak counts for three different levels of aggregation. The color code corresponds to the different cluster classified and depicted in Figure 4.

The G- and D-band intensities were obtained from their maximum peak counts. G-/D-band intensity ratio averages at three aggregation levels are 5±0.6 for regions with low aggregation, 9.2±0.8 in regions of medium aggregation and 25±1 in regions of high aggregation, as shown in Figure 5. It can be seen that there are three different values of relation, related with the aggregation state of the sample. The color code presented in Figure 5 correlates with the colors assigned to each cluster associated to a different value of G-/D-band intensity.

3.6. Spectra of debundled single-walled carbon nanotubes

Exfoliation of carbon nanotubes has been attempted by ultrasonication in the presence of organic solvents [31] or aqueous solutions of surfactants [34], copolymers [35], polyelectrolytes [36] and DNA molecules [37]. In previous work [29], the suitability of surfactants to disperse carbon nanotubes without interfering with the Raman signal has been demonstrated. The interaction of linear ionic surfactants such as SDS and CTAB with the nanotube surface is weaker than in the case of Triton X-100 by virtue of its aromaticity. Molecules having a benzene ring structure adsorb more strongly to the graphitic surface due to π-π stacking interactions [38].

SWNTs were dispersed in a 5 wt/vol% Triton X-100 solution with the aid of an ultrasonic probe as explained in sample treatment. Again, a Raman image of the sample was acquired and subsequently submitted to K-NN cluster analysis similarly to that previously described. Figure 6 shows the results obtained. Figure 6a depicts the Raman image which reflects the intensity of the G band, while Figure 6b classified the different points of the image in two clusters, whose corresponding spectra are shown in Figure 6c. TEM images corroborated the more debundled state of this sample, as can be seen in Figure 6d. In this case, the differences in G-/D-band intensity ratio are less significant being the values obtained 4.59 and 4.34 for the two different classified clusters. Thus, it can be concluded that a suitable control of aggregation state of the sample is

crucial for a representative value of G-/D-band intensity ratio. In fact, this parameter has proved to be effective for the characterization of mixtures of single- and multi-walled carbon nanotubes in a reproducible way when carbon nanotubes samples are dispersed in a surfactant solution [29].

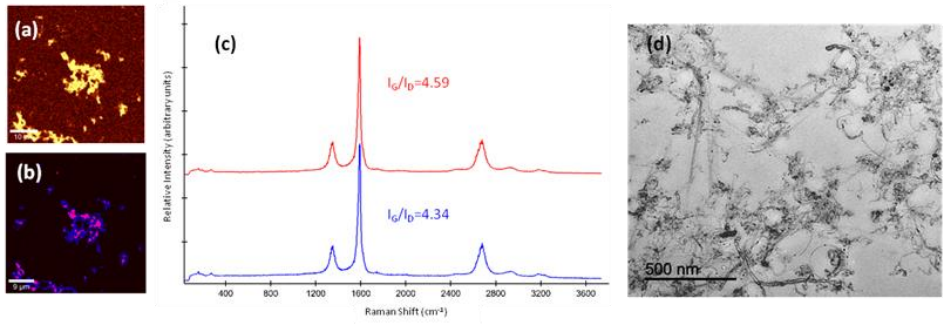

Figure 6. (a) Raman image which reflects the intensity of G-band in a sample of well-dispersed SWNTs in 5 wt/v% Triton X-100 drop-dried on a glass support, (b) assignation of regions to the different clusters when the set of spectra was submitted to K-NN analysis, (c) Raman spectra corresponding to each cluster and I_G/I_D calculated for each spectrum, (d) TEM photograph carried out with JEOL JEM-1400 transmission electron microscope of a SWNT sample dispersed and ultrasonicated in 5 wt/v% Triton X-100 prepared placing one drop of the dispersion onto a copper TEM grid with a Carbowax forward.

A Raman image was also acquired in a region containing just some SWNTs. Figure 7e shows the optical microscope photograph of the scanned surface and Figure 7d shows an AFM image of the sample. Raman image (shown in Fig.7a) was composed by 100 points per line and 100 lines per image at a scan area of 8 x 8 μm measured with an integration time of 0.1 s. Similarly to that described above, the set of spectra were submitted to K-NN cluster analysis, which classified them in three different regions (see in Fig. 7b cluster classification and the corresponding spectra in Fig. 7c). In this case it should be point out that the more significant differences found that lead to the classification of the spectra in clusters were differences in G- and G'-band wavenumbers. As can be seen in the

insets of Figure 7c, the G-band positions of the spectra are 1568, 1571 and 1575 cm^{-1}, respectively for the blue, green and red spectra, while the G' band appears at 2681, 2687 and 2690 cm^{-1}. It seems that the spectrum corresponding to the interior of the carbon nanotubes shows the features at lower wavenumbers.

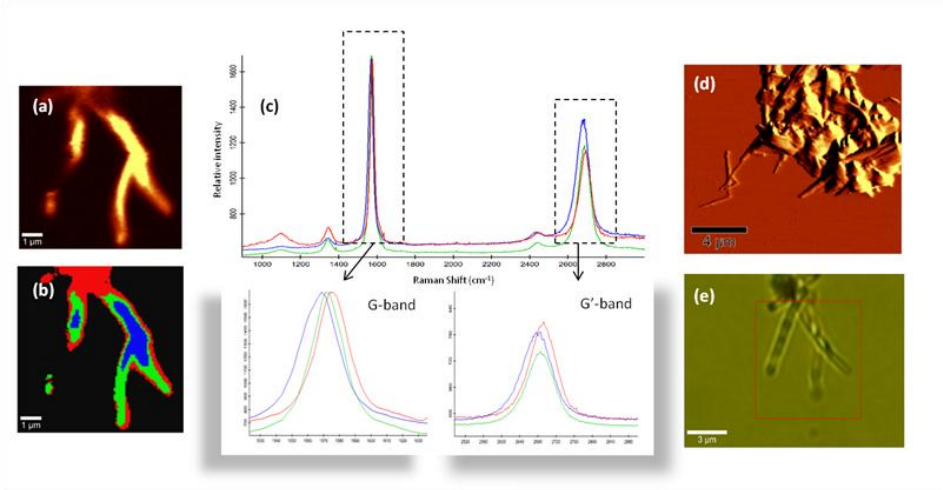

Figure 7. (a) Raman image which reflects the intensity of G-band in a sample of well-dispersed SWNTs in 5 wt/v% Triton X-100 drop-dried on a glass support, (b) assignation of regions to the different clusters when the set of spectra was submitted to K-NN analysis, (c) Raman spectra corresponding to each cluster, the insets shows the wavenumbers at which appear the G- and G'-band in each cluster, (d) AFM image of the sample, (e) photography acquired with an optical microscope employing a 20x objective of the SWNTs sample.

3.7. Influence of aggregation state in multi-walled carbon nanotubes

Raman spectrum of MWNTs has been less studied than SWNTs. In order to elucidate if these changes due to aggregation also take place when measuring the spectrum of a sample of multiwalled ones, similar measurements were performed. When acquiring the spectrum of solid (without any preparation treatment) as received multiwalled carbon nanotubes, differences in G-/D-band

intensity ratio were also observed although less significant than in previous studies (Figure 8).

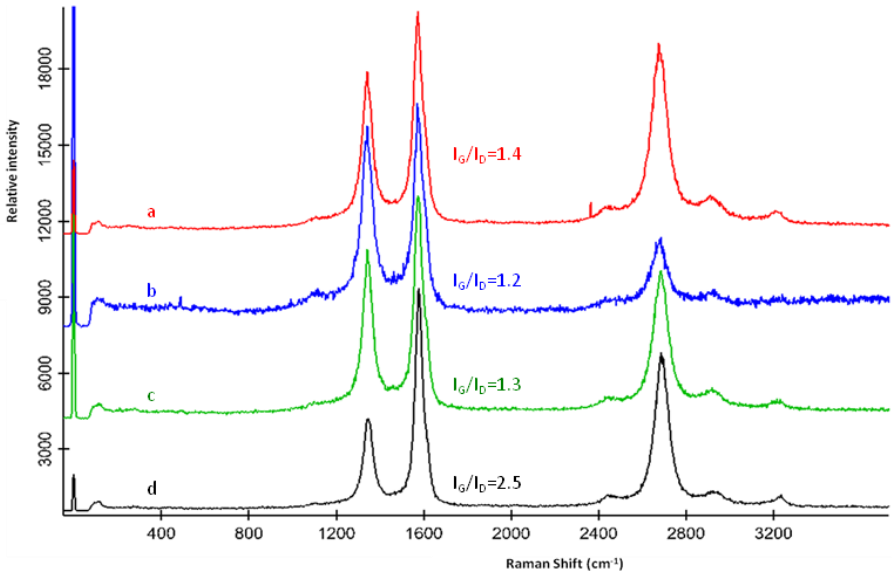

Figure 8. Raman spectra of solid multi walled carbon nanotubes acquired in the same sample at different points (a-d). Spectra were taken with an integration time of 1 second and accumulating 20 spectra with an EMCCD Gain output amplifier.

In order to corroborate it, we measured a Raman image of MWNTs dispersed in methanol and drop-dried on a glass support (Figure 9a), measuring a total of 90 points per line and 90 lines per image at a surface of 72 x 72 μm with an integration time of 0.05 s. The set of spectra were submitted to analogous K-NN analysis than that described for SWNTs. In this case it can be concluded that aggregation affects in less extent to the G-/D-band intensity ratio. Figure 9b shows the different regions of the clusters corresponding to the Raman spectra in Fig. 9c with the same colour code.

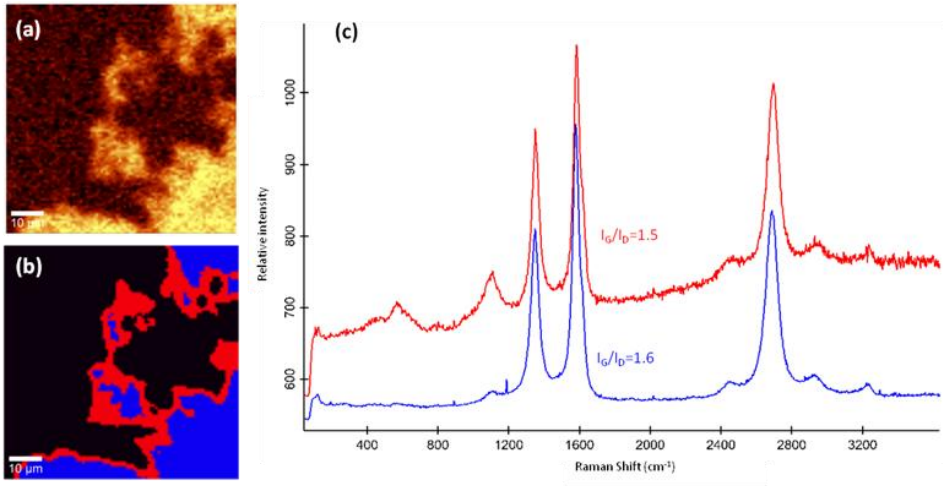

Figure 9. (a) Raman image which reflects the intensity of G-band in a sample of MWNTs dispersed in ethanol and drop-dried on a glass support, (b) assignation of regions to the different clusters when the set of spectra was submitted to K-NN analysis, (c) Raman spectra corresponding to each cluster and I_G/I_D calculated for each spectrum.

In the case of MWNTs, most of the characteristic bands of SWNTs such as the RBM Raman feature are not usually observed owing to the larger diameter of the outer tubes and the ensemble average of inner tube diameter broadens the signal. The less influence of bundle state of the sample on MWNTs features may be attributed to the presence of several layers. In the case of SWNTs the bands associated to isolated nanotubes are associated with a single-layer, while in the case of bundles of SWNTs the signal is influenced by the nanotubes present around them.

4. Conclusions

The need of carefully consider the aggregation state of a sample of single-walled carbon nanotubes when measuring Raman spectrum has been demonstrated, because of their influence in G-/D-band intensity ratio, which has been usually employed to discuss sample purity. The possible influence of

laser beam or sample focusing has been discarded. K-nearest neighbors classified a set of spectra of a region of carbon nanotubes with different aggregation state into three different clusters, according to their G-/D-band intensity ratio. Thus, regarding the variability introduced by aggregation, a sample pretreatment is proposed which consists in the dispersion of carbon nanotubes with the aid of surfactants, such as Triton X-100, and the subsequent measurement of the free carbon nanotubes placed in a glass substrate. It has been proved that when analyzing debundled carbon nanotubes the reproducibility of the measurements is consistent. The influence of aggregation in the case of MWNTs has been also studied finding that this sample is less sensitive to changes produced by this variable than in the case of SWNTs.

Acknowledgements

The authors wish to thank Spain's Ministry of Innovation and Science for funding Project CTQ2007-60426 and Junta de Andalucía for Project FQM02300. A.I. López-Lorente also wishes to thank the Ministry for the award of a Research Training Fellowship (Grant AP2008-02939).

References

[1] H. Wang, J. Luo, F. Schäffel, M. H. Rümmeli, G. A. D. Briggs and J. H. Warner, *Nanotechnology*, 2011, **22**, 245305.

[2] R.P. Raffaelle, B.J. Landi, J.D. Harris, S.G. Bailey and A.F. Hepp, *Mater. Sci. Eng. B*, 2005, **116**, 233–243.

[3] S.A. Miller, V.Y. Young and C.R. Martin, *J. Am. Chem. Soc*., 2001, **123**, 12335-12342.

[4] N. Sinha, J. Ma and J. T. W. Yeow, *J. Nanosci. Nanotech,* 2006, **6**, 573–590.

[5] P. J. F. Harris, *International Materials Reviews*, 2004, **49**, 31-43.

[6] J. M. Planeix, N. Coustel, B. Coq, V. Brotons, P. S. Kumbhar, R. Dutartre, P. Geneste, P. Bernier and P. M. Ajayan, *J. Am. Chem. Soc.*, 1994, **116**, 7935–7936.

[7] A.I. López-Lorente, B.M. Simonet and M. Valcárcel, *Anal. Chem.*, 2010, **82**, 5399-5407.

[8] A. Hagen and T. Hertel, *Nano Lett.*, 2003, **3**, 383-388.

[9] V.A. Sinani, M.K. Gheith, A.A. Yaroslavov, A.A. Rakhnyanskaya, K. Sun, A.A. Mamedov, J.P. Wicksted and N.A. Kotov, *J. Am. Chem. Soc.*, 2005, **127**, 3463-3472.

[10] A. Hartschuh, H.N. Pedrosa, L. Novotny and T.D. Krauss, *Science*, 2003, **301**, 1354-1356.

[11] A. Jorio, M.A. Pimenta, A.G. Souza Filho, R. Saito, G. Dresselhaus and M.S. Dresselhaus, *New J. Phys,.*2003, **5**, 1.1-1.17.

[12] C.G. Salzmann, B.T.T. Chu, G. Tobias, S.A. Llewellyn and M.L.H. Green, *Carbon*, 2007, **45**, 907-912.

[13] A.I. López-Lorente, B.M. Simonet and M. Valcárcel, *Talanta*, 2013, **105**, 75-79.

[14] A.I. López-Lorente. M.L. Polo-Luque, M. Valcárcel, *Anal. Chem.*, 2013, DOI: 10.1021/ac402256p

[15] Y. Miyata, K. Mizuno and H. Kataura, *J. Nanomater.*, 2011, **2011**, 786763-786770.

[16] S. Reich, C. Thomsen and J. Maultzsch, Carbon Nanotubes: Basic Concepts and Physical Properties, John Wiley & Sons, Berlin, 2004, Germany

[17] A.C. Dillon, T. Gennett, K.M. Jones, J.L. Alleman, P.A. Parilla and M.J. Heben, *Adv. Mater.*, 1999, **11**, 1354–1358.

[18] M.E. Itkis, D.E. Perea, R. Jung, S. Niyogi and R.C. Haddon, *J. Am. Chem. Soc.*, 2005, **127**, 3439–3448.

[19] H. Kataura, Y. Kumazawa, Y. Maniwa, Y. Ohtsuka, R. Sen, S. Suzuki and Y. Achiba, *Carbon*, 2000, **38**, 1691–1697.

[20] D.A. Heller, P.W. Barone, J.P. Swanson, R.M. Mayrhofer and M.S. Strano, *J. Phys. Chem. B*, 2004, **108**, 6905-6909.

[21] V.N. Popov and P. Lambin, *Phys. Rev. B*, 2006, **73**, 165425/1-165425/11.

[22] D. Yoon, J.B. Choi, C.S. Han, Y.J. Kim and S. Baik, *Carbon*, 2008, **46**, 1530-1534.

[23] N. Izard, D. Riehl and E. Anglaret, *Phys. Rev. B*, 2005, **71**, 195417.

[24] A. Kumatani and P. A. Warburton, *Appl. Phys. Lett.*, 2008, **92**, 243123.

[25] J.F. Cárdenas, *Carbon*, 2008, **46**, 1327-1330.

[26] K.K. Kim, J.S. Park, S.J. Kim, H.Z. Geng, K.H. An, C.M. Yang, K. Sato, R. Saito and Y.H. Lee, *Phys. Rev. B.*, 2007, **76**, 205426/1-205426/8.

[27] L.M. Ericson and P.E. Pehrsson, *J. Phys. Chem. B*, 2005, **109**, 20276-20280.

[28] T. Liu, Z. Xiao and B. Wang, *Carbon*, 2009, **47**, 3529-3537.

[29] A.I. López-Lorente, B.M. Simonet and M. Valcárcel, *Analyst*, 2013, **138**, 2378-2385.

[30] M.S. Dresselhaus, G. Dresselhaus, R. Saito and A. Jorio, *Phys. Rep.*, 2005, **409**, 47-99.

[31] K.R. Moonoosawmy, P. Kruse, J. Phys. Chem. C 113 (2009) 5133-5140.

[32] P. Corio, P.S. Santos, M.A. Pimenta and M.S. Desselhaus, *Chem. Phys. Lett.*, 2002, **360**, 557-564.

[33] J. Judek, C. Jastrzebski, A. Malopeszy, M. Mazurkiewicz, L. Stobinski and M. Zdrojek, *Phys. Status Solidi A*, 2012, **2**, 313-316.

[34] V. C. Moore, M. S. Strano, E. H. Haroz, R. H. Hauge and R. E. Smalley, *Nano Lett.*, 2003, **3**, 1379-1382.

[35] I. Cotiuga, F. Picchioni, U. S. Agarwal, D. Wouters, J. Loos and P. J. Lemstra, *Macromol. Rapid Commun.*, 2006, **27**, 1073-1078.

[36] Y. Liu, L. Gao, S. Zheng, Y. Wang, J. Sun, H. Kajiura, Y. Li and K. Noda, Nanotechnology, 2007, **18**, 365702.

[37] M. Zheng, A. Jagota, E. D. Semke, B. A. Diner, R. S. Mclean, S. R. Lustig, R. E. Richardson and N. G. Tasii, *Nat. Mater.*, 2003, **2**, 338-342.

[38] R. Rastogi, R. Kaushal, S. K. Tripathi, A. L. Sharma, I. Kaur and L. M. Bharadwaj, *J. Colloid Interface Sci.*, 2008, **328**, 421-428.

Capítulo 6

Qualitative detection and quantitative determination of single-walled carbon nanotubes in mixtures of carbon nanotubes with a portable Raman spectrometer

Analyst 138 (2013) 2378-2385

RSC Publishing

Analyst

138 (2013) 2378-2385

Qualitative detection and quantitative determination of single-walled carbon nanotubes in mixtures of carbon nanotubes with a portable Raman spectrometer

A. I. López-Lorente, B. M. Simonet, M. Valcárcel

Department of Analytical Chemistry, University of Córdoba, E-14071 Córdoba, Spain.

The main aim of this work is to develop a one-step method for the characterization of mixtures of single- and multi-walled carbon nanotubes using a simple and inexpensive tool, a portable Raman spectrometer. In order to overcome the problem of heat dissipation in solid samples, the suitability of three surfactants—SDS, Triton X-100 and CTAB—to disperse nanotubes has been evaluated. A systematic study of the wavenumbers and relative intensity of the D and G bands has been carried out with six samples of multiwalled carbon nanotubes (MWNTs) and one of single-walled carbon nanotubes (SWNTs) dispersed in these surfactants, and this has been compared with solid samples. Finally, the possibility to identify and (semi)quantify the presence of SWNTs in a mixture containing MWNTs has been demonstrated.

Keywords: carbon nanotube, Raman spectroscopy, characterization, SWNTs, MWNTs, surfactants.

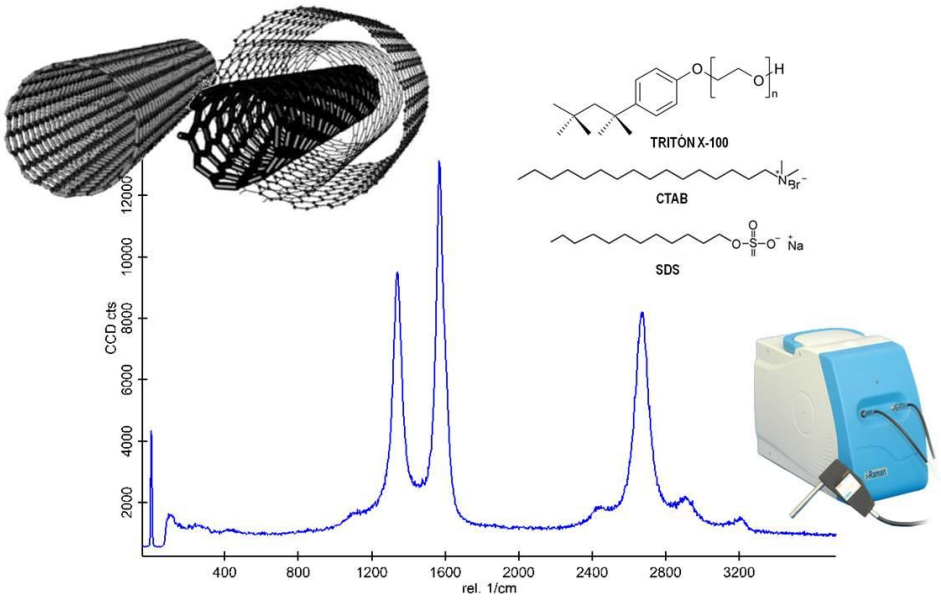
TRITÓN X-100
CTAB
SDS
CCD cts
2000
4000
6000
8000
10000
12000
400
800
1200
1600
2000
2400
2800
3200
rel. 1/cm

1. Introduction

Carbon nanotubes (CNTs) have aroused much attention in many fields of application due to their exceptional electrical, optical and mechanical properties. A bottleneck for a more widespread industrial application is the characterization and identification of CNTs with different properties, since most of the synthetic procedures lead to heterogeneous samples. Depending on the synthetic method, the technique used for the separation from the amorphous by-products, the subsequent cleaning steps, and, finally, different functionalizations, a variety of different CNT are obtained that have very diverse properties [1]. Thus, there is a need for new analytical methodologies, based on simple instrumentation, for a rapid characterization of the products of these synthetic processes as well as the control of raw materials.

CNTs dispersions have been characterized by UV-Visible absorption spectroscopy [2], near infrared (NIR) fluorescence spectroscopy [3], or just by visual inspection of the darkness of the dispersions [4]. UV-Vis absorption spectroscopy has been used to quantify different SWNTs dispersions [5], although it is difficult to separate contributions from SWNTs and other species such as carbonaceous impurities or dispersing agents. NIR luminescence studies [6] are limited to individually dispersed nanotubes due to the quenching effect of metallic ones as well as the surfactant influence on the peak. Microscopy-based techniques [7] provide exact information about type and characteristics (shape, size, etc.), however, they present shortcomings in sample preparation such as the aggregation of the nanoparticles as well as the statistical uncertainty due to the human subjectivity implied when deciding which parts of the grid are photographed. Separation techniques (i.e. electrophoresis) have also been employed for the separation of single-walled carbon nanotubes, based on tube length or diameter-selective CE separation [8].

With regard to these techniques, Raman spectroscopy has emerged as a powerful technique for the characterization of carbon nanotubes since Raman measurements are simple, can be performed at room temperature and under ambient pressure, are quick, non-destructive and non-invasive [9], and it is possible to find sophisticated laboratory equipment as well as less expensive portable ones. Raman scattering from SWCNTs is a resonant phenomena which generates an intense and easily measurable signal. Their widespread acceptance relies on their usefulness to provide information about vibrational properties that can be correlated with the structure and electronic properties of the nanotubes. The most significant Raman spectral features for carbon nanotubes are the radial breathing mode (RBM, 100–300 cm^{-1}), the disorder peak (D peak, ~1350 cm^{-1}), the tangential mode (G band, 1400–1700 cm^{-1}), and the second order overtone of the D peak (G', 2500–2800 cm^{-1}).

Carbon nanotubes tend to form aggregates, and exfoliation of these bundles has been attempted by ultrasonication in the presence of organic solvents (e.g. o-dichlorobenzene, benzyl chloride [10]) or aqueous solutions of surfactants [11], copolymers [12], polyelectrolytes [13] and DNA molecules [14]. Raman spectroscopy has been employed for the characterization of the disaggregation state of CNT bundles dispersed with the aid of surfactants such as sodium dodecylbenzene sulfonate (SDBS) [4, 15, 16], sodium deoxycholate (DOC) [17], sodium cholate (SC) [18], sodium dodecylsulfate (SDS) [19,20] and Triton X-100 [19].

In this paper, a rapid technique with affordable equipment has been developed for the characterization of mixtures of single and multiwalled carbon nanotubes. Surfactant dispersions are employed in order to overcome the limitations of the portable Raman spectrometer for its use from an analytical point of view. The suitability of sodium dodecylsulfate (SDS), Triton X-100 and cetyltrimethylammonium bromide (CTAB) surfactants have been evaluated. A

systematic study of the wavenumbers and relative intensity of the D and G bands has been carried out with six samples of multiwalled carbon nanotubes and one of single-walled. Measurements of dispersions have been compared with solid samples of the same nanotubes. Finally, the discriminated contribution of SWNTs to the Raman spectra of mixtures of both single- and multi-walled nanotubes has been demonstrated, which allows their identification and quantification. The added value of this work is the use of an inexpensive portable Raman spectrometer for the rapid and simple identification of single-walled carbon nanotubes within a sample of multiwalled ones, which can be applied as a screening method for the quality control of raw samples.

2. Materials and methods

2.1. Chemicals

Different types of carbon nanotubes have been used. Table 1 shows the main characteristics of each kind of nanotube. MWNTs-1, 2, 3 were provided by Cheap Tubes (USA), MWNTs-4 were provided by Bayer Material Science (Germany), MWNTs-5 were bought from NTP (China), MWNTs-6 from Nanocyl (Belgium). SWNTs were provided by NTP.

Carbon nanotube dispersions were prepared with the aid of surfactants. Triton X-100 and cetyltrimethylammonium bromide (CTAB) were provided by Fluka, (Buchs, Switzerland) and sodium dodecylsulfate (SDS) 98.5% was bought from Sigma-Aldrich (Madrid, Spain).

2.2. Equipment

Raman spectra were recorded with a portable Raman spectrometer system provided by B&W TEK Inc., known as i-Raman BWS415 with a wavelength of 785 nm and a maximum laser output power at the system's excitation port of 354

mW ± 15%. OPUS 5.0 from BrukerOptik GmbH was employed for data treatment and spectra analysis.

Carbon nanotubes were dispersed by using an ultrasound bath without heating (Ultrason model, Selecta, 50 W, 60 Hz). A precision analytical scale (Ohaus, Explorer model) was also employed.

Table 1. Characteristics of the carbon nanotubes subject of study

	Diameter (nm)	Length (μm)	Functionalization
MWNTs-1	10-30	10-30	2.5 (wt)% OH
MWNTs-2	10-30	10-30	1.6 (wt)% COOH
MWNTs-3	10-30	10-30	-
MWNTs-4	5-20	1-10	-
MWNTs-5	10-20	5-15	-
MWNTs-6	9.5	1.5	-
SWNTs	<2	5-15	-

For Raman measurements of solid samples, a confocal Raman equipment (alpha500, manufactured by WITec GmbH) was employed. For excitation, a frequency double Nd:YAG laser at 532 nm (second harmonic generation) was used, which resulted in a penetration depth in silicon of about 0.5 mm. Raman spectra were collected using a 600 g mm^{-1} diffraction grating. The laser beam was focused on the sample surface using a 100x/0.95 Nikon objective. Laser powers were measured directly on the sample stage and were typically between 0.5 and 1.5 mW.

2.3. Preparation of the dispersions

5 mg of carbon nanotubes were combined with 2 mL of a 10 wt/vol% SDS solution, a 10 wt/vol% Triton X-100 solution or 10 wt/vol% CTAB solutions. Carbon nanotubes were placed in a mortar and crushed with a few microlitres of the surfactant solution in order to achieve a better dispersion. The mixture (with

the final volume of surfactant solution) was then dispersed by ultrasonic irradiation in a bath sonicator (60 Hz) for 10 min. The ultrasonic irradiation was optimized in order to provide a good dispersion of carbon nanotubes in the surfactant solution without damaging them. Fig. 1 shows a typical TEM photograph of MWNTs-6 dispersed in Triton X-100 as an example.

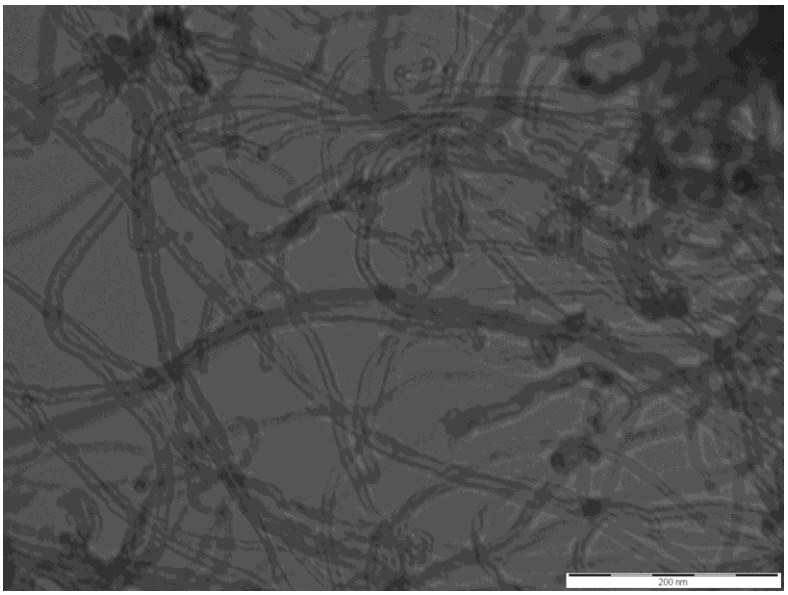

Figure 1. Transmission electron microscopy (TEM) photograph carried out with Philips CM-10 electron microscope. The sample was prepared by placing one drop of a dilute solution of dispersed MWNTs-6 in Triton X-100 onto a copper TEM grid with a Carbowax forward.

2.4. Proposed methodology

For recording Raman spectra, dispersions were pipetted into a 100 mL polyethylene home-made vial with a diameter of 0.5 cm. Raman spectra of solutions were recorded on the portable Raman spectrometer described above, by accumulating six spectra with collection times of 50 s each with a laser power of 354 mW.

3. Results and discussion

Carbon nanotube samples can be damaged during data capture in Raman spectroscopy due to their poor heat dissipation despite the use of low laser power settings. The first studies in this work were carried out directly with solid samples with the portable equipment, but this resulted in damage to the carbon nanotubes. Measurements of carbon nanotube powder were achieved with a confocal Raman spectrometer coupled to an optical microscope which allows sample focusing. This equipment is more than ten times more expensive than the portable one. As the aim of this work was the development of a simple and cost-effective methodology, we decided to change the procedure of spectra acquisition by measuring dispersions of carbon nanotubes, which is feasible with the portable Raman spectrometer since Raman spectra of surfactant or polymer-suspended SWNTs are similar to those in aqueous solution [21]. Surfactants facilitate sample heat dissipation due to the much larger thermal conductivity of liquids with respect to the air.

Different surfactants have been evaluated for this task, namely anionic sodium dodecylsulfate (SDS), cationic cetyltrimethylammonium bromide (CTAB) and neutral Triton X-100.

3.1. Optimization of the amount of surfactant for dispersions

The first step was the optimization of the best conditions for the preparation of the dispersions of carbon nanotubes and their stability. To this end, the surfactants previously mentioned were studied at different concentrations of each and a variety of conditions of agitation/radiation. In order to study the optimum amount of surfactant necessary to achieve a homogeneous dispersion of carbon nanotubes, without interfering in the subsequent Raman measurements, dispersions in a range of surfactant concentration from 0.5% to 20%wt/vol were prepared, with sample concentration at intervals from 0.5 to 2.5

mg mL^{-1}. Ultrasound radiation times varied from 5 minutes to 1 hour. Evaluation of the best conditions for the dispersion was accomplished by means of absorbance and turbidimetry measurements. Because lower concentrations of surfactant were not able to completely disperse carbon nanotubes, the criterion followed to recommend the concentration of surfactant was the determination of the maximum amount of surfactant compatible with the Raman detection. For the three surfactants, concentrations higher than 15% result in a background noise of the spectrum as well as the presence of surfactant peaks. The fact that high concentrations of surfactant result in aggregation of CNTs due to a large degree of circular micelle formation has been described [22]. Therefore, for further studies a concentration of 10% was recommended (Fig. 2a).

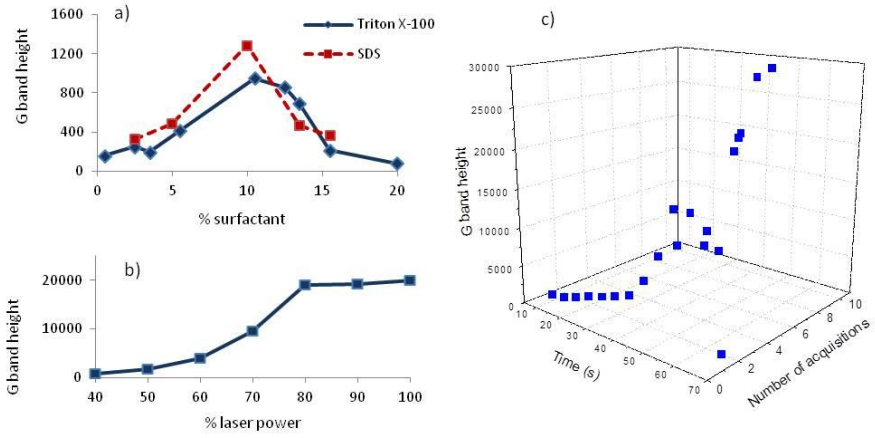

Figure 2. (a) Dependence of the intensity of the G band with the % of surfactant employed for the dispersion in the case of SDS and Triton X-100; (b) influence of laser power on the intensity of the G band; (c) influence of time of measurement as well as number of acquisitions on the intensity of the G band.

The selected concentrations for the three surfactants are below the critical micellar concentrations (cmc), which are tabulated by Sigma-Aldrich [23] to be 0.2–0.9 mM for Triton X-100, 1 mM for CTAB and 7–10 mM for SDS.

We recorded spectra of the surfactants employed for the dispersion and compared them with the spectrum of the carbon nanotubes dispersed with the aid of them. The bands of the surfactant do not appear in the spectrum of the samples of carbon nanotubes with the same concentration of surfactant. This fact allows carbon nanotube dispersions spectra to be recorded. As an example, Fig. 3 shows the spectra of a 10% aqueous solution of SDS (which is below the cmc) and a carbon nanotube (MWNTs-1) dispersion in 10% SDS. As can be seen, there is no influence of the surfactant in the spectrum of the nanoparticles, so it was not necessary to subtract its spectrum from the dispersion one.

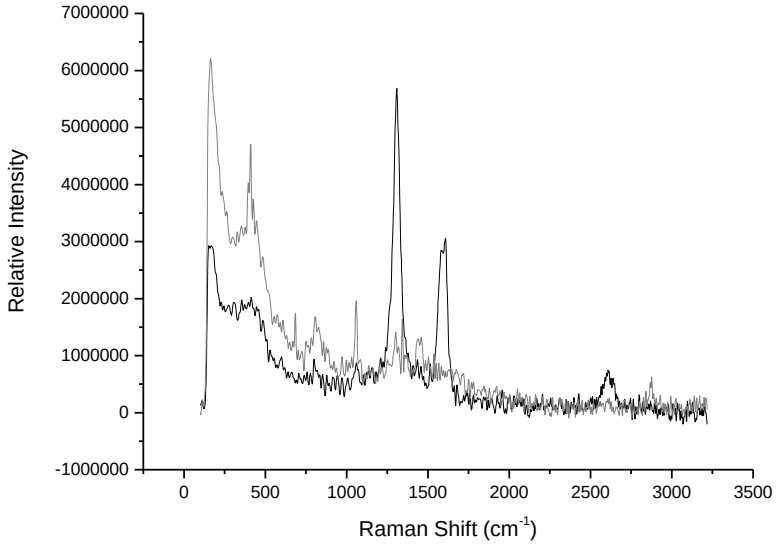

Figure 3. Raman spectrum of a solution of 10%wt/vol SDS in water (grey) and 2.5 mgmL^{-1} MWNTs-1 dispersed in 10%wt/vol SDS (black).

The mechanism of dispersion is that surfactant molecules orient themselves in such a way that the hydrophobic tail groups face the nanotube surface, while hydrophilic head groups face the aqueous phase, producing a lowering of the nanotube–water interfacial tension [24].

It is thought that the interaction of linear ionic surfactants (SDS and CTAB) with the nanotube surface may be weaker than that of the neutral surfactant (Triton X-100), since they do not contain aromatic rings. In fact, the concentrations of each surfactant employed for dispersions were 0.16 mM for Triton X-100, 0.27 mM CTAB and 0.34 mM in the case of SDS. Thus, the dispersing power of surfactants follows the order: SDS < CTAB < Triton X-100. This behavior agrees with other studies; it has been described in the literature that CTAB can better suspend the nanotubes at minimum concentration (because it has a longer alkyl chain length) than SDS, and so the adsorption was induced exclusively by hydrophobic interactions [22]. Moreover, Triton X-100 has been said to have the highest dispersing power by virtue of its aromaticity [24]. Molecules having the benzene ring structure adsorb more strongly to the graphitic surface due to π–π stacking type interactions [24]. The amount of adsorbed surfactant depends on graphite–surfactant interactions, surface structure and both length of alkyl chains, head group size and charge of the surfactant [25] affect their dispersing power. Hydrophobic tail groups are placed usually flat on the graphitic surface, since methylene units of hydrocarbon chains are well coordinated with graphitic unit cells [24]. Longer tails means high spatial volume and more steric impediment, thus providing greater repulsive forces between individual carbon nanotubes. Besides this, surfactants with unsaturated bonds in their tail groups contribute more towards nanotube dispersion [24].

Regarding the dispersion of carbon nanotubes, 10 minutes of ultrasound irradiation has demonstrated to be sufficient in order to obtain homogenous and stable dispersion of samples, although the amount dispersed was different

depending on carbon nanotube–surfactant combination. In spite of the amount of surfactant used to disperse the sample, it is not possible to assure the absence of remaining aggregates. However, under the recommended conditions, Raman measurements were reproducible and characteristic of the carbon nanotube.

3.2. Optimization of laser power

As has been previously explained, the main difficulty found when measuring the Raman spectra of solid samples of carbon nanotubes is the heat degradation of the sample due to the laser radiation. In fact, the portable Raman equipment does not allow achieving this, since it is less flexible in regulating the power of the laser. Measurements of solid carbon nanotubes were carried out with the second equipment, by carefully regulating the laser power needed to avoid not only damages on the sample but also the appearance of interferences due to fluorescence of the sample (a drawback which has to be taken into account when measuring powder samples). These disadvantages have been overcome by dispersing the nanotubes in aqueous suspensions with the aid of surfactants. Solutions allow better heat dissipation which decreases the requirements of laser conditions.

The influence of laser power on the spectra of the nanotubes has been studied. We found that at low laser power we could not record the spectrum. When increasing the laser power the spectrum was more sensitive (Fig. 2b), peaks were higher and we did not notice differences in the shape of the entire spectrum or loss of a peak with the power. The influence of laser irradiation over the Raman features in carbon nanotubes samples has been described in literature [10, 26]. However, in our case the ratio I_D/I_G was not affected by laser power. In any case, measurements have been carried out using the same laser power for all the samples with dispersed carbon nanotubes. For them, the optimum laser power

was found to be the maximum allowed by the equipment, which was 354 mW with a laser wavelength of 785 nm.

On the other hand, the influence of heating (as consequence of laser irradiation) has been also described, which leads to an increase in D peaks [10]. In order to evaluate this possible influence, measurements with samples dispersed in surfactants were performed with the sample heated at different temperatures between the range 25–60ºC. In order to minimize the heating effect of the laser in the sample, measurements were also carried out on a rotating sample. The trend in the I_D/I_G ratios became unaltered since all measurements used the same laser power. In fact, it has been described that laser irradiation purifies carbon nanotubes during the first power sweep and an almost constant I_D/I_G ratio is observed after the irradiation process in subsequent measurements [27].

In the case of solid samples, laser power was reduced to 1.0 mW for a laser wavelength of 532 nm using a 100x objective lens. The laser power to measure Raman spectra of CNT bundles without burning the sample should be much lower than for isolated nanotubes because of the poor inter-tube thermal conductivity in CNT bundles [28].

3.3. Optimization of acquisition time and the accumulated spectra

Spectra were performed with an acquisition time ranging from 10 to 65 s with a number of acquisitions ranging from 1 to 10 (Fig. 2c). The minimum time of acquisition necessary to visualize the spectrum has been proved to be 10 s, being necessary to accumulate more than one spectrum in order to achieve a good signal-to-noise ratio. A compromise between the duration of the acquisition and the quality of the spectrum has to be reached, with 10 acquisitions being enough to record an acceptable spectrum. Thus, the best conditions in terms of shape of the spectrum and duration of the acquisition

were 50 seconds accumulating a sum of 6 spectra. In further studies these were the performance conditions.

3.4. Influence of pH

In order to investigate the possible influence of the pH of the media when recording the spectrum owing to the presence of groups such as –OH or –COOH, we measured the spectrum of samples of carbon nanotubes with the mentioned groups at different pH values. We did not notice differences in the spectrum, so in further studies we did not take this into account.

3.5. Evaluation of D/G band intensity ratio

Dispersions of the different carbon nanotubes were prepared and measured under the optimum conditions. The ratio of intensity of D/G bands was calculated for each nanotube with the different surfactants. The intensity ratio of the G and D peaks (I_D/I_G) refers to the ratio of the height of each peak after subtracting the baseline. Fig. 4 shows the calculated ratio values. As can be seen, in the case of multiwalled carbon nanotubes the intensity of the D band is in all cases higher than the intensity of the G band, resulting in ratio values greater than 1. However, in the case of single-walled carbon nanotubes the ratio decreases to values around $I_D/I_G=0.5$, depending on the surfactant employed for dispersion.

MWNTs-4 when dispersed provided the highest ratio, which means a low intensity for the G feature with respect to the D band. Differences between surfactants may be attributed to the different dispersion capabilities of each of them for the particular case of each type of nanotube. In fact, values of D/G ratio have been not calculated for MWNTs-5 dispersed in CTAB and MWNTs-6 in Triton X-100, since nanotube dispersions did not provide a good spectrum where these bands could be correctly identified. The influence of the degree of

alignment in MWNTs on the I_D/I_G ratio has been reported [29], thus, differences found between nanotubes and within the same type of nanotubes dispersed with different surfactants can be explained on this basis.

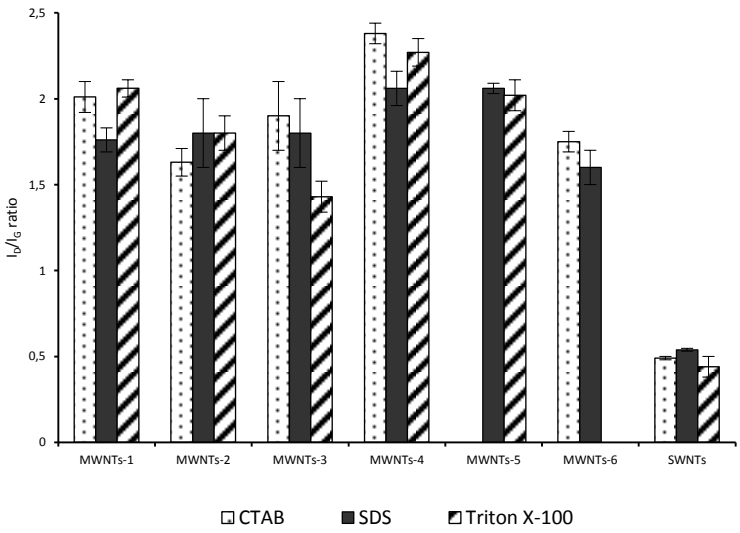

Figure 4. I_D/I_G ratio for each type of carbon nanotubes studied.

In SWNTs, the G band is, along with RBM bands, one of the strongest features in Raman spectra, and both are first-order Raman modes. However, the D band is a second-order Raman scattering and is weaker. It should be pointed out that an inverse behavior of the intensity of these first and second order Raman modes is observed in the case of the six different multi-walled carbon nanotubes studied in this work with respect to SWNTs, which can be related to the higher quantity of structural defects because of their multiple graphite layers.

3.6. Evaluation of D and G band wavenumbers

The D band is related to disorder present in the carbon aromatic structure. From the experimental results, it can be assumed that the position of the D bands for carbon nanotubes with different characteristics differs. Fig. 5(A1) shows the Raman shift at which the D band appears for the carbon nanotubes subjected to the present study.

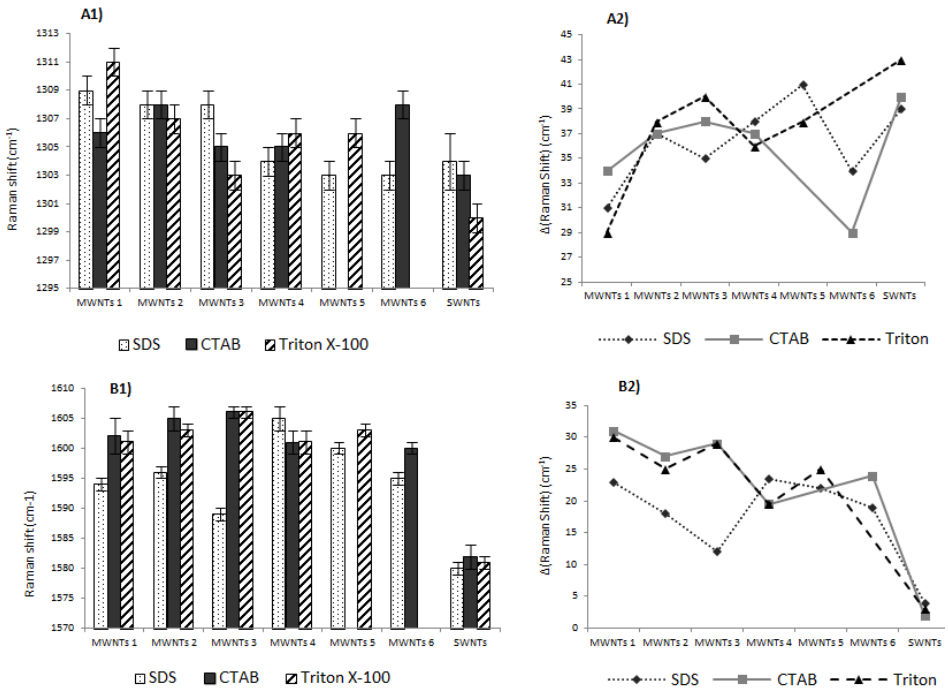

Figure 5. (1) Raman shift values at which D band (A1) and G band (B1) features appear when measuring dispersion of the different carbon nanotubes with each surfactant. (2) Deviation of the Raman shift wavenumbers (in absolute value) of the D band, downshift, (A2) and the G band, upshift, (B2) from dispersions with respect to solid samples.

As previously commented, the G band is a first-order Raman mode which is the strongest feature in the Raman spectra of SWNTs. It originates from sp^2 carbon sites present in the sample [30]. In SWNTs it is usually split into features around

1580 cm^{-1}. However, the splitting of the G band in MWNTs is small in intensity and smeared out due to the effect of the diameter distribution within the individual MWNTs. The G band exhibits a weakly asymmetric lineshape appearing as a single peak at a frequency closer to that of graphite of 1582 cm^{-1} [31]. In this study the splitting of the G band has not been observed. Fig. 5(B1) depicts the Raman shift for the G feature in the Raman spectra of dispersed carbon nanotubes with each surfactant. SWNT G peak appears at lower wavenumbers compared with that of MWNTs.

3.7. Comparison of D and G band wavenumbers with solid carbon nanotubes spectra

The most prominent variation of spectra of solid carbon nanotubes with respect to surfactant-dispersed solutions is a shift of Raman features, including D and G bands which are the object of this study. The average positions of the D peaks in the spectra are 1340 cm^{-1} (MWNTs-1), 1345 cm^{-1} (MWNTs-2), 1343 cm^{-1} (MWNTs-3), 1342 cm^{-1} (MWNTs-4), 1344 cm^{-1} (MWNTs-5), 1337 cm^{-1} (MWNTs-6) and 1343 cm^{-1} (SWNTs) when recorded using 532 nm excitation (solid samples). However the positions of D peaks in the spectra of dispersed nanotubes using a 785 nm excitation wavelength were found at values ranging from 1300–1311 cm^{-1}, as depicted in Fig. 5(A1), depending on the nature of the nanotube and the dispersant. Thus, the D band shows a shift in the range of 30–40 cm^{-1} (see Fig. 5(A2)) from solid samples (532 nm laser wavelength) to dispersed nanotubes (785 nm laser wavelength).

In the case of the G band, the average positions in solid carbon nanotubes are 1571 cm^{-1} (MWNTs-1), 1578 cm^{-1} (MWNTs-2), 1577 cm^{-1} (MWNTs-3), 1581 cm^{-1} (MWNTs-4), 1578 cm^{-1} (MWNTs-5), 1575 cm^{-1} (MWNTs-6) and 1584 cm^{-1} (SWNTs). The positions of G peaks in the spectra of dispersed nanotubes using a 785 nm excitation wavelength were found at values ranging from 1589–1606 cm^{-1}, as depicted in Fig. 5(B1), depending on the nature of the nanotube and

the dispersant. Again a shift in the range of 0–30 cm^{-1} (see Fig. 5(B2)) from solid samples to dispersed nanotubes can be observed. It should be noted that in the case of SWNTs there is no significant shift between solid and dispersed samples that being the main difference in the case of dispersed SWNTs, without dependence of the surfactant employed, in which the G band appeared in all cases at lower wavenumbers than MWNTs dispersions.

The observed downshift and upshift in the case of D and G bands, respectively, may be attributed to the influence of laser wavelength and debundling of carbon nanotubes.

Firstly, it should be taken into account that measurements in the case of solid samples were performed with a laser at a wavelength of 532 nm, and in the case of dispersion at a wavelength of 785 nm. The shift of Raman features depending on the laser wavelength has been described previously [29]. The fact that several weak Raman signals vary in phonon frequency when changing laser excitation energy has been reported [32-34], such as the D band at 1350 cm^{-1} whose frequency changes by 53 cm^{-1} as a result of changing the laser energy [28].

On the other hand, different transition energies have been observed for individual suspended SWNTs wrapped by a surfactant and SWNTs in bundles, where the transition energies for bundled SWNTs are shifted towards lower energies [35-37]. A shift of Raman bands in MWNTs to higher wavenumbers upon debundling, on account of reduced intertube interactions, has also been reported [38].

Moreover, an upshift of RBM bands has been described when SWNTs are dispersed in suspensions with respect to dry powder, which has been assigned to molecular interactions between the surfactant molecules and the nanotubes [19]. In our case, the observed upshift of the G band and downshift of the D band could be attributed to the same phenomenon. The hydrophobic parts of

all the surfactants employed as dispersing agents in this study are similar to those of alkanes, so they will exert molecular pressure with similar cohesive energy density to long alkanes. This agrees with the finding of Wood and Wagner [39] who showed an upshift of the G′ band of carbon nanotubes dispersed in fluids when increasing the cohesive energy density, due to the internal pressure of molecular liquids.

3.8. Characterization of mixtures of single- and multiwalled carbon nanotubes

The suitability of Raman spectroscopy to identify and quantify the presence of single walled carbon nanotubes within a dispersion of multi walled carbon nanotubes has been investigated. For that purpose we prepared mixtures with different quantities of SWNTs and carbon nanotubes modified with hydroxyl groups (MWNTs-1) ranging from 0–8 mg of each CNTs in 4 mL of 10% SDS solution. The spectra showed the presence of the different carbon nanotubes by variation of the relative intensity of the D/G bands which resulted in 0.53 in pure SWNTs and 2.01 for pure MWNTs-1.

Fig. 6 shows the relation found between the percentage of SWNTs in the mixture of carbon nanotubes and the ratio of height of D/G bands. Results of the relation of full width at half maximum (FWHM) of the D/G bands agreed with these results, showing a linear relationship that can be employed to determine the quantity of carbon nanotubes of each type that are present in an unknown sample. This information may be very useful to characterize industrial samples that are composed of a mixture of nanotubes of different types.

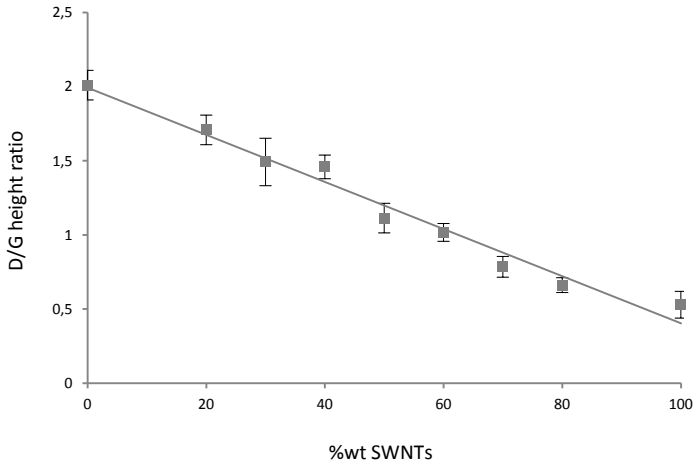

Figure 6. Relationship between the percentage of SWNTs present in the sample of carbon nanotubes mixtures and the height of the D/G band ratio.

In addition to the influence that the presence of SWNTs in a MWNTs sample has demonstrated on the height of the D/G band ratio (Fig. 6), a variation has also been observed in the G band lineshape. Raman features have been analyzed by a Lorentzian fit of the spectra. It has been described that in the case of the lower frequency G band feature (G^-) for metallic SWNTs, a better fit can be achieved by a Breit–Wigner–Fano lineshape, while in the case of semiconducting SWNTs the G^- band remains well fit by a Lorentzian [28]. In the present study, we have both metallic and semiconducting SWNTs in our sample, thus the fitting has been performed according to the Lorentzian lineshape both for SWNTs and MWNTs:

$$y = y_0 + \frac{2A}{\pi}\frac{w}{4(x - x_c)^2 + w^2}$$

In the case of the G peak a shoulder is observed when varying the percentage of SWNTs and MWNTs within the mixture. The G bands of spectra of dispersions with different proportions of both types of carbon nanotubes have been

analyzed and deconvoluted by using a Lorentzian fitting lineshape, and the contribution of both single and multiwalled carbon nanotubes have been shown (Fig. 7).

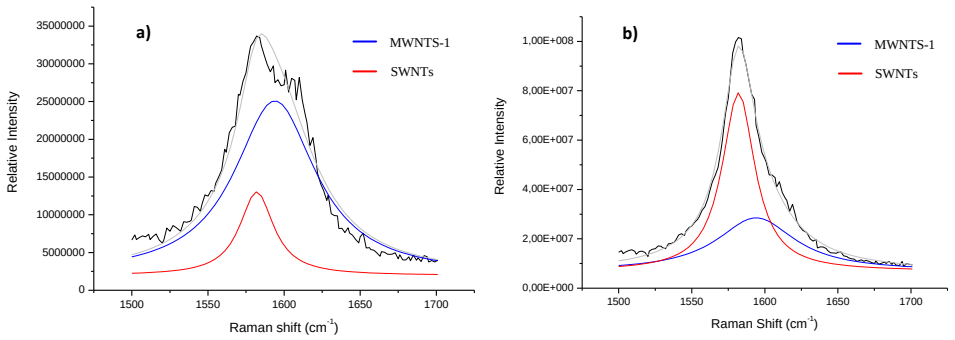

Figure 7. G band feature for (a) mixture with 20%wt/vol of SWNTs and (b) 80%wt/vol of SWNTs in a mixture with MWNTs-1. The peak has been fitted with a Lorentzian lineshape and deconvoluted to show the contribution of each type of nanotube to the G band feature.

4. Conclusions

A detailed study of the Raman spectra of a variety of surfactant dispersed carbon nanotubes including the experimental optimization and the study of the results achieved allows us to develop a simple (one step) and reliable method for the characterization of mixtures of single- and multi-walled carbon nanotubes based on the relative intensity of the D and G bands as a measurement parameter.

The main contributions of this work with regards to other methods described in the literature with the same aim are based on the following factors: (i) the simplicity of the procedure; (ii) the inexpensive instrument involved; (iii) the portability of the instrument, (iv) the systematic study of the Raman wavenumbers and the intensity ratio of D and G bands for CNTs suspended in

three different surfactants and (v) the feasibility to detect and (semi)quantify SWNTs in the presence of MWNTs both by using I_D/I_G ratio and by the effect on the G band lineshape.

The results achieved demonstrate the feasibility of the proposed methodology as fit for purpose. This topic is of great relevance in both nanoscience and nanotechnology realms since one of their bottlenecks, not fully solved to date, is the batch-to-batch reproducibility of commercially supplied nanomaterials. Any contribution to develop simple procedures for quick and reliable quality control of incoming nanomaterials in research laboratories and nanotechnological industries should be obviously welcome.

Acknowledgements

The authors wish to thank Spain's Ministry of Innovation and Science for funding Project CTQ2007-60426 and Junta de Andalucía for Project FQM02300. A. I. López-Lorente also wishes to thank the Ministry for the award of a Research Training Fellowship (Grant AP2008-02939).

References

[1] H. Dai, Acc. Chem. Res., 2002, 35, 1035–1044.

[2] M. J. O'Connell, S. M. Bachilo, C. B. Huffman, V. C. Moore, M. S. Strano, E. H. Haroz, K. L. Rialon, P. J. Boul, W. H. Noon, C. Kittrell, J. Ma, R. H. Hauge, R. B. Weisman and R. E. Smalley, Science, 2002, 297, 593–596.

[3] R. B. Weisman, Anal. Bioanal. Chem., 2010, 396, 1015–1023.

[4] C. G. Salzmann, B. T. T. Chu, G. Tobias, S. A. Llewellyn and M. L. H. Green, Carbon, 2007, 45, 907–912.

[5] V. A. Sinani, M. K. Gheith, A. A. Yaroslavov, A. A. Rakhnyanskaya, K. Sun, A. A. Mamedov, J. P. Wicksted and N. A. Kotov, J. Am. Chem. Soc., 2005, 127, 3463–3472.

[6] A. Hartschuh, H. N. Pedrosa, L. Novotny and T. D. Krauss, Science, 2003, 301, 1354–1356.

[7] A. E. Porter, M. Gass, K. Muller, J. N. Skepper, P. A. Midgleyand M. Welland, Nat. Nanotechnol., 2007, 2, 713–717.

[8] A. I. López-Lorente, B. M. Simonet and M. Valcárcel, TrAC, Trends Anal. Chem., 2011, 30, 58–71.

[9] A. Jorio, M. A. Pimenta, A. G. Souza Filho, R. Saito, G. Dresselhaus and M. S. Dresselhaus, New J. Phys., 2003, 5, 1.1–1.17.

[10] K. R. Moonoosawmy and P. Kruse, J. Phys. Chem. C, 2009, 113, 5133–5140.

[11] V. C. Moore, M. S. Strano, E. H. Haroz, R. H. Hauge and R. E. Smalley, Nano Lett., 2003, 3, 1379–1382.

[12] I. Cotiuga, F. Picchioni, U. S. Agarwal, D. Wouters, J. Loos and P. J. Lemstra, Macromol. Rapid Commun., 2006, 27, 1073–1078.

[13] Y. Liu, L. Gao, S. Zheng, Y. Wang, J. Sun, H. Kajiura, Y. Li and K. Noda, Nanotechnology, 2007, 18, 365702.

[14] M. Zheng, A. Jagota, E. D. Semke, B. A. Diner, R. S. Mclean, S. R. Lustig, R. E. Richardson and N. G. Tassi, Nat. Mater., 2003, 2, 338–342.

[15] T. Liu, Z. Xiao and B. Wang, Carbon, 2009, 47, 3529–3537.

[16] D. Movia, E. Del Canto and S. Giordani, Phys. Status Solidi B, 2009, 246, 2704–2707.

[17] J. R. Simpson, J. A. Fagan, M. L. Becker, E. K. Hobbie and A. R. H. Walker, Carbon, 2009, 47, 3238–3241.

[18] A. Kumatani and P. A. Warburton, Appl. Phys. Lett., 2008, 92, 243123/1–243123/3.

[19] N. Izard, D. Riehl and E. Anglaret, Phys. Rev. B: Condens. Matter Mater. Phys., 2005, 71, 195417/1–195417/7.

[20] A. W. Musumeci, E. R. Waclawik and R. L. Frost, Spectrochim. Acta, Part A, 2008, 71, 140–142.

[21] A. Y. Glamazda, U. Dettlaff-Weglikowska, V. S. Leontiev, P. V. Mateichenko and V. A. Karachevtsev, Fullerenes, Nanotubes, Carbon Nanostruct., 2006, 14, 221–225.

[22] J. Y. Shin, T. Premkumar and K. E. Geckeler, Chem.–Eur. J., 2008, 14, 6044–6048.

[23] http://www.sigmaaldrich.com/img/assets/15402/Detergent_Selection_Table.pdf

[24] R. Rastogi, R. Kaushal, S. K. Tripathi, A. L. Sharma, I. Kaur and L. M. Bharadwaj, J. Colloid Interface Sci., 2008, 328, 421–428.

[25] V. C. Moore, M. S. Strano, E. H. Haroz, R. H. Hauge and R. E. Smalley, Nano Lett., 2003, 3, 1379–1382.

[26] P. Corio, P. S. Santos, M. A. Pimenta and M. S. Dresselhaus, Chem. Phys. Lett., 2002, 360, 557–564.

[27] J. Judek, C. Jastrzebski, A. Malopeszy, M. Mazurkiewicz, L. Stobinski and M. Zdrojek, Phys. Status Solidi A, 2012, 2, 313–316.

[28] M. S. Dresselhaus, G. Dresselhaus, R. Saito and A. Jorio, Phys. Rep., 2005, 409, 47–99.

[29] H. M. Heise, R. Kuckuck, A. K. Ojha, A. Srivastava, V. Srivastava and B. P. Asthana, J. Raman Spectrosc., 2009, 40, 344–353.

[30] A. C. Ferrari, Diamond Relat. Mater., 2002, 11, 1053–1061.

[31] A. M. Rao, A. Jorio, M. A. Pimenta, M. S. S. Dantas, R. Saito, G. Dresselhaus and M. S. Dresselhaus, Phys. Rev. Lett., 2000, 84, 1820–1823.

[32] M. S. Dresselhaus, G. Dresselhaus, A. Jorio, A. G. Souza Filho and R. Saito, Carbon, 2002, 40, 2043–2061.

[33] M. S. Dresselhaus and P. C. Eklund, Adv. Phys., 2000, 49, 705–814.

[34] J. Kürti, V. Zólyomi, A. Grüneis and H. Kuzmany, Phys. Rev. B: Condens. Matter Mater. Phys., 2002, 65, 165433/1–165433/9.

[35] R. Graupner, J. Raman Spectrosc., 2007, 38, 673–683.

[36] L. M. Ericson and P. E. Pehrsson, J. Phys. Chem. B, 2005, 109, 20276–20280.

[37] C. Fantini, A. Jorio, M. Souza, M. S. Strano, M. S. Dresselhaus and M. A. Pimenta, Phys. Rev. Lett., 2004, 93, 147406.

[38] L. Bokobza and J. Zhang, eXPRESS Polym. Lett., 2012, 6, 601–608.

[39] J. R. Wood and H. D. Wagner, Appl. Phys. Lett., 2000, 76, 2883/1–2883/3.

IV.2. ESPECTROSCOPIA INFRARROJA

La espectroscopia infrarroja (IR) es una técnica instrumental que proporciona información sobre los grupos funcionales y la estructura química de una molécula. La reflectancia total atenuada (ATR) se basa en la formación de una onda evanescente en el límite entre dos superficies con diferente índice de refracción.

Los cambios significativos que se observan en las propiedades ópticas de las moléculas cuando están adsorbidas sobre superficies metálicas han potenciado un interés creciente por las espectroscopias amplificadas por superficie[1]. Como se verá posteriormente en el bloque V.2. el ejemplo más conocido es la dispersión Raman amplificada por superficies (SERS). Por otro lado, Hartstein[2] y colaboradores describieron un incremento de la señal infrarroja de moléculas adsorbidas en superficies metálicas en un factor de hasta 10^4 veces, efecto que fue posteriormente denominado como absorción infrarroja amplificada por superficies (SEIRA) por Osawa y Ikeda[3], por analogía con SERS.

Se han descrito dos mecanismos que contribuyen al incremento de la señal –electromagnético y químico- tanto en espectroscopia SERS como SEIRA. En el caso de SEIRA, el mecanismo electromagnético asume un incremento del campo eléctrico local en la superficie de la nanopartícula, mientras que el

[1] R.P. Van Duyne, Science 306 (2004) 985-986.
[2] A. Harstein, J.R. Kirtley, J.C. Tsang, Phys. Rev. Lett. 45 (1980) 201-204.
[3] M. Osawa, M. Ikeda, J. Phys. Chem. 95 (1991) 9914-9919.

mecanismo químico supone un aumento del coeficiente de absorción debido a interacciones químicas entre las moléculas y la superficie metálica[4].

En el **capítulo 7** se muestra el potencial de la espectroscopia infrarroja como herramienta para la caracterización de nanopartículas de oro en disolución. Se ha monitorizado la síntesis in-situ de nanopartículas de oro mediada por acero inoxidable que se ha propuesto anteriormente en el capítulo 3 de esta memoria de Tesis Doctoral mediante espectroscopia infrarroja por reflexión total atenuada (IR-ATR). El acero inoxidable que forma las paredes de la celda ATR induce la reducción del ácido tetracloroaúrico. A medida que las nanopartículas de oro se depositan en la superficie ATR de SiO_2, se observa un incremento de la señal del agua debido al efecto SEIRA producido por las nanopartículas. Además, se ha demostrado que es posible investigar cambios de estado de agregación de la disolución de nanopartículas así como estudiar la sedimentación de nanopartículas de oro sin ligandos en superficie y con ligandos citrato utilizando esta técnica.

[4] M. Baia, F. Toderas, L. Baia, D. Maniu, S. Astilean, Chem. Phys. Chem. 10 (2009) 1106-1111.

Capítulo 7

Infrared attenuated total reflection spectroscopy as a tool for the characterization of gold nanoparticles in solution

Submitted to Analytical Chemistry

Analytical Chemistry

Submitted

Infrared attenuated total reflection spectroscopy as a tool for the characterization of gold nanoparticles in solution

A. I. López-Lorente[1], M. Sieger[2], M. Valcárcel[1], B. Mizaikoff[2]

[1]*Department of Analytical Chemistry, University of Córdoba, E-14071 Córdoba, Spain.*

[2]*Institute of Analytical and Bioanalytical Chemistry, University of Ulm, Ulm, Germany.*

In-situ synthesis of bare gold nanoparticles mediated by stainless steel as reducing agent was monitored via infrared attenuated total reflection (IR-ATR) spectroscopy. Gold nanoparticles are directly synthesized within the liquid cell of the ATR unit taking immediate advantage of the stainless steel walls of the ATR cell. As nanoparticles are formed, a layer of particles deposits at the SiO_2 ATR waveguide surface. Incidentally, the absorption bands of water increased resulting from surface enhanced infrared absorption (SEIRA) effects arising from the presence of the gold nanoparticles within the evanescent field. Next to the influence of the Au(III) precursor concentration and the temperature, the suitability of IR-ATR spectroscopy as an innovative tool for investigating changes of nanoparticles in solution such as aggregation promoted by an increase of the ionic strength or pH decrease, as well as for detailing the sedimentation process of gold nanoparticles was confirmed.

Keywords: attenuated total reflection, ATR, infrared spectroscopy, surface-enhanced infrared absorption, SEIRA, gold nanoparticles, nanoparticle synthesis, aggregation.

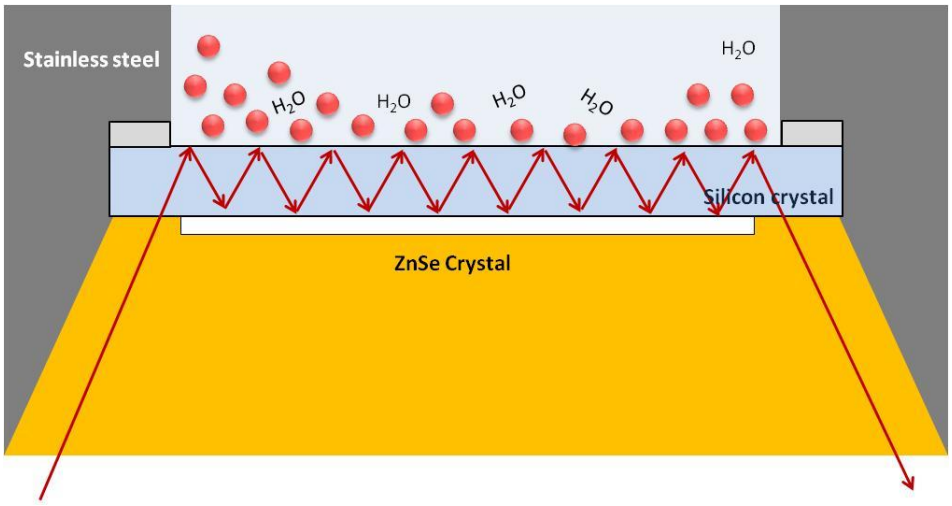
Stainless steel
H_2O
H_2O
H_2O
H_2O
H_2O
Silicon crystal
ZnSe Crystal

1. Introduction

Metallic nanoparticles and especially gold nanoparticles (AuNPs) provide exceptional properties, which have promoted their use in many fields of application including biomedical imaging and diagnostic assays [1], biological applications [2], as catalysts [3], and for applications based on the enhanced optical properties of nanoparticles such as enhanced Rayleigh scattering or surface-enhanced Raman scattering (SERS) of adsorbed molecules [4].

Increasing interest has also been attributed to the diversity of synthetic procedures for the generation of AuNPs [5], which demand for advanced characterization tools for nanoparticles synthesized at a wide variety of conditions. Microscopic techniques are among of the most commonly employed techniques, although they suffer from several drawbacks being e.g., time-consuming in order to assure sample representativeness, and potential problems related to the aggregation of nanoparticles when studied in solution. Optical analysis techniques have proved useful for the characterization of nanoparticles in particular taking advantage of the pronounced surface plasmon resonances attributed to gold nanoparticles. Dynamic light scattering (DLS) is a common method for the size characterization of nanoparticles [6]. In addition, Raman spectroscopy has been applied for the characterization and quantification of gold nanoparticles previously extracted by ionic liquids [7]. Separation techniques including electrophoresis [8] have also been extensively employed for the characterization of synthesized gold nanoparticles. Finally, inductively coupled plasma mass spectrometry [9] (ICP-MS) has been used to quantitatively determine the presence of gold nanoparticles.

In general, gold nanoparticles do not show pronounced mid-infrared (3-20 μm; MIR) absorptions, unless they are functionalized at the surface with organic ligands giving rise to characteristic IR spectra. Consequently, AuNPs with cetyltrimethylammonium bromide (CTAB) molecules adsorbed in ionic liquid

media [10] have been characterized by Fourier transformation infrared (FT-IR) spectroscopy. Furthermore, IR spectra of 2-(12-mercaptododecyloxy)methyl-15-crown-5-ether modified gold nanoparticles [11], 4-mercaptobenzoic acid modified AuNPs [12], and AuNPs-metallocarbonyl conjugates [13] have been published. Infrared attenuated total reflectance (IR-ATR) spectroscopy has been used to quantitatively determine competitive molecular adsorption of thiolated poly(ethylene glycol) at gold nanoparticle surfaces [14]. However, to date infrared spectroscopy has not been used for the characterization of bare gold nanoparticles without any surface modification.

Hartstein et al. [15] reported for the first time on the so-called surface enhanced infrared absorption (SEIRA) effect occurring at corrugated noble metal surfaces. Two enhancement mechanisms – electromagnetic and chemical enhancement - are considered as the main contributions to the observed enhancement in SEIRA spectroscopy [16]. Electromagnetic mechanisms increase the local electric field at the surface, while chemical enhancement assumes an increase of the absorption due to chemical interactions between molecules and gold nanoparticles [17]. SEIRA effects have been used for the determination of molecules such as p-nitrobenzoic acid [18], carbon monoxide [19], octadecanethiol [20-22], 4-pyridinethiol [23], and p-mercaptoaniline [24].

In the present study, photoenhanced adsorption of water at gold nanoparticles has been utilized for *in-situ* monitorization of the synthesis of bare gold nanoparticles via surface-enhanced infrared attenuated total reflection (SEIRA-ATR) spectroscopy. Gold nanoparticles were directly grown within the liquid cell of the ATR unit from a tetrachloroauric acid solution mediated by the stainless steel housing of the ATR cell following a mechanism previously discussed by the authors [25,26]. As nanoparticles are formed and deposited at the surface of the ATR waveguide, an enhancement of the water absorption features is observed, which correlates with the amount of AuNPs present at the surface. A similar

effect has been observed in the case of gold nanoparticles synthesized in D_2O with the absorption bands of deuterium oxide revealing similar enhancement during the formation of AuNPs. Moreover, the suitability of SEIRA-ATR spectroscopy for the investigation of gold nanoparticle solutions has been confirmed by studying effect of salts and pH on the aggregation state of gold nanoparticles in solution, as well as monitoring the involved sedimentation processes. Thus, herein IR spectroscopy is proposed as a novel alternative tool that can be applied for the characterization of AuNPs, being a simple, non-expensive and non-destructive technique.

2. Methods

2.1. Materials and reagents

$HAuCl_4$ solution (Sigma Aldrich) and gold(III) chloride were used to synthesize the gold nanoparticles. Prior to synthesis, the material was washed with a mixture of nitric acid and hydrochloric acid (PANREAC). A flat piece of 304-stainless steel was used as solid reducing agent of gold precursor in order to form gold nanoparticles. Sodium citrate dehydrate 99.5% (Sigma Aldrich) was used to synthesize citrate-coated gold nanoparticles. Silver nitrate, potassium nitrate, and sodium chloride purchased from Sigma-Aldrich were used to investigate the aggregation of the nanoparticles. Hexadecyltrimethylamonium chloride (CTAC) was obtained from Fluka. Deuterium oxide (D_2O) was provided by VWR. All stock solutions were prepared in Milli-Q water.

2.2. Synthesis of bare gold nanoparticles

Gold nanoparticles were synthesized following the procedure described elsewhere [25,26], in which stainless steel is used as solid reductant. All glassware was cleaned with freshly prepared aqua regia (HNO_3:HCl = 1:3 mixture) and then rinsed thoroughly with distilled H_2O prior to use. A piece of

304-stainless steel (12.9 mm^2 of total surface) was introduced into 100 µL of a 0.2 mg mL^{-1} aqueous solution of $HAuCl_4$. The reaction is carried out at room temperature; the stainless steel substrate was simultaneously used as stirrer during the reaction.

2.3. Synthesis of bare gold nanoparticles inside the ATR liquid cell

Gold nanoparticles were also directly synthesized inside the liquid cell of the ATR unit by taking direct advantage of the stainless steel, which forms the walls of the ATR cell. In this case, no stainless steel piece is added to the solution of tetrachloroauric acid, which is used as a gold(III) precursor. Once the tetrachloroauric acid solution is located within the ATR unit, the immediate onset of the formation of gold nanoparticles is observed. Thus obtained AuNPs sediment at the ATR crystal surface facilitating direct monitoring via the infrared analysis techniques detailed below. The reaction was performed at different temperatures: room temperature (i.e., 22ºC), 40ºC, 50ºC, and 60ºC, as controlled by a thermostat unit.

2.4. Synthesis of citrate-coated gold nanoparticles

Gold nanoparticles obtained via $HAuCl_4$ reduction mediated by sodium citrate were also prepared according to the method described by Turkevich et al. [27] applying some modifications, as described elsewhere [7]. Firstly, all glassware were cleaned with freshly prepared aqua regia (HNO_3:HCl 1:3 mixture), and then rinsed thoroughly with distilled H_2O prior to use. Tetrachloroauric acid and sodium citrate solutions were filtered through a 0.45 µm nylon membrane prior use. Once a 0.01% solution of $HAuCl_4$ was boiling, 0.254 mL of a 1% sodium citrate solution were added. The system was then left to react while stirring for a period of 15 min. Afterwards, 5mL of 0.01% $HAuCl_4$ solution were added to the system followed by 0.254 mL of 1% sodium citrate solution, and again stirred while heating for 15 min. Then, the heater was switched off, and the solution

was stirred until cooling to room temperature. Thus obtained AuNPs were stored at 4ºC in an amber bottle.

2.5. Infrared spectroscopic analysis

Infrared measurements were performed using a Vertex 70 FT-IR spectrometer equipped with a BioATRCell-II unit and a liquid nitrogen cooled mercury-cadmium-telluride (MCT) detector (Bruker Optics, Ettlingen, Germany). Figure 1 shows a scheme of the IR measurement setup. Data acquisition and processing was performed using the OPUS 6.5 software package (Bruker Optics, Ettlingen, Germany). Spectra were acquired by averaging 300 scans in the spectral window of 4000 to 400 cm^{-1} at a spectral resolution of 4 cm^{-1}. Prior to analyzing each set of samples, a background spectrum of the tetrachloroauric acid solution was collected when monitoring the subsequent *in-situ* synthesis of AuNPs. If AuNPs were synthesized *ex-situ*, prior to a sample measurement a background spectrum of deposited AuNPs at time zero was recorded. Finally, measurements of the synthesis of gold nanoparticles in D_2O media were acquired averaging 500 scans within 4000 to 400 cm^{-1} at 4 cm^{-1} spectral resolution.

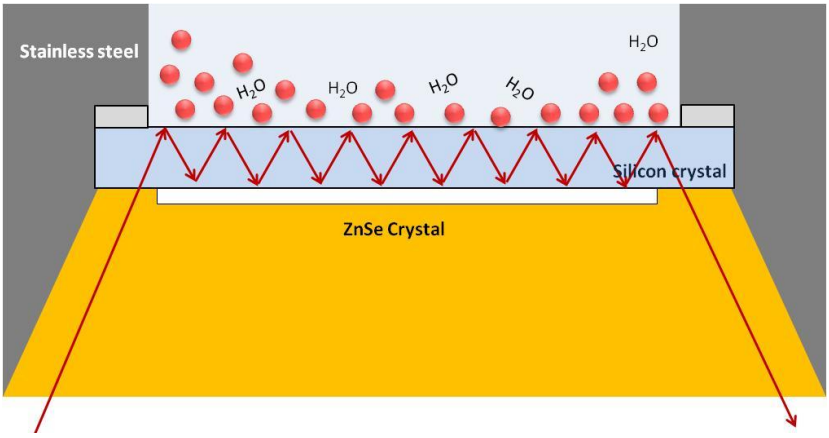

Figure 1. Scheme of the ATR unit employed in this work. As it can be seen the walls of the cell are composed of stainless steel, which acts as reducing agent leading to the in-situ formation of gold nanoparticles from tetrachloroauric acid solution.

3. Results and discussion

3.1. *In-situ* synthesis of gold nanoparticles within the IR-ATR liquid cell

Gold nanoparticles were directly synthesized inside the ATR unit taking advantage of the stainless steel ring establishing the confining walls of the liquid cell, as previously demonstrated by the authors [25,26]. While AuNPs form, the sediment at the ATR waveguide surface until Coulomb repulsion from already adsorbed AuNPs lead to an equilibrium.

Gold nanoparticles are characterized by a strong plasmon resonance in the UV/Vis region as a consequence of the collective oscillation of electrons within the conduction band. However, in the MIR gold nanoparticles do not show a pronounced absorption. Despite the IR-inactivity of AuNPs, it was found that their formation may still be monitored via IR spectroscopy by analyzing the increase of the water absorption features during the synthesis process, which arises from the SEIRA effect. Figure 2 shows a series of *in-situ* IR-ATR spectra recorded during gold nanoparticles being synthesized within the ATR unit.

According to literature [28], the vibrational modes of water in the infrared region are the H_2O bending mode at 1644 cm^{-1}, the combination of H_2O bending and libration mode at 2128 cm^{-1}, and a pronounced vibration around 3404 cm^{-1}, which is composed of the overtone of the bending mode at 3250 cm^{-1}, the symmetric OH stretch at 3450 cm^{-1} and the antisymmetric OH stretch at 3600 cm^{-1} [22]. As gold nanoparticles are formed and deposited at the ATR waveguide surface, an increase of the H_2O bending and the OH stretching bands is observed despite the decrease of water molecules present within the evanescent field being displaced by gold nanoparticles. This increase is attributed to an enhancement of the water absorptions within the evanescent field resulting from the presence of AuNPs. While the magnitude of the enhancement certainly decreases with increasing the distance from the

waveguide surface (i.e., the nanoparticulated Au film), it compensates for the decreasing number of water molecules steadily displaced by AuNPs. The hypothesis of enhancing the IR signature of water via the formation of AuNPs is further corroborated by the observed increase of the water absorption signal vs. the background spectrum.

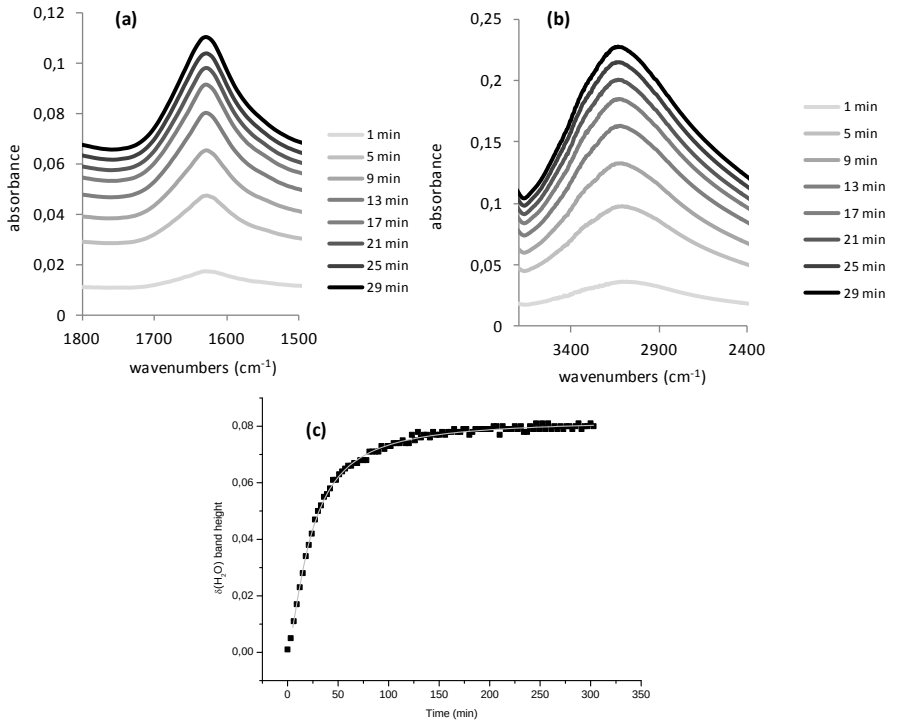

Figure 2. *In situ* ATR-SEIRA spectra during the synthesis of gold nanoparticles inside the ATR unit in a water environment (from a 200 mg dL^{-1} $HAuCl_4$ solution).(a) H_2O bending mode, (b) OH stretch. To see the SEIRA effect of gold nanoparticles over water bands, a spectrum of tetrachloroauric acid solution in water just before the synthesis starts was used as background reference. Thus, the water features shown in the spectra are directly the enhancement produced as gold nanoparticles are obtained. (c) Height of the $\delta(H_2O)$ bending vibration band at 1644 cm^{-1} and best-fit function of the band height versus time. At t=0 the $HAuCl_4$ solution was injected into the ATR unit.

For monitoring the kinetics of the synthesis, and of the deposition of AuNPs at the ATR waveguide surface, the peak height of the water bending mode ($\delta(H_2O)$)was analyzed in detail. Figure 2a shows the peak height of the H_2O bending mode vs. time with t=0 indicating the initiation of the *in-situ* synthesis of gold nanoparticles from tetrachloroauric acid solution. The obtained data points readily fit to a Langmuir model, which describes a random adsorption process within the first monolayer (Figure 2c). The obtained goodness-of-the-fit was r^2=0.997.

The band corresponding to the OH stretching vibration likewise showed revealed an increase during the synthesis of gold nanoparticles (figure 2b). Plotting the peak height vs. time again fits a Langmuir isotherm.

In order to further study the *in-situ* formation of gold nanoparticles within the ATR cell, a stainless steel O-ring of similar dimensions was glued onto a piece of silicon wafer, in order to simulate the scenario inside the ATR liquid cell (i.e., mock-up ATR cell; MU-ATR) enabling access to subsequent scanning electron microscopy (SEM) studies of the obtained AuNPs without additional manipulation. Similar to the *in-situ* synthesis monitored by IR-ATR spectroscopy, a small amount of $HAuCl_4$ (200 mg dL^{-1}) was added to the MU-ATR in order to synthesize AuNPs. The reaction was stopped after 20 min and 100 min, respectively, by removing the aqueous solution followed by rinsing with dried air.

After 20 min, sub-monolayer coverage with few agglomerates of AuNPs was determined at the Si wafer surface, as expected from the *in-situ* IR-ATR studies. After 100 min, the AuNPs in solution show significant agglomeration with already adsorbed gold nanoparticles, as can be seen in Figure 3. MU-ATR microscopic studies were compared with the results obtained by IR. During the process of deposition of AuNPs on the ATR crystal, their distribution, size and shape of the NPs as well as their interaction change. This morphological

development causes changes of the electromagnetic field near the ATR active surface. Firstly, a monolayer of AuNPs is formed at the surface, which leads to a strong water bending and OH stretching signal enhancement in the first few minutes. They are SEIRA active due to an enhanced near-field around the NPs, which decays with increasing distance from the particle surface. As previously explained, the near-field enhancement around the AuNPs overcompensates the loss of water molecules replaced by AuNPs during their adsorption on the surface. Once gold nanoparticles are deposited on the surface, aggregates or islands of nanoparticles are observed, as can be seen from SEM images (Figure 3), along with no further increase of water features bands. At such islands, the electromagnetic near-field distribution changes as the consequential absorption of IR radiation [21].

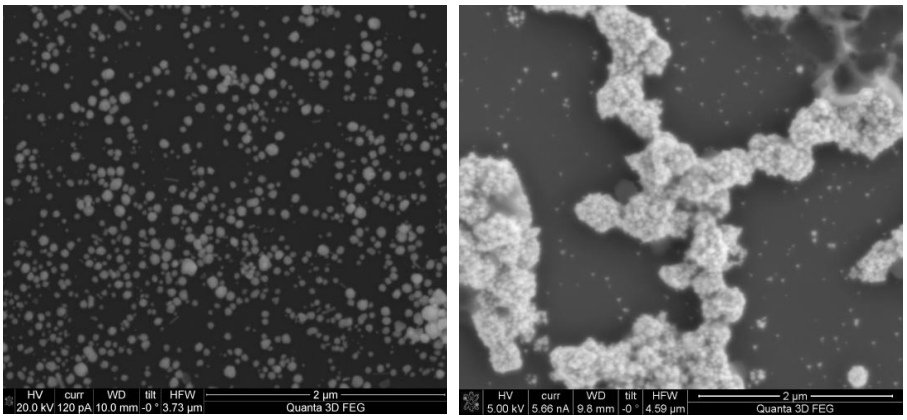

Figure 3. Scanning electron microscopy images of in situ synthesized gold nanoparticles: (left) after 20 min, (right) after 100 min.

3.2. Influence of the gold(III) precursor concentration

The influence of the concentration of the gold(III) precursor (i.e., tetrachloroauric acid) was performed. While the kinetics of the reaction follow a different rate

depending on the concentration, in all cases the obtained rate functions may be fitted with a Langmuir isotherm.

If the concentration of gold precursor within the ATR unit is high (i.e., 200 $mgdL^{-1}$), the increase of the absorption features related to the water spectrum is rapidly observed (i.e., within 1 min). At lower concentrations (i.e., 66 $mgdL^{-1}$), the formation of gold nanoparticles is correspondingly slower, which is reflected in the IR spectrum (Figure S1). Figure S2 shows the H_2O bending region at different times of reaction. Initially, AuNPs deposited at the surface appear isolated with only few particles agglomerated. With increasing reaction time, packed island of connected nanoparticles are evident. This behavior agrees with findings previously reported in literature [22] for the water OH stretching band during the adsorption of a submonolayer of AuNPs at a substrate initially treated with (aminopropyl)triethoxysilane (APTES).

3.3. Influence of the temperature

If AuNPs are synthesized outside the ATR unit by inserting a piece of stainless steel piece into the solution [25], an increase of the rate of production of gold nanoparticles is observed with increasing temperature. The *in-situ* synthesis was performed at different temperatures (23, 40, 50, and 60ºC) to spectroscopically study this behavior. With increasing temperature the enhancement of water bands appears more rapidly, which in turn indicates that AuNPs are formed more rapidly.

3.4. Reproducibility

A study of the reproducibility of the *in-situ* AuNPs synthesis and the observed SEIRA-ATR water signal was performed by repeating the analysis four times during different days for the synthesis procedure based on a 200 mg dL^{-1}

$HAuCl_4$ solution at 60ºC. The relative standard deviation calculated from the H_2O bending peak height was 10.55%.

3.5. *In-situ* synthesis of gold nanoparticles in D_2O

The synthesis of the gold nanoparticles mediated by stainless steel inside the ATR unit was finally also performed in D_2O, again using $AuCl_3$. The aim of this study was to potentially observe the SEIRA effect on the associated D_2O bands in a different spectral regime for confirmation of the observed effects. No significant difference was noted concerning the formation of AuNPs during the chemical reaction compared to the studies in H_2O. Similarly to the observations in water, as gold nanoparticles were emerging the absorption signals of the υ(OD) and the δ(D_2O) band appear with enhanced intensity. Again, thus obtained data was fitted using a Langmuir model with a goodness-of-the-fit of r^2=0.994 (see Figure S3).

The same behavior was observed when performing the synthesis in a 1:1 mixture of H_2O and D_2O resulting in the corresponding simultaneous enhancement of water and deuterium oxide infrared features, respectively.

3.6. Influence of the ionic strength

As IR spectra are also sensitive to variations of the chemical environmental, next to non-destructively monitoring the synthesis of gold nanoparticles one may furthermore analyze changes in aggregation or stability of the obtained AuNP dispersions. The aggregation of AuNPs causes coupling of their plasmonic modes, thereby resulting in a red shift and broadening of the longitudinal plasmon resonance band in the optical spectrum, as evident in the UV/Vis absorption spectra shown in Figure 4 (top). It is known that variation of the ionic strength is a particle-independent strategy to affect the repulsion distance between charged particles. Increasing the ionic strength decreases the Debye

length, thus also decreasing the averaged distance between particles [29]. Two hypotheses have been proposed to explain the observed change in the color of such solutions when increasing the ionic strength: (i) the gold nanoparticles physically coalesce to form larger particles, and (ii) the mean interaction distance is reduced such that their surface plasmons may interact [29].

Herein, the effect of the addition of silver(I) nitrate and potassium nitrate was investigated. As gold nanoparticles are synthesized and deposited within the evanescent field at the ATR waveguide surface, an enhancement of the water absorption features is observed. If the ionic strength of the solution is altered by addition of salts, a sudden increase of the absorption of the water bands is observed, without any further change with time.

While AuNPs synthesized *in-situ* using the stainless steel assisted method do not contain citrate ligands bound to the nanoparticle surface, chloride ions are present in abundance and may shield the obtained nanoparticles. Such a chloride shell may prevent nanoparticle agglomeration, and may also facilitate the stabilization of the solution due to the achieved spacing between individual NPs. When adding silver nitrate to the solution, which increases the ionic strength, the enhancement of the water bands terminates (see Figure 4 bottom). Apparently, silver ions interact with chloride ions, and thus, the AuNPs will be destabilized and rapidly deposit at the waveguide surface. Once deposited as islands on the surface the increase in water vibration bands stopped, analogous to that observed at longer times of deposition of AuNPs during their synthesis.

A similar behavior was observed when adding potassium nitrate; once nanoparticles aggregate, an increase in water signal is observed followed by no further changes of the IR absorption band.

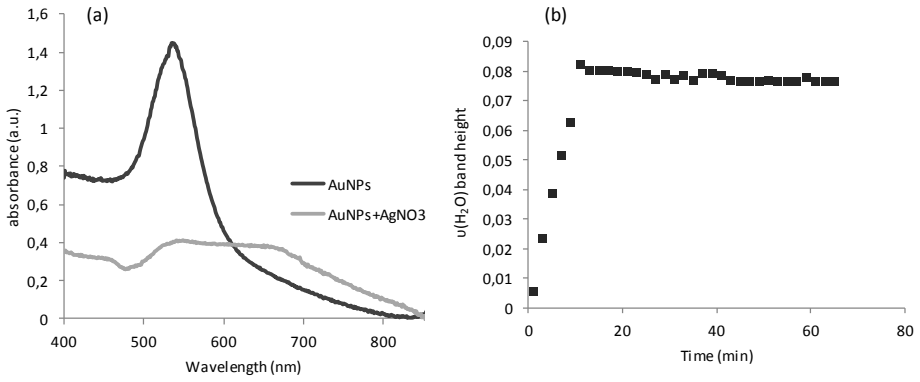

Figure 4. (a) UV-Vis spectra of the gold nanoparticles solution prior and after the addition of NaCl increasing the ionic strength of the solution which leads to the aggregation of the AuNPs. (b) Plot of the water OH stretching band height versus time. At minute 11, 10 µL of 1M $AgNO_3$ solution were added.

3.7. Influence of the pH value

The influence of a decrease in pH during the synthesis of gold nanoparticles within the ATR unit was investigated by adding HNO_3 during the synthesis. 10 µL of a 10% (v/v) HNO_3 solution were added to 40 µL of 200 mg dL^{-1} $HAuCl_4$ solution previously placed into the ATR liquid cell. It has been described that low pH values induce the aggregation of gold nanoparticles [30]. Again, the suitability of IR-ATR spectroscopy to determine changes in aggregation state of the synthesizing gold nanoparticles was demonstrated observing a behavior similar to that when increasing ionic strength.

3.8. Investigating the sedimentation behavior of *ex-situ* synthesized unmodified and citrate coated gold nanoparticles via IR-ATR spectroscopy

Studying the sedimentation behavior of gold nanoparticles has been reported via UV/Vis spectroscopy under normal gravitational force [31]. The optical detection of sedimenting particles in solution enables accurately determining

the particle size distribution in a polydisperse nanoparticle sample [31]. Herein, IR-ATR spectroscopy is demonstrated as an alternative tool for monitoring gravitational sedimentation of gold nanoparticles. Hence, the sedimentation rate of both unmodified gold nanoparticles obtained via stainless steel assisted reduction outside the ATR liquid cell, and citrate-capped gold nanoparticles was compared. In order to achieve acceptable sedimentation rates, CTAC was added, as previously reported in the literature [32]. Cationic surfactant causes aggregation by neutralizing the negative charge at the nanoparticle surface.

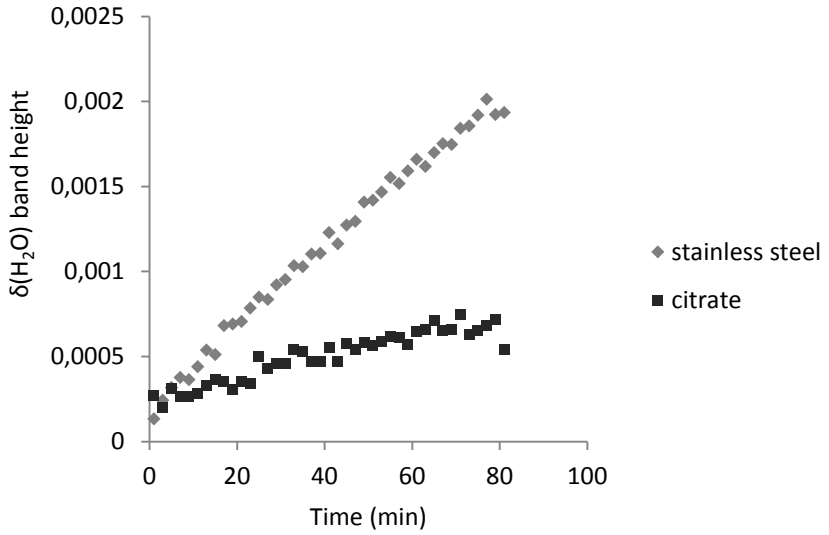

Figure 5. Plot of H_2O bending band height versus time during the sedimentation of citrate-coated and bare gold nanoparticles in CTAC media. To see the SEIRA effect while depositing of gold nanoparticles over water bands, a spectrum of the gold nanoparticles solution at t=0 was measured and used as background reference. Thus, the water features shown in the spectra are directly the enhancement produced as gold nanoparticles settle.

Experiments were carried out by placing a mixture of 20 µL of stainless steel assisted bare gold nanoparticles synthesized outside the cell with 20 µL of 0.1 mol L^{-1} CTAC solution on the ATR unit. An increase of water band features is

again observed with time, such enhancement being faster in the presence of CTAC in solution. A similar experiment was conducted by placing a mixture of 20 µL of citrate-coated gold nanoparticles with 20 µL of 0.1 mol L^{-1} CTAC solution on the ATR unit. Figure 5 shows a comparison of the behavior of both types of nanoparticles during their sedimentation on the ATR surface.

4. Conclusions

Thus, we propose the use of FTIR-ATR spectroscopy as tool for the study of gold nanoparticles solutions. IR-ATR was used to monitor the *in-situ* synthesis of gold nanoparticles in the ATR unit mediated by the stainless steel forming the walls of the cell. As gold nanoparticles are synthesized they cover the evanescent field replacing water molecules. Despite being no IR active, we can observe gold nanoparticles deposition by the enhancement they produce over water featured bands. This surface-enhancement, SEIRA effect, overcompensates the lost of water molecules on the surface active region, and allows the determination of gold nanoparticles presence. Moreover, IR-ATR can be used not only to monitor particle density at the ATR surface, but also to control chemical changes in solution that may affect the gold nanoparticles. Finally, it has been shown that IR-ATR spectroscopy can be used to evaluate the sedimentation process of gold nanoparticles on the surface.

Acknowledgments

A.I. López-Lorente and M. Valcárcel wish to thank Spain's Ministry of Innovation and Science for funding Project CTQ2011-23790 and Junta de Andalucía for Project FQM4801. A.I. López-Lorente also wishes to thank the Ministry for the award of a Research Training Fellowship (Grant AP2008-02939), and gratefully acknowledges funding of her stay in Germany at the University of Ulm to conduct the research reported in the present study.

The authors declare no competing financial interest.

References

[1] Cai, W.; Gao, T.; Hong, H.; Sun, J. *Nanotechnol. Sci. Appl.* **2008**, *1*, 17-32.

[2] Sperling, R.A.; Rivera-Gil, P.; Zhang, F.; Zanella, M.; Parak, W.J. *Chem. Soc. Rev.* **2008**, *37*, 1896-1908.

[3] Eustis, S.; El-Sayed, M.A. *Chem. Soc. Rev.* **2006**, *35*, 209-217.

[4] López-Lorente, A.I.; Simonet, B.M.; Valcárcel, M. *Comprehensive Analytical Chemistry* **2012**, *59*, 33-89.

[5] Pang, X.; Zhao, L.; Han, W.; Xin, X.; Lin, Z. *Nature Nanotechnology* **2013**, *8*, 426-431.

[6] Kato, H.; Suzuki, M.; Fujita, K.; Horie, M.; Endoh, S.; Yoshida, Y.; Iwahashi, H.; Takahashi, K.; Nakamura, A.; Kinugasa, S. *Toxicol. In Vitro* **2009**, *23*, 927-934.

[7] López-Lorente, A.I.; Simonet, B.M.; Valcárcel, M. *Analyst* **2012**, *137*, 3528-3534.

[8] López-Lorente, A.I.; Simonet, B.M.; Valcárcel, M. *TrAC, Trends Anal. Chem.* **2011**, *30*, 58-71.

[9] Allabashi, R.; Stach, W.; de la Escosura-Muñiz, A.; Liste-Calleja, L.; Merkoçi, A. *J. Nanopart. Res.* **2009**, *11*, 2003-2011.

[10] Wang, B.; Wang, X.; Lou, W.; Hao, J. *J. Coll. Interf. Sci.* **2011**, *362*, 5-14.

[11] Lin, S.Y.; Liu, S.W.; Lin, C.M.; Chen, C.H. *Anal. Chem.* **2002**, *74*, 330-335.

[12] Park, J.H.; Park, J.; Dembereldorj, U.; Cho, K.; Lee, K.; Yang, S.I.; Lee, S.Y.; Joo, S.-W. *Anal. Bioanal. Chem.* **2011**, *401*, 1631–1639.

[13] Rudolf, B.; Salmain, M.; Grobelny, J.; Celichowski, G.; Tomaszewska, E. *Colloids and Surfaces A: Physicochem. Eng. Aspects* **2011**, *385*, 241– 248.

[14] Tsai, D.-H.; Davila-Morris, M.; DelRio, F.W.; Guha, S.; Zachariah, M.R.; Hackley, V.A. *Langmuir* **2011**, *27*, 9302–9313.

[15] Harstein, A.; Kirtley, J.R.; Tsang, J.C. *Phys. Rev.. Lett.* **1980**, *45*, 201-204.

[16] Baia, M.; Toderas, F.; Baia, L.; Maniu, D.; Astilean, S. *Chem. Phys. Chem.* **2009**, *10*, 1106-1111.

[17] Osawa, M. *Top. Appl. Phys*. **2001**, *81*, 163-187.

[18] Jensen, T.R.; Van Duyne, R.P.; Johnson, S.A.; Maroni, V.A. *Appl. Spectrosc.* **2000**, *54*, 371-377.

[19] Miyake, H.; Ye, S.; Osawa, M. *Electrochem. Commun.* **2002**, *4*, 973-977.

[20] Pucci, A.; Neubrech, F.; Weber, D.; Hong, S.; Toury, T.; Lamy de la Chapelle, M. *Phys. Status Solidi B* **2010**, *247*, 2071-2074.

[21] Enders, D.; Nagao, T.; Pucci, A.; Nakayama, T.; Aono, M. *Phys. Chem. Chem. Phys.* **2011**, *13*, 4935-4941.

[22] Enders, D.; Nagao, T.; Nakayama, T.; Aono, M. *Surf. Interface Anal.* **2008**, *40*, 1681-1683.

[23] Zhang, Z.; Imac, T. *J. Colloid Interface Sci.* **2001**, *233*, 107-111.

[24] Kundu, J.; Le, F.; Nordlander, P.; Halas, N.J. *Chem. Phys. Lett.* **2008**, *452*, 115-119.

[25] López-Lorente, A.I.; Simonet, B.M.; Valcárcel, M.; Mizaikoff, B. *Anal. Chim. Acta* **2013**, *788*, 122-128.

[26] López-Lorente, A.I.; Simonet, B.M.; Valcárcel, M.; Eppler, S.; Schindl, S.; Kranz, C.; Mizaikoff, M. *Talanta* **2014**, *118*, 321-327.

[27] Turkevich, J.; Stevenson, P.C.; Hillier, J. *Discuss. Faraday Soc.* **1951**, *11*, 55-75.

[28] Venyaminov, S.Y.; Pendegast, F.G. *Anal. Biochem.* **1997**, *248*, 234-245.

[29] Burns, C.; Spendel, W.U.; Puckett, S.; Pacey, G.E. *Talanta* **2006**, *69*, 873-876.

[30] Nam, J.; Won, N.; Jin, H.; Chung, H.; Kim, S. *J. Am. Chem. Soc.* **2009**, *131*, 13639-13645.

[31] Alexander, C.M.; Dabrowiak, J.C.; Goodisman, J. *J. Colloid Interf. Sci.* **2013**, *396*, 53-62.

[32] Norman Jr., T.J.; Grant, C.D.; Magana, D.; Zhang, Z.; Liu, J.; Cao, D.; Bridges, F.; Van Buuren, A. *J. Phys. Chem. B* **2002**, *106*, 7005-7012.

SUPPORTING INFORMATION

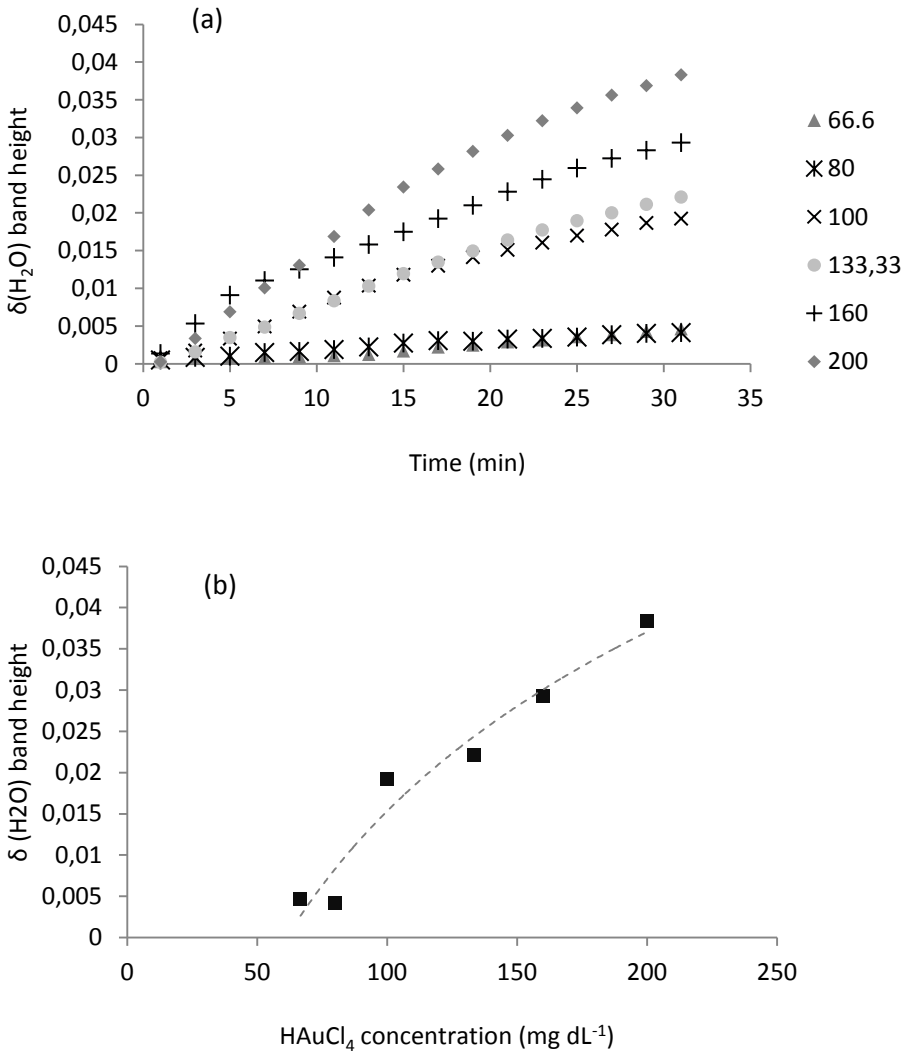

Figure S1. (a) Water δ(H_2O) band height evolution with time during the synthesis of gold nanoparticles from a tetrachloroauric acid solution at a concentration of: 66.6, 80, 100, 133.3, 160 and 200 mg dL^{-1}. (b) Plot of δ(H_2O) band height versus $HAuCl_4$ water solution concentration at a time of 31 minutes.

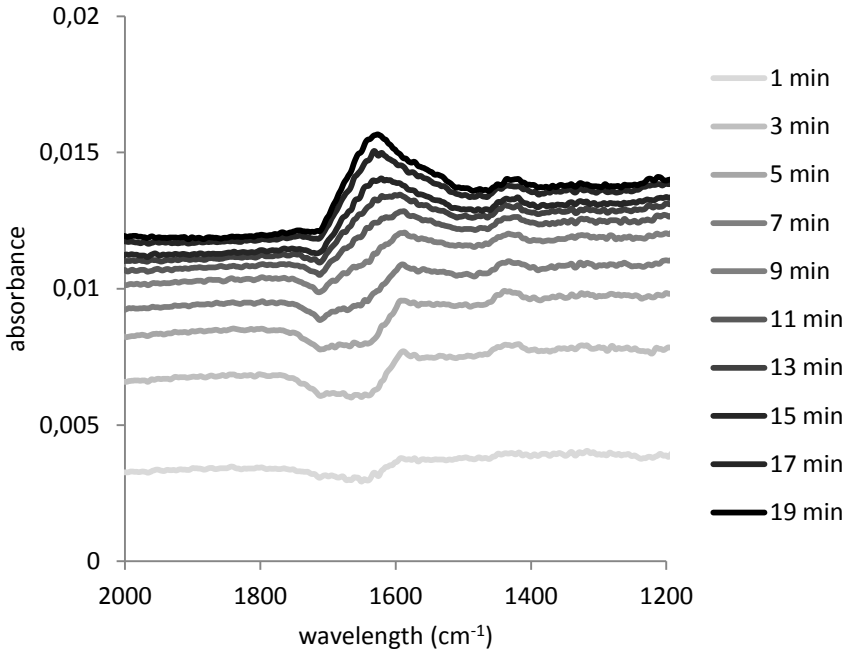

Figure S2. In situ ATR-IR spectra of gold nanoparticles on the ATR surface during the synthesis procedure. Spectra were acquired each 120 second after the filling of the ATR unit with a 66.6 mg dL^{-1} solution of $HAuCl_4$.

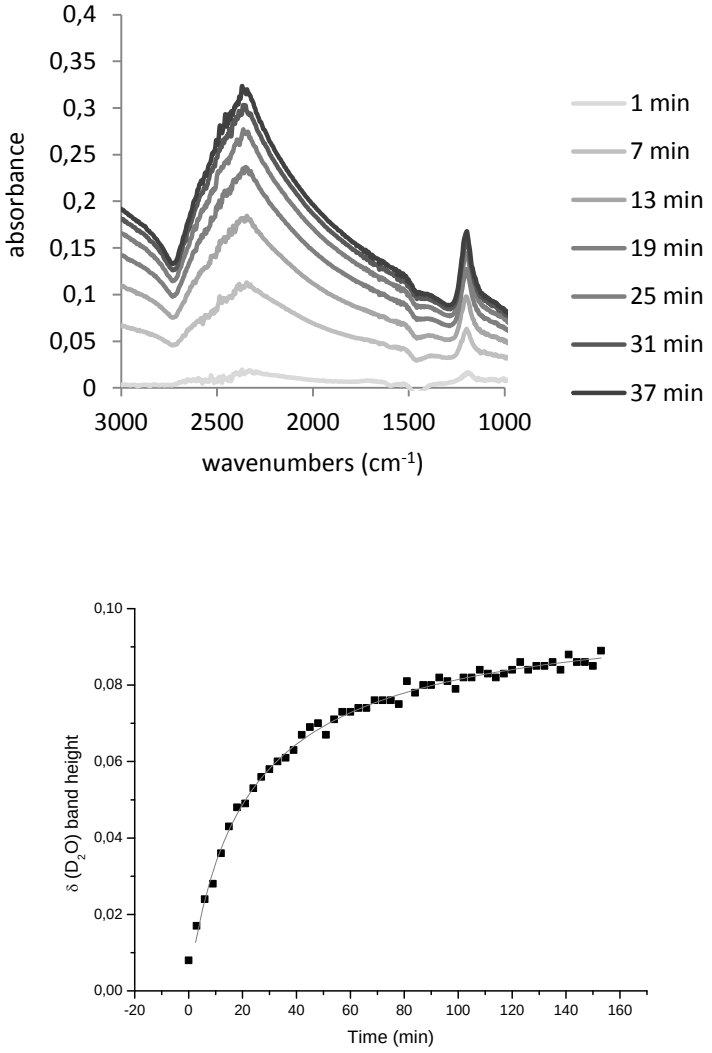

Figure S3. Top: *In situ* ATR-SEIRA spectra during the synthesis of gold nanoparticles inside the ATR unit in a D_2O environment (from a 200 mg dL^{-1} $HAuCl_4$ solution). To see the SEIRA effect of gold nanoparticles over deuterium oxide bands, a spectrum of gold(III) chloride solution in deuterium oxide just before the synthesis starts was used as background reference. Thus, the D_2O features shown in the spectra are directly the enhancement produced as gold nanoparticles are obtained. Bottom: δ (D_2O) band height evolution with time as gold nanoparticles are synthesized on the ATR cell and deposited on the SiO_2 surface.

IV.3. ELECTROFORESIS CAPILAR

De entre las diversas técnicas que se emplean para la caracterización de nanopartículas, la electroforesis capilar ha mostrado un gran potencial dado que es rápida y tiene un bajo consumo de muestra y reactivos. La electroforesis capilar se ha utilizado para separar una gran variedad de nanomateriales de diferente tamaño. La electroforesis capilar de zona (CZE) es fácilmente aplicable al estudio de nanopartículas con cargas superficiales, que forman dobles capas, siendo su comportamiento en el sistema electroforético similar al de las especies moleculares cargadas. La carga puede ser resultado de la estabilización coloidal con un ligando o de la introducción de grupos orgánicos cargados (por ejemplo a través de la formación de derivados de tioles).

Las nanopartículas de oro sintetizadas con citrato forman una doble capa con los iones citrato adsorbidos en la superficie de la nanopartícula, lo que evita la aglomeración e interacciones de adsorción con la pared del capilar cuando está negativamente cargada. Se ha encontrado que AuNPs con diferentes diámetros tienen tiempos de migración diferentes, lo que se ha utilizado para la separación de nanopartículas en función del tamaño. Asimismo, se ha llevado a cabo la separación de nanopartículas de oro y plata en función de la forma de las mismas.

El **capítulo 8** proporciona una visión general de las técnicas electroforéticas empleadas para la caracterización y determinación de nanopartículas de diferente naturaleza. Se ha estructurado en función del analito diana, que pueden ser las nanopartículas o derivados de las mismas. Aunque no se ha

incluido en esta Memoria, más información sobre las técnicas electroforéticas y dielectroforéticas utilizadas para el análisis de nanomateriales puede encontrarse en el capítulo de libro de la referencia [1].

El **capítulo 9** presenta una metodología para la separación y preconcentración de nanopartículas de oro y plata cubiertas con citrato mediante electroforesis capilar, en base a la interacción selectiva con compuestos tiólicos añadidos como aditivos al buffer electroforético. Las nanopartículas de oro y plata se sintetizaron con similar tamaño, ambas rodeadas por ligandos citrato, por lo que mostraron el mismo tiempo de migración cuando no se añadieron aditivos al buffer acuoso. Para aumentar el tiempo de interacción de las nanopartículas con el buffer, y favorecer así su funcionalización, se utilizó la modalidad electroforética de preconcentración con un gran volumen de muestra "large volumen sample stacking (LVSS)" obteniéndose una mejor sensibilidad y separación.

[1] A.I. López-Lorente, B.M. Simonet, M. Valcárcel, Comprehensive Analytical Chemistry 59 (2012) 33-89.

Capítulo 8

Electrophoretic methods for the analysis of nanoparticles

Trends Analytical Chemistry 30 (2011) 58-71

TrAC Trends in Analytical Chemistry

30 (2011) 58-71

Characterization, Analysis and Risks of Nanomaterials in environmental and Food Samples

Electrophoretic methods for the analysis of nanoparticles

A. I. López-Lorente, B. M. Simonet, M. Valcárcel

Department of Analytical Chemistry, University of Córdoba. 14071 Córdoba, Spain.

With the development of nanotechnology, there is a need for methodologies to determine and characterize nanomaterials. Electrophoresis has emerged as a useful tool, which has been employed in various formats (e.g., capillary-zone electrophoresis, gel electrophoresis or isotachophoresis) for the size- or shape-based separation of different types of nanoparticles (NPs) (e.g., metallic, semi-metallic or carbon). This article reviews the main progress in electrophoresis techniques in order to achieve separation of NPs.

Keywords: Capillary-zone electrophoresis; Carbon nanoparticle; Electrophoresis; Gel electrophoresis; Isotachophoresis; Metallic nanoparticle; Nanomaterial; Nanoparticle; Semi-metallic nanoparticle; Separation

1. Introduction

Nanotechnology is a growing area that attracts much attention due to the excellent properties of nanomaterials. Thanks to their potential, nanoparticles (NPs) – which are said to be particles that have at least one dimension in the nanoscale (1–100 nm) – attract widespread attention in many scientific fields.

The sizes and the shapes of NPs are important factors that determine their physical and chemical properties. The difficulty in generating the desired size, shape, and monodispersity of NPs creates the need for new, refined techniques for synthesizing them. Synthesis of NPs is an active area of research, increasing their uses, with the potential for great advances in everyday life due to nanotechnology.

In addition, new tools are required for characterizing NPs [1]. Electron microscopy is one of the tools employed most in characterizing the size distribution of NPs. Transmission electron microscopy (TEM) suffers from the drawback of needing a lot of time for each analysis in order to assure sample representativeness. And, one of the most important shortcomings to be resolved in sample preparation is the aggregation of the NPs, which makes it difficult to analyze individual NPs. Moreover, there is statistical uncertainty because of the human subjectivity implied when deciding which parts of the grid are photographed.

To separate free from functionalized NPs, the use of size-exclusion chromatography (SEC) has been proposed. SEC has the advantages of being faster or coupling to optical spectroscopy, but there may be irreversible adsorption onto the stationary phase in some cases.

High-performance liquid chromatography (HPLC) have been also used in combination with TEM, although the resolution is not high enough [2].

For these reasons, from the diverse techniques employed for NP characterization, capillary electrophoresis (CE) has emerged as useful, potentially faster than electron microscopy, with fewer surface effects than in other techniques (e.g., SEC). Another advantage of CE is low consumption of sample and reagents.

CE has been used to separate a variety of differently sized materials, including inorganic oxide [3], latex [4], polystyrene [5], gold [6] and silver [7] NPs, carbon nanotubes (CNTs) [8], quantum dots (QDs) [9], etc. Capillary-zone electrophoresis (CZE) is easily applicable for the investigation of NPs due to their surface charges, which form electrical double layers, so their separation behavior is similar to that of charged molecular species in CZE. In other circumstances, when the electrical double layer is not enough to stabilize the NPs in the electrophoretic system, covalent functionalization is required. This strategy is useful if the covalent bond does not affect to the core of the NP.

Gel electrophoresis has been extensively used in separating biological targets (e.g., DNA and proteins) with a remarkable resolution. This tool has gained exposure since it was employed for separation of nanomaterials [10] and [11]. However, several reasons may hinder use of polyacrylamide gel in preparative electrophoresis (e.g., pore size, which is typically ~3-5 nm or the heterogeneity in pore sizes). Preparative electrophoresis using agarose gels of ~100-nm pore size has proved to separate gold NPs (AuNPs) based on size and shape.

Isoelectric focusing (IEF) is commonly employed to determine the isoelectric point of proteins and enzymes. Proteins move under the influence of an electric field in a pH gradient and come to rest at the isoelectric point. Colloid metal and semiconductor particles of different sizes derivatized with carboxylic groups can be rapidly separated from their mixtures in a home-made miniscale IEF unit [12]. The method is fast, inexpensive and highly sensitive. It shows potential

for future modification and development in improving the monodispersity of colloidal particles.

This article is a general overview on determination and analysis of NPs by CE, focusing on the different strategies carried out in order to facilitate the determination of NPs of different sorts. Recently, several overviews have given theoretical descriptions of the physical mechanism involved in the electrophoretic transport of NPs and colloids [13], [14], [15] and [16]. We have structured the article according to the target analyte, which may be the NP itself or a derivative of the NP. To improve electrophoretic resolution, there have been different approaches (e.g., functionalization of NPs, and use of gels or surfactants). In order to present a systematic view of strategies for solubilization and methodologies used to enhance resolution, this overview has been classified according to the nature of the NP. To be resolved by CE, NPs must be soluble, charged and stable in the background electrolyte (BGE) under the electrophoretic conditions.

2. Separation of nanoparticles by capillary electrophoresis

In this section, we describe the electrophoretic methodologies developed for the separation of NPs originally uncharged. Although strategies used to solubilize and separate NPs are similar, in our opinion, a classification according to the nature of the NP helps readers to have a general overview of the strategies, which can involve the solubilization, the detection or the electrophoretic separation.

2.1. Noble-metal nanoparticles

Metallic NPs (MNPs) display fascinating properties quite different from those of individual atoms, surfaces or bulk materials. For example, AuNPs have a characteristic red color, while silver nanospheres are yellow. This color is due to

the collective oscillation of the electrons in the conduction band, known as the surface-plasmon oscillation, whose frequency is usually in the visible region for gold and silver, giving rise to the strong surface-plasmon resonance (SPR) absorption. This property allows the determination of these NPs with UV/Vis detection. In this way, we need to take into account that characteristic absorption spectra are susceptible to be changed by the interaction of NPs with ligands. It means that the components of the BGE can change the color of the NPs. The change is normally a decrease of absorption. As a result, the UV/Vis detector has low sensitivity.

To be separated, MNPs must present a stable charge in the electrophoretic system. The charge can be the result of a colloidal stabilization with a ligand or the introduction of charged organic groups (e.g., through formation of thiol derivatives). AuNPs are normally synthesized by reduction of gold with citrate. As a result, a colloidal AuNP is obtained that arises from the sorption of citrate ions onto the NP surface during the preparation process that leads to the formation of an electric double layer, whose potential stabilizes NPs, preventing agglomeration and avoiding adsorptive interactions with the capillary wall when it is negatively charged.

Schnabel et al. [6] characterized colloidal AuNPs according to size by CZE using acetate buffer at pH 5.0 without any sieving additive. As they observed relatively broad peaks caused by the dispersion of the samples, a marker was introduced in order to simultaneously measure the electroosmotic flow (EOF) mobility and reduce possible bias of the colloid particle mobility data. They found a reduction of the ionic mobilities with decreasing ionic strength due to the increase of the thickness of the double layer affecting smaller particles more. Although the dependence on particle radius is complex, they demonstrated that electrophoretic properties can serve as a measure for size-based characterization.

Another strategy involves chemical functionalization of the MNPs. This can be a covalent bound or a hydrophobic interaction (e.g., with surfactant). For example, separation of MNPs by incorporating carboxylic groups was proposed using self-assembled bifunctional surfactant molecules. In this way, Gole et al. [12] developed a method for isolating MNPs (gold and silver) according to size by using a miniscale IEF technique. The pH at which the ionization of carboxylic groups begins is a strong function of the surface curvature of the colloidal particles, and, because it critically affects the number of surfactant molecules surrounding the NP, this property can be used to separate mixtures of colloidal particles according to their sizes.

Surfactants have been widely employed as stabilizers for the size-selective preparation of MNPs, since they prevent agglomeration by electrostatic repulsion. Hence, the use of NPs stabilized by ionic surfactants may be more feasible for separation by CE. In this sense, Liu et al. [2] demonstrated that adding sodium dodecyl sulfate (SDS) surfactant to the running buffer enhances the capability of CE to separate AuNPs. Increasing the SDS concentration increases the electrophoretic mobility of AuNPs, as there is an increase in the total charges of all the NPs because there are more SDS molecules available for adsorption. The interaction between the hydrophobic tail of SDS and the gold surfaces causes the adsorption of SDS onto the surface of the NPs in the CE capillary, which results in an exchange from citrate to SDS of the stabilizing reagent of the AuNPs. The charge of the NPs will, therefore, relate to the number of molecules of SDS on the surface (change in the charge-to-size ratio), although, once a certain SDS concentration is reached, the amount of charge on a NP is no longer limited by the SDS ions present in the media. Fig. 1 shows an electropherogram of the separation of AuNPs of different sizes following the proposed procedure, which includes SDS in the electrophoretic buffer. It is important to remark that the SDS molecules form a stable complex with the NP, so acting as ligands, and the new species of NP-SDS molecules are separated

according to their *m/z* ratio. This separation is then a CZE separation and not a micellar electrokinetic chromatography (MEKC) separation. To be considered an MEKC separation, kinetic equilibrium between NP and micelle is necessary.

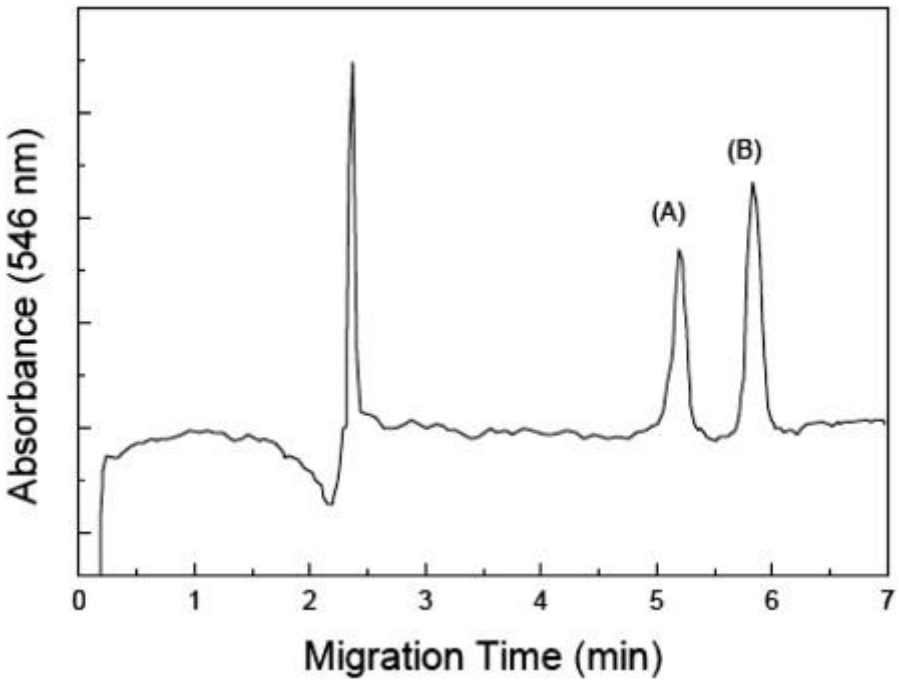

Figure 1. Electropherogram of the separation of differently-sized AuNPs. SDS, 70 mM; CAPS, 10 mM; pH 10.0; applied voltage, 20 kV. (A) 5.3 nm and (B) 19 nm (Reproduced from [2] with permission).

The proposed electrophoretic conditions for characterization of AuNPs [2] were SDS (70 mM) and 3-cyclohexylamino-1-propanesulfonic acid (CAPS; 10 mM) at pH 10.0 as BGE and an applied voltage of 20 kV. With slight changes in the electrophoretic conditions (pH 11.0 and voltage of 18 kV) [17], the authors also analyzed the size distribution of AuNPs while simultaneously obtaining physical properties (e.g., absorbance). They found that AuNPs with different diameters

have different migration times, and suggested a linear relationship between electrophoretic mobility and the radius of AuNPs, assuming the number of SDS molecules associated with an AuNPs is proportional to its surface area.

The same group recently developed a high-efficiency CE method for characterizing the sizes of AuNPs [18] using the reversed-electrode polarity-stacking mode (REPSM) of CE for on-line enhancement of detection and separation of AuNPs. Buffer and voltage were the same as in previous articles but, by using REPSM for sample concentration, the sensitivity toward the AuNPs improved by up to 260-fold. They optimized the length of time for which the REPSM was applied, the concentration of the buffer and the SDS and the pH for detection of AuNPs and Au/Ag core/shell NPs. With optimized on-line enhancement conditions, the limits of detection (LODs) of the AuNPs and Au/Ag NPs increased 30-fold and 140-fold, respectively [19]. They also employed CE to analyze the sizes of AuNPs fabricated through seed-assisted growth [20]. For that study, they did not employ REPSM in order to provide an adequate separation window because of the increase in the sample-plug length.

Furthermore, it was demonstrated that introducing sodium dihydrogenphosphate as salt additive in the AuNP sample changed the retention times and separation resolution of the analytes [21]. Although the authors stated that separation takes place by MEKC, we think that there is no partition of the NP into the micelle, and the surfactant interacts with the NP surface providing it with charge. A similar method was employed to characterize the size of Au/Ag core/shell NPs [22].

Another strategy is functionalization of AuNPs with thiol derivatives. An effective CE technique for separating samples of negatively charged, polydisperse, water-soluble gold monolayer-protected cluster (AuMPC) protected by monolayers of *N*-acetyl-L-cysteine was developed by Lo et al. [23]. The separation mechanisms of the AuMPC in CZE suggest that the larger core sizes of AuMPC

emerge first from the capillary. The electrophoretic separation depends on pH, buffer concentration and organic modifiers. The addition of aliphatic alcohols to the run buffer can improve the separation of AuMPC by reducing the EOF and changing the selectivity between the AuMPCs. The enhancement of resolution is attributed to the more significant difference in the charge-to-size ratio between the AuMPCs. In order to resolve the polydisperse AuMPCs completely, organic modifiers are recommended in the run buffer so that the differences in ν_i/z_i between the AuMPCs are further enhanced. Different organic modifiers show different effects, and ethanol was found to be the best organic modifier to separate the polydisperse AuMPC product. In this case, the earlier-migrating peaks are larger-core AuMPCs and the later-migrating peaks are smaller.

A different approach is functionalization of AuNPs with mercaptoacetic acids, which have been separated by isotachophoresis CZE [24]. The citrate-ligated AuNPs were not suitable for this application, because the ligand was desorbed, and the NP solutions were degraded, so mercaptocarboxylic acids were used, because the chemisorption of thiols on the gold surface improves stability. Isotachophoresis was also employed for calibration-free determination of the concentration of charged colloidal NPs [25].

Gel electrophoresis has succeeded in characterizing NPs, although, in most cases, they were previously derivatized. For example, Arnaud et al. [26] employed an IEF technique in a polyacrylamide pH gradient gel to analyze the size distribution of AuNPs functionalized with mercaptosuccinic acid. The isoelectric point of the NPs is shown to be size dependent, allowing fractionation by electrophoresis. The possibility to change the surface charge of the NPs by changing the number density of thiol molecules at the surface of the AuNPs allows a net separation of the particles depending on their size. Compared to other techniques of fractionation (e.g., SEC used for the separation of AuNPs), the IEF technique provides better size distribution, reaching a

standard deviation of about 6% for a colloidal dispersion with an average size of 4.9 nm.

Furthermore, Xu et al. [10] employed agarose gel preparative electrophoresis to separate AuNPs based on size, shape, and charge. The ability to separate AuNPs by shape was also shown by purifying a mixture of gold spheres, plates, and long rods. In order to introduce charges to NP surfaces, 11-mercaptoundecanoic acid was employed as capping agent. The introduction of carboxylate groups gives negative charges and NPs migrate to the anodic electrode at the same time, and that improves the stability of NPs through electrostatic repulsion.

Hanauer et al. [11] demonstrated separation of AuNPs and silver NPs (AgNPs) according to their size and shape by agarose gel electrophoresis after coating them with a charged polymer layer, polyethylene glycol (PEG), which is covalently attached at one end to the metal surface via a thiol group ("PEGylation"). The other end of the polymer chain may carry different functional groups (e.g., -COOH, -SH, $-NH_2$, or $-OCH_3$), which are exploited for controlling the overall particle charge and mobility. They found that an SH-PEG-COOH coating gives the best separation of silver nanorods, while using the other functional groups or mixing them with $-OCH_3$ in various proportions leads to a less-pronounced separation. The separation is monitored optically by plasmon resonance of noble-metal particles and confirmed by TEM.

AgNPs have been also the subject of CE characterization. Liu et al. [7] separated AgNPs reduced with citrate, whose concentration has strong influence on NP size and morphology. During separation by CE of NPs with different diameters, the presence of a high concentration of ions in the running electrolyte may be required to tune the charge-to-size parameters of the particles and to optimize separation efficiency. It was demonstrated that, as in the case of AuNPs, in addition to preventing AgNPs from coagulating during the separation process,

the use of ionic surfactants (e.g. SDS) enhances the resolution of the separation of the AgNPs by CE, as depicted in Fig. 2.

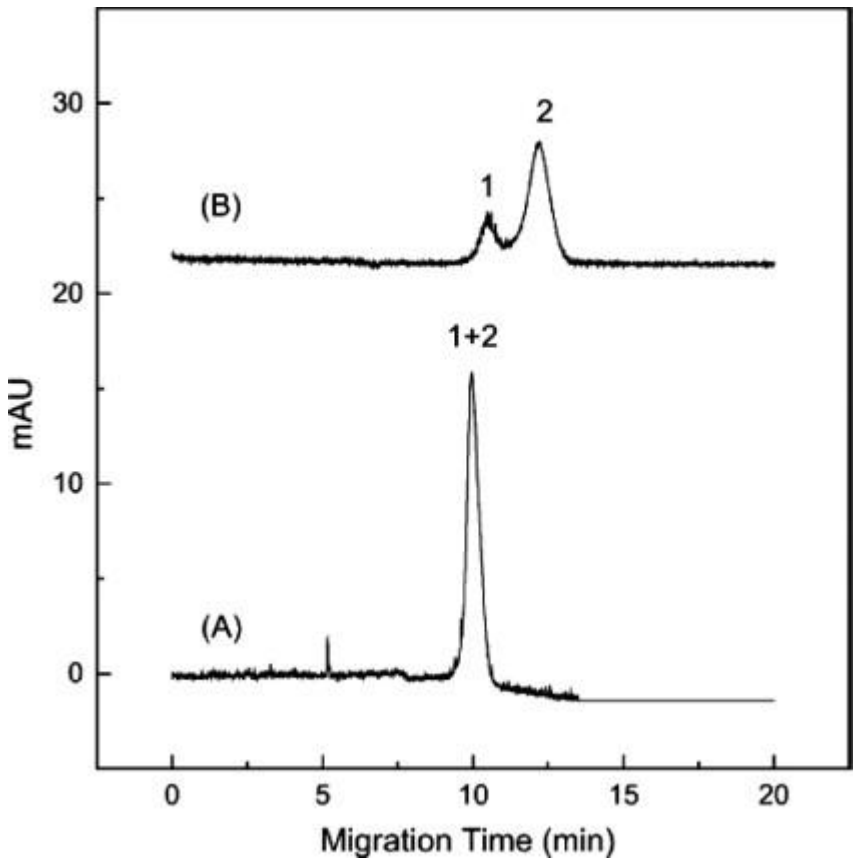

Figure 2. Electropherograms of silver NPs ("1" = 17.0-nm diameter particles; "2" = 49.7-nm particles) as a function of SDS surfactant concentration. The separation was obtained using a running electrolyte of SDS at (A) 0 mM, (B) 20 mM. CE separation conditions: 10 mM Tris (pH 8.5); applied voltage: 20 kV (Reproduced from [7] with permission).

2.2. Quantum dots

QDs are NPs that exhibit optical properties advantageous to researchers, particularly in the field of fluorescence detection. Typically, QDs contain an inorganic, fluorescent central core surrounded by an outer shell designed for core protection from chemical and photo-oxidation. Semiconductor QDs, comprising a few thousand atoms, are typically in the size range 1–10 nm in diameter, which makes their properties different from those of bulk crystals or single atoms. The outer shell of QDs serves to eliminate non-radiative pathways, increasing photo-emission, and providing a means to attach ligands giving the QDs specific properties for solubility and intermolecular interaction.

Characterization of QDs and bioconjugates has mostly been performed using UV/fluorescence spectroscopy, microscopy [scanning electron microscopy (SEM) or TEM] and slab-gel electrophoresis techniques. Reports have shown that the optical and chemical properties of QDs are influenced by pH, solvent polarity, electrostatic interactions, presence of divalent cations, ionic strength, and the application of various coating or ligand cappings.

Song et al. [9] presented a new method for highly efficient size separation of water-soluble CdTe QDs based on capillary gel electrophoresis (CGE) using a polymer solution as sieving medium to overcome the limitation of CZE when differentiating QDs with tiny differences in size. QDs were synthesized using 3-mercaptopropionic acid, which covers their surface and stabilizes the colloidal solution of QDs. The solution was alkaline, so CdTe QDs possessed negative charges due to dissociation of carboxylic groups on their surface and migrated to the anode in the electric field.

In linear polyacrylamide sieving medium, the migration time of QDs increased with their size and was found to depend on the pH. As it is shown in Fig. 3, Song et al. [9] proved that CGE is an efficient tool for characterization and size-

dependent separation of water-soluble NPs. Compared to other separation methods (e.g., HPLC or CZE), CGE is characterized by high resolution, speed, automation, and small sample and reagent requirements. CGE is also used to purify crude QDs with polydispersity for special applications (e.g., nanodevices) and it may be extended to other water-soluble NPs.

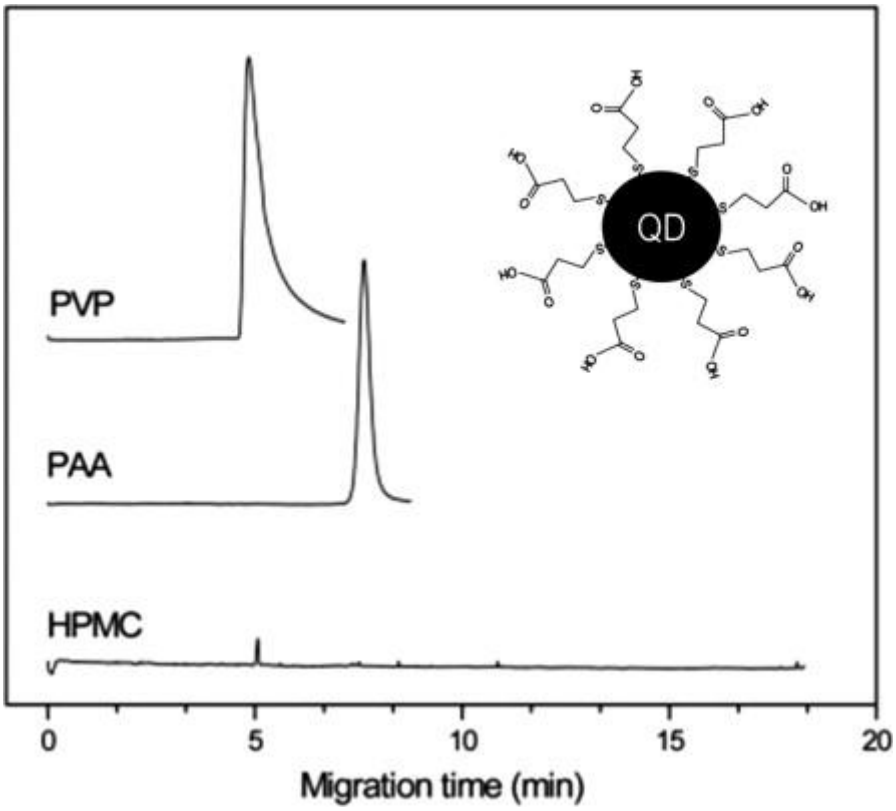

Figure 3. Electropherograms of quantum dots (QDs) using different polymer solutions as sieving media. Sample was CdTe QD with 1.9-nm diameter. Three sieving media, 2% PVP, 5% PAA, and 0.2% HPMC, were used. Coated capillary with 30-cm effective (40 cm total) length and 75-μm ID. Running buffer, 2xTB (pH 8.8), was used. Applied voltage was −16 kV, and electrokinetic injection at −10 kV for 10 s was used. Detection wavelength was 250 nm. The inset shows the surface structure of CdTe QD (Adapted from [9] with permission).

Commercially available QDs were characterized by Pereira et al. [27] using CE. Sodium mercaptopropionate CdTe/CdS QDs and carboxylic acid CdSe/ZnS QDs yielded high separation efficiencies when using sodium phosphate (5–25 mM, pH 7.5–11) as buffer electrolyte.

Recently, our group proposed a method based on formation of a double surfactant layer. First, QDs are covered with trioctylphosphine oxide/trioctylphosphine (TOPO/TOP) surfactant and afterwards with SDS molecules. The complex obtained is separated by CZE. The results demonstrated a relationship between diameter size of QDs and migration time. Distribution size was related to the bandwidth of the electrophoretic peak.

2.3. Carbon nanotubes

Much progress has been made in CNT production methods, which include DC arc, laser ablation, and catalytic gas-phase growth. These methods typically produce 50–95% yields of nanotubes, with the mass balance comprising amorphous carbon, graphitic material and fullerenes. Nanotubes may vary in length, diameter and chirality. Many of their interesting properties depend on these structural parameters. Among other purification techniques [e.g., solvent treatment followed by ultrafiltration, flocculation, use of oxidation and acid washing coupled with centrifugation, SEC or field-flow fractionation (FFF)], electrophoretic methods have shown potential for purification of nanotubes by size. The rapid, high-resolution separations available with CE have the potential to separate a nanotube sample into discrete fractions of uniformly-sized tubes.

In the case of CNTs, electrophoretic methods have been employed mainly as a purification tool, due to the great interest in obtaining samples with CNTs of the same electric properties (metallic or semiconductor) or chirality, in order to be used in many applications in which performance strongly depends on CNT

purity. Dielectrophoresis has been widely employed for separation of these NPs, based on their electronic properties.

As well as in the case of AuNPs, surfactants have been employed in the electrophoretic separation of single-walled CNTs (SWCNTs) suspended in SDS slightly above the critical micelle concentration [28]. The hydrophobic SDS tails are expected to specifically interact with the SWCNT surface, providing it with a negative charge. The resultant electrostatic repulsion between SWCNTs stabilizes them against van der Waals attraction. The right dispersion of SWCNTs with surfactant is the key point for their reliable separation by CE. SWCNTs have a high tendency to aggregate, so reliable dispersion of SWCNTs needs auxiliary energy (e.g., ultrasound irradiation). However, intensive ultrasound irradiation can result in the chemical modification of SWCNTs. Although surfactants are involved in the separation, as there is no partition of a neutral solute into the micelle, it cannot be considered as MEKC. The authors employed CE with absorbance and Raman detection, and fractions collected were analyzed by atomic force microscopy (AFM). Electropherograms showed sharp peaks attributed to nanotube fractions, since characteristic Raman bands of SWCNTs were observed, confirming the identification. CE proved to be suitable for separation of SWCNTs into discrete fractions according to tube length and for removal of non-nanotube material. Diameter-dependent mobility may hold some potential for separations of chiral tubes from those with armchair or zigzag configuration.

Moreover, a CE methodology was performed on polymer-stabilized bundles and SDS suspensions of high-pressure carbon monoxide-produced SWCNTs [29]. Detection was performed by Raman spectroscopy, by using the radial breathing mode (RBM) bands, which are the most sensitive to SWCNT diameter. CE was performed on samples containing a broad distribution of SWCNT diameters, and Raman allowed observation of composition-dependent changes in SWCNT

fractions over the course of the separation. CE was capable of separating poly(vinylpyrrolidone)-stabilized SWCNT bundles into fractions containing bundles of different electronic properties, which may also depend on variations in bundle size. CE on SDS suspensions can separate large aggregates from smaller bundles and produce a relatively pure fraction of individual isolated SWCNTs.

Isolating metallic single-walled NTs (SWNTs) from a suspension of metallic and semi-metallic SWNTs is really interesting since, for many electronic applications, there is a need of homogeneity in the electronic properties of CNTs. Krupke et al. [8] developed a method using alternating current dielectrophoresis, which takes advantage of the difference of the relative dielectric constants of the two species with respect to the solvent, resulting in an opposite movement of metallic and semiconducting tubes along the electric field gradient. Metallic tubes are attracted toward a microelectrode array, leaving semiconducting tubes in the solvent. They reported that the interaction between SWNTs and the surfactant induces a nanotube surface conductance that gives rise to a unique dependence of the nanotube dielectrophoresis on the frequency of the electric field [30].

Other work focusing on the dielectrophoretic properties of SWNTs has mostly concentrated on using this technique to align nanotubes [31] and [32], to position them specifically [33] or to remove impurities [34]. Lutz et al. [35] demonstrated that it is possible to work with a macroscopic cell to perform dielectrophoresis of SWNTs, so that a commercial use of the process becomes conceivable. In addition, Peng et al. [36] reported type separation and diameter enrichment of semiconducting SWNTs with dielectrophoresis-FFF (DEP-FFF). The fractions could be collected for further analysis or application. In-solution, band-gap fluorescence was used to study the correlation between the band gap of semiconducting SWNTs and retention time in the DEP system.

Enrichment was observed of semiconducting SWNTs with various diameters and band gaps. Hong et al. [37] also achieved complete separation between metallic and semiconducting species at the electric-field frequency of 10 MHz only when the surface charge of nanotubes was neutralized.

Metallic SWNTs has been functionalized with *p*-hydroxybenzene diazonium salt [38] at 45° C with high selectivity. Deprotonation in alkaline solution induces a negative charge on the functionalized SWNT for electrophoretic separation. This concept was applied to enrich metallic and semiconducting fractions separately using the induced differences in electrophoretic mobilities. Free-solution electrophoresis was utilized to separate selectively reacted samples into immobile and negative electrophoretic mobility fractions. Raman spectroscopy and ultraviolet-visible-near-infrared (UV-vis-NIR) absorption spectroscopy confirmed both separation of reacted and unreacted SWNTs and, after annealing, enrichment of metallic and semiconducting SWNTs in two distinct fractions.

Suárez et al. [39] used CE to analyze dispersions of CNTs as SDS surfactant-coated species (Fig. 3). The addition of small amounts of hydroxypropyl methyl cellulose (HPMC) together with the surfactant, SDS, was found critical to achieve reproducible dispersion of nanotubes and to obtain a homogeneous, stable sample solution. Different from other works, these authors proposed separation of the sample using a gel and a BGE without surfactant molecules. The proposed BGE comprised a polymer, 0.025% (w/v) HPMC solution, prepared in 5 mM ammonium acetate at pH 8.03. This procedure was effective in detecting small differences in the physico-chemical surface properties of the nanotubes.

The same group [40] performed separation of previously solubilized SWNTs, in this case with the aid of ionic liquids and ultrasound assisted, by using a 50 mM formic acid solution at pH 2.0 as BGE and a potential of −10 kV. Under these conditions, separation was completed within only 4 min. As it can be seen in Fig.

4, in the analysis of commercial SWNT bundles, 18 peaks were identified. The two types of bundles studied exhibited distinct, highly characteristic electrophoretic profiles that could be used to control SWNT purity (Fig. 4).

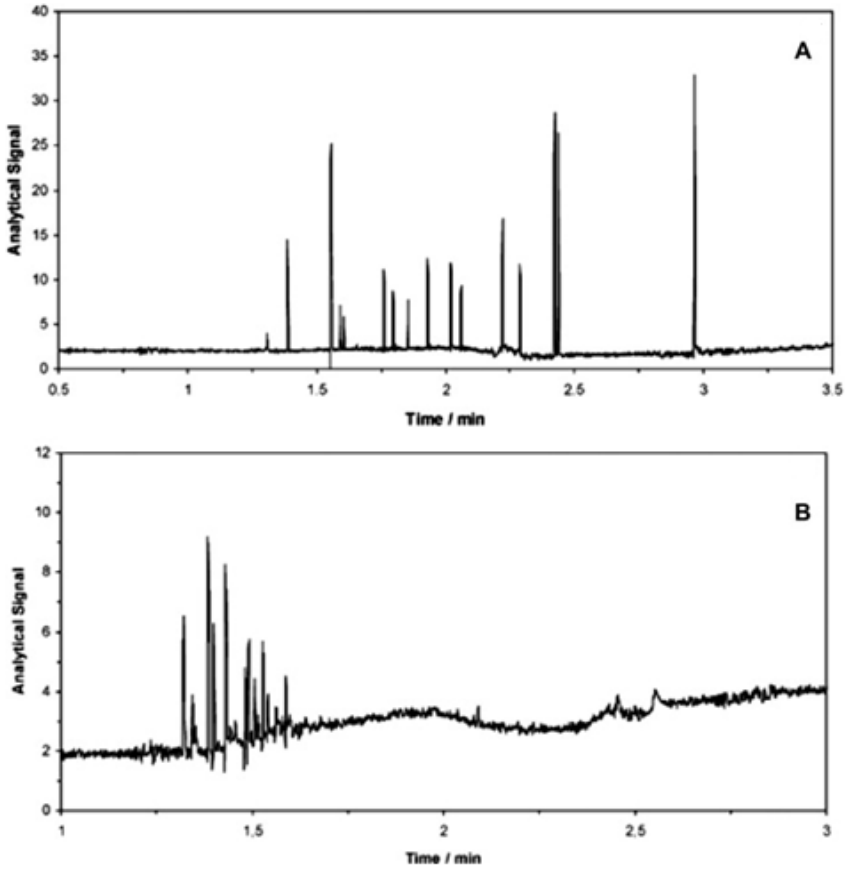

Figure 4. Electropherograms used to analyze commercial bundles of single-walled nanotubes (SWNTs) for quality and purity by using the recommended operating conditions. The size distribution was as follows: (A) diameters of 1.2-1.5 nm and (B) lengths of 2-20 μm. Electropherogram corresponding to the separation of SWNT-2 dispersed in SDS and without prior dispersion in the ionic liquid (Reproduced from [40] with permission).

Finally, Baker et al. [41] studied the influence of buffer composition on the separation of the mixture of negatively-charged carbon NPs (as a consequence of oxidative treatment) by varying buffer selection, pH and concentration. Their carbonaceous material was collected from the incomplete combustion of paraffin oil in a flame. Buffers employed were glycine, $NaHCO_3$, $KHCO_3$ or sodium phosphate. The electrophoretic pattern was affected by both co-ion and counter-ion in the buffer solution, influencing selectivity and peak shape. The mobility of selected species in the mixture of NPs showed strong dependence upon the ionic strength of the solution.

Over the past few years, several studies showed that fullerene derivatives can be used as biologically-active compounds in medicinal chemistry. Tamisier-Karolak et al. [42] developed an analytical method for measuring amounts of a dendro[60]fullerene (DF), which is a highly water-soluble [60]fullerene derivative. For that purpose, CZE was employed. Preliminary assays showed that DF has almost the same mobility as the EOF, but in the opposite direction. Attempts were made to reduce the EOF and positive results were obtained by adding hydroxypropylcellulose to the BGE. The optimal conditions in terms of rapid, efficient separation were obtained for pH 6 using a 75 mM phosphate buffer, although it increased ionic dispersion. Lower pH values were associated with unbalanced mobility and less concentrated buffers led to a large increase in running times. The EOF decrease was large enough when using 0.075% HP-cellulose in a phosphate buffer-methanol (70/30 v/v).

In another study, Chan et al. [43] developed an approach to CE for the analysis of two NPs (i.e. carboxyfullerene and dendrofullerene in both standard solutions and a serum matrix). These highly soluble, charged C_{60} derivatives were characterized by CZE using bare or dynamically-coated fused-silica capillaries. The resolution of both NPs was slightly lower with the coated capillary; however, their migration times were faster. While separation of the dendrofullerene NPs

using MEKC resulted in a greater number of observable peaks, the peak profile of carboxyfullerene was basically unchanged, regardless of whether or not SDS micelles were added to the running buffers. Fig. 5 shows the calibration of carboxyfullerene in serum using CZE.

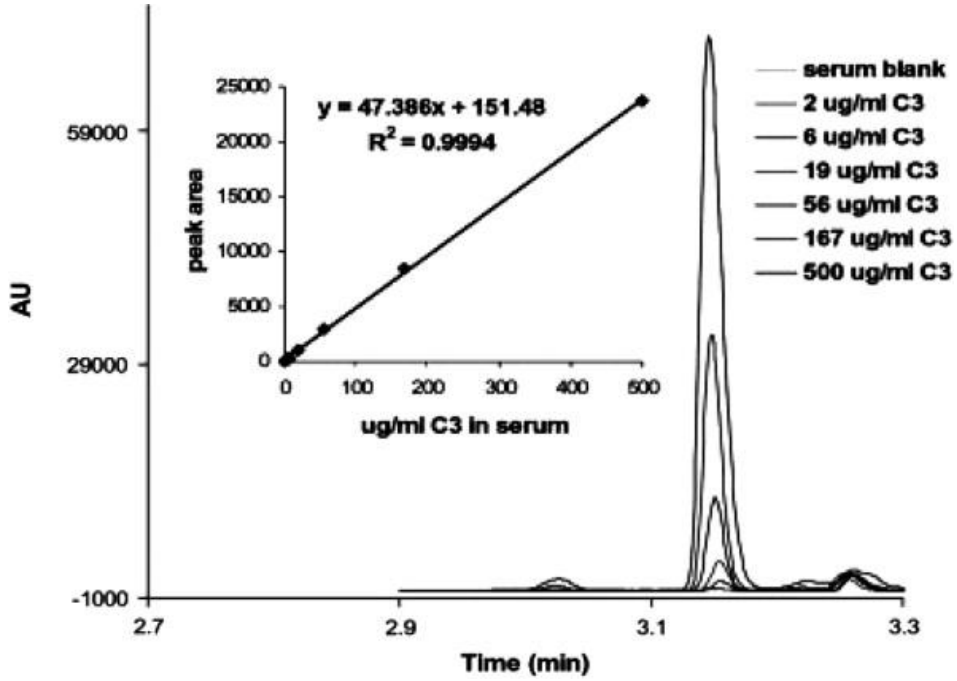

Figure 5. Calibration of carboxyfullerene (C3) in serum using capillary zone electrophoresis. Capillary: 50 mm, 40 cm with dynamic coating; buffer: 40 mM sodium phosphate (pH 7.4); voltage: −14 kV. Serum samples were diluted five-fold with SDS solution (80 mM final SDS concentration). The C3 concentrations refer to the undiluted samples (Reproduced from [43] with permission).

The analysis of fullerenes in CE was also investigated by Treubig et al. [44]. SDS was used to solubilize fullerenes C_{60}, C_{70}, and a mixture of C_{60} and C_{70} in water. The behavior of the solutions of the C_{60}–SDS and C_{70}–SDS complexes was examined by CE with on-line UV–Vis diode-array detection.

2.4. Other types of nanoparticles

One of the first attempts in using CE for characterizing particles was performed by Jones et al. [45], who separated different latex particles (with different numbers of attached carboxylate or sulfate groups). Particles were in the μm–nm size range and were separated according to numbers and kinds of functional groups attached to the particles. They studied the influence of capillary inner diameter, finding that a 75-μm column provided an increase in resistance and a decrease in current for a constant applied potential and column length, which eliminated overheating and boiling problems found in capillaries of larger diameter. Reduction of total column length and distance from injection to detector also proved crucial to reducing peak width and improving resolution between components in the latex mixture.

For many biotechnology applications of CE, sample introduction by electromigration appears to be used more often than hydrodynamic flow. However, in this case, the authors employed hydrodynamic sample introduction in order to avoid discrimination against sample components due to different net charges and sizes of the particles.

Petersen at al. [46] investigated the effects of capillary temperature control and electrophoretic heterogeneity on parameters characterizing separation of particles by CZE. They found that maintenance of constant capillary temperature by a thermostatted system significantly reduced the large dependence on voltage of mobility, selectivity, efficiency and resolution, observed in a non-thermostatted system. Electrophoretic heterogeneity in the particle samples was determined to be the major source of zone broadening on the thermostatted system.

Sub-μm and μm-sized metal-oxide particles (e.g., TiO_2, Al_2O_3, and Fe_2O_3) have also been characterized by CE [47]. The use of different electrolyte solutions

(e.g., sodium nitrate) leads to an electrolyte system without specific surface adsorption of ions but with essentially only electrostatic interactions between electrolyte ions and the surface of metal-oxide particles. The use of unbuffered solutions, along with the tendency of metal-oxide particles to form aggregates, prohibits accurate determination of electrophoretic mobility, so, using the model, there was only general agreement between the predicted electrophoretic mobilities and the measured values.

Furthermore, the effects of phosphate, carbonate, and borate-anion and sodium-ion concentration on the electrophoretic mobility of titania, hematite, and alumina oxide particles was investigated [48]. All three anion types have significant effects on the electrophoretic mobility of each of the oxides, with borate anions yielding the highest degree of selectivity between titania and alumina.

Several types of NPs have been studied in order to gain insight into the mechanisms of size-dependent separation of NPs and micro-particles in electrophoresis {e.g., sulfated polystyrene latex microspheres [49], polystyrene nanospheres [5], fluorescently-labeled latex particles [4], iron-oxide NPs [3], carboxylate-functionalized silicon NPs [50]} and dielectrophoresis [51].

Vanifatova et al. [52] performed size separation of five unmodified polystyrene nanosphere standards with diameters of 50–600 nm in phosphate-buffer solutions as carrier electrolyte. The electrophoretic mobility increased with particle diameter and optical spectra were shown to differ for particles of different size. The polymerization process left behind a number of acidic functional groups, which, because of their polar character, tended to accumulate at the polymer-solution interface. Particles of this kind bear a slightly negative surface charge due to ionization of such groups, so they can be separated by CZE. Besides, acquisition of additional charge due to ion adsorption from a carrier electrolyte is possible for these particles. It was found that migration

behavior of polystyrene spheres is mainly determined by their electrophoretic properties.

Selective separation of silica nanospheres, which is a function of separation conditions (e.g., pH or phosphate concentration of a carrier electrolyte), has been also studied [53], finding a decrease in electro-osmotic mobility with increasing phosphate concentration over the whole range studied. This decrease occurred only when acidic buffer solutions were used as carrier electrolyte. d'Orlyé et al. [54] characterized cationic maghemite NPs with diameters of 6–10 nm by CE with UV detection. They were dispersed in acidic, citrated or basic aqueous media. Particular interest was paid to the investigation of ferrofluids in their positively-charged form, since cationic colloids had received little attention through experimental difficulties. A strategy for capillary-wall modification was chosen in order to prevent particle adsorption while preserving high analytical performance. Size-dependent electrophoretic mobility was demonstrated and, although there was a very narrow size range, partial separation was obtained with selectivity varying as a function of the ionic strength of the electrolyte.

3. Analysis of bioderivatives of nanoparticles

In this section, we show some examples of separating derivatives of NPs. The difference with some examples described above is that, in this case, functionalization is not a strategy to achieve the resolution needed for the separation, or a way to introduce charges onto the NPs. The following NPs are directly synthesized with functionality, which is exploited, and, in some cases, their uses depend on this derivatization.

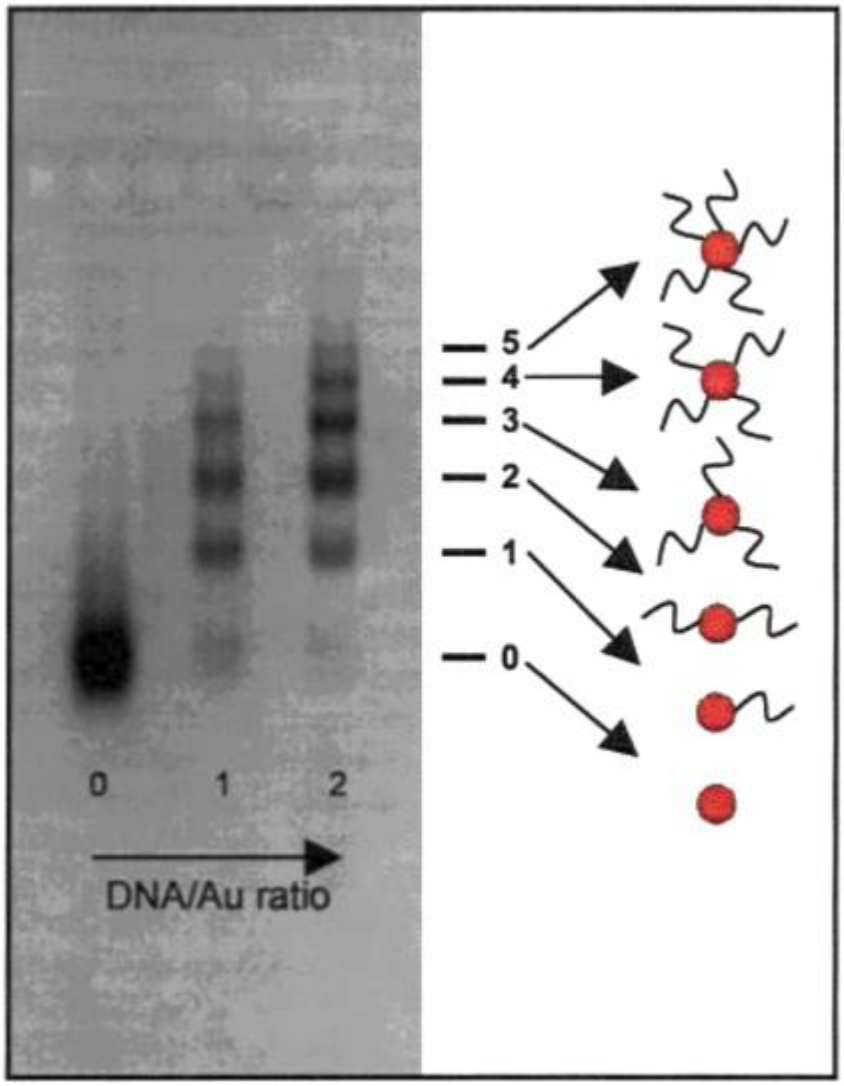

Figure 6. Electrophoretic mobility of 5 nm Au/100b HS-ssDNA conjugates (3% gel). The first lane (left to right) corresponds to 5-nm particles (single band). When ~1 equiv of DNA is added to the Au particles second lane), discrete bands appear (namely 0, 1, 2, 3, ...). When the DNA amount is doubled (third lane), the intensity of the discrete bands changes and additional retarded bands appear (4, 5). Because of the discrete character, each band can be directly assigned to a unique number of DNA strands per particle (Reproduced from [55] with permission).

Zanchet et al. [55] demonstrated the electrophoretic isolation of discrete gold nanocrystal/DNA conjugates, as can be seen in Fig. 6. By adjusting the DNA:Au ratio, they were able to control the average number of DNA strands per particle, but there would always be a distribution of oligonucleotides present. Thus, it was necessary to have a technique for separation and isolation of conjugates that was very sensitive to the number of bound strands. They used Au particles of 5 nm and 10 nm mean diameter and alkanethiol-modified single-stranded (HS-ss) DNA 18–100 bases long. The conjugates were prepared by adding the DNA to the Au colloid and were analyzed in 2–3% agarose gels.

The success of the electrophoretic isolation of nanocrystal/DNA conjugates depends on several factors (e.g., the need for the NP sample to be homogeneous in charge and particle-size distribution in order to obtain narrow bands). Employing purified conjugates, which gave more control and greater understanding of the system, they showed that particle/DNA hybrid properties dominated the mobility and that dimers, trimers, and intermediate building blocks could be identified in the gel. A drawback was that it was not possible to isolate or probe large DNA conjugated NPs structures by gel electrophoresis because of the finite pore size of the gel [56].

CZE was employed [57] to characterize nm-sized thiolated α-cyclodextrin-capped AuNPs (α-CD-S-AuNPs). The addition of tetrabutylammonium (Bu_4N^+) ions to the run buffer greatly narrowed the migration peak of α-CD-S-AuNP. The optimal run buffer was determined to be 10 mM Bu_4N^+ in 30 mM phosphate buffer at pH 12 and an applied voltage of 15 kV. Bu_4N^+ was successfully employed to narrow the peak width of α-CD-S-AuNP, as it could form inclusion complexes with α-CD-S-AuNPs via the hydrophobic cavities of the surface-attached thiolated α-CDs, thus inducing their inter-linkage. Moreover, functionalized AuNPs with one, two, and three PEG molecules per NP have been separated using gel electrophoresis [58].

Further proof of the potential of CE as a characterization tool is in the separation of QD bioconjugates for future bio-applications. Huang et al. [59] presented a very efficient, sensitive method for characterizing QD bioconjugates based on CE with laser-induced fluorescent (LIF) detection. They prepared CdTe QDs in aqueous phase by a chemical route with mercaptopropionic acid as ligand, and then coupled them to proteins using a bifunctional linkage reagent or electrostatic attraction. These bioconjugates were analyzed by CE with LIF detection, and they were efficiently separated from free QDs by optimizing the buffer pH.

Vicente et al. [60] also employed CE with LIF detection to separate different bioconjugated CdSe/ZnS QDs. The QD nanocrystals studied were conjugated to the biomolecules (i.e. streptavidin, biotin, and immunoglobulin G). The bioconjugated QDs showed different electrophoretic mobilities, which appeared to depend upon the biomolecule that was attached to the QD and the buffer solution used. The use of a polymeric additive in the CE run buffer improved the resolution of the bioconjugates. The use of QDs with different emission properties allowed selective monitoring of two different wavelengths while using one single excitation source. This allowed the monitoring of overlapping peaks in the electropherogram when newly-formed products resulting from the interaction of the two bioconjugated QDs appeared.

In addition, d'Orlyé et al. [61] studied the charge-based separation of cationic bifunctional maghemite/silica core-shell NPs. The inner wall of a silica capillary was modified so as to obtain a positive surface charge and thus allow the CE characterization of cationic particle populations. Eight amino/polyethylene glycol (PEG)-functionalized core/shell particle populations were synthesized, homogeneous in size, but differing in their surface-charge density according to the molar ratio between the two silane derivatization agents. Particle-size

distribution was calculated theoretically by Pyell [62] directly from dielectrophoresis data.

Vetcher et al. [63] showed that aqueous dispersions of SWCNTs, prepared with the aid of nucleic acids (NAs) (e.g., RNA or DNA), can be separated into fractions using agarose gel electrophoresis. In a discharge electric field, SWCNT/NA complexes migrated in the gel in the direction of positive potential to form well-defined bands. Raman spectroscopy as a function of band position showed that SWCNTs having different spectroscopic properties possessed different electrophoretic mobilities. The migration patterns for SWCNT/RNA and SWCNT/DNA complexes differed. Parallel elution of the SWCNT/NA complexes from the gel during electrophoresis and subsequent characterization by AFM revealed differences in SWCNT diameter, length and curvature.

4. Applications of capillary-electrophoresis separation of nanoparticles

As stated above, electrophoresis is a powerful tool for characterizing NPs in size, shape or charge. The electrophoretic separation of NPs involves formation of a charged derivative. The migration time will be affected by the chemical nature of the NP because the number of ligand molecules attached to the NP surface will be a function of the chemical bond established between the NP and the ligand but also of the dimensions of the NP. However, the velocity that NPs achieve in the electrophoretic system will depend of their m/z ratio but also on their hydrodynamic size due to the friction or Stokes forces established in the capillary. We would point out that non-symmetric NPs (e.g., CNTs) can be oriented in the capillary thanks to the interaction of the electrical field with the dipolar moment or electronic configuration of the NP. The orientation critically affects the friction forces experienced by the NP. In conclusion, migration time will be affected by: size and shape of the NP, chemical nature of the NP, electronic configuration of the NP, and the ligand or stabilizers added to the medium. Although it is difficult to relate a priori the migration time to the

properties and the characteristics of NPs, we describe below selected examples of applications.

In the case of MNPs, which have been used in catalysis, their catalytic activity depends on their shape and size, since they dramatically affect their physical and chemical properties, so there is interest in determining the size of MNPs, but also in separating fractions of homogeneously-sized MNPs [2].

The vast potential of colloidal nanocrystals conjugated with DNA as probes for biological diagnostics has been reported. However, in order to exploit them, it is necessary to control the number of oligonucleotides attached to each nanocrystal, which can be investigated by CE due to the shift in the electrophoretic mobility of NPs as a consequence of DNA binding [55]. The conformation and the packing of the DNA can influence the accessibility of the oligonucleotides for hybridization. Electrophoretic mobility of gold nanocrystals with attached nucleotides can be determined by gel electrophoresis, and the diameter of the conjugates determined depends on the conformation giving information about the nature of the attachment [64]. Moreover, DNA-DNA-hybridization reactions on silica functionalized with oligonucleotides are found to affect the amplitude and the direction of the dielectrophoretic mobility of the particles at nanomolar target ssDNA concentrations, which can be used for the detection of the hybridization event [65].

CE also allowed determination of the conjugation efficiency of antibodies and proteins to iron-oxide NPs prior to derivatization of the conjugates with naphthalene-2,3-dicarboxaldehyde reagent and detected by LIF [66]. As the CE-LIF technique requires negligible amounts of sample, it is suitable for controlling the functionalization of these NPs before use in diagnosis.

This technique can be also employed to verify the fractionation efficiency of other methodologies developed (e.g., electrolyte-induced fractionation of gold nanoclusters) [67].

The increasing use of NPs in industrial applications will inevitably lead to the release of such materials into the environment. Accurately assessing the environmental risks posed by NPs requires effective quantitative analytical methods to determine their mobility, reactivity, ecotoxicity and persistence, many of which have still to be developed [68]. In this sense, a method based on the preconcentration of carboxylated SWCNTs (c-SWNTs), by using a filter modified with multi-walled CNTs (MWCNTs), and their further electrophoretic analysis was developed in order to determine them in environmental water samples [69]. Electrophoretic separation of c-SWCNTs was accomplished using a 50 mM ammonium acetate solution at pH 7.5 as a BGE and a potential of 15 kV.

5. Detection

The most common detection techniques in CE used with NPs are UV/Vis and fluorescence spectroscopy. However, inductively coupled plasma with mass spectrometry (ICP-MS), Raman spectroscopy or near-infrared (NIR)-fluorescence are promising options. ICP-MS is useful for detection of metal, semiconducting and oxide-derivative NPs, and the Raman and NIR-fluorescence are valuable for the characterization of carbon NPs (e.g., CNTs).

The plasmon-resonance absorption of noble-metal NPs has absorption coefficient orders of magnitude greater than strongly absorbing dyes. Anisotropic shapes have plasmon-resonance absorptions that are even greater, leading to increased detection sensitivity. MNPs generate enhanced electromagnetic fields that affect the local environment. The field is determined by the geometry of the MNP and can enhance the fluorescence of the metal itself, the Raman signal of a molecule on the surface, and the scattering of light.

The free electrons in the metal (d electrons in silver and gold) are free to travel through the material. The mean free path in gold and silver is ~50 nm, so, in particles smaller than this, no scattering is expected from the bulk. Thus, all interactions are expected to be with the surface. When the wavelength of light is much greater than the size of the NP, it can set up standing resonance conditions. Light in resonance with the surface-plasmon oscillation causes the free electrons in the metal to oscillate. As the wave-front of the light passes, the electron density in the particle is polarized to one surface and oscillates in resonance with the light frequency, causing a standing oscillation. When the shape or the size of the NP changes, the surface geometry changes, causing a shift in the electric-field density on the surface. This causes a change in the oscillation frequency of the electrons, generating different cross-sections for the optical properties, including absorption and scattering [70]. The most useful detectors for the analysis of this kind of NPs are therefore UV/Vis detectors, which are limited by the small pathlength of the capillary. An alternative of higher sensitivity should be ICP-MS but the performance of coupling between CE and ICP-MS is still not well developed due to the small amount of sample introduced into the capillary and the low flow rate of the electrophoretic separation. In order to maintain electrophoretic resolution, it is necessary to develop a plasma with a small lead volume and equipment with high-speed measurement.

QDs are highly fluorescent NPs characterized by having a symmetric, narrow bandwidth of ~30 nm full width at half maximal fluorescence, which enables emission of pure color. Since the spectroscopic properties of QDs are size-dependent, they are continuously tunable in the preparation procedures. The smaller the QD the more blue-shifted ("hypsochrom") are absorption and emission. QDs are now studied in various fields, including biology, electronics and optoelectronics. They are starting to compete with conventional organic fluorescent labels and can be directly detected by LIF, while non-fluorescent NPs

and their conjugates need to be derivatized in order to acquire fluorescence. The combination of LIF with CE is probably the most useful for the determination of QDs, because they present broad excitation spectra that make it possible to excite all the QDs with the unique wavelength coming from the laser source.

The optical properties of SWCNTs have attracted growing interest since the recent observation of near-infrared luminescence from well-separated, surfactant-suspended semiconducting SWNTs [71]. All current methods for producing SWNTs lead to heterogeneous samples containing mixtures of metallic and semiconducting species with a variety of lengths and defects. This diversity of SWNT structures complicates precise spectroscopic characterization [72]. Photoluminescence studies performed on individual SWNTs revealed the single-NT line-width of emission spectra and the presence of spectral variations within a given *(n,m)* type [73]. However, luminescence measurements are limited to semiconducting SWNTs.

By contrast, Raman scattering has been used to study individual semiconducting and metallic SWNTs [74], but such experiments remain constrained by the weakness of the signal and the need to use near-resonant laser sources. Rayleigh scattering has also been studied to record optical spectra from individual structure-assigned SWNTs [75].

However, Raman spectroscopy is the most widely used technique to study CNTs, primarily focused on SWCNTs. Raman scattering from SWCNTs is a resonant phenomena that generates an intense, easily measurable signal. Their popularity relies on their usefulness to provide information on not only the vibrational properties but also the structure and the electronic properties of SWCNTs. The most significant spectral features for SWCNTs are the RBM (100–300 cm^{-1}), the disorder peak (D peak, ~1350 cm^{-1}), the tangential mode (G band, 1400–

1700 cm^{-1}), and the second-order overtone of the D peak (D′, 2500-2800 cm^{-1}).

Although there are advantages in the combination of Raman spectroscopy with CE, its use is limited because the complexity of the coupling. In addition to a special optical system, it is difficult to make compatible the electrophoretic mobility of the NPs with the acquisition time required to record the Raman spectrum. At-line coupling is the best combination for this purpose. In spite of the advantage that different detectors offer in the analysis of NPs, UV/Vis and fluorescence detectors are still used most.

6. Future trends

CE analysis of NPs will be focused on improvement of the coupling of CE systems with detectors (e.g., ICP-MS, Raman spectrometry and NIR fluorescence). Another important trend is development of new complexant agents that provide charge to NPs and avoid their aggregation without modifying their structure. With respect to the analysis of metallic and semi-metallic NPs, the development of fundamental theory, which shows the theoretical relation between migration time and size, will be of interest for the rapid, direct determination and characterization of NPs.

Finally, we need to point out the lack of standards. Their development and implementation would help to relate the electrophoretic behavior in separation of NPs to the characteristics and the properties of NPs.

In spite of the limitations of electrophoretic methods, their use offers important advantages that justify their development.

Acknowledgements

The authors wish to thank Spain's Ministry of Innovation and Science for funding Project CTQ2007-60426 and *Junta de Andalucía* for Project FQM02300. A.I. López-Lorente also wishes to thank the Ministry for the award of a Research Training Fellowship (Grant AP2008-02939).

References

[1] M. Valcárcel, B.M. Simonet, S. Cárdenas, Anal. Bioanal. Chem. 391 (2008) 1881.

[2] F.K. Liu, G.T. Wei, Anal. Chim. Acta 510 (2004) 77.

[3] N.G. Vanifatova, B.Y. Spivakov, J. Mattusch, U. Franck, R. Wennrich, Talanta 66 (2005) 605.

[4] H. Ahmadzadeh, R. Dua, A.D. Presley, E.A. Arriaga, J. Chromatogr., A 1064 (2005) 107.

[5] Y.H. Rezenom, A.D. Wellman, L. Tilstra, C.D. Medley, S.D. Gilman, Analyst (Cambridge, UK) 132 (2007) 1215.

[6] U. Schnabel, C.H. Fischer, E. Kenndler, J. Microcolumn Sep. 9 (1997) 529.

[7] F.K. Liu, F.H. Ko, P.W. Huang, C.H. Wu, T.C. Chu, J. Chromatogr., A 1062 (2005) 139.

[8] R. Krupke, F. Hennrich, H. von Löhneysen, M.M. Kappes, Science (Washington, DC) 301 (2003) 344.

[9] X. Song, L. Li, H. Qian, N. Fang, J. Ren, Electrophoresis 27 (2006) 1341.

[10] X. Xu, K. Caswell, E. Tucker, S. Kabisatpathy, K.L. Brodhacker, W.A. Scrivens, J. Chromatogr., A 1167 (2007) 35.

[11] M. Hanauer, S. Pierrat, I. Zins, A. Lotz, C. Sönnichsen, Nano Lett. 7 (2007) 2881.

[12] A.M. Gole, C. Sathivel, A. Lachke, M. Sastry, J. Chromatogr., A 848 (1999) 485.

[13] U. Pyell, Electrophoresis 31 (2010) 814.

[14] N. Surugau, P.L. Urban, J. Sep. Sci. 32 (2009) 1889.

[15] M.A. Rodriguez, D.W. Armstrong, J. Chromatogr., B 800 (2004) 7.

[16] S.P. Radko, A. Chrambach, Electrophoresis 23 (2002) 1957.

[17] F.K. Liu, Y.Y. Lin, C.H. Wu, Anal. Chim. Acta 528 (2005) 249.

[18] F.K. Liu, J. Chromatogr., A 1167 (2007) 231.

[19] K.H. Lin, T.C. Chu, F.K. Liu, J. Chromatogr., A 1161 (2007) 314.

[20] T.H. Chang, F.K. Liu, Y.C. Chang, T.C. Chu, Chromatographia 67 (2008) 723.

[21] F.K. Liu, J. Chromatogr., A 1216 (2009) 2554.

[22] F.K. Liu, M.H. Tsai, Y.C. Hsu, T.C. Chu, J. Chromatogr., A 1133 (2006) 340.

[23] C.K. Lo, M.C. Paau, D. Xiao, M.M.F. Choi, Electrophoresis 29 (2008) 2330.

[24] W. Bücking, T. Nann, IEE Proc. Nanobiotechnol. 153 (2006) 47.

[25] U. Pyell, W. Bücking, C. Huhn, B. Herrmann, A. Merkoulov, J. Mannhardt, H. Jungclas, T. Nann, Anal. Bioanal. Chem. 395 (2009) 1681.

[26] I. Arnaud, J.P. Abid, C. Roussel, H.H. Girault, Chem. Comm. (2005) 787.

[27] M. Pereira, E.P.C. Lai, B. Hollebone, Electrophoresis 28 (2007) 2874.

[28] S.K. Doorn, R.E. Fields, H. Hu, M.A. Hamon, R.C. Haddon, J.P. Selegue, V. Majidi, J. Am. Chem. Soc. 124 (2002) 3169.

[29] S.K. Doorn, M.S. Strano, M.J. O'Connell, E.H. Haroz, K.L. Rialon, R.H. Hauge, R.E. Smalley, J. Phys. Chem. B 107 (2003) 6063.

[30] R. Krupke, F. Hennrich, M.M. Kappes, H. von Löhneysen, Nano Lett. 4 (2004) 1395.

[31] X.Q. Chen, T. Saito, H. Yamada, K. Matsushige, Appl. Phys. Lett. 78 (2001) 3714.

[32] M.S. Kumar, T.H. Kim, S.H. Lee, S.M. Song, J.W. Yang, K.S. Nahm, E.K. Suh, Chem. Phys. Lett. 383 (2004) 235.

[33] R. Krupke, F. Hennrich, H.B. Weber, M.M. Kappes, H. von Löhneysen, Nano Lett. 3 (2003) 1019.

[34] K. Yamamoto, S. Akita, Y. Nakayama, J. Phys. D: Appl. Phys. 31 (1998) L34.

[35] T. Lutz, K.J. Donovan, Carbon 43 (2005) 2508.

[36] H. Peng, N.T. Alvarez, C. Kittrell, R.H. Hauge, H.K. Schmidt, J. Am. Chem. Soc. 128 (2006) 8396.

[37] S. Hong, S. Jung, J. Choi, Y. Kim, S. Baik, Langmuir 23 (2007) 4749.

[38] W.J. Kim, M.L. Usrey, M.S. Strano, Chem. Mater. 19 (2007) 1571.

[39] B. Suárez, B.M. Simonet, S. Cárdenas, M. Valcárcel, J. Chromatogr., A 1128 (2006) 282.

[40] M. López-Pastor, A. Domínguez-Vidal, M.J. Ayora-Cañada, B.M. Simonet, B. Lendl, M. Valcárcel, Anal. Chem. 80 (2008) 2672.

[41] J.S. Baker, L.A. Colón, J. Chromatogr., A 1216 (2009) 9048.

[42] S.L. Tamisier-Karolak, S. Pagliarusco, C. Herrenknecht, M. Brettreich, A. Hirsch, R. Céolin, R.V. Bensasson, H. Szwarc, F. Moussa, Electrophoresis 22 (2001) 4341.

[43] K.C. Chan, A.K. Patri, T.D. Veenstra, S.E. McNeil, H.J. Issaq, Electrophoresis 28 (2007) 1518.

[44] J.M. Treubig Jr., P.R. Brown, J. Chromatogr., A 873 (2000) 257.

[45] H.K. Jones, N.E. Ballou, Anal. Chem. 62 (1990) 2484.

[46] S.L. Petersen, N.E. Ballou, Anal. Chem. 64 (1992) 1676.

[47] C. Quang, S.L. Petersen, G.R. Ducatte, N.E. Ballou, J. Chromatogr., A 732 (1996) 377.

[48] G.R. Ducatte, N.E. Ballou, C. Quang, S.L. Petersen, J. Microcolumn Sep. 8 (1996) 403.

[49] S.P. Radko, M. Stastna, A. Chrambach, Electrophoresis 21 (2000) 3583.

[50] D.A. Eckhoff, J.N. Stuart, J.D.B. Sutin, J.V. Sweedler, E. Gratton, J. Chem. Phys. 125 (2006) 081103.

[51] A.T.J. Kadaksham, P. Singh, N. Aubry, Electrophoresis 25 (2004) 3625.

[52] N.G. Vanifatova, B.Y. Spivakov, J. Mattusch, R. Wennrich, J. Chromatogr., A 898 (2000) 257.

[53] N.G. Vanifatova, B.Y. Spivakov, J. Mattusch, R. Wennrich, Talanta 59 (2003) 345.

[54] F. D'Orlyé, A. Varenne, P. Gareil, Electrophoresis 29 (2008) 3768.

[55] D. Zanchet, C.M. Micheel, W.J. Parak, D. Gerion, A.P. Alivisatos, Nano Lett. 1 (2001) 32.

[56] D. Zanchet, C.M. Micheel, W.J. Parak, D. Gerion, S.C. Williams, A.P. Alivisatos, J. Phys. Chem. B 106 (2002) 11758.

[57] M.C. Paau, C.K. Lo, X. Yang, M.M.F. Choi, J. Chromatogr., A 1216 (2009) 8557.

[58] R.A. Sperling, T. Pellegrino, J.K. Li, W.H. Chang, W.J. Parak, Adv. Funct. Mater. 16 (2006) 943.

[59] X.H. Huang, J. Weng, F. Sang, X. Song, C. Cao, J. Ren, J. Chromatogr., A 1113 (2006) 251.

[60] G. Vicente, L.A. Colón, Anal. Chem. 80 (2008) 1988.

[61] F. D'Orlyé, A. Varenne, T. Georgelin, J.M. Siaugue, B. Teste, S. Descroix, P. Gareil, Electrophoresis 30 (2009) 2572.

[62] U. Pyell, Electrophoresis 29 (2008) 576.

[63] A.A. Vetcher, S. Srinivasan, I.A. Vetcher, S.M. Abramov, M. Kozlov, R.H. Baughman, S.D. Levene, Nanotechnology 17 (2006) 4263.

[64] W.J. Parak, T. Pellegrino, C.M. Micheel, D. Gerion, S.C. Williams, A.P. Alivisatos, Nano Lett. 3 (2003) 33.

[65] Z. Gagnon, S. Senapati, J. Gordon, H.C. Chang, Electrophoresis 29 (2008) 4808.

[66] F.H. Wang, T. Yoshitake, D.K. Kim, M. Muhammed, B. Bjelke, J. Kehr, J. Nanopart. Res. 5 (2003) 137.

[67] C.K. Lo, M.C. Paau, D. Xiao, M.M.F. Choi, Anal. Chem. 80 (2008) 2439.

[68] B.M. Simonet, M. Valcárcel, Anal. Bioanal. Chem. 393 (2009) 17.

[69] B. Suárez, Y. Moliner-Martínez, S. Cárdenas, B.M. Simonet, M. Valcárcel, Environ. Sci. Technol. 42 (2008) 6100.

[70] S. Eustis, M.A. El-Sayed, Chem. Soc. Rev. 35 (2006) 209.

[71] M.J. O'Connell, S.M. Bachilo, C.B. Huffman, V.C. Moore, M.S. Strano, E.H. Haroz, K.L. Rialon, P.J. Boul, W.H. Noon, C. Kittrell, J. Ma, R.H. Hauge, R.B. Weisman, R.E. Smalley, Science (Washington, DC) 297 (2002) 593.

[72] S. Berciaud, L. Cognet, P. Poulin, R.B. Weisman, B. Lounis, Nano Lett. 7 (2007) 1203.

[73] A. Hartschuh, H.N. Pedrosa, L. Novotny, T.D. Krauss, Science (Washington, DC) 301 (2003) 1354.

[74] N. Anderson, A. Hartschuh, S. Cronin, L. Novotny, J. Am. Chem. Soc. 127 (2005) 2533.

[75] M.Y. Sfeir, T. Beetz, F. Wang, L. Huang, X.M.H. Huang, M. Huang, J. Hone, S. O'Brien, J.A. Misewich, T.F. Heinz, L. Wu, Y. Zhu, L.E. Brus, Science (Washington, DC) 312 (2006) 554

Capítulo 9

Capillary electrophoretic separation of citrate-capped silver and gold nanoparticles by interaction with thiol compounds as additives in buffer solution

Submitted to Journal of Chromatography A

Journal of Chromatography A

Submitted

Capillary electrophoresis separation of citrate-capped silver and gold nanoparticles by interaction with thiol compounds as additives in buffer solution

A.I. López-Lorente, M.L. Soriano, M. Valcárcel

Department of Analytical Chemistry, University of Córdoba, E-14071 Córdoba, Spain.

This paper reports an innovative and simple method to separate and preconcentrate metallic nanoparticles (NPs) in aqueous medium by capillary electrophoresis (CE) accordingly to their nature, based on ligand-exchange microreaction. Both gold (AuNPs) and silver NPs (AgNPs) were synthesized with same size, shape and shell (citrate) and characterized by microscopic and spectroscopic techniques. We have demonstrated the separation of these nanoparticles, which show same migration times in capillary electrophoresis, by the addition of thiol compounds in the buffer solution capable of interacting with NP surface establishing different migration times because of the differences on the core-shell charges. "Large-sample volume stacking" methodology combined with thiol compounds as additives was also used for both preconcentrating and improving the separation of metallic NPs of similar size.

Keywords: capillary electrophoresis, gold nanoparticles, silver nanoparticles, thiol compounds, ligand-exchange reaction, large-volume sample stacking.

1. Introduction

Metallic nanoparticles possess exceptional properties which have promoted their use in many fields, such as biomedical imaging and diagnostic tests [1], biological applications [2], catalysis [3], bactericides and for other analytical applications owing to their enhanced optical properties such as absorption, enhanced Rayleigh scattering or surface-enhanced Raman scattering of molecules adsorbed on NP surfaces [4].

The great social interest aroused by nanotechnology has promoted an intense use of metallic NPs in many areas, including consumer products. Such extensive uses and their unforeseen hazards give rise to the need of developing new methodologies for separation and characterization of such nanoparticles. Microscopic techniques are one of the most commonly employed techniques, although they suffer from the drawback of being time-consuming in order to assure sample representativeness. Dynamic light scattering is a common method for the size characterization of nanoparticles [5], although it is difficult to infer further physical properties from an ensemble of NPs. Size-exclusion chromatography (SEC) has been attempted to size and shape separation of gold nanoparticles, obtaining low resolutions [6]. Experimentally, small AuNPs exhibit a strong UV absorption feature which decays approximately exponentially into the visible, with a superimposed localized surface plasmon resonance (LSPR) band at about 520 nm that decreases in intensity and energy with decreasing AuNP size [7], which also depends on their shape and attached ligands and has been used for their characterization.

Capillary electrophoresis (CE) has emerged as a useful separation technique, owing to the surface charges of colloidal nanoparticles [8, 9]. Nanoparticle charges arise from the sorption of citrate onto its surface during the synthesis forming an electrical double layer which stabilizes the nanoparticles and prevent their agglomeration. Thus, metallic NPs behave in a similar manner to that of

charged molecular species, their separation being based on their charge-to-size ratio. When the electrical double layer is not enough to stabilize the NPs in the electrophoretic system, covalent functionalization or stabilization with the aid of surfactants is required.

CE has been used to separate a variety of differently sized materials, including inorganic oxide [10], latex [11], silver and gold NPs [12], carbon nanotubes (CNTs) [13], quantum dots (QDs) [14], etc. The dependence of electrophoretic mobility of the nanoparticles with their size has been widely studied, CE being used as a tool for monitoring the synthesis of NPs [15], characterizing the size of synthesized nanoparticles [16, 17] and subsequently employed for the size-dependent separation of nanoparticles as a consequence of the deformation of the electric double layer around the NP, which depends on the size of the particles and buffer ionic strength [18]. Most of works regarding the electrophoretic separation of gold and silver nanoparticles have been based on nanoparticles size or shape separation. However, as far as we are concerned, similar sized and shaped gold and silver nanoparticles with the same ligand shell have not been separated until now.

On the other hand, according to the well-established gold-thiol chemistry in the formation of self-assembled monolayers (SAMs) [19], ligand exchange reaction is a simple and versatile approach for tuning the characteristics of NPs while maintains the size and dispersity of the precursor particles, especially in case of organic molecules containing thiol groups [20]. A good strategy for incorporating more thiolate linkers into the ligand must take into account the packing efficiency and stability of surface-modified NPs [21, 22]. When covalently functionalized, the extinction maximum of AuNPs with thiol SAMs is slightly red shifted as additional ligands bind to the surface. The extinction maximum wavelength red shifts as molecular packing density and/or alkanethiol chain length increases [23].

This paper reports the separation and in-line preconcentration of citrate-capped AgNPs and AuNPs using capillary electrophoresis based on the introduction of various thiol derivatives in the buffer solution. The basis of the separation lies in the different mobilities found for two analytes (citrate-capped NPs of similar size with same mobility) before and after derivatization (functionalized nanoparticles) with different thiol additives present in the separation buffer rather than differences in nanoparticles size. Typically, microreactions are employed close to the start of an isolation procedure to enhance the recovery of analytes, to ensure their stability during the isolation process, or to increase the selectivity of the method for the target compounds. Furthermore, the combination of capillary electrophoresis with multi-wavelength PDA detection provides a useful tool for separation and detection of different types of NPs, even their aggregation state.

A drawback of capillary electrophoresis is the low sensibility of UV detection systems. Because of the small dimensions of CE capillaries, only very small sample volumes can be loaded. Moreover, the path length in CE is usually reduced compared, for example, with liquid chromatography. In order to preconcentrate in-line the sample and enable a better interaction of NPs with the additive present in electrophoretic buffer, "large-volume sample stacking" (LVSS) approach was successfully employed. In this modality, the capillary is filled with a high-conductivity buffer, and then, the sample solution is injected to a certain length into it and a negative polarity applied. At that point, EOF moves towards the inlet while anionic analytes move towards detection end stacking at one side of the boundary between the sample zone and BGE. The subsequent separation occurs in the normal CE mode [24].

2. Materials and methods

2.1. Apparatus

Capillary electrophoresis was performed on a Beckman Coulter (Palo Alto, CA, USA) P/ACE MDQ instrument equipped with an on-column UV detector and a diode array detector (DAD). The instrumental setup was governed, and data acquired and processed, by using the software 32 Karat.

UV-Vis measurements were performed using a halogen lamp as excitation and the monochromator and photonic detector of a PTI fluorescence Master system as a detector. TEM photographs were carried out with Philips CM-10 electron microscope.

2.2. Reagents

Tetrachloroauric acid solution ($HAuCl_4$), silver nitrate (>99%), sodium citrate dihydrate (99.5%), sodium dodecyl sulfate (SDS, 98%), 3-(cyclohexylamino)-1-propanesulfonic acid (CAPS, ≥98%), thiomalic acid (TMA, 97%) and sodium hydroxide were supplied by Sigma-Aldrich; thioctic acid (TA, ≥98%) was purchased from Fluka; methanol (with a purity ≥99.9%) from J.T. Baker; nitric acid (≥69%) and sulfuric acid (95-98%) from PANREAC. Ultrapure water used for all the experiments was obtained from a Milli-Q system.

2.3. Synthesis of gold nanoparticles

Gold nanoparticles were synthesized according to the method proposed by Turkevich et al. [25] with some modifications, as described elsewhere [26]. Prior use all glass materials were washed with a mixture of nitric acid and hydrochloric acid (1:3 v/v). $HAuCl_4$ and sodium citrate solutions were filtered through a 0.45 μm nylon membrane. For the synthesis 50 mL of a 0.01% (w/v) $HAuCl_4$ solution was heated while being magnetically stirred. After reaching the

boiling point, 0.254 mL of a 1% (w/v) of sodium citrate solution was added to the solution. The mixture was left stirring for 15 min while boiling. Then, 5 mL of 0.01% (w/v) $HAuCl_4$ solution and 0.254 mL of a 1% (w/v) of sodium citrate solution were added to the mixture and stirred for 15 min. Then, the heater was switched off and the system kept stirring until reach room temperature. 10 mL of the resulted solution were consequently centrifuged at 2515 g for 10 minutes removing the colorless supernatant (from 10 mL to 2 mL of solution). The final reddish solution containing gold nanoparticles was stored in an amber bottle at 4ºC until use.

2.4. Functionalization of gold nanoparticles with thioctic acid

Solution of citrated nanoparticles was treated with a large excess of TA (1:3 Au/thiol) by adding small amounts of TA while changing the pH to 8 to redissolve the pinkish suspension. As a normal thiol derivate, chemical adsorption to the particle surface through Au-S bonding is expected. When not flocculation was observed, the solution was left stirring for 12 hours and purified by steps of washing with ultrapure water and ethyl acetate followed by centrifugation (14489 g) to remove unbound thioctic acid. The nanoparticles remained stable and did not agglomerate in alkaline aqueous solution at room temperature over a period of 6 months.

2.5. Synthesis of silver nanoparticles

Silver colloid solution was prepared according to Lee and Meisel´s method [27]. Silver nitrate (9 mg, 0.053 mmol) was dissolved in 50 mL of ultrapure water and brought to boiling point. 5 mL of a 1% w/v sodium citrate solution was then added keeping the reaction under stirring and refluxed conditions for 90 minutes. A greenish yellow suspension was obtained after cooling the reaction to ambient temperature. Silver nanoparticles were purified and preconcentrated

by centrifugation at 2515 g for 10 minutes. The final solution containing the purified silver nanoparticles was stored in an amber bottle at 4ºC.

2.6. Capillary electrophoresis procedures

CE separations were accomplished by using a fused-silica capillary 75 µm of inner diameter with an effective length between inlet and detector of 50 cm (total length of 57 cm). Photometric measurements were made both at 420 and 539 nm in all cases. Initially, the capillary was sequentially conditioned using 1M HCl (5 min), 0.1M NaOH (10 min) and ultrapure water (5 min). Between runs, the capillary was sequentially washed with 1M HCl (1 min), 0.1M NaOH (2 min), ultrapure water (5 min) and background electrolyte (5 min).

The initial background electrolyte (BGE) was a mixture of 40 mM sodium dodecyl sulfate (SDS) and 10 mM 3-(cyclohexylamino)-1-propanesulfonic acid (CAPS) with 0.1% of methanol, adjusted to pH 9.7 using NaOH. All solutions were filtered through a 0.45 µm membrane filter before use. Gold and silver nanoparticles solution was introduced into the capillary by applying 0.5 psi for 50 s. Separation was then accomplished using an applied voltage of +20 kV. The temperature of the capillary cartridge was set to 25ºC.

Two buffer additives were evaluated in order to achieve the separation of Au and Ag nanoparticles according to their selective interaction with the organic molecule according to their nature, as depicted in figure 1. The effect of thioctic (TA) and thiomalic acids (TMA) has been evaluated in a range of 0.1-0.4% (w/v) present in the buffer solution.

In order to improve the separation, LVSS electrophoretic modality was performed. In this case, the sample was introduced into the capillary by applying 0.5 psi for 50 s, then, a small plug of buffer is introduced (0.5 psi for 20 s). Subsequently, a high negative voltage (-20 kV) was applied for 4 minutes, and

finally the polarity is returned to positive. Separation was then accomplished using an applied voltage of +20 kV. The temperature of the capillary cartridge was set to 25ºC.

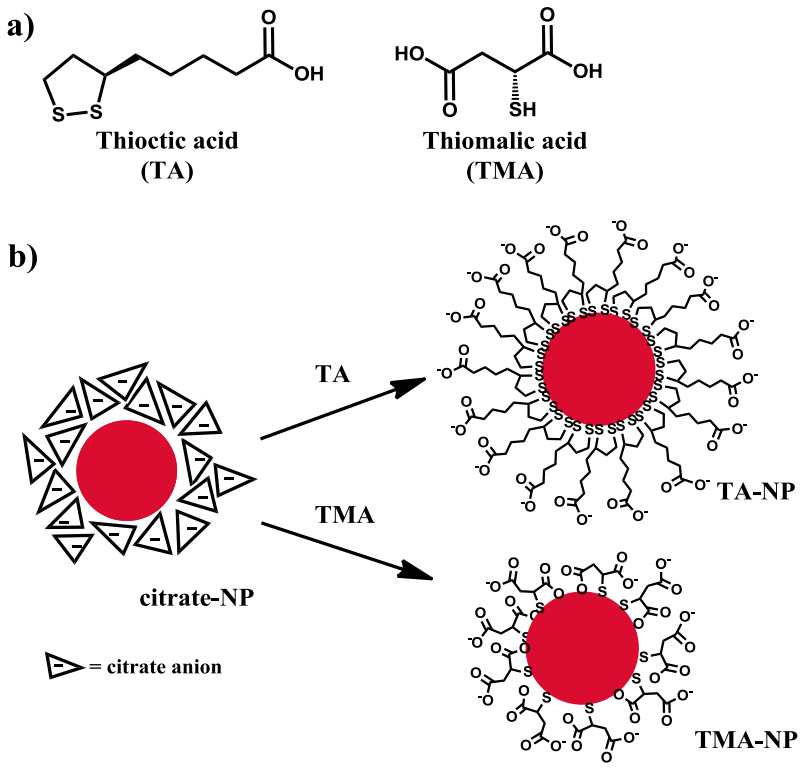

Figure 1. (a) Molecular structures of two thiol derivatives employed as buffer additives in order to achieve Au and AgNPs separation. (b) Metallic nanoparticle functionalization scheme: 1) TA-NPs; 2) TMA-NPs (drawing are not to scale).

3. Results and discussion

3.1. Characterization of gold and silver nanoparticles

To verify the formation of NPs and their size and shape, localized surface plasmon resonance (LSPR) and TEM images were evaluated. Metallic NPs exhibit strong extinction properties in the visible region, which are sensitive to variations in the NP shape, size, environment and their state of aggregation. Fig.

2a displays the UV–visible absorption spectra of typically spherically shaped Au and Ag colloid solutions. The LSPR of AuNPs appears at 537 nm whereas for AgNPs is centered at 420 nm. Preliminary studies confirm their stability in water and in BGE, and even in pH values ranging from 5-8 due to the not appearance of other red-shifted bands. Solutions of citrate-capped gold and silver nanoparticles were clear and stable for months.

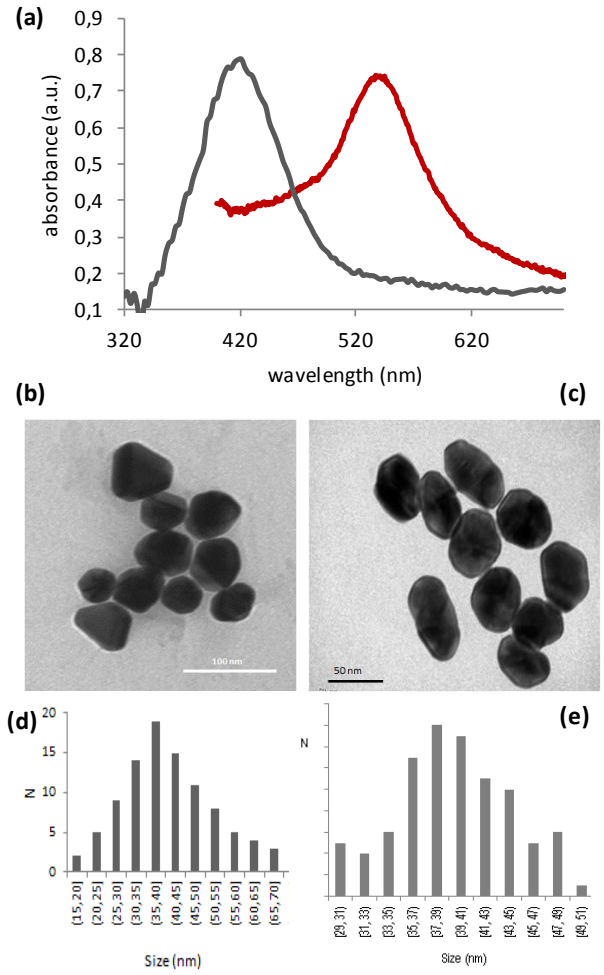

Figure 2. (a) Ultraviolet-visible spectra of citrated AgNPs (grey) and AuNPs (red). (b) Representative TEM images of citrate-capped AgNPs and (c) of AuNPs. (d) Size distribution of AgNPs and (e) AuNPs calculated from their corresponding TEM images.

Structural analysis of both types of NPs via TEM (figure 2b and c) reveals the polygonal almost nearly spherical shape of NPs with diameters of 41±7 nm and 39±6 nm for Ag and AuNPs, respectively.

In order to provide a comprehensive understanding of carboxylated SAM formation of AuNPs when ligand exchange takes place, functionalized AuNPs with a thioctic acid were also prepared by ligand exchange of citrate-AuNPs and characterized.

With regard to functionalized nanoparticles with thioctic acid (TA-AuNPs) in ultrapure water solution (Figure S1) the LSPR appears centered at 539 nm, being this slight red shifted value a consequence of the relatively higher molecular packing density compared with citrate ligand [23, 28]. Although both citrate-AuNPs and TA-AuNPs are statistically identical in terms of core and size (figure S2), both types of NPs reveal diverse stabilities in various pH environments. Flocculation of TA-AuNPs were observed when pH value was lower than 7, therefore, solutions of TA-AuNPs were stable in alkaline BGE.

3.2. Electrophoretic mobility studies

The composition of electrophoretic buffer employed for the CE characterization of the nanoparticles was 40 mM of SDS and 10 mM of CAPS, following the recommended procedure by Liu et al [29]. The pH of the buffer was alkaline (9.7) in order to preserve nanoparticle stability since at lower pH flocculation of derivatized NPs was observed. Furthermore, addition of methanol to the running buffer was investigated and a significant influence of its content on migration time of the metallic NPs was observed, as depicted in Figure 3 for example in the case of TA-AuNPs. When increasing the amount of methanol added to the BGE, NPs appeared at shorten migration times. In the case of citrate-capped AuNPs we observed a migration time of 9.93 min in absence of methanol, while in the case of 0.1% (v/v) of methanol in BGE the migration time

observed was 7.9 min. An optimal value of 0.1% (v/v) of methanol in the buffer was selected since higher amounts resulted in irreproducibility of the measurements. Accordingly with Debye-Hückel-Henry theory [30], since size, shape and effective charge of NPs remain invariable; viscosity of the buffer must change during addition of methanol if the electrophoretic mobility of NPs changes. Organic modifiers such as methanol or other organic solvents added to the aqueous buffer affect the degree of ionization of the NPs and normally decreases the migration time.

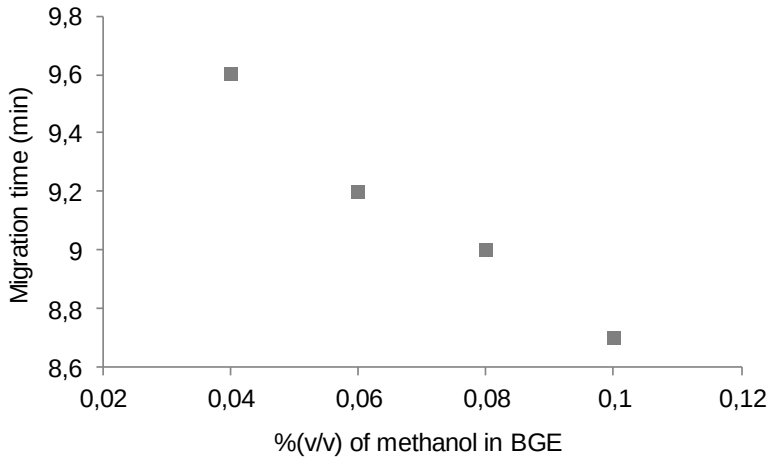

Figure 3. Dependence of migration time of TA-AuNPs with the amount (% v/v) of methanol added to the BGE composed of 40 mM of SDS and 10 mM of CAPS at a pH of 9.7.

3.2.1. Citrate-capped Au and AgNPs

Citrate-capped gold and silver nanoparticles have been separately analyzed by capillary electrophoresis following the procedure previously described. Characteristic bands for gold and silver NPs were observed at 539 and 420 nm, respectively, showing migration times of 7.9 and 8.2 minutes, respectively, as shown in Table 1.

Citrate ions are responsible for nanoparticle reduction and the subsequent capping of their surfaces [31]. Thus, these nanoparticles have surface charges forming an electric double layer, and, therefore, their separation is based on a similar mechanism than that of charged molecular species. Differently sized particles display different electrophoretic mobilities since their charge-to-size ratios differ. In this case, the mobility of both types of nanoparticles is expected to be almost the same since the size of silver and gold NPs is similar, and both types of nanoparticles are surrounded by the same ligand layer, citrate.

In addition, a mixture of both types of NPs was analyzed. Figure 4 shows the spectrum contour graph in which the absorbance of Ag and AuNPs can be observed as well as the electropherogram obtained at 539 nm. Both gold and silver NPs appear at the same migration time being not possible to distinguish each nanoparticle contribution to the peak. Interestingly, in a sample composed by a mixture of both types of NPs their migration times appear at longer time (9.3 minutes) than when those NPs are individually introduced in the electrophoretic system; however no aggregation of NPs were observed in any case.

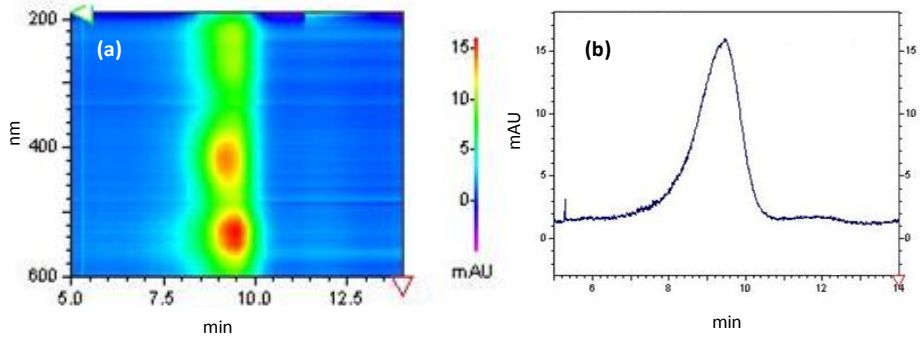

Figure 4. (a) Contour graph showing the relation between absorbance intensity at each wavelength versus migration time for a mixture of citrate-capped gold and silver nanoparticles; (b) electropherogram at 539 nm, corresponding to AuNPs.

In order to achieve electrophoretic separation of nanoparticles accordingly to the core nature, derivatization of the NPs by in-capillary microreaction with buffer additives was attempted.

3.2.2. Thioctic acid modified AuNPs (TA-AuNPs)

In order to investigate the electrophoretic behavior of gold nanoparticles when functionalized with thiol derivatives, TA-modified gold NPs were analyzed following the same techniques than in previous experiments. The introduction of carboxylate groups will make gold nanoparticles bear negative charges at pH 9.7 (similar to that when capped with citrate) and migrate to the anodic electrode in an electric field. Furthermore, carboxylate groups will substantially improve the stability of nanoparticles through electrostatic repulsion. In that way, considering the interaction of disulfide ring with gold atoms [28, 32, 33] the remaining COO^- group will be responsible for the NP charge (see figure 1). In this case the resonance plasmon band of gold nanoparticles functionalized with TA appears sharper and at a larger migration time -8.7 minutes- than unfunctionalized NPs. The presence of such ligand attached to NP surface modifies their charge-to-size ratio, affecting to their electrophoretic mobilities and, thus, to their migration times.

A possible explanation of this behavior falls to the self-assembly of lineal thiols onto a metallic surface which produces SAMs more highly ordered and oriented with increased molecular packing density than with citrate ligand [28, 34]. The mechanism of formation of SAMs is not completely understood [35], being influenced by nanoparticle surface energy, non-covalent ligand chain interaction or binding moiety. In the first step citrate molecules which are electrostatically bound to NP surface are displaced by thiolate ligands due to their high binding affinity (S-Au bond) [36]. Ligands attached at the surface form a double layer imposing steric impediment and intermolecular forces enabling or preventing

SAM reorganization. In this sense, longer alkanethiol chains are more quickly stabilized [37]. Finally, defects sites are eliminated.

3.3. Effect of thiol molecules in BGE on the separation

3.3.1. Influence of thioctic acid in electrophoretic mobility of AuNPs

Inside capillary, the interaction of citrate-AuNPs with TA added into the electrophoretic buffer was investigated to confirm the selective functionalization of AuNPs. Concentrations of TA ranging from 0.1 to 0.4% were evaluated. Ligand exchange reaction takes place in capillary since as much TA was present in the BGE, a shift in the electrophoretic peak is observed at longer migration time. According to gold-thiol chemistry, the undefined ionic species on the electrostatically-attached citrate-gold nanoparticle surface could be easily replaced with a self-assembled monolayer of TA originated from the disulfide adsorption through Au-S bonds.

The migration time will be affected by the chemical nature of the nanoparticle since the number of ligand molecules which are attached to the nanoparticle surface will vary in function of the chemical bond established between the NP and the ligand, but also it depends on the dimensions of the NP. The velocity that NPs will achieve in the electrophoretic system will depend on their m/z ratio as well as on their hydrodynamic size owing to the friction or Stokes forces established in the capillary. As can be seen in Figure 5, migration time of AuNPs increases when higher amount of TA added in the BGE. These results suggest that assembled TA molecules on the surface of AuNPs increased the SAM packing density if compared with the large binding moiety of citrate.

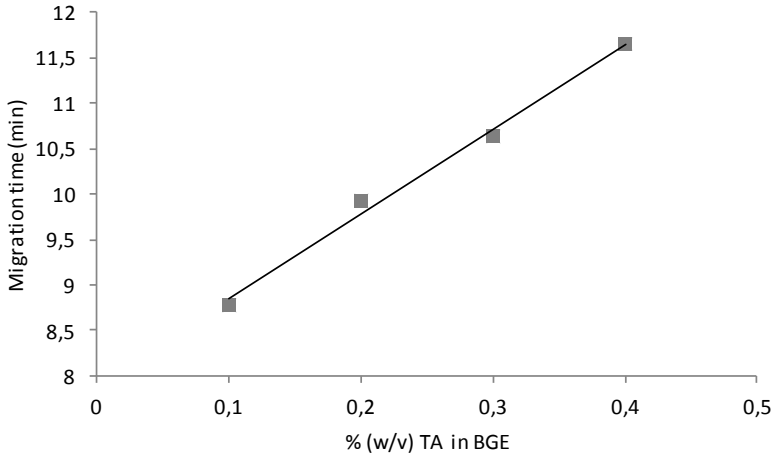

Figure 5. Dependence of migration time of AuNPs with the amount of TA added in the electrophoretic buffer in the range 0.1-0.4% (w/v).

3.3.2. Influence of thioctic acid on the separation of AuNPs and AgNPs

Separation of gold and silver NPs by their interaction with TA present in electrophoretic buffer was assayed. As TA only has a carboxylic group, NPs are also negatively charged in the capillary after ligand exchange. Data indicate that AuNPs appear at higher migration time than AgNPs. As can be observed in Figure 6, part of AuNPs (assigned as partially functionalized) migrate more slowly achieving separation with respect to AgNPs. These results are consistent with the formation of disulfide SAMs with AuNPs only. Baseline separation of gold and silver NPs was not possible when increasing the amount of TA because of the partially functionalization of also AgNPs traduced in the longer migration time observed for both metallic NPs, appearing at 14.8 minutes.

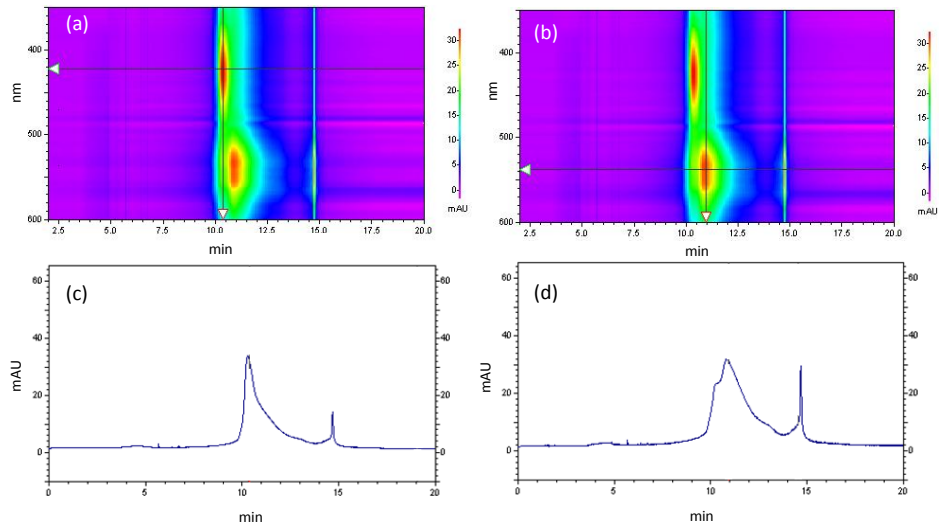

Figure 6. (a and b) Contour graph showing the relation between intensity of absorbance at each wavelength versus migration time for a mixture of citrate capped gold nanoparticles when using a BGE in which 0.1% of TA has been added; (c) electropherogram observed at 420 nm, and (d) electropherogram obtained at 539 nm.

3.3.3. Influence of thiomalic acid on the separation of AuNPs and AgNPs

The effect of the addition of thiomalic acid as additive in the electrophoretic buffer was also investigated. TMA is, as well as TA, soluble in alkaline aqueous solution, its addition into the electrophoretic buffer being possible. Structural similarities to TA can be observed although the presence of two dissociable carboxylic groups will enable the electrostatic repulsion required to preserve colloidal stability after functionalization [20], while having a single thiol conferring their interaction with metallic nanoparticles.

In that case, migration of AgNPs became slower than for AuNPs, appearing at 9.9 min while AuNPs at 8.6 min. (Table 1). This fact may be a consequence of functionalization of AgNPs due to the highest affinity of this organic molecule for silver atoms. Multiple ligand binding can be performed through thiol and one of the carboxylate groups to silver atoms (see figure 1). Due to the shorten

length of the chain, the packing density is expected to be lower and this explain the migration time value.

3.4. Separation of AuNPs and AgNPs using large-volume sample stacking modality using TMA as buffer additive

Since ligand exchange reactions on NP surface are both kinetically and thermodynamically controlled [38], the incubation time required is critical to optimize SAM packing density.

To corroborate the selective functionalization of NPs inside capillary, LVSS modality was employed to increase the reaction time inside the capillary with the aim of obtaining a better separation of peaks. In this way, an improvement in terms of sensitivity was also obtained as a consequence of the stacking of the nanoparticles prior separation. For these experiments, TMA was selected as additive. In this electrophoretic modality, a large volume of sample is introduced in the capillary. In our case, a plug of buffer is introduced after the sample in order to increase the sample-additive interaction. Subsequently, a high negative voltage was applied for 4 minutes for increasing the time of the derivatization, and finally the polarity is returned to positive to start the separation.

A good separation of NPs accordingly to their core-nature is achieved when using our methodology together with LVSS, although baseline separation is not completely achieved. As can be seen in Table 1, which summarizes the conditions investigated with the corresponding migration times obtained in each case, AgNPs appear at a migration time of 9.7 min, while AuNPs show a peak at 7.9 min.

In summary, in order to achieve better separation of gold and silver NPs, an optimized concentration of 0.1% (w/v) of TMA as buffer additive with the use of LVSS mode is recommended.

Table 1. Electrophoretic studies performed with different additives in BGE and the migration times observed for Au and AgNPs.

Section	Type of CE technique	Analyte	BGE[(a)] additive 0.1%(w/v)	Migration time Au (min)	Migration time Ag (min)	Final remarks
3.2.1	CZE	AuNPs	-	7.9	-	AuNPs show a peak at 539 nm
3.2.1	CZE	AgNPs	-	-	8.2	AgNPs show a peak at 420 nm
3.2.1	CZE	AuNPs + AgNPs	-	9.3	9.3	Both NPs appear at the same migration time
3.2.2	CZE	TA-AuNPs	-	8.7	-	TA-AuNPs show longer t_m than unfunctionalized
3.3.1	CZE	AuNPs	TA	8.7	-	AuNPs are functionalized inside the capillary
3.3.2	CZE	AuNPs + AgNPs	TA	10.9/ 14.8	10.3	AuNPs appear at longer t_m
3.3.3	CZE	AuNPs + AgNPs	TMA	8.6	9.9	Separation of Au and AgNPs
3.4.	CZE with LVSS	AuNPs + AgNPs	TMA	7.9	9.7	Improved sensitivity and separation

[(a)]BGE: 40 mM SDS, 10 mM CAPS, 0.1% methanol at pH 9.7

4. Conclusions

A novel method for selectively separating citrate-capped gold and silver nanoparticles is achieved by making use of microreaction technology, in which selective derivatization of their cores takes place inside capillary while certain thiol compounds were added into the electrophoretic buffer. Both thioctic and thiomalic acids were used for such purpose due to the high affinity of sulfur for metal atoms, being possible the selective formation of Au-S or Ag-S bonds.

Functionalized nanoparticles with more highly ordered and oriented SAMs than citrate ligand showed longer migration time owing to their increase molecular packing density enabling the separation of both types of nanoparticles according to their nature rather than size or shape separation. The proposed method was improved for performing at once the preconcentration and separation of metallic nanoparticles by applying "large-volume sample stacking" modality in order to increase the incubation time of the ligand-exchange reaction inside the capillary at the same time than in-line preconcentration takes place.

Acknowledgments

The authors wish to thank Spain's Ministry of Innovation and Science for funding Project CTQ2011-23790 and Junta de Andalucía for Project FQM4801. A.I. López-Lorente also wishes to thank the Ministry for the award of a Research Training Fellowship (Grant AP2008-02939).

The authors declare no competing financial interest.

References

[1] W. Cai, T. Gao, H. Hong, J. Sun, Nanotechnol. Sci. Appl. 1 (2008) 17.

[2] R.A. Sperling, P. Rivera-Gil, F. Zhang, M. Zanella, W.J. Parak, Chem. Soc. Rev. 37 (2008) 1896.

[3] S. Eustis, M.A. El-Sayed, Chem. Soc. Rev. 35 (2006) 209.

[4] A.I. López-Lorente, B.M. Simonet, M. Valcárcel, B. Mizaikoff, Anal. Chim. Acta 788 (2013) 122.

[5] H. Kato, M. Suzuki, K. Fujita, M. Horie, S. Endoh, Y. Yoshida, H. Iwahashi, K. Takahashi, A. Nakamura, S. Kinugasa, Toxicol. In Vitro 23 (2009) 927.

[6] G.T. Wei, F.K. Liu, J. Chromatogr. A 836 (1999) 253.

[7] M. J. Hostetler, J. E. Wingate, C. J. Zhong, J. E. Harris, R. W. Vachet, M. R. Clark, J. D. Londono, S. J. Green, J. J. Stokes, G. D. Wignall, G. L. Glish, M. D. Porter, N. D. Evans, R. W. Murray, Langmuir 14 (1998) 17.

[8] A.I. López-Lorente, B.M. Simonet, M. Valcárcel, TrAC Trends. Anal. Chem. 30 (2011) 58.

[9] A.I. López-Lorente, B.M. Simonet, M. Valcárcel, in: M. Farré, D. Barceló (Eds.), Analysis and Risk of Nanomaterials in Environmental and Food Samples. Comprehensive Analytical Chemistry 59 (2012) 33.

[10] N.G. Vanifatova, B.Y. Spivakov, J. Mattusch, U. Franck, R. Wennrich, Talanta 66 (2005) 605.

[11] H. Ahmadzadeh, R. Dua, A.D. Presley, E.A. Arriaga, J. Chromatogr. A 1064 (2005) 107.

[12] F.K. Liu, J. Chromatogr. A, 1216 (2009) 9034.

[13] R. Krupke, F. Hennrich, H. von Löhneysen, M.M. Kappes, Science (Washington, DC) 301 (2003) 344.

[14] C. Carrillo-Carrión, Y. Moliner-Martínez, B.M. Simonet, M. Valcárcel, Anal. Chem. 83 (2011) 2807.

[15] T.H. Chang, F.K. Liu, Y.C. Chang, T.C. Chu, Chromatographia 67 (2008) 723.

[16] F.K. Liu, Y.Y. Lin, C.H. Wu, Anal. Chim. Acta 528 (2005) 249.

[17] F.K. Liu, J. Chromatogr. A 1167 (2007) 231.

[18] K.H. Lin, T.C. Chu, F.K. Liu, J. Chromatogr. A 1161 (2007) 314.

[19] A. Badia, R.B. Lennox, L. Reven, Acc. Chem. Res. 33 (2000) 475.

[20] T. Zhu, K. Vasilev, M. Kreiter, S. Mittler, W. Knoll, Langmuir 19 (2003) 9518.

[21] L.O. Srisombat, J.-S. Park, S. Zhang, T. R. Lee, Langmuir 24 (2008) 7750.

[22] W. Hou, M. Dasog, R. W. J. Scott, Langmuir 25 (2009) 12954.

[23] M.R. Ivanov, A.J. Haes, Analyst, 136 (2011) 54.

[24] S. Almeda, L. Arce, M. Valcárcel, Current Anal. Chem. 6 (2010) 126.

[25] J. Turkevich, P.C. Stevenson, J. Hillier, J. Discuss. Faraday Soc. 11 (1951) 55.

[26] A.I. López-Lorente, B.M. Simonet, M. Valcárcel, Analyst 137 (2012) 3528.

[27] P.C. Lee, D. Meisel, J. Phys. Chem., 86 (1982) 3391.

[28] A.A. Volkert, V. Subramaniam, M.R. Ivanov, A.M. Goodman, A.J. Haes, ACS Nano 5 (2011) 4570.

[29] F.K. Liu, M.H. Tsai, Y.C. Hsu, T.C. Chu, J. Chromatogr. A 1133 (2006) 340.

[30] J.P. Landers, Handbook of Capillary Electrophoresis, CRC Press Inc., New York, 2nd ed., 1997.

[31] F.K. Liu, F.H. Ko, P.W. Huang, C.H. Wu, T.C. Chu, J. Chromatrogr. A 1062 (2005) 139.

[32] M. Rooth, A.M. Shaw, J. Phys. Chem. C 111 (2007) 15363.

[33] J.M. Abad, S.F.L. Mertens, M. Pita, V.M. Fernandez, D.J. Schiffrin, J. Am. Chem. Soc. 127 (2005) 5689.

[34] J. Tournebize, A. Boudier, A. Sapin-Minet, P. Maincent, P. Leroy, R. Schneider, ACS Appl. Mater. Interfaces 4 (2012) 5790.

[35] J.C. Love, L.A. Estroff, J.K. Kriebel, R.G. Nuzzo, G.M. Whitesides, Chemical Reviews 105 (2005) 1103.

[36] R.D. Felice, A. Selloni, J. Chem. Phys. 120 (2004) 4906.

[37] L.H. Dubois, R.G. Nuzzo, Annu. Rev. Phys. Chem. 43 (1992) 437.

[38] G. Cao, Nanostructures and Nanomaterials: Synthesis, Properties and Applications, Imperial College Press, London, 1st ed., 2004.

SUPPORTING INFORMATION

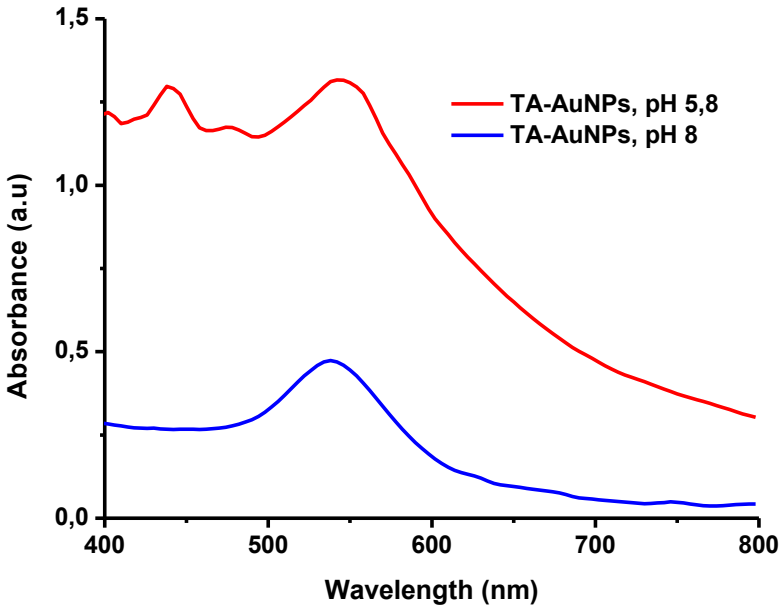

Figure S1. Ultraviolet-visible spectra of thioctic acid functionalized gold nanoparticles at pH 5,8 and 8. As can be seen at low pH gold nanoparticles became unstable while at higher pH values the spectrum shows a band centered at about 539 nm.

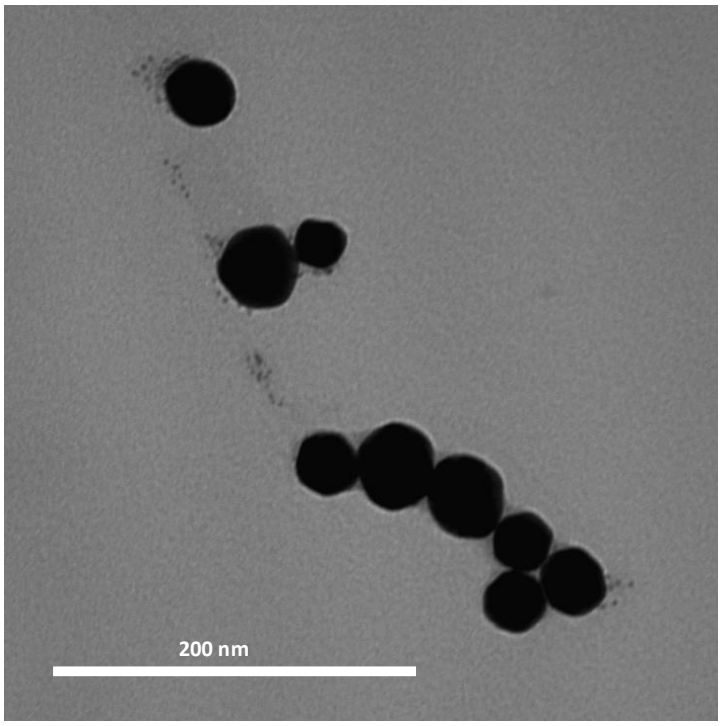

Figure S2. TEM image of spherically shaped thioctic acid functionalized gold nanoparticles.

DETERMINACIÓN DE NANOPARTÍCULAS

en muestras ambientales y biológicas

DETERMINATION OF NANOPARTICLES

in environmental and biological samples

V

BLOQUE V

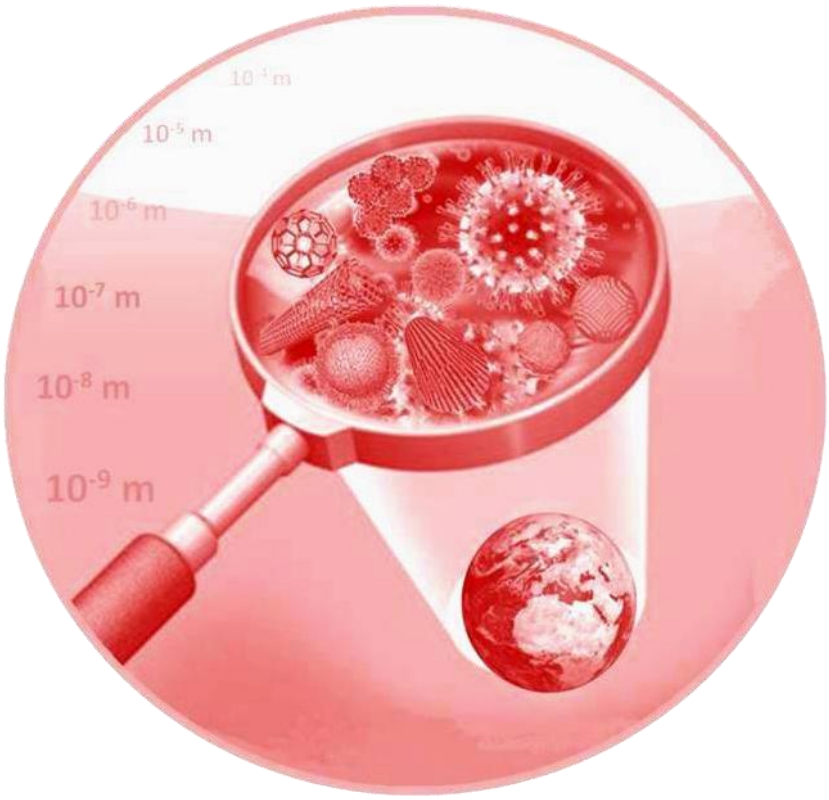

El aumento en la producción y utilización de nanopartículas manufacturadas dará lugar a su acumulación en aire, suelo, agua y organismos. Por ejemplo, las nanopartículas pueden causar daño en los pulmones[1], asimismo se ha descrito que AuNPs con un diámetro de 18 nm tienen una importante penetración en células.[2] Sin embargo, poco se conoce de la presencia de nanomateriales en organismos o en el medio ambiente dada la falta de técnicas analíticas para su determinación y cuantificación. La situación se agrava aún más en el caso de matrices biológicas.

Este bloque V presenta los métodos de determinación de nanopartículas –nanotubos de carbono monocapa carboxilados (c-SWNTs) y AuNPs- en muestras ambientales de agua de río y biológicas, como tejido de hígado de pollo, que se han desarrollado en la presente Tesis Doctoral. Se seleccionaron AuNPs ya que se ha descrito que pueden acumularse en riñones o hígado en función de las cargas superficiales. Por otro lado, los c-SWNTs son solubles en agua, siendo la carboxilación una práctica común en la industria. Cuanto más dispersos estén los CNTs más tiempo permanecerán en el medio acuoso, pudiéndolos encontrar como contaminantes en muestras acuosas.

Se han desarrollado diversos procedimientos como la microextracción líquido-líquido utilizando líquidos iónicos, la microfiltración sobre un sustrato SERS formado por nanopartículas de oro y la preconcentración sobre membranas modificadas con MWNTs. Como sistema de detección se emplearon las espectroscopias UV-Vis y Raman.

[1] G. Oberdorster, Z. Sharp, V. Atudorei, A. Elder, R. Gelein, W. Kreyling, C. Cox, Inhalation Toxicol. 16 (2004) 437-445.
[2] E.E. Connor, J. Mwamuka, A. Gole, C.J. Murphy, M.D. Wyatt, Small 1 (2005) 325-327.

V.1. MICROEXTRACCIÓN LÍQUIDO-LÍQUIDO CON LÍQUIDO IÓNICO

Los líquidos iónicos (ILs) tienen unas propiedades fisicoquímicas únicas, como una presión de vapor no detectable y una estabilidad térmica relativamente alta, por lo que continúan atrayendo un gran interés como medio alternativo para reacciones y separaciones. Wei et al.[3] demostraron la posibilidad de extraer nanomateriales (nanopartículas y nanohilos de oro, Cu y CuO nanométrico) de fases acuosas al líquido iónico BMIM PF_6 mediante un proceso de partición con efectos de sales. Posteriormente, nanocristales de CdTe se han extraído en BMIM Tf_2N[4]. Los autores atribuyeron esta extracción a un proceso de intercambio de cationes en la interfaz agua-líquido iónico.

Por otro lado, se ha descrito la interacción de líquidos iónicos con catión imidazolio con nanotubos de carbono monocapa[5], protegiéndolos de las fuertes interacciones π-π entre nanotubos. Los líquidos iónicos abren, por tanto, la puerta al análisis de nanomateriales en matrices complejas.

El **capítulo 10** muestra un método de extracción y preconcentración de nanopartículas de oro mediante el uso combinado de tensioactivos catiónicos y líquidos iónicos con grupo imidazolio gracias a la interacción del catión imidazolio con las AuNPs. Para la detección se ha empleado tanto espectroscopia UV-Vis como Raman. Se ha aplicado a muestras de agua de río e hígado de pollo.

[3] G.T. Wei, Z. Yang, C.Y. Lee, H.Y. Yang, C.R.C. Wang, *J. Am. Chem. Soc.* 126 (2004) 5036–5037
[4] T.Nakashima,T. Kawai, *Chem. Commun.* (2005) 1643–1645
[5] J. Wang, H. Chu, Y. Li, ACS Nano 2 (2008) 2540-2546.

El método desarrollado en el capítulo anterior se ha adaptado para la extracción de c-SWNTs en muestras de agua de río, como se describe en el **capítulo 11**. De nuevo la combinación de líquidos iónicos con tensioactivos catiónicos permitió la extracción cuantitativa del nanomaterial. Los c-SWNTs presentan unas bandas características en Raman, como ya se ha visto previamente en el bloque de caracterización de NPs, que se utilizaron para cuantificar la presencia de los mismos.

Capítulo 10

Rapid analysis of gold nanoparticles in liver and river water samples

Analyst 137 (2012) 3528-3534

RSC Publishing

Analyst

137 (2012) 3528-3534

Rapid analysis of gold nanoparticles in liver and river water samples

A. I. López-Lorente, B. M. Simonet, M. Valcárcel

Department of Analytical Chemistry, University of Córdoba, E-14071 Córdoba, Spain.

This paper describes a simple approach to determine gold nanoparticles in liver and river water samples. The method of purification of nanoparticles from the matrix is based on the stabilization of gold nanoparticles with a cationic surfactant followed by a microliquid–liquid extraction in ionic liquid. Finally, the extracted nanoparticles can be analysed by UV/Vis detection or Raman spectroscopy. The precision of the proposed method for the analysis of liver tissue and river water samples was 9.7% and 18% respectively for UV/Vis analysis. The sensitivity was 1.17×10^{-12} M for the analysis of 3 mL of liver homogenate or river water sample.

Keywords: gold nanoparticles, Raman spectroscopy, UV/Vis spectroscopy, liver samples, river water samples

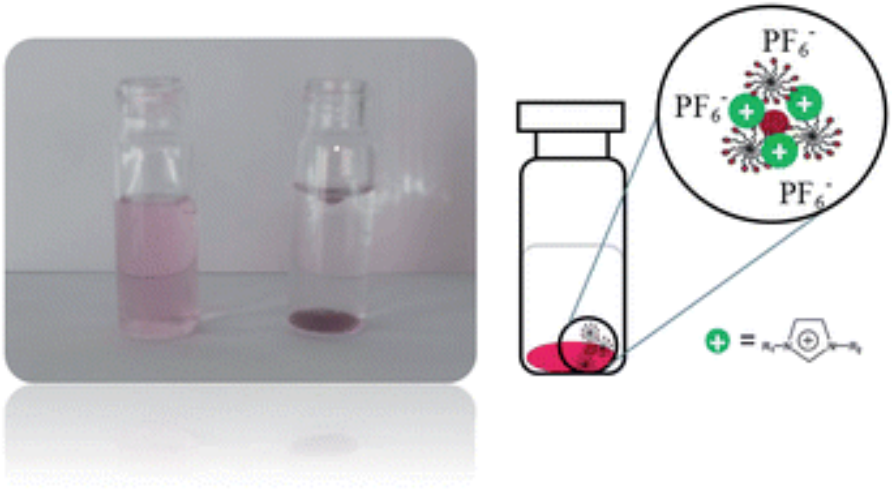
PF_6^-
PF_6^-
PF_6^-

1. Introduction

Nanotechnology is a rapidly expanding area. In fact, large numbers of nanoparticles (NPs) are actually used in a wide range of areas including cosmetics, medicine, food and food packaging, bioremediation, paints, coatings, electronics, fuel catalysts and water treatment [1, 2]. Currently, nanoparticles used in products include metals, metal oxides and alloys, carbon based materials such as fullerenes, nanotubes and nanofibres, silicates and quantum dots as well as polymer composites [3-6]. Although nanosized particles have always occurred in nature, the latest developments in the use and production of nanoparticles have raised concerns over their potential release and impact on the environment, in this way the amount and kind of nanoparticles can affect the environment. As nanoparticles are expected to be used in a wide range of product types, it is likely that a range of environmental regulatory frameworks will apply to them [7, 8]. However, at present, regulations are not very restrictive.

From the analytical point of view, described methods and models for nanoparticles in both environmental and biological samples have been questioned. There are the following needs: (i) analysis of biological samples in order to study toxicity and (ii) methods to analyse environmental samples to establish the potential risk and environmental control.

Nowadays, there is a lack of nanoparticle monitoring data from the environment. Therefore, it is difficult to know the real concentration and the potential risk. One way to assess the potential levels of NPs released into the environment and, hence, levels for testing, is to use environmental exposure models [9, 10]. For example, Boxall et al. have estimated the potential concentrations of several kinds of NPs arising from consumer products by using simple algorithms [10]. The predictions point out that gold is expected to reach a concentration of 0.14 ppb in water samples and 6.0 ppb in soil. Based on this, gold nanoparticles (AuNPs) were selected as target analyte in this paper.

With regards to biological samples, gold nanoparticles are also of high interest [11, 12]. There is no doubt that nanoparticles, especially gold nanoparticles, offer a huge potential in the field of nanomedicine and nanotechnologies in the future because they provide several opportunities in imaging, diagnostics, and also therapies [13-15]. In order to develop these applications and to achieve safe and well characterized tools for nanomedicine, it is of high importance to thoroughly study the in vivo biodistribution of NPs as this will allow determination of the concentration in secondary organs, which may eventually cause adverse health effects [16]. An interesting study [17], points out that commercially available 1.9 nm gold nanoparticles are biodistributed and accumulated in different organs depending on their charge. In general, positively charged particles accumulate more in the kidneys while negative and non-charged particles showed a higher accumulation in the liver [17]. Based on this data, liver tissues were selected as the sample for this study because gold nanoparticles stabilized with citrate, and thus presenting a negative charge, are the most used to date.

Therefore, as was indicated before, the aim of this work is to evaluate the determination of gold nanoparticles in river water samples and liver samples by using a portable Raman and a UV/ Vis spectrometer as detectors. The extraction of gold nanoparticles from real samples was performed by combining cationic surfactant with ionic liquids which present a high affinity to solubilise nanoparticles thanks to the interaction of the imidazolium group with the gold nanoparticles.

2. Materials and methods

2.1. Chemicals

$HAuCl_4$ (Sigma Aldrich) and sodium citrate dihydrate 99.5% (Sigma Aldrich) were used to synthesize the gold nanoparticles. Before synthesis the glassware

material was washed with a 1:3 mixture of nitric acid and hydrochloric acid (Panreac).

1-Hexyl-3-methyl-imidazolium hexafluorophosphate (HMIM PF_6) and 1-butyl-3-methyl-imidazolium hexafluorophosphate (BMIM PF_6) (Merck) were selected as the ionic liquids (ILs) to extract gold nanoparticles from the samples. Hexadecyltrimethylammonium chloride (CTAC), hexadecyltrimethylammonium bromide (CTAB) and Triton X-100 (Fluka) were used as surfactants to enhance liquid–liquid extraction. Trichloroacetic acid (TCA) (Panreac, Barcelona, Spain) and ethylenediaminetetraacetic acid (EDTA) (Sigma, St. Louis, MO, USA) were used to treat biological samples.

All the reagent stock solutions were prepared in Milli-Q water. Water river samples were obtained from Guadalquivir (Córdoba). Chicken liver tissue was obtained from a local butchery.

2.2. Synthesis of gold nanoparticles

Gold nanoparticles were synthesized according to the method of Turkevich et al. [18] with slight modifications. Firstly, the glass material was washed with a 1:3 mixture of nitric acid and hydrochloric acid. Solutions of $HAuCl_4$ and sodium citrate were prepared in Milli-Q water. For the synthesis 50 mL of a 0.01% $HAuCl_4$ solution was heated with magnetic stirring. After reaching the boiling point, 0.254 mL of a 1% sodium citrate solution was added. Then the system was left for 15 min under stirring. Afterwards, 5 mL of 0.01% $HAuCl_4$ solution and 0.254 mL of 1% sodium citrate solution were added to the system. After reaction for 15 min the heater was switched off and the system was stirred and allowed to reach room temperature. The final solution containing gold nanoparticles was stored in the freezer in an amber bottle at 4ºC.

2.3. Equipment

Gold nanoparticles were analysed by absorbance and Raman spectroscopy. UV/Vis measurements were performed using a halogen lamp as excitation and the monochromator and photonic detector of a PTI fluorescence Master system as a detector.

Raman measurements were performed with a portable Raman spectrometer system provided by B&W TEK Inc., known as i-Raman BWS415 with a wavelength of 785 nm and a maximum laser output power at the system's excitation port of 354 mW±15%. OPUS 5.0 from BrukerOptik GmbH software was employed for data treatment and spectra analysis as well as the Unscrambler® 9.1 software (Camo).

2.4. Sample treatment

Treatment for water samples. 3 mL of river sample containing 1.67 mM of CTAC and spiked with gold nanoparticles was treated with 0.3 g of ionic liquid (BMIM PF_6). The system was manually shaken for 30 s. Then the system was allowed to stand in order to achieve separation of the ionic liquid from the water phase. Periodically we checked that the concentration of the stock solution was constant by UV/Vis measurements. The calibration standards were prepared by dilution of the stock solution. Potential losses of gold nanoparticles with dilution were discarded in the studied range, since we obtained a linear response of the concentration with the UV/Vis spectrum.

Absorbance measurements were performed with 100 µL of the ionic liquid phase containing the extracted gold nanoparticles in an ultramicro Hellma cell with an optical length of 10 mm, measuring the difference between the absorbance at the maximum of the peak (about 537 nm) and the base of the peak, in order to amend baseline shifts between measurements.

For Raman measurements 100 µL of the extract was located in a home-made vial with a diameter of 5 mm. Raman measurements were performed with a laser power of 354 mW. A 1 second CCD exposure was used, with averaging of the Raman signal over 10 signal acquisitions. For spiking, a certain volume of a stock solution of gold nanoparticles was added to the river water samples, the solution was homogenized and mixed for 4 hours. Fig. 1 shows the phase separation and the preconcentration of gold nanoparticles in the water-insoluble ionic liquid.

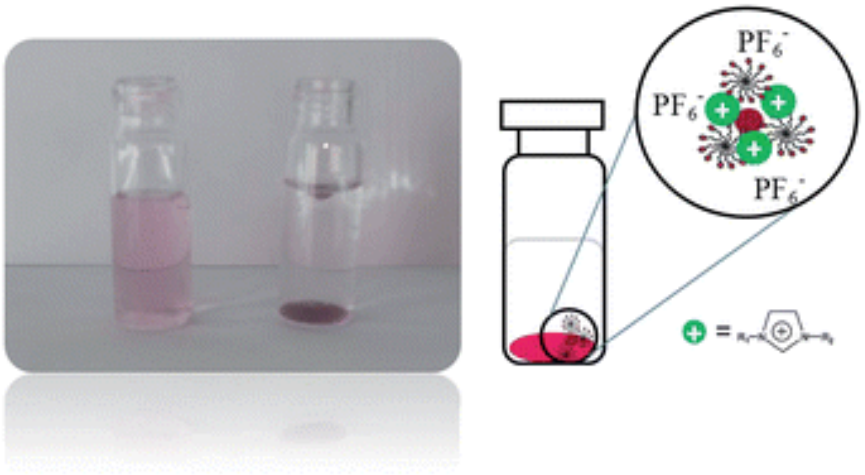

Figure 1. Photograph of the water solution containing gold nanoparticles before and after extraction and preconcentration treatment with 0.3 g of water-insoluble ionic liquid (left). Scheme of the extraction process which implies the use of a cationic surfactant (CTAC) and the ionic liquid with an imidazolium group (right).

Treatment of liver tissue. Chicken liver samples were dried with acetone and pulverised to form a uniform blend. For analysis, 3 mL of water containing TCA (0.15 M), in order to denature the proteins which precipitate and may interfere with the measurements, and EDTA (3.33 mM), as a complexing agent for possible interfering ions, were mixed with 2 mg of powdered chicken liver

sample. The obtained homogenated tissue was then spiked with an aqueous stock solution of gold nanoparticles and the mixture was stirred for 1 h to promote the interactions of the gold nanoparticles with the biological compounds. Afterwards, the solid phase was separated by centrifugation at 1370 g for 5 min. The supernatant was treated with surfactant (1.67 mM CTAC) and ionic liquid (0.3 g) to extract the gold nanoparticles. The method then continued as in the treatment for water samples.

In order to ensure homogeneous distribution of AuNPs in the material, two sets of experiments were compared. One was carried out as described in the experimental section. Three independent homogenates were spiked and analyzed following the recommended procedure. In a second set of experiments the three homogenates were spiked and afterwards mixed for one hour. After this time three aliquots were analyzed. Because the results of the two sets of experiments were comparable, the sample was deemed to be homogeneous.

3. Results and discussion

3.1. Characterization of gold nanoparticles

Gold nanoparticles were characterized by high resolution transmission electron microscopy (HTEM) and UV/Vis spectroscopy. Fig. 2 shows the characteristic HTEM image and the size distribution of the gold nanoparticles. The size of the nanoparticles ranged between 31 and 58 nm with an average size of 39±6 nm. The characterization was completed by measuring the UV/Vis spectrum of the gold nanoparticle solution. Fig. 3 shows the spectrum of gold nanoparticles. By using the spectrum, the average diameter was calculated according to the procedure described by Haiss et al. [19], resulting in an average diameter of 33 nm, a result which agrees with that obtained by HTEM. The diameter was calculated taking into account the ratio between the absorbance at the

maximum of the surface Plasmon resonance (537 nm) and the absorbance at 450 nm, following the equation described by Haiss [19].

$$d = \exp\left[(B_1 \cdot (A_{spr}/A_{450})) - B_2\right]$$

where $B_1 = 3.55$ and $B_2 = 3.11$ experimentally calculated by Haiss [19].

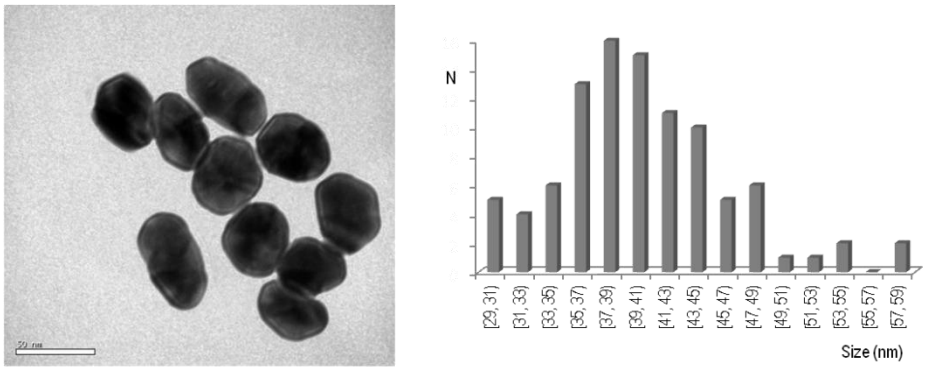

Figure 2. Characterization of gold nanoparticles. HTEM photograph (left) and size distribution (right).

The concentration of the stock solution was determined also according to ref. 19 from the UV/Vis spectrum. By using the calculated diameter of the nanoparticles, we can estimate the ε_{450} and calculate the particle concentration in mol per litre from the absorption A at 450 nm for a standard path length of 1 cm according to $c = A_{450}/\varepsilon_{450}$ [19]. The range of concentrations from the different syntheses was between 1 and 8×10^{-10} M.

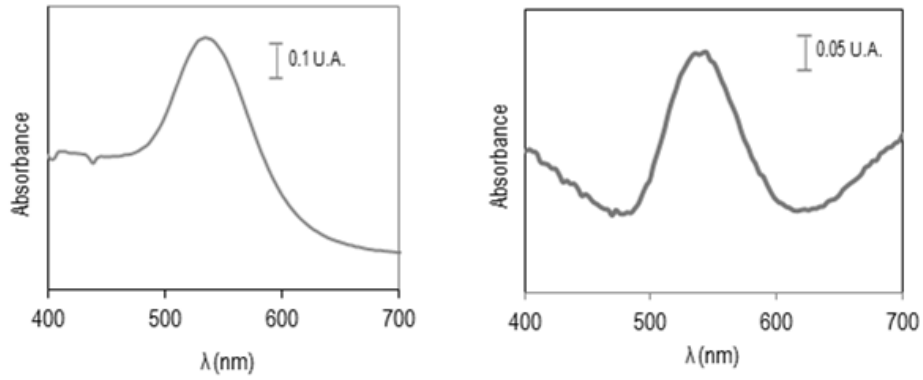

Figure 3. UV/vis spectrum of the gold nanoparticles in water (left) and UV/vis spectrum of the gold nanoparticles extracted in ionic liquid dispersed with the aid of the surfactant (right).

3.2. Optimization of the extraction procedure

The first variable studied was the nature of the ionic liquid. Although four different kinds of ionic liquids, which are liquids at room temperature and present very low solubility in water, were studied, only those with an imidazolium group provided good preliminary results. 1-hexyl-3-methylimidazolium hexafluorophosphate and 1-butyl-3-methylimidazolium hexafluorophosphate were effective for the extraction, while 1-ethyl-3-methyl pyridine bis(trifluoromethylsulfonyl)imide and 1-hexyl-3-methylimidazolium bis(trifluoromethylsulfonyl)imide were discarded, the first because we did not notice a statistically significant decrease of the absorbance in the aqueous phase. The second was discarded because although nanoparticles were extracted there were problems with measurement due to solution viscosity and changes in the refraction index. The study was then developed by using HMIM and BMIM as extractants. The anion of the ionic liquid was hexfluorophosphate in order to lower the water solubility of the IL. It must be pointed out that the

chosen ionic liquids showed that once extraction took place, the aqueous phase absorbance value was statistically equal to the blank, allowing the quantitative extraction of gold nanoparticles from the aqueous solutions. However, the presence of aggregates in the interface between the water and the IL was observed. This phenomenon was attributed to the presence of citrate ligands attached to the surface of the gold nanoparticles. Therefore, the effect of adding cationic surfactant was studied. It must be remarked that once nanoparticles were aggregated it was not possible to redisperse them. Therefore it was proposed first to stabilize the nanoparticles with the surfactant and then to extract them with the ionic liquid. In a first stage, surfactant micelles coat the nanoparticles and interact with them in the aqueous medium and in a second stage they are extracted by the ionic liquid by the formation of ionic pairs with the ionic liquid anion. As different ionic liquids show different extraction capacities, it is probable that mixed micelles were formed in which, in addition to the surfactant, there are also ionic liquid cations interacting with the nanoparticle. It is clear that the interaction of ammonium groups with the gold nanoparticles is responsible for the stability. Similar results were recently obtained by Wei and co-workers [20].

By using HMIM PF_6, the effect of different kind of surfactants: cationic such as CTAB and CTAC, anionic SDS and nonionic Triton X-100 was studied. Cationic surfactants were the only ones that allowed the extraction procedure. In the case of CTAB, in general, a concentration of 0.5 mM CTAB was not enough to quantitatively extract gold nanoparticles. On the other hand, concentrations ranging from 1 to 2 mM were efficient. The use of a higher amount of surfactant was discarded because it resulted in the presence of turbidity in the IL phase. Therefore a concentration of 2 mM of CTAB was recommended for analysis. The precision determined from 5 consecutive measurements was 2.8%. Similar results were obtained with CTAC, the concentration of which was also optimized

at 2 mM. With CTAC the precision was 9.3% but the sensitivity, expressed as the slope of a calibration graph, was 20 times better with CTAC than CTAB.

The suitability of the ionic liquid 1-butyl-3-methylimidazolium hexafluorophosphate was studied. As there are mixed micelles with the cation of the ionic liquid and the surfactant, the presence of butyl or hexyl groups changes the apolar character of the cations and their capacity to interact with the surfactant. Surfactant concentration was again optimized and the chosen concentration was 1.67 mM CTAC. It is important to indicate that surfactant concentration is referred to as the aqueous phase and that these studies were performed by UV/Vis spectroscopy. The choice of the best ionic liquid for the extraction was made on the basis of reproducibility and simplicity of operation. Both ionic liquids show good results, but finally BMIM PF_6 was chosen for further studies.

Moreover, the quantity of ionic liquid appropriate for the extraction in relation to a constant volume of aqueous sample was studied. In order to improve the reproducibility, due to ionic liquid viscosity, it was added to the system by weight. By using 3 mL of spiked water sample the amount of IL was studied in the range 0.1–0.5 g. The best sensitivity was obtained with 0.3 g of IL.

The extraction time was also studied but the results point out that only a slight influence was observed. In general, 15–20 min was long enough to separate the phases. Alternatively this time can be reduced by centrifugation of the mixture at low velocity (3000 rpm).

3.3. Analytical features

Standards prepared with Milli-Q water were analyzed under the selected conditions. There is a linear section until a concentration of 1.72×10^{-11} M due to aggregation problems at higher concentrations. The limit of detection was only

$1.7x10^{-12}$ M and the precision 9.3%. It must be indicated that the molar absorption coefficient of gold nanoparticles in the ionic liquid was 2.5 times lower than in water. This fact decreases the sensitivity of the method. However, the extraction is necessary in order to remove the interferences from the sample matrix.

We do not demonstrate a selective extraction of gold nanoparticles in the IL. We show that it is possible to extract the gold nanoparticles in the IL and to determine their concentration by Raman or UV/Vis spectroscopy. It must be remarked that direct analysis is not possible due to the presence of organic compounds interfering with the spectroscopic measurement. Obtained results point out that the extraction of gold nanoparticles in the ionic liquid is quantitative since once the extraction process is completed, the absorbance value of the aqueous phase is statistically equal to the blank and, on the other hand, a second extraction of the liquid phase with IL does not provide a signal due to the gold nanoparticles. Thus, assuming quantitative extraction, the preconcentration factor is defined by the volume of the aqueous and ionic liquid phases. It is 13.7 when working under the recommended conditions. However, we have proved, using only 0.1 g of ionic liquid, that it is possible to reach a preconcentration factor of 41.1.

As an alternative to UV/Vis detection, a portable Raman spectrometer, was used to record gold nanoparticles. As can be seen in Fig. 4, gold nanoparticles have a well-defined peak in Raman spectroscopy. The figure shows the spectrum obtained in the same experimental conditions with the ionic liquid, a sample control, nanoparticles in aqueous media and nanoparticles extracted and preconcentrated in the IL. The sample control corresponds to the preconcentration and analysis of a solution of sodium citrate. It is clear from these results that the peak corresponds to gold nanoparticles.

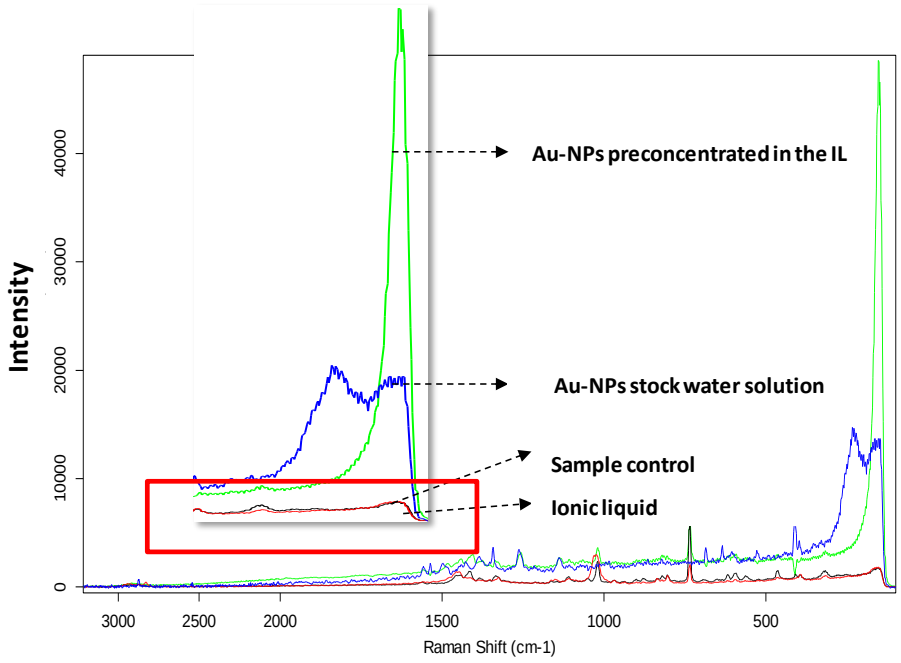

Figure 4. Raman response of gold nanoparticles.

Duval reported that Raman spectra of gold and silver nanomaterials always show a band, in the low-frequency range, due to the excitation of the acoustic vibrations of the roughness features of the nanoparticles. Using group theory they showed that among the two types of vibrational modes, torsional and spheroidal, only the latter ones can scatter light. The quadrupolar spheroidal vibrations of the nanoparticles are detected by Raman scattering due to their strong interaction with the dipolar Plasmon [21]. In the case of silver and gold nanoparticles with diameters between 4 and 50 nm, the fundamental radial mode (breathing mode) yields the dominant response in time-resolved experiments [22-24]. The observation of new low frequency Raman bands in the 3–40 cm^{-1} range in samples formed by silver or gold nanoparticles embedded in either a phosphate glass or amorphous silica matrix has been also described

previously. The authors attribute the lower frequency band to the light scattering by the quadrupolar vibrational mode of the nanoparticles and the others are ascribed to light scattering by the nanoparticle radial modes: the breathing mode and its harmonics [25].

In addition, it was verified that the peak was a function of gold nanoparticle concentration. In order to discard possible SERS effects, we added increasing amounts of citrate to the medium, as well as IL. However, the Raman peak was not affected by these compounds, therefore it was concluded that the peak was due to the presence of gold nanoparticles, and because it was not affected by other organic compounds present in the standard solution a possible SERS effect was discarded.

A set of 12 standards (in a range of concentrations between 0.1 and $3.5x10^{-11}$ M in gold nanoparticles) was extracted and analysed by Raman spectroscopy and formed the so-called training group. The results were submitted to principal component analysis (PCA) finding that 2 variables were enough for a probability of 99.9%, as can be seen in Fig. 5. PCA is a useful tool for carrying out dimensional reduction of data while retaining most of the variation within the dataset [26], as well as evaluating the cross-correlation among the variables. The data are projected in a new space defined by the principal components. The principal components (PCs) obtained are not correlated to each other and are also called eigenvectors or loadings. They are linear combinations of the original measurement variables in the dataset. The order of the PCs describes their relative importance (variance or eigenvalues), which are progressively lower, and ideally the variation in the dataset can be described sufficiently by a few PCs whose eigenvalues are most significant, as in this case in which two PCs are enough.

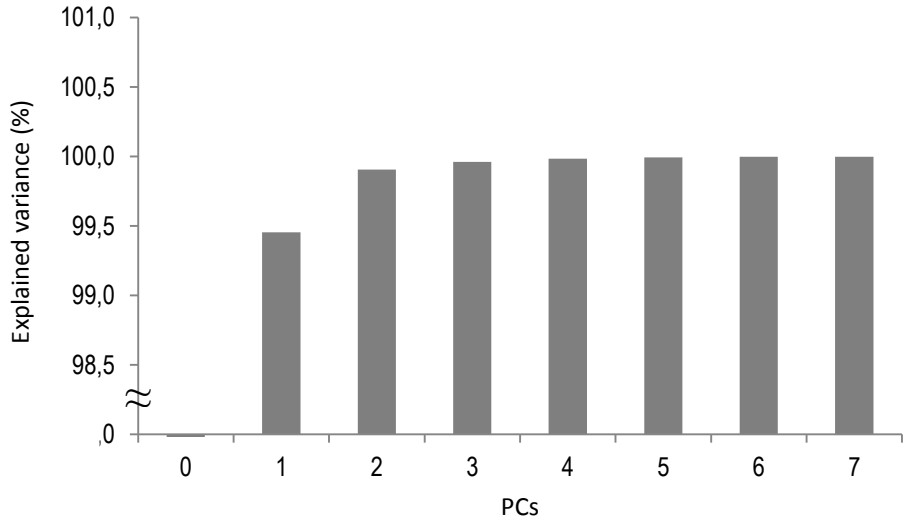

Figure 5. Representation of the accumulated explained variance according to the number of principal components considered.

Calibration was then performed by partial least square modelling (PLS). The aim of PLS is the construction of a model to describe the response variables (in this case gold nanoparticles concentration) in terms of the observed variables (Raman spectra) from a set of training data. The least squares model is given by:

$$Y = XB + E$$

where Y is the dependent variable (concentration), X the independent variable (Raman spectra), B the matrix of regression parameters for each component in Y, and E is the matrix of residuals (differences between measured and predicted variables) [27]. PLS considers both the X and Y matrices ensuring that the factors correlate the X matrix to the concentration.

The data structure of the PLS model was applied to the whole training group that is composed of the regions of the Raman spectrum between 119–229 cm^{-1}

and 1085–1305 cm^{-1}, since those are the regions where the most featured bands of the spectrum appear. The concentration of gold nanoparticles was the output variable in the PLS model.

The training group was used to construct the PLS model, while a testing group was used to test the accuracy of the model. The testing group included spectral measurement of 6 standards at different concentrations (in the same range as the training group), the data from the testing groups were set aside during model development. The representation of concentration found with the PLS model versus the concentration added were statistically comparable for a probability of 95% with the theoretical graph y=x. This result points out the usefulness of the Raman peak of gold nanoparticles to monitor their concentration.

3.4. Analysis of river water samples

A total of 36 river samples spiked at 6 concentration levels (between 0 and $3.5x10^{-11}$ M) were used to test the efficiency of the proposed methodology, divided again into training and testing groups for PLS calibration in the case of Raman spectroscopy analysis. When using UV/Vis detection the recoveries ranged from 79–103%, and the precision determined from 8 consecutive measurements was 18%. These samples were also analyzed by Raman spectroscopy obtaining an acceptable agreement. In this case, the representation of concentration found versus concentration added in the testing samples (in the same concentration range as the training samples) gives the regression line $y=0.8885X + 1x10^{-12}$ (Fig. 6). Although the system presents an important error, it is the first approach described in the literature for the preconcentration of gold nanoparticles.

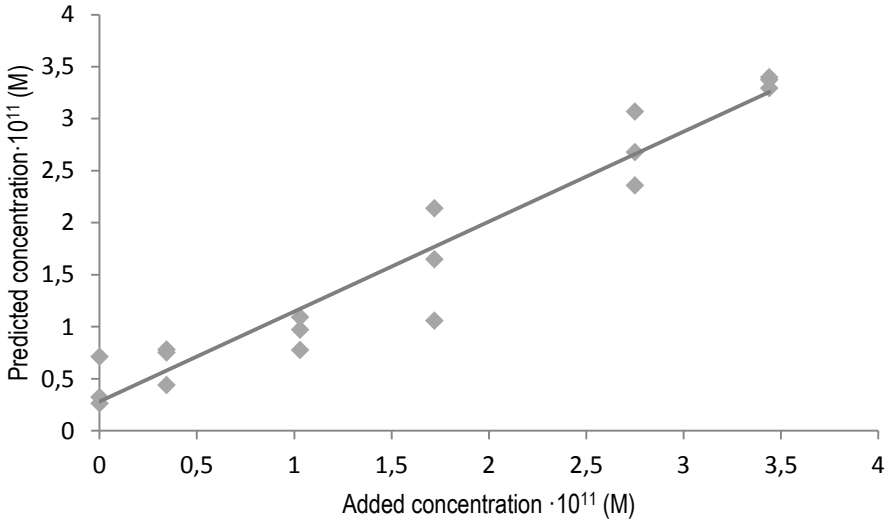

Figure 6. Predicted value of concentration versus added concentration of gold nanoparticles in spiked river water samples. The added concentration refers to the spiking level.

3.5. Analysis of liver tissue

In the case of liver tissue, samples spiked at four different concentrations (between 0.95 and $7.6x10^{-11}$ M) were analyzed both by UV/Vis and Raman spectroscopy. UV/Vis detection did not provide good results. As can be seen, in Fig. 7 there is a big difference between the response of the standard and the tissue. At higher concentrations the signal decreases due to possible aggregation problems. We may have to take into consideration that the concentration in this case is higher than the concentration in water samples, and this problem could be solved by diluting the sample prior to extraction with the ionic liquid. The precision of the method for the analysis of gold nanoparticles in tissues was 9.7% in the linear range.

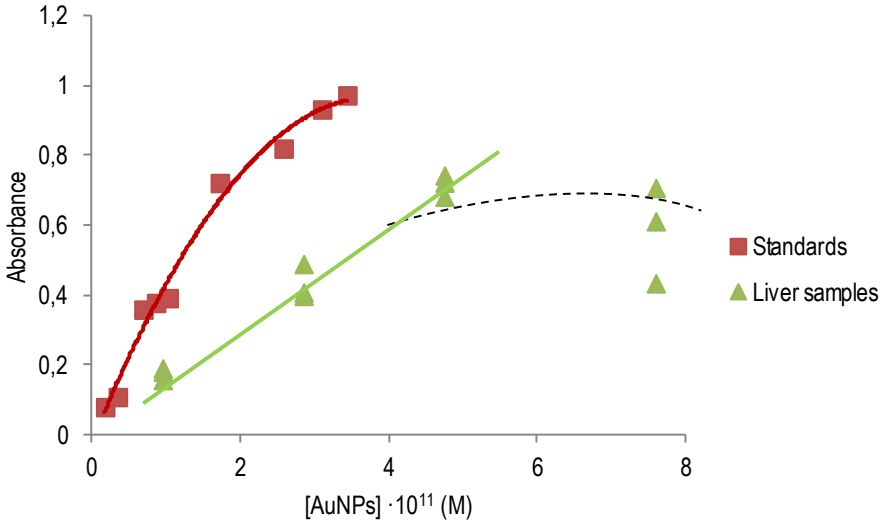

Figure 7. Comparison of analytical response of standards and liver tissues analyzed with the recommended procedure and UV/Vis detection.

However, when the samples were analyzed by Raman spectroscopy, the regression line of the graph predicted concentration versus added concentration yielded the equation $Y=0.9565X + 2x10^{-12}$, which is comparable with the theoretical line Y=X for a probability of 95%. As can be observed in Fig. 8, the model data points lie relatively close to the 45° line indicating small prediction error. The PLS model was developed with the training group of spiked liver tissue samples, and the testing group showed the results showed in Fig. 8. Based on the results, it can be affirmed that the low analytical signal observed with UV/Vis detection is due to the presence of interferences which affect the photometric measurement, and not to a low recovery of the gold nanoparticles from the liver matrix. It can be then concluded that interferences do not affect Raman spectroscopy.

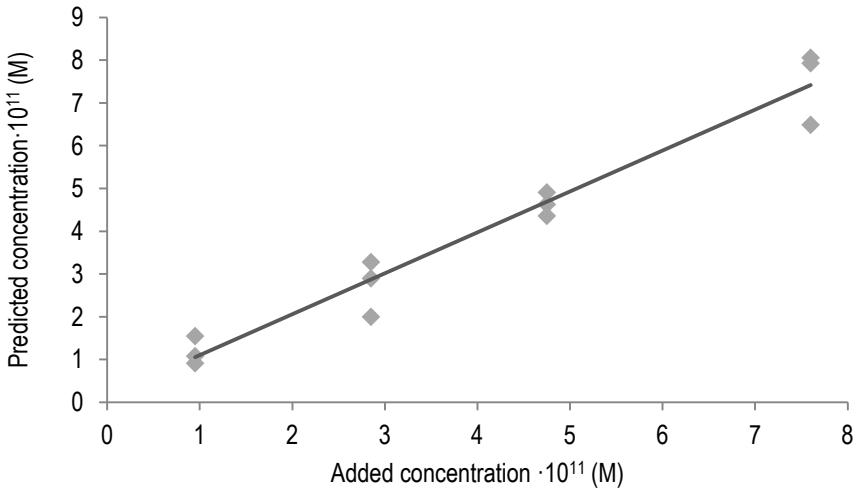

Figure 8. Predicted value of concentration versus added concentration of gold nanoparticles in spiked chicken liver tissue samples. The added concentration refers to the spiking level.

4. Conclusions

It has been demonstrated that ionic liquid with cationic surfactant is a good combination to extract gold nanoparticles from river water and liver tissues samples. Thanks to the high affinity of the imidazolium group for the gold nanoparticle surface, it is possible to preconcentrate the dispersed nanoparticles in a low volume of ionic liquid. The basis of this procedure could be extended to other nanoparticles and samples. As regards detection, although gold nanoparticles present a well defined characteristic UV/Vis spectrum, it has been also demonstrated that they present a characteristic peak in Raman spectroscopy, which can be used as an analytical signal. For example, in the case of liver samples the use of the Raman peak as an analytical signal presents clear advantages over the band of plasmon resonance.

The analysis of nanoparticles in real samples is difficult in part because it is not possible to know the ligand coating that nanoparticles have. In this work gold nanoparticles covered with citrate were selected as a model because they are the most widely used in applications. In both water and liver samples, after spiking the sample, the nanoparticles were left in the medium for 4 hours in order to promote possible ligand changes between compounds of the sample and citrate. In our opinion, the liquid–liquid extraction is a good procedure because it works with excess of ligand, then it is reasonable to think that ligands can be exchanged by the cation of the IL. Although this process, probably, takes place in all of the cases, it must be remarked that the kinetics can be different depending on the ligand. Then, when there are nanoparticles with a different ligand the kinetics as well as the amount of surfactant must be re-studied or re-optimized.

Although it has been shown that it is possible to determine gold nanoparticles stabilized with citrate from water river samples and liver samples, in real samples in which the ligands bound to the nanoparticles are not known it will be necessary to study the working conditions in order to assure the quantitative extraction of the gold nanoparticles. There is no doubt that liquid–liquid extraction with ionic liquids is a good way to approach the analysis of these kinds of samples and analytes.

Acknowledgements

The authors wish to thank Spain's Ministry of Innovation and Science for funding Project CTQ2007-60426 and Junta de Andalucía for Project FQM02300. A.I. López-Lorente also wishes to thank the Ministry for the award of a Research Training Fellowship (grant AP2008-02939).

References

[1] S. Kokura, O. Handa, T. Takagi, I. Tomohisa, N. Takeshi, Y. Yuji and T. Yoshukawa, Nanomedicine, 2010, 6, 570–574.

[2] A. Weir, P. Westerhoff, L. Fabricius, K. Hristovski and N. von Goetz, Environ. Sci. Technol., 2012, 46, 2242–2250.

[3] R. Kessler, Environ. Health Perspect., 2011, 119, a120–a125.

[4] O. D. Gendrikson, I. V. Safenkova, A. V. Zherdev, B. B. Dzantiev and V. O. Popov, Biofizika, 2011, 56, 965–994.

[5] M. A. Bolzinger, S. Briancon and Y. Chevalier, Wiley Interdiscip. Rev.: Nanomed. Nanobiotechnol., 2011, 3, 463–478.

[6] A. Llevot and D. Astruc, Chem. Soc. Rev., 2012, 41, 242–257.

[7] P. Christian, F. Von der Kammer, M. Baalousha and T. Hofmann, Ecotoxicology, 2008, 17, 326–343.

[8] B. Alistair, T. Karen and C. Qasim, Nanomedicine, 2007, 2, 919–927.

[9] A. Sanchez, S. Recillas, X. Font, E. Casals, E. Gonzalez and V. Puntes, TrAC, Trends Anal. Chem., 2011, 30, 507–516.

[10] A. B. A. Boxall, Q. Chaudhry, A. Jones, B. Jefferson and C. D. Watts, Current and Future Predicted Environmental Exposure to Engineered Nanoparticles, Report to Defra, 2008.

[11] R. Arvizo, R. Bhattacharya and P. Mukherjee, Expert Opin. Drug Delivery, 2010, 7, 753–763.

[12] E. Boisselier and D. Astruc, Chem. Soc. Rev., 2009, 38, 1759–1782.

[13] W. Lu, A. K. Singh, S. A. Khan, D. Senapati, H. Yu and P. C. Ray, J. Am. Chem. Soc., 2010, 132, 18103–18114.

[14] R. A. Rippel and A. M. Seifalian, J. Nanosci. Nanotechnol., 2011, 11, 3740–3748.

[15] S. R. Butle and P. R. Baheti, Int. J. Pharm. Sci. Rev. Res., 2011, 10, 54–59.

[16] M. A. K. Abdelhalim and M. Mahmoud Mady, Lipids Health Dis., 2011, 10, 195.

[17] C. Schleh, M. Semmler-Behnke, J. Lipka, A. Wenk, S. Hirn, M. Schäffler, G. Schnid, U. Simon and W. G. Kreyling, Nanotoxicology, 2012, 6, 36–46.

[18] J. Turkevich, P. C. Stevenson and J. Hillier, Discuss. Faraday Soc., 1951, 11, 55–75.

[19] W. Haiss, N. T. K. Thanh, J. Aveyard and D. G. Fernig, Anal. Chem., 2007, 79, 4215–4221.

[20] G. T. Wei, Z. Yang, C. Y. Lee, H. Y. Yang and C. R. C. Wang, J. Am. Chem. Soc., 2004, 126, 5036–5037.

[21] E. Duval, Phys. Rev. B: Condens. Matter Mater. Phys., 1992, 46, 5795–5797.

[22] N. Del Fatti, C. Voisin, F. Chevy, F. Vallee and C. Flytzanis, J. Chem. Phys., 1999, 110, 11484–11487.

[23] J. H. Hodak, A. Henglein and G. V. Hartland, J. Phys. Chem. B, 2000, 104, 5053–5055.

[24] C. Voisin, N. Del Fatti, D. Christofilos and F. Vallee, J. Phys. Chem. B, 2001, 105, 2264–2280.

[25] H. Portales, L. Saviot, E. Duval, M. Fujii, S. Hayashi, N. Del Fattiand F. Vallee, J. Chem. Phys., 2001, 115, 3444–3447.

[26] K. R. Beebe, R. J. Pell and M. B. Seasholtz, Chemometrics: A Practical Guide, John Wiley & Sons, Inc., New York, 1998.

[27] P. Knief, C. Clarke, E. Herzog, M. Davoren, F. M. Lyng, A. D. Meadea and H. J. Byrne, Analyst, 2009, 134, 1182–1191.

Capítulo 11

Determination of carboxylic SWCNTs in river water by microextraction in ionic liquid and determination by Raman spectroscopy

Talanta 105 (2013) 75-79

Talanta

105 (2013) 75-79

Determination of carboxylic SWCNTs in river water by microextraction in ionic liquid and determination by Raman spectroscopy

A. I. López-Lorente, B. M. Simonet, M. Valcárcel

Department of Analytical Chemistry, University of Córdoba, E-14071 Córdoba, Spain

The paper proposes a simple approach for the preconcentration of carboxylated single-walled carbon nanotubes and their determination in river water samples. The method is based on a microliquid–liquid extraction into an ionic liquid (bmim PF_6) in the presence of a cationic surfactant (CTAC). 10 µL of the ionic liquid phase are microfiltrated by using a home-made filtration device having a small diameter. The membrane was of cellulose with a pore size of 5 µm. Finally, the carbon nanotubes retained in the membrane are directly analyzed by Raman spectroscopy, which allows their direct characterization and quantification. The limit of detection was 0.050 mg L^{-1}. The precision, for a 1.4 mg L^{-1} concentration of carbon nanotubes, is 3.2%.

Keywords: Carboxylated single-walled carbon nanotubes; Raman spectroscopy; Preconcentration; Ionic liquid; Cellulose membranes; Water samples.

1. Introduction

The increasing use of nanoparticles in industrial applications will inevitably lead to the release of such materials into the environment. However, very little is known on emissions of engineered nanomaterials to the environment due to a lack of quantitative techniques for monitoring nanomaterials emissions and determining its concentrations in the environment. Exposure might occur during the production, use and disposal of CNTs and CNT-containing products. CNTs may be released into the aquatic environment from point sources, such as factories, landfills and wastewater effluents or from nonpoint sources, such as storm-water runoff, attrition from composites and from wet deposition from the atmosphere [1]. It has been described the fact that a considerable part of the CNTs, utilized in mass consumer products such as batteries and textiles, can be dispersed in the technosphere or the environment, e.g. by wear and tear from products as well as recycling processes which could cause occupational exposure [2]. It can be assumed that environmental and human exposure to CNTs is likely to occur. Moreover, Gottschalk et al. calculated predicted environmental concentrations based on a probabilistic material flow analysis from a life-cycle perspective of engineered nanomaterials containing products. A concentration of carbon nanotubes in STP effluent in the ng L^{-1} range in Europe has been predicted [3] and [4].

The properties of nanomaterials raise concerns about adverse effects on biological systems, which, at the cellular level, include structural arrangements that resemble nanomaterials and nanostructures in terms of their function [5]. This is the subject of considerable debate regarding the open questions on toxicology and environmental impact [6] and [7].

Effectively monitoring nanoparticles in environmental samples entails meeting several requirements. One is using analytical methods capable of detecting environmentally relevant concentrations, which fall in the nanogram per litre

range, and another is avoiding the potential interference of natural nanoparticles frequently present in environmental samples [8]. Separation of nanoparticles is one of the most critical steps in their analytical processing. Available methods for this purpose are still unrefined.

For carbon nanotubes (CNTs), their extremely low solubility in water, variable sizes of the particles, small diameters and the complexity of aggregates formed make characterizations of these nanomaterials extremely difficult in aqueous exposure experiments [9]. CNTs are usually functionalized to prevent them from sticking together and make them water soluble. Functionalization (e.g. carboxylation) is also a common practice in industry in the case of CNT-polymer matrices in order to achieve better dispersion, alignment and strong interfacial interactions [10]. Oxidized CNT is an important and widely used derivative of CNTs both for dispersing CNTs in aqueous systems and further functionalizing them via carboxyl group reactions [11]. It is assumed that the better de-bundled and individually suspended the CNTs are, the longer they remain in the water column [12]. Thus, oxidized CNTs may be one of the most possible forms of CNT pollutant in aqueous environment [13] and hence the importance of determining them. In the case of CNTs (both single and multi-walled), Nowack and Bucheli [14] reported that no method existed for their quantification in natural media. However, a recent approach to the extraction of carboxylic carbon nanotubes from surface water uses a filter modified with multiwalled carbon nanotubes as a preconcentrator and determines them by capillary electrophoresis. It has the limitation that does not provide information about the carbon nanotubes and also standards are needed [15].

On the other hand, ionic liquids (ILs) have attached more and more attention over the last few years. Wei et al. [16] demonstrated the possibility to extract nanomaterials (nanoparticles and nanowires of Au, Cu and CuO) from aqueous phases to the $[C_4MIM][PF_6]$ ionic liquid. CdTe nanocrystals have been also

extracted in [C_4MIM][Tf_2N] [17]. Recently, a method for the preconcentration of gold nanoparticles from river water samples and liver tissue in ionic liquid has been also developed [18]. It has been described the dispersion of carbon nanotubes (SWNTs) in ionic liquid through weak van der Waals interaction. The ionic liquid can effectively shield the strong π-π stacking interaction among SWNTs and disperse them [19]. The aim of this work is to use the affinity of carbon nanotubes to ionic liquids from an analytical point of view, to extract this nanomaterial from water samples and their subsequent quantification by Raman spectroscopy. As far as we are concerned this is the first time ionic liquid are used for microextraction of carbon nanotubes.

2. Experimental

2.1. Materials and reagents

SWNTs were obtained from Shenzhen Nanotech Port Co. Ltd (NTP) (China), with a purity over 90%, an outer diameter of <2 nm, a length of 5–15 μm and a special surface area of 500–700 m^2/g. H_2SO_4 and HNO_3 were purchased from Panreac (Barcelona, Spain). 1-butyl-3methyl-imidazolium hexafluorophosphate (BMIM PF_6) (MERCK) was selected as the ionic liquid (IL) to extract the carboxylated single-walled carbon nanotubes from the samples. Hexadecyltrimethylamonium chloride (CTAC) and hexadecyltrimethylamonium bromide (CTAB) were obtained from Fluka. Cellulose membranes of 5.0 μm pore sizes were purchased from Millipore. Chemicals were used as received with safety precautions taken as according to their respective MSDS.

2.2. Equipments

Raman measurements were performed with a portable Raman spectrometer system provided by B&W TEK Inc., known as inno-Ram with a wavelength of 785 nm and a maximum laser output power at system's excitation port of

348 mW and 285 mW in the probe. For measurements the laser power at the probe was 28.5 mW in order to avoid sample damage. UV/Vis measurements were performed using a halogen lamp as excitation and the monochromator and photonic detector of a PTI QuantaMasterTM Spectrofluorometer (Photon Technology International) system as a detector with FeliX32 software.

2.3. Functionalization of single-walled carbon nanotubes

Carboxylated carbon nanotubes (c-SWNTs) were prepared by adding into a glass flask 100 mg of single-walled carbon nanotubes to 20 mL of H_2SO_4/HNO_3 mixture (3:1). The mixture was refluxed for 1 h. Afterwards, diluted fractions of the mixture were centrifuged at 10000 rpm for 10 min and washed with water until the supernatant phase ceased to have acidic pH. Finally, carboxylated derivates were dried at 60ºC in a heater. After the acid treatment, the SWNTs were negatively charged by covalently attached carboxylic (-COOH) groups on the sidewalls and the open ends which make them highly soluble in water. The method of carboxylation is based on the described by Xue and Cui [20] with some modifications.

2.4. c-SWNTs preconcentration procedure

2 mL of river water sample containing 3.12 mM of CTAC (from a 0.1 M stock solution) at a pH=1.4, adjusted with HCl 1 M, were treated with 0.1 g of ionic liquid (BMIM PF_6). The system was manually shaken for 30 s. Then the system is allowed to stand in order to achieve ionic liquid from water phase separation. The river water samples were fortified with certain volume of a stock solution of carboxylated single-walled carbon nanotubes, the solution was homogenized and mixed for 2 h. The pH of the solution is acid due to the carboxylic groups in carbon nanotubes and it was adjusted to 1.4 for the extraction. For Raman measurements 10 µL of the extract were filtered through a Millipore cellulose membrane with a pore size of 5 µm, where the nanotubes are homogeneously

retained. Carbon nanotubes are retained in the membrane owing to their length and flexibility by physic impediment, since there is a network of pores in the membrane and not straight holes. The viscosity of ionic liquid phase in this case helps to their retention. A home-made designed microfiltration device with sandwich configuration (Fig. 1) was employed. The diameter of filtration is 1.3 mm. Both, the volume of ionic liquid phase and the diameter of filtration were optimized in order to have an appropriate signal in Raman spectroscopy. For samples with very low concentration (<0.8 mg L^{-1}), a modified procedure is proposed. Maintaining the proportion of ionic liquid to water, the volumes can be increased. Finally, instead of 10 µL, a major volume is filtrated on the cellulose membrane.

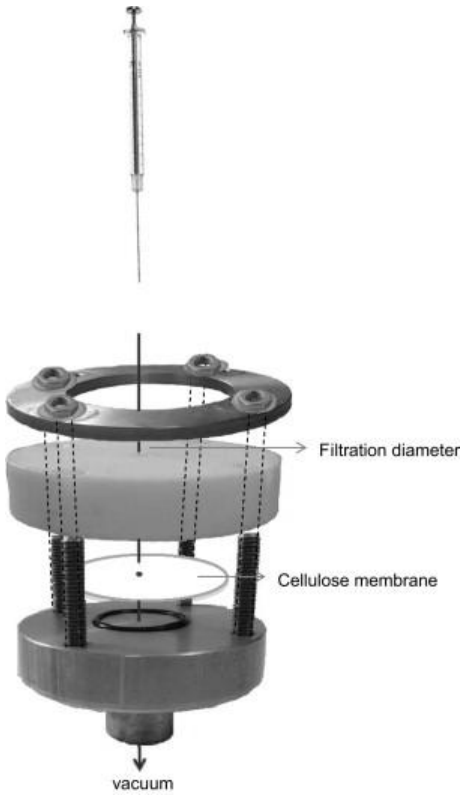

Figure 1. Scheme of the microfiltration device.

Raman measurements were performed with a 785 nm laser with a power of 28.5 mW. A 1-sec CCD exposure was used, averaging the Raman signal over 10 signal acquisitions. Raman measurements were acquired from five randomly selected locations within each membrane and repeated over three samples, giving a total of 15 Raman measurements for each nanotube concentration. For these measurements a 20x objective was employed, resulting in an area of measurement in each spot of 109 μm of diameter. It should be remarked the homogeneity of carbon nanotubes in the membrane since spectra measured at different points of the sample provide a similar signal.

3. Results and discussion

3.1. Selection of the ionic liquid

The interaction of imidazolium-based ionic liquid with single-walled carbon nanotubes through weak van der Waals interaction has been described [19]. The ionic liquids can effectively shield the strong π-π stacking interaction among SWNTs. The objective of this work was to take advantage of this affinity in order to develop an extraction procedure which allows preconcentration of the analyte (carboxylated carbon nanotubes), so the main requirement that ionic liquid must fulfill is a low solubility in water although both water-soluble and insoluble ionic liquids containing 1-butyl-3-methyl imidazolium cation has been proved to interact with carbon nanotubes. Ionic liquids' solubility is dependent on its anion, presenting a low solubility in water those composed by hexafluorophospate (PF_6^-), so they are suitable for the purpose of our work. For this reason, the selected ionic liquid was 1-butyl-3-methylimidazolium hexafluorophosphate (BMIM PF_6). Additionally, it has been demonstrated the suitability of 1-hexyl-3-methylimidazolium hexafluorophosphate (HMIM PF_6) to perform the extraction procedure.

3.2. Effect of the amount of cationic surfactant

The negatively charged nanotubes are covered by cationic surfactant molecules forming ionic pairs. Thus, the effect of the amount of a cationic surfactant, CTAB and CTAC, on the extraction procedure was studied. Similar results were obtained for both surfactants in terms of carbon nanotube extractions; however CTAC was selected because it produces lower modifications in the viscosity of the ionic liquid. The influence was studied in a range 0.4-35 mM of CTAC. The signal of carbon nanotubes extracted on ionic liquid increased when increasing the amount of CTAC up to 3.12 mM, being observed a better dispersion of the nanotubes within the ionic liquid. From these results, the optimum amount of CTAC was selected to be 3.12 mM.

3.3. Effect of the pH

We have observed that when carboxylated single-walled carbon nanotubes are put in contact with ionic liquid, the extraction is not quantitative and carbon nanotubes are not homogeneously distributed in the ionic liquid phase. As the carboxylated carbon nanotubes are negatively charged it may influence the low efficiency of the extraction. Thus, pH is thought to be a variable that may condition the performance of the extraction. By decreasing the pH the negative charge of the nanotubes may be neutralized and the protonated carboxylate specie extracted in the ionic liquid phase. We studied the influence of the pH in the range 0.72-3.32 (3.32 is the pH of the initial solution), adjusting the pH with a solution of HCl 1 M. The best results were obtained for a pH of 1.37, at which most of the carboxylic groups will be protonated. We discarded the adjustment of the pH as the only step to improve the extraction by neutralizing the charges due to the fact that although the extraction was quantitative, the ionic liquid phase with the carbon nanotubes within it showed to be more homogeneous when CTAC was present.

Consequently, we also studied the influence of the pH in the extraction with CTAC present in the media at the optimized concentration. The study was conducted in a range 1.10-3.46, finding that in this case the pH plays a less significant role in the efficiency of the extraction. Nevertheless, prior extraction with ionic liquid the pH was adjusted to 1.4. Probably CTAC molecules surrounding the carbon nanotubes are not enough to neutralize the negative charges due to steric impediment, thus a decrease of pH benefits the extraction.

3.4. Selection of the nature of the membrane

The microfiltration of the extracted nanotubes in the ionic liquid was assayed with membranes of different nature: cellulose, PTFE and PVDF, with a diameter of pore of 5.0 μm. Carbon nanotubes are retained in the membrane owing to their length and flexibility by physic impediment. Moreover, the viscosity of the ionic liquid creates a lattice of carbon nanotubes that remains retained on the membrane after vacuum filtration. Excess of ionic liquid is removed by filtration and the one that remains adsorbed on carbon nanotubes surface is used to normalize spectra of carbon nanotubes.

PVDF and cellulose membranes showed less operational problems maintaining their integrity after the filtration procedure, while the PTFE ones tended to wrinkle. A cellulose membrane was finally selected because it was easier to handle and the nanotubes were homogeneously distributed. This membrane do not interfere in Raman measurements and it is not damaged during the laser irradiation.

3.5. Raman spectra of carbon nanotubes in ionic liquid retained in the membrane

The most significant Raman spectral features for single-walled carbon nanotubes are the radial breathing mode (RBM, 100-300 cm^{-1}), the disorder

peak (D peak, ~1350 cm^{-1}), the tangential mode (G band, 1400–1700 cm^{-1}), and the second-order overtone of the D peak (G', 2500–2800 cm^{-1}) [21]. The RBM band is originated from the out-of-plane tangential acoustic modes of monolayer graphene sheet and all carbon atoms vibrate in phase along the radial direction [22]. It is the characteristic mode for SWNTs, although can sometimes be observed in MWNTs with a small diameter inner tube (less than 2 nm) when good resonance condition is established [23]. The G-band, in the case of SWNTs, comprises several tangential modes due to stretching vibrations in SWNT sidewall C-C bonds. Two double resonance features commonly found in the Raman spectra of CNTs bundles are the D-band feature, stemming from the disorder-induced mode in graphite with the same name [24], and its second harmonic, the G' band. In nanotubes, both the D-band and the G'-band are sensitive to the CNT diameter and chirality, since these features depend sensitively on how the 2D electronic and phonon structure is folded into a 1D structure. In the case of carboxylated carbon nanotubes a difference in the spectrum with respect to pristine carbon nanotubes is a distinctive D-band to G-band intensity ratio [25].

In the spectra obtained with this procedure the most predominant bands are D and G, while the RBM was barely distinguishable (see Fig. 2). The intensity of the D band has been used in order to quantify the samples. Ionic liquid bands also appear in the spectrum, such as a characteristic one at 739 cm^{-1} produced by the symmetric stretching of PF_6^- anion, which was used as internal reference to normalize the spectra. It must be pointed out that there is no effect of the surfactant on the Raman spectrum of carbon nanotube after the filtration step.

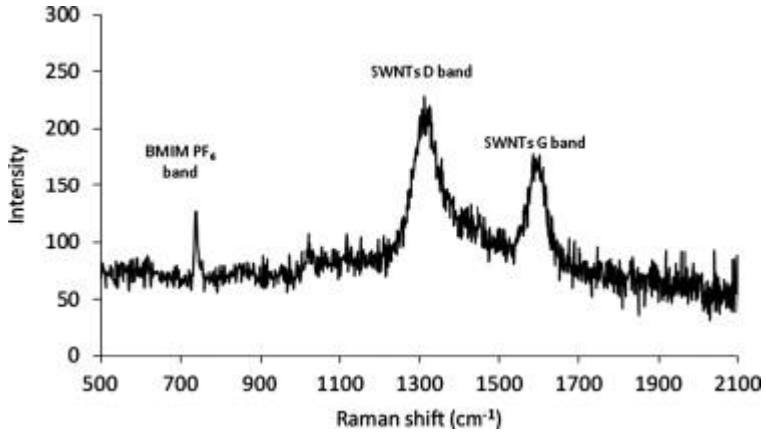

Figure 2. Raman spectrum of carboxylated single-walled carbon nanotubes preconcentrated in ionic liquid and microfiltrated on a cellulose membrane. The peak at 739 cm^{-1} corresponds to the ionic liquid (BMIM PF_6). The bands at 1313 and 1595 cm^{-1} correspond to the D and G band of carbon nanotubes, respectively.

The instrumental variables for measurement were optimized. We studied the influence of laser power in the spectra. The optimum laser power was found to be 28.5 mW with a laser wavelength of 785 nm. This power was selected due to the fact that it proved to be enough to record a good spectrum higher laser powers resulting into sample damage.

Furthermore, spectra were performed with an acquisition time ranging from 0.5 to 20 s and a number of acquisitions ranging from 1 to 10. The minimum time of acquisition necessary to visualize the spectrum has been proved to be 1 s, but it is necessary to accumulate more than one spectrum in order to achieve a good signal-to-noise ratio. A compromise between the duration of the acquisition and the quality of the spectrum has to be reached being 10 acquisitions enough to record an acceptable spectrum. Thus, the better conditions in terms of shape of the spectrum and duration of the acquisition were 1 s accumulating a sum of 10 spectra.

3.6. Analytical features of the proposed method

The analytical performance of the proposed method was studied in order to evaluate its usefulness for quantitative analyses. Calibration graphs of the analytical signal versus concentration for standard solutions were registered. The intensity of the D band of carbon nanotubes in the Raman spectra divided by the intensity of the ionic liquid band at 739 cm^{-1} was adopted as analytical signal.

The calibration curve was determined for concentrations ranging from 0.6 to 4 mg L^{-1}. Each concentration level was analyzed in triplicates (measuring each sample at five randomly selected location in the membrane), and the response was linear in the range of concentrations tested (R^2=0.9856). The precision of the measurements was evaluated at a concentration of 1.4 mg L^{-1} obtaining a relative standard deviation (n=5) of 3.2%. The detection and quantification limits were calculated as three and 10 times the signal of S_a between the scope and were 0.169 and 0.565 mg L^{-1}, respectively. In the case of the modified procedure for large volume (samples with a concentration <0.8 mg L^{-1}), the limit of detection was 0.050 mg L^{-1}. The interval of linearity was from 0.07 to 0.8 mg L^{-1}, which was the measured interval. In this case the RSD for a concentration of 0.8 mg L^{-1} was 12.6%, higher than with the normal procedure, but with this modified protocol we can determine carbon nanotubes at lower concentrations. The analytical features of the developed method are summarized in Table 1.

Table 1. Analytical features of the method

Calibration equation	S=(0.54±0.03)[c-SWNTs]+(0.39±0.01)
R^2	0.9856
Lineal range	0.4-4 mgL^{-1}
LOD[a]	0.169 mg L^{-1}
LOD[b] (Large volume procedure)	0.050 mg L^{-1}
RSD[c] (%)	3.2%
RSD[d] (%) (Large volume procedure)	12.6%

[c-SWNTs]: Concentration of c-SWNTs in the aqueous media in mgL^{-1}.
[a,b]Limit of detection, determined as $(3S_a)/b$, for y=bx+a.
[c]Relative standard deviation, determined from five measurements of 1.4 mgL^{-1} c-SWNTs.
[d]Relative standard deviation, determined from five measurements of 0.8 mgL^{-1} c-SWNTs.

3.7. Application to the determination of water-soluble carboxylated carbon nanotubes in river water samples.

In order to check the analytical usefulness of the proposed method, samples of water from Guadalquivir river were fortified and analyzed following the recommended procedure. Before fortification the samples were analyzed and no carbon nanotubes were found in them since the analytical signal was equal to zero.

To demonstrate the accuracy of the proposed method, a recovery test of the analysis of spiked samples was also carried out. For the recovery study, four fortification levels were assayed being the recoveries values shown in Table 2. The obtained results displayed good agreement obtaining acceptable recoveries between 70.1% and 101.7% depending on the concentration level. Each sample was analyzed in triplicate in order to evaluate the precision of the method. The coefficients of variation ranged from 8.98% to 3.63%.

Table 2. Recovery study of spiked river samples.

Sample	Added concentration (mgL^{-1})	Found concentration[a] (mgL^{-1})	Recovery (%)	RSD(%)
1	0.94	0.68±0.08	70.1-81.2	8.98
2	1.41	1.11±0.07	73.8-84.6	4.98
3	1.88	1.83±0.08	92.8-101.7	3.63
4	2.35	2.2±0.1	93.9-100.3	4.04

[a]Average of three independent spiked samples±CI ($p < 0.05$).

Interferences of other components of the matrix have not shown effect on the performance of the extraction procedure. Selectivity is achieved in the first place by the use of ionic liquid for the extraction acting as a sieve for other components present in water samples.

4. Conclusions

It has been demonstrated that ionic liquid with a cationic surfactant are a good combination for the extraction of carboxylated single-walled carbon nanotubes from river water samples. Thanks to the high affinity of imidazolium group for the carbon nanotube, it is possible to preconcentrate the nanotubes in a low volume of ionic liquid. Regards detection, carbon nanotubes present a characteristic Raman spectrum which has been used as analytical signal. It should be remarked that the use of a cationic surfactant is crucial for avoiding the carbon nanotube aggregation within the ionic liquid phase and then for obtaining a homogeneous dispersion of carbon nanotubes on the membrane, which allow for quantitative and reproducible Raman measurements of the extracted nanomaterials.

The limit of detection achieved with the proposed methodology is 50 μg L^{-1}, which is higher than the estimated concentrations reported until date. However this work can be considered as a first approximation to the quantification of this nanomaterial in water matrices. It could be applied as screening method to control the release of this nanomaterial in the source points of contamination, such as factories, landfills and wastewater effluents, where concentrations of carbon nanotubes will be considerably higher.

Acknowledgments

The authors wish to thank Spain's Ministry of Innovation and Science for funding Project CTQ2007-60426 and Junta de Andalucía for Project FQM02300. A.I. López-Lorente also wishes to thank the Ministry for the award of a Research Training Fellowship (Grant AP2008-02939).

References

[1] M. R. Wiesner, G. V. Lowry, P. Alvarez, D. Dionysiou, P. Biswas ,Environ. Sci. Technol. 40 (2006) 4336–4345.

[2] A. R. Köhler, C. Som, A. Helland, F. Gottschalk, J. Clean. Prod. 16 (2008) 927–937.

[3] F. Gottschalk, T. Sonderer, R. W. Scholz, B. Nowack, Environ. Sci. Technol. 43 (2009) 9216–9222.

[4] F. Gottschalk, T. Sonderer, R. W. Scholz, B. Nowack, Environ. Toxicol. Chem. 29 (2010) 1036–1048.

[5] M. Farré, K. Gajda-Schrantz, L. Kantiani, D. Barceló, Anal. Bioanal. Chem. 393 (2009) 81–95.

[6] G. Oberdörster, E. Oberdörster, J. Oberdörster, Environ. Health Perspect. 113 (2005) 823–839.

[7] K. Donaldson, L. Tran, L. A. Jimenez, R. Duffin, D. E. Newby, N. Mills, W. MacNee, V. Stone, Fibre Toxicol. 2 (2005) 10.

[8] B. M. Simonet, M. Valcárcel, Anal. Bioanal. Chem. 393 (2009) 17–21.

[9] M. Hassellöv, J. W. Readman, J. F. Ranville, K. Tiede, Ecotoxicology 17 (2008) 344–361.

[10] N. G. Sahoo, S. Rana, J. W. Cho, L. Li, S. H. Chan, Prog. Polym. Sci. 35 (2010) 837–867.

[11] Y. P. Sun, K. Fu, Y. Lin, W. Huang, Acc. Chem. Res. 35 (2002) 1096–1104.

[12] I. Schwyzer, R. Kaegi, L. Sigg, A. Magrez, B. Nowack, Environ. Pollut. 159 (2011) 1641–1648.

[13] S. T. Yang, H. Wang, Y. Wang, Y. Wang, H. Nie, Y. Liu, Chemosphere 82 (2011) 621–626.

[14] B. Nowack, T. D. Bucheli, Environ. Pollut. 150 (2007) 5–22.

[15] B. Suárez, Y. Moliner-Martínez, S. Cárdenas, B. M. Simonet, M. Valcárcel, Environ. Sci. Technol. 42 (2008) 6100–6104.

[16] G. T. Wei, Z. Yang, C. Y. Lee, H. Y. Yang, C. R. C. Wang, J. Am. Chem. Soc. 126 (2004) 5036–5037.

[17] T. Nakashima, T. Kawai, Chem. Commun. (2005) 1643–1645.

[18] A. I. López-Lorente, B. M. Simonet, M. Valcárcel, Analyst 137 (2012) 3528–3534.

[19] J. Wang, H. Chu, Y. Li, ACS Nano 2 (2008) 2540–2546.

[20] W. Xue, T. Cui, Nanotechnology 18 (2007) 145709/1–145709/7.

[21] M. S. Dresselhaus, G. Dresselhaus, R. Saito, A. Jorio, Phys. Rep. 409 (2005) 47.

[22] Z. Liu, J. Zhang, B. Gao, Chem. Commun. (2009) 6902.

[23] J. M. Benoit, J. P. Buisson, O. Chauvet, C. Godon, S. Lefrant, Phys. Rev. B66 (2002) 073417.

[24] F. Tuinstra, J. L. Koening, J. Phys. Chem. 53 (1970) 1126.

[25] N. Lachman, X. Sui, T. Bendikov, H. Cohen, H. D. Wagner, Carbon 50 (2012) 1734.

V.2. DETERMINACIÓN MEDIANTE ESPECTROSCOPIA RAMAN AMPLIFICADA EN SUPERFICIE (SERS)

El descubrimiento de la dispersión Raman amplificada en superficie (SERS) abrió una nueva vía para la espectroscopia Raman. En los últimos años el interés por SERS se ha revivido, dado el descubrimiento de la detección de una sola molécula mediante SERS y los avances alcanzados en Nanociencia y Nanotecnología. Un impedimento clave para un uso más común de sensores basados en SERS es la falta de estrategias sencillas y robustas de fabricación de sustratos SERS reproducibles con un elevado y estable incremento Raman[1].

Después de un amplio debate, actualmente se acepta que al efecto SERS contribuyen dos mecanismos: uno electromagnético y otro químico, siendo el primero el responsable en mayor medida del aumento observado. El incremento electromagnético está causado por la excitación de la oscilación colectiva de los electrones de conducción en una nanopartícula metálica[2], lo que resulta en un incremento del campo local que experimenta una molécula adsorbida en la superficie de la nanopartícula. El efecto químico es otro mecanismo independiente que aumenta la dispersión Raman del analito adsorbido en la superficie metálica[3]. La proximidad entre el metal y las moléculas de analito adsorbidas en la superficie provoca un acoplamiento electrónico por un mecanismo de transferencia de carga.

[1] H. Ko, S. Singamaneni, V.V. Tsukruk, Small 4 (2008) 1576–1599.
[2] A. Knoll, Ann. Rev. Phys. Chem. 49 (1998) 569–638.
[3] A. Otto, J. Raman Spectrosc. 36 (2005) 497–509.

El **capítulo 12** describe el uso de las nanopartículas de oro sin ligandos en superficie obtenidos mediante el método de síntesis propuesto en el capítulo 3 para formar un sustrato SERS que permite la determinación sensible de nanotubos de carbono carboxilados (c-SWNTs). Asimismo se ha comparado la eficiencia de dichas nanopartículas con AuNPs cubiertas con citrato. Dada la simplicidad del procedimiento y las pequeñas cantidades de NPs que se necesitan, para cada medida se prepara un nuevo sustrato evitándose limitaciones de tiempo de vida y reutilización del sustrato.

Capítulo 12

Bare gold nanoparticles mediated surface-enhanced Raman spectroscopic determination and quantification of carboxylated single-walled carbon nanotubes

Analytica Chimica Acta 788 (2013) 122-128

Analytica Chimica Acta

788 (2013) 122-128

Bare gold nanoparticles mediated surface-enhanced Raman spectroscopic determination and quantification of carboxylated single-walled carbon nanotubes

A. I. López-Lorente[a], B. M. Simonet[a], M. Valcárcel[a], B. Mizaikoff[b]

[a] *Department of Analytical Chemistry, University of Córdoba, E-14071 Córdoba, Spain*
[b] *Institute of Analytical and Bioanalytical Chemistry, University of Ulm, Ulm, Germany*

The paper proposes a simple and portable approach for the surface enhanced Raman scattering (SERS) spectroscopy in situ determination of carboxylated single walled carbon nanotubes (SWNTs) in river water samples. The method is based on the subsequent microfiltration of a bare gold nanoparticles solution and the water sample containing soluble carbon nanotubes by using a home-made filtration device with a small filtration diameter. An acetate cellulose membrane with a pore size of 0.2 μm first traps gold nanoparticles to form the SERS-active substrate and then concentrates the carbon nanotubes. The measured SERS intensity data were closely fit with a Langmuir isotherm. A portable Raman spectrometer was employed to measure SERS spectra, which enables in situ determination of SWNTs in river waters. The limit of detection was 10 μg L^{-1}. The precision, for a 10 mg L^{-1} concentration of carbon nanotubes, is 1.19% intra-membrane and 10.5% inter-membrane.

Keywords: Carboxylated single walled carbon nanotubes, Surface-enhanced Raman scattering, Gold nanoparticles, Cellulose membrane.

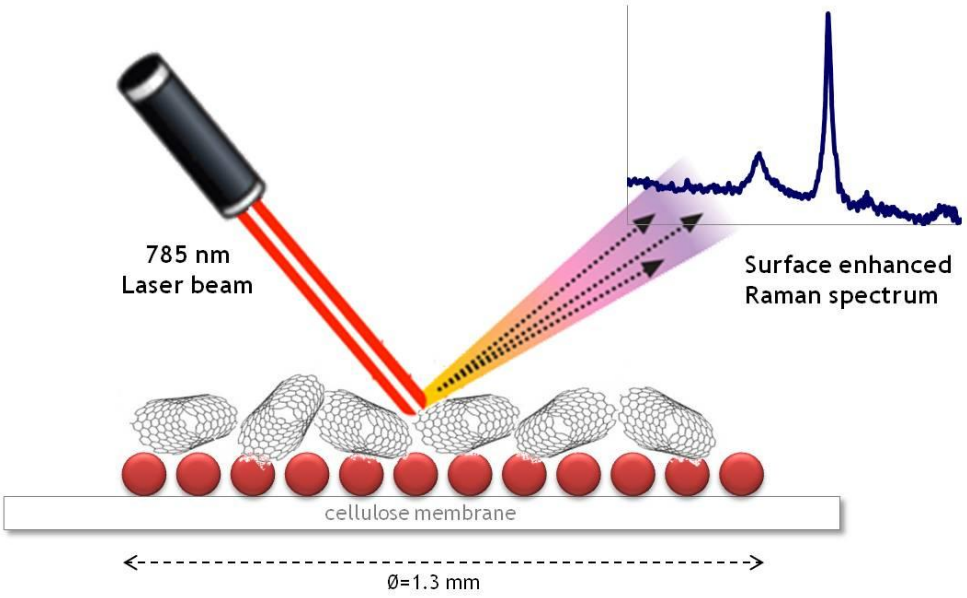
785 nm
Laser beam
Surface enhanced
Raman spectrum
cellulose membrane
Ø=1.3 mm

1. Introduction

Carbon nanotubes (CNTs) have attracted much attention since their discovery [1]. The increasing use and disposal of these nanoparticles (NPs) will lead to their accumulation in the environment. The effectively monitoring of their occurrence requires the development of quantitative analytical techniques for determining their concentration in the environment. Probabilistic material flow analysis from a life-cycle perspective of engineered nanomateriales containing products has been used in order to predict the environmental concentration at which carbon nanotubes may be present. In this sense, Gottschalk et al. [2,3] predicted CNTs concentration at the ng L^{-1} range in sewage treatment plant (STP) effluent in Europe, which is a constraint from the point of view of the actual analytical methods available for CNT detection.

Carbon nanotubes are highly water insoluble and tend to aggregate, which hampers their characterization and determination in aqueous environments [4]. In order to reduce aggregation and improve their solubility, different strategies of carbon nanotube functionalization have been developed [5–7]. Among them, carboxylation is commonly employed in industry to achieve aqueous dispersion of CNTs and further functionalization via carboxyl group [8]. As much de-bundled and individually suspended CNTs are, they will remain longer in the water column [9]. Oxidized carbon nanotubes are, thus, likely to be present in aqueous environmental compartments [10] and hence the importance of developing methodologies for their determination and quantification. There are still few approaches to their quantification in natural media. Carboxylic carbon nanotubes from surface waters have been preconcentrated by using a filter modified with carbon nanotubes and subsequently determined by capillary electrophoresis [11]. In addition, carboxylated single walled carbon nanotubes (c-SWNTs) in waters have been subjected to microliquid–liquid extraction in

ionic liquid, microfiltrated in a membrane and finally determined by Raman spectroscopy [12].

Surface-enhanced Raman scattering (SERS) spectroscopy is a powerful technique for carbon nanotube characterization. SERS enhancement is produced at the so-called hot spots, consisting of two or more coupled metallic nanoparticles with closely spaced features [13]. Two mechanisms –electromagnetic and chemical– are responsible for the enhancement, the electromagnetic being the most predominant [14]. SERS substrates have been traditionally composed by highly ordered arrays of metallic nanoparticles in order to obtain high sensitivity and reproducibility [15]. An impediment for a widespread use of SERS-based sensors is the lack of facile fabrication strategies for reproducible SERS substrates with large and stable Raman enhancement [15]. SERS studies of carbon nanotubes using metallic periodic structures have been described [13,16–18], in order to investigate defects [19] and transformations [20,21] in CNT structure as well as the influence of different conditions (i.e. low temperature) [22] on the feature bands which appear in the SERS spectrum [23]. Other attempts have included the mixture of Au hydrosols and SWNTs to form a solid film [24], the deposition of a nanometric Ag layer by electron-beam metal evaporation at high pressure [25] and the use of metal-coated filter paper to study defect, diameter and SERS mechanism of SWNTs [26]. Furthermore, a modified silver electrode has been also used as substrate [27]. Recently, a 3D substrate formed by gold nanoparticles deposited at the end of vertically aligned CNTs has been described [28].

In this work, a simple SERS substrate is fabricated by using a home-made microfiltration device that allows the subsequent microfiltration of gold nanoparticles – forming the SERS active substrate – and c-SWNTs water solutions on an acetate cellulose membrane. Due to the simplicity of the procedure and the low quantities of nanoparticles needed, a new substrate is

prepared for each measurement which overcomes the limitations of substrate shelf-life and reusability. The suitability of gold nanoparticles obtained by using a new synthetic procedure in which stainless steel acts as reductant agent, leading to nanoparticles without ligands or stabilizers on their surface, has been proved. Moreover, its performance has been compared with those of gold nanoparticles synthesized by citrate reduction method. The procedure shows relatively low variability being possible to fit the data with a Langmuir isotherm. Thus, the potential of the proposed procedure to quantify carboxylic carbon nanotubes in water has been demonstrated.

2. Methods

2.1. Materials and reagents

SWNTs were obtained from Shenzhen Nanotech Port Co. Ltd (NTP) (China), with a purity over 90%, an outer diameter of <2 nm, a length of 5–15 μm and a special surface area of 500–700 m^2 g^{-1}. H_2SO_4 and HNO_3 were purchased from Panreac (Barcelona, Spain). Acetate of cellulose membranes of 0.2 μm pore size and nylon membranes with a pore size of 0.45 μm were purchased from Sartorius Stedim Biotech (Germany) and Supelco (USA), respectively. $HAuCl_4$ (Sigma Aldrich), sodium citrate dihydrate 99.5% (Sigma Aldrich) were used to synthesize the gold nanoparticles. Before synthesis the materials were washed with a mixture 1:3 of nitric acid and hydrochloric acid (PANREAC). Chemicals were used as received with safety precautions taken as according to their respective material safety data sheet.

2.2. Equipment

Raman measurements were performed with a portable Raman spectrometer system provided by B&W TEK Inc., known as inno-Ram with a wavelength of 785 nm and a maximum laser output power of 285 mW in the probe. For

measurements the laser power at the probe was 5.7 mW in order to avoid sample damage.

UV/vis measurements were performed using a halogen lamp as excitation and the monochromator and photonic detector of a PTI fluorescence Master system as a detector. TEM images were recorded using a PHILIPS CM-10 system. Characterization of the nanoparticles was performed using an AFM 5500 by Agilent equipped with NCL-W Point probe-Silicon SPM-cantilevers. For AFM studies at AuNPs, a piece of silicon wafer was covered with AuNP suspension, dried, and then imaged by AFM in tapping mode with a resonance frequency of 190 kHz and a force constant of 48 N m^{-1}. SEM measurements were performed with a Quanta 3D FEG, FEI Company (Eindhoven, Nederland) equipped with an EDX detector.

2.3. Stainless-steel assisted synthesis of gold nanoparticles

Gold nanoparticles were synthesized by using a new proposed method [29], which is based on the reduction of the $HAuCl_4$ by H_2 mediated by the iron contained in stainless steel at ambient conditions. All glassware was cleaned with freshly prepared aqua regia (HNO_3:HCl 1:3 mixture) and then rinsed thoroughly with distilled H_2O prior to use. A piece of 304-stainless steel (12.9 mm^2 of total surface) was introduced into 100 µL of a 0.2 mg mL^{-1} aqueous solution of $HAuCl_4$. The dimensions of the vial employed were diameter 1.3 cm and 3.3 cm height. Despite the reaction takes place at room temperature, in order to reduce reaction time, synthesis was conducted at 50 ºC. The stainless steel substrate is simultaneously used as stirrer during the reaction.

2.4. Citrate reduction synthesis of gold nanoparticles

Gold nanoparticles were synthesized according to the method proposed by Turkevich et al. [30] with some modifications, as described elsewhere [31].

Firstly, the glass material was washed with a mixture 1:3 of nitric acid and hydrochloric acid and then rinsed with distilled water and dry prior use. Solutions of $HAuCl_4$ and sodium citrate were prepared in Milli-Q water and filtered through a 0.45 μm nylon membrane prior use. For the synthesis 50 mL of a 0.01% $HAuCl_4$ solution were heated while being magnetically stirred. After the boiling point, 0.254 mL of a 1% of sodium citrate solution was added to react. Then the system was left for 15 min under stirring. Afterwards, 5 mL of 0.01% $HAuCl_4$ solution and 0.254 mL of a 1% of sodium citrate solution were added to the system. After 15 min of reaction the heater was switch off and the system was stirred until reach room temperature. The final solution containing gold nanoparticles was stored in an amber bottle at 4ºC.

2.5. Functionalization of single-walled carbon nanotubes

Carboxylated carbon nanotubes (c-SWNTs) were prepared by adding 100 mg of single-walled carbon nanotubes to 20 mL of a 3:1 H_2SO_4/HNO_3 mixture into a glass flask as described in [12]. The mixture was then refluxed for 1 h; diluted fractions of it were centrifuged at 10,062 g for 10 min and washed with water. The centrifugation process was repeated until the supernatant phase stopped having acidic pH. Finally, carboxylated derivates were dried at 60ºC in a heater. After acid treatment, SWNTs present covalently attached carboxylic (-COOH) groups on the sidewalls and the open ends, being negatively charged, which make them highly water soluble. The carboxylation method is based on that described by Xue and Cui [32] with slight modifications.

2.6. SERS measurements

SERS measurements were performed on a substrate composed of gold nanoparticles on commercial acetate of cellulose (pore size of 0.2 μm) or nylon (pore size of 0.45 μm) membranes. The membrane is placed on a home-made microfiltration device (with a diameter of filtration of 1.3 mm) and a suitable

amount of gold nanoparticles is placed on it. The membrane traps the gold nanoparticles forming a SERS active substrate. Then, an adequate volume of aqueous sample containing the water soluble carboxylated single-walled carbon nanotubes is passed through the membrane and nanotubes are adsorbed and concentrated on the previously deposited gold nanoparticles.

The membrane is analyzed using SERS detection by means of a portable Raman spectrometer with a 785 nm diode laser. For each carbon nanotube concentration three different membranes were prepared. SERS measurements were acquired from three randomly selected places within the membrane, resulting in a total of nine SERS signals. The laser power was set to 5.7 mW. A 1-s acquisition was employed for measurements averaging the signal of 10 acquisitions. The intensity of carbon nanotubes G band around 1583 cm^{-1} has been selected as analytical signal and subsequently used in order to quantify the samples.

3. Results and discussion

3.1. Characterization of stainless-steel assisted gold nanoparticles

Bare gold nanoparticles obtained by the stainless steel assisted procedure have been characterized by ultraviolet–visible spectroscopy, scanning electron microscopy (SEM), transmission electron microscopy (TEM), and atomic force microscopy (AFM) in order to determine their size and shape (Fig. 1). AuNPs appear homogeneous in shape and size and of polygonal yet nearly spherical shape. The size distribution of these nanoparticles is narrow being well dispersed with neither aggregates nor rods observed. AFM studies allowed the calculation of the nominal colloid size which was 21 ± 9 nm.

Gold nanoparticles were also characterized by ultraviolet–visible spectroscopy. Their average diameter was calculated according to the procedure described by

Haiss et al. [33], resulting in an approximated diameter of 26 nm, value which is in the range provided by AFM studies. The concentration of the stock solution was also determined from the UV/vis spectrum according to Haiss [33]. By using the calculated diameter of the nanoparticles, ε_{450} can be estimated as well as the concentration in mol L^{-1} from the absorption A at 450 nm. The calculated concentration of gold nanoparticles was 1.5×10^{-10} M, which is in the same range than concentrations obtained for nanoparticles synthesized by other procedures [31].

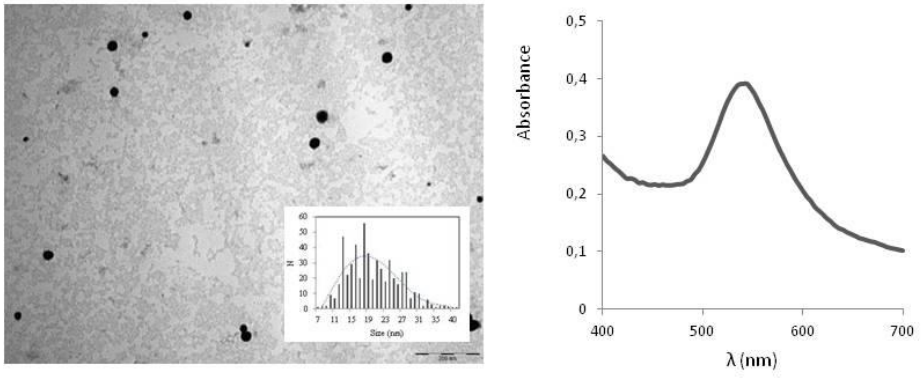

Figure 1. (a) TEM image of individual gold nanoparticles obtained through stainless steel assisted synthesis, the inset shows their size distribution resulting in d_{ave} = 20±6 nm. (b) UV–vis spectrum of the synthesized gold nanoparticles.

3.2. SERS spectra of carboxylated single walled carbon nanotubes (c-SWNTs)

Single walled carbon nanotubes Raman spectra are featured by the following bands: (i) the radial breathing mode (RBM, 100–300 cm^{-1}), in which all carbon atoms vibrate in phase along the radial direction [34], (ii) the disorder peak (D peak, ~1350 cm^{-1}), stemming from the disorder-induced mode in graphite with the same name [35], (iii) the tangential mode (G band, 1400–1700 cm^{-1}), which

comprises several tangential modes due to stretching vibrations in SWNT sidewall C-C bonds, and (iv) the second-order overtone of the D peak (G' ~2500–2800 cm^{-1}) [36]. The RBM is characteristic of SWNTs, although can sometimes be observed in MWNTs with a small diameter inner tube if good resonance condition is established [37]. The spectral difference of carboxylated carbon nanotubes compared with pristine carbon nanotubes is a distinctive D-band to G-band intensity ratio [38].

When carbon nanotubes are in contact with metallic nanoparticles two effects might contribute to the enhancement of their Raman signal. Firstly, the collective oscillation of electrons in metallic nanoparticles leads to the so-called plasmon resonance. This plasmon can resonate with the energy of the excitation laser, exhibiting, thus, high local optical fields (electromagnetic field enhancement). On the other hand, the electronic interaction between carbon nanotubes and metal nanostructures can result in an increased Raman signal ("chemical" enhancement) [14]. SERS spectrum of carbon nanotubes has been described [26] to show both an enhancement of SWNTs Raman bands, but also the appearance of new bands. An increase in G band has been also observed by Pauzauskie et al. [39] when having c-SWNTs placed in a small electric field, which supports the electromagnetic mechanism. In this work, the SERS intensity of the G band around 1583 cm^{-1} has been selected as analytical signal and subsequently used in order to quantify the samples.

The instrumental variables for Raman measurement have been optimized. Firstly, the influence of laser power in the spectra has been studied, finding that, the optimum laser power was 5.7 mW with a laser wavelength of 785 nm. Moreover, spectra were recorded with an acquisition time ranging from 0.5 to 20 s and a number of acquisitions ranging from 1 to 10. The best conditions in terms of sensitivity of the spectrum and duration of the acquisition were 1 s accumulating a sum of 10 spectra.

3.3. Optimization of the amount of gold nanoparticles in SERS substrate

The amount of gold nanoparticles deposited in the membrane will affect the SERS activity of the substrate. A study of the optimal volume of gold nanoparticles has been carried out by loading increasing volumes of gold nanoparticles through the membrane and then loading 5 µL of 40 mg L^{-1} carboxylated single-walled carbon nanotubes. The intensity of the band decreases when loading volumes of gold nanoparticles higher than 10 µL.

The optimization process was repeated at a lower carbon nanotube concentration (8 mg L^{-1}), finding in this case that higher amount of gold nanoparticles led to better sensitivity to the detriment of reproducibility, since calculated RSD in filters with high concentration of gold nanoparticles were significantly higher. They also produced fluorescence interferences which mask CNT bands preventing them from being determined. Regarding these experiments, the optimum volume of gold nanoparticles loaded in the membrane was 5 µL.

Moreover, the deposition order of gold nanoparticles and carbon nanotubes was studied. The best results were obtained when gold nanoparticles are placed below carbon nanotubes, so this configuration was selected for further measurements.

3.4. Optimization of sample volume

The dependence of the Raman signal upon sample loading has been also studied. A lineal increase in G-band intensity when loading between 5 µL and 25 µL of carboxylated single-walled carbon nanotubes (5 mg L^{-1}) has been found. In order to reach a lower limit of detection, higher volumes of carbon nanotubes solutions at lower concentration were passed through the membrane by means of a flow system by using a peristaltic pump. In fact, a volume of 5 mL of a

10 μg L^{-1} c-SWNTs solution was loaded into the membrane allowing measuring the Raman signal. A compromise between sensitivity and operational feasibility (i.e. regarding loading times) must be adopted according to the concentration range of our samples. It could be thought that the limit of detection may be improved by increasing the volume of carbon nanotubes above 5 mL. However there is a limit of concentration that can be measured since as much diluted carbon nanotubes are, higher interferences due to nanotube fluorescence are observed, masking the signal of CNTs featured bands. For simplicity, experiments have been performed with a sample volume of 5 μL.

3.5. Selection of the nature of the membrane

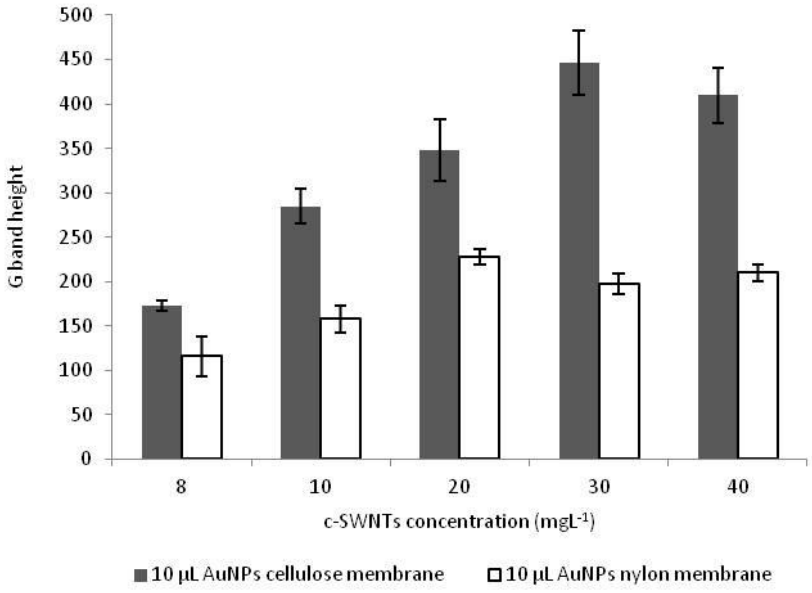

Figure 2. Comparison of G band height when measuring SERS spectra of c-SWNTs in membranes of different nature: cellulose (0.2 μm pore size) and nylon (0.45 μm pore size). Measurements were performed at different carbon nanotube concentration (filtrating 5 μL of sample solution) into a membrane previously loaded with 10 μL of gold nanoparticles.

Previously described studies have been carried out with acetate of cellulose membranes with a diameter of pore of 0.2 μm. A comparison with nylon membranes with pore size of 0.45 μm has been conducted. Cellulose membranes have been found to be more suitable for the SERS measurements, since the yield of retention of gold nanoparticles in the nylon membrane is lower than in the case of cellulose membranes due to the higher pore size. Fig. 2 shows the SERS signal of samples at different concentrations of carbon nanotubes when passed through a cellulose or nylon membrane previously loaded with 10 μL of gold nanoparticles.

3.6. Raman enhancement of bare gold nanoparticles coated membrane

In order to establish the SERS enhancement factor of the gold nanoparticles coated membranes, the Raman signal of 5 μL of 100 mg L^{-1} solution of c-SWNTs placed onto a membrane without gold nanoparticles was measured and compared with the signal obtained when placing 5 μL of 8 mg L^{-1} solution of c-SWNTs onto a membrane previously loaded with gold nanoparticles. Fig. 3 shows both spectra.

The enhancement factor of the membrane can be calculated by using the following equation [40]:

$$EF = \left(\frac{I_{SERS}}{I_{Raman}}\right)\left(\frac{N_{Raman}}{N_{SERS}}\right)$$

where the intensity I is the height of the G-band of carbon nanotubes at 1583 cm^{-1} and N represents the total number of analyte molecules deposited in the substrate. In our case, instead of the number of molecules, we have used the mass of carbon nanotubes passed through the membrane. An enhancement factor of 39 ± 1 was determined. This result improves that obtained in fractal silver surfaces (increased by a factor ~1.4–1.7) [41], with Ag nanoparticles formed at SWNTs surfaces (~5–10 times increase) [42], and other described in literature by using silver, gold and Ag-core Au-shell nanoparticles, which ranged

from 2.2 to 12.4 when nanoparticles and carbon nanotubes are placed on a glass coverslips [43]. In addition, the last mentioned work [43] employed metallic nanoparticles whose plasmon resonance matches the wavelength of the Raman excitation sources. In this work, a 785 nm laser has been employed to carry out SERS measurements due to the fact that experiments with a 532 nm laser did not succeed because of the high fluorescence signal stemming from carbon nanotubes, such interference being higher as nanotubes are more isolated. Taking into account that the laser wavelength is not resonant with gold nanoparticles plasmon, obtained results demonstrate the high SERS performance of studied bare gold nanoparticles.

As it can be seen in Fig. 3, the tangential mode is greatly enhanced and narrowed, which is in agreement with previous reports on carbon nanotubes SERS spectra [43,44].

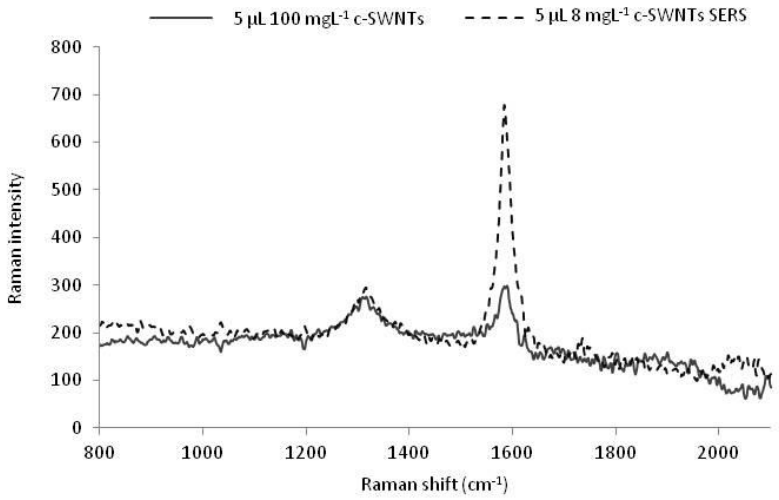

Figure 3. Measured Raman spectra for c-SWNTs with and without gold nanoparticles loaded in the membrane. Raman spectrum was measured passing through the membrane 5 µL of 100 mg L^{-1} solution of c-SWNTs. SERS spectrum was performed passing 5 µL of 8 mg L^{-1} c-SWNTs solution through a membrane previously loaded with 5 µL of gold nanoparticles.

3.7. Comparison of SERS enhancement of bare AuNPs with citrate-coated AuNPs

The SERS performance of gold nanoparticles synthesized with stainless steel as reducing agent was compared with that achieved when using citrate-coated gold nanoparticles. For this task, 5 µL of citrate-coated gold nanoparticles, at the same concentration as that of bare gold nanoparticles, were microfiltered on 0.2 µm pore size acetate of cellulose membrane and measured with the same conditions.

As it can be seen in Fig. 4, the SERS signal obtained with both types of gold nanoparticles is of the same order of magnitude. At higher carbon nanotube concentrations citrate gold nanoparticles provided a slightly increased signal compared with bare gold nanoparticles. However, the reproducibility of membranes composed of citrate-coated gold nanoparticles is worse as regards the RSD obtained both for measurements within the membrane and between different membranes prepared in the same conditions, due to the fact that the distribution of citrate-coated gold nanoparticles throughout the membrane is less homogeneous, some small aggregates concentrated in some regions of the membrane being observed.

Thus, since the SERS response is similar for both types of AuNPs, and taking into account the better reproducibility achieved with stainless steel assisted bare gold nanoparticles, these can be considered a good substrate to perform quantitative SERS measurements.

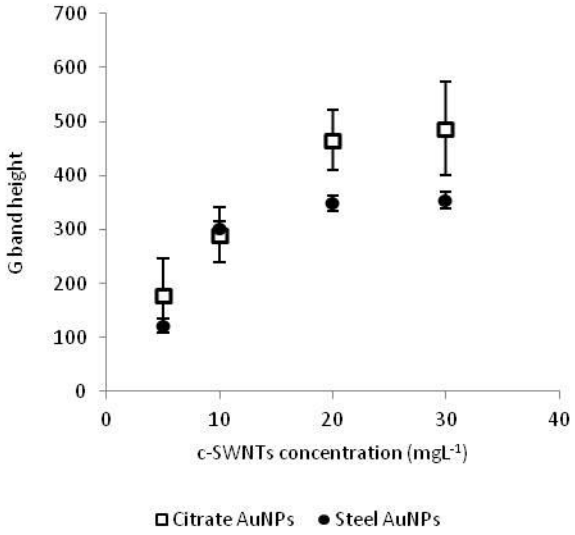

Figure 4. Comparison of SERS response (in terms of carbon nanotube G band height) at different concentrations of c-SWNTs provided by citrate-coated and stainless steel assisted synthesized gold nanoparticles.

3.8. Analytical features of the proposed method

The analytical performance of the proposed method was studied in order to evaluate its usefulness for quantitative analyses. The analytical signal – peak height of the 1583 cm^{-1} Raman G-band –was plotted against c-SWNTs concentration for standard solutions (Fig. 5).

The calibration curve was determined for concentrations ranging from 5 to 30 mg L^{-1}. Each concentration level was analyzed in triplicates (measuring each sample at three randomly selected locations within the membrane). Thus, the data points represent the mean value corresponding to three independent membranes, being the value of each individual membrane the average of three measurements at different spots. Error bars depict the standard deviation of the mean value. The response was fitted with the Langmuir isotherm and the fit was

found to be excellent in the range of concentrations tested (R^2 = 0.99459). Langmuir equation is y = (a * b * x(1−c))/(1±b * x(1−c)), for which calculated parameters are the followings: a = 351.51, b = 0.0011, c = −2.826. As it can be seen in Fig. 5, at concentrations above 15 mg L^{-1} the dependence of the signal with concentration is almost horizontal. In those cases, samples should be diluted in order to be quantified.

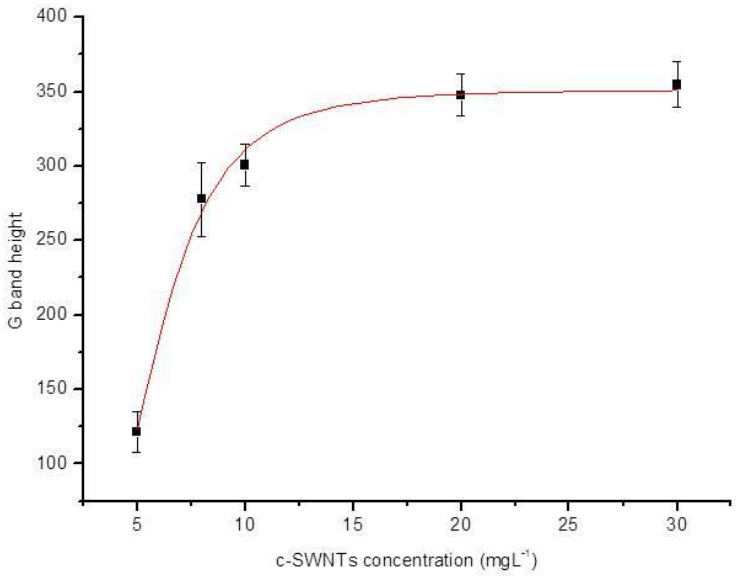

Figure 5. Plot of c-SWNTs Raman G band height for different carbon nanotube concentrations using acetate of cellulose membrane and the optimized conditions. Red line corresponds to the calculated Langmuir equation to which data set has been fitted.

The precision of the measurements was evaluated at a concentration of 10 mg L^{-1} obtaining a relative standard deviations (n = 5) of 1.19% for measurements within a membrane and 10.5% for measurements in different membranes. The analytical features of the method developed are summarized in Table 1.

As it has been previously mentioned, the feasibility of detecting low concentrations of carbon nanotubes by increasing the volume of sample loaded in the membrane has been proved. The detection limit is restricted by the fact that as much diluted carbon nanotubes are, higher interferences due to nanotubes fluorescence are observed. Thus, the detection limit achieved with this procedure was 10 μg L^{-1}. This methodology has proved to be more sensitive than previous described methods in which a preconcentration step prior measurement is needed [12].

Table 1. Analytical features of the method

Calibration equation (Langmuir isotherm)[a]	y = (a*b*x^(1-c))/(1 + b*x^(1-c))
R^2	0.99459
LOD	10 μg L^{-1}
RSD[b] (%) (intra-membrane)	1.19%
RSD[c] (%) (inter-membrane)	10.5%

[a] Where a=351.51638 ±7.45067; b=0.00114±0.0008; c=-2.82639±0.3938 and x=c-SWNTs concentration in mgL^{-1}.

[b]Relative standard deviation, determined from five measurements of 5 μL 10 mgL^{-1} c-SWNTs within the same membrane.

[c]Relative standard deviation, determined from the average value of five measurements of 5 μL 10 mgL^{-1} c-SWNTs in different membranes.

3.9. Application to the determination of water-soluble carboxylated carbon nanotubes in river water samples

In order to check the analytical usefulness of the proposed method, water samples from Guadalquivir river were analyzed following the recommended procedure. No carbon nanotubes were found in them since the analytical signal

was equal to zero. Therefore, river water samples were spiked and analyzed using the proposed methodology.

In order to demonstrate the accuracy of the proposed method, a recovery test of the analysis of spiked river water samples was also carried out. For the recovery study, four fortification levels were assayed; the recoveries values are shown in Table 2. The obtained recoveries were between 86.5% and 105.5% depending on the concentration level. Each sample was analyzed in triplicate in order to evaluate the precision of the method. The coefficients of variation ranged from 4.02% to 5.16%.

Prior analysis, samples were sonicated for 5 min using Vibracell^{TM} 75041 ultrasonic probe (750 W, 20 kHz, Bioblock Scientific, Illkirch, France) equipped with a 3 mm probe set at 20% of amplitude in order to obtain a good dispersion of the nanotubes in the sample and assure its homogeneity.

Table 2. Recovery study of spiked river samples.

Sample	Added concentration (mgL^{-1})	Found concentration[a] (mgL^{-1})	Recovery (%)	RSD(%)
1	5	4.5±0.3	86.5-93.8	4.02
2	8	8.0±0.6	96.1-105.1	4.50
3	10	10.3±0.7	97.8-105.5	4.13
4	15	14±1	91.2-100.5	5.16

[a]Average of three independent spiked samples±CI ($p < 0.05$).

4. Conclusions

In this work a simple approach to the determination of c-SWNTs in water samples is presented. A home-made microfiltration device allows the subsequent microfiltration upon acetate of cellulose membranes of bare gold nanoparticles in solution –obtained through a new synthetic procedure involving stainless steel as reductant-, which will form a SERS active substrate, and a certain volume of water sample containing c-SWNTs. The presence of metallic nanoparticles produces an enhancement of Raman spectra of carbon nanotubes, enabling the sensitive detection of these nanomaterials by means of a portable Raman spectrometer. The performance of these new bare gold nanoparticles as SERS substrate has been compared with those coated with citrate ligands. Due to the simplicity of the procedure and the low quantities of gold nanoparticles needed, a new substrate is prepared for each measure which overcomes the limitations of substrate shelf-life and reusability.

The limit of detection achieved with the proposed methodology is 10 μg L^{-1}, which is higher than the predicted concentrations for carbon nanotubes occurrence in effluent water reported until date. Nevertheless, the presented procedure is capable of detecting and quantifying small quantities of carbon nanotubes in water samples without implying any preconcentration step. Detection limit could be improved if problems related to carbon nanotube fluorescence when isolated are overcome. Anyway, this simple, affordable and portable procedure could be used to the in situ monitorization of the release of these nanostructures from point's source of contamination, such as factories, landfills and wastewater effluents, where concentrations of carbon nanotubes are expected to be considerably higher. In this work, the two facets of analytical nanoscience and nanotechnology are covered. Nanoparticles are considered both objects of analysis (carbon nanotubes) and analytical tools (gold nanoparticles) improving the detection.

Conflict of interest

The authors declare no competing financial interest.

Acknowledgments

The authors wish to thank Spain's Ministry of Innovation and Science for funding Project CTQ2007-60426 and Junta de Andalucía for Project FQM02300. A.I. López-Lorente also wishes to thank the Ministry for the award of a Research Training Fellowship (Grant AP2008-02939).

References

[1] S. Iijima, Nature 354 (1991) 56–58.

[2] F. Gottschalk, T. Sonderer, R.W. Scholz, B. Nowack, Environ. Sci. Technol. 43 (2009) 9216–9222.

[3] F. Gottschalk, T. Sonderer, R.W. Scholz, B. Nowack, Environ. Toxicol. Chem. 29 (2010) 1036–1048.

[4] M. Hassellöv, J.W. Readman, J.F. Ranville, K. Tiede, Ecotoxicology 17 (2008) 344–361.

[5] A. Hirsch, O. Vostrowsky, Top. Curr. Chem. 245 (2005) 193–237.

[6] H. Kuzmany, A. Kukovecz, F. Simon, M. Holzweber, Ch. Kramberger, T. Pichler, Synth. Met. 141 (2004) 113–122.

[7] K. Balasubramanian, M. Burghard, Small 1 (2005) 180–192.

[8] Y.P. Sun, K. Fu, Y. Lin, W. Huang, Acc. Chem. Res. 35 (2002) 1096–1104.

[9] I. Schwyzer, R. Kaegi, L. Sigg, A. Magrez, B. Nowack, Environ. Pollut. 159 (2011) 1641–1648.

[10] S.T. Yang, H. Wang, Y. Wang, Y. Wang, H. Nie, Y. Liu, Chemosphere 82 (2011) 621–626.

[11] B. Suárez, Y. Moliner-Martínez, S. Cárdenas, B.M. Simonet, M. Valcárcel, Environ. Sci. Technol. 42 (2008) 6100–6104.

[12] A.I. López-Lorente, B.M. Simonet, M. Valcárcel, Talanta 105 (2013) 75–79.

[13] X. Lang, T. Qiu, W. Zhang, C. Ji, J. Wang, P.K. Chu, J. Phys. D: Appl. Phys. 43 (455302) (2010), 4pp.

[14] K. Jneipp, H. Kneipp, M.S. Dresselhaus, S. Lefrant, Philos. Trans. R. Soc. Lond. A 362 (2004) 2361–2373.

[15] H. Ko, S. Singamaneni, V. Tsukruk, Small 4 (2008) 1576–1599.

[16] H. Grebel, Z. Iqbal, A. Lan, Chem. Phys. Lett. 348 (2001) 203–208.

[17] X.Y. Dou, Z.P. Zhou, P.H. Tan, L. Song, L.F. Liu, X.W. Zhao, S.D. Luo, X.Q. Yan, D.F. Liu, J.X. Wang, Y. Gao, Z.X. Zhang, H.J. Yuan, W.Y. Zhou, S.S. Xie, Physica E 27 (2005) 469–473.

[18] C. Zhang, K. Abdijalilov, H. Grebel, J. Chem. Phys. 127 (2007), 044701/1-5.

[19] N. Al-Attar, I. Kopf, E. Kennedy, K. Flavin, S. Giaordani, J.H. Rice, Chem. Phys. Lett. 535 (2012) 146–151.

[20] S. Lefrant, I. Baltog, M. Baibarac, J.Y. Mevellec, O. Chauvet, Carbon 40 (2002) 2201–2211.

[21] S. Lefrant, I. Baltog, M. Baibarac, J. Raman Spectrosc. 36 (2005) 676–698.

[22] S. Gohil, S. Ghosh, Appl. Phys. Lett. 96 (2010), 143108/1–3.

[23] M. Baibarac, J.M. Benoit, S. Lefrant, I. Baltog, J. Schreiber, P. Bernier, O. Chauvet, Synth. Met. 121 (2001) 1199–1200.

[24] Y. Ouyang, Y. Fang, J. Mol. Struct. 705 (2004) 71–74.

[25] R. Kumar, H. Zhou, S.B. Cronin, Appl. Phys. Lett. 91 (2007), 223105/1–3.

[26] Z. Niu, Y. Fang, J. Colloid Interface Sci. 303 (2006) 224–228.

[27] X. Hou, Y. Fang, Spectrochim. Acta A 69 (2008) 1140–1145.

[28] S. Lee, M.G. Hahm, R. Vajtai, D.P. Hashim, T. Thurakitseree, A.C. Chipara, P.M. Ajayan, J.H. Hafner, Adv. Mater. 24 (2012) 5261–5266.

[29] A.I. López-Lorente, B.M. Simonet, M. Valcárcel, S. Eppler, R. Schindl, C. Kranz, B. Mizaikoff, Talanta 118 (2014) 321-327.

[30] J. Turkevich, P.C. Stevenson, J. Hillier, J. Discuss. Faraday Soc. 11 (1951) 55–75.

[31] A.I. López-Lorente, B.M. Simonet, M. Valcárcel, Analyst 137 (2012) 3528–3534.

[32] W. Xue, T. Cui, Nanotechnology 18 (2007) 145709/1–145709/145709.

[33] W. Haiss, N.T.K. Thanh, J. Aveyard, D.G. Fernig, Anal. Chem. 79 (2007) 4215–4221.

[34] Z. Liu, J. Zhang, B. Gao, Chem. Commun. 45 (2009) 6902–6918.

[35] F. Tuinstra, J.L. Koening, J. Phys. Chem. 53 (1970) 1126–1130.

[36] M.S. Dresselhaus, G. Dresselhaus, R. Saito, A. Jorio, Phys. Rep. 409 (2005) 47–99.

[37] J.M. Benoit, J.P. Buisson, O. Chauvet, C. Godon, S. Lefrant, Phys. Rev. B 66 (2002) 073417.

[38] N. Lachman, X. Sui, T. Bendikov, H. Cohen, H.D. Wagner, Carbon 50 (2012) 1734–1739.

[39] P.J. Pauzauskie, A. Jamshidi, J.M. Zaug, S. Baker, T.Y.J. Han, J.H. Satcher Jr., M.C. Wu, Adv. OptoElectron. (2012) (Article ID 869829, 4pp.).

[40] W. Yu, I.M. White, Analyst 137 (2012) 1168–1173.

[41] T. Livneh, M. Moskovits, J. Appl. Phys. 92 (2002) 3517–3523.

[42] J. Maley, G. Schatte, J. Yang, R. Sammynaiken, J. Nanotechnol. 2011 (2011) 408151, 7pp.

[43] G.V.P. Kumar, J. Raman Spectrosc. 40 (2009) 2069–2073.

[44] Y.C. Zhao, W.J. Ma, L. Song, Z. Liu, G.T. Liu, Z.X. Zhang, Y.L. Yang, Y.J. Guo, D.L. Ma, S.S. Xie, L.F. Sun, J. Nanosci. Nanotechnol. 9 (2009) 1308-1311.

V.3. PRECONCENTRACIÓN EN MEMBRANAS MODIFICADAS CON NANOTUBOS DE CARBONO

Las excelentes propiedades sorbentes de los nanotubos de carbono han impulsado el desarrollo de membranas basadas en este nanomaterial, que constituyen excelentes soportes para procesos analíticos como la separación o preconcentración de materiales de muestras complejas mediante filtración.

El **capítulo 13** es una revisión del potencial de membranas de nanotubos de carbono en Química Analítica. Por un lado, se han descrito membranas con nanotubos de carbono alineados verticalmente, bien embebidos en una matriz o formadas exclusivamente por CNTs; y por otro, membranas formadas por entramados de CNTs sobre membranas inertes o los denominados buckypapers, constituidos exclusivamente por CNTs. A continuación se muestran las principales aplicaciones analíticas de cada tipo de membrana.

En el **capítulo 14** se describe la aplicación de membranas de MWNTs depositados en una membrana inerte de celulosa a partir de una dispersión en tensioactivos de los mismos para la preconcentración y determinación de c-SWNTs en muestras ambientales, con posterior cuantificación mediante espectroscopia Raman directamente en la membrana. Los analitos (c-SWNTs) se retienen en la membrana gracias a las interacciones π-π con los MWNTs. En este

caso como señal analítica se ha empleado la relación de bandas G y D, de manera análoga al método de caracterización de mezclas de CNTs descrito en el capítulo 6.

Capítulo 13

The potential of carbon nanotube membranes for analytical separations

Analytical Chemistry 82 (2010) 5399-5407

Analytical Chemistry

82 (2010) 5399-5407

analytical chemistry feature

The Potential of Carbon Nanotube Membranes for Analytical Separations

A. I. López-Lorente, B. M. Simonet, M. Valcárcel

Department of Analytical Chemistry, University of Córdoba. 14071 Córdoba, Spain.

Advances in nanotechnology have enabled the development of nanoporous membranes based on carbon nanotubes, which, by virtue of their exceptional properties, constitute excellent supports for analytical processes, including the selective separation of some molecules.

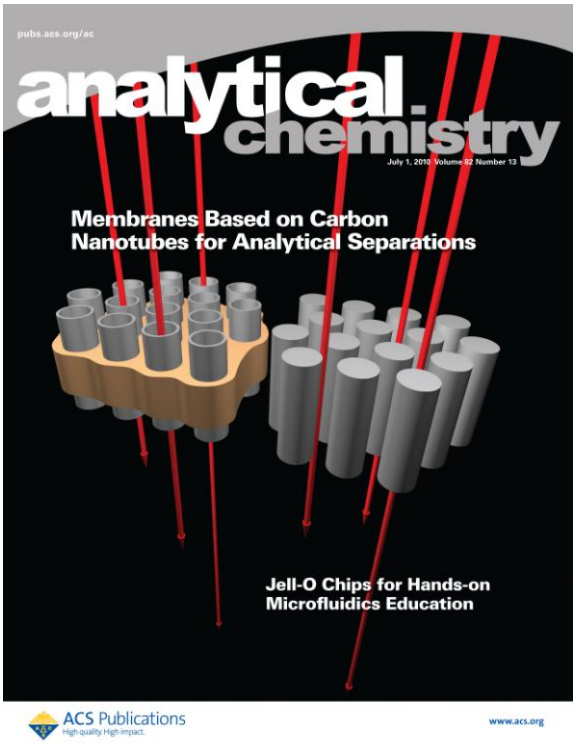

Optimizing a membrane separation process requires careful control of pore size and uniformity in the membrane. In this respect, the inner core of carbon nanotubes (CNTs) provides an effective alternative to existing ordered porous structures such as anodized alumina or polycarbonate membranes at pore diameters of 0.3 nm to 0.6 μm. One major advantage of CNTs is that they provide a uniform membrane pore size (typically 6−7 nm with multiwalled nanotubes [MWNTs] and 1.3−2 nm with double-walled nanotubes [DWNTs]) that can be fine-tuned via the catalyst particle size. CNT-based membranes have opened up new prospects for analytical chemistry, such as selective separation of microorganisms [1], nanoparticles [2,3], or biomolecules [4] from complex samples by filtration.

Since their discovery in 1991, CNTs have aroused much attention from researchers in a number of fields. Thus, their favorable adsorption properties have fostered use as sorbent materials in many analytical processes, e.g., as sorbents in solid-phase (micro)extraction, stationary phases in GC and LC, or pseudostationary phases in CE. More recently, CNT-based membranes have been found to possess unique fluid properties; thus, some properties of fluids confined at molecular dimensions diverge from those in the bulk fluid.

The starting point for the development of CNT membranes was the study of fluid flow through CNTs by molecular simulation, which revealed that water molecules can be carried through nanotubes in a membrane [5] by effect of the tight hydrogen bonding network present inside each tube. Transport rates are extremely high when the membrane is placed under the influence of an osmotic gradient [6]. These theoretical discoveries have been implemented in real membranes for efficient water desalting/desalination by reverse osmosis [7].

Additional theoretical studies on the analytical possibilities of these membranes include one on electrophoretic transport of single-stranded RNA molecules

through 1.5-nm-wide pores in CNT membranes [8]. Conformational dynamics controlled RNA entry into the nanotube pores, while hydrophobic attachment of RNA bases onto pores controlled its exit. Another study predicted binary permeance of CH_4/H_2 mixtures through defect-free (10,10) single-walled nanotubes (SWNTs) acting as a membrane at room temperature [9]. CNTs seem to be highly selective for CH_4 over H_2 when a mixture of these gases permeates through the membrane. For instance, the binary selectivity for the membrane with a pressure drop of 197.4 kPa and a CH_4 fraction in feed of ~0.3 was 20. Finally, a study using molecular dynamics assessed the possibility of separating different atom species by using twisted CNTs [10].

Molecular dynamic simulations have predicted excellent fluxes for gases and water through CNT membranes; this useful property, based on CNTs' hydrophobic nature, has promoted the development of membranes containing embedded nanotubes. Liquid flow is 4−5 orders of magnitude faster than predicted by conventional fluid-flow theory [11] because of the presence of an almost frictionless interface at CNT walls. The presence of MWNTs in membranes increased selectivity in the filtration of H_2/CH_4 mixtures through nanocomposite fabricated membranes [12]. In addition, CNT membranes can be turned into "gatekeepers" by functionalizing CNT tips [13,14]; this, as explained later on, carefully controls fluxes and improves selectivity. More recently, membranes based on DWNTs have been fabricated in reduced diameters comparable to those used in molecular simulation tests, and mass transport of water through them has been confirmed [15].

Mass transport in nanoporous media can be useful for many technologically important reasons. So far, membranes have been used to deliver therapeutic molecules such as drugs and genes through cellular matrices [8], to treat nicotine addiction and opioid withdrawal symptoms transdermally [16], and to

introduce volatile analytes into mass spectrometers by directly fitting the membrane in place of a capillary tube [17].

This Feature provides an overview of the state of the art and analytical potential of CNT membranes. Though we cannot provide a comprehensive review here, interested readers can find further information about nanofluidic transport through CNTs elsewhere [18]. This article has been structured in accordance with the two main arrangements of CNTs in membranes: vertically aligned or as bundles.

1. Membranes with Vertically Aligned Carbon Nanotubes

The synthesis and characterization of ordered nanoporous materials is an active research area because producing an appropriate membrane structure with a highly ordered vertical orientation of pores is a major challenge. At present, the problem is usually addressed by embedding CNTs in a matrix (e.g., a polymer or silicon nitride) and using them as such to form the membrane.

CNT membranes contain two different types of pores: those between individual nanotubes and those in the nanotube lumina. This allows membranes to be established from open-ended nanotubes or from the interstitial spaces between nanotubes.

1.1. Aligned Carbon Nanotubes Embedded in a Matrix

In some CNT membranes, the interstitial spaces are filled with silicon nitride [19] or polymers (polystyrene [20], polysulfone [21]). The spacing between CNTs is filled with a continuous matrix, and the usually closed ends of the nanotubes are etched open, so filtration occurs through the open nanotubes, the only available pathway for mass transport. Synthesis of this type of membrane involves chemical vapor deposition (CVD) of nanotubes onto a support such as quartz or a silicon chip (Figure 1, ia-ic), followed by filling of the volume

between nanotubes with a polymer or silicon nitride (Figure 1, id) and, in free-standing membranes, removal of the film from the substrate (Figure 1, ie). Finally, excess matrix material is removed, and CNT tips are opened by oxidation with H_2O plasma.

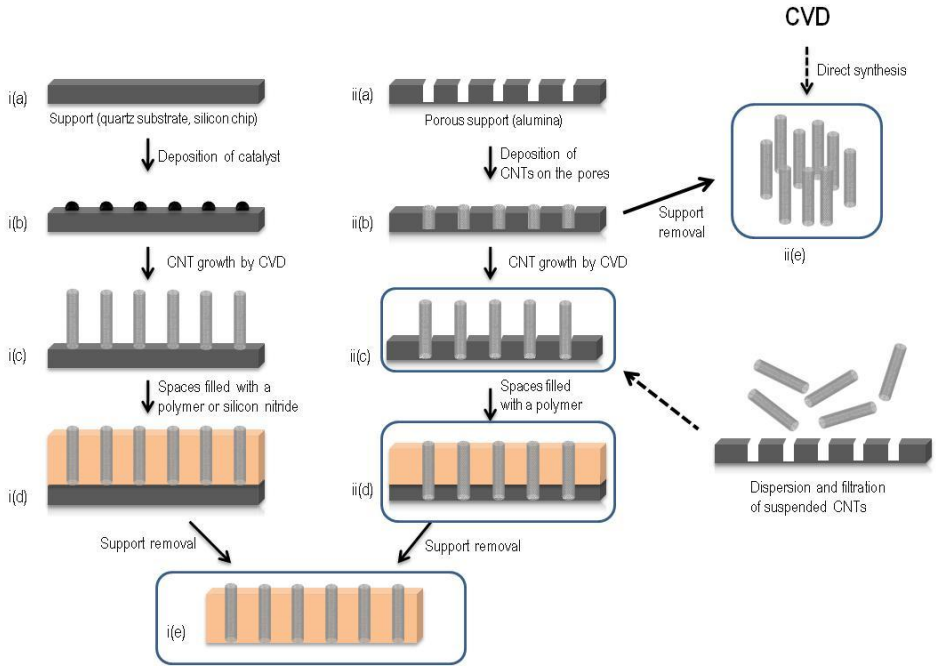

Figure 1. (i) Simplified scheme of the synthetic procedure for free-standing membranes with vertically aligned CNTs embedded in a polymeric (polystyrene)[17] or silicon nitride[13] matrix. The quartz substrates for CVD growth are removed at the end. (ii) Method for fabricating vertically aligned CNT membranes by CVD growth of nanotubes within the pores of an alumina substrate. Membranes can be directly used (iic) or spaces within CNTs filled with a polymer (iid). In addition, the alumina template can be removed (ie). Membranes consisting exclusively of vertically aligned CNTs (iie) can be obtained by removing the alumina template once nanotubes have been deposited into pores. Finally, (iic) membranes can be obtained by CNT dispersion and filtration of the solution through a porous membrane.

The difficulty of using free-standing [20] and silicon chip supported [22] CNT membranes in large-scale industrial applications has spurred the development

of alternative, vertically aligned CNT membranes on porous alumina supports, which can be scaled up as needed [23]. The support may have disk geometry or a tubular or multichannel structure. Nanotubes are grown on its pores (Figure 1, iib-iic), and the inner CNT gaps in the membrane filled with polystyrene (Figure1, iid). The synthetic procedure differs in how excess polymer is removed from the surface and CNT tips are opened (by mechanical polishing). Some authors have successfully used a combination of self-assembly and filtration to fabricate a SWNT/polymer (polysulfone) nanocomposite membrane [21].

In general, membranes consisting of MWNTs have pore diameters of 6−7 nm. However, interest is growing in producing membranes with smaller nanopores-those in the same size range as the molecules—to facilitate fast transport and size selectivity for gas mixtures. Pore sizes of 1.3−2 nm can readily be produced by growing DWNTs on a silicon chip [22].

Table 1 summarizes the characteristics of vertically aligned CNT membranes. Unlike conventional ceramic membranes, which typically have tortuosity factors and porosities of ~3−5 and 0.3−0.6, respectively, CNT membranes have a near-unity tortuosity factor but very low areal porosity, which suggest the presence of straight pores and large gaps between nanotubes, respectively. CNT membranes with porous alumina as support are the least porous because of their low areal density. The enhancement over the Knudsen diffusion model increases with decreasing pore size or increasing Knudsen number (i.e., the ratio of molecular mean free path to pore diameter). Knudsen diffusion occurs when the mean free path of the gas molecules is larger than the pore radius of the membrane and there are more collisions with the pore walls than between gas molecules. The enhancement indicates that the gas transport takes place primarily through the carbon nanotubes, with very little transport through the ultrathin polymer matrix. Membranes on porous alumina supports have low areal tube densities relative to membranes on dense silicon and quartz supports.

Table 1. Comparison of CNT Membranes

Study	Mi et al.[23]	Hinds et al.[20]	Holt et al.[19]	Kim et al.[21]
Membrane structure	Porous alumina support	Free-standing (removed from dense quartz support)	Silicon wafer	PTFE filter
Matrix	Polystyrene	Polystyrene	Silicon nitride	Polysulfone
CNT layer thickness (μm)	~10	5-10	5	6
CNT areal density (#/cm^2)	1.87x10^9	6x10^{10}	2.5x10^{11}	7±1.75x10^{10}
CNT structure	Multiwalled	Multiwalled	Double-walled	Single-walled
CNT outer diameter (nm)	20	NA	2	-
Pore diameter (d_p) (nm)	6.3	7.5	1.6	1.2
CNT tortuosity factor (τ)	1.26	1.1	1	-
Areal porosity (ε)	6.2x10^{-4}	2.7x10^{-2}	5.0x10^{-3}	-
Knudsen number (λ/d_p)	1.2-2.2	~1	10-70	-
Enhancement over Knudsen model	~4	~1	16-120	-

Carboxylated CNTs obtained by oxidation can be easily derivatized by carbodiimide chemistry with a molecule that binds to a bulky receptor that can open or close the pore entrance (Figure 2). For example, a desthiobiotin (DSB) derivative [13] attached to the membrane binds reversibly to streptavidin and improves the selectivity of chemical transport across the membrane [14]. Incubating a streptavidin-coordinated membrane with biotin caused

streptavidin to be released and the flux of methyl viologen (MV^{2+}) restored, allowing reversible binding to regulate transport through the membrane.

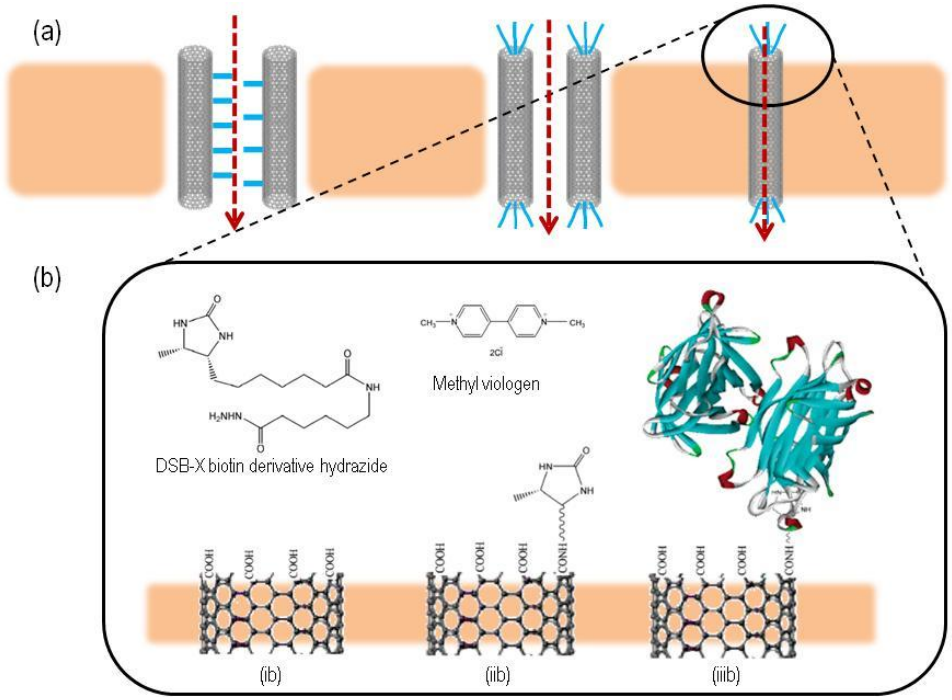

Figure 2. (a) Pore types present in a CNT membrane: within and between nanotubes. (b) More detailed view demonstrating binding of streptavidin to DSB-functionalized tips of CNTs at the surface of a CNT−polystyrene composite membrane. (ib) Open tips of CNTs with carboxylic end groups; (iib) DSB-X biotin hydrazine functionalized tip of a CNT; (iiib) Streptavidin bound to the functionalized membrane. The structures of DSB-X biotin hydrazine and methyl viologen are also shown. Adapted from ref. 13.

Many applications require increasing the density of tethered molecules with modest separation factors [14] such as MV^{2+} and $Ru(bipy)_3^{2+}$ (1.7−3.6) relative to porous alumina, in which separation coefficients can be as high as 1500 [24]. Electrochemical grafting of functional diazonium salts to exposed CNT tips increases functionalization of the latter—and the density of functional molecules

as a result. One important constraint is that the molecules binding to CNT pores should be small enough not to block the core themselves. Moreover, membranes consisting of an array of aligned CNTs and functionalized with charged molecular tethers exhibit voltage gated control of ionic transport through the cores of CNTs. The selectivity between $Ru(bipy)_3^{2+}$ and MV^{2+} flux can be as high as 23 with −130 mV bias applied to the membrane as a working electrode [25].

As noted earlier, despite their hydrophobicity, CNT membranes have the exceptional property of allowing fast flow of a fluid such as water, a result of the formation of water wires and clusters held by tight hydrogen bonds. Also, water wire formation is believed to be important for proton transport, which was 40× higher within 0.8-nm-diameter CNTs than in bulk water [26]. This property expedites filtration of aqueous solutions, which, together with CNTs' extraordinary ability to adsorb nonpolar analytes via π-π interactions, can facilitate some steps of the analytical process. In fact, Raman spectroscopy measurements [27] have suggested that gas molecules are adsorbed in the inner pores of MWNTs, so sorption must occur on the polymer binding matrix or in membrane defects. An ideal membrane must possess a high selectivity and high permeance; both properties are dictated by the affinity of the molecules to be adsorbed and the relative speed with which they can diffuse through the membrane. CNT membranes, which have proved highly compliant with both requirements, may thus be the ideal platforms for analytical separations.

Polymeric membranes containing CNTs have proved useful for transporting gas molecules such as N_2 [13,14] or aqueous ions such as $Ru(NH_3)_6^{3+}$ [20], $Ru(bpy)_3^{2+}$ [13,14,25,28], and MV^{2+} [13,14,25]. For instance, a $Ru(NH_3)_6^{3+}$ flux of 0.07 μmol/cm^{2}h can be raised to 0.9 μmol/cm^{2}h by treating the membrane with acid. This flux level is comparable to that of ordered alumina membranes [29]. Also, the flux of MV^{2+} before binding of streptavidin to a DSB-functionalized CNT

membrane [13], 4.8 nmol/cm^{2}h, was reduced to 0.2 nmol/cm^{2}h upon binding; this result testifies to the ability to control the flux by adjusting the membrane properties. CNT membranes on silicon nitride have been used to remove some small ions such as Cl^-, K^+, $Ru(bipy)_3^{2+}$, Ca^{2+}, and $Fe(CN)_6^{3-}$ from aqueous solutions [30,31].

In the place of a capillary tube, a membrane with CNTs grown within the pores of anodic aluminum oxide was directly coupled to a mass spectrometer [17] to introduce volatile analytes; the membrane exhibited preferential transmission of methane. Conductance decreased with increasing total pressure, but the effect decreased progressively for the following sequence of gases: $CH_4 > N_2 > O_2 > Ar > CO_2$.

1.2. Membranes Consisting Exclusively of Aligned Carbon Nanotubes

The membranes consisting of vertically aligned CNTs described above posses a matrix that fills the spaces between CNTs and/or the support onto which nanotubes are grown and is subsequently removed in some cases. By contrast, the membranes described in this section contain no binder or support. Most are obtained by growing CNTs by CVD on a substrate [2,32] such as the pores of a microporous alumina template [33,34] or glass [35]; the nanotubes are peeled off the membrane at the end of the process (Figure 1, iie). Alumina templates, for instance, can be removed by leaching with a NaOH solution [34]. New synthetic procedures producing aligned CNTs without a support [36] may in the near future enable the direct synthesis of CNT membranes. Figure 3 shows scanning electron micrographs of membranes with alumina template.

This type of membrane can also be obtained with other methods such as continuous spray pyrolysis [37], which creates hollow carbon cylinders up to a few centimeters in diameter and several centimeters long with walls consisting of micrometer-length aligned MWNTs. Alternatively, membranes can be

produced by self-assembly of oxidized SWNTs. The surface of a soaked glass substrate immersed in a SWNT water dispersion forms a thin film through natural vaporization of water. Nanotubes are uniaxially aligned in the direction of the air/water/substrate triple line [38], and the membrane is peeled off by stirring the glass in water.

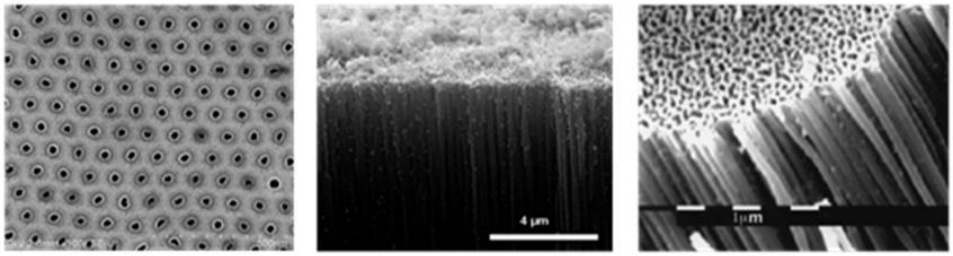

(a) (b) (c)

Figure 3. (a) Scanning electron micrograph of a CNT membrane surface after ion milling. The dark areas in the image are open pores, the light rim around the pore is the CNT, and the remainder substrate the aluminum oxide film. (b) Cross-sectional scanning electron image of a CNT-modified anodized alumina membrane with pore size 200 nm. (c) Scanning electron micrograph of a template-synthesized carbon tubular membrane after the alumina template is dissolved. The edge (lower part of the image) with the tubules and the surface (upper part) are shown. Adapted with permission from refs. 17, 33, and 34.

One other way of obtaining an array of CNTs is to grow them by CVD into dense membranes via the capillary forces of solvent evaporation and then allow them to collapse [2]. These membranes have an average spacing between CNTs after shrinkage of ~3 nm-comparable to the pore size of the nanotubes-and a density 8−270x higher than that of previous membranes. Because the interstitial pores are not sealed, gases can permeate through both the nanotubes and their interstitial pores.

These free-standing membranes contain a parallel array of CNTs that spans their full thickness. Well-aligned CNTs cannot always be obtained; in some cases, the material deposits mainly as bundles of curved CNTs [34]. Electroosmotic flow (EOF) can be driven across by separating two electrolyte solutions with the membrane and using an electrode in each solution to pass a constant ionic current through the nanotubes [39,40]. Based on the EOF direction, the nanotubes have negative surface charge that can be boosted by electrochemical derivatization with *p*-aminobenzoic acid. On the other hand, membranes with positive surface charge can be prepared by electrochemical derivatization with 2-(4-aminophenyl)ethylamine.

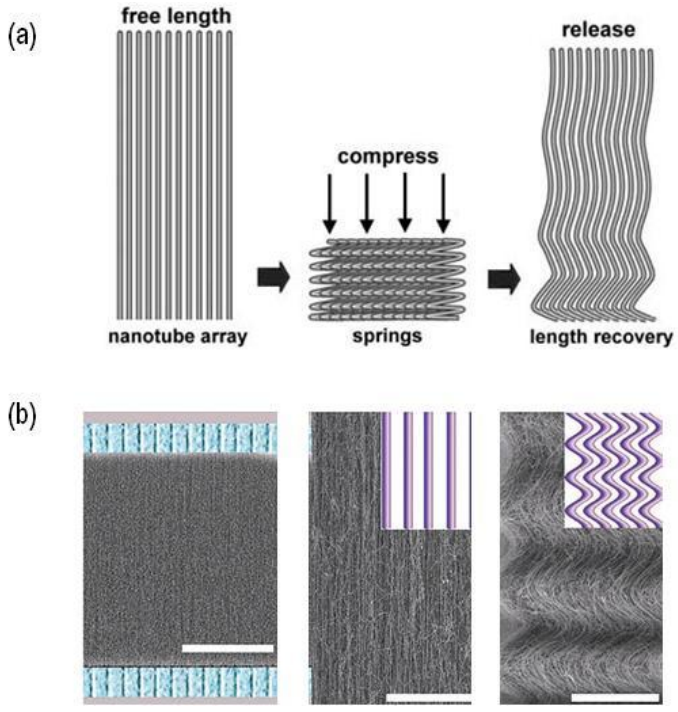

Figure 4. (a) Compression testing of aligned CNT films. A schematic illustration shows a nanotube array compressed to folded springs and then regaining its free length upon release of the compressive load. (b) Scanning electron micrographs of a membrane both compressed and uncompressed. Adapted with permission from refs. 41 and 42.

This type of membrane is super-compressible [41] and fully elastic; the pores can be tuned simply by mechanical compression and release (Figure 4) [42]. This unique property has enabled the separation of species of different sizes within the tunable pore size range by simply adjusting the membrane thickness by uniaxial compression, eliminating the need to replace the filter.

An advantage of CNT membranes over conventional filters is that they can easily be cleaned by ultrasonication and autoclaving (or purging) to restore their filtering efficiency. Other water-filtration membranes (e.g., cellulose nitrate/acetate membranes) cannot be reused because they adsorb bacteria heavily during filtration. Moreover, CNTs are thermally stable, so their membranes can be used at higher temperatures than conventional polymer membrane filters (~400 °C versus ~50 °C). In summary, the exceptional thermal and mechanical stability of nanotubes and the high surface area and easy and cost-effective fabrication of nanotube membranes make them competitive with commercially available ceramic and polymer-based separation membranes.

The membranes described in this section have been used in a variety of applications including nanofiltration of gold nanoparticles and N_2 adsorption [2]. Because no filler is used, they also allow permeation through the interstitial spaces. Cylindrical membranes of this type are useful for removing multiple components of heavy hydrocarbons from petroleum and for filtering bacterial contaminants such as *E. coli* or the nanometer-sized poliovirus from water [37]. Filtering seems to occur mostly through interstitial spaces; however, there might be some additional transport through the inner hollow channels of the nanotubes. These membranes have also been used to separate a larger molecule (triisopropyl orthoformate) from a smaller molecule (*n*-hexane) during pervaporation [2]. This testifies to their potential for separating not only gases—the permeance of which is roughly 450x higher than predicted from Knudsen theory—but also liquid mixtures.

2. Membranes with Bundles of Carbon Nanotubes

Unlike those in membranes described in the previous section, CNTs are not aligned vertically in membranes containing bundles of nanotubes. As a result, filtration does not rely on size exclusion or sieving in the inner core of the tubes but rather on the sorption capabilities of the material.

2.1. Bundles of Carbon Nanotubes on Inert Membranes

Unlike buckypapers (below), CNT-modified membranes require an inert membrane. There are two different types of filters: those with electrostatic and those with covalent interaction of CNTs with the membrane. Because CNT bundles are not aligned, they can form aggregates and facilitate interaction of the analytes with both their walls and the interstitial spaces. Adsorption of the analytes is favored by π-π electrostatic interactions and the typically large surface area of CNTs.

CNT-modified filters are usually prepared by passing a dispersed solution of CNTs through a membrane. The nanotubes are dispersed by means of a surfactant such as SDS [43] or Triton X-100 [3] or DMSO [1]; alternatively, MWNTs functionalized with poly(diallyldimethylammonium) chloride [44] can be filtered directly. These membranes are available in various formats including cellulose ester membranes [44], PVDF [1], nylon-encased filters [3], or qualitative filter paper [43]. When DMSO or a surfactant is used to disperse the CNTs, the dispersant must be removed by passing an appropriate solvent such as methanol or ethanol through the membrane.

Some crucial properties of CNTs such as their high surface area, tendency to aggregate and form highly porous structures, and antibacterial action (of SWNTs) have been exploited to develop membranes incorporating nanotube bundles. Among other applications, these membranes have enabled 1) selective

isolation and preconcentration of acidic proteins such as BSA [44] (increased sample loading and elution flow rates resulted in a 146-fold improvement in the sorption capacity of BSA); 2) preconcentration and determination of carboxylic SWNTs from spiked environmental water samples [3] (separated electrophoretically with recoveries of 70−85% and precision of 6.4−7.3%); 3) retention of bacteria, which were effectively inactivated upon contact with a SWNT filter, and removal of viruses, which were captured by nanotube bundles inside the SWNT layer [1]; and 4) enrichment of phthalate esters, bisphenol A, 4-*n*-nonylphenol, 4-*tert*-octylphenol, and chlorophenols from variable volumes of solution [43]. A comparative study showed that a system comprising two stacked SWNT disks containing 60 mg of nanotubes exhibited extraction capabilities on a par with those of a commercial C_{22} disk loaded with 500 mg of sorbent for nonpolar or moderately polar compounds. The former system proved more powerful than the latter in extracting polar analytes and exhibited easier desorption after loading [43].

A membrane-protected CNT micro-solid phase extraction device [45] was prepared by enclosing MWNTs within a polypropylene sheet membrane envelope that was heat-sealed to secure the contents. The device was used to extract organophosphorus pesticides from a stirred solution. The porous membrane filtered out extraneous materials, so no further cleanup was required. After extraction, the analytes were desorbed in hexane and analyzed by GC/MS. The method exhibited good linearity over the concentration range 0.1−50 μg/L, RSD values of 2−8%, and low limits of detection (1−7 pg/g) [45]; it also proved an accurate, rapid, cost-effective alternative to other microextraction techniques.

Though they do not necessarily contain an inert membrane, we have included nanocomposite membranes in this section because the CNTs within are embedded in a polymer matrix that acts as a support for nanotube bundles. The unique electronic, adsorptive, mechanical, and thermal properties of CNTs can

make these nanocomposite membranes useful for a number of applications that may benefit from cooperative and synergistic effects between the polymer and carbon phases. The following are a few examples among many illustrating the potential of nanocomposite membranes. Nanocomposites of MWNTs with poly(bisphenol A-co-4-nitrophtalic anhydride-co-1,3-phenylene diamine) [12] and CNTs with poly(vinyl alcohol) (PVA) [46] have been used to successfully separate H_2/CH_4 and benzene/cyclohexane mixtures, respectively. Using a high molecular weight CNT concentration resulted in significantly improved permeability and selectivity for H_2, CO_2, and CH_4 [12]. With 10% CNT loading, for example, the H_2/CH_4 selectivity was ~8 and the CO_2/CH_4 selectivity 3.8. Incorporating CNTs previously dispersed with β-cyclodextrin by grinding into PVA membranes was found to boost permeate flux and increase separation factors; for example, 50/50 (w/w) benzene/cyclohexane mixtures exhibited a permeation flux of 61.0 g/m^2h and a separation factor of 41.2 at 333 K [46].

2.2. Membranes Consisting Exclusively of Carbon Nanotube Bundles (Buckypapers)

Nanometer-sized CNTs have a tendency to self-aggregate via strong van der Waals forces. This intrinsic property of CNTs can be used to obtain paper-like sheets called “buckypapers” from dispersed nanotubes in solution.

Buckypapers are self-supporting entangled assemblies of CNTs arranged as a planar film held together by van der Waals interactions at tube−tube junctions. The greatest difference between buckypapers and CNT-modified filters is that the inert membrane used to prepare the paper in the former—usually by filtration—is removed at the end of the process. As a result, buckypapers consist solely of packed bundles of CNTs. Ideally, buckypapers should have all CNTs connected with one another to form a network structure and the nanotubes should be long and straight [47].

This type of membrane has been prepared using DWNTs [48-50] (Figure 5), SWNTs [51-53], and MWNTs [54,55]; the most popular method involves dispersion and filtration of a suspension of CNTs. Unfunctionalized nanotubes tend to agglomerate in solvents, which hinders their filtration. The resulting buckypapers are often brittle and tend to crack upon drying. Acid oxidation [51] improves dispersion but introduces extensive surface functionalization. One alternative procedure uses a surfactant such as Triton X-100 or SDS or a solvent such as dimethylformamide [54,56] or acetyl acetone [56]; any residual surfactant or solvent remaining after the buckypaper has been prepared should be carefully removed. PTFE [49], ceramic [51], and Whatman nylon filters [54] have been used for filtration. The ensuing filtration procedures have some advantages including homogeneity in the films and the ability to control their thickness with nanometric accuracy via the nanotube concentration used and suspension volume filtered.

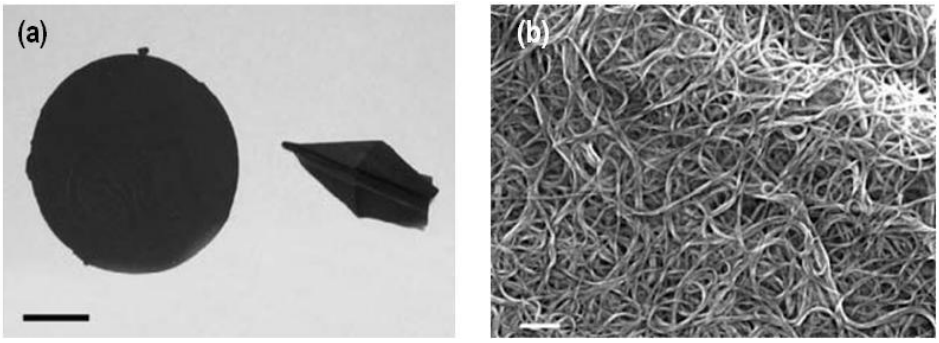

Figure 5. Production of pure, clean DWNTs in a high yield. (a) Photograph of DWNT buckypaper. The paper (left) is tough and flexible enough to fold into an origami airplane (right). Scale bar: 1 cm. (b) Scanning electron micrograph of DWNT paper showing CNT bundles. Scale bar: 300 nm. Adapted with permission from ref. 48.

The pore structure of MWNT buckypapers is independent of the type of solvent, sonication time, and buckypaper surface density used [56]. However, control

over the structure is a prerequisite for engineering buckypaper-based separation technology applications [54]. The pore characteristics of buckypapers can be controlled via the length distribution of their CNTs.

Buckypaper-like membranes have also been fabricated in other ways (Figure 6). Evaporation of a small amount of a SWNT/oleum dispersion [53] from a Petri dish formed a SWNT film, and a large-area double-walled film was obtained by spreading purified DWNTs with ethanol or acetone [50]. Another study accomplished fabrication of buckypaper from unfunctionalized MWNTs without the aid of a surfactant or surface modification technique by using a frit compression method [55]. Also, aligned buckypaper was obtained by operatively rotating CNTs in vertically oriented arrays (forests) to make self-supporting 5-cm-wide, 1-m-long transparent sheets [57].

A macroscopic manipulation procedure for aligned CNT arrays called "domino pushing" allowed the "dry", in situ preparation of aligned, thick buckypapers with large areas [47]. The procedure involves three steps: 1) covering the CNT array with a piece of microporous membrane and forcing the array down in one direction, which attracts nanotubes together via van der Waals forces to form an aligned buckypaper; 2) peeling off the membrane from the silicon substrate; and 3) spreading ethanol to facilitate peeling of the aligned buckypaper off the membrane.

Finally, in a novel approach called "hydroentangling" [58], dry CNT powder is directly laid onto a porous support, and the drag force of water jets overcomes van der Waals forces to generate entangled CNT structures. The thickness of hydroentangled CNT membranes can be easily controlled by selectively adjusting the amount of powder that is laid on the support. In addition to separation applications, the electrochemical properties of these membranes may also be suitable for developing electroanalytical electrodes.

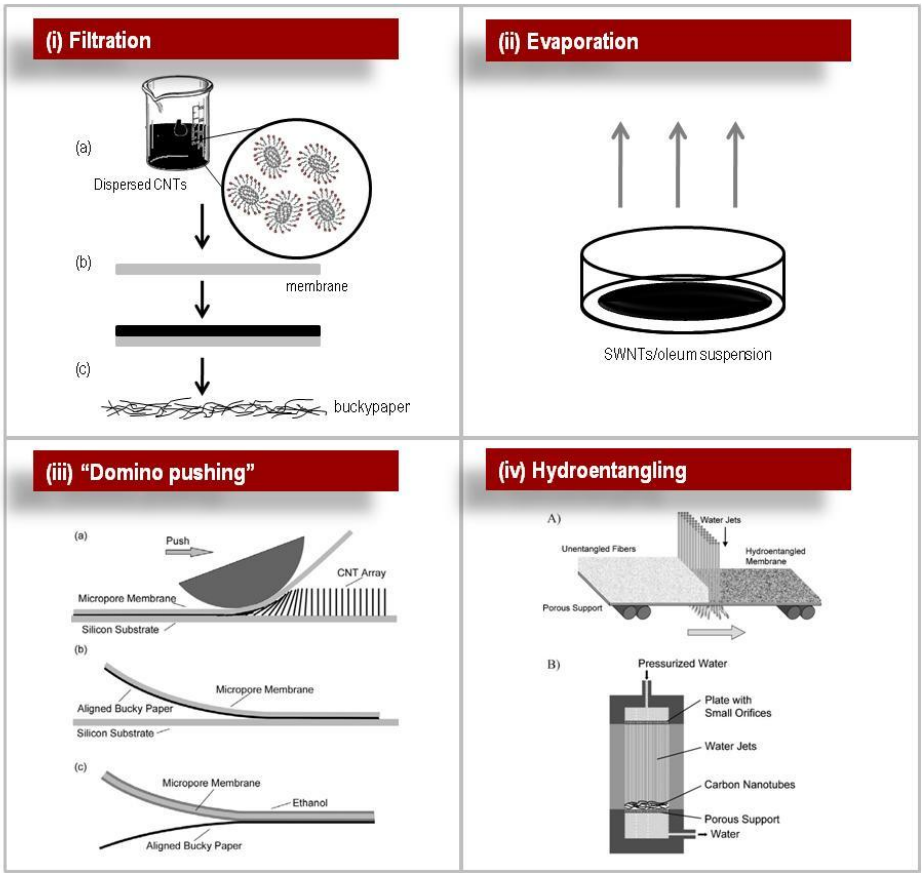

Figure 6. Most common buckypaper synthetic procedures. (i) Filtration involves three steps: (a) dispersion; (b) filtration; and (c) peeling off the membrane. (ii) Evaporation of a small amount of a SWNT/oleum suspension. (iii) Scheme of the domino pushing method: (a) formation of aligned buckypaper; (b) peeling of the buckypaper off the silicon substrate; (c) peeling of the buckypaper off the microporous membrane. (iv) Hydroentangling of CNTs: (A) continuous hydroentangling; (B) bench-top hydroentangling setup used to obtain batches of hydroentangled CNT membranes. Adapted with permission from refs. 47 and 58.

The effective diffusivity of six common laboratory gases (O_2, N_2, H_2, He, CO_2, CH_4) through buckypapers thicker than 186 μm was in the 3−12 × 10^{-9} m^2/s range and correlated with the kinetic diameter of the gases [56]. Transparent, conductive SWNT films [52] were used to construct an electric field activated

optical modulator, which is an optical analog to the nanotube-based field effect transistor. A packed bed of MWNTs completely removed CO_2 from a flowing stream of CO_2/N_2 and exhibited rapid uptake kinetics for CO_2 [59].

3. Conclusions

In summary, Table 2 shows a comparison and the main analytical applications of each kind of membrane discussed in this article.

CNT membranes provide an effective alternative to commercially available membrane filters for analytical separations. Their combination of excellent flow and adsorptive properties allows the rapid filtration of polar solutions. Also, membranes consisting of vertically aligned CNTs possess quite good selectivity by virtue of their filtration mechanism of size exclusion or sieving through open-ended CNTs and/or interstitial spaces. Their selectivity can be further improved by functionalization. In some cases, their tunability via pore size allows strict control over pore diameters by pressure.

One disadvantage of membranes consisting exclusively of CNT bundles is their poor selectivity; thus, nonpolar compounds (particularly aromatic compounds) are retained via π-π interactions. By contrast, this type of membrane is much easier to prepare than those consisting of vertically aligned nanotubes. Finally, buckypapers provide a promising alternative platform for analytical separation but are still brittle and prone to cracking upon drying, so they will require more research before they can be rendered as useful as their CNT-based counterparts. Although buckypapers are still at the development stage, they may find a host of applications in the near future like vertically aligned and CNT-modified membranes have since their inception.

Table 2. Main Analytical Applications of the Different Kind of Membranes

	Type of membrane	Filtration mechanism	Selectivity	Stability	Applications	Ref.
Membranes with vertically aligned CNTs	Aligned CNTs embedded on a matrix	Size exclusion or sieving through open CNTs	Modest separation factors; increased by CNT tip functionalization; membranes with smaller diameters, size exclusion	Good	Transport of N_2	13,14
					Transport of $[Ru(NH_3)_6^{3+}$, $Ru(bpy)_3^{2+}$ and $MV^{2+}]$	20,13,14
					Removal of ions (Cl^-, $Ru(bpy)_3^{2+}$, Ca^{2+}, $Fe(CN)_6^{3-}$) from aqueous solutions	30,31
	Aligned CNTs only	Size exclusion or sieving through open CNTs or their interstitial space	Good; achieved by compression (pore-tunable property) or CNT wall functionalization	Moderate	Separation of CH_4 from H_2	9
					N_2 adsorption	2
					Water desalination	7
					Selective filtration of proteins	42
					Elimination of multiple components of heavy hydrocarbons from petroleum	37
					Filtration of bacterial contaminants	37
					Nucleic acid transport	8
					Transport of $Ru(NH_3)_6^{3+}$, $Ru(bpy)_3^{2+}$ and MV^{2+}	6
					Nanofiltration of gold nanoparticles	2
Membranes with bundles of CNTs	Bundles of CNTs on inert membranes	Based on sorption capabilities	Low; separation is based on π-π electrostatic interactions	Good	Separation of CH_4 from H_2	12
					Separation of benzene/cyclohexane	46
					Removal of viral and bacterial pathogens from water	1
					Selective isolation of acidic proteins	44
					Preconcentration of organophosphorous pesticides	45
					Preconcentration of carboxylic SWNTs	3
					Preconcentration of phthalate esters, bisphenol A, 4-*n*-nonylphenol, 4-*tert*-octylphenol, and chlorophenols	43
	Buckypaper	Based on sorption capabilities	Low; separation is based on π-π electrostatic interactions	Poor*	Removal of CO_2 from a flowing stream of CO_2/N_2	59

*Often brittle and cracking upon drying.

Acknowledgment

The authors wish to thank Spain's Ministry of Innovation and Science for funding Project CTQ2007-60426 and Junta de Andalucía for Project FQM02300. A. I. López-Lorente also wishes to thank La Caixa for award of a research fellowship.

References

[1] Brady-Estévez, A. S.; Kang, S.; Elimelech, M. *Small* **2008**, *4*, 481–484.

[2] Yu, M.; Funke, H. H.; Falconen, J. L.; Noble, R. D. *Nano Lett.* **2009**, *9*, 225–229.

[3] Suárez, B.; Moliner-Martínez, Y.; Cárdenas, S.; Simonet, B. M.; Valcárcel, M. *Environ. Sci. Technol.* **2008**, *42*, 6100–6104.

[4] Miller, S. A.; Young, V. Y.; Martin, C. R. *J. Am. Chem. Soc.* **2001**, *123*, 12,335–12,342.

[5] Hummer, G.; Rasaiah, J. C.; Noworyta, J. P. *Nature* **2001**, *414*, 188–190.

[6] Kalra, A.; Garde, S.; Hummer, G. *Proc. Natl. Acad. Sci. U.S.A.* **2003**, *100*, 10,175–10,180.

[7] Corry, B. *J. Phys. Chem. B* **2008**, *112*, 1427–1434.

[8] Yeh, I. C.; Hummer, G. *Proc. Natl. Acad. Sci. U.S.A.* **2004**, *101*, 12,177–12,182.

[9] Chen, H.; Sholl, D. S. *J. Membr. Sci.* **2006**, *269*, 152–160.

[10] Wang, Q. *Carbon* **2009**, *47*, 2752–2760.

[11] Majumder, M.; Chopra, N.; Andrews, R.; Hinds, B. J. *Nature* **2005**, *438*, 44.

[12] Weng, T. H.; Tseng, H. H.; Wey, M. Y. *Int. J. Hydrog. Energ.* **2009**, *34*, 8707–8715.

[13] Nednoor, P.; Chopra, N.; Gavalas, V.; Bachas, L. G.; Hinds, B. J. *Chem. Mater.* **2005**, *17*, 3595–3599.

[14] Majumder, M.; Chopra, N.; Hinds, B. J. *J. Am. Chem. Soc.* **2005**, *127*, 9062–9070.

[15] Verweij, H.; Schillo, M. C.; Li, J. *Small* **2007**, *3*, 1996–2004.

[16] Strasinger, C. L.; Scheff, N. N.; Wu, J.; Hinds, B. J.; Stinchcomb, A. L. *Subst. Abuse: Res. Treat.* **2009**, *3*, 31–39.

[17] Miranda, L. D.; Short, R. T.; van Amerom, F. H. W.; Bell, R. J.; Byrne, R. H. *J. Membr. Sci.* **2009**, *344*, 26–31.

[18] Holt, J. K. *Adv. Mater.* **2009**, *21*, 3542–3550.

[19] Holt, J. K.; Noy, A.; Huser, T.; Eaglesham, D.; Bakajin, O. *Nano Lett.* **2004**, *4*, 2245–2250.

[20] Hinds, B. J.; Chopra, N.; Rantell, T.; Andrews, R.; Gavalas, V.; Bachas, L. G. *Science* **2004**, *303*, 62–65.

[21] Kim, S.; Jinschek, J. R.; Chen, H.; Sholl, D. S.; Marand, E. *Nano Lett.* **2007**, *7*, 2806–2811.

[22] Holt, J. K.; Park, H. G.; Wang, Y.; Stadermann, M.; Artyukhin, A. B.; Grigoropoulos, C. P.; Noy, A.; Bakajin, O. *Science* **2006**, *312*, 1034–1037.

[23] Mi, W.; Lin, Y. S.; Li, Y. *J. Membr. Sci.* **2007**, *304*, 1–7.

[24] Jirage, K. B.; Hulteen, J. C.; Martin, C. R. *Science* **1997**, *278*, 655–658.

[25] Majumder, M.; Zhan, X.; Andrews, R.; Hinds, B. J. *Langmuir* **2007**, *23*, 8624–8631.

[26] Dellago, C.; Naor, M. M.; Hummer, G. *Phys. Rev. Lett.* **2003**, *90*, 105902.

[27] Matranga, C.; Bockrath, B.; Chopra, N.; Hinds, B. J.; Andrews, R. *Langmuir* **2006**, *22*, 1235–1240.

[28] Majumder, M.; Keis, K.; Zhan, X.; Meadows, C.; Cole, J.; Hinds, B. J. *J. Membr. Sci.* **2008**, *316*, 89–96.

[29] Ago, H.; Komatsu, T.; Ohsima, S.; Kuruki, Y.; Yumura, M. *Appl. Phys. Lett.* **2000**, *77*, 79–81.

[30] Fornasiero, F.; Park, H. G.; Holt, J. K.; Stadermann, M.; Grigoropoulos, C. P.; Noy, A.; Bakajin, O. *Mater. Res. Soc. Symp. Proc.* **2008**, 1106–1111.

[31] Fornasiero, F.; Park, H. G.; Holt, J. K.; Stedermann, M.; Grigoropoulos, C. P.; Noy, A.; Bakajin, O. *Proc. Natl. Acad. Sci. U.S.A.* **2008**, *105*, 17,250–17,225.

[32] Wang, Z.; Ci, L.; Chen, L.; Nayak, S.; Ajayan, P. M.; Koratkar, N. *Nano Lett.* **2007**, *7*, 697–702.

[33] Che, G.; Lakshmi, B. B.; Fisher, E. R.; Martin, C. R. *Nature* **1998**, *393*, 346–349.

[34] Vermisoglou, E. C.; Pilatos, G.; Romanos, G. E.; Karanikolos, G. N.; Boukos, N.; Mertis, K.; Kakizis, N.; Kanellopoulos, N. K. *Microporous Mesoporous Mater.* **2008**, *110*, 25–36.

[35] Ren, Z. F.; Huang, Z. P.; Xu, J. W.; Wang, J. H.; Bush, P.; Siegal, M. P.; Provencio, P. N. *Science* **1998**, *282*, 1105–1107.

[36] Andrews, R.; Jacques, D.; Rao, A. M.; Derbyshire, F.; Qian, D.; Fan, X.; Dickey, E. C.; Chen, J. *Chem. Phys. Lett.* **1999**, *303*, 467–474.

[37] Srivastava, A.; Srivastava, O. N.; Talapatra, S.; Vajtai, R.; Ajayan, P. M. *Nat. Mater.* **2004**, *3*, 610–614.

[38] Shimoda, H.; Fleming, L.; Horton, K.; Zhou, O. *Physica B* **2002**, *323*, 135–136.

[39] Miller, S. A.; Martin, C. R. *J. Electroanal. Chem.* **2002**, *522*, 66–69.

[40] Miller, S. A.; Martin, C. R. *J. Am. Chem. Soc.* **2004**, *126*, 6226–6227.

[41] Cao, A. Y.; Dickrell, P. L.; Sawyer, W. G.; Ghasemi-Nejhad, M. N.; Ajayan, P. M. *Science* **2005**, *310*, 1307–1310.

[42] Li, X.; Zhun, G.; Dordick, J. S.; Ajayan, P. M. *Small* **2007**, *3*, 595–599.

[43] Niu, H. Y.; Cai, Y. Q.; Shi, Y. L.; Wei, F. S.; Liu, J. M.; Jiang, G. B. *Anal. Bioanal. Chem.* **2008**, *392*, 927–935.

[44] Du, Z.; Yu, Y.; Wang, J. *Anal. Bioanal. Chem.* **2008**, *392*, 937–946.

[45] Basheer, C.; Alnedhary, A. A.; Rao, B. S. M.; Valliyaveettil, S.; Lee, H. K. *Anal. Chem.* **2006**, *78*, 2853–2858.

[46] Peng, F.; Hu, C.; Jiang, Z. *J. Membr. Sci.* **2007**, *297*, 236–242.

[47] Wang, D.; Song, P.; Liu, C.; Wu, W.; Fan, S. *Nanotechnology* **2008**, *19*, 075609/1-6.

[48] Endo, M.; Muramatsu, H.; Hayashi, T.; Kim, Y. A.; Terrones, M.; Dresselhaus, M. S. *Nature* **2005**, *433*, 476.

[49] Kim, Y. A.; Muramatsu, H.; Hayashi, T.; Endo, M.; Terrones, M.; Dresselhaus, M. S. *Chem. Vap. Deposition* **2006**, *12*, 327–330.

[50] Jia, Y.; Wei, J. Q.; Shu, Q. K.; Chang, J. G.; Wang, K. L.; Wang, Z. C.; Luo, J. B.; Liu, W. J.; Zheng, M. X.; Wu, D. H. *Chin. Sci. Bull.* **2007**, *52*, 997–1000.

[51] Kulesza, S.; Szroeder, P.; Patyk, J. K.; Szatkowski, J.; Kozanecki, M. *Carbon* **2006**, *44*, 2178–2183.

[52] Wu, Z.; Chen, Z.; Du, X.; Logan, J. M.; Sippel, J.; Nikolov, M.; Kamaras, K.; Reynolds, J. R.; Tanner, D. B.; Hebard, A. F.; Rinzler, A. G. *Science* **2004**, *305*, 1273–1276.

[53] Sreekumar, T. V.; Liu, T.; Kumar, S.; Ericson, L. M.; Hauge, R. H.; Smalley, R. E. *Chem. Mater.* **2003**, *15*, 175–178.

[54] Kukovecz, A.; Smajda, R.; Konya, Z.; Kiricsi, I. *Carbon* **2007**, *45*, 1696–1716.

[55] Whitby, R. L. D.; Fukuda, T.; Maekawa, T.; James, S. L.; Mikhalovsky, S. V. *Carbon* **2008**, *46*, 949–956.

[56] Smajda, R.; Kukovecz, A.; Konya, Z.; Kiricsi, I. *Carbon* **2007**, *45*, 1176–1184.

[57] Zhang, M.; Fang, S.; Zakhidov, A. A.; Lee, S. B.; Aliev, A. E.; Williams, C. D.; Atkinson, K. R.; Baughman, R. H. *Science* **2005**, *309*, 1215–1219.

[58] Zhang, X. *Adv. Mater.* **2008**, *20*, 4140–4144.

[59] Andrews, R.; Jagtoyen, M.; Grulke, E.; Lee, K. H.; Mao, Z.; Sinnott, S. B. NASA Conference Publication (2001).

Capítulo 14

Sequential preconcentration and on-membrane Raman determination of carboxylic single-walled carbon nanotubes in river water samples

Analytical Chemistry 85 (2013) 10338-10343

Analytical Chemistry

85 (2013) 10338-10343

Sequential preconcentration and on-membrane Raman determination of carboxylic single-walled carbon nanotubes in river water samples

A. I. López-Lorente, M. L. Polo-Luque, M. Valcárcel

Department of Analytical Chemistry, University of Córdoba, E-14071 Córdoba, Spain.

This article proposes a simple and sensitive approach for the preconcentration and determination of carboxylated single-walled carbon nanotubes (c-SWNTs) in environmental samples using membranes modified with multiwalled carbon nanotubes (MWNTs). The method is based on the preconcentration of c-SWNTs and their direct on-filter Raman spectroscopic analysis. The preconcentration of c-SWNTs is performed by microfiltrating the sample through a cellulose membrane modified with MWNTs fabricated from a surfactant dispersion of the same. The analytes are retained in the membrane through π-π interactions with MWNTs forming the membrane. The G-/ D-band ratio of the carbon nanotubes has been used as an analytical parameter to quantify the presence of c-SWNTs, which mainly contribute to the intensity of the G band. The limit of detection was found to be 1 $\mu g \cdot L^{-1}$, and the precision, for a 10 $\mu g \cdot L^{-1}$ concentration of c-SWNTs, was 4.74% intramembrane and 6.3% intermembrane. The optimized procedure was successfully applied to the determination of traces of c-SWNTs in river water samples.

Keywords: multiwalled carbon nanotubes membranes, carboxylic single walled carbon nanotubes, Raman spectroscopy.

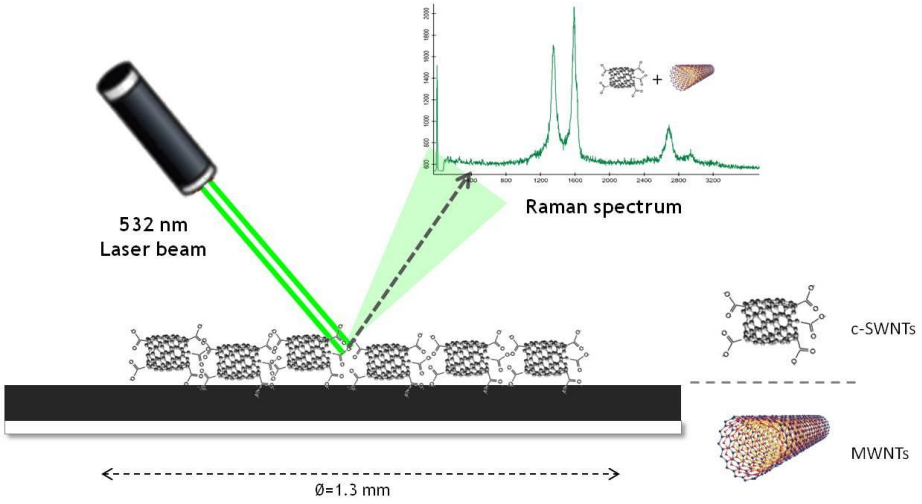
532 nm
Laser beam
Raman spectrum
c-SWNTs
MWNTs
Ø=1.3 mm

1. Introduction

Since their discovery in 1991 [1], carbon nanotubes (CNTs) have aroused great interest. The increasing use and disposal of these nanomaterials in different applications will lead to their accumulation in environmental matrixes. Despite the widespread use of nanomaterials, there is still a lack of analytical techniques to monitor their occurrence in environmental sectors. Probabilistic material flow analysis from a life-cycle perspective of engineered nanomaterials containing products has been used to predict the environmental concentration at which carbon nanotubes are expected to be present. In fact, Gottschalk et al. [2,3] predicted low CNTs concentrations in effluent from sewage treatment plants in Europe, which is a constraint from the point of view of the actual analytical methods available for CNT detection. Thus, analytical methods devoted to the determination of nanomaterials should satisfy several requirements such as being capable of detecting environmentally relevant concentrations as well as avoiding the potential interference of natural nanoparticles commonly present in environmental samples [4].

Carbon nanotubes are water-insoluble and tend to aggregate. Carboxylation is commonly used in industry to obtain stable water dispersions of nanotubes and to further CNT functionalize CNTs with carboxylic groups. The better debundled and individually suspended the CNTs are, the longer they remain in the water column [5]. Thus, oxidized CNTs might be one of the most likely forms of CNT pollutant in aqueous environment [6], making their determination highly important.

The potential of using CNT membranes to perform analytical separations has been demonstrated using membranes with both vertically aligned CNTs and CNT bundles [7]. CNT-modified membranes can be prepared by electrostatic or covalent interaction of CNTs with the corresponding membranes. Analyte adsorption is favored by π-π electrostatic interactions and the typically large

surface area of CNTs. Such CNT-modified filters are usually prepared by passing a dispersed solution of CNTs through a membrane. The nanotubes are dispersed by means of a surfactant such as sodium dodecyl sulfate (SDS) [8] or Triton X-100 [9] or solvents such as dimethyl sulfoxide (DMSO) [10]; alternatively, MWNTs functionalized with poly(diallyldimethylammonium chloride) [11] can be directly used. These membranes are available in various formats including cellulose ester membranes, poly(vinylidene difluoride) (PVDF) membranes, nylon-encased filters, and qualitative filter paper [7]. Commercially available MWNT-modified nylon filters have been used for the preconcentration and elution of c-SWNTs with electrophoretic determination [9].

Raman spectroscopy has emerged as a powerful technique for the characterization of carbon nanotubes [12], because Raman measurements are simple; can be performed at room temperature and under ambient pressure; and are rapid, nondestructive, and noninvasive [13]. In this sense, carboxylated single-walled carbon nanotubes (c-SWNTs) have been determined from environmental waters by their liquid-liquid microextraction in ionic liquids with imidazolium cation and subsequently quantified by Raman spectroscopy [14]. Moreover, c-SWNTs have been also determined by surface-enhanced Raman scattering (SERS) measurements on bare gold nanoparticles as a substrate [15].

In this work, a c-SWNTs preconcentration procedure is proposed that uses MWNT-modified cellulose acetate membranes. c-SWNTs are retained in the membrane through π-π interactions with carbon nanotubes forming the membrane. Moreover, in this case, c-SWNTs are directly measured on-membrane by Raman spectroscopy. The G-/D-band height ratio (obtained from the combined spectrum of both types of CNTs) is employed for the quantification of water samples containing c-SWNTs, because a higher ratio is observed when the amount of c-SWNTs deposited over MWNTs is increased. This simple procedure enables the sensitive determination of samples at low c-

SWNTs concentrations. MWNT membranes preconcentrate c-SWNTs and also facilitate their quantification by Raman spectroscopy.

2. Methods

2.1. Materials and reagents

SWNTs were obtained from Shenzhen Nanotech Port Co. Ltd (NTP) (Shenzhen, China), with a purity over 90%, an outer diameter of <2 nm, a length of 5-15 μm and a specific surface area of 500-700 m^2/g. MWNTs were provided by Bayer Material Science (Leverkusen, Germany), with a diameter between 5 and 20 nm and a length between 1 and 10 μm. H_2SO_4 and HNO_3 were purchased from Panreac (Barcelona, Spain). Triton X-100 was provided by Fluka, (Buchs, Switzerland). Cellulose acetate membranes of 0.2-μm pore size were purchased from Sartorius Stedim Biotech (Göttingen, Germany). Methanol, humic acids, and potassium hydroxide were purchased from Sigma-Aldrich.

2.2. Equipment

For Raman measurements, a confocal Raman spectrometer (alpha500; WITec GmbH, Ulm, Germany) was employed. For excitation, a frequency-double Nd:YAG laser at 532 nm (second harmonic generation) was used, which resulted in a penetration depth in silicon of about 0.5 μm. Raman spectra were collected using a 600 g mm^{-1} diffraction grating. The laser beam was focused on the sample surface using a 20x/0.4 Zeiss objective. Laser powers were measured directly on the sample stage and were typically between 0.5 and 1.5 mW. Raman spectra were collected with an integration time of 1 s, accumulating a total of 10 spectra.

A Vibracell 75041 ultrasonic probe (750 W, 20 KHz, Bioblock Scientific, Illkirch, France) equipped with a 3-mm probe was also employed to prepare the dispersions.

2.3. Functionalization of single-walled carbon nanotubes for method characterization

Carboxylated single-walled carbon nanotubes (c-SWNTs) were prepared by adding 100 mg of single-walled carbon nanotubes to 20 mL of a 3:1 H_2SO_4/HNO_3 mixture in a glass flask as described in ref [14], adapted from ref [16]. The mixture was refluxed for 1 h; after that, diluted fractions were centrifuged at 10000 rpm for 10 minutes and washed with water. The centrifugation process was repeated until the supernatant phase became neutral. Finally, carboxylated derivates were dried at 60ºC in a heater. After acid treatment, the SWNTs had covalently attached carboxylic (–COOH) groups on the sidewalls and the open ends, which, being negatively charged, made them highly water-soluble.

2.4. Preparation of multiwalled-carbon-nanotube-modified membranes

MWNTs (50 mg) were dispersed in 50 mL of a 0.5 % (w/v) Triton X-100 solution. Carbon nanotubes were dispersed by 5 min of ultrasonication using a Vibracell 75041 ultrasonic probe (750W, 20 KHz, Bioblock Scientific, Illkirch, France) equipped with a 3-mm probe set at 35% of amplitude to obtain a good dispersion of the nanotubes in the sample and ensure its homogeneity. Pulses of energy of 20 s on and 10 s off were employed in order to avoid sample heating.

Cellulose acetate membranes of 0.2 µm were modified with MWNTs. Five microliters of the MWNT solution in Triton X-100 were subjected to microfiltration using a homemade microfiltration device designed to allow filtration on a small surface (1.3-mm diameter of filtration). MWNTs are retained on the membrane, forming an entanglement of nanotubes that retains and preconcentrates carboxylated single-walled carbon nanotubes.

2.5. Preconcentration procedure

Carboxylic carbon nanotubes were preconcentrated from water matrixes (standards and river water samples) using a membrane modified with MWNTs that acted as a sorbent (see Figure 1). Water samples of 5 mL were subjected to microfiltration through a filtration diameter of 1.3 mm using the homemade device previously described. The filtration procedure was automated using a peristaltic pump that passes the water sample through the membrane at a constant flow rate.

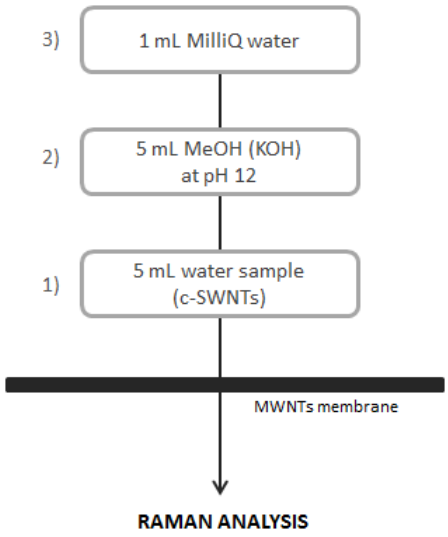

Figure 1. Scheme of the c-SWNTs preconcentration procedure.

After loading the water sample had been loaded, 5 mL of a KOH solution in methanol at pH 12 was passed through the membrane to remove possible interferences from components of the water sample such as humic acids. Then, 1 mL of water was subsequently passed. Then, the membrane was ready for Raman analysis to quantify the amount of c-SWNTs retained.

2.6. Raman spectroscopic analysis

Raman measurements were performed with a 532-nm laser. Both the acquisition time and the number of accumulated spectra for measuring a single Raman spectrum were optimized. A 1-s CCD exposure was used, with averaging of the Raman signal over 10 signal acquisitions. Raman measurements were acquired from five randomly selected locations within each membrane and repeated over three samples, giving a total of 15 Raman measurements for each nanotube concentration. For these measurements, a 20x objective was employed, resulting in a 109-μm-diameter area of measurement in each spot. It should be remarked the carbon nanotubes were confirmed to be homogeneously dispersed in the membrane because the spectra measured at different points of a sample provide similar signals.

The G-/D-band intensity ratio of carbon nanotubes was selected as the analytical signal. As the amount of c-SWNTs in the membrane increased, this ratio increased in comparison to that of an MWNTs membrane without c-SWNTs present. The use of the relationship between bands overcomes problems of reproducibility of Raman spectroscopy in quantitative analysis, regarding focusing or laser power between different samples.

3. Results and discussion

3.1. Foundation of the proposed method

The proposed method is based on the dual roles played by MWNTs retained in a membrane. First, they act as active components to increase the retention of the analytes (c-SWNTs) as a result of the well-known π-π interactions between them. Second, MWNTs facilitate Raman determination of the analytes owing to the fact that they are the spectral reference to show the presence of c-SWNTs in

the filter because of the increment of the G band as a function of the amount of analyte retained. The indicator parameter used is the G-/D-band intensity ratio.

3.2. Raman spectra of MWNTs and c-SWNTs

Raman spectra of single-walled carbon nanotubes show the radial breathing mode (RBM, 100-300 cm^{-1}), in which all carbon atoms vibrate in phase along the radial direction [17]. Moreover, the disorder peak (D peak, ~1350 cm^{-1}), stemming from the disorder-induced mode in graphite with the same name [18], and the tangential mode (G band, 1400-1700 cm^{-1}) also appear in the spectra, with these two bands being the most intense and the ones used in this work for quantification. The G band is composed of several peaks: G^+ associated with carbon-atom vibrations along the nanotube axis and G^- associated with vibrations of carbon atoms along the circumferential direction of the SWNTs. Its line shape depends on the metallic or semiconducting nature of the SWNT sample [19]. Finally, the second-order overtone of the D peak (G', 2500-2800 cm^{-1}) [19] can also be observed. The RBM band is characteristic of SWNTs and is sometimes observed in MWNTs with a small-diameter inner tube under good resonance conditions [20]. The spectral difference of carboxylated carbon nanotubes compared with pristine carbon nanotubes is a distinctive D-/G-band intensity ratio [21], whereas no spectral bands can be ascribed to COO^- groups.

For Raman scattering, MWCNTs can be said to be an ensemble of carbon nanotubes with diameters ranging from small to very large [13]. As a consequence of the large diameters of the outer tubes, many differences from SWNTs to graphite spectra are not as evident for MWNTs, such as for the above-mentioned RBM bands, as well as differences in G-band line shape. The splitting of the G band in MWNTs is small in intensity and smeared out by the effects of the diameter distribution [19]. As can be seen in Figure 2, a change in the G-band line shape is observed, along with variations in the G-/D-band

intensity ratio. Similar behavior has been observed in mixtures of SWNTs and MWNTs in surfactant solutions [12].

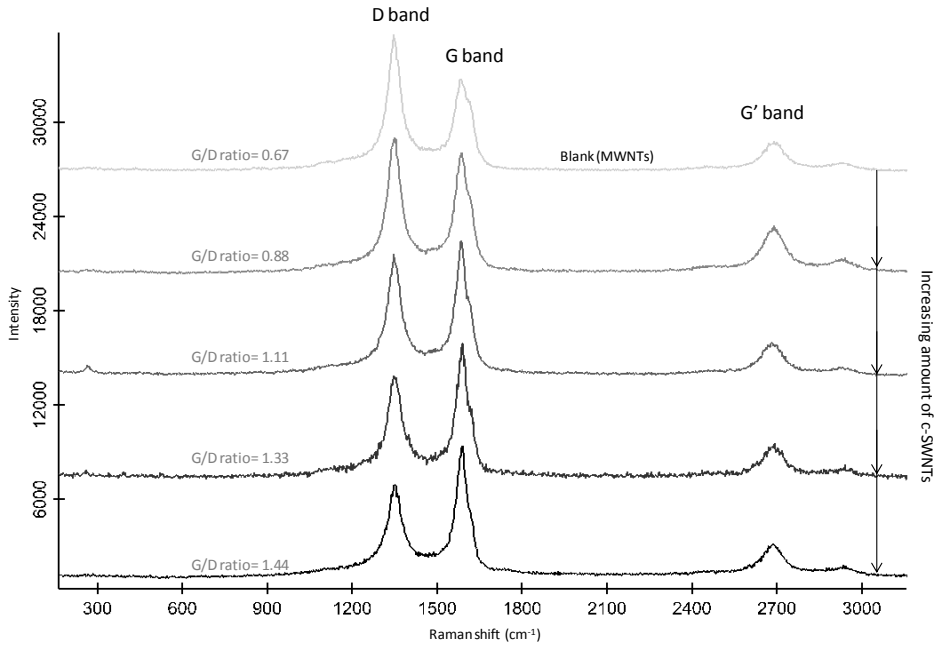

Figure 2. Evolution of G-/D-band height ratio with increasing amount of c-SWNT solution subjected to microfiltration through an MWNT-modified membrane.

In the case of MWNTs and SWNTs employed in this work, the G-/D-band ratios show different values. In the case of MWNTs, the intensity of the disorder peak (D band) is higher than that of the tangential mode (G band), whereas in the case of c-SWNTs, the behavior is the opposite, as was previously observed for surfactant solutions of carbon nanotubes [12]. As can be seen in Figure 2, when the amount of c-SWNTs retained on the membrane increased, the G-/D-band intensity ratio evolved, increasing in value as a result of a higher c-SWNTs contribution. This effect was employed to quantify the c-SWNTs preconcentrated on MWNTs-modified membranes. The use of the band ratio

overcomes limitations of Raman spectroscopy for quantitative analysis when directly measuring intensities of signal.

In our case, the possible use of RBM bands to quantify the samples was discarded because the absolute intensities of the radial breathing mode are dramatically reduced after functionalization [22] and, as can be seen in Figure 2, under our conditions, they were barely distinguishable.

3.3. Optimization of the procedure to disperse MWNTs

First, the procedure for the dispersion of MWNTs was optimized. Previous studies [12] confirmed the suitability of sodium dodecyl sulfate (SDS), cetyltrimethylammonium bromide (CTAB), and Triton X-100 for dispersing carbon nanotubes. Triton X-100 was the surfactant selected in this work for achieving a dispersion of MWNTs to enable the formation of a homogeneous modified membrane. To this end, Triton X-100 solutions were studied at different concentrations and a variety of conditions of agitation and/or radiation. To determine the optimum amount of surfactant necessary to achieve a homogeneous dispersion of carbon nanotubes, dispersions with a range of surfactant concentrations from 0.5 to 20% (w/v) were prepared, with a sample concentration of 1 $mg \cdot mL^{-1}$. Ultrasonication was performed with an ultrasonic probe (750W, 20 KHz) at 35% amplitude. Pulses of energy of 20 s on and 10 s off were employed to avoid sample heating. Five minutes proved to be sufficient to reach a stable solution of homogeneously dispersed MWNTs. A Triton X-100 concentration of 0.5% (w/v) was found to enable the stable dispersion of MWNTs and was selected for preparing modified membranes.

3.4. Selection of the nature and pore size of the membranes

To prepare MWNTs-modified membranes, the nature of the membrane that acts as the support of the MWNTs has to be selected. The suitabilities of

cellulose acetate, polyamide, polycarbonate, and polytetrafluoroethylene (PTFE) membranes were investigated. PTFE membranes were directly eliminated because they have a hydrophobic nature and a water solution of MWNTs did not pass through them. Cellulose acetate membranes provided better results in terms of the homogeneity of the MWNTs distribution, as observed by optical microscope photographs (see Figure 3), and cellulose acetate was thus selected as the supporting membrane material for the deposition of MWNTs. Such membranes do not interfere in Raman measurements and are not damaged during laser irradiation.

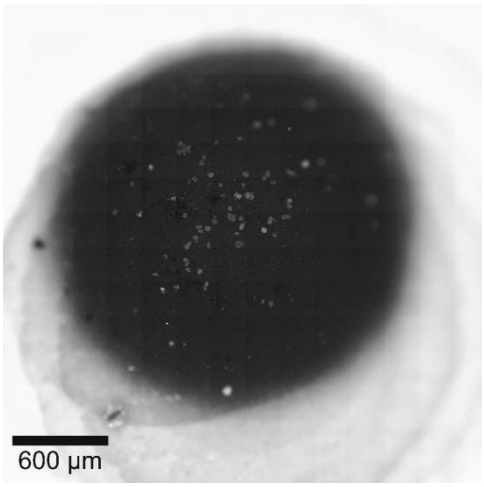

Figure 3. Optical microscope photograph of the MWNT-modified membrane selected as the sorbent for the preconcentration and determination of c-SWNTs**.**

Cellulose acetate membranes with different pore sizes, namely, 0.2 and 5 µm, were studied. Although both showed a homogeneous distribution of MWNTs, in the case of 5-µm pore-size membranes, the retention of MWNTs was not quantitative, and part of the MWNTs in the dispersion passed through the membrane. Thus, 0.2-µm-pore-size membrane was selected for further experiments.

3.5. Optimization of the amount of MWNTs dispersion to prepare the modified membranes

The amount of MWNTs forming the modified membranes plays a crucial role in the subsequent quantification of c-SWNTs present in the filtrated water samples, because the G-/D-band intensity ratio is affected by the signals of both MWNTs and c-SWNTs. Thus, the amount of MWNTs loaded on the membrane was optimized. A 1 $mg \cdot mL^{-1}$ solution of MWNTs dispersed in 0.5% Triton X-100 solution was employed to prepare the membranes. A volume range between 1 and 20 µL was investigated, for a fixed amount of c-SWNTs loaded onto the different membranes (2 mL of water solution of 40 $\mu g \cdot L^{-1}$ concentration of c-SWNTs).

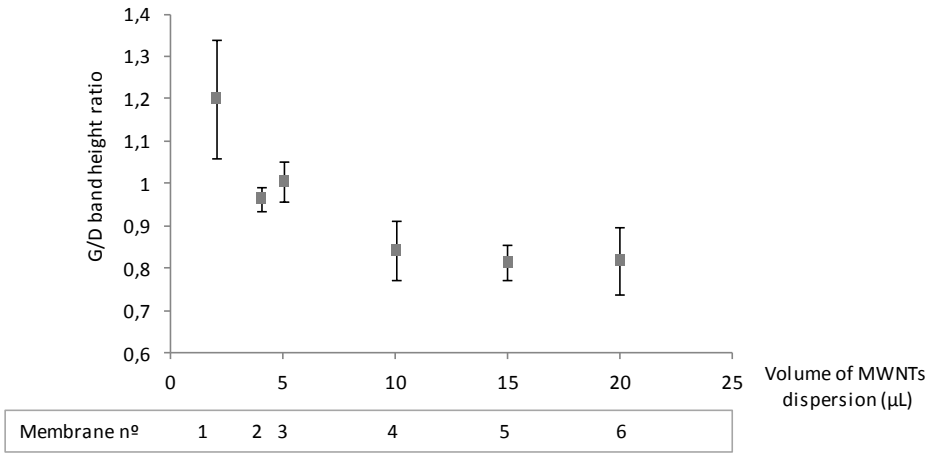

Figure 4. Study of the influence of the volume of the MWNT dispersion in 0.5% Triton X-100 loaded onto the membrane to form the modified membranes in terms of G-/D-band height ratio for a fixed concentration of c-SWNTs standard solution subjected to microfiltration on different membranes.

As can be seen in Figure 4, for a lower amount of MWNTs for the same c-SWNTs quantity in the membrane, there is a major contribution of the latter

to the analytical signal because the G-/D-band intensity ratio is higher. Thus, lower amounts of MWNTs, on the one hand, favor the more sensitive detection of c-SWNTs and, on the other hand, avoid saturation of the membrane when the water samples are loaded. However, very low amounts of MWNTs solution lead to less homogeneous membranes, decreasing the reproducibility of the measurements.

Moreover, MWNT solutions at different concentrations, in the range between 0.1 and 1 $mg \cdot mL^{-1}$, were prepared, and 5-µL samples were loaded onto the cellulose membrane. Finally, 5 µL of 1 $mg \cdot mL^{-1}$ MWNT solution was selected to form homogeneous MWNT-modified cellulose membranes.

3.6. Optimization of sample volume

The volume of water sample loaded onto the membrane was also studied. Using membranes prepared at the previously optimized conditions, different volumes of a 40 $\mu g \cdot L^{-1}$ solution were subjected to microfiltration in the range between 1 and 30 mL. The study was repeated for a 1 $\mu g \cdot L^{-1}$ solution of c-SWNTs. When the volume of c-SWNTs solution subjected to microfiltration on the membrane was increased, the signal of G-/D-band height ratio increased until a certain volume, when saturation of c-SWNTs on the membrane occurred in the case of studies at higher concentration levels. The behavior found fitted a Langmuir isotherm model, which reflects the adsorption of the c-SWNTs onto the MWNTs forming the membrane. Equilibrium has to be reached between loading higher volumes of sample, with the consequent time consumption, to increase the sensitivity of the method and achieving rapid and reproducible measurements. For further experiments, 5 mL was selected as the volume of the water sample loaded onto the membrane.

3.7. Study of influence of water sample pH and ionic strength

We studied the influence of the sample pH on the c-SWNT preconcentration stage. Freshly prepared original c-SWNTs suspensions have an initial pH between 3 and 5. Changing the pH of a 40 $\mu g \cdot L^{-1}$ c-SWNT water solution in the pH range between 2 and 10 does not give rise to considerable effects in the preconcentration stage.

On the other hand, increasing the ionic strength by adding greater amounts of NaCl did not improve the preconcentration of c-SWNTs on the MWNT-modified membranes.

3.8. Study of humic acids as potential interferents

In environmental waters, carbon nanotubes can be stabilized through interactions with natural ligands, such as humic acids. Hence, we studied the potential effect of humic acids in the concentration range from 0 to 40 $mg \cdot L^{-1}$. As shown in Figure 5, increasing the concentration of humic acids in water samples significantly lowered the signal of c-SWNTs. To overcome the limitation of the humic acid content in the sample affecting the analytical signal, prior to analysis, 5 mL of a KOH solution in methanol at pH 12 was passed through the membrane to remove humic acids retained on it. Later, 1 mL of ultrapure water was passed, and the membrane was ready for subsequent Raman analysis. The recoveries obtained after this cleanup step were similar to those obtained in standards in which no humic acids were present.

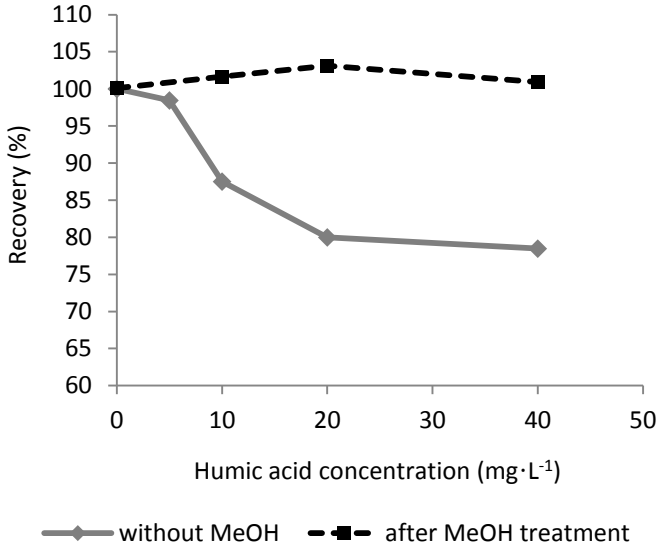

Figure 5. Recoveries obtained for standards with different spiked humic acid concentrations (5, 10, 20, and 40 $mg \cdot L^{-1}$) compared to standards without humic acid content. Solid line, procedure without methanol basic solution cleaning step; dotted line, after introduction of a cleaning step with methanol basic solution (pH 12) to remove humic acids retained in the membrane.

The possible influence of other compounds present in sediment-loaded water of flowing rivers, such as aluminosilicates or sand, was not tested. In principle, such compounds should not interfere in Raman spectra of CNTs because their spectral features appear in a lower-frequency region than the range at which the carbon nanotubes D- and G- bands appear. Anyway, when passing the KOH solution in methanol through the membrane, aluminosilicates [23] may be solubilized and removed, preventing collapse of the membrane. In fact, as explained below, no interferences were found when spiked river water samples were analyzed.

3.9. Analytical features of the proposed method

The analytical performance of the proposed method was studied to evaluate its usefulness for quantitative analyses. The analytical signal, namely, the ratio of the peak height of the 1583 cm^{-1} Raman G band to the peak height of the 1350 cm^{-1} D band, was plotted against the c-SWNTs concentration for standard solutions.

The calibration curve was determined for concentrations ranging from 0 to 15 $\mu g \cdot L^{-1}$. Each concentration level was analyzed in triplicate (measuring each sample at five randomly selected locations in the membrane). Thus, the data points represent mean values corresponding to three independent membranes, where the value for each individual membrane is the average of five measurements at different spots. The response was linear in the range of concentrations tested (R^2 = 0.990). Concentrations above that range resulted in saturation of the membrane, and the corresponding response was fit to a Langmuir isotherm.

The precision of the measurements was evaluated at a concentration of 10 $\mu g \cdot L^{-1}$, giving a relative standard deviation (n = 5) of 4.74 % for measurements within a membrane and 6.3% for measurements in different membranes. The analytical features of the method developed are summarized in Table 1.

The detection and quantification limits were calculated as 3 and 10 times the signal of S_a between the scope and were 1.007 and 3.36 $\mu g \cdot L^{-1}$, respectively. The limit of detection is restricted by the fact that, as less concentrated CNT solutions are, higher interferences due to nanotubes fluorescence are observed. Despite the loading of larger volumes, the more isolated distribution of c-SWNTs at low concentrations within the membrane led to high fluorescence interferences.

Table 1. Analytical features of the method.

Calibration equation	S = (0.038±0.001)[c-SWNTs][a]+(0.66±0.01)
R^2	0.990
Lineal range	1-15 μg·L^{-1}
LOD[b]	1.007 μg·L^{-1}
RSD[c] (%) (intramembrane)	4.7%
RSD[d] (%) (intermembrane)	6.3%

[a][c-SWNTs] represents the concentration of c-SWNTs in the aqueous medium in μg·L^{-1}.
[b]Limit of detection, determined as ($3S_a$)/b, for y=bx+a.
[c]Relative standard deviation, determined from five measurements of 5 mL 10 μg·L^{-1} c-SWNTs within the same membrane.
[c]Relative standard deviation, determined from the average value of five measurements of 5 mL 10 μg·L^{-1} c-SWNTs in different membranes.

3.10. Application to the determination of carboxylated carbon nanotubes in river water samples

To validate the proposed method, water samples from Guadalquivir River were analyzed following the recommended procedure. No carbon nanotubes were found in the samples. Therefore, the samples were spiked and analyzed using the proposed methodology.

To demonstrate the accuracy of the proposed method, a recovery test of the analysis of spiked river water samples was also carried out. For the recovery study, four fortification levels were assayed; the recoveries values are reported in Table 2. The obtained recoveries were between 80.6% and 111% depending on the concentration level. Each sample was analyzed in triplicate to evaluate the precision of the method. The coefficients of variation ranged from 8.98% to 15.4%.

If the G-/D-band intensity ratio of an unknown CNT samples needs to be calculated, a two-filter assay can be carried out, using a nonmodified membrane to calculate G-/D-band intensity ratio and an MWNT-modified membrane to quantify the amount of CNTs present.

Table 2. Recovery study of spiked river samples.

	Concentration of c-SWNTs ($\mu g \cdot L^{-1}$)			
Sample	added	found[a]	Recovery (%)	RSD (%)
1	2	2.0±0.3	89.3-111	15.4
2	5	4.9±0.5	80.6-107.6	10.7
3	10	9±1	85.6-110.3	12.5
4	15	14±1	88.3-106.2	8.98

[a]Average of three independent spiked samples±CI ($p < 0.05$).

4. Conclusions

A simple and sensitive c-SWNTs preconcentration procedure has been proposed. MWNT-modified membranes have been fabricated using commercially available cellulose acetate membranes and surfactant dispersions of MWNTs. c-SWNTs were retained in the membranes through π-π interactions with the multiwalled carbon nanotubes forming the membrane. On-membrane Raman measurements were directly performed to quantify the presence of c-SWNTs by using carbon nanotubes G-/D-band intensity ratio as the analytical signal. The use of this parameter overcomes limitations of Raman spectroscopy for quantitative analysis.

This simple procedure enabled the sensitive determination of samples at low c-SWNTs concentrations. The limit of detection achieved with the proposed

procedure improves upon most of those reported to date. This method was applied to the determination of c-SWNTs in river water samples. Moreover, the availability of portable Raman spectrometers could enable in situ monitoring of the release of these materials at source points of contaminations.

Finally, in this work, the two facets of analytical nanoscience and nanotechnology have been covered. On one hand, MWNTs are used as analytical tools to form modified membranes that improve the preconcentration stage. On the other hand, c-SWNTs are considered the target of the analysis, that is, in this case, this nanomaterial is considered an object to be determined and quantified.

Acknowledgments

The authors thank Spain's Ministry of Innovation and Science for funding Project CTQ2011-23790 and Junta de Andalucía for Project FQM4801. A.I.L.-L. also thanks the Ministry for the award of a Research Training Fellowship (Grant AP2008-02939).

The authors declare no competing financial interest.

References

[1] Iijima, S.; *Nature* **1991**, *354*, 56–58.

[2] Gottschalk, F.; Sonderer, T.; Scholz, R.W.; Nowack, B. *Environ. Sci. Technol.* **2009**, *43*, 9216–9222.

[3] Gottschalk, F.; Sonderer, T.; Scholz, R.W.; Nowack, B. *Environ. Toxicol. Chem.* **2010**, *29*, 1036–1048.

[4] Simonet, B.M.; Valcárcel, M.; *Anal. Bioanal. Chem.* **2009**, 393, 17–21.

[5] Schwyzer, I.; Kaegi, R.; Sigg, L.; Magrez, A.; Nowack, B. *Environ. Pollut.* **2011**, *159*, 1641–1648.

[6] Yang, S.T.; Wang, H.; Wang, Y.; Wang, Y.; Nie, H.; Liu, Y. *Chemosphere* **2011**, *82*, 621–626.

[7] López-Lorente, A.I.; Simonet, B.M.; Valcárcel, M.; *Anal. Chem.* **2010**, 82, 5399–5407.

[8] Niu, H. Y.; Cai, Y. Q.; Shi, Y. L.; Wei, F. S.; Liu, J. M.; Jiang, G. B. *Anal. Bioanal. Chem.* **2008**, *392*, 927–935.

[9] Suárez, B.; Moliner-Martínez, Y.; Cárdenas, S.; Simonet, B. M.; Valcárcel, M. *Environ. Sci. Technol.* **2008**, *42*, 6100–6104.

[10] Brady-Estévez, A. S.; Kang, S.; Elimelech, M. *Small* **2008**, *4*, 481–484.

[11] Du, Z.; Yu, Y.; Wang, J. *Anal. Bioanal. Chem.* **2008**, *392*, 937–946.

[12] López-Lorente, A.I.; Simonet, B.M.; Valcárcel, M.; *Analyst* **2013**, 138, 2378–2385.

[13] Jorio, A.; Pimenta, M.A.; Souza Filho, A.G.; Saito, R.; Dresselhaus G.; Dresselhaus, M.S.; *New J. Phys.* **2003**, 5, 1.1–1.17.

[14] López-Lorente, A.I.; Simonet, B.M.; Valcárcel, M. *Talanta* **2013**, *105*, 75–79.

[15] López-Lorente, A.I.; Simonet, B.M.; Valcárcel, M. *Anal. Chim. Acta* **2013**, 788, 122–128.

[16] Xue, W.; Cui, T.; *Nanotechnology* **2007**, 18, 145709/1–145709/7.

[17] Liu, Z.; Zhang, J.; Gao, B.; *Chem. Commun.* **2009**, 45, 6902–6918.

[18] Tuinstra, F.; Koening, J.L.; *J. Phys. Chem.* **1970**, 53, 1126–1130.

[19] Dresselhaus, M.S.; Dresselhaus, G.; Saito, R.; Jorio, A.; *Physics Reports* **2005**, 409, 47–99.

[20] Benoit, J.M.; Buisson, J.P.; Chauvet, O.; Godon, C.; Lefrant, S. *Phys. Rev. B* **2002**, *66*, 073417.

[21] Lachman, N.; Sui, X.; Bendikov, T.; Cohen, H.; Wagner, H.D. *Carbon* **2012**, *50*, 1734–1739.

[22] Hussain, S.; Jha, P.; Chouksey, A.; Raman, R.; Islam, S.S.; Islam, T.; Choudhary, P.K.; Harsh; J. *Modern Physics* **2011**, 2, 538-543.

[23] Gasteiger, H.A.; Frederick, W.J.; Streisel, R.C.; *Ind. Eng. Chem. Res.* **1992**, 31*,* 1183-1190.

RESULTADOS Y DISCUSIÓN

VI

BLOQUE VI

RESULTS AND DISCUSSION

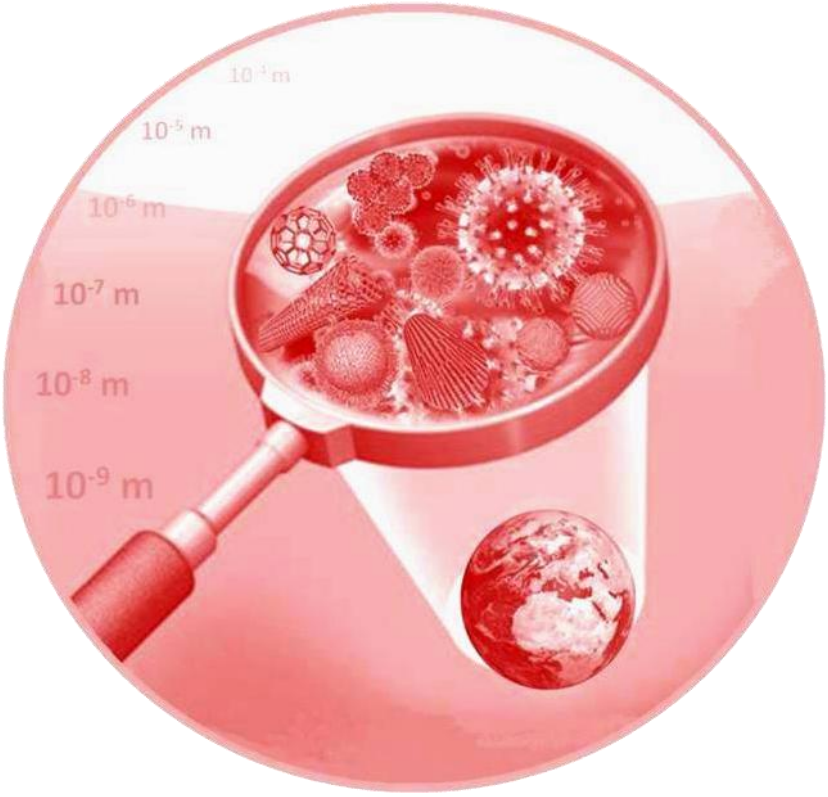

The main results of the research developed in this Doctoral Thesis are summarized in this part. Since the Memory is a compilation of articles and the specific results of each paper have been previously discussed, the aim of this section is to give an integral approach to the experimental work performed and presented along the Memory, by comparing the strengths and drawbacks of each of them.

This block has been structured differently from the general scheme of the Thesis. It is divided into three sections, the first devoted to carbon nanostructures, another focused on metallic nanoparticles, and, finally, a section dealing with the different facets of nanoparticles in Analytical Nanoscience and Nanotechnology (AN&N), this is, objects or tools, introducing a third facet, as interface between those, which is the use of nanoparticles as tools for the determination of other nanomaterials. The two first sections have been in turn divided into methods of characterization and/or determination of nanoparticles.

Table VI.1 gathers the different groups in which the developed work can be classified and supports the scheme of this block.

Table VI.1. Classification of different approaches to the determination/characterization of NPs developed in this Doctoral Thesis

TYPES OF NANOPARTICLES	ANALYTICAL OBJECTIVE	ANALYTICAL NANOSCIENCE AND NANOTECHNOLOGY	
		NANOPARTICLES AS OBJECTS	NANOPARTICLES AS TOOLS(*)
CARBON NANOPARTICLES	CHARACTERIZATION	• SWNTs Raman characterization: influence of aggregation (chapter 5) • Mixtures of surfactant-dispersed SWNTs and MWNTs (chapter 6)	-
	DETERMINATION	• c-SWNTs by MWNTs modified membranes (chapter 14) • c-SWNTs by ionic liquid microextraction (chapter 11) • c-SWNTs by SERS (chapter 12)	• MWNTs modified membrane for determining c-SWNTs (chapter 14)
METALLIC NANOPARTICLES	CHARACTERIZATION	• Synthesis of bare AuNPs (chapter 3 and 4) • Bare AuNPs by IR-ATR (chapter 7) • Citrate coated AuNPs and AgNPs by CE (chapter 9)	-
	DETERMINATION	• AuNPs by ionic liquid microextraction (chapter 10)	• AuNPs as SERS substrates for determining c-SWNTs (chapter 12)

(*) Use of nanoparticles for the determination of other nanomaterials

The main targets of this Thesis are the development of methods of both characterization and determination of nanoparticles. As can be seen in Figure VI.1 characterization encompasses determination, which has analytes as targets. Objects or systems are characterized, being related with knowledge in the primary data-information (provided by analytes)-knowledge hierarchy. In the analytical-chemical context information is related to qualitative and quantitative results, while knowledge is related with reports. Characterization can be defined as the identification and/or quantification of specific properties or characteristics of the sample or material[1]. On the other hand, determination can be considered as the application of the complete analytical process for detecting, identifying and quantifying an analytical parameter[2].

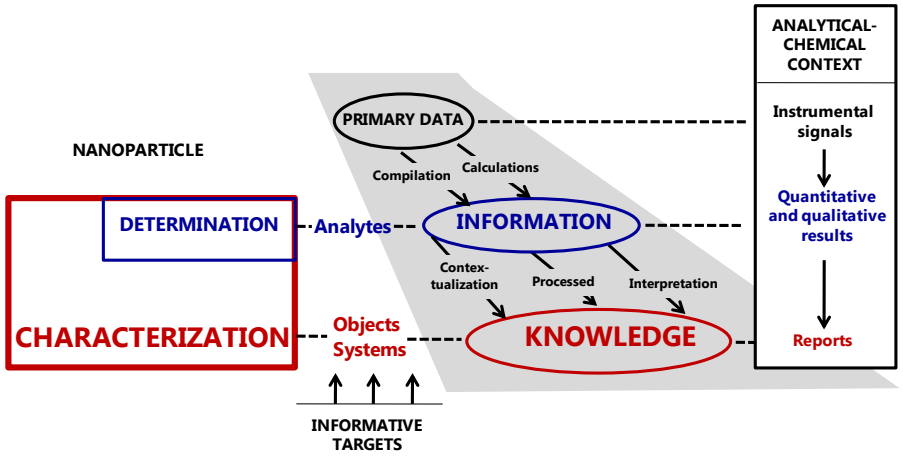

Figure VI.1. Differentiation between characterization and determination in the analytical-chemical context and their relationship with primary data-information-knowledge hierarchy.

Several techniques have been used to address the characterization and determination of carbon nanomaterials (carbon nanotubes) and metallic

[1] E. Prichard, Analytical measurement terminology (2001), LGC/RSC.
[2] L. Cuadros, L. Gámiz, A. Carrasco, C. Ruiz, Glossary of Analytical Terms, 1ª ed. GRASEQA.

nanoparticles (gold and silver nanoparticles). Figure VI.2 summarizes the main techniques employed for this task. The edges of the tetrahedron show techniques used for characterization/determination of carbon nanotubes or gold nanoparticles. SERS is included in the face comprised between carbon nanotubes-gold nanoparticles-determination vertexes since it employed gold nanoparticles as tools for the determination of carbon nanotubes. As can be seen, Raman spectroscopy is the predominant technique used for carbon nanotubes, while in the case of gold nanoparticles a broader range of techniques have been used, especially for studying those bare gold nanoparticles obtained through a new synthetic route proposed in this Thesis.

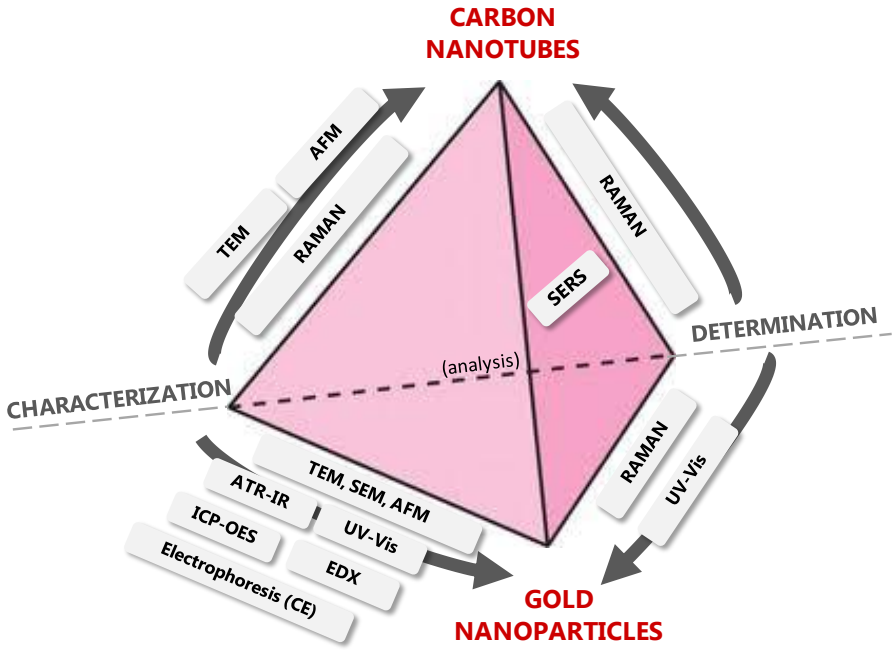

Figure VI.2. Techniques employed for the characterization and determination of the main nanostructures subject of this Thesis: carbon nanotubes and gold nanoparticles.

VI.1. CARBON NANOPARTICLES

Raman spectroscopy is a powerful technique for the characterization and determination of carbon nanotubes. The resonant Raman scattering from carbon nanotubes generates an intense and easily measurable signal. Raman measurements are simple, can be performed at room temperature and under ambient pressure, being non-destructive, hence its widespread use.

Traditional Raman studies of CNTs have focused on the radial breathing mode (RBM, 100-300 cm^{-1}), which appears in the case of SWNTs, a mode where all atoms vibrate in phase in the radial direction. Its frequency inversely depends on the diameter of the tube[3]. The two other energy regions of most interest in Raman spectra of CNTs are the disorder peak, D mode, around 1350 cm^{-1} and the tangential mode, G band, around 1400-1700 cm^{-1}. In addition, the second-order overtone of the D peak, G' band, is also observed around 2500-2800 cm^{-1}.

Characterization/determination of carbon nanotubes was carried out with various types of Raman spectrometers showing different performances. Table VI.2 summarizes the main characteristics of each spectrometer and measurements performed with each of them. As described in block 2 of this Thesis ("Analytical tools"), two portable Raman equipments have been used along the experimental work, i-Raman BWS415 (Raman portable 1) for characterization of SWNTs and MWNTs and inno-Ram (Raman portable 2) for determination of c-SWNTs, both of B&W TEK Inc. Moreover, a confocal Raman spectrometer has been also employed both for the characterization and determination of CNTs.

[3] C. Thomsen, S. Reich, J. Maultzsch, Phil. Trans. R. Soc. Lond. A 362 (2004) 2337–2359.

Table VI.2. Comparison of the characteristics and performance of Raman spectrometers employed along this Thesis.

	Portable Raman spectrometer 1	Portable Raman spectrometer 2	Confocal Raman microscope
Characterization	✓		✓
Determination		✓	✓
Type of sample	Surfactant dispersion of CNTs (liquid sample) (C-6)	c-SWNTs extracted in IL deposited on cellulose membrane (C-11)	Solid CNTs (C-5 and C-6)
			Drop-dried CNTs from ethanol and surfactant dispersion (C-5)
		c-SWNTs deposited on SERS substrate (C-12)	c-SWNTs deposited on MWNTs membrane (C-14)
Laser wavelength	785 nm (red)	785 nm (red)	532 nm (green)
Laser power	354 mW	5.7 mW (C-12) 28.5 mW (C-11)	0.5-1.5 mW
Raman images	x	x	✓
¿Solid sample measurements?	No	Yes	Yes
Optical microscope for sample focusing	No	Yes	Yes
Measurements conditions (single spectrum)	50 sec 6 acq	1 sec 10 acq	1 sec 10/20 acq
Measurements conditions (Raman images)	-	-	0.05-0.1 s integration time

1.1. Characterization of carbon nanotubes

In this Thesis, both SWNTs and MWNTs of different nature have been characterized by using Raman spectroscopy. Table 1 of Chapter 6 shows the characteristics of the carbon nanotubes subject to study: six types of MWNTs and one of SWNTs.

As can be seen in Table VI.2 two different Raman spectrometers have been employed for this task. Carbon nanotubes samples can be damaged during data capture. Measurements of solid samples of CNTs with the portable Raman spectrometer 1 resulted in sample damage, since it does not allow setting very low laser power. Measurements of carbon nanotube powders were achieved with a confocal Raman spectrometer coupled to an optical microscope which allows sample focusing. However, this equipment is more than ten times more expensive than the portable one.

Different strategies have been carried out in order to prepare CNTs for Raman characterization, namely:

- As received solid CNTs were placed on a microscope glass slide for measurements of solid samples (Chapter 5 and 6).
- As received SWNTs were dispersed in ethanol and ultrasonicated in an ultrasound bath (50 W, 10 min). The dispersion was then drop-dried on a microscope glass slide. Nanotubes aggregated as ethanol was evaporating, although the size of aggregates was smaller than in an untreated solid sample (Chapter 5).
- SWNTs were also dispersed in 5 wt/vol% Triton X-100 solution by using an ultrasonic probe for 10 min (750 W, 20 KHz) equipped with a 3 mm probe set at 20% amplitude. Pulses of energy of 20 s on and 20 s off were employed in order to avoid sample heating. Once dispersed, the dispersion was drop-dried on a glass slide (Chapter 5).

- SWNTs and MWNTs were dispersed in a 10 wt/vol% SDS, Triton X-100 and CTAB solutions. CNTs were placed in a mortar and crushed with a few microlitres of the surfactant solution in order to achieve a better dispersion. The solution was then dispersed by ultrasonic irradiation in a bath sonicator (60 Hz) for 10 min. In this case measurements were directly performed on the dispersion, which was placed on a polyethylene home-made vial with a diameter of 0.5 cm (Chapter 6).

Different surfactants have been evaluated to achieve CNTs dispersion, namely anionic sodium dodecylsulfate (SDS), cationic cetyltrimethylammonium bromide (CTAB) and neutral Triton X-100. The selected concentration was 10%wt/vol, higher concentrations resulting in background noise. This concentration is below the critical micellar concentration for all of them. The mechanism of dispersion entails that surfactant molecules orient themselves with the hydrophobic tail group facing the nanotube surface and the hydrophilic head groups to the aqueous phase[4]. The dispersing power of surfactants was proved to be: Triton X-100>CTAB>SDS. CTAB has a longer alkyl chain length than SDS, so the adsorption may be induced by hydrophobic interactions. Triton X-100 has the higher dispersing power by virtue of its aromaticity, thank to π-π stacking type interactions.

As previously mentioned, two ultrasonication strategies have been employed: an ultrasonication bath, which provide softer conditions (50 W, 60 Hz), and an ultrasonic probe (750 W, 20 KHz). The last apparatus enables better dispersion of nanomaterials needing less surfactant concentration. No degradation or shortening of CNTs was observed after sonication treatment at selected conditions.

[4] R. Rastogi, R. Kaushal, S.K. Tripathi, A.L. Sharma, I. Kaur, L.M. Bharadwaj, J. Colloid Interf. Sci. 328 (2008) 421-428.

Table VI.3. Raman wavenumbers of D- and G-bands and I_D/I_G ratio for the different CNT surfactant dispersions and solid CNTs samples.

	SDS			Triton X-100			CTAB			Solid	
	D-band wavenumber (cm^{-1})	G-band wavenumber (cm^{-1})	I_D/I_G ratio	D-band wavenumber (cm^{-1})	G-band wavenumber (cm^{-1})	I_D/I_G ratio	D-band wavenumber (cm^{-1})	G-band wavenumber (cm^{-1})	I_D/I_G ratio	D-band wavenumber (cm^{-1})	G-band wavenumber (cm^{-1})
MWNTs-1	1309±1	1594±1	1.76±0.07	1311±1	1601±2	2.06±0.05	1306±1	1602±3	2.01±0.09	1340±1	1571±1
MWNTs-2	1308±1	1596±1	1.8±0.2	1307±1	1603±1	1.8±0.1	1308±1	1605±2	1.63±0.08	1345±2	1578±3
MWNTs-3	1308±1	1589±1	1.8±0.2	1303±1	1606±1	1.43±0.09	1305±1	1606±1	1.9±0.2	1343±2	1577±2
MWNTs-4	1304±1	1605±2	2.1±0.1	1306±2	1601±2	2.27±0.08	1305±1	1601±2	2.38±0.06	1342±1	1581±1
MWNTs-5	1303±1	1600±1	2.06±0.03	1306±1	1603±1	2.02±0.09	-	-	-	1344±2	1578±3
MWNTs-6	1303±1	1595±1	1.06±0.1	-	-	-	1308±1	1600±1	1.75±0.06	1337±2	1576±1
SWNTs	1304±2	1580±1	0.539±0.008	1300±1	1581±1	0.44±0.06	1303±1	1582±2	0.49±0.01	1343±3	1584±4

The D-/G-band intensity ratio was calculated for each nanotube dispersed with different surfactants, as well as the D- and G-band wavenumbers evaluated for both suspensions and solid CNTs samples. Table VI.3 summarizes the values found. As can be seen, in the case of MWNTs, D-to G-band intensity ratio values are greater than 1, whereas in the case of SWNTs this ratio decreases to values around 0.5, depending on the surfactant employed for dispersion.

The most prominent variation in the spectra of solid to surfactant-dispersed CNTs is a shift of Raman features. The D band shows a shift in the range of 30-40 cm^{-1} from solid to dispersed samples. Again a shift of 0-30 cm^{-1} is observed for G-band. In the case of SWNTs, G-band from dispersed to solid samples showed no significant shift, appearing that of dispersed ones at lower wavenumbers as compared with MWNTs dispersions. The observed downshift and upshift may be attributed to the influence of laser wavelength[5] (measurements of solid samples were performed with a 532 nm laser and dispersions at 785 nm) and debundling of carbon nanotubes. In fact, different transitions energies have been observed for individual suspended SWNTs wrapped by surfactants and SWNTs in bundles[6] as well as a shift to higher wavenumbers of MWNTs upon debundling[7].

The suitability of Raman spectroscopy to identify and quantify the presence of SWNTs in MWNTs mixtures has been proved. A linear relationship exists between the percentage of SWNTs in the mixture and D-/G-band intensity or full width at half maximum ratios. A variation in G band lineshape has also been observed. G band was fit to a Lorentzian lineshape, a shoulder being observed when varying the percentage of SWNTs. The presence of both SWNTs and

[5] H.M. Heise, R. Kuckuck, A.K. Ojha, A. Srivastava, V. Srivastava, B.P. Asthana, J. Raman Spectrosc. 40 (2009) 344-353.
[6] R. Graupner, J. Raman Spectrosc. 38 (2007) 673-683.
[7] M. Dresselhaus, G. Dresselhaus, R. Saito, A. Jorio, Phys. Rep. 409 (2005) 47-99.

MWNTs was analyzed by deconvoluting their contribution to the band lineshape (see Figure VI.3).

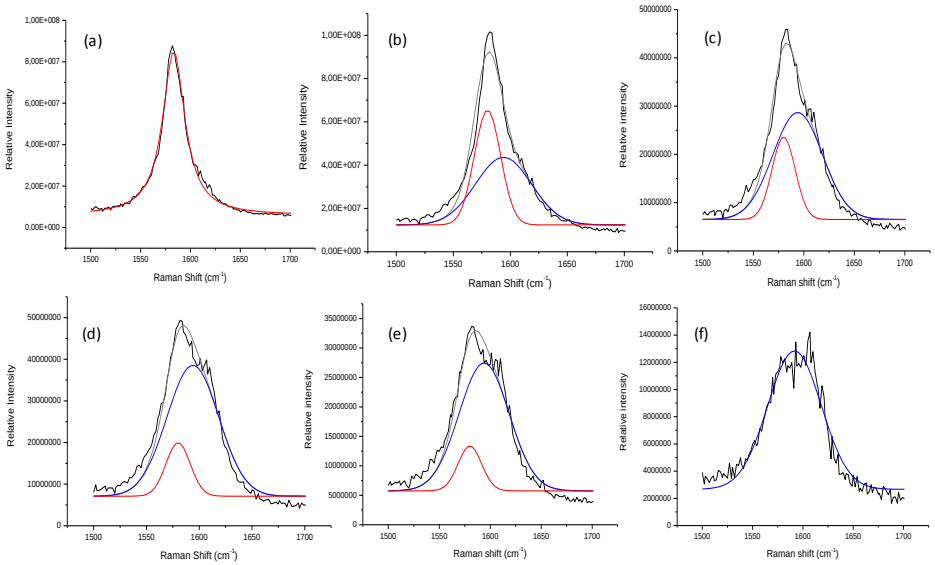

Figure VI.3. G band feature for (a) 100%wt/vol SWNTs dispersion, (b) 80%wt/vol SWNTs, (c) 60%wt/vol SWNTs, (d) 40%wt/vol SWNTs, (e) 20%wt/vol SWNTs and (f) 0% SWNTs (100%wt/vol MWNTs) surfactant dispersion. The peak has been fitted with a Lorentzian lineshape and deconvoluted to show the contribution of each type of nanotube to the G band feature.

Furthermore, it has been demonstrated (see Chapter 5 of this Thesis) that aggregation state of SWNTs has to be taken into account when measuring Raman spectrum since it affects to the G-/D-band intensity ratio, usually employed to discuss sample purity. Once discarded the influence of laser beam or sample focusing, the impact of aggregation was proved by K-nearest neighbors' classification of a Raman image composed by a set of spectra with different aggregation state into three different classes according to G-/D-band intensity ratio. When analyzing debundled SWNTs, previously dispersed with the aid of surfactants, the reproducibility of the measurements was consistent. MWNTs samples showed to be less sensitive to changes of aggregation state.

1.2. Determination of carbon nanotubes

Carboxylation is commonly employed in industry to achieve aqueous dispersion of CNTs. As much debundled CNTs are, the longer they remain in the water column and may be present in aqueous environmental compartments. In this Doctoral Thesis three methods have been developed for the determination of carboxylated single walled carbon nanotubes (c-SWNTs) in river water samples. The different strategies for achieving this task are compared in Table VI.4.

Table VI.4. Comparison of the different strategies for the determination of c-SWNTs in river water samples.

	Chapter 14	Chapter 11	Chapter 12
Analyte	c-SWNTs	c-SWNTs	c-SWNTs
Mediated by	MWNTs	Ionic liquids	AuNPs
Detection	Confocal Raman	Raman (portable 2)	SERS (Raman portable 2)
Analytical signal	G-/D-band intensity ratio	CNTs D band to PF_6^- band ratio	G band intensity
Measurement platform	Cellulose membranes 0.2 μm pore size	Cellulose membranes 5 μm pore size	Cellulose membranes 0.2 μm pore size
Laser wavelength	532 nm	785 nm	785 nm
Laser power	0.5-1.5 mW	28.5 mW	5.7 mW
Measurement conditions	1 s, 10 acq	1 s, 10 acq	1s, 10 acq
Interference study	Yes	No	No
LOD	1.007 μg L^{-1}	50 μg L^{-1}	10 μg L^{-1}
RSD (%)	6.3	12.6	10.5
Recoveries from spiked river water (%)	80.6-111	70.1-101.7	86.5-105.5

As can be seen in Table VI.4, Raman spectroscopy is again the technique selected for the determination of c-SWNTs. The portable Raman spectrometer 2 and the confocal Raman microscope have been used for this task (see Table VI.2). The portable Raman spectrometer could have been also employed for the determination of c-SWNTs retained in MWNTs membranes (chapter 14); however, confocal Raman spectrometer showed less versatility in the case of the determination by extraction in ionic liquid and/or SERS determination due to higher fluorescence problems since it is equipped with a more energetic laser (532 nm). In fact, in the case of SERS detection, the use of a 532 nm laser would have matched AuNPs plasmon resonance increasing the enhancement factor observed thanks to contribution not only of chemical mechanism but also electromagnetic one. It was discarded due to those mentioned fluorescence interferences. Lower limits of detection have not been achieved due to the fact that as much isolated CNTs are, the higher fluorescence interferences are found.

Different strategies for the extraction/preconcentration of c-SWNTs have been employed (Figure VI.4), namely:

(a) Preconcentration by microfiltration of the sample through a cellulose membrane modified with MWNTs fabricated from a surfactant dispersion of them. c-SWNTs are retained over the MWNTs layer thanks to π-π interactions (Chapter 14).

(b) Microliquid-liquid extraction into an ionic liquid (bmim PF_6) in the presence of a cationic surfactant (CTAC). Thanks to the high affinity of imidazolium group for the carbon nanotube, it is possible to preconcentrate the nanotubes in a low volume of ionic liquid. The addition of a cationic surfactant revealed to be crucial for quantitative extraction of c-SWNTs. Cationic surfactant forms ionic pairs with negatively charged CNTs enabling their extraction. A low volume of ionic liquid phase is then microfiltrated on a cellulose membrane of 5 μm pore size for Raman analysis (Chapter 11).

(c) Subsequent microfiltration of bare gold nanoparticles (forming a SERS active substrate) and c-SWNTs water solution on cellulose acetate membranes, where CNTs are preconcentrated on gold nanoparticles (Chapter 12).

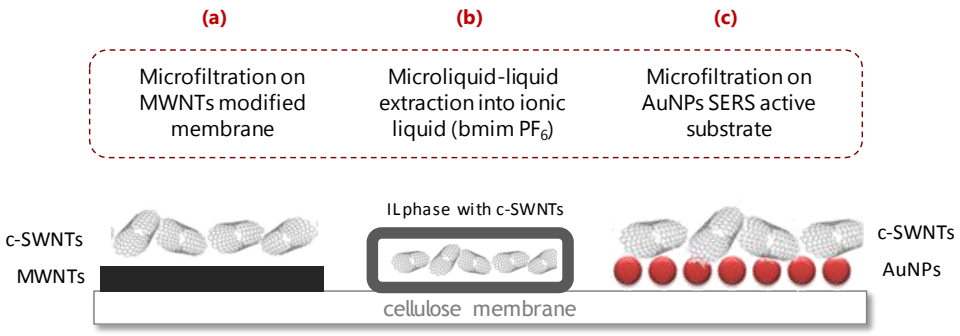

Figure VI.4. Strategies employed for the extraction/preconcentration and subsequent Raman determination of c-SWNTs.

Analytical signals used are based on CNTs characteristic Raman spectrum, but differ for each method. In the case of MWNT-modified membranes, the method is based on the dual role that MWNTs play. They act as active components in order to increase the retention of the analytes thanks to the well known π-π interactions between them, but also facilitate Raman determination owing to the fact that they are the spectral reference to show the presence of c-SWNTs in the filter since G-/D-band intensity ratio increases as much c-SWNTs are retained, this parameter being used as analytical signal. The variation observed for G-/D-band intensity ratio agrees to that noticed when measuring Raman spectra of surfactant mixtures with different proportions of SWNTs and MWNTs, which was employed in chapter 6 for characterization of the mixtures.

In the case of ionic liquid extraction procedure, the intensity of D band was used for quantification. Ionic liquid band at 739 cm^{-1} produced by symmetric stretching of PF_6^- anion was employed as internal reference. Thus, the intensity

of CNTs D-band divided by the intensity of ionic liquid band was adopted as analytical signal. Finally, for SERS measurements, the intensity of CNTs G-band around 1583 cm^{-1} was selected as analytical signal and subsequently used to quantify the samples. In this case, data were closely fit with a Langmuir isotherm.

The method described by using MWNTs modified membranes is the only one in which an interference study of humic acids has been performed. In order to overcome limitation of humic acid content in the sample affecting analytical signal, a clean-up step was introduced which removed such interferences. Nevertheless, in all cases a recovery study from spiked river water was carried out observing acceptable recoveries values, which mean that interferences of other components of the matrix have not effect of the performance of the procedure (see Table VI.4). In the case of ionic liquid extraction, selectivity is also achieved by the use of an ionic liquid acting as a sieve for other components present in water samples.

Regarding the limits of detection (LODs) achieved with the proposed methodologies, it should be pointed out that all of them fall in the μgL^{-1} range (ppb), as can be seen in Table VI.4. However, CNTs concentrations at the ngL^{-1} range are predicted in Europe[8]. LODs could be improved if problems of CNT fluorescence when isolated were overcome. Nevertheless, there is a lack of analytical methods for the determination of these nanostructures in environmental matrices and those proposed methodologies can be considered as a first approximation to their quantification in water matrices. They could be used for the in situ monitorization of the release of carbon nanotubes from point's source of contamination, where the concentrations of CNTs are expected to be considerably higher.

[8] F. Gottschalk, T. Sonderer, R.W. Scholz, B. Nowack, Environ. Toxicol. Chem. 29 (2010) 1036-1048.

VI.2. METALLIC NANOPARTICLES

Metallic nanoparticles used along this Doctoral Thesis have been synthesized in the laboratory, by using well-established methodologies as well as new synthesis procedures proposed herein. That is the case of bare gold nanoparticles obtained through a simple, environmentally friendly, one-pot method. Bare AuNPs have been synthesized from tetrachloroauric acid solution using stainless steel as solid reducing agent, as previously detailed in chapter 3. The proposed method yields bare gold nanoparticles at atmospheric pressure and room temperature for potentially producing large quantities.

Moreover, the synthesis procedure has been adapted for continuous flow production of bare gold nanoparticles in a stainless steel tubular reactor, as described in chapter 4. Gold(III) is reduced by the own stainless steel of the tubular reactor to form gold nanoparticles, which are collected at the end of the coil. By controlling the conditions of the synthesis (i.e. flow rates, temperature) the size of the nanoparticles can be tuned.

Bare gold nanoparticles obtained both in batch and continuous flow procedures have been characterized by several techniques, together with citrate coated silver and gold nanoparticles obtained through citrate reduction (and those functionalized with thioctic acid), as described in "Analytical Tools" block of this Thesis (block II). The next section summarizes the characterization techniques employed for this task.

2.1. Characterization of metallic nanoparticles

The different techniques employed for the characterization of the diverse types of gold nanoparticles studied along this Doctoral Thesis are summarized in Figure VI.5.

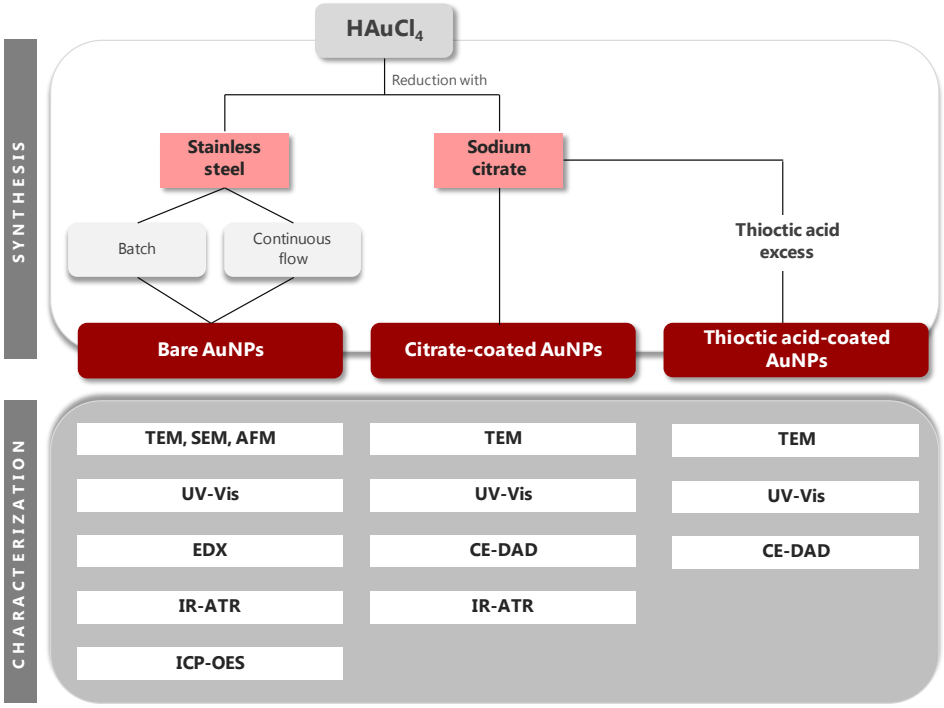

Figure VI.5. Synthetic procedures employed along this Doctoral Thesis and the different types of gold nanoparticles obtained (top). Techniques used for the characterization of gold nanoparticles with different surface (bottom).

Microscopic techniques such as TEM, SEM or AFM have been employed for the characterization of the nanoparticles. Bare gold nanoparticles were investigated by TEM and SEM, which showed to be homogeneous in shape and size and of polygonal yet nearly spherical shape. The average diameter was determined to be 20±6 nm, corroborated by AFM studies (21±9 nm). Continuous flow

synthesized bare AuNPs were also investigated by TEM microscopy calculating their size distribution. No aggregates were observed in the solutions, consisting of separated AuNPs. Those NPs obtained at 80ºC and 0.240 $mLmin^{-1}$ flow rate are more polydispersed than those obtained at 40 or 60ºC. As described with more detail in chapter 4, the average diameter of nanoparticles is higher at lower flow rates.

TEM and high resolution transmission electron microscopy (HTEM) have been also used for the characterization of citrate coated gold and silver nanoparticles (see chapters 9 and 10). The size of citrate coated gold nanoparticles ranged between 31 and 58 nm with an average size of 39±6 nm. The size of citrated coated silver nanoparticles was also determined by TEM measurements being 41±7 nm. TEM images of thioctic acid-functionalized AuNPs used in chapter 9 revealed an average diameter of around 35 nm.

Ultraviolet-visible spectroscopy has been also used for the characterization of metallic nanoparticles thanks to their surface plasmon resonance absorption band. Metallic NPs exhibit strong extinction properties in the visible region which are sensitive to variations in NP shape, size, environment and state of aggregation.

The kinetic of the synthesis of bare gold nanoparticles has been directly monitored via UV-Vis spectroscopy in a cuvette. It has been also employed to study the influence of variables such as gold precursor concentration, flow rate or temperature in the continuous flow synthesis of those bare AuNPs. The intensity of absorbance of AuNPs varies with flow rate, slower flows leading to higher absorption, which means higher concentration. In addition, a wavelength shift of surface resonance peak is observed as a consequence of the formation of nanoparticles with different size, obtaining smaller nanoparticles at higher flow rates. Moreover, broadening of absorbance band at high flow rates is also observed which suggests that nanoparticles became polydisperse. Wavelength

shift related to different AuNPs diameter was also observed when varying temperature.

Furthermore, UV-Vis spectroscopy has been also used for characterizing citrate-coated gold and silver nanoparticles as well as thioctic acid-functionalized gold nanoparticles (TA-AuNPs), as shown with more detail in chapter 9. Citrate-coated AuNPs showed a band at 537 nm, while AgNPs showed a band around 420 nm. The concentration of AuNPs solution can be calculated from the UV-Vis spectrum[9], as shown in chapter 10. Finally, the UV-visible spectrum of functionalized TA-AuNPs in ultrapure water solution showed a broad peak at 539 nm, this red shift being consequence of the relatively higher molecular packing density compared with citrate ligands.

Photoenhanced absorption of water on gold nanoparticles has been employed for the in-situ monitorization of the synthesis of bare gold nanoparticles by ***infrared attenuated total reflection (IR-ATR) spectroscopy*** (chapter 7). AuNPs are directly synthesized within the liquid cell of the ATR unit taking immediate advantage of the stainless steel walls of the ATR cell. According to literature[10], the vibrational modes of water in the infrared region are the H_2O bending mode at 1644 cm^{-1}, the combination of H_2O bending and libration at 2128 cm^{-1}, and one around 3404 cm^{-1}. As gold nanoparticles were formed and deposited on the ATR surface, an increase in the H_2O bending and the OH stretching bands was observed, despite a decrease in the amount of water molecules present in the evanescent field during the deposition and exchange of water molecules by gold nanoparticles. This increase can be attributed to the so-called surface enhanced infrared absorption (SEIRA) effect arising from the presence of water molecules in the enhanced field created by AuNPs. A similar effect was observed in the case of AuNPs synthesized in D_2O with the

[9] W. Haiss, N.T.K. Thanh, J. Aveyard, D.G. Fernig, Anal. Chem. 79 (2007) 4215-4221.
[10] S.Y. Venyaminov, F.G. Pendegast, Anal. Biochem. 248 (1997) 234-245.

absorption bands of deuterium oxide revealing similar enhancement during the formation of AuNPs.

Moreover, IR-ATR potential to monitor gravitational sedimentation of gold nanoparticles has been shown. For this aim, the sedimentation rate of both bare gold nanoparticles obtained through stainless steel assisted reduction and citrate-capped gold nanoparticles was measured. CTAC was added in order to increase NPs sedimentation rate[11].

Inductively coupled plasma optical emission spectroscopy (ICP-OES) has been used to analyze which metals were present in solution after the synthesis of bare gold nanoparticles with a piece of stainless steel. It was found that in addition to Au –forming the NPs- Fe is the dominant metal species complemented by trace levels of Cr, Ni, Mn and Mo.

In order to investigate if metals released from stainless steel are subsequently incorporated into the AuNPs obtained through the proposed synthetic procedure, ***energy dispersive X-ray spectroscopy*** (EDX) studies were performed, corroborating that the obtained NPs were composed only by gold. In the case of continuous flow synthesized AuNPs, EDX analysis revealed that small amounts of iron were present in solution and could have been incorporated into the NPs, nevertheless the relative concentration found of gold to iron is about 20:1.

Citrate-coated gold and silver nanoparticles have been separated in aqueous medium by ***capillary electrophoresis***, as previously explained with more detail in chapter 9. Au and AgNPs were synthesized with the same size, shape and shell (citrate), showing similar migration time when analyzing a mixture of both of them with a 40 mM SDS, 10 mM CAPS electrophoretic buffer (BGE) with 0.1%

[11] T.J. Norman Jr., C.D. Grant, D. Magana, Z. Zhang, J. Liu, D. Cao, F. Bridges, A. Van Buuren, J. Phys. Chem. B 106 (2002) 7005-7012.

methanol at pH 9.7. The pH of the buffer was alkaline in order to preserve nanoparticle stability, while the addition of methanol decreased the migration time of the NPs. Citrate ions are responsible both for nanoparticle reduction and capping of their surfaces[12]. Thus, these NPs have surface charges forming an electric double layer and, therefore, their separation is based on a similar mechanism than that of charged molecular species.

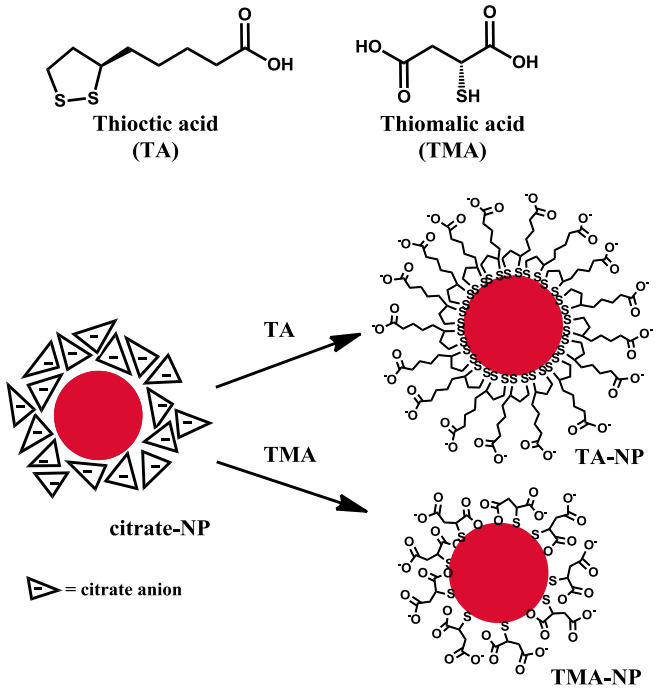

Figure VI.6. Molecular structures of thiol derivatives (thioctic and thiomalic acids) added to the BGE in order to achieve Au and AgNPs separation. Scheme of the ligand-exchange reaction resulting in NPs with different molecular packing density (drawing are not to scale).

Thiol derivatives were introduced as additives in the BGE enabling the separation of Au and AgNPs by selective interaction with the metallic surface of the nanoparticles –through the formation of Au-S or Ag-S bonds- establishing

[12] F.K. Liu, F.H. Ko, P.W. Huang, C.H. Wu, T.C. Chu, J. Chromatogr. A 1062 (2005) 139-145.

different migration times because of the differences on core-shell charges when functionalized (see Figure VI.6.). Thus, separation takes place because of the different nature of the core of the nanoparticle and not owing to their different size, as usually reported in literature. Two thiol compounds have been investigated, namely thioctic and thiomalic acids. Disulfide ring of thioctic acid may interact with gold atoms, the remaining COO^- group being responsible for the NP charge[13]. The self-assembly of thiols will produce SAMs with increased molecular packing density than citrate ligands, showing slower migration times. Thiomalic acid possesses two carboxylic groups, having a single thiol which enables their interaction with metallic NPs. AgNPs showed higher affinity, since multiple ligand binding can be performed through thiol and one carboxylate group, appearing at longer times in the electropherogram.

Thioctic acid functionalized gold NPs (TA-AuNPs) were also analyzed, by using the BGE without the addition of thiol compounds. Migration time observed agrees with observations when AuNPs interact with thioctic acid present in BGE decreasing their electrophoretic mobility.

Since ligand exchange reactions on NP surface are both kinetically and thermodynamically controlled, the incubation time is critical[14]. In order to increase the reaction time inside the capillary and, thus, functionalization of nanoparticles, large-volume sample stacking was used, observing an improvement in terms of sensitivity and separation of the peaks.

[13] A.A. Volkert, V. Subramaniam, M.R. Ivanov, A.M. Goodman, A.J. Haes, ACS Nano 5 (2011) 4570-4580.
[14] G. Cao, Nanostructures and Nanomaterials: Synthesis, Properties and Applications, Imperial College Press, London, 1st ed., 2004.

2.2. Determination of gold nanoparticles

Predictions have pointed out that gold nanoparticles arising from consumer products are expected to reach a concentration of 0.14 $\mu g \cdot L^{-1}$ (ppb) in water samples[15]. On the other hand, a study has reported that commercially available 1.9 nm gold nanoparticles are biodistributed and accumulated in different organs depending on their charge, those negatively charged and non-charged nanoparticles being accumulated in the liver[16].

Citrate-coated gold nanoparticles have been determined in liver and river water samples by stabilization with a cationic surfactant followed by microliquid-liquid extraction in ionic liquid (Chapter 10). Ionic liquids present a high affinity to gold nanoparticles thanks to their interaction with imidazolium group. The extracted nanoparticles can be analyzed by UV-Vis or Raman spectroscopy (by using the so-called portable Raman spectrometer 1 previously described).

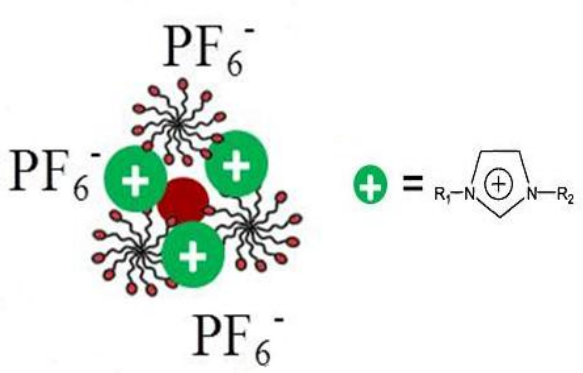

Figure VI.7. Scheme of the extraction process which implies the use of a cationic surfactant (CTAC) and ionic liquid with imidazolium cation.

[15] A.B.A Boxall, Q. Chaudhry, A. Jones, B. Jefferson, C.D. Watts, Current and future predicted environmental exposure to engineered nanoparticles, Report to Defra, 2008.
[16] C. Schleh, M. Semmler-Behnke, J. Lipka, A. Wenk, S. Hirn, M. Schäffler, G. Schnid, U. Simon and W. G. Kreyling, Nanotoxicology, 2012, 6, 36–46.

Sample treatment for each type of sample –river water and liver tissue- has been previously described in chapter 10. In a first stage, surfactant micelles coat the nanoparticle interacting with them in aqueous phase, and, later, they are extracted by the formation of ionic pairs with the ionic liquid anion. Probably mixed micelles are formed in which, in addition to the surfactant, there are also ionic liquids cations interacting with the nanoparticle (see Figure VI.7).

AuNPs extracted in ionic liquid have been determined by UV-Vis absorption, although their absorption coefficient in ionic liquid is 2.5 times lower than in water. Nevertheless, the extraction procedure is necessary in order to remove sample matrix interferences. In addition, Raman spectroscopy has been also used for their determination. Calibration was performed by partial least square modelling (PLS) after principal component analysis (PCA). It was applied to river water samples, as well as liver tissue. In the latter case, a low analytical signal was observed with UV-Vis detection due to the presence of interferences. Such interferences did not affect Raman measurements.

This IL-based extraction method is similar to that previously described for extraction of c-SWNTs (chapter 11). In both cases, the use of a cationic surfactant proved to be crucial since both types of NPs were negatively charged. However, regarding subsequent detection, in the case of CNTs their Raman features enabled direct calibration, while for AuNPs PCA-PLS calibration was chosen in order to extract more information from the Raman spectra.

VI.3. FACETS OF NANOPARTICLES IN ANALYTICAL NANOSCIENCE AND NANOTECHNOLOGY

The different consideration of nanoparticles and nanostructured materials as objects (analytes) or tools involved in the analytical process has been repeatedly mentioned throughout the Memory of this Doctoral Thesis. Generally, nanomaterials in the Analytical Nanoscience and Nanotechnology (AN&N) scope are considered as analytical objects or analytical tools. However, a third classification, as interface between the two previous, is proposed herein, which is the use of nanomaterials in analytical processes for the characterization and/or determination of other nanomaterials. In this sense, this Thesis covers points 1 and 3 of Figure VI.8 as they will be commented below.

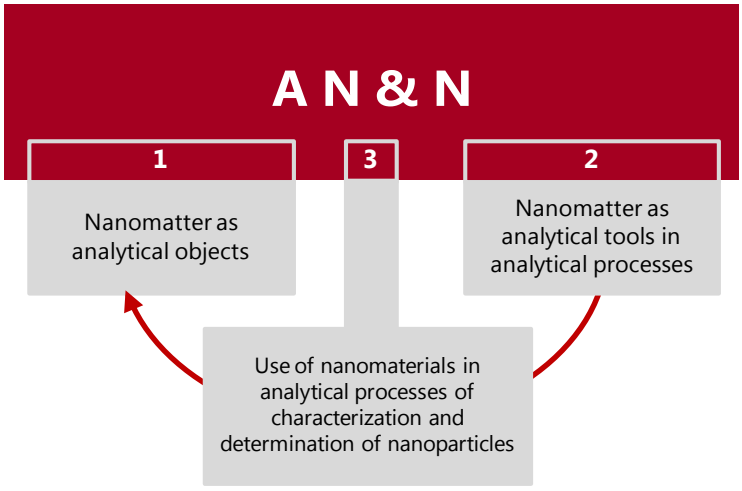

Figure VI.8. Different facets of nanoparticles in Analytical Nanoscience and Nanotechnology (AN&N) scope.

3.1. Nanomatter as analytical objects

This facet of nanomaterials in Analytical Chemistry has been the basis of this Doctoral Thesis. In this sense, the main objective of the Thesis was the development of methods for the characterization and determination of nanostructures such as carbon nanotubes or metallic nanoparticles.

As summarized in Table VI.1, and previously discussed along this block, carbon nanoparticles have been characterized mainly by using Raman spectroscopy. This technique has also enabled their determination after extraction/preconcentration with the aid of different (nano)materials, namely: ionic liquids, AuNPs forming the SERS substrate or MWNTs modified membranes.

On the other hand, metallic nanoparticles have been characterized by several techniques including microscopic (TEM, SEM, AFM), spectroscopic (UV-Vis, IR-ATR, ICP-OES, EDX) and separation techniques such as capillary electrophoresis, which allowed the separation of citrate-coated Au and AgNPs of the same size on the basis of the different nature of their core by their functionalization with thiol derivatives. Furthermore, gold nanoparticles stabilized with cationic surfactant (CTAC) in a first stage, and subsequently extracted in ionic liquid were determined by UV-Vis and Raman spectroscopy.

3.2. Use of nanomaterials in analytical processes of characterization and determination of nanoparticles

The synergy between nanotechnology and analytical sciences is self-apparent. In this sense, nanoparticles can be used to improve methodologies devoted to characterization of nanostructures of different or similar nature (e.g. by

functionalizing an atomic force microscopy tip with a multiwalled carbon nanotube in order to boost image resolution)[17].

This third facet of nanoparticles in AN&N has been also afforded in this Thesis. Both bare and citrate coated gold nanoparticles proved their suitability to act as SERS substrates. The performance of both types of nanoparticles was assayed for the determination of c-SWNTs in river water (chapter 12). In this case, gold nanoparticles act as analytical tool improving the detection of carbon nanotubes. The presence of metallic nanoparticles produces an enhancement of the Raman spectra of carbon nanotubes, enabling the sensitive detection of these nanomaterials by means of a portable Raman spectrometer.

Two enhancement mechanisms –electromagnetic and chemical- are thought to contribute to the total enhancement. The electromagnetic mechanism is produced by the resonant excitation of AuNPs surface plasmon, which increases the electromagnetic field strength at nanoparticles' surface giving up to 10^{12} enhancement. On the other hand, the chemical mechanism relies on the formation of charge complexes between analyte and metallic NPs producing enhancements of 10-100 times[18]. In our case, a 785 nm laser was employed due to the fact that experiments with 532 nm laser, which would match AuNPs' plasmon resonance, lead to high fluorescence interferences. Thus, the enhancement observed (~39 times) is produced by chemical mechanism, the performance showed by bare AuNPs being quite acceptable in such conditions, even better than many previously described in literature.

Another example of this third facet is the use of MWNT-modified membranes for the determination of c-SWNTs. The basis of the method is the different spectral features, in terms of G-/D-band intensity ratio, shown by each type of

[17] B. Bhushan, T. Kasai, C.V. Nguyen, M. Meyyappan, Microsyst. Technol. 10 (2004) 633-639.
[18] H. Ko, S. Singamaneni, V.V. Tsukruk, Small 10 (2008) 1576-1599.

nanotubes. When increasing the amount of c-SWNTs deposited over the MWNT-modified membrane, G-/D-band intensity ratio linearly increases enabling their quantification. The use of this parameter overcomes limitations of Raman spectroscopy for quantitative analysis. As can be seen in Table VI.4 the limit of detection achieved with this method is better than obtained with SERS detection or ionic liquid extraction. The limit is imposed by c-SWNTs fluorescence, which increases as much isolated CNTs are on the membrane. However, in this case, this problem is palliated by the presence of a background of MWNTs forming the membrane, which subdue fluorescence stemming from c-SWNTs. As a consequence, it enabled the use of a 532 nm wavelength laser, which had been not possible in the case of SERS determination or IL-extraction of c-SWNTs. Nevertheless, the same portable Raman spectrometer with a 785 nm laser employed in those two previous works could also have been employed in that of MWNTs membranes, enabling in-situ measurements.

CONCLUSIONES

CONCLUSIONS

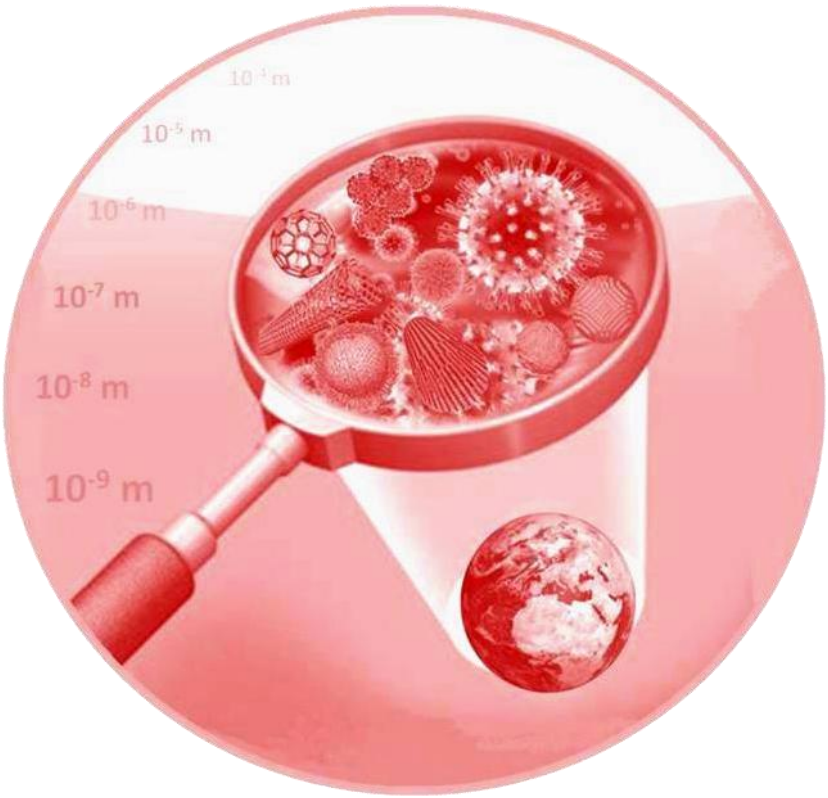

La investigación realizada en la presente Tesis Doctoral se ha centrado en el desarrollo de métodos analíticos enfocados a la caracterización y determinación de nanopartículas y nanomateriales en muestras biológicas y medioambientales. Se han caracterizado nanomateriales de diversa naturaleza, entre ellos nanopartículas de oro obtenidas a través nuevos procedimientos de síntesis propuestos durante el desarrollo experimental de esta Tesis. Siguiendo el esquema general de esta Memoria, las conclusiones principales de cada uno de los aspectos abordados se recogen a continuación.

En cuanto a la **síntesis de nanopartículas**, cabe destacar que se ha propuesto un nuevo método de síntesis sencillo, responsable con el medio ambiente, económico y en un solo paso, para llevar a cabo la síntesis de nanopartículas de oro sin recubrimiento superficial altamente estables. La principal aportación es el empleo de un agente reductor sólido –acero inoxidable- que puede recuperarse de la disolución y reutilizarse, evitando el uso de agentes químicos. El proceso conduce a nanopartículas de oro de forma casi esférica de 20 nm de diámetro sin ligandos en su superficie, libres de impurezas de compuestos químicos. Las nanopartículas se han caracterizado mediante SEM, TEM, AFM y EDX. La síntesis puede llevarse a cabo a presión atmosférica y temperatura ambiente, aunque se ha demostrado que elevadas temperaturas incrementan la producción de nanopartículas. Cabe destacar que las nanopartículas obtenidas son muy estables sin necesidad de añadir agentes estabilizantes, mediada por los iones presentes en la disolución.

El procedimiento de síntesis es fácilmente escalable como se comprobó adaptándolo para la producción en flujo continuo de las nanopartículas de oro en un reactor tubular de acero inoxidable. El sistema permite la producción de

nanopartículas estables de forma altamente reproducible empleando componentes disponibles comercialmente. Se trata de un sistema en una única fase, en el que no es necesario mezclar disoluciones. Controlando las condiciones de la síntesis (velocidad de flujo y temperatura), puede modificarse el tamaño de las nanopartículas, como se demostró mediante estudios de UV-Vis y TEM. Este método puede ser útil para la producción a gran escala de nanopartículas de oro sin ligandos en su superficie.

Respecto a la **caracterización de nanopartículas**, cabe destacar que además de otras técnicas (como las microscópicas) también utilizadas para caracterizar las nanopartículas sintetizadas, las principales aportaciones de esta Tesis en este sentido abarcan tres técnicas: las espectroscopias Raman e IR-ATR y la electroforesis capilar.

(1) La espectroscopia Raman se ha empleado para la caracterización de nanotubos de carbono:

- Se ha demostrado la necesidad de tener en cuenta el estado de agregación de una muestra de SWNTs cuando se llevan a cabo medidas Raman, ya que influye en la relación de intensidades de las bandas G y D. En el caso de MWNTs la influencia de dicha variable es menos significativa.
- Una vez descartada la posible influencia del haz de láser o del enfoque, mediante análisis de clústeres K-NN se clasificó un conjunto de espectros con diferente estado de agregación de acuerdo a su relación de intensidades de las bandas G y D.
- Se ha propuesto la dispersión de los SWNTs con ayuda de tensioactivos antes del análisis, ya que cuando se analizaron nanotubos no agregados se observó que las medidas eran reproducibles.
- Se ha realizado un estudio detallado de los espectros Raman de siete tipos diferentes de nanotubos de carbono en disoluciones de

tensioactivos –CTAB, SDS y Tritón X-100-, y los resultados obtenidos se han comparado con medidas sólidas de los diferentes tipos de nanotubos.

- Se han analizado mezclas de SWNTs y MWNTs dispersos en tensioactivos usando un espectrómetro Raman portátil, siendo posible detectar y (semi)cuantificar la presencia de SWNTs en la mezcla usando tanto la relación de intensidades de las bandas D y G como la influencia sobre el perfil de la banda G.

(2) La espectroscopia infrarroja con reflexión total atenuada ha demostrado ser una herramienta útil para la caracterización de disoluciones de nanopartículas de oro.

- Se ha empleado IR-ATR para monitorizar *in-situ* la síntesis de nanopartículas dentro de la celda ATR mediada por el acero inoxidable que forma las paredes de la celda.
- Conforme son sintetizadas, las nanopartículas cubren el campo evanescente reemplazando a las moléculas de agua. A pesar de no ser activas en IR, puede observarse la deposición de las AuNPs mediante el incremento que producen en las bandas del agua. Este incremento, denominado efecto SEIRA, compensa la pérdida de moléculas de agua en la región activa, y permite determinar la presencia de las AuNPs.
- La espectroscopia IR puede usarse también para controlar cambios químicos en la disolución que afectan a las nanopartículas, como procesos de agregación consecuencia de cambios de pH o fuerza iónica.
- Se ha demostrado que la espectroscopia IR puede usarse para evaluar el proceso de sedimentación de AuNPs con diferentes recubrimientos superficiales sobre la superficie ATR.

(3) La electroforesis capilar, por otra parte, se ha empleado para la separación de nanopartículas de oro y plata cubiertas por citrato.

- Nanopartículas de Au y Ag de similar tamaño cubiertas de citrato mostraron una movilidad electroforética similar cuando se usó un buffer compuesto por SDS y CAPS con un 0.1% de metanol a un pH de 9.7.
- Cuando se introdujeron compuestos tiólicos –ácido tióctico (lipóico o 6,8-ditioctanoico) y ácido tiomálico (mercaptosuccínico)- como aditivos en el buffer, se observó la separación de las nanopartículas gracias a la interacción selectiva con estos compuestos.
- Para aumentar la interacción de las NPs con el buffer, permitiendo la funcionalización de las mismas, se empleó la modalidad electroforética de preconcentración de un gran volumen de muestra (*"large volumen sample stacking"*), mejorándose la separación.

Finalmente, en lo que respecta a la **determinación de nanopartículas**, se han desarrollado tres estrategias para la cuantificación de c-SWNTs en muestras de agua de río usando en todos los casos la espectroscopia Raman como técnica cuantitativa. AuNPs han sido también determinadas mediante espectroscopia UV-Vis y Raman.

(1) Se ha usado la microextracción líquido-líquido de nanopartículas en líquido iónico para la determinación de AuNPs y c-SWNTs.

- Los líquidos iónicos con grupo imidazolio y los tensioactivos catiónicos son una buena combinación para extraer tanto AuNPs como c-SWNTs de muestras de agua de río, y, en el caso de las primeras, de muestras de tejido de hígado de pollo. Gracias a la alta afinidad del grupo imidazolio por la nanopartículas es posible preconcentrarlas en un pequeño volumen, extrayéndolas de la matriz de la muestra.

- En cuanto a la detección de AuNPs, tanto la espectroscopia UV-Vis, gracias al plasmón superficial de las NPs, como la espectroscopia Raman han demostrado su potencial para la cuantificación de las mismas. En el caso de las muestras de tejido de hígado, Raman mostró ser menos sensible a las interferencias de la matriz. Se llevó a cabo PCA seguido de calibración por PLS.
- En el caso de c-SWNTs, éstos presentan un espectro Raman característico, empleándose la intensidad de la banda D dividida entre la intensidad de la banda de tensión del PF_6^- como señal analítica.

(2) La espectroscopia Raman amplificada por superficies, usando las AuNPs sin ligandos superficiales propuestas anteriormente como substrato SERS, permitieron la determinación sensible de c-SWNTS.

- El substrato SERS se formó mediante la microfiltración de la disolución de AuNPs sobre una membrana de celulosa. Dada la simplicidad del procedimiento y las pequeñas cantidades de AuNPs necesitadas, se prepara un nuevo substrato para cada medida, superando las limitaciones de tiempo de vida media y reusabilidad.
- Los c-SWNTs son depositados mediante microfiltración en el substrato SERS, que produce un incremento de su espectro Raman, permitiendo la detección de pequeñas cantidades de nanotubos de carbono en muestras acuosas, utilizando como señal analítica la intensidad de la banda G de los CNTs.

(3) Membranas modificadas con MWNTs permitieron la preconcentración y determinación directamente sobre la membrana de c-SWNTs en muestras de agua de río.

- Las membranas de celulosa modificadas con MWNTs se prepararon a partir de dispersiones de MWNTs en tensioactivo Tritón X-100.

- Los c-SWNTs son microfiltrados y retenidos en la membrana mediante interacciones π-π con los MWNTs.
- La medida directa en la membrana de la variación de las intensidades relativas de las bandas G y D de los CNTs conforme se retienen cantidades mayores de c-SWNTs se usó como señal analítica, mejorando los límites de detección y superando las limitaciones de la espectroscopia Raman para el análisis cuantitativo.
- Se llevó a cabo un estudio de la interferencia de ácidos húmicos, adaptando la metodología con el fin de evitar dichas interferencias.

The research performed in this Doctoral Thesis is centered on the development of analytical methods focused on the characterization and determination of nanoparticles and nanomaterials in biological and environmental samples. Nanomaterials of different nature have been subjected to characterization, gold nanoparticles obtained through new synthetic procedures proposed during the experimental work of this Thesis being among them. According to the general scheme of this Memory, the main conclusions of each of the issues addressed are presented as follows.

*Regarding the **synthesis of nanoparticles**, it should be pointed out that a simple, environmentally friendly, inexpensive, one-pot method to synthesize highly stable bare gold nanoparticles has been proposed. The main contribution is the use of a solid reducing agent -stainless steel- which can be recovered from solution and reused, avoiding the use of harsh chemicals. The process leads to 20 nm size, nearly spherical shaped gold nanoparticles without ligands in their surface, in which impurities of chemical compounds are absent. Nanoparticles have been characterized by SEM, TEM, AFM and EDX. The synthesis can be carried out at atmospheric pressure and room temperature, although it has been demonstrated that higher temperatures increased the production of the nanoparticles. A highlight of the procedure is that bare gold nanoparticles produced proved to be very stable without needing further stabilizing agents, just mediated by the chloride ions present in solution shielding the nanoparticles.*

The synthesis procedure is easily scalable as proved by adapting it for continuous flow synthesis of gold nanoparticles in a stainless steel tubular reactor. The system enables high throughput production of highly reproducible

and stable bare gold nanoparticles by using commercially available components. It is a single-phase system, avoiding mixing of solutions. By controlling the conditions of the synthesis (flow rates, temperature), the size of the nanoparticles may be tuned as demonstrated by UV-Vis and TEM studies. This method can be useful for the scale-up production of gold nanoparticles without ligands in their surface.

*Concerning the **characterization of nanoparticles**, it should be remarked that, in addition to other techniques (i.e. microscopic) also used for characterizing synthesized nanomaterials, the main contributions of this Thesis in this respect comprises three techniques, namely: Raman and IR-ATR spectroscopies and capillary electrophoresis.*

(1) Raman spectroscopy has been employed for the characterization of carbon nanotubes:

- *The need of carefully consider the aggregation state of a sample of SWNTs when recording Raman spectra has been demonstrated, since it influences G-/D-band intensity ratio. In the case of MWNTs this variable showed less influence.*
- *Once discarded the possible influence of laser beam or sample focusing, K-NN neighbors classified a set of spectra with different aggregation according to their G-/D-band intensity ratio.*
- *Dispersion of SWNTs prior analysis with the aid of surfactants was proposed, since when analyzing debundled carbon nanotubes the reproducibility of measurements was consistent.*
- *A detailed study of the Raman spectra of seven types of CNTs in different surfactant solutions –CTAB, SDS and Triton X-100- has been carried out, and the results obtained compared with solid measurements of the different types of CNTs.*

- *Mixtures of SWNTs and MWNTs dispersed in surfactant solutions have been analyzed by using a portable Raman spectrometer. The detection and (semi)quantification of the presence of SWNTs in the mixture was possible by using both the D-/G-band intensity ratio and the effect on the G band lineshape.*

(2) Infrared attenuated total reflection spectroscopy has proved to be a suitable tool for the characterization of gold nanoparticles solutions.

- *IR-ATR was used to monitor the in-situ synthesis of AuNPs in the liquid cell of the ATR unit mediated by the stainless steel walls of the ATR cell.*
- *As gold nanoparticles were synthesized, they covered the evanescent field replacing water molecules. Despite being no IR active, gold nanoparticles deposition was observed by the enhancement they produced over water featured bands. This surface-enhancement, SEIRA effect, overcompensated the lost of water molecules on the surface active region, and allowed the determination of the presence of gold nanoparticles.*
- *IR can be also used to control chemical changes in solution that may affects the gold nanoparticles, such as aggregation processes as a consequence of changes of pH or ionic strength.*
- *It has been shown that IR spectroscopy can be used to evaluate the sedimentation process of gold nanoparticles with different surface coatings on the ATR surface.*

(3) Capillary electrophoresis has been also employed for the separation of citrate-capped gold and silver nanoparticles.

- *Au and AgNPs of similar size covered with citrate showed similar electrophoretic mobility when using a buffer composed by SDS and CAPS with 0.1% of methanol at a pH of 9.7.*

- *When introducing thiol derivatives –thioctic (lipoic or 6,8-dioctanoic) and thiomalic (mercaptosuccinic) acids- as additives to the buffer, separation of NPs was observed thanks to the selective interaction of the NPs with these compounds.*
- *In order to increase the interaction of NPs with buffer, enabling functionalization of the nanoparticles, large volume sample stacking electrophoretic modality was employed, improving their separation.*

*Finally, regarding the **determination of nanoparticles**, three strategies have been developed for quantifying c-SWNTs in river water samples by using in all the cases Raman spectroscopy as analytical technique. AuNPs have been also determined by UV-Vis and Raman spectroscopy.*

(1) Liquid-liquid microextraction of nanoparticles in ionic liquid phase has been used for the determination of both AuNPs and c-SWNTs.

- *Imidazolium-based ionic liquids with cationic surfactant proved to be a good combination to extract both AuNPs and c-SWNTs from river water samples, and, in the case of the former, chicken liver tissue samples. NPs were preconcentrated in a low volume thanks to the high affinity of imidazolium group towards them, being extracted from the sample matrix.*
- *Regards detection of AuNPs, both UV-Vis spectroscopy, thanks to NPs surface plasmon, and Raman spectroscopy, proved to be suitable for their quantification. In the case of liver tissue samples, Raman showed to be less sensitive to matrix interferences. PCA followed by PLS calibration was employed.*
- *In the case of c-SWNTs, they show a characteristic Raman spectrum. The ratio between D-band and PF_6^- stretching band intensities was employed as analytical signal.*

(2) Surface enhanced Raman spectroscopy, by using the previously proposed bare AuNPs as SERS substrate, enabled the sensitive determination of c-SWNTs.

- *The SERS active substrate is formed by microfiltration on a cellulose membrane of the bare AuNPs solution. Due to the simplicity of the procedure and low quantities of AuNPs needed, a new substrate is prepared for each measurement overcoming limitations of substrate shelf-life and reusability.*
- *c-SWNTs are deposited by microfiltration on the SERS substrate which produces an enhancement of their Raman spectrum, allowing the detection of small quantities of carbon nanotubes in water samples, by using as analytical signal CNTs G-band intensity.*

(3) Membranes modified with MWNTs enabled the sequential preconcentration and on-membrane determination of c-SWNTs in river water samples.

- *MWNT-modified cellulose membranes were prepared from aqueous surfactant dispersions of MWNTs in Triton X-100.*
- *c-SWNTs were microfiltrated and retained in the membrane through π-π interactions with MWNTs.*
- *Variation of G-/D-band intensity ratio as increasing amounts of c-SWNTs were retained and directly measured on-membrane was used as analytical signal, improving the detection limits and overcoming limitations of Raman spectroscopy for quantitative analysis.*
- *An interference study of humic acid was performed the methodology being adapted to avoid such interferences.*

AUTOEVALUACIÓN CIENTÍFICA

SCIENTIFIC SELF-ASSESSMENT

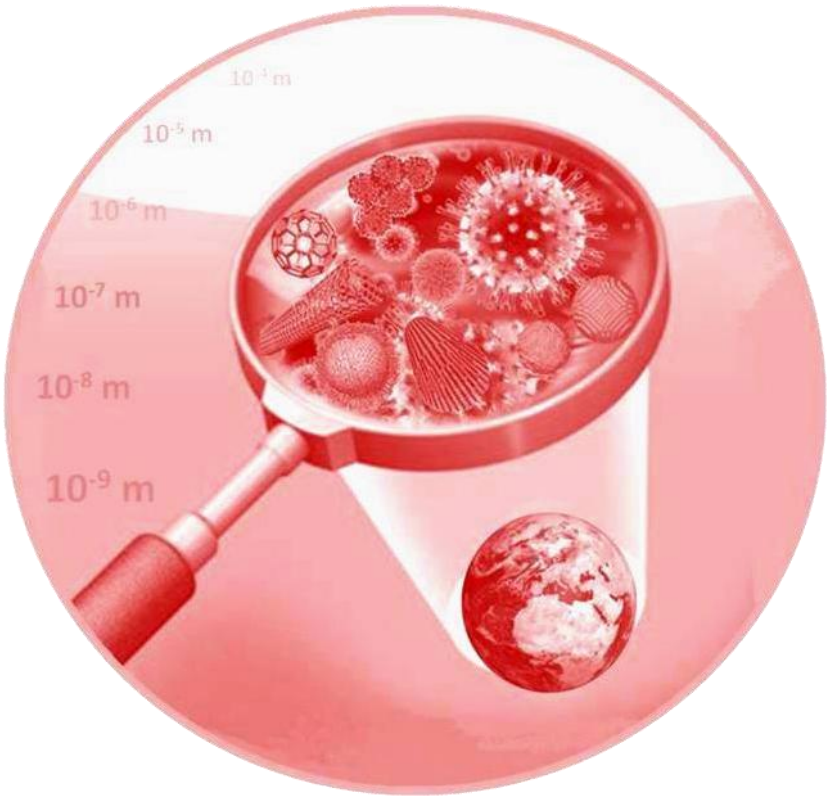

La redacción de esta Memoria, junto con la experiencia adquirida durante el desarrollo de esta Tesis Doctoral, ha proporcionado una visión general y objetiva del trabajo presentado. En esta sección se ha llevado a cabo una autoevaluación crítica de los resultados obtenidos con el fin de valorar, por un lado, las principales aportaciones del trabajo a la comunidad científica, así como analizar las limitaciones con vistas a planificar futuras investigaciones.

Las principales aportaciones de esta Tesis Doctoral están dirigidas a la síntesis, caracterización y determinación de nanopartículas de diferente naturaleza.

En el caso de la **síntesis de nanopartículas**, se ha propuesto un nuevo procedimiento de síntesis, que ha sido adaptado para la producción de AuNPs en continuo de manera sencilla, respetuosa con el medio ambiente y que genera nanopartículas de oro sin ligandos en superficie altamente estables. En el caso del uso del reactor de flujo continuo tiene lugar la producción de nanopartículas reproducibles, con el tamaño deseado, sin necesidad de mezclar disoluciones.

Sin embargo, la polidispersidad de las nanopartículas podría mejorarse. Aunque es comparable con las obtenidas mediante otros métodos de síntesis usados comúnmente, puede verse influenciada por la ausencia de ligandos unidos a la superficie de las nanopartículas que controlen su crecimiento. No obstante, como se comentó anteriormente, flujos medios en el reactor conducen a la formación de nanopartículas con una distribución de tamaños más estrecha. Además, podrían realizarse más estudios para profundizar en el mecanismo de producción de las nanopartículas. En el caso de la producción en flujo continuo, podría estudiarse en profundidad el tiempo de vida media del reactor a fin de

evaluar si puede influir en el tamaño y composición de las nanopartículas sintetizadas.

En cuanto a la **caracterización de nanopartículas**, aparte de las microscopías, los nanotubos de carbono se han analizado mediante espectroscopia Raman, mientras que las disoluciones de nanopartículas de oro se han caracterizado por espectroscopia infrarroja y electroforesis capilar. La espectroscopia Raman ha demostrado ser una herramienta simple y barata para la identificación rápida de SWNTs en mezclas de MWNTs. La baja capacidad de disipación de calor de los CNTs limita su medida en estado sólido, a menos que el equipo permita utilizar potencias de láser muy bajas. En este sentido, el uso de un espectrómetro Raman confocal con un detector de carga acoplada con multiplicador de electrones (EMCCD) mejora la sensibilidad, a pesar de usar potencias de láser bajas. El problema se ha solucionado también mediante la dispersión de los CNTs en tensioactivos, lo que permite el uso de equipos Raman más económicos. Sería útil llevar a cabo la comparación de los espectros Raman de dispersiones de CNTs en tensioactivos y de los mismos sólidos a la misma longitud de onda del láser (las dispersiones se midieron con un láser de 785 nm y los sólidos con uno de 532 nm).

La principal limitación para la caracterización de nanopartículas de oro mediante electroforesis capilar es el pequeño paso óptico del capilar, lo que reduce la sensibilidad. Para intentar solucionar esta limitación, se usó un equipo de electroforesis con una fibra óptica que transmite la señal al detector, así como el empleo del método de preconcentración de un gran volumen de muestra (*"large volume sample stacking"*) para mejorar, por un lado, la sensibilidad y, por otro, la interacción de las nanopartículas con el buffer electroforético. Se usó un capilar de 75 µm de diámetro para evitar el bloqueo del mismo cuando se inyectaron bolos de nanopartículas altamente concentradas.

Por otro lado, cuando se empleó la espectroscopia infrarroja para caracterizar las disoluciones de AuNPs, el principal inconveniente es la baja velocidad de sedimentación de las NPs en la superficie ATR. Aunque se añadió CTAC con el fin de acelerar su deposición, si se pudiera incrementar aún más la velocidad, esta técnica podría emplearse para la rápida determinación y cuantificación de AuNPs.

La dispersión de luz dinámica (DLS, en inglés) es una herramienta analítica usada comúnmente para determinar el tamaño hidrodinámico de nanopartículas y coloides en medio líquido. En nuestro caso, no hemos tenido acceso a esta técnica, que sin duda hubiese resultado muy interesante para contrastar y completar la caracterización de las nanopartículas utilizadas durante el desarrollo de esta Tesis Doctoral.

En lo que respecta a la **determinación de nanopartículas**, la espectroscopia Raman ha demostrado igualmente ser una herramienta eficaz para este fin. Se han determinado c-SWNTs, por un lado, mediante microextracción líquido-líquido en líquido iónico, que permitió su preconcentración, evitando interferencias de la matriz de la muestra ya que los CNTs son extraídos en la fase de líquido iónico. En segundo lugar, se han determinado mediante espectroscopia SERS gracias al incremento proporcionado por las nanopartículas de oro sintetizadas con acero inoxidable. La formación del substrato SERS es sencilla, necesitándose pequeñas cantidad de nanopartículas. Finalmente, se han retenido y cuantificado c-SWNTs con mejor sensibilidad directamente sobre membranas modificadas con MWNTs. En todos estos métodos se empleó un dispositivo de microfiltración casero con un pequeño diámetro de filtración, lo que mejoró la preconcentración de los CNTs en los diferentes soportes donde se depositaron. La retención de los c-SWNTs en membranas (modificadas con diferentes materiales: MWNTs, substrato SERS de

nanopartículas de oro) mejoró la sensibilidad de los métodos permitiendo llevar a cabo medidas Raman cuantitativas.

Una limitación de estas metodologías es la interferencia de la fluorescencia evitando obtener mejores límites de detección, que están en el rango de los μgL^{-1} mientras que las predicciones teóricas sitúan la presencia de CNTs en muestras acuosas medioambientales en el rango de los ngL^{-1}. En cualquier caso, estos métodos pueden considerarse como una primera aproximación a la cuantificación de dichos nanomateriales en matrices acuosas. Gracias al uso de un espectrómetro Raman portátil podrían aplicarse como métodos de cribado para controlar las posibles emisiones de dichos materiales en puntos de contaminación como factorías, vertederos o efluentes de aguas residuales, en donde se encontrarán en mayor concentración. En el caso de las medidas SERS, se podría haber obtenido un mayor incremento de la señal si se hubiese empleado un láser con una longitud de onda en resonancia con el plasmón superficial de las AuNPs. Se probó con un láser de 532 nm, observándose mayores incrementos de señal, que iban acompañados de una mayor interferencia de la fluorescencia. La curva de calibrado de las medidas SERS se ajusta a una isoterma de Langmuir, por lo que a la hora de cuantificar las muestras debemos asegurar que la concentración se encuentra en la región linear, diluyendo la muestra en caso necesario.

Solamente en el caso de la preconcentración de c-SWNTs en las membranas modificadas con MWNTs se llevó a cabo un estudio de la interferencia de los ácidos húmicos. No obstante, en todos los casos se hicieron estudios de recuperación de muestras de agua de río encontrándose valores aceptables. En el caso de la microextracción en líquido iónico la selectividad se mejora mediante el proceso de extracción así como mediante la medida Raman característica de los CNTs. Otras especies de carbono podrían interferir en la señal, en este sentido, en lugar de usar para la cuantificación la banda D

mostrada a modo de ejemplo en este trabajo, que es más sensible a la presencia de defectos e impurezas de carbono, el empleo de la banda G sería más selectivo.

El uso de la relación de intensidades de las bandas G y D en el caso de las membranas modificadas con MWNTs presenta la ventaja de que dicho parámetro es independiente de las condiciones de medida, como la potencia del láser o el enfoque, superando las limitaciones de la espectroscopia Raman en análisis cuantitativo. Para aplicarlo a una muestra de CNTs con una relación de intensidades de las bandas G y D desconocida, debe llevarse a cabo la medida en primer lugar en una membrana sin modificar para calcular la relación de intensidades, y, posteriormente, en una membrana modificada con MWNTs para cuantificar la presencia de los CNTs.

Por último, las nanopartículas de oro se han determinado mediante microextracción en líquido iónico, no sólo de muestras de agua de río sino también de tejido de hígado de pollo. La extracción es cuantitativa y las nanopartículas extraídas en la fase de líquido iónico fueron analizadas por espectroscopia UV-Vis y Raman, estando esta última menos afectada por la interferencias de la matriz en el caso de la muestras de tejido de hígado. Hasta donde sabemos, la señal Raman de las nanopartículas de oro no se había explotado hasta ahora desde un punto de vista analítico.

El coeficiente de absorción molar de las AuNPs en el medio de líquido iónico es 2.5 veces menor que en agua, lo que disminuye la sensibilidad del método. Sin embargo, la extracción es necesaria para eliminar interferencias de la matriz de la muestra. Para calcular la concentración de las AuNPs, se utilizó el método propuesto por Haiss et al.[1], que tiene la limitación de que los ligandos de la superficie de las nanopartículas –citrato en este caso- pueden afectar a las

[1] W. Haiss, N.T.K. Thanh, J. Aveyard, D.G. Fernig, Anal. Chem. 79 (2007) 4215-4221.

propiedades ópticas de las mismas. Por otro lado, las bandas Raman de las nanopartículas de oro no han sido ampliamente descritas. Se empleó, por tanto, PCA seguido de calibración por PLS usando dos regiones del espectro para no perder información, lo que dificulta la calibración y el tratamiento de los datos en comparación con la calibración directa usada en el caso de la detección de c-SWNTs.

El análisis de nanopartículas en muestras reales es difícil, en parte porque no es posible conocer qué ligandos están unidos a las nanopartículas. Se seleccionaron AuNPs cubiertas por citrato, ya que son las más ampliamente usadas en aplicaciones. Tanto en el caso de muestras de agua de río como de hígado de pollo, tras fortificar la muestra, las nanopartículas se dejaron en contacto con el medio 4 horas para promover posibles intercambios de ligandos entre componentes de la muestra y citrato. En nuestra opinión, la extracción líquido-líquido es un buen procedimiento ya que se trabaja en condiciones de exceso de ligando, por lo que es razonable pensar que dichos ligandos pueden ser intercambiados por el catión del líquido iónico. Aunque este proceso, probablemente, tenga lugar en todos los casos, cabe destacar que la cinética puede ser diferente dependiendo del ligando. Por tanto, habría que estudiar la cinética y re-optimizar la cantidad de tensioactivo cuando se empleen nanopartículas con ligandos diferentes.

The preparation of this Memory, together with the experience gained during the development of this Doctoral Thesis, has provided an objective overview of the work presented herein. In this section, a critical assessment of the results achieved has been conducted to evaluate, on the one hand, the main contributions that the work can provide to the scientific community and, on the other hand, the drawbacks and shortcomings with a view to planning further investigations.

The main contributions of this Thesis are devoted to the synthesis, characterization and determination of nanoparticles of different nature.

*In the case of the **synthesis of nanoparticles**, a novel synthetic procedure, which has been adapted for continuous flow production of AuNPs, has been proposed with the highlights of being simple, environmentally friendly, leading to highly stable bare gold nanoparticles. In the case of the use of the continuous flow reactor, high throughput production of tailor-made bare AuNPs takes place without mixing solutions with good reproducibility.*

However, the polydispersity of the nanoparticles could be improved. Although it is comparable with other commonly employed synthetic routes, the absence of ligands attached into the nanoparticles' surface controlling their growth may influence it. Nevertheless, as previously reported, medium flow rates conditions in the reactor led to AuNPs with a narrower size distribution. Moreover, further studies could be performed to delve into the mechanism of the production of AuNPs. In the case of continuous flow production, the half-life time of the reactor could be studied in depth in order to evaluate if the composition and size of AuNPs obtained change after several use of the reactor.

*Regarding the **characterization of nanoparticles**, apart from microscopic techniques, carbon nanotubes have been analyzed by Raman spectroscopy, while gold nanoparticles solutions have been characterized by infrared spectroscopy and capillary electrophoresis. Raman spectroscopy proved to be a simple and inexpensive tool for the rapid identification of SWNTs in mixtures of MWNTs. The poor heat dissipation of CNTs limits their measurement in solid state, unless the equipment allows setting very low laser power. In this sense, the use of a confocal Raman spectrometer with an electron multiplying charge coupled device (EMCCD) provides increased sensibility, although using very low laser powers. This problem has been also overcome by dispersing the CNTs in surfactants, enabling the use of less expensive Raman equipments. It would be useful to compare CNTs surfactant dispersions and solid sample spectra measured with the same laser wavelength (herein dispersion were measured with a 785 nm laser and solid samples with a 532 nm one).*

The main limitation found in the characterization of gold nanoparticles with capillary electrophoresis is the small pathlength of the capillary, which leads to a low sensibility. CE equipment with an optic fiber coupled to the detector was employed in order to overcome this drawback as well as the use of large volume sample stacking for both increasing the sensitivity and the interaction of the nanoparticles with buffer solution. A 75-μm capillary was used in order to avoid its blockage when injecting highly concentrated NPs plugs.

On the other hand, when using infrared spectroscopy to characterize AuNPs solutions, the main shortcoming is the low rate of sedimentation of NPs on the ATR surface. Although CTAC was added in order to accelerate their deposition, if the rate could be further increased this technique might be used for the rapid determination and quantification of AuNPs.

Dynamic light scattering (DLS) is an analytical tool routinely used for measuring the hydrodynamic size of nanoparticles and colloids in liquid environments. In

our case, we did not have access to this technique, which certainly would have been very interesting in order to contrast and complete the characterization of nanoparticles used during the development of this Thesis.

*Concerning the **determination of nanoparticles**, Raman spectroscopy has also revealed as a powerful tool for this task. c-SWNTs have been determined, on the one side, by liquid-liquid microextraction in ionic liquid, which enabled their preconcentration, avoiding interferences of sample matrix since the NPs are extracted into the ionic liquid phase. Secondly, they have been determined by SERS spectroscopy taking advantage of the enhancement properties of bare gold nanoparticles produced with the stainless steel. The formation of the SERS substrate is simple, low quantities of gold nanoparticles being needed for its preparation. Finally, MWNT-modified membranes also allowed the retention and quantification of c-SWNTs directly on the membrane with better sensitivity. Common to all these methods is the use of a home-made microfiltration device with a small diameter of filtration, which improved the preconcentration of CNTs in the different platforms where they were deposited. The retention of c-SWNTs on membranes (modified with different materials: MWNTs, AuNPs SERS substrate) increased the sensitivity of the methods, enabling quantitative Raman measurements to be performed.*

Fluorescence interference is the major limitation of these methodologies, which prevent from achieving better limits of detection, which fall in the μgL^{-1} range, while theoretical predictions expect CNT concentration in aqueous environmental samples in the ngL^{-1} range. Nevertheless, these methods can be considered as a first approximation to the quantification of these nanomaterials in water matrices. Thanks to the use of portable Raman spectrometers, those procedures could be applied as screening methods to control the release of such materials in source points of contaminations such as factories, landfills or wastewater effluents where the concentrations are expected to be higher. In the

case of SERS measurements, a greater increase would have been obtained if a laser in resonance with AuNPs plasmon had been used. We proved with a 532 nm laser, observing larger signal enhancements, however, higher fluorescence interferences were also found. The calibration curve of SERS measurements fits a Langmuir isotherm, thus, when quantifying samples, we should ensure that our concentration falls in the linear region, or dilute the sample if necessary.

Only in the case of the preconcentration of c-SWNTs on MWNTs modified membranes, an interference study was performed using humic acids. Nevertheless, recoveries studies with river water samples were performed in all the cases finding acceptable values. Regarding ionic liquid microextraction, selectivity is improved by the extraction step as well as the fact that Raman signal are characteristic of CNTs. Other carbonaceous materials could interfere in the signal, in this sense, instead of using D band for quantification, as shown as example in that work, which is more sensitive to defects and carbonaceous impurities, the use of G band would be more selective.

The use of G-/D-band intensity ratio as analytical signal in the case of MWNTs modified membranes shows the advantage that this parameter does not depend on Raman conditions, such as laser power or sample focusing, overcoming limitations of Raman spectroscopy for quantitative analysis. If the G-/D-band intensity ratio of an unknown CNT sample need to be calculated, a two-filter assay can be carried out, using a nonmodified membrane to determine the G-/D-band intensity ratio followed by a MWNT-modified membrane to quantify the amount of CNTs present.

Finally, gold nanoparticles have been determined by microextraction in ionic liquids not only in river water samples but also in liver tissue. The extraction proved to be quantitative and NPs extracted within the IL phase were analyzed by UV-Vis and Raman spectroscopy, the latter being less affected by matrix interferences in the case of liver tissue samples. To our knowledge, the Raman

signal of gold nanoparticles had not been exploited until now from an analytical point of view.

The molar absorption coefficient of AuNPs in the ionic liquid is 2.5 times lower than in water, which decreases the sensitivity of the method. However, the extraction is necessary in order to remove interferences from the sample matrix. In order to calculate the concentration of gold nanoparticles, the method proposed by Haiss et al.[1] *was followed, which has some limitations due to the fact that ligands coating the nanoparticles –citrate in this case- may affect their optical properties. On the other hand, Raman spectral features of gold nanoparticles have not been widely described. Thus, PCA followed by PLS calibration was employed using two regions of the spectrum in order not to lose information, which difficult calibration and data treatment in comparison with direct calibration employed in the case of c-SWNTs detection.*

The analysis of nanoparticles in real samples is difficult, in part because it is not possible to know the ligand coating that nanoparticles have. Citrate-capped AuNPs were selected because they are the most widely used in applications. In the case of both river water and liver samples, after spiking the sample, nanoparticles were left in the medium for 4 hours in order to promote possible ligand changes between compounds of the sample and citrate. In our opinion, the liquid–liquid extraction is a good procedure because it works with excess of ligand, then it is reasonable to think that ligands can be exchanged by the cation of the IL. Although this process, probably, takes place in all cases, it must be remarked that the kinetics can be different depending on the ligand. Then, when analyzing nanoparticles with a different ligand, the kinetics as well as the amount of surfactant must be re-studied or re-optimized.

[1] W. Haiss, N.T.K. Thanh, J. Aveyard, D.G. Fernig, Anal. Chem. 79 (2007) 4215-4221.

ANEXOS

Producción científica

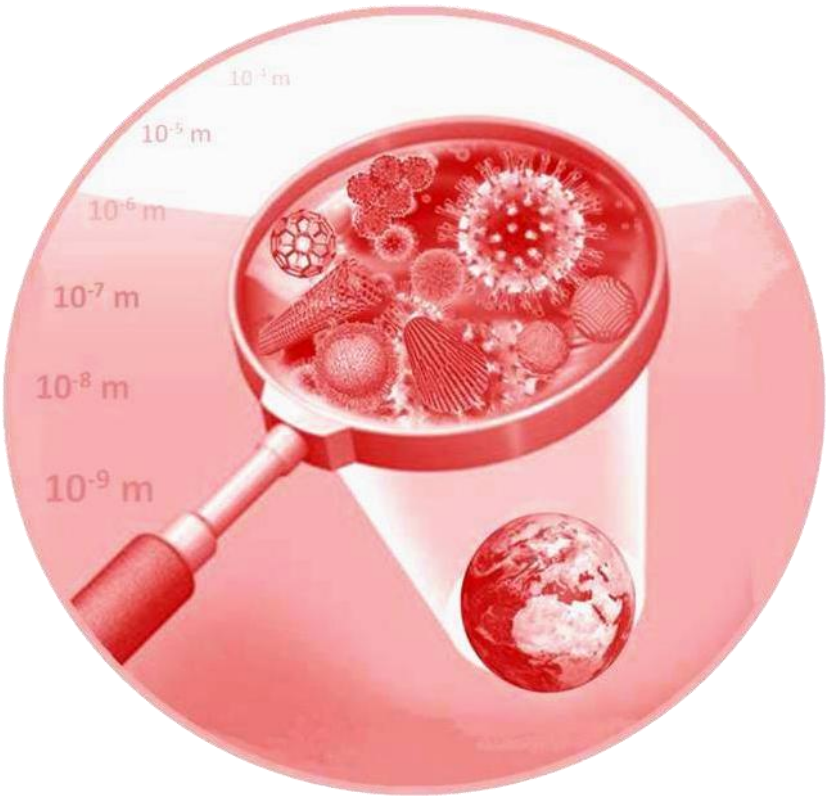

Anexo A

Publicaciones científicas derivadas de la Tesis Doctoral

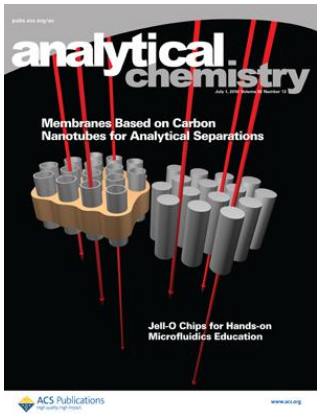

1. The potential of carbon nanotube membranes for analytical separations.

A.I. López-Lorente, B.M. Simonet, M. Valcárcel

Analytical Chemistry 82 (2010) 5399-5407.

Feature article. Portada de la revista del mes de Julio de 2010.

2. Electrophoretic methods for the analysis of nanoparticles.

A.I. López-Lorente, B.M. Simonet, M. Valcárcel

Trends Analytical Chemistry (TrAC) 30 (2011) 58-71.

3. Analytical potential of hybrid nanoparticles.

A.I. López-Lorente, B.M. Simonet, M. Valcárcel

Analytical Bioanalytical Chemistry 399 (2011) 43-54.

4. Determination of nanoparticles in biological matrices.

A.I. López-Lorente, B.M. Simonet, M. Valcárcel

Frontiers in Bioscience E4 (2012) 41024-41042.

5. Analysis of nanoparticles based on electrophoretic separations.

A.I. López-Lorente, B.M. Simonet, M. Valcárcel

Comprehensive Analytical Chemistry 59 (2012) 33-89 (Capítulo de libro).

6. Rapid analysis of gold nanoparticles in liver and river water samples.

A. I. López-Lorente, B. M. Simonet, M. Valcárcel

Analyst 137 (2012) 3528-3534.

7. Determination of carboxylic SWCNTs in river water by microextraction in ionic liquid and determination by Raman spectroscopy.

A.I. López-Lorente, B.M. Simonet, M. Valcárcel

Talanta 105 (2013) 75-79.

8. Qualitative detection and quantitative determination of single-walled carbon nanotubes in mixtures of carbon nanotubes with a portable Raman spectrometer.

A.I. López-Lorente, B.M. Simonet, M. Valcárcel

Analyst 138 (2013) 2378-2385.

9. Bare gold nanoparticles mediated surface-enhanced Raman spectroscopic determination and quantification of carboxylated single-walled carbon nanotubes.

A. I. López-Lorente, B. M. Simonet, M. Valcárcel, B. Mizaikoff

Analytica Chimica Acta 788 (2013) 122-128.

10. Sequential preconcentration and on-membrane Raman determination of carboxylic single-walled carbon nanotubes in river water samples.

A.I. López-Lorente, M.L. Polo-Luque, M. Valcárcel

Analytical Chemistry 85 (2013) 10338-10343.

11. Characterization of stainless steel assisted bare gold nanoparticles and their analytical potential.

A.I. López-Lorente, B.M. Simonet, M. Valcárcel, S. Eppler, R. Schindl, C. Kranz, B. Mizaikoff.

Talanta 118 (2014) 321-327.

12. Raman spectroscopic characterization of single-walled carbon nanotubes: influence of sample aggregation state.

A.I. López-Lorente, B.M. Simonet, M. Valcárcel

Analyst (2013) DOI: 10.1039/C3AN00642E.

13. Continuous flow synthesis and characterization of tailor-made bare gold nanoparticles for analytical applications.

A. I. López-Lorente, M. Valcárcel, B. Mizaikoff

En revisión en la revista Microchimica Acta.

14. Capillary electrophoretic separation of citrate-capped silver and gold nanoparticles by interaction with thiol compounds as additives in buffer solution.

A.I. López-Lorente, M.L. Soriano, M. Valcárcel

En revisión en la revista Journal of Chromatography A.

15. Infrared attenuated total reflection spectroscopy as a tool for the characterization of gold nanoparticles in solution.

A.I. López-Lorente, M. Sieger, M. Valcárcel, B. Mizaikoff

En revisión en la revista Analytical Chemistry.

Anexo B

Presentación de comunicaciones a congresos

Comunicaciones orales

1. Comunicación Flash y póster

López-Lorente, A.I.; Simonet, B.M.; Valcárcel, M.

Preconcentración y determinación de nanopartículas de oro en muestras ambientales y biológicas.

III Workshop Nanociencia y Nanotecnología Analíticas, Oviedo, Septiembre-2009.

2. Comunicación Flash y póster

López-Lorente, A.I.; Simonet, B.M.; Valcárcel, M.

Potencial de las membranas con nanotubos de carbono para las separaciones analíticas.

IV Workshop Nanociencia y Nanotecnología Analíticas, Zaragoza (España), Septiembre-2010.

3. Oral

López-Lorente, A.I.

Contribuciones analíticas a la caracterización y determinación de nanopartículas.

II Congreso de Investigadores en Formación de la Universidad de Córdoba, Córdoba (España), Mayo-2012.

4. Oral

López-Lorente, A.I.; Simonet, B.M.; Valcárcel, M.; Mizaikoff, B.

New stainless steel assisted synthesis of bare gold nanoparticles and application to SERS determination of carbon nanotubes.

IV Encuentro sobre Nanociencia y Nanotecnología de Investigadores y Tecnólogos Andaluces (NanoUCO), Córdoba (España), Febrero-2013.

5. Oral

López-Lorente, A.I.; Simonet, B.M.; Valcárcel, M.

Determination of carboxylic SWCNTs in river water by microextraction in ionic liquid and determination by Raman spectroscopy.

XVIII Reunión de la Sociedad Española de Química Analítica, Úbeda (España), Junio-2013.

6. Conferencia invitada

López-Lorente, A.I.; Simonet, B.M.; Valcárcel, M.; Mizaikoff, B.

Catalytic and sustainable synthesis and applications of bare gold nanoparticles.

VI Workshop Nanociencia y Nanotecnología Analíticas, Alcalá de Henares (España), Julio-2013.

7. Oral

López-Lorente, A.I.; Valcárcel, M.; Mizaikoff, B.

Bare gold nanoparticles mediated surface-enhanced Raman spectroscopic (SERS) determination and quantification of carboxylated single-walled carbon nanotubes.

II Simposio de Jóvenes Investigadores en Espectroscopia Aplicada, Granada (España), Julio-2013.

8. Oral

López-Lorente, A.I.; Simonet, B.M.; Valcárcel, M.

Determination of carboxylic SWCNTs in river water by microextraction in ionic liquid and determination by Raman spectroscopy.

XVII Euroanalysis, Warsaw (Polonia), Agosto-2013.

Comunicaciones póster

9. Póster

López-Lorente, A.I.; Simonet, B.M.; Valcárcel, M.

Filtros modificados con nanotubos de carbono como nuevo sistema de extracción en fase sólida en disco.

II Workshop Nanociencia y Nanotecnología Analíticas, Tarragona (España), Septiembre-2008

10. Póster

López-Lorente, A.I.; Simonet, B.M.; Valcárcel, M.

Filtros modificados con nanotubos de carbono como nuevo sistema de preconcentración.

I Encuentro sobre Nanociencia y Nanotecnología de Investigadores y Tecnólogos de la Universidad de Córdoba. (NanoUCO), Córdoba (España), Diciembre-2008.

11. Póster

López-Lorente, A.I.; Simonet, B.M.; Valcárcel, M.

Determinación rápida de nanopartículas de oro en muestras ambientales y biológicas.

II Encuentro sobre Nanociencia y Nanotecnología de Investigadores y Tecnólogos de la Universidad de Córdoba. (NanoUCO), Córdoba (España), Enero-2010.

12. Póster

López-Lorente, A.I.; Simonet, B.M.; Valcárcel, M.

Caracterización rápida de nanotubos de carbono mediante un espectrómetro Raman portátil.

II Encuentro sobre Nanociencia y Nanotecnología de Investigadores y Tecnólogos de la Universidad de Córdoba. (NanoUCO), Córdoba (España), Enero-2010.

13. Póster

López-Lorente, A.I.; Simonet, B.M.; Valcárcel, M.

Método de screening para la detección rápida de MWNTs en productos de síntesis de SWNTs.

XII Encuentro del Grupo Regional Andaluz de la Sociedad Española de Química Analítica. Córdoba (España), Junio-2010.

14. Póster

López-Lorente, A.I.; Simonet, B.M.; Valcárcel, M.

Raman spectroscopy as tool for the characterization of mixtures of carbon nanotubes.

VI Conferencia Ibérica de espectroscopia. XII Encuentro Nacional de espectroscopia, Oporto (Portugal), Septiembre-2010.

15. Póster

López-Lorente, A.I.; Simonet, B.M.; Valcárcel, M.

Potencial de las nanopartículas híbridas.

IV Workshop Nanociencia y Nanotecnología Analíticas, Zaragoza (España), Septiembre-2010.

16. Póster

López-Lorente, A.I.; Simonet, B.M.; Valcárcel, M.

Caracterización de nanotubos de carbono mediante equipos Raman portátiles.

IV Workshop Nanociencia y Nanotecnología Analíticas, Zaragoza (España), Septiembre-2010.

17. Póster

López-Lorente, A.I.; Simonet, B.M.; Valcárcel, M.

Influencia del estado de agregación en el espectro Raman de nanotubos de carbono monocapa (SWNTs.)

III Encuentro sobre Nanociencia y Nanotecnología de Investigadores y Tecnólogos Andaluces (NanoUCO), Córdoba (España), Febrero-2011.

18. Póster

López-Lorente, A.I.; Simonet, B.M.; Valcárcel, M.

Potencial de las nanopartículas híbridas en química analítica.

III Encuentro sobre Nanociencia y Nanotecnología de Investigadores y Tecnólogos Andaluces (NanoUCO), Córdoba (España), Febrero-2011.

19. Póster

López-Lorente, A.I.; Simonet, B.M.; Valcárcel, M.

Influence of the aggregation state in the Raman spectrum of single-walled carbon nanotubes (SWNTs).

8th WITec Symposium Confocal Raman Imaging, Ulm (Alemania), Octubre-2011.

20. Póster

López-Lorente, A.I.; Simonet, B.M.; Valcárcel, M.

Preconcentration and determination of water soluble carbon nanotubes (CNTs) by microliquid-liquid extraction and Raman detection.

XXIII Reunión Nacional-VII Congreso Ibérico de Espectroscopia, Córdoba (España), Septiembre-2012.

21. Póster

López-Lorente, A.I.; Simonet, B.M.; Valcárcel, M.

Influence of the aggregation state in the Raman spectrum of single-walled carbon nanotubes (SWNTs).

XXIII Reunión Nacional-VII Congreso Ibérico de Espectroscopia, Córdoba (España), Septiembre-2012.

22. Póster

López-Lorente, A.I.; Valcárcel, M.; Mizaikoff, B.

Continuous flow synthesis of bare gold nanoparticles and their application to the determination of carbon nanotubes by SERS.

XVII Euroanalysis, Warsaw (Polonia), Agosto-2013.

23. Póster

López-Lorente, A.I.; Sieger, M.; Valcárcel, M.; Mizaikoff, B.

Attenuated total reflection infrared (ATR-IR) spectroscopy in-situ monitorization of the synthesis of bare gold nanoparticles.

Trends in Nanotechnology International Conference (TNT2013), Sevilla (España), Septiembre-2013.

Anexo C

Pósters

FILTROS MODIFICADOS CON NANOTUBOS DE CARBONO COMO NUEVO SISTEMA DE EXTRACCIÓN EN FASE SÓLIDA EN DISCO

A. López, B.M. Simonet, M. Valcárcel

Departamento de Química Analítica, Universidad de Córdoba. Edificio Anexo C3, Campus de Rabanales, 14071 Córdoba.

E-mail: qa1meobj@uco.es

OBJETIVOS

- Establecer procedimientos simples de síntesis de filtros modificados con nanotubos de carbono dispersados y evaluar sus propiedades adsortivas.
- Estudiar la aplicabilidad analítica de los filtros modificados como sistema de extracción en fase sólida en disco

INTRODUCCIÓN

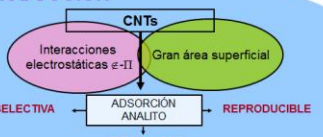

FILTROS MODIFICADOS	CARTUCHOS SPE
Pequeñas cantidades de CNTs	Mayor cantidad de sorbente empaquetado
Pequeños volúmenes de muestra	Mayor cantidad de muestra
Compatible con flujos grandes (no sobrepresión)	No compatible con flujos altos
Eficacia superior	Menor adsorción de analitos
Fácil acoplamiento sistema flujos	Integración más complicada

PROCEDIMIENTO DE SÍNTESIS

RECOMENDADO

1. Dispersar los CNTs en Tritón X-100 al 0.5% asistido por ultrasonidos
2. Filtrar a vacío por succión la dispersión de CNTs.
3. Eliminar el tensioactivo con metanol
4. Secar con aire

CARACTERÍSTICAS CNTs				
Tipo	Diámetro (nm)	Longitud (μm)	Pureza	Carbono amorfo
MWCNTs (1)	10-30	5-15	≥95%	<3%
MWCNTs (2)	5-20	1-10	≥95%	No detectado por TEM
SWNTs	< 2	5-15	≥90%(CNTs), ≥50% (SWNTs)	<5%

Concentración de tensioactivo (%) necesaria para dispersar los CNTs (concentración 1,33 gL^{-1})			
	MWCNTs (1)	MWCNTs (2)	SWNTs
Tritón X-100	0,5	0,5	0,5
SDS	0,6	0,6	Con 5% no se dispersaron

COMPARACIÓN CNTs			
LODs lidocaina (ppm)			
	MWNTs (1)	MWNTs (2)	SWNTs
Tritón X-100	0,005	0,1	0,05
SDS	>0,005	0,1	-

La estructura química del CNT condiciona mucho su poder adsorbente

10 mL de muestra → FILTRAR MUESTRA

Elución con 0,5 ml de eluente modificado con patrón interno en caso de requerirse → ELUIR

ANALIZAR

Análisis por CE/MS

CNTs AGREGADOS

SUPERFICIE CNTs

INTERSTICIOS AGREGADOS CNTs

ADSORCIÓN ANALITOS

MAYOR GRADO DE INTERACCIÓN MOLECULAR

CNTs DISPERSADOS

SUPERFICIE CNTs

La dispersión previa de los CNTs elimina la presencia de agregados aumentando el área eficaz de interacción de los CNTs

El tensioactivo Tritón X-100 ofrece mejores dispersiones que los tensioactivos iónicos tipo SDS o CTAB

IMPORTANTE

LOS FILTROS MODIFICADOS CON CNTs OFRECEN MAYORES VALORES DE PRECONCENTRACIÓN QUE COLUMNAS DE SPE CONTENIENDO MAYORES CANTIDADES DE CNTs EMPAQUETADOS

PROCEDIMIENTO EXPERIMENTAL

ANALITOS ENSAYADOS

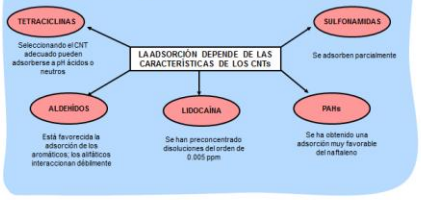

CONCLUSIONES

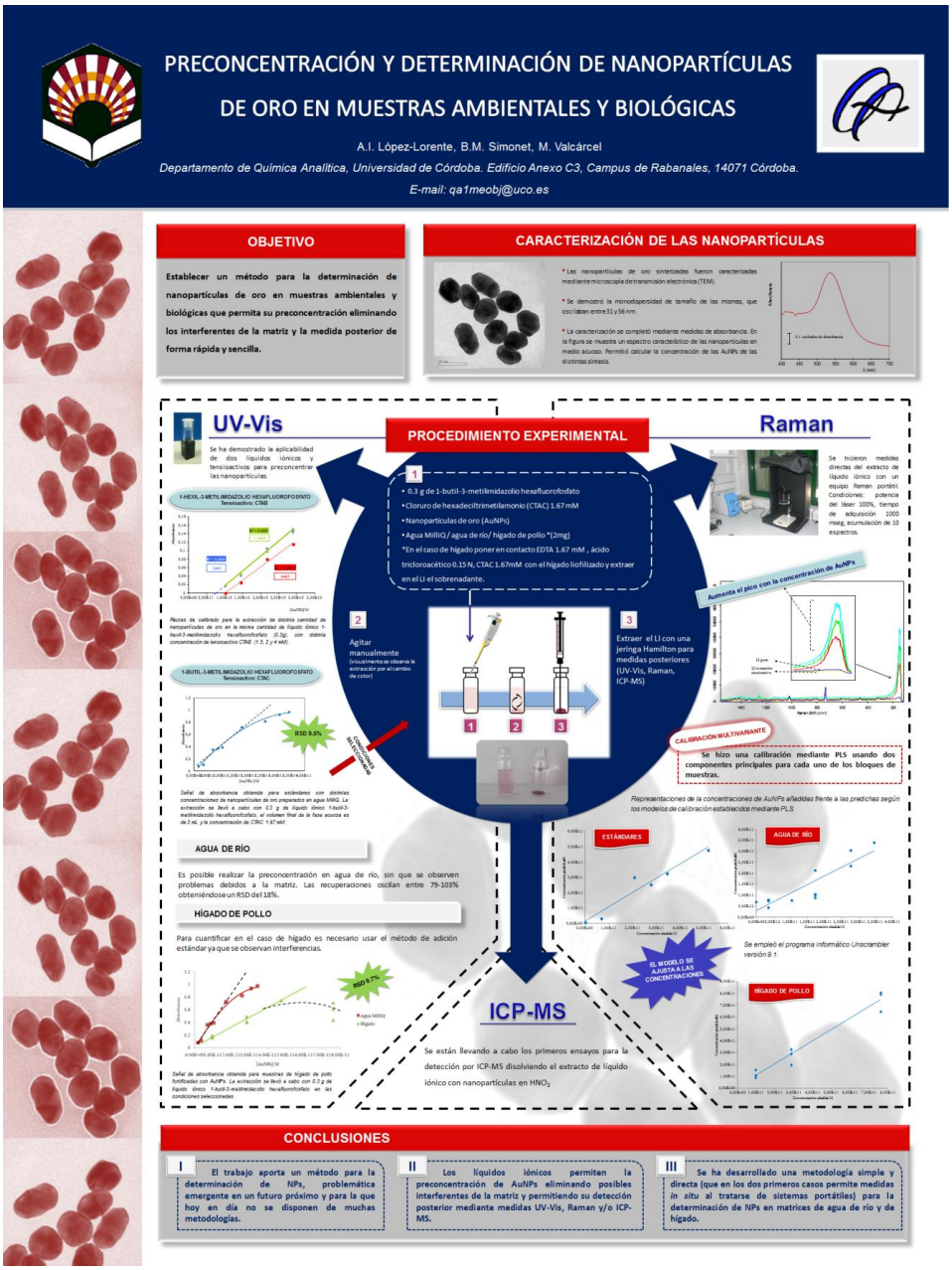
PRECONCENTRACIÓN Y DETERMINACIÓN DE NANOPARTÍCULAS DE ORO EN MUESTRAS AMBIENTALES Y BIOLÓGICAS
A.I. López-Lorente, B.M. Simonet, M. Valcárcel
Departamento de Química Analítica, Universidad de Córdoba. Edificio Anexo C3, Campus de Rabanales, 14071 Córdoba.
E-mail: qa1meobj@uco.es
OBJETIVO
Establecer un método para la determinación de nanopartículas de oro en muestras ambientales y biológicas que permita su preconcentración eliminando los interferentes de la matriz y la medida posterior de forma rápida y sencilla.
CARACTERIZACIÓN DE LAS NANOPARTÍCULAS
PROCEDIMIENTO EXPERIMENTAL
UV-Vis
Raman
1
• 0.3 g de 1-butil-3-metilimidazolio hexafluorofosfato
• Cloruro de hexadeciltrimetilamonio (CTAC) 1.67 mM
• Nanopartículas de oro (AuNPs)
• Agua MilliQ / agua de río/ hígado de pollo *(2mg)
*En el caso de hígado poner en contacto EDTA 1.67 mM , ácido tricloroacético 0.15 N, CTAC 1.67mM con el hígado liofilizado y extraer en el LI el sobrenadante.
2
Agitar manualmente
3
Extraer el LI con una jeringa Hamilton para medidas posteriores (UV-Vis, Raman, ICP-MS)
Aumenta el pico con la concentración de AuNPs
CALIBRACIÓN MULTIVARIANTE
Se hizo una calibración mediante PLS usando dos componentes principales para cada uno de los bloques de muestras.
Representaciones de la concentraciones de AuNPs añadidas frente a las predichas según los modelos de calibración establecidos mediante PLS.
ESTÁNDARES
AGUA DE RÍO
HÍGADO DE POLLO
EL MODELO SE AJUSTA A LAS CONCENTRACIONES
Se empleó el programa informático Unscrambler versión 9.1.
AGUA DE RÍO
Es posible realizar la preconcentración en agua de río, sin que se observen problemas debidos a la matriz. Las recuperaciones oscilan entre 79-103% obteniéndose un RSD del 18%.
HÍGADO DE POLLO
Para cuantificar en el caso de hígado es necesario usar el método de adición estándar ya que se observan interferencias.
ICP-MS
Se están llevando a cabo los primeros ensayos para la detección por ICP-MS disolviendo el extracto de líquido iónico con nanopartículas en HNO3
CONCLUSIONES
I El trabajo aporta un método para la determinación de NPs, problemática emergente en un futuro próximo y para la que hoy en día no se disponen de muchas metodologías.
II Los líquidos iónicos permiten la preconcentración de AuNPs eliminando posibles interferentes de la matriz y permitiendo su detección posterior mediante medidas UV-Vis, Raman y/o ICP-MS.
III Se ha desarrollado una metodología simple y directa (que en los dos primeros casos permite medidas in situ al tratarse de sistemas portátiles) para la determinación de NPs en matrices de agua de río y de hígado.

CARACTERIZACIÓN RÁPIDA DE NANOTUBOS DE CARBONO MEDIANTE UN ESPECTRÓMETRO RAMAN PORTÁTIL

A.I. López-Lorente, B.M. Simonet, M. Valcárcel

Departamento de Química Analítica, Universidad de Córdoba. Edificio Anexo C3, Campus de Rabanales, 14071 Córdoba.

E-mail: qa1meobj@uco.es

ESPECTRO RAMAN DE LOS NANOTUBOS DE CARBONO

Los nanotubos de carbono (CNTs) son sistemas unidimensionales (1D), lo que origina un confinamiento, y consecuente cuantización, de los estados de energía electrónica y vibracional en la dirección radial que da lugar a la aparición de singularidades de van Hove (vHSs) en la densidad de estados electrónicos que son distintas para cada nanotubo. Las transiciones ópticas en los CNTs ocurren entre vHSs de las respectivas bandas electrónicas de valencia y conducción, siendo pues transiciones discretas. En la espectroscopia Raman normalmente se excita la muestra con láseres de energías que coinciden en el rango de algunas de las transiciones ópticas de los CNTs, por lo que cabría esperar que dicha espectroscopia pudiera proporcionar información sobre la estructura de los mismos. La enorme potencialidad de la técnica reside en que tiene lugar un proceso Raman resonante que depende del diámetro del nanotubo. La resonancia, que se debe a que la energía del fotón excitatriz coincide con alguna de las transiciones electrónicas entre singularidades de van Hove de los CNTs, se traduce en una intensificación de los correspondientes espectros Raman. Como a esta intensificación se añade el elevado número de estados electrónicos que se encuentran agrupados en cada una de las vHSs, la intensificación total de los espectros Raman (resonantes) de CNTs puede llegar a ser de hasta 10^6 por lo que es posible estudiar incluso nanotubos aislados.

Banda G o modos tangenciales, aparecen alrededor de 1600 cm^{-1}. Provienen de vibraciones dentro del plano de las láminas de grafito. Por tanto, en los CNTs se corresponden con movimientos de los átomos de carbono perpendiculares a la dirección radial. Su perfil indica el carácter metálico o semiconductor de los CNTs.

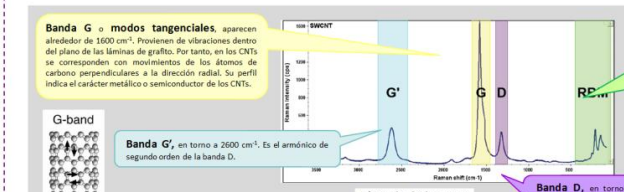

"Radial breathing modes" (RBMs), aparecen en la zona del espectro en torno a 150 cm^{-1}. Su frecuencia es proporcional a la inversa del diámetro del nanotubo. Todos los átomos de carbono se desplazan en fase y en la dirección radial del nanotubo. Son característicos de los SWNTs.

G-band

Banda G', en torno a 2600 cm^{-1}. Es el armónico de segundo orden de la banda D.

RBM

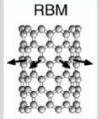

Información sobre la estructura fina de las bandas de valencia y conducción de los CNTs.

Banda D, en torno a 1300 cm^{-1}. Su origen está relacionado con el desorden y los defectos en la estructura de los CNTs.

ASPECTOS NEGATIVOS

- Raman portátil dificultad enfoque manual muestra sólida
- Fluorescencia muestra dificulta la medida
- Degradación de los CNTs al incidir el láser

ASPECTOS POSITIVOS

- Raman herramienta útil para la caracterización de CNTs
- Proporciona gran información de forma rápida

MEDIDA DE LOS ESPECTROS RAMAN DE NANOTUBOS DISPERSADOS

Se han registrado espectros Raman de nanotubos de carbono dispersados en distintos tensioactivos: Dodecilsulfato sódico (SDS), Tritón X-100 y bromuro de hexadeciltrimetilamonio (CTAB).

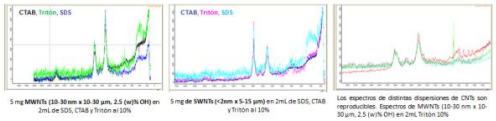

5 mg **MWNTs (10-30 nm x 10-30 µm, 2.5 (w)% OH)** en 2mL de SDS, CTAB y Tritón al 10%

5 mg de **SWNTs (<2nm x 5-15 µm)** en 2mL de SDS, CTAB y Tritón al 10%

Los espectros de distintas dispersiones de CNTs son reproducibles. Espectros de MWNTs (10-30 nm x 10-30 µm, 2.5 (w)% OH) en 2mL Tritón 10%

CARACTERIZACIÓN CNTs

Nanotubos de distintas características generan espectros Raman diferentes

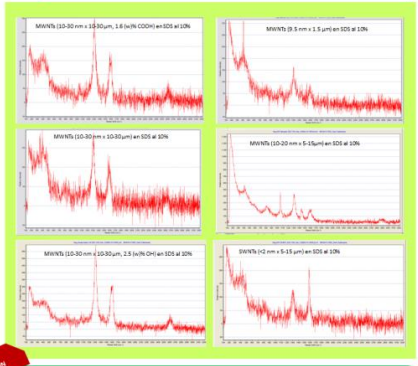

LA PRESENCIA DE TENSIOACTIVO NO AFECTA A LA SEÑAL RAMAN DE LOS CNTs Y FACILITA EL ENFOQUE DE LA MUESTRA Y OBTENCIÓN DEL ESPECTRO

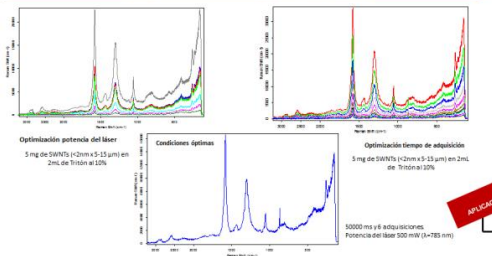

APLICACIÓN

Caracterización de mezclas de CNTs mediante medidas cinéticas por su distinta capacidad de dispersión en tensioactivos

MÉTODO DE SCREENING PARA LA DETECCIÓN RÁPIDA DE MWNTS EN PRODUCTOS DE SÍNTESIS DE SWNTS

A.I. López-Lorente, B.M. Simonet, M. Valcárcel
Departamento de Química Analítica, Universidad de Córdoba. Edificio Anexo C3, Campus de Rabanales, 14071 Córdoba.
E-mail: qa1meobj@uco.es

OBJETIVO

Desarrollar un método rápido para la monitorización de MWNTs como subproducto en productos de SWNTs. Desarrollar una metodología compatible con un equipo Raman portátil.

INTRODUCCIÓN

La espectroscopia Raman es una poderosa herramienta capaz de proporcionar gran información de estos sistemas. Por lo general las muestras están constituidas por una mezcla de nanotubos de carbono, de modo que el espectro Raman corresponde a un promedio de espectros de los distintos nanotubos. Las transiciones ópticas en los CNTs ocurren entre singularidades de van Hove de las bandas electrónicas de valencia y conducción. Las bandas más características de los CNTs que se han utilizado en este trabajo son la banda correspondiente a la vibración fundamental de elongación tangencial denominada G, sobre 1600 cm^{-1}, así como la banda D de segundo orden en la zona de 1300 cm^{-1}.

Banda G o modos tangenciales, aparecen alrededor de 1600 cm^{-1}. Provienen de vibraciones dentro del plano de las láminas de grafito. Su perfil indica el carácter metálico o semiconductor de los CNTs.

Banda G', en torno a 2600 cm^{-1}. Es el armónico de segundo orden de la banda D.

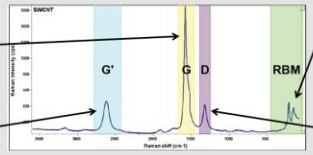

"Radial breathing modes" (RBMs), aparecen en la zona del espectro en torno a 150 cm^{-1}. Su frecuencia es proporcional a la inversa del diámetro del nanotubo. Son informativas en el caso de SWNTs.

Banda D, en torno a 1300 cm^{-1}. Su origen está relacionado con el desorden y los defectos en la estructura de los CNTs.

ESPECTROS RAMAN DE CNTs DISPERSADOS CON TENSIOACTIVO

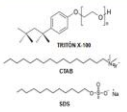

La dispersión con tensioactivos permite obtener el espectro de CNTs de forma rápida, sin interferencias del tensioactivo y minimizando problemas de fluorescencia y degradación de la muestra como consecuencia de una mejor disipación de calor, por lo que permite emplear potencias de láser mayores.

Se ha demostrado que el espectro obtenido puede correlacionarse con el espectro de muestras sólidas.

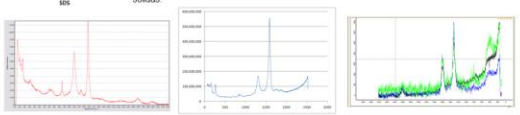

Espectro Raman de SWNTs dispersados en tensioactivo (SDS) y sólidos, respectivamente

Espectro Raman de MWNTs funcionalizados con grupos OH dispersos con distintos tensioactivos: SDS, CTAB y Triton X-100

CONDICIONES ÓPTIMAS MEDIDA

- Longitud de onda del láser: 785 nm
- Potencia del láser: 499.95 mW
- Tiempo de adquisición: 50 s
- Espectros acumulados: 6

NATURALEZA CNTs

Se han analizado CNTs de distinta naturaleza encontrándose espectros característicos para cada uno de ellos.

	Diámetro (nm)	Longitud (µm)	Funcionalización
MWNTs-1	10-30	10-30	2.5 (wt)% OH
MWNTs-2	10-30	10-30	1.6 (wt)% COOH
MWNTs-3	10-30	10-30	-
MWNTs-4	5-20	1-10	-
MWNTs-5	10-20	5-15	-
MWNTs-6	9.5	1.5	-
MWNTs-7	110-170	2	-
SWNTs	<2	5-15	-

Cada CNT posee una relación de las bandas D/G característica. Además en los SWNTs aparecen las bandas RBM y la banda G está desplazada unos pocos nm.

MEZCLAS DE CNTs

Dado que cada tipo de nanotubo origina un espectro Raman característico, investigamos la posibilidad de identificar y (semi)cuantificar la presencia de nanotubos de carbono de distinta naturaleza en una dispersión de CNTs de distinto tipo. Para ello preparamos mezclas con distinta cantidad de SWNTs y MWNTs modificados con grupos hidroxilos. La figura muestra la variación de la relación de las bandas D y G al variar la proporción de cada tipo de nanotubo, relación que resultó ser 0.378 para los SWNTs puros y 2.4587 para MWNTs-1 en ausencia de otro tipo de nanotubo. Se observa que existe una relación lineal entre la altura o área de as bandas D/G y el % de SWNTs.

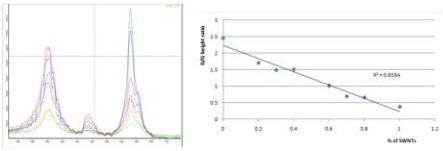

CONCLUSIONES

LA PRESENCIA DE TENSIOACTIVO NO AFECTA A LA SEÑAL RAMAN DE LOS CNTs Y FACILITA EL ENFOQUE DE LA MUESTRA Y OBTENCIÓN DEL ESPECTRO → NANOTUBOS DE DISTINTAS CARACTERÍSTICAS GENERAN ESPECTROS RAMAN DIFERENTES → SE HA DESARROLLADO UNA METODOLOGÍA RÁPIDA Y SIMPLE DE ANÁLISIS DE CNTs MEDIANTE UN EQUIPO PORTÁTIL DE RAMAN → A PARTIR DE LA RELACIÓN DE BANDAS D Y G SE HA DETERMINADO LA PRESENCIA DE MWNTs EN PRODUCTOS DE SÍNTESIS DE SWNTs

RAMAN SPECTROSCOPY AS TOOL FOR THE CHARACTERIZATION OF MIXTURES OF CARBON NANOTUBES

A.I. López-Lorente, B.M. Simonet, M. Valcárcel

Department of Analytical Chemistry, University of Córdoba. E-14071 Córdoba, Spain.

E-mail: qa1meobj@uco.es

INTRODUCTION

Raman spectroscopy is the most widely used technique to study carbon nanotubes, primarily focused on single-walled carbon nanotubes (SWCNTs). Raman scattering from SWCNTs is a resonant phenomena which generates an intense and easily measurable signal. Their popularity relies on their usefulness to provide information not only on the vibrational properties but also on the structure and electronic properties of the nanotubes. The most significant spectral features for SWCNTs are the radial breathing mode (RBM, 100-300 cm^{-1}), the disorder peak (D peak, ~1350 cm^{-1}), the tangenthial mode (G band, 1400-1700 cm^{-1}), and the second-order overtone of the D peak (D', 2500-2800 cm^{-1}).

G band or **tangenthial modes**, around1600 cm^{-1}, is closely related to vibrations in all sp^2 carbon materials. The most important aspect of the G-band is the characteristic Raman lineshape which differs in accordance with whether the nanotube is semiconducting or metallic, allowing to readily distinguishing between both types.

G' band, around 2600 cm^{-1}. It is the second order armonic of D band.

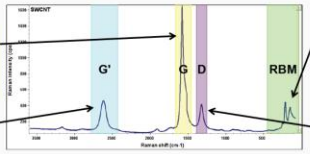

"Radial breathing modes" (RBMs), appears at wavenumbers of above 150 cm^{-1}. Its frecuency is proportional to the inverse of the nanotube diameter. They give inclimation in the case of SWNTs.

D band, about 1300 cm^{-1}. Its origin is related with the disorder and defects on the nanotube structure.

EXPERIMENTAL

	Diameter(nm)	Length (μm)	Funtionalization
MWNTs-1	10-30	10-30	2.5 (wt)% OH
MWNTs-2	10-30	10-30	1.6 (wt)% COOH
MWNTs-3	10-30	10-30	-
MWNTs-4	5-20	1-10	-
MWNTs-5	10-20	5-15	-
MWNTs-6	9.5	1.5	-
MWNTs-7	110-170	2	-
SWNTs	<2	5-15	-

CNTs NATURE

CNTs of different nature have been analyzed which provided characteristic spectra for each type. Each CNT posseses a characteristic D/G band relationship. Moreover, in the case of SWNTs appear RBM bands and there is a displacement of G band.

OPTIMAL MEASUREMENT CONDITIONS

- Laser wavelength: 785 nm
- Laser power: 499.95 mW
- Adquisition time: 50 s
- Coadded spectra: 6

RESULTS

CNTs RAMAN SPECTRA DISPERSED WITH SURFACTANTS

Carbon nanotubes samples can be damaged during data capture due to the poor heat dissipation of carbon nanotubes. In order to avoid this problem, carbon nanotubes were dispersed in aqueous solution with the aid of surfactants to facilitate sample heat dissipation due to the much larger thermal conductivity of the liquids with respect to the air. We have evaluated different surfactants for this task, namely sodium dodecyl sulphate (SDS), Triton X-100 and CTAB.

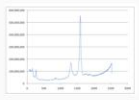

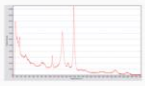

Figures. Raman spectrum of dispersed SWNTs in SDS and solids, respectively

Type of CNT	Band	SDS	CTAB	Triton X-100
MWNTs-1	D	1389±2	1386±2	1391±1
	G	1594±12	1582±7	1601±2
	G'	2618±1	2618±1	2622±1
MWNTs-2	D	1381±1	1381±1	1387±1
	G	1596±1	1585±3	1603±1
	G'	2613±3	2622±1	2622±1
MWNTs-3	D	1385±1	1385±1	1383±1
	G	1589±1	1586±1	1606±1
	G'	2615±1	-	-
MWNTs-4	D	1384±1	1385±1	1386±2
	G	1603±3	1601±2	1601±2
	G'	-	-	-
MWNTs-5	D	1383±1	-	1386±1
	G	1600±1	-	1603±1
	G'	-	-	-
MWNTs-6	D	1383±1	1386±1	-
	G	1595±1	1600±1	-
	G'	-	-	-
MWNTs-7	D	-	1386±1	1386±1
	G	-	1600±1	1595±1
	G'	-	-	2616±1
SWNTs	D	1384±5	1383±1	1386±1
	G	1581±5	1582±2	1591±1
	G'	-	-	2596±1

MIXTURES OF CARBON NANOTUBES

There is a relationship between the percentage of SWNTs in the mixture and the ratio of height of D/G bands. These results suggest that Raman can be employed to determine the quantity of carbon nanotubes of each nature present in an unknown sample.

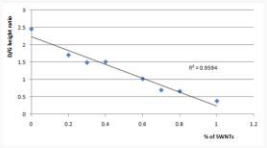

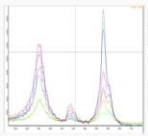

Above: Relationship between the percentage of SWNTs present in the sample and the height of D/G band ratio.

Below: Variation of the intensity of D and G band with the proportion of MWNTs-1 and SWNTs

CONCLUSIONS

THE PRESENCE OF SURFACTANT DOES NOT AFECT TO THE CNT RAMAN SIGNAL AND FACILITATE THE FOCUSING OF THE SAMPLE AND COLLECTION OF SPECTRUM

→

CARBON NANOTUBES WITH DIFFERENT CHARACTERISTICS GENERATE DIFFERENT RAMAN SPECTRUM

→

A FAST AND SIMPLE METHODOLOGY HAS BEEN DEVELOPED FOR THE ANALYSIS OF CNTs THROUGH A PORTABLE RAMAN EQUIPMENT

→

D/G BAND RELATIONSHIP HAS BEEN EMPLOYED FOR THE DETERMINATION OF THE PRESENCE OF MWNTs IN PRODUCTS OF SYNTHESIS OF SWNTs

CARACTERIZACIÓN DE NANOTUBOS DE CARBONO MEDIANTE EQUIPOS DE ESPECTROSCOPIA RAMAN PORTÁTILES

A.I. López-Lorente, B.M. Simonet, M. Valcárcel

Departamento de Química Analítica, Universidad de Córdoba. Edificio Anexo C3, Campus de Rabanales, 14071 Córdoba.

E-mail: qa1meobj@uco.es

OBJETIVO

Desarrollar un método rápido para la monitorización de la tipología de nanotubo de carbono mediante un equipo Raman portátil.

INTRODUCCIÓN

La espectroscopia Raman es una poderosa herramienta capaz de proporcionar gran información de estos sistemas. Por lo general las muestras están constituidas por una mezcla de nanotubos de carbono, de modo que el espectro Raman corresponde a un promedio de espectros de los distintos nanotubos. Las transiciones ópticas en los CNTs ocurren entre singularidades de van Hove de las bandas electrónicas de valencia y conducción. Las bandas más características de los CNTs que se han utilizado en este trabajo son la banda correspondiente a la vibración fundamental de elongación tangencial denominada G, sobre 1600 cm^{-1}, así como la banda D de segundo orden en la zona de 1300 cm^{-1}.

Banda G o modos tangenciales aparecen alrededor de 1600 cm^{-1}. Provienen de vibraciones dentro del plano de las láminas de grafito. Su perfil indica el carácter metálico o semiconductor de los CNTs.

Banda G', en torno a 2600 cm^{-1}. Es el armónico de segundo orden de la banda D.

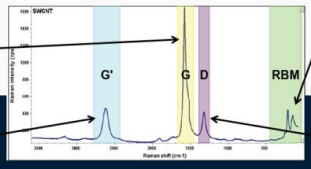

"Radial breathing modes" (RBMs), aparecen en la zona del espectro en torno a 150 cm^{-1}. Su frecuencia es proporcional a la inversa del diámetro del nanotubo. Son informativas en el caso de SWNTs.

Banda D, en torno a 1300 cm^{-1}. Su origen está relacionado con el desorden y los defectos en la estructura de los CNTs.

EXPERIMENTAL

CONDICIONES ÓPTIMAS DE MEDIDA

- Longitud de onda del láser: 785 nm
- Potencia del láser: 499.95 mW
- Tiempo de adquisición: 50 s
- Espectros acumulados: 6

NATURALEZA CNTs

Se han analizado CNTs de distinta naturaleza encontrándose espectros característicos para cada uno de ellos. Cada CNT posee una relación de las bandas D/G característica. Además en los SWNTs aparecen las bandas RBM y la banda G está desplazada unos pocos nm.

	Diámetro (nm)	Longitud (µm)	Funcionalización
MWNTs-1	10-30	10-30	2.5 (wt)% OH
MWNTs-2	10-30	10-30	1.6 (wt)% COOH
MWNTs-3	10-30	10-30	-
MWNTs-4	5-20	1-10	-
MWNTs-5	10-20	5-15	-
MWNTs-6	9.5	1.5	-
MWNTs-7	110-170	2	-
SWNTs	<2	5-15	-

RESULTADOS

ESPECTROS RAMAN DE CNTs DISPERSADOS CON TENSIOACTIVO

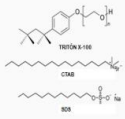

La dispersión con tensioactivos permite obtener el espectro de CNTs de forma rápida, sin interferencias del tensioactivo y minimizando problemas de fluorescencia y degradación de la muestra como consecuencia de una mejor disipación de calor, por lo que permite emplear potencias de láser mayores. Se ha demostrado que el espectro obtenido puede correlacionarse con el espectro de muestras sólidas.

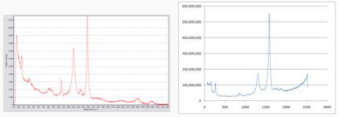

Figuras. Espectro Raman de SWNTs dispersados en tensioactivo (SDS) y sólidos, respectivamente

MEZCLAS DE NANOTUBOS DE CARBONO

Dado que cada tipo de nanotubo origina un espectro Raman característico, investigamos la posibilidad de identificar y (semi)cuantificar la presencia de nanotubos de carbono de distinta naturaleza en una dispersión de CNTs de distinto tipo. Para ello preparamos mezclas con distinta cantidad de SWNTs y MWNTs modificados con grupos hidroxilos.

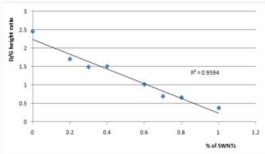

La figura muestra la variación de la relación de las bandas D y G al variar la proporción de cada tipo de nanotubo, relación que resultó ser 0,378 para los SWNTs puros y 2,4587 para MWNTs-1 en ausencia de otro tipo de nanotubo. Se observa que existe una relación lineal entre la altura o área de as bandas D/G y el % de SWNTs.

CONCLUSIONES

LA PRESENCIA DE TENSIOACTIVO NO AFECTA A LA SEÑAL RAMAN DE LOS CNTs Y FACILITA EL ENFOQUE DE LA MUESTRA Y OBTENCIÓN DEL ESPECTRO

→ NANOTUBOS DE DISTINTAS CARACTERÍSTICAS GENERAN ESPECTROS RAMAN DIFERENTES

→ SE HA DESARROLLADO UNA METODOLOGÍA RÁPIDA Y SIMPLE DE ANÁLISIS DE CNTs MEDIANTE UN EQUIPO PORTÁTIL DE RAMAN

→ A PARTIR DE LA RELACION DE BANDAS D Y G SE HA DETERMINADO LA PRESENCIA DE MWNTs EN PRODUCTOS DE SÍNTESIS DE SWNTs

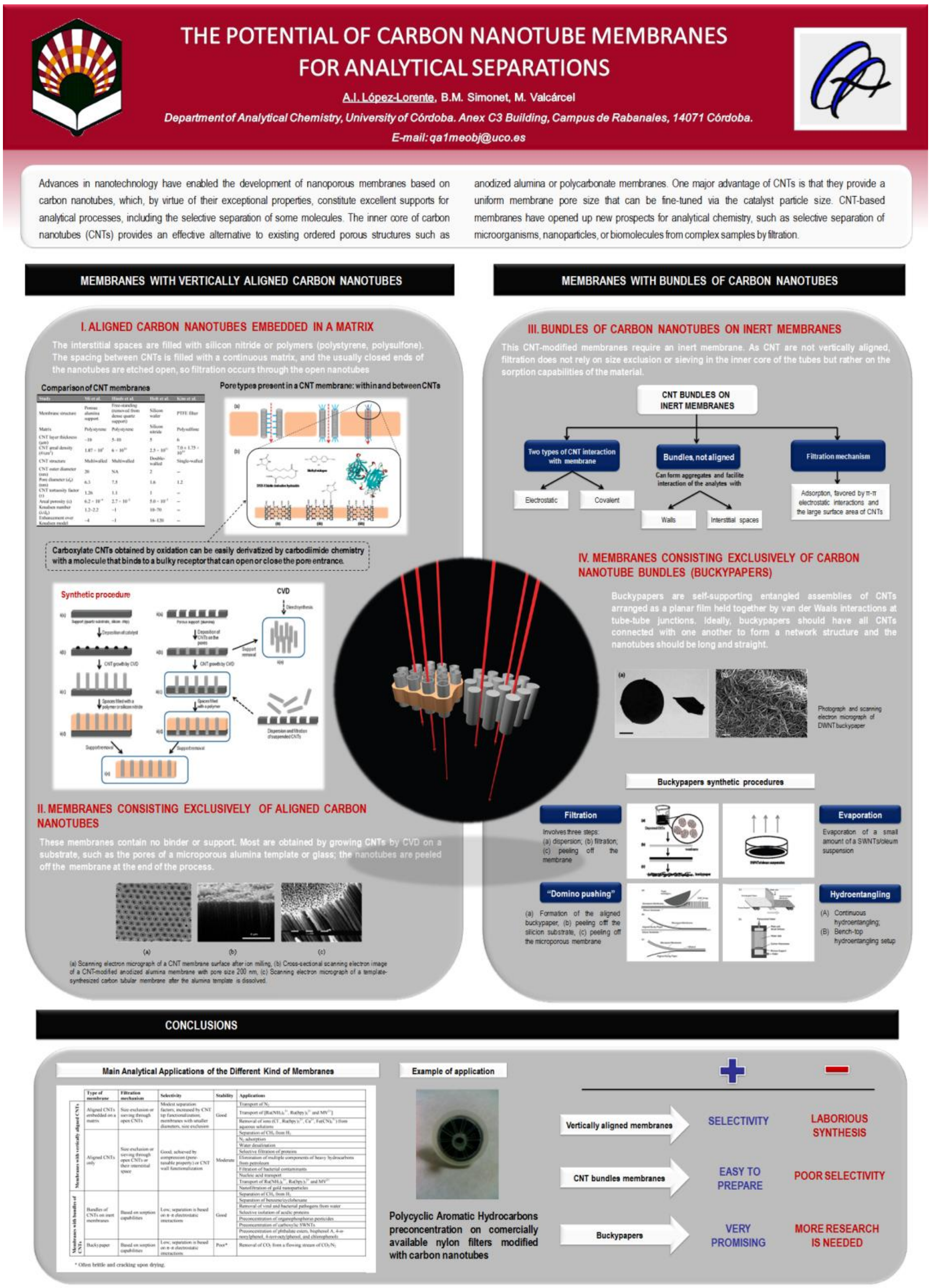
THE POTENTIAL OF CARBON NANOTUBE MEMBRANES FOR ANALYTICAL SEPARATIONS
A.I. López-Lorente, B.M. Simonet, M. Valcárcel
Department of Analytical Chemistry, University of Córdoba. Anex C3 Building, Campus de Rabanales, 14071 Córdoba.
E-mail: qa1meobj@uco.es
Advances in nanotechnology have enabled the development of nanoporous membranes based on carbon nanotubes, which, by virtue of their exceptional properties, constitute excellent supports for analytical processes, including the selective separation of some molecules. The inner core of carbon nanotubes (CNTs) provides an effective alternative to existing ordered porous structures such as anodized alumina or polycarbonate membranes. One major advantage of CNTs is that they provide a uniform membrane pore size that can be fine-tuned via the catalyst particle size. CNT-based membranes have opened up new prospects for analytical chemistry, such as selective separation of microorganisms, nanoparticles, or biomolecules from complex samples by filtration.
MEMBRANES WITH VERTICALLY ALIGNED CARBON NANOTUBES
I. ALIGNED CARBON NANOTUBES EMBEDDED IN A MATRIX
The interstitial spaces are filled with silicon nitride or polymers (polystyrene, polysulfone). The spacing between CNTs is filled with a continuous matrix, and the usually closed ends of the nanotubes are etched open, so filtration occurs through the open nanotubes
Comparison of CNT membranes
Pore types present in a CNT membrane: within and between CNTs
Carboxylate CNTs obtained by oxidation can be easily derivatized by carbodiimide chemistry with a molecule that binds to a bulky receptor that can open or close the pore entrance.
Synthetic procedure
CVD
II. MEMBRANES CONSISTING EXCLUSIVELY OF ALIGNED CARBON NANOTUBES
These membranes contain no binder or support. Most are obtained by growing CNTs by CVD on a substrate, such as the pores of a microporous alumina template or glass; the nanotubes are peeled off the membrane at the end of the process.
(a) (b) (c)
(a) Scanning electron micrograph of a CNT membrane surface after ion milling, (b) Cross-sectional scanning electron image of a CNT-modified anodized alumina membrane with pore size 200 nm, (c) Scanning electron micrograph of a template-synthesized carbon tubular membrane after the alumina template is dissolved.
MEMBRANES WITH BUNDLES OF CARBON NANOTUBES
III. BUNDLES OF CARBON NANOTUBES ON INERT MEMBRANES
This CNT-modified membranes require an inert membrane. As CNT are not vertically aligned, filtration does not rely on size exclusion or sieving in the inner core of the tubes but rather on the sorption capabilities of the material.
CNT BUNDLES ON INERT MEMBRANES
Two types of CNT interaction with membrane
Electrostatic
Covalent
Bundles, not aligned
Can form aggregates and facilite interaction of the analytes with
Walls
Interstitial spaces
Filtration mechanism
Adsorption, favored by π-π electrostatic interactions and the large surface area of CNTs
IV. MEMBRANES CONSISTING EXCLUSIVELY OF CARBON NANOTUBE BUNDLES (BUCKYPAPERS)
Buckypapers are self-supporting entangled assemblies of CNTs arranged as a planar film held together by van der Waals interactions at tube-tube junctions. Ideally, buckypapers should have all CNTs connected with one another to form a network structure and the nanotubes should be long and straight.
Photograph and scanning electron micrograph of DWNT buckypaper
Buckypapers synthetic procedures
Filtration
Involves three steps: (a) dispersion; (b) filtration; (c) peeling off the membrane
Evaporation
Evaporation of a small amount of a SWNTs/oleum suspension
"Domino pushing"
(a) Formation of the aligned buckypaper, (b) peeling off the silicion substrate, (c) peeling off the microporous membrane
Hydroentangling
(A) Continuous hydroentangling; (B) Bench-top hydroentangling setup
CONCLUSIONS
Main Analytical Applications of the Different Kind of Membranes
Example of application
Polycyclic Aromatic Hydrocarbons preconcentration on comercially available nylon filters modified with carbon nanotubes
+
−
Vertically aligned membranes
SELECTIVITY
LABORIOUS SYNTHESIS
CNT bundles membranes
EASY TO PREPARE
POOR SELECTIVITY
Buckypapers
VERY PROMISING
MORE RESEARCH IS NEEDED

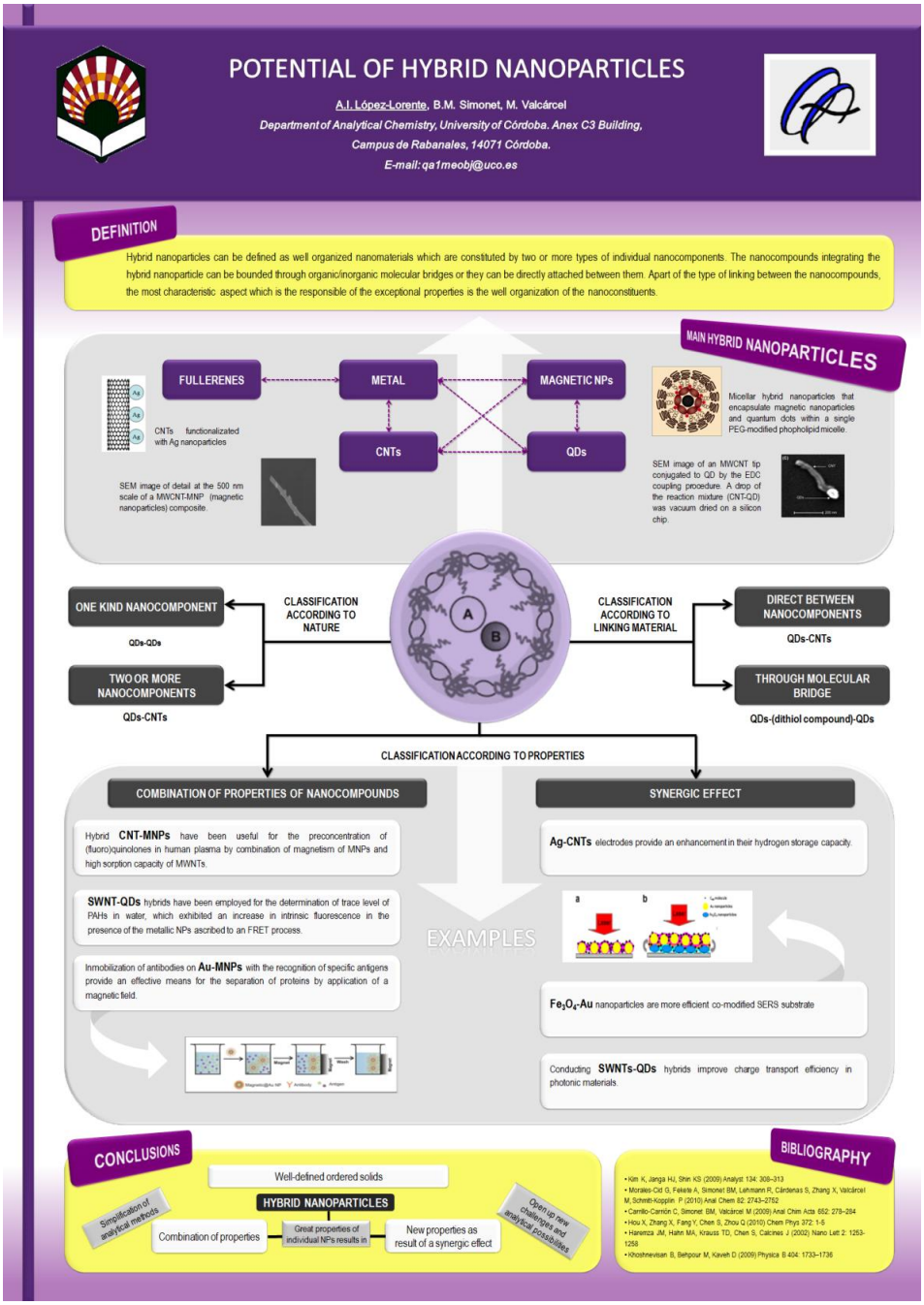
POTENTIAL OF HYBRID NANOPARTICLES
A.I. López-Lorente, B.M. Simonet, M. Valcárcel
Department of Analytical Chemistry, University of Córdoba. Anex C3 Building, Campus de Rabanales, 14071 Córdoba.
E-mail: qa1meobj@uco.es
DEFINITION
Hybrid nanoparticles can be defined as well organized nanomaterials which are constituted by two or more types of individual nanocomponents. The nanocompounds integrating the hybrid nanoparticle can be bounded through organic/inorganic molecular bridges or they can be directly attached between them. Apart of the type of linking between the nanocompounds, the most characteristic aspect which is the responsible of the exceptional properties is the well organization of the nanoconstituents.
MAIN HYBRID NANOPARTICLES
FULLERENES
METAL
MAGNETIC NPs
CNTs
QDs
CNTs functionalized with Ag nanoparticles
SEM image of detail at the 500 nm scale of a MWCNT-MNP (magnetic nanoparticles) composite.
Micellar hybrid nanoparticles that encapsulate magnetic nanoparticles and quantum dots within a single PEG-modified phopholipid micelle.
SEM image of an MWCNT tip conjugated to QD by the EDC coupling procedure. A drop of the reaction mixture (CNT-QD) was vacuum dried on a silicon chip.
CLASSIFICATION ACCORDING TO NATURE
ONE KIND NANOCOMPONENT
QDs-QDs
TWO OR MORE NANOCOMPONENTS
QDs-CNTs
CLASSIFICATION ACCORDING TO LINKING MATERIAL
DIRECT BETWEEN NANOCOMPONENTS
QDs-CNTs
THROUGH MOLECULAR BRIDGE
QDs-(dithiol compound)-QDs
CLASSIFICATION ACCORDING TO PROPERTIES
COMBINATION OF PROPERTIES OF NANOCOMPOUNDS
Hybrid CNT-MNPs have been useful for the preconcentration of (fluoro)quinolones in human plasma by combination of magnetism of MNPs and high sorption capacity of MWNTs.
SWNT-QDs hybrids have been employed for the determination of trace level of PAHs in water, which exhibited an increase in intrinsic fluorescence in the presence of the metallic NPs ascribed to an FRET process.
Inmobilization of antibodies on Au-MNPs with the recognition of specific antigens provide an effective means for the separation of proteins by application of a magnetic field.
SYNERGIC EFFECT
Ag-CNTs electrodes provide an enhancement in their hydrogen storage capacity.
EXAMPLES
Fe3O4-Au nanoparticles are more efficient co-modified SERS substrate
Conducting SWNTs-QDs hybrids improve charge transport efficiency in photonic materials.
CONCLUSIONS
Well-defined ordered solids
HYBRID NANOPARTICLES
Simplification of analytical methods
Combination of properties
Great properties of individual NPs results in
New properties as result of a synergic effect
Open up new challenges and analytical possibilities
BIBLIOGRAPHY
• Kim K, Janga HJ, Shin KS (2009) Analyst 134: 308–313
• Morales-Cid G, Fekete A, Simonet BM, Lehmann R, Cárdenas S, Zhang X, Valcárcel M, Schmitt-Kopplin P (2010) Anal Chem 82: 2743–2752
• Carrillo-Carrión C, Simonet BM, Valcárcel M (2009) Anal Chim Acta 652: 278–284
• Hou X, Zhang X, Fang Y, Chen S, Zhou Q (2010) Chem Phys 372: 1-5
• Haremza JM, Hahn MA, Krauss TD, Chen S, Calcines J (2002) Nano Lett 2: 1253-1258
• Khoshnevisan B, Behpour M, Kaveh D (2009) Physica B 404: 1733–1736

INFLUENCE OF THE AGGREGATION STATE IN THE RAMAN SPECTRUM OF SINGLE-WALLED CARBON NANOTUBES (SWNTs)

A.I. López-Lorente, B.M. Simonet, M. Valcárcel

Analytical Chemistry Department, University of Córdoba. Annex C3 Building, Campus of Rabanales, 14071 Córdoba.

E-mail: qa1meobj@uco.es

Raman spectroscopy is one of the most employed techniques for CNT characterization. The most significant spectral features for SWNTs are the radial breathing mode (RBM, 100-300 cm^{-1}), the disorder peak (D peak, ~1350 cm^{-1}), the tangential mode (G band, 1400-1700 cm^{-1}), and the second-order overtone of the D peak (D', 2500-2800 cm^{-1}). SWNTs spectrum dependence in function of their aggregation state has been demonstrated, by observing a change in the relative intensities of D and G bands.

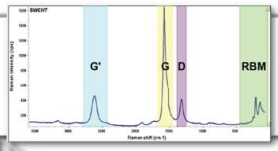

I CNTs RAMAN SPECTRUM DOES NOT DRAMATICALLY CHANGE WHEN INCREASING LASER POWER

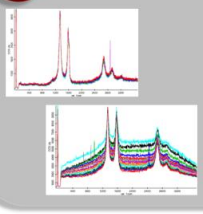

Spectra were measured by gradually increasing the laser power and, although it was found that baseline increases, differences in the relative intensity of the bands were not found. Laser was focused on the same point of the sample during a certain time and changes as a consequence of sample degradation were not neither detected.

II FOCUSING DOES NOT AFFECT D AND G BANDS INTENSITY RELATIONSHIP

A depth image revealed that there are no significant differences in the Raman spectrum of carbon nanotubes when modifying focusing of the lens. A proportional increase or decrease in sensitivity is observed for all the bands in the spectrum.

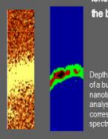

Depth Raman image of a bundle of carbon nanotubes. Cluster analysis of the image corresponding spectra

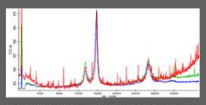

Raman spectra corresponding to the region of the image at the left obtained by cluster analysis of the showed Raman image.

III D AND G BANDS INTENSITY RELATIONSHIP VARY AS A FUNCTION OF CARBON NANOTUBE AGGREGATION STATE

Powder carbon nanotube Raman images were recorded by placing them over a glass plate. The set of spectra that conform the image were analyzed by K-NN cluster analysis, which classified the spectra in different groups as a function of the relative intensities of the bands.

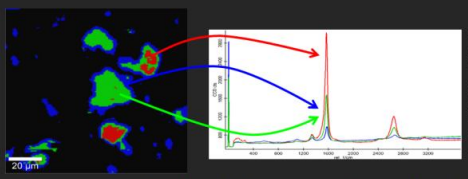

Raman spectra corresponding to the region that appear in the left image and which have been obtained by K-NN cluster analysis on the basis of a Raman image composed by Raman spectra acquired with a 20x objective and an integrating time of 0.03 s.

As it can be seen in the coloured image generated as a function of the different areas, differences in spectra are observed depending on the position of the nanotubes in the sample: in the inside of the aggregates or at their ends, where it is expected to be more debundled.

IV D BAND VARIATIONS ARE OBSERVED FOR AN ISOLATED NANOTUBE, RELATED TO DEFECT AMONG THE NANOTUBE AXIS

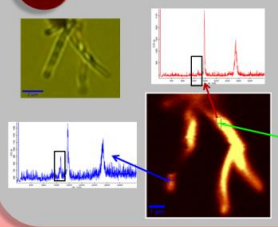

As it can be seen in the spectra of different locations in the Raman image, depending on the position a higher or lower contribution of D band to the spectrum is observed. Such band is related to the defects present in the nanotube as well as the presence of sp^3 bonds on them.

In the left a photograph obtained with a confocal Raman microscope with a 20x objective is shown. The central picture is a Raman image build by using Raman spectra, some of which have been extracted of the image at different locations.

CONCLUSIONS

I. It has been demonstrated that SWNTs aggregation rate can be evaluated by means of high resolution Raman spectroscopy. Differences in the spectra are significant.

II. The next step is to be able to apply this recognition system to manufactured samples where material's properties depend on the aggregation state of carbon nanotubes.

III. Although this fact has been widely described in literature, it can not have still been evaluated by means of an analytical technique.

IV. This is the first step where high resolution Raman spectroscopy potential for this kind of applications is demonstrated.

Determination of carboxylic SWCNTs in river water by microextraction in ionic liquid and determination by Raman spectroscopy

Ángela I. López-Lorente, Bartolomé M. Simonet, Miguel Valcárcel

Analytical Chemistry Department, University of Córdoba. Annex C3 Building, Campus of Rabanales, 14071 Córdoba. E-mail: qa1meobj@uco.es

Abstract

- A simple approach for the preconcentration of carboxylated single walled carbon nanotubes and their determination in river water samples is proposed.

Microliquid-liquid extraction into an ionic liquid in the presence of a cationic surfactant

Ionic liquid phase is microfiltrated by using a home-made filtration device on a cellulose membrane.

Carbon nanotubes retained in the membrane are directly analyzed by Raman spectroscopy, which allows their direct characterization and quantification

- The limit of detection was 0.050 mg L^{-1}. The precision, for a 1.4 mg L^{-1} concentration of carbon nanotubes, is 3.2%.

SWNTs functionalization and study of variables

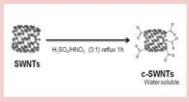

After the acid treatment, the SWNTs were negatively charged by covalently attached carboxylic (-COOH) groups on the sidewalls and the open ends, which make them highly soluble in water.

RECOMMENDED VARIABLES	
Selection of ionic liquid	BMIM PF_6
Effect of amount and nature of cationic surfactant	CTAC 3.12 mM
Effect of pH	1.4
Selection of membrane	Cellulose

cSWNTs preconcentration procedure

2 mL of river water sample containing 3.12 mM of CTAC at pH=1.4, were treated with 0.1 g of BMIM PF_6

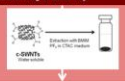

The river water samples were fortified with certain volume of a stock solution of c-SWNTs, the solution was homogenized and mixed for 2 hours.

10 µL of the extract were filtered through a Millipore cellulose membrane with a pore size of 5 µm*.

A home-made designed microfiltration device with sandwich configuration was employed (filtration ⌀= 1.3 mm).

*For samples with very low concentration (<0.8 mgL^{-1}), a modified procedure maintaining the proportion of ionic liquid to water and increasing the volumes is proposed. A major volume is filtrated on the cellulose membrane.

Figure. Scheme of the home-made microfiltration device

Raman spectra of cSWCNTs in IL

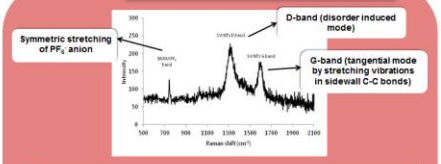

RAMAN MEASUREMENTS CONDITIONS	
785 nm laser	1-second CCD exposure
28.5 mW power	10 signal acquisitions
20x objective	Acquired from five locations within each membrane and repeated over three samples

Analytical features

The analytical signal employed was the intensity of the D band of carbon nanotubes in the Raman spectra divided by the intensity of the ionic liquid band at 739 cm^{-1} using the average of the five locations. There is no effect of the surfactant on the Raman spectrum after the filtration step.

Calibration equation	S=(0.54±0.03)[c-SWNTs]+(0.39±0.01)
R^2	0.9856
Lineal range	0.4-4 mgL^{-1}
LOD[a]	0.169 mg L^{-1}
LOD[b] (Large volume procedure)	0.050 mg L^{-1}
RSD[c] (%)	3.2%
RSD[d] (%) (Large volume procedure)	12.6%

[c-SWNTs]: Concentration of c-SWNTs in the aqueous media in mgL^{-1}.
[a]Limit of detection, determined as ($3S_a$)/b, for y=bx+a.
[c]Relative standard deviation, determined from five measurements of 1.4 mgL^{-1} c-SWNTs.
[d]Relative standard deviation, determined from five measurements of 0.8 mgL^{-1} c-SWNTs.

Application to river water samples

Samples of water from Guadalquivir river were spiked and analyzed following the recommended procedure. Before spiking the samples were analyzed and no carbon nanotubes were found in them. Recovery test was performed in order to study accuracy of the analysis of spiked samples.

Fortification level	Added concentration (mgL^{-1})	Found concentration[a] (mgL^{-1})	Recovery (%)	RSD(%)
1	0.94	0.68±0.08	70.1-81.2	8.98
2	1.41	1.11±0.07	73.8-84.6	4.98
3	1.88	1.83±0.08	92.8-101.7	3.63
4	2.35	2.2±0.1	93.9-100.3	4.04

[a]Average of three independent spiked samples±CI ($p < 0.05$).

Conclusions

I. Thanks to the high affinity of imidazolium group for the carbon nanotube, it is possible to preconcentrate the nanotubes in a low volume of ionic liquid

II. Regards detection, carbon nanotubes present a characteristic Raman spectrum which has been used as analytical signal.

III. It should be remarked that the use of a cationic surfactant is crucial for obtaining a homogeneous dispersion of carbon nanotubes on the membrane

IV. It has been demonstrated that ionic liquid with cationic surfactant is a good combination to extract carboxylated single-walled carbon nanotubes from river water samples.

Continuous flow synthesis of bare gold nanoparticles and their application to the determination of carbon nanotubes by SERS

Ángela I. López-Lorente[a], Miguel Valcárcel[a], Boris Mizaikoff[b]

[a]Analytical Chemistry Department, University of Córdoba. Córdoba. E-mail: qa1meobl@uco.es. [b]Institute of Analytical and Bioanalytical Chemistry, University of Ulm, Ulm, Germany.

Abstract

• A simple approach for the SERS determination of carboxylated single walled carbon nanotubes in river water samples is proposed.

Flow synthesis of bare gold nanoparticles by using stainless steel as solid reducing agent

Characterization of bare gold nanoparticles

Bare AuNPs are microfiltrated on a membrane forming the SERS active substrate.

c-SWNTS are determined and quantified by SERS spectroscopy using a portable Raman spectrometer

Flow synthesis of bare gold nanoparticles

• $HAuCl_4$ solution is introduced into a stainless steel tubular coil (1/8" o.d., 2 mm i.d., 1.5 m length) using a peristaltic pump.

• The stainless steel coil, which assists the reduction of gold(III) into nanoparticles, is immersed in a thermostatic bath in order to control the reaction temperature.

VARIABLES STUDIED
Concentration of gold precursor
Flow rate
Temperature

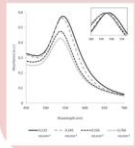

Uv-vis spectra of solutions of gold nanoparticles obtained through the proposed synthesis at a temperature of 40ºC at different flow rates: 0.135, 0.240, 0.556 and 0.766 mL·min⁻¹. The inset shows the maximum of the peak normalized where a shift in wavelength with flow rate can be observed.

Characterization of bare AuNPs

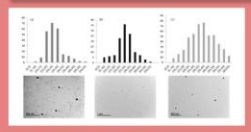

TEM image and the corresponding particle size distribution analysis of the Au nanoparticles synthesized in the tubular reactor (a) 60ºC 0.135 mL·min⁻¹, (b) 40ºC 0.556 mL·min⁻¹, (c) 80ºC 0.240 mL·min⁻¹.

Flow rate (mL·min⁻¹)	Temperature (ºC)	Particle size (nm) Average diameter	Standard deviation
0.041	40	33	16
0.240	40	33	10
0.556	40	27	8
0.135	60	29	7
0.556	60	24	9
1.081	60	23	10
0.240	80	35	12
0.556	80	28	11
1.487	80	26	9

SERS determination of cSWCNTs

RAMAN MEASUREMENTS CONDITIONS	
785 nm laser	1-second CCD exposure
28.5 mW power	10 signal acquisitions

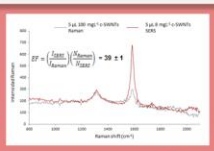

$EF = \left(\frac{I_{SERS}}{I_{Raman}}\right)\left(\frac{N_{Raman}}{N_{SERS}}\right) = 39 \pm 1$

Measured Raman spectra for c-SWNTs with and without gold nanoparticles loaded in the membrane.

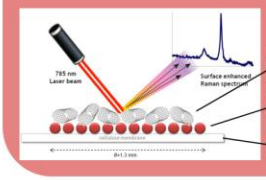

Microfiltration of water sample containing c-SWNTs (2)

Microfiltration of bare AuNPs forming SERS substrate (1)

Cellulose acetate membrane (pore size 0.2 µm)

Analytical features

The analytical signal employed was the peak height of the 1583 cm^{-1} Raman G band of carbon nanotubes. Each concentration level was analyzed in triplicate (measuring each sample at three randomly selected locations within the membrane).

Calibration equation (Langmuir isotherm)[a]	y = (a*b*x^(1-c))/(1 + b*x^(1-c))
R^2	0.99459
LOD	10 µg L^{-1}
RSD[b] (%) (intra-membrane)	1.19%
RSD[c] (%) (inter-membrane)	10.5%

[a] Where a = 351.51638±7.45067; b = 0.00114±0.0008; c = −2.82639±0.3938 and x = c-SWNTs concentration in mg L^{-1}.
[b] Relative standard deviation, determined from five measurements of 5 µL 10 mg L^{-1} c-SWNTs within the same membrane.
[c] Relative standard deviation, determined from the average value of five measurements of 5 µL 10 mg L^{-1} c-SWNTs in different membranes.

Application to river water samples

Samples of water from Guadalquivir river were spiked and analyzed following the recommended procedure. Before spiking the samples were analyzed and no carbon nanotubes were found in them. Recovery test was performed in order to study accuracy of the analysis of spiked samples.

Fortification level	Added concentration (mgL⁻¹)	Found concentration[a] (mgL⁻¹)	Recovery (%)	RSD(%)
1	5	4.5 ± 0.3	86.5-93.8	4.02
2	8	8.0 ± 0.6	96.1-105.1	4.50
3	10	10.3 ± 0.7	97.8-105.5	4.13
4	15	14 ± 1	91.2-100.5	5.16

[a]Average of three independent spiked samples±CI ($p < 0.05$).

Conclusions

I. AuNPs can be synthesized in a continuous flow tubular reactor in which the own stainless steel walls of the reactor acts as reducing agent.

II. A simple SERS approach to the determination of c-SWNTs in water samples is presented using the synthesized bare gold nanoparticles.

III. This simple, affordable and portable procedure could be used to the in situ monitorization of the release of these nanostructures from point's source of contamination

IV. In this work, the two facets of analytical nanoscience & nanotechnology are covered. NPs are considered both objects of analysis (CNTs) and analytical tools (AuNPs) improving the detection.

Attenuated total reflection infrared (ATR-IR) spectroscopy in-situ monitoring of the synthesis of bare gold nanoparticles

Ángela I. López-Lorente[a], Markus Sieger[b], Miguel Valcárcel[a], Boris Mizaikoff[b]

[a]Analytical Chemistry Department, University of Córdoba. Córdoba. E-mail: qa1meobj@uco.es. [b] Institute of Analytical and Bioanalytical Chemistry, University of Ulm, Ulm, Germany.

Stainless steel synthesis of bare AuNPs

• AuNPs are synthesized from tetrachloroauric acid solution using stainless steel as solid reducing agent[1].

• Bare AuNPs without any ligand in their surface are obtained, with an average diameter of 20 nm.

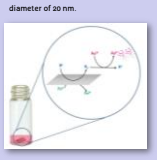

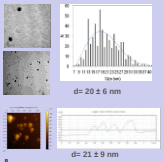

[1] A.I. López-Lorente, B.M. Simonet, M. Valcárcel, B. Mizaikoff. Anal. Chim. Acta 788 (2013) 122-128.

In-situ ATR unit synthesis of AuNPs

• AuNPs were directly synthesized inside the ATR unit by means of the stainless steel which forms the unit walls.

• IR measurements were performed using a Vertex 70 FT-IR spectrometer equipped with a BioATRCell-II unit.

• A stainless steel O-ring was glued on a piece of silicon. $HAuCl_4$ was added and the formation of AuNPs investigated by SEM.

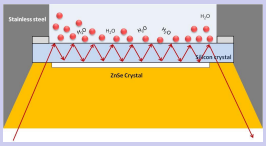

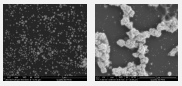

Scanning electron microscopy images of in-situ synthesized gold nanoparticles: (left) after 20 min, (right) after 100 min.

ATR-IR monitorisation of the *in-situ* synthesis

• While synthesizing, AuNPs adsorb in the SiO_2 ATR surface. Despite the IR inactivity of AuNPs, their formation can be monitored by measuring the increase in water absorption bands by SEIRA effect.

• As AuNPs are formed and deposited on the ATR surface, an increase in the H2O bending and the OH stretching bands is observed, despite a decrease in the amount of water molecules present in the euanescent field during the deposition and exchange of water molecules by AuNPs.

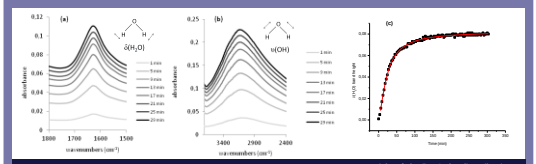

H_2O bending mode | OH stretch | Height of the $\delta(H_2O)$ bending vibration band at 1644 cm^{-1} and best-fit function of the band height versus time.

Influence of gold(III) precursor concentration and temperature

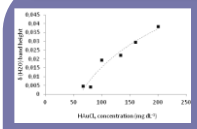

• The kinetic of the reaction follows a different rate depending on the concentration of gold(III) precursor: $HAuCl_4$.

FIGURE: Plot of $\delta(H_2O)$ band height versus $HAuCl_4$ water solution concentration at a time of 31 minutes.

• When increasing the temperature, the enhancement of water bands is observed faster, meaning that NPs are formed more rapidly.

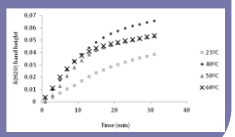

Synthesis of AuNPs in D_2O media

• Similarly to that observed in water media, as gold nanoparticles are synthesized in deuterium oxide media, absorption signals of ν(OD) and ν(CH) emerge with enhanced intensity.

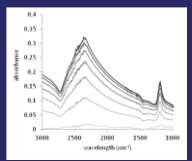

In-situ ATR-SEIRA spectra during the synthesis of AuNPs inside the ATR unit in a D_2O environment. The D_2O features shown in the spectra are directly the enhancement produced as AuNPs are obtained.

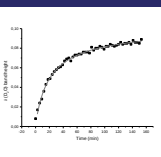

δ (D_2O) band height evolution with time as gold nanoparticles are synthesized in the ATR cell and deposited on the SiO_2 surface. Points were fitted to a Langmuir model.

Study of aggregation and sedimentation of AuNPs

• Increasing ionic strength of the solution containing AuNPs results in NP aggregation

• The gravitational sedimentation of AuNPs was monitored. CTAC was added in order to increase the sedimentation rate.

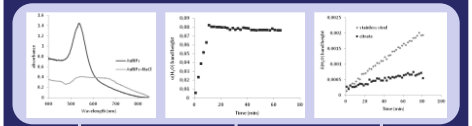

UV-Vis spectra of the gold nanoparticles solution prior and after the addition of NaCl increasing the ionic strength of the solution which leads to the aggregation of the AuNPs.

Plot of the water OH stretching band height versus time. At minute 11, 10 µL of 1M $AgNO_3$ solution were added.

Plot of water bending band height versus time during the sedimentation of citrate-coated and bare gold nanoparticles in CTAC media.

Conclusions

I. We propose the use of ATR-FTIR spectroscopy as tool for the study of gold nanoparticles solutions.

II. ATR-IR was used to monitor the *in-situ* synthesis of gold nanoparticles in the ATR unit by measuring an enhancement of water bands due to SEIRA effect.

III. IR can be also used to control chemical changes in solution that may affect the gold nanoparticles.

IV. It has been shown that IR spectroscopy can be used to evaluate the sedimentation process of gold nanoparticles on the surface.

Contribuciones analíticas a la caracterización y determinación de nanopartículas

Ángela Inmaculada López Lorente. Departamento de Química Analítica. Universidad de Córdoba

NANOCIENCIA Y NANOTECNOLOGÍA ANALÍTICAS

La **NANOCIENCIA** es la ciencia de la síntesis, análisis y manipulación de materiales en la nanoescala, donde las propiedades son muy diferentes a las que encontramos en la escala convencional.

Una **NANOPARTÍCULA** es una partícula que cuenta con una o más dimensiones menores que 100 nanómetros (1 nm=10^{-9} m).

NANOTUBOS DE CARBONO: MWNTs (multicapa), SWNTs (monocapa), c-SWNTs (carboxilados)

NANOPARTÍCULAS METÁLICAS: AuNPs (Sin recubrimiento), AuNPs (Con citrato), AgNPs

CONTENIDO DE LA TESIS

- Microextracción líquido-líquido con líquidos iónicos
- Membranas modificadas con nanotubos de carbono
- Espectroscopia Raman amplificada por superficie (SERS)
- Técnicas de separación Electroforesis capilar
- Técnicas microscópicas (TEM, SEM, AFM)
- Técnicas espectroscópicas (Raman e infrarrojo)

DETERMINACIÓN — CARACTERIZACIÓN — SÍNTESIS

DETERMINACIÓN de c-SWNTs MEDIANTE SERS USANDO AuNPs SIN RECUBRIMIENTO

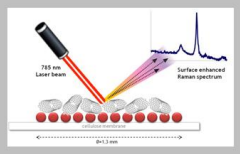

- AuNPs se usaron como herramienta para determinar c-SWNTs en agua de río mediante espectroscopia Raman amplificada por superficie (SERS).
- AuNPs fueron microfiltradas en membranas de celulosa formando el substrato SERS.
- Espectrómetro Raman portátil permite la determinación in-situ de los c-SWNTs en puntos de contaminación.

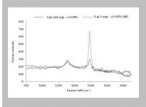

Incremento de la señal Raman de c-SWNTs en presencia de las AuNPs.

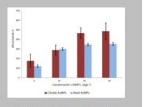

Comparación de AuNPs cubiertas con citrato convencionales con las propuestas en esta tesis.

CARACTERÍSTICAS ANALÍTICAS DEL MÉTODO

Ecuación calibrado (isoterma de Langmuir)*	$y = [a*b*x*(1-c)]/(1 + b*x*(1-c))$
R^2	0.99459
LOD	10 µg L^{-1}
RSD* (%) (intra-membrana)	1.19%
RSD* (%) (inter-membrana)	10.5%

*Donde a=0.51658 ±7.45067; b=0.0011405±0.0008; c=2.8269801.3938 y x= concentración de c-SWNTs en mg·L^{-1}.

SÍNTESIS DE NANOPARTÍCULAS DE ORO SIN RECUBRIMIENTO CATALIZADAS POR ACERO INOXIDABLE

SÍNTESIS INNOVADORA PROPUESTA

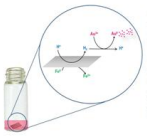

- Se ha propuesto una nueva síntesis de AuNPs sin ligandos en superficie catalizada por acero inoxidable como reductor sólido.
- Síntesis económica, fácilmente escalable, respetuosa con el medio ambiente.
- AuNPs estables, sin recubrimiento que interfiera en futuras aplicaciones.

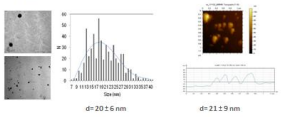

SÍNTESIS EN FLUJO CONTINUO

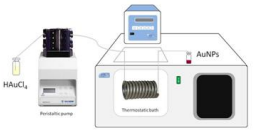

- Se ha diseñado un sistema para la síntesis en flujo continuo usando un reactor tubular de acero inoxidable que actúa de agente reductor.
- Controlando las condiciones del sistema (temperatura, flujo) podemos seleccionar el tamaño de las AuNPs sintetizadas.

CARACTERIZACIÓN y MONITORIZACIÓN IN-SITU de la SÍNTESIS de AuNPs SIN RECUBRIMIENTO MEDIANTE ATR-IR

ATR=Attenuated total reflectance infrared spectroscopy

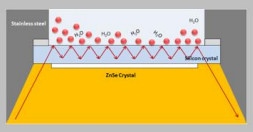

- AuNPs son sintetizadas en la celda ATR mediante el acero inoxidable de las paredes. La síntesis puede ser monitorizada in-situ.
- ATR-IR permite investigar cambios de agregación de AuNPs por variaciones de fuerza iónica o pH, así como el estudio de la sedimentación de AuNPs.

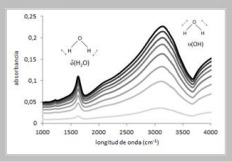

Al depositarse las AuNPs en la superficie ATR producen una amplificación de la señal del agua (efecto SCIRA), a pesar del menor número de moléculas de agua en la superficie ya que son reemplazadas por AuNPs.